THEORETICAL STUDIES OF ELECTRONICALLY ADIABATIC AND NON-ADIABATIC CHEMICAL REACTION DYNAMICS

Thesis by

Joel Mark Bowman

In Partial Fulfillment of the Requirements

For the Degree of

Doctor of Philosophy

California Institute of Technology

Pasadena, California

1975

(Submitted September 18, 1974)

To my wife Karen and my friend Mike.

ACKNOWLEDGMENTS

It is a pleasure to thank Professor Aron Kuppermann for his guidance as my research advisor. His interest in my work and his enthusiasm for science greatly aided my research efforts.

I thank George C. Schatz for his collaboration on several publications and manuscripts and for many stimulating and useful discussions.

I thank Dr. Michael Baer for many discussions on many subjects.

I thank all of my contemporaries in the Kuppermann group for broadening my appreciation of experimental science.

I also wish to thank Professor William A. Goddard III, Professor Vincent McKoy and members of their research groups for their willingness to discuss subjects related to my research.

I thank Mike Coggiola, my best best friend, especially. His encouragement and support during the early days of my research were crucial to its eventual completion; and his constant help continues.

Finally, and with great affection I thank my wife Karen for her enormous help in preparing figures for this thesis, for her forbearance and understanding.

I thank California Institute of Technology for scholarships and teaching assistantships. I thank the National Science Foundation, the Shell Oil Company, and the Air Force Office of Scientific Research for financial aid.

I thank Linda Bryant for her expert, intelligent and efficient typing of Parts II and III of this thesis.

ABSTRACT

Part I presents several sets of comparisons of semi-classical, quasi-classical and exact quantum reactive scattering calculations for collinear chemical reactions. The possibility of modifying the standard quasi-classical method according to a quantum criterion is investigated. The systems studied are $H + H_2$, $F + H_2$, and $F + D_2$. In addition, a theoretical investigation of the semi-classical S matrix is made.

Details of a quasi-classical current density analysis of the $H + H_2$ reaction are presented and a comparison with exact quantum results is made.

A direct test of two versions of the vibrationally adiabatic theory of chemical reactions is made in Part II for the $H + H_2$ reaction. The adiabaticity of the symmetric stretch motion of the H_3 transition state is focussed upon. In addition, a determination of the completeness of adiabatic basis sets for scattering calculations is made.

The theory of electronically non-adiabatic chemical reactions is presented in Part III. Quantum calculations of the collinear $H^+ + H_2 \rightarrow H_2 + H^+$ reaction are described. A model and a realistic potential energy surface are employed in these calculations.

A fictitious electronically non-adiabatic $H + H_2$ collinear chemical reaction is treated quantum mechanically. Two potential energy surfaces and a coupling surface are developed for this purpose.

The reaction $Ba(^1S) + ON_2(X^1\Sigma) \rightarrow BaO(X^1\Sigma) + N_2(X^1\Sigma_g^+)$, $BaO(a^3\Pi) + N_2(X^1\Sigma_g^+)$ is studied quantum mechanically. The singlet and triplet potential energy surfaces are devised as is a spin-orbit

coupling surface. Electronically adiabatic and non-adiabatic transition probabilities are calculated as a function of the initial translational energy of the reagents.

TABLE OF CONTENTS

PART I

Theoretical Studies of Electronically Adiabatic Chemical Reaction Dynamics

PART II

A Direct Test of the Vibrationally Adiabatic Theory of Chemical Reactions

PART III

Theoretical Studies of Electronically Non-Adiabatic Chemical Reaction Dynamics

PART I

THEORETICAL STUDIES OF ELECTRONICALLY ADIABATIC CHEMICAL REACTION DYNAMICS

INTRODUCTION

INTRODUCTION

A theoretical description of molecular reaction dynamics requires two, usually independent, efforts. The first effort is concerned with the construction of the potential energy surface(s) describing the various molecular reaction channels; this is within the domain of molecular quantum mechanics calculations. The second effort deals with the solution of the equations of motion of the nuclei; this is the domain of molecular dynamics calculations.

An ab initio approach to molecular quantum mechanics and molecular dynamics calculations does of course lead to predictions about the reaction dynamics which will agree exactly with experiments. However, such an approach is in general not feasible (or perhaps even desirable) due to the great numerical difficulties involved in doing exact calculations. As a result of this, many, varied approximate approaches to chemical reaction dynamics calculations have been developed. A description, examination, and comparison of several approximate approaches to various aspects of molecular dynamics calculations (on a single potential energy surface) is presented in this part of the thesis. Also, and most importantly, a comparison between calculations based on the approximate methods and the exact quantal one is made.

The format of this part of the thesis consists of a presentation of seven manuscripts, four of which have been published, and two Appendices.

Paper I. 1 presents a comparison between exact quantum and quasi-classical reaction probabilities for the collinear $H + H_2$ exchange reaction. Also presented is a comparison of thermal rate constants. The calculations reported in this paper as well as all others are for collinear collisions only. This has been done, first, so that the many calculations reported could be feasibly done. Second, the testing of approximate methods for collinear collisions does contain enough reality so that the conclusions reached will probably be valid for three-dimensional calculations. Third, many atom-molecule reactions do proceed through a collinear transition state, at least at low collision energies.

Paper I. 2 examines the possibility of making a modification of the quasi-classical trajectory method by selecting initial conditions of the trajectory ensemble according to a quantal criterion. This suggestion, made by Careless and Hyatt, is shown to be inconsistent with a general condition of scattering calculations.

The semi-classical expressions for transition probabilities given in new scattering theories developed by W. H. Miller and R. A. Marcus are derived in paper I. 3. The derivation is based on a coordinate representation of the Feynman propagator and is given in terms of a general diatom internal coordinate. Also, a new derivation of the classical limit of the Feynman propagator is given.

An extensive comparison of quasi-classical, semi-classical, and exact quantum transition probabilities for the $H + H_2$ exchange

reaction is given in paper I. 4. A difficulty associated with the semi-classical method is revealed and stressed. Also, the idea of reverse quasi-classical trajectory calculations is introduced as a means of improving the agreement between exact and quasi-classical results.

A comparison of quantal and classical current density, streamline, and current density profile plots is made in paper I. 5 for the H + H_2 exchange reaction. An examination of the regions of configuration space sampled by the classical and quantal current densities, etc., is made for five values of the collision energy.

In papers I. 6 and I. 7 extensive comparisons are made between quasi-classical, uniform semi-classical, and exact quantum reaction probabilities for the F + H_2 and F + D_2 exchange reactions, respectively. The utility of reverse quasi-classical trajectory calculations is stressed, as is the fact that forward and reverse quasi-classical transition probabilities do not obey microscopic reversibility.

A symmetry property of a transition probability discussed in paper I. 2 is derived in Appendix 1. The analytical continuation of the semi-classical S-matrix into the complex plane by means of a simple power series representation is discussed in Appendix 2. The expressions obtained are very similar to those given by Miller previously. Also, some numerical results are presented.

I.1 CLASSICAL AND QUANTUM REACTION PROBABILITIES AND THERMAL RATE CONSTANTS FOR THE COLLINEAR H + H_2 EXCHANGE REACTION WITH VIBRATIONAL EXCITATION *

* This paper appeared in Chemical Physics Letters 12, 1 (1971).

CLASSICAL AND QUANTUM REACTION PROBABILITIES AND THERMAL RATE CONSTANTS FOR THE COLLINEAR H + H_2 EXCHANGE REACTION WITH VIBRATIONAL EXCITATION*

JOEL M. BOWMAN AND ARON KUPPERMANN
Division of Chemistry and Chemical Engineering**
A. A. Noyes Laboratory of Chemical Physics
California Institute of Technology
Pasadena, California 91109

Classical trajectory calculations for the collinear H + H_2 exchange reaction were performed using the same potential energy surface previously adopted for exact quantum mechanical calculations. Reactions of both ground state and vibrationally excited state reagent were considered, over a relative kinetic energy range sufficient to produce vibrational excitation of products. At energies close to threshold the classical and quantum mechanical reaction probabilities differ sufficiently to cause a major difference in the corresponding thermal rate constants at low temperatures. Effective reaction thresholds differ by 0.07 eV for ground state and 0.09 eV for excited state reagent. At energies substantially above threshold the quantum reaction probabilities oscillate around the corresponding classical ones. However, some classical curves

* This work was supported in part by the United States Atomic Energy Commission, Report Code No. CALT-767P4-87.

**Contribution No. 4330

also show oscillatory behavior, suggesting caution in the assignment of oscillations in the quantum curves to quantum effects.

Comparisons between exact classical and quantum mechanical calculations for the collinear H + H_2 exchange reaction have been previously reported. Mortensen [1] studied this collinear reaction and three of its isotopic variations classically and quantum mechanically. McCullough and Wyatt [2] reported a time-dependent quantum and classical calculation of this collinear reaction at four energies. In neither of these comparisons was the energy sufficiently high for a detailed comparison of the role of vibrational energy in classical and quantum calculations to be made.

In this paper we present such a comparison. We have performed quasi-classical trajectory calculations [3] and compare the results with the exact quantum calculations of Truhlar and Kuppermann [4]. The corresponding total reaction probability from the ground and first excited vibrational states of H_2 is compared, as well as reaction probabilities into individual vibrational quantum states of products. The relative collision energy was varied from 0.20 to 1.28 eV and 0.07 to 0.70 eV for collisions of the ground and first excited vibrational state of the diatomic reagent, respectively. At these energies the first three vibrational states of product H_2 are accessible. The potential energy surface used, identical in both the classical and quantum calculations, was a Wall-Porter [5] type, fit by Truhlar and Kuppermann [4] to the ab-initio H_3 surface of Shavitt, Stevens, Minn, and Karplus [6] and scaled to give the "correct" barrier height of 0.424 eV [7].

In a quasi-classical trajectory calculation one can choose to quantize the initial vibrational energy of the reactant diatom, but the final diatom energies are not quantized. One can, nevertheless, for purposes of comparison with the quantum mechanical results, assign a quantum number to the final diatom in several ways. We choose the following one. If $\Delta E(n) = E(n+1) - E(n)$ is the quantum mechanical energy difference between vibrational states n + 1 and n and E_{cl}^{v} is one of a continuum of classical final diatom vibrational energies such that $E(n) \leq E_{cl}^{v} < E(n+1)$, we assign to this diatom the quantum number v = n if $E(n) \leq E_{cl}^{v} < \frac{1}{2}\Delta E(n)$, or v = n + 1 if $E(n) + \frac{1}{2}\Delta E(n) < E_{cl}^{v} \leq E(n+1)$. If $E_{cl}^{v} \leq E(0)$, we set v = 0. Using this assignment we can obtain the probability P_{ij}^{R} for reaction from the $i^{\underline{th}}$ vibrational state of the reactant to the $j^{\underline{th}}$ vibrational state of the product from the quasi-classical trajectory calculations. This method of assignment optimized the agreement between classical and quantum results.

In Fig. 1 we exhibit the classical and quantum total reaction probability, P_{0}^{R}, for reactant H_2 in its v = 0 vibrational state as a function of relative collision energy. In this figure as well as in Figs. 2 and 3, the classical points are accurate to plus or minus 0.03 or better due to the statistical fluctuations associated with the trajectory calculation method [3]. The T1 and T2 marks on the abscissa correspond to relative collision energies at which vibrational excitation of H_2 to its v = 1 and v = 2 states respectively becomes energetically possible. As the collision energy exceeds

0.30 eV, both the classical and quantum reaction probability start to decrease with increasing energy. The classical curve drops monotonically, whereas the quantum one shows marked oscillatory structure and appears to oscillate about the classical curve. At energies between 0.28 and 0.30 eV the two curves are in good agreement, but at energies less than 0.28 eV, they diverge slowly.

The exact threshold energies at which $P_0^R = 0$ is zero for the quantum case and must equal or exceed 0.151 eV (at which value the classical kinetic energy at the saddle point is zero) in the classical one. However, if we arbitrarily define an "effective" threshold kinetic energy as that corresponding to $P_0^R = 0.01$, it is 0.19 eV for the quantum calculation and about 0.26 eV for the classical one, corresponding to a difference of about 0.07 eV (1.6 Kcal/mole).

In Fig. 2 we have plotted the classical and quantum total reaction probability, P_1^R, for reactant H_2 in its v = 1 vibrational state as a function of relative collision energy. The mark T2 designates the energy at which excitation to the v = 2 vibrational state becomes energetically accessible. At collision energies between 0.40 and 0.70 eV, the classical reaction probability displays, as before, the behavior of the oscillation-averaged quantum curve. From 0.20 to 0.40 eV, the two reaction probabilities show semi-quantitatively the same trend. At energies between 0.13 and 0.20 eV the dip in the classical reaction probability is qualitatively similar to, though more pronounced than, the one in the quantum reaction probability. We note that this curious oscillation in the reaction probability is manifestly not a quantum effect as it appears classically also. Thus,

one should be cautious when assigning oscillations in quantum results to quantum effects. At energies less than 0.13 eV the two curves show, as for the v = 0 case, a rapid decrease with decreasing energy, but in the present case they differ more from one another. In this case the quantum $P_1^R = 0.01$ effective reaction threshold is 0.02 eV and the classical one about 0.11 eV, although even at zero relative kinetic energy the total energy (0.79 eV) is sufficient for the reaction to proceed. Therefore, some kinetic energy is still necessary for the reaction probability to be appreciable, more in the classical case than in the quantum one. The difference in these effective threshold energies for v = 1 is now 0.09 eV, compared to 0.07 eV for the v = 0 case.

In Fig. 3 we have plotted four reaction probabilities, P_{00}^R, P_{10}^R, P_{11}^R, and P_{12}^R versus collision energy. The P_{00}^R, P_{10}^R, and P_{11}^R, classical curves show decreasing monotonic behavior with increasing energy for collision energies greater than 0.30 eV and the corresponding quantum curves show pronounced oscillatory behavior about the classical ones. At the energies just above threshold the classical P_{10}^R and P_{11}^R curves show very rapid variation with energy. This indicates a very abrupt variation in the extent of non-adiabaticity in the reactive collisions. This effect is not seen quantum mechanically. We are uncertain as to how much credence should be given to this portion of the classical curves because of the way in which quantum numbers were assigned to classical vibrators.

For example, the classical reaction probability P_{12}^{R} is substantial at energies less than T2, because of this method of assignment. Again we see threshold differences of 0.07 to 0.09 eV.

Truhlar and Kuppermann [8] have recently calculated the thermal rate constant for this collinear reaction from their quantum reaction probabilities. Using the same expression for the rate constant, but replacing the quantum reaction probabilities with the corresponding classical ones, we calculated the classical thermal rate constant. Figure 4 shows a plot of the ratios of the classical to quantum rate constants as a function of 1/T for temperatures ranging from 150 to 1200°K. Table I shows this comparison more quantitatively. The classical activation energy, derived from the classical rate constant, is 0.30 eV, and the quantum activation energy is 0.299 eV [8]. The quantum results were reported with an accuracy of 2% or better and the present classical ones are accurate to about 10%. The two rate constants are seen to approach each other at high temperatures and to diverge significantly at temperatures below 250°K. The small difference in the quantum and classical reaction thresholds is responsible for this marked low temperature difference.

In summary, we have found that at the higher collision energies considered here, there is qualitative agreement between the classical and the oscillation-averaged quantum reaction probabilities discussed here. Quantitatively, however, a difference of a factor of two is not uncommon. In addition, a marked difference exists between

classical and quantum rate constants due to the difference between the corresponding reaction probabilities near threshold. We feel that, although these results were obtained from collinear calculations, the qualitative conclusions will still hold for 3-dimensional reactions.

REFERENCES

[1] E. M. Mortensen, J. Chem. Phys. 49 (1968) 3526.

[2] E. A. McCullough and R. E. Wyatt, J. Chem. Phys. 54 (1971) 3578, 3592.

[3] For details of the method see, e.g., M. Karplus, R. N. Porter, and R. D. Sharma, J. Chem. Phys. 43 (1965) 3259.

[4] D. G. Truhlar and A. Kuppermann: (a) J. Chem. Phys. 52 (1970) 3841; (b) to be published.

[5] F. T. Wall and R. N. Porter, J. Chem. Phys. 6 (1962) 3256.

[6] I. Shavitt, R. M. Stevens, F. L. Minn, and M. Karplus, J. Chem. Phys. 48 (1968) 2700.

[7] I. Shavitt, J. Chem. Phys. 49 (1968) 4048.

[8] D. G. Truhlar and A. Kuppermann, Chem. Phys. Letters 9 (1971) 269.

FIGURE CAPTIONS

Figure 1. Classical (open circles) and quantum (full circles) total reaction probability, P_0^R, for the collinear reaction $H + H_2 (v = 0) \rightarrow H_2(v = 0, 1, 2) + H$ as a function of relative collision energy E_0.

Figure 2. Classical (open circles) and quantum (full circles) total reaction probability, P_1^R, for the collinear reaction $H + H_2 (v = 1) \rightarrow H_2 (v = 0, 1, 2) + H$ as a function of relative collision energy E_1.

Figure 3. Classical (open circles) and quantum (full circles) reaction probabilities P_{ij}^R as a function of relative collision energy E_i.

Figure 4. Ratio of classical to quantum rate constant as a function of 1/T.

Table I. Exact quantum $k_{qm}(T)$ and classical $k_{cl}(T)$ rate constants in cm/(molecule-sec) and their ratio.*

T(°K)	$k_{cl}(T)$	$k_{qm}(T)$	$k_{cl}(T)/k_{qm}(T)$
200	0.86(-2)	0.201(0)	0.43(-1)
300	0.19(1)	0.585(1)	0.32(0)
400	0.31(2)	0.593(2)	0.52(0)
500	0.17(3)	0.266(3)	0.64(0)
600	0.52(3)	0.752(3)	0.69(0)
700	0.12(4)	0.161(4)	0.74(0)
800	0.22(4)	0.290(4)	0.76(0)
900	0.37(4)	0.463(4)	0.80(0)
1000	0.55(4)	0.677(4)	0.81(0)
1100	0.77(4)	0.928(4)	0.83(0)
1200	0.10(5)	0.121(5)	0.83(0)

* The numbers in parentheses are powers of ten which multiply the numbers preceding them.

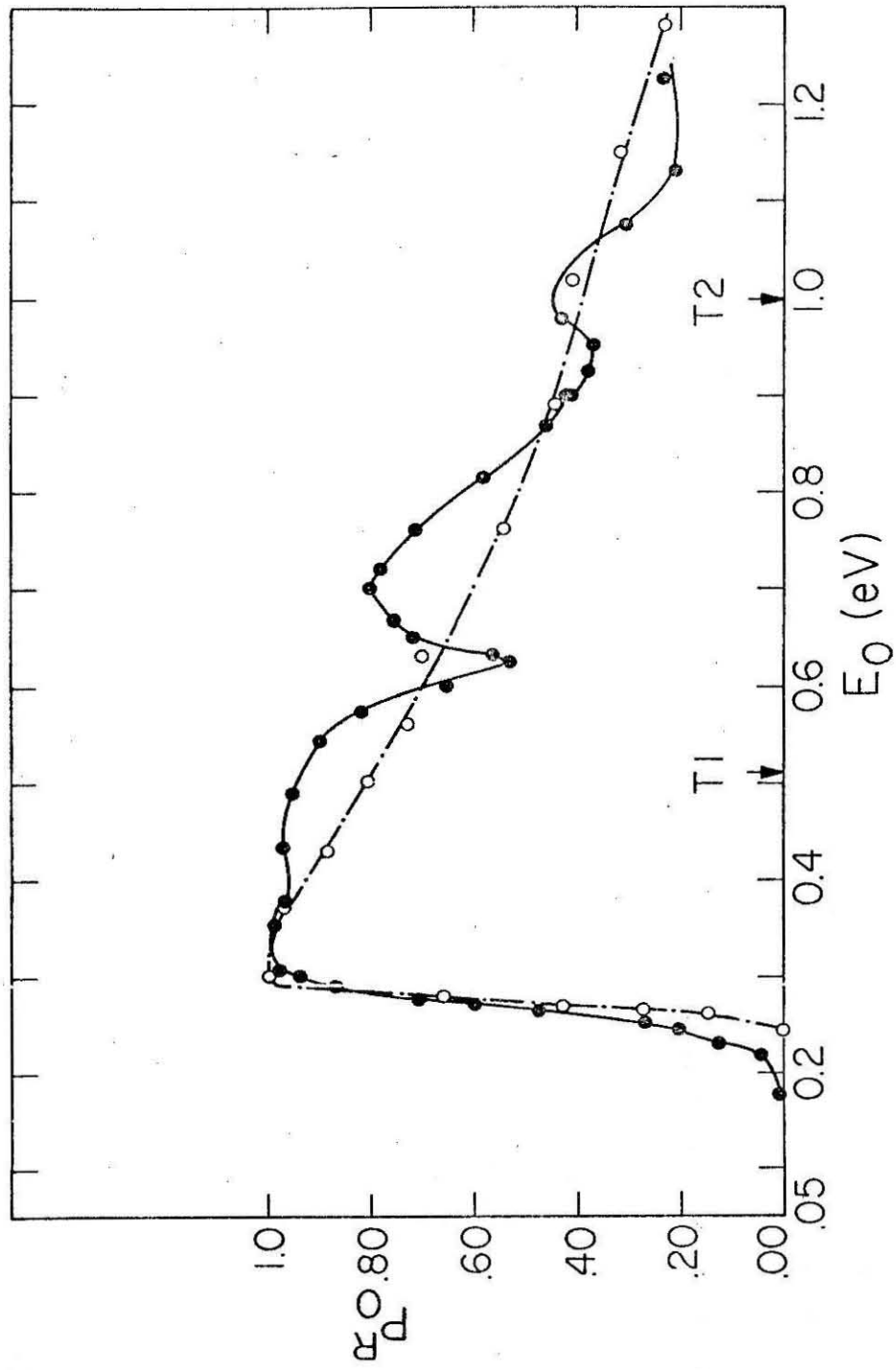

Figure 1

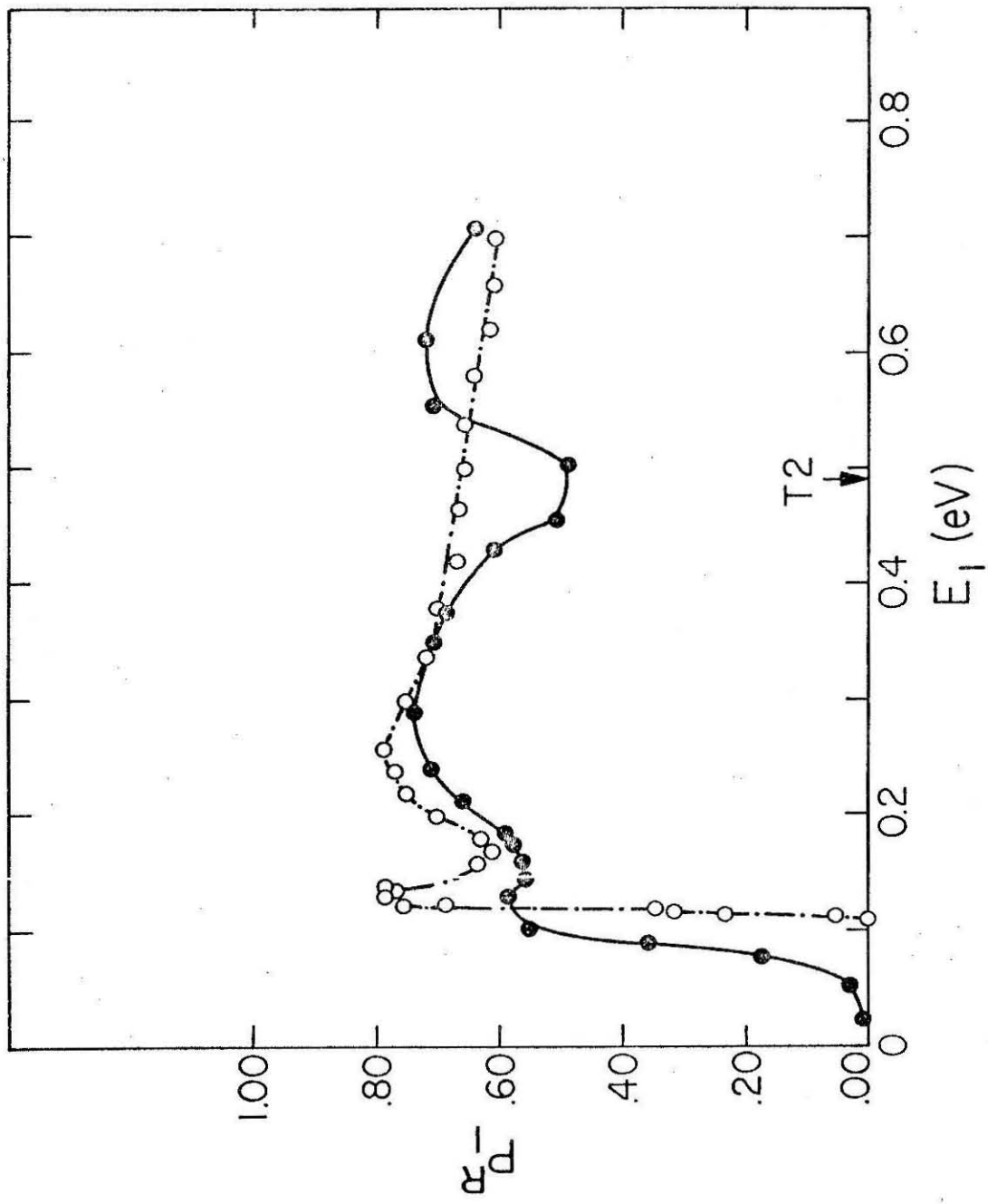

Figure 2

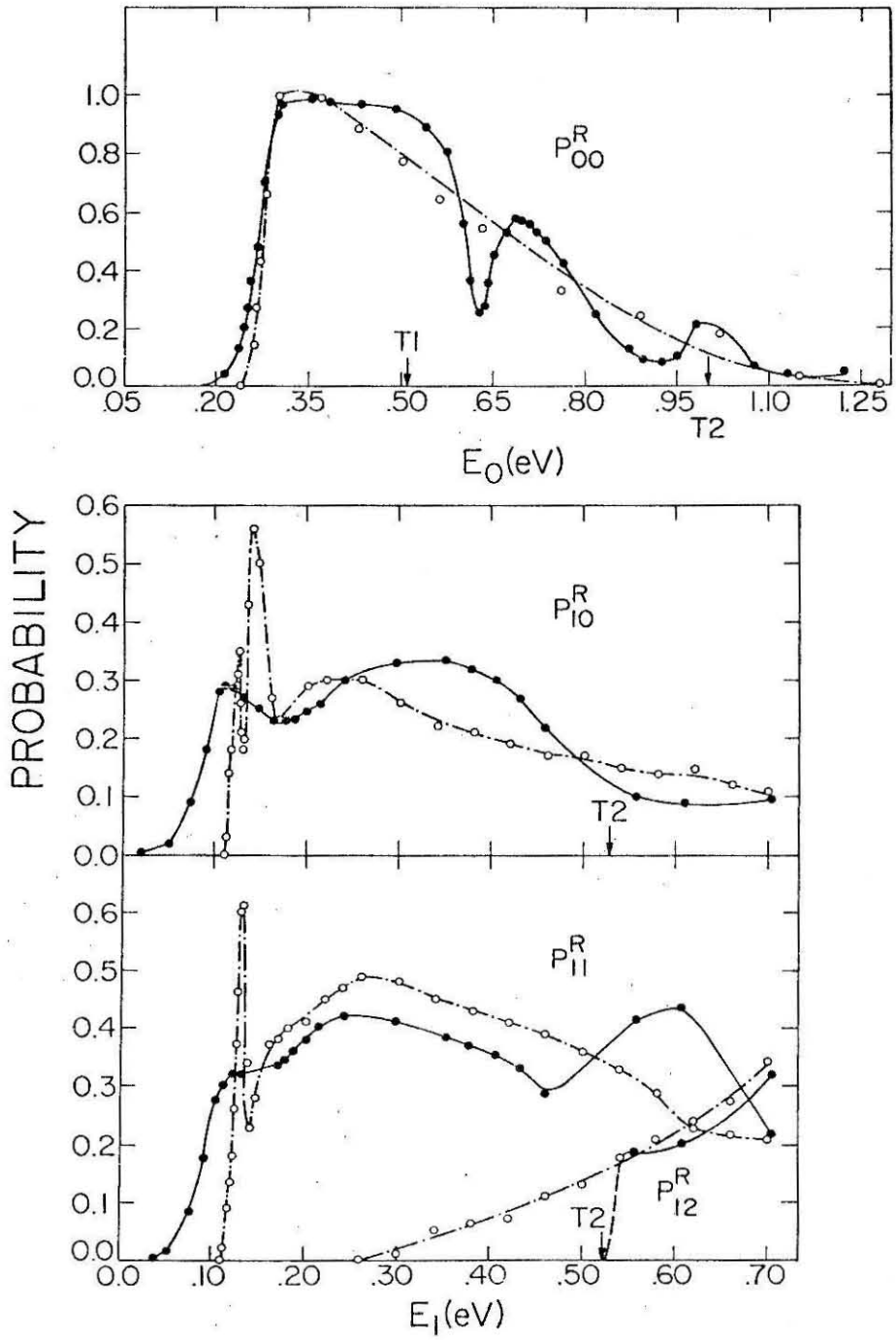

Figure 3

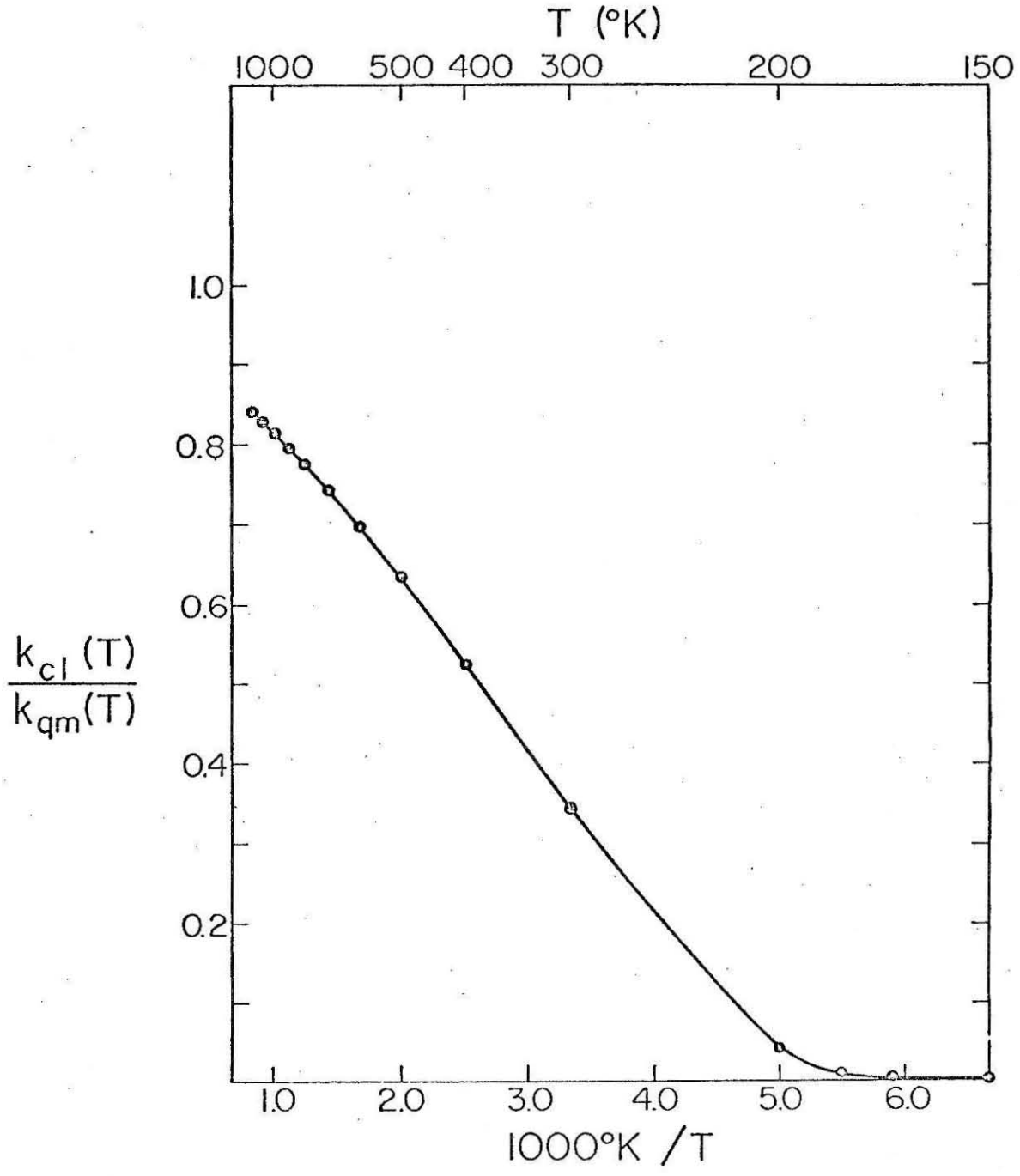
T (°K)
1000
500
400
300
200
150
1.0
0.8
0.6
0.4
0.2
$\frac{k_{cl}(T)}{k_{qm}(T)}$
1.0
2.0
3.0
4.0
5.0
6.0
1000°K /T

Figure 4

I.2 QUANTUM INITIAL CONDITIONS IN QUASI-CLASSICAL TRAJECTORY CALCULATIONS.*

* This paper appeared in Chemical Physics Letters 19, 21 (1973).

QUANTUM INITIAL CONDITIONS IN QUASI-CLASSICAL TRAJECTORY CALCULATIONS.*

JOEL M. BOWMAN,** ARON KUPPERMANN, and GEORGE C. SCHATZ
Arthur Amos Noyes Laboratory of Chemical Physics†
California Institute of Technology, Pasadena, California 91109, USA

Received

The quantum distribution of initial conditions suggested recently by Careless and Hyatt as a means of "phase-averaging" classical trajectories is shown to lead to reaction probabilities which depend on the initial distance between the reagents even when this distance is sufficiently large for the corresponding interaction energy to vanish. We used that distribution to calculate reaction probabilities for the collinear $H + H_2$ exchange reaction on a potential energy surface for which quasi-classical and exact quantum results had been previously obtained. The dependence of the resulting reaction probabilities on the arbitrarily chosen value of the initial atom-molecule separation was substantial. We conclude that the use of such quantum distributions for initial conditions is physically unacceptable.

* This work was supported in part by the United States Atomic Energy Commission, Report Code No. CALT.-767P4-101.

** Work performed in partial fulfillment of the requirements for the Ph. D. Degree in Chemistry at the California Institute of Technology.

† Contribution No. 4596.

1. INTRODUCTION

In a recent paper [1], Careless and Hyatt reported reaction probabilities from a classical trajectory study of the collinear $H + H_2$ exchange reaction on an LEPS surface. In addition to the standard "phase-averaging" (i.e., averaging over the initial reagent molecule's vibrational phase) in which the initial internuclear distance of reagent H_2 (treated a classical harmonic oscillator with zero-point vibrational energy) is selected according to the classical distribution function (CDF), they phase-averaged according to a quantum distribution function (QDF), the probability density of the ground vibrational state. The total reaction probability they obtained from the QDF oscillated with energy around the one obtained from the CDF. This, as they observed, was reminiscent of the oscillations of the exact quantum reaction probability curve around the standard quasi-classical one obtained for an H_3 surface different than but similar to theirs [2], and suggested that the use of the QDF may be a way to introduce quantum effects in classical trajectory calculations.

In this paper we investigate the properties and usefulness of the QDF-classical trajectory method.

2. CLASSICAL AND QUANTUM INITIAL DISTRIBUTIONS FUNCTIONS

Let $F_C(r)$ and $F_Q(r)$ be respectively the CDF and QDF of the initial internuclear distance, r, of a reagent diatomic molecule in a bound state having a quantized vibrational energy. Let the corresponding classical turning points be r_{min} and r_{max}. By definition the quantities $K^+(r)$ and $K^-(r)$ are set equal to one if the trajectory corresponding to r is reactive and to zero otherwise. The superscript +(-) corresponds to the reagent initially expanding

(contracting). The CDF and QDF total reaction probabilities of this molecule with a third atom in a linear world, P_C and P_Q respectively, are given by [3]

$$P_\alpha = \int_{r_{min}}^{r_{max}} dr\,[K^+(r) + K^-(r)]\,F_\alpha(r) \,/\, 2\int_{r_{min}}^{r_{max}} dr\,F_\alpha(r), \quad \alpha = C, Q. \quad (1)$$

The CDF is normalized according to

$$\int_{r_{min}}^{r_{max}} dr\,F_C(r) = 1$$

but due to barrier penetration the corresponding QDF integral for the same integration limits is less than unity.

The CDF and QDF total reaction probabilities can also be obtained by sampling the initial diatom internuclear separation from the CDF and QDF respectively and determining the fraction of trajectories leading to reaction. This technique is equivalent to the one given by Eq. (1), and as a consistency check of our numerical results both were employed for some calculations.

3. CONDITIONS ON INITIAL DISTRIBUTION FUNCTIONS

Let x stand for an internal coordinate of the diatomic molecule. It can be the internuclear distance, r, or the angle variable, q [4]. The distribution function $F(x, t)$ of x at time t should satisfy the condition that as long as the third atom is not interacting with the molecule this function does not have an explicit time dependence, i.e., $[\,\partial F(x, t)/\partial t\,]_x = 0$. If this is not the case the resulting reaction probabilities would in general be a function of the initial atom-molecule separation, R, even though at this separation the interaction

energy vanishes [5]. Such a result would not be physically meaningful [6]. We will show that $[\partial F/\partial t]_x$ vanishes if and only if at an arbitrary initial time t_0 $F(x, t_0)$ is the classical distribution function [$F_C(r)$ or $F_C(q)$] and therefore that any other initial distribution function, including the quantum one [$F_Q(r)$ or $F_Q(q)$], is not acceptable.

Let p_x be the momentum canonically conjugate to x (i.e., either the cartesian momentum p_r for $x = r$ or the action variable n [4] for $x = q$). Let $\rho(x, p_x, t)$ be the density function (at time t and point (x, p_x) of phase space) representing an ensemble of isolated diatomic molecules. The distribution function $F(x, t)$ in x-configuration space is related to ρ by

$$F(x, t) = \int dp_x \rho(x, p_x, t) \tag{2}$$

where x and p_x are taken as usual to be independent. From this we get

$$(\frac{\partial F}{\partial t})_x = \int dp_x (\frac{\partial \rho}{\partial t})_{x, p_x} .$$

The quantity $(\partial\rho/\partial t)_{x, p_x}$, describing the rate of change of ρ with time at a fixed point in phase space, can be obtained from Liouville's theorem [7] according to which $d\rho/dt$ vanishes. As a result

$$(\frac{\partial F}{\partial t})_x = -\int dp_x [(\frac{\partial \rho}{\partial x})_{p_x, t} \frac{dx}{dt} + (\frac{\partial \rho}{\partial p_x})_{x, t} \frac{dp_x}{dt}] . \tag{3}$$

It is now convenient to use angle-action variables, i.e., $x = q$ and $p_x = n$. The corresponding equations of motion are [4]

$$\frac{dq}{dt} = \omega \; ; \; \frac{dn}{dt} = 0 \tag{4}$$

where ω is the positive constant angular frequency of the vibrational motion of the molecule. Therefore,

$$q = \omega t + c \; ; \; n = m \tag{5}$$

where c and m are integration constants, the latter being uniquely determined by the energy of the molecule [4]. Let the ensemble of molecules being considered be restricted to lie "on the energy shell" (i.e., have energies in the range) E to E + dE. Then, in view of Eq. (5) we may write

$$\rho(q, n, t) = f(q, t)\, \delta(n-m) \; . \tag{6}$$

From this and Eq. (2) we have that

$$F(q, t) = f(q, t) \tag{7}$$

and with the aid of Eqs. (4), (6), and (7), Eq. (3) becomes

$$\left(\frac{\partial F}{\partial t}\right)_q = -\omega \left(\frac{\partial F}{\partial q}\right)_t \; . \tag{8}$$

This is the general partial differential equation which any distribution function F(q, t) on the energy shell must satisfy. In addition F should be normalized in the q-range 0 to 2π corresponding to one vibration period, i.e.,

$$\int_0^{2\pi} dq\, F(q, t) = 1 \; . \tag{9}$$

Since we wish to find the conditions under which $F(q, t_o)$ must be equal to $F_C(q)$, we first obtain an expression for the latter. By definition $F_C(q)\, dq$ is equal to the fraction of time spent by an isolated diatom in the range q to q + dq, i.e.,

$$F_C(q)\,dq = \frac{dt}{\tau}$$

where τ, the molecular vibration period, is related to ω by

$$\tau = \frac{2\pi}{\omega} \quad . \tag{10}$$

The last three expressions together with Eq. (5) furnish

$$F_C(q) = \frac{1}{2\pi} \quad . \tag{11}$$

The theorem we wish to prove is that a necessary and sufficient condition for $[\partial F(q, t)/\partial t]_q$ to vanish for all q and t is that $F(q, t_0)$ be $1/2\pi$ (i.e., $F_C(q)$). That the condition is necessary follows from Eq. (8) by setting $[\partial F/\partial t]_q$ equal to zero. According to the resulting expression, F is independent of both q and t, i.e., it is a constant whose value, due to the normalization condition (9), must be $1/2\pi$. Therefore, F(q, t) at all times, and in particular at time t_0, must be equal to $1/2\pi$. To show that the condition is sufficient, we assume that $F(q, t_0) = 1/2\pi$ and solve Eq. (8) subject to this initial condition. It follows that $[\partial^n F(q, t_0)/\partial t^n]_q$ vanishes at $t = t_0$ for all n. Therefore, a power series expansion of F(q, t) in the variable t around $t = t_0$ furnishes $F(q, t) = F(q, t_0) = 1/2\pi$ from which we conclude that $[\partial F/\partial t]_q$ vanishes at all q and t, Q.E.D.

If we now change from the angle-action variables (q, n) to the cartesian ones (r, p_r), the distribution function F(q, t) transforms into F(r, t) and it is straightforward to prove that a necessary and sufficient condition for $[\partial F/\partial t]_r$ to vanish at r and t is that for an arbitrary t_0 we have $F(r, t_0) = F_C(r)$. Indeed, since

$$F(r, t)\,|dr| = F(q, t)\,dq$$

we get from Eq. (4)

$$F(r, t) = F(q, t) \frac{\omega}{|v(r)|} \tag{12}$$

where v is the cartesian velocity given by

$$v(r) = \pm \left\{\frac{2}{\mu} [E - V(r)]\right\}^{\frac{1}{2}} ,$$

μ being the reduced mass of the diatom and V(r) its potential energy function. (The absolute value signs were introduced to force F(r, t) to be positive.) On the energy shell n is a constant and therefore r is a function of q only. Thus, a necessary and sufficient condition for $[\partial F/\partial t]_r$ to vanish is that $[\partial F/\partial t]_q$ vanish, i.e., that $F(q, t_0)$ equal $1/2\pi$. Due to Eqs. (12) and (10) this is equivalent to

$$F(r, t_0) = \frac{1}{\tau} \frac{1}{|v(r)|} . \tag{13}$$

Since the classical distribution function $F_C(r)$ must, by definition, satisfy

$$F_C(r)\, dr = \frac{dt}{\tau}$$

we get finally that

$$F(r, t_0) = F_C(r) .$$

Thus, we have proved that the one and only initial distribution leading to an F(r, t) which has no explicit time dependence is the classical one, $F_C(r)$, and therefore this distribution function is the only physically acceptable one. For any other initial distribution, including the quantum one, the resulting reaction probabilities will be periodic functions of the

atom-molecule separation, R, with period $V\tau$, where V is the initial relative velocity. This is an immediate consequence of the fact that the diatom's internal motion is periodic with period τ. Furthermore, the function $P_Q(R)$ will be symmetric about a point $\overline{R}$ due to the fact that $F_Q(q)$ is symmetric about the point $q = \pi$.

Although these conclusions were derived for the particular case of a collinear atom-molecule exchange reaction, their generalization to three dimensions and to more complicated reactions is straightforward.

4. NUMERICAL RESULTS AND DISCUSSION

In order to determine the magnitude of the dependence of the total reaction probability on R for the QDF we computed P_Q as a function of the initial relative kinetic energy, E_0, for several values of R for the $H + H_2$ exchange reaction, with the H_2 molecule initially in its ground vibrational state. The potential energy surface used was a Wall-Porter fit to the scaled SSMK surface [8], and was the same one for which exact quantum and quasi-classical reaction probabilities had previously been obtained [9, 2].

We also performed some calculations using the CDF by both the sampling method described at the end of Section 2 and by the integration method. The latter is a modification of Eq. (1), obtained by replacing the initial H_2 internuclear distance variable r with the angle variable, q. The resulting expression is

$$P_C = \sum_i (\Delta q)_i / 2\pi \tag{14}$$

where the $(\Delta q)_i$ represent the lengths of the regions in q-space which lead to reaction. Most of the QDF calculations were made using the integration

method with Eq. (1) unaltered. For one energy the sampling technique was also used.

For an initial relative kinetic energy, equal to 0.64 eV P_C and P_Q were obtained by these methods for four values of R between 4.621 bohr and $4.621 + \tau V$ bohr (6.592 bohr) and the results are given in Table 1 for a set of 100 trajectories per value of R. As seen the CDF results are independent of R as expected whereas the QDF ones depend significantly on this variable. Furthermore the latter dependence is periodic with period τV and the integration and sampling methods of calculation give the same results (to within the accuracy of either calculation), as predicted. In Fig. 1 we have plotted P_Q (computed from Eq. (1)) as a function of R over the range 4.78 bohr to $4.78 + \tau V$ bohr (6.75 bohr) and for E_0 equal to 0.64 eV to illustrate the nature and magnitude of the R-dependence. The range of the abscissa has been chosen so that the symmetric shape of the curve is clearly displayed. The point of symmetry, $\overline{R}$, (5.76 bohr in the present example) is calculated from the expression $\overline{R} = R_0 + \frac{V}{\omega} [(q_2 + q_1)/2 - \pi]$ where q_1 and q_2 are the limits of the q region over which all trajectories are reactive for $R = R_0$. The range of P_Q for this energy is 0.50 to 0.83 compared to the value of 0.65 for P_C. This is a substantial dependence of P_Q on R.

In Fig. 2 we have plotted, as a function of E_0, the QDF total reaction probability at three values of R and the CDF total reaction probability. In addition, for comparison purposes, we display the exact quantum curve obtained previously for the same surface [9]. The QDF results again clearly exhibit a substantial variation with R, even though the range of values of P_Q for each E_0 indicated in the figure is not the maximum one [10].

Depending on the arbitrarily chosen value of R some of the P_Q versus E_0 curves can display an oscillatory behavior. However, the position and amplitude of these oscillations are themselves dependent on R, and appear in general unrelated to those of the exact probabilities, as displayed in Fig. 2.

We conclude that, in the absence of a reasonable criterion for choosing the initial atom-molecule separation, the use of a quantum distribution of initial conditions to phase-average classical trajectories is neither theoretically justifiable nor physically acceptable.

Table 1

Classical (CDF), P_C, and "quantum" (QDF), P_Q, total reaction probabilities at four values of the initial atom-molecule separation, R, for an initial relative kinetic energy of 0.64 eV.

R (bohr)	P_C		P_Q	
	Integration[a]	Sampling[b]	Integration[c]	Sampling[b]
4.621	0.65	0.65	0.76	0.76
5.278	0.65	0.66	0.53	0.54
5.935	0.65	0.66	0.68	0.70
6.592	0.65	0.66	0.76	0.76

a) Method using Eq. (14).

b) Method described at the end of Section 2.

c) Method using Eq. (1).

REFERENCES

[1] P. M. Careless and D. Hyatt, Chem. Phys. Letters 14 (1972) 358.

[2] J. M. Bowman and A. Kuppermann, Chem. Phys. Letters 12 (1971) 1.

[3] In the event that $K^{+}(r)$ and $K^{-}(r)$ are non-integrable functions the sampling method described in the next paragraph can still be used.

[4] H. Goldstein, Classical mechanics (Addison-Wesley, Reading, Mass., 1950) pp. 288-294.

[5] This dependence results from the fact that as the atom-molecule system approaches the region of interaction, i.e., R is decreasing with time, the distribution of x is changing.

[6] Two special cases for which there should not be an R dependence even though $\partial F(x, t)/\partial t \neq 0$ are obviously the ones for which either no trajectory or every trajectory leads to reaction.

[7] Ref. [4], pp. 266-268.

[8] The potential energy surface is described in detail in [8] and references therein.

[9] D. G. Truhlar and Aron Kuppermann, J. Chem. Phys. 56 (1972) 2232.

[10] To obtain, at each E_0, the maximum spread in $P_Q(R)$ would require sampling a finer grid of values of R, in the manner done to obtain the results displayed in Fig. 1 for $E_0 = 0.64$ eV. The small spread observed for $E_0 = 0.30$ eV is due to the fact that for this energy essentially all trajectories are reactive (see [5]).

FIGURE CAPTIONS

Fig. 1. "Quantum" (QDF) total reaction probability, P_Q, as a function of the initial atom-molecule separation, R, for an initial relative kinetic energy of 0.64 eV. The arrow indicates the position of the symmetry point, $\overline{R}$ = 5.76 bohr. The error bars are a measure of the uncertainties associated with the number of trajectories (100) used for each R.

Fig. 2. Exact quantum (dashed-dotted curve), quasi-classical (CDF) (solid curve), and "quantum" (QDF) (triangles, circles, and squares) total reaction probabilities as a function of initial relative kinetic energy, E_0. The initial atom-molecule separations, R, for the latter are given in the figure insert.

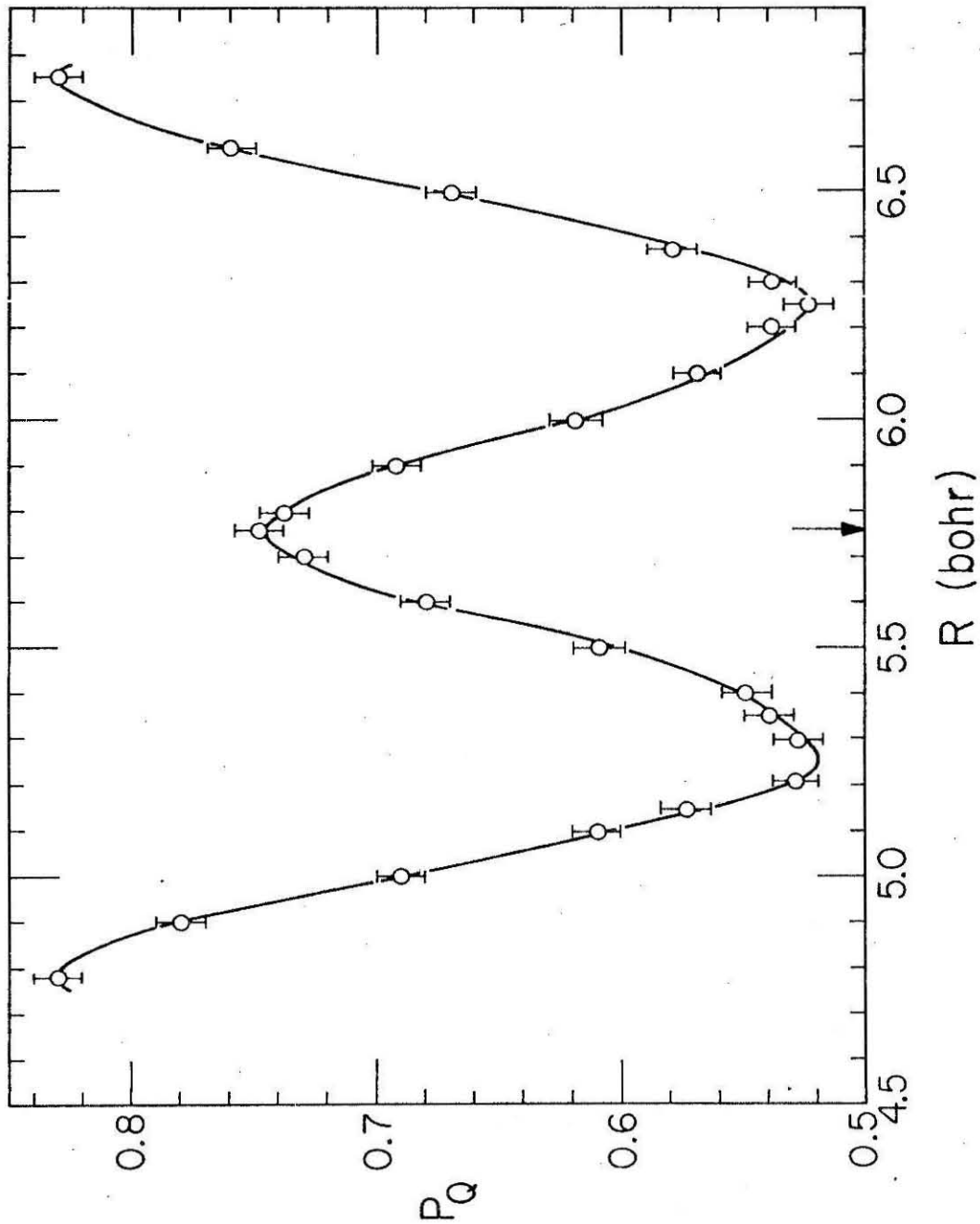

Figure 1

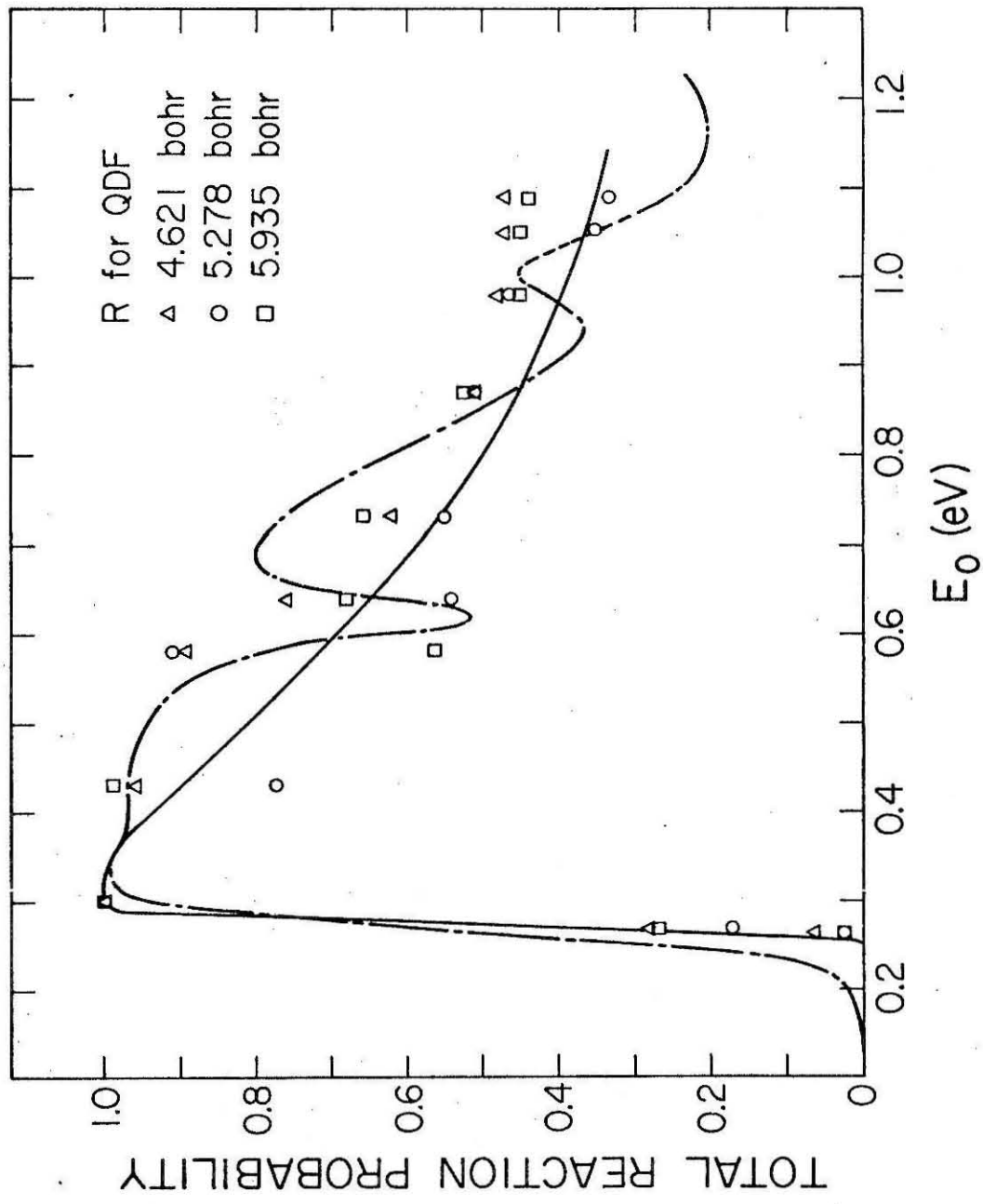
R for QDF
4.621 bohr
5.278 bohr
5.935 bohr
TOTAL REACTION PROBABILITY
0
0.2
0.4
0.6
0.8
1.0
0.2
0.4
0.6
0.8
1.0
1.2
E_0 (eV)

Figure 2

I.3 SEMI-CLASSICAL S MATRIX THEORY OF REACTIVE AND NON-REACTIVE ATOM-MOLECULE COLLISIONS. *

* This paper appeared in Chemical Physics 2, 158 (1973).

SEMI-CLASSICAL S MATRIX THEORY OF REACTIVE AND NON-REACTIVE ATOM-MOLECULE COLLISIONS. *

J. M. BOWMAN** and ARON KUPPERMANN

Arthur Amos Noyes Laboratory of Chemical Physics, †
California Institute of Technology, Pasadena, California 91109

Received

Expressions for the transition probabilities in collinear collisions of an atom with a diatomic molecule in the uniform, primitive, and classical semi-classical approximations of W. H. Miller are rederived from a new integral representation of a semi-classical S matrix. This derivation treats reactive and non-reactive collisions in a unified manner and gives additional insight into the nature of the semi-classical approximation. The derivation and resulting expressions are given in terms of a general internal diatom coordinate which can be chosen for computational convenience. The new integral expression is compared with ones given previously.

* Work supported in part by the United States Atomic Energy Commission Report Code No. CALT - 767P4-116

** Work performed in partial fulfillment of the requirements for the Ph. D. degree in chemistry at the California Institute of Technology.

† Contribution Number 4715

1. Introduction

Semi-classical expressions for the scattering matrix pertinent to molecular collisions based on exact classical trajectories have been given by Miller [1], Marcus and co-workers [2], Levine and Johnson [3], and Eu [4]. It was argued that such semi-classical expressions would yield results in agreement with exact quantum ones for molecular scattering processes. A semi-classical scattering theory in which the relative motion is treated classically (exactly) and the internal motion quantum mechanically has been developed by Pechukas [5a] and Pechukas and Davis [5b].

Miller has dealt mostly with closed forms for the semi-classical S matrix which result in a hierarchy of expressions of increasing range of validity termed the "classical," "primitive," and "uniform" approximations [1b]. They are appealing in their simplicity and ease of interpretation. Applications of these expressions to model non-reactive collisions [1b, 1c] gave encouraging results and stimulated interest in its applications to reactive collisions [6, 7, 8]. Additional results of numerical calculations we have performed for the collinear $H+H_2$ and $F+H_2$ systems will be published elsewhere [9, 10].

Marcus [2a] and Connor and Marcus [2b] developed their theory by focussing attention on the JWKB solution to the scattering wavefunction and extracting the semi-classical S matrix from it. The many points of contact with Miller's theory indicate that the two theories are essentially equivalent. Wong and Marcus [2c] have applied their theory to the inelastic scattering of a particle by a harmonic oscillator and found excellent agreement with the quantum results of Secrest and Johnson [11].

Johnson and Levine [3] gave an expression for the semi-classical S operator and proceeded to give its matrix elements in terms of either

JWKB or exact wavefunctions for the unperturbed initial and final internal states of the system. This expression differs from Miller's and Marcus' and co-workers' and it represents an approximation to the semi-classical S matrix.

These previous treatments of the semi-classical S matrix have focussed on an action-angle-variables description [12a] of the internal diatom's coordinates and momenta. Miller and co-workers have modified their theory to include other coordinates and momenta [1a, 6].

In the present paper we give a unified derivation of a semi-classical S matrix for collinear reactive and non-reactive collisions between an atom and a diatomic molecule in which a generalized internal coordinate and momentum are used to describe the motion of the latter. The uniform, primitive, and classical semi-classical approximations for the transition probabilities are rederived in terms of these variables. A new integral expression for the semi-classical S matrix is also derived. This expression is of limited use; however, in some cases it is the only expression having some validity. In addition, we give a new derivation of the classical limit of the propagator in the Appendix.

2. Theory

Let us consider, for convenience, the collinear collision of an atom with a diatomic molecule and derive an expression for a semi-classical S matrix for reactive and non-reactive transitions. This derivation can easily be extended to collisions in three physical dimensions.

The exact S matrix for atom-molecule collisions is [13a]

$$S_{m\beta n\alpha} = \lim_{t \to +\infty} \langle \chi_{m\beta}(t) | \Psi^{+}_{n\alpha}(t) \rangle \qquad \alpha, \beta = 1, 2 \qquad (2.1)$$

where $\chi_{m\beta}(t)$ is some non-interacting state of the system describing separated collision partners in arrangement channel β and $\Psi^{+}_{n\alpha}(t')$ is the scattering state which for $t' \to -\infty$ describes the non-interacting reagent state $\chi_{n\alpha}(t')$. For collinear collisions n^{α} and m^{β} are, respectively, the vibrational quantum numbers of the reactant and product diatoms.

For arrangement channel 1(2) we define $R^{1(2)}$ as the distance from the atom A(C) to the center of mass of the diatom BC(AB) and denote the internal diatom coordinate as $x^{1(2)}$ which is left general (i.e., it can be the internuclear distance, the angle variable or some other convenient internal coordinate) for most of the discussion. In terms of these variables, the time, and the propagator $K(R^{\beta}, x^{\beta}, t; R^{\alpha'}, x^{\alpha'}, t')$‡ eq. (2.1) can be written as [13a]

$$S_{m\beta n\alpha} = \lim_{\substack{t\to+\infty \\ t'\to-\infty}} \iiint\!\!\int dR^{\beta} dx^{\beta} dR^{\alpha'} dx^{\alpha'}\, \chi^{*}_{m\beta}(R^{\beta}, x^{\beta}, t) K(R^{\beta}, x^{\beta}, t; R^{\alpha'}, x^{\alpha'}, t') \times \chi_{n\alpha}(R^{\alpha'}, x^{\alpha'}, t') \qquad \alpha, \beta = 1, 2 \quad , \tag{2.2}$$

where K is the amplitude for the system to propagate from space-time point $R^{\alpha'}, x^{\alpha'}, t'$ to space-time point R^{β}, x^{β}, t.

A semi-classical approximation to (2.2) results if semi-classical expressions for $\chi_{m\beta}(R^{\beta}, x^{\beta}, t)$, $\chi_{n\alpha}(R^{\alpha'}, x^{\alpha'}, t')$ and $K(R^{\beta}, x^{\beta}, t; R^{\alpha'}, x^{\alpha'}, t')$ are used. The first one can be written as

$$\chi^{sc}_{m\beta}(R^{\beta}, x^{\beta}, t) = \Psi^{sc}(R^{\beta}, t)\, \eta^{sc}_{m\beta}(x^{\beta}, t) \tag{2.3}$$

and an analogous expression holds for $\chi_{n\alpha}$. The wavefunctions Ψ^{sc} and $\eta^{sc}_{m\beta}$ are defined in eqs. (2.5), (2.12) and (2.15) below. Let us now define an interaction region which extends from R^{α}_{0} (before collision) to R^{β}_{1} (after collision) such that for $R^{\alpha'}$ and R^{β} greater than R^{α}_{0} and R^{β}_{1} respectively the interaction between the atom and the diatom is negligible. Let us also define

‡ In reference [13] p. 300, $K(R, r, t; R', r', t') = i\,G^{+}(R, r, t; R', r', t')$ where G^{+} is the retarded Green's function. K is also called the Feynman propagator.

two times t_0 and t_1 which are required to satisfy the "boundary conditions" $R^{\alpha}(t_0) = R_0^{\alpha}$ and $R^{\beta}(t_1) = R_1^{\beta}$, where $R^{\alpha}(t)$ and $R^{\beta}(t)$ are given by the classical equations of motion. Thus for times $t' < t_0$ and $t > t_1$ the partners propagate freely. We take the semi-classical approximation to $S_{m\beta n\alpha}$ to be

$$S^{sc}_{m^{\beta}n^{\alpha}} = \lim_{\ell\to\infty} \int_{R_1^{\beta}}^{R_1^{\beta}+\ell} dR^{\beta} \int_{x^{\beta}_{min}}^{x^{\beta}_{max}} dx_1^{\beta} \int_{x^{\alpha}_{min}}^{x^{\alpha}_{max}} dx_0^{\alpha} \int_{R_0^{\alpha}}^{R_0^{\alpha}+\ell} dR^{\alpha'}$$

$$\Psi^{*sc}(R^{\beta}, t)K^{sc}(R^{\beta}, t; R_1^{\beta}, t_1)\eta^{*sc}_{m^{\beta}}(x_1^{\beta}, t_1) \tag{2.4}$$

$$\times\, K^{sc}(R_1^{\beta}, x_1^{\beta}, t_1; R_0^{\alpha}, x_0^{\alpha}, t_0)\eta^{sc}_{n^{\alpha}}(x_0^{\alpha}, t_0)K^{sc}(R_0^{\alpha}, t_0; R^{\alpha'}, t')\Psi^{sc}(R^{\alpha'}, t').$$

In this expression, $K^{sc}(R_0^{\alpha}, t_0; R^{\alpha'}, t')$ describes the propagation associated with the relative motion of the separated collision partners before collision, $K^{sc}(R_1^{\beta}, x_1^{\beta}, t_1; R_0^{\alpha}, x_0^{\alpha}, t_0)$ the propagation associated with the motion occurring during the interaction, and $K^{sc}(R^{\beta}, t; R_1^{\beta}, t_1)$ the propagation associated with the relative motion thereafter. Only the second of these semi-classical propagators contains the internal coordinates. The finite integration limits associated with these coordinates correspond to the classical turning points of the diatom before and after collision. The integrations over $R^{\alpha'}$ and R^{β} are performed with these variables considered independent of t' and t respectively. We stress that in our description the quantities R_0^{α} and R_1^{β} are fixed parameters and the times t_0 and t_1 are functions of the other parameters which define the trajectories. Ultimately the semi-classical S matrix must not depend in a significant way on the choice of the parameters R_0^{α} and R_1^{β}.

The wavefunctions $\Psi^{sc}(R^{\alpha'}, t')$ and $\Psi^{sc}(R^{\beta}, t)$ appearing in the last two expressions are normalized over lines of length ℓ and are given by

$$\Psi^{sc}(R^{\alpha'}, t') = \ell^{-\frac{1}{2}} \exp\left[i(P_R^{\alpha'} R^{\alpha'} - E^{\alpha}_{n^{\alpha}} t')/\hbar\right]$$

$$\Psi^{sc}(R^{\beta}, t) = \ell^{-\frac{1}{2}} \exp\left[i\,(P_R^{\beta} R^{\beta} - E^{\beta}_{m^{\beta}}\, t)\,/\,\hbar\right] \quad , \tag{2.5}$$

where $P_R^{\alpha'}$ and P_R^{β} are the relative momenta of the system before and after collision respectively and $E_{n\alpha}^{\alpha}$ and $E_{m\beta}^{3}$ are the associated kinetic energies. The semi-classical propagators $K^{sc}(R_0^{\alpha}, t_0; R^{\alpha'}, t')$ and $K^{sc}(R^{\beta}, t; R_1^{\beta}, t_1)$, also normalized over lines of length ℓ, are given by [14b]

$$K^{sc}(R_0^{\alpha}, t_0; R^{\alpha'}, t') = \ell^{-\frac{1}{2}} \exp\{i[\, p_{R_0}^{\alpha} (R_0^{\alpha} - R^{\alpha'}) - E_k^{\alpha}(t_0 - t')\,]/\hbar\}$$
$$K^{sc}(R^{\beta}, t; R_1^{\beta}, t_1) = \ell^{-\frac{1}{2}} \exp\{i[\, p_{R_1}^{\beta} (R^{\beta} - R_1^{\beta}) - E_k^{\beta}(t - t_1)\,]/\hbar\} \qquad (2.6)$$

where $p_{R_0}^{\alpha} = p_R^{\alpha}(t_0)$ and $p_{R_1}^{\beta} = p_R^{\beta}(t_1)$ are the momenta canonically conjugate to R^{α} and R^{β} at times t_0 and t_1 respectively. They are given by

$$p_{R_0}^{\alpha} = \mu^{\alpha} \frac{dR^{\alpha}}{dt} = \mu^{\alpha}(R_0^{\alpha} - R^{\alpha'})/(t_0 - t')$$
$$p_{R_1}^{\beta} = \mu^{\beta}(R^{\beta} - R_1^{\beta})/(t - t_1)$$

where $\mu^1(\mu^2)$ is the reduced mass of the A + BC (C + AB) system. $E_k^{\alpha}(E_k^{\beta})$ is the relative kinetic energy of the system before (after) collision. According to eq. (2.6), $|K^{sc}(R_0^{\alpha}, t_0; R^{\alpha'}, t')|^2$ and $|K^{sc}(R^{\beta}, t; R_1^{\beta}, t_1)|^2$ are constants. The reason for this is that A and BC do not interact for distances R^{α} greater than R_0^{α} before collision and C and AB do not interact for distances R^{β} greater than R_1^{β} after collision; hence, the probabilities $|K^{sc}(R_0^{\alpha}, t_0; R^{\alpha'}, t')|^2$ and $|K^{sc}(R^{\beta}, t; R_1^{\beta}, t_1)|^2$ for the system to propagate from one space-time point to another in these regions are constants. The semi-classical propagator associated with the interaction is given by [1a, 15, 16]

$$K^{sc}(R_1^{\beta}, x_1^{\beta}, t_1; R_0^{\alpha}, x_0^{\alpha}, t_0) = (2\pi i\hbar)^{-\frac{1}{2}} [\partial p_{x_0}^{\alpha}/\partial x_1^{\beta}]^{\frac{1}{2}} \exp[\, i\Phi_{\beta\alpha}^{sc}(R_1^{\beta}, x_1^{\beta}, t_1; R_0^{\alpha}, x_0^{\alpha}, t_0)/\hbar\,] , \qquad (2.7)$$

where [6]

$$\Phi^{sc}_{\alpha\beta}(R_1^\beta, x_1^\beta, t_1; R_0^\alpha, x_0^\alpha, t_0) = \Phi^{sc}_{\alpha\alpha}(R_1^\alpha, x_1^\alpha, t_1; R_0^\alpha, x_0^\alpha, t_0) + F_1(R_1^\beta, x_1^\beta, R_1^\alpha, x_1^\alpha)\delta_{\beta\alpha} \tag{2.8a}$$

with

$$\Phi^{sc}_{\alpha\alpha} = \int_{t_0}^{t_1} dt\ L[R^\alpha(t), \dot{R}^\alpha(t), x^\alpha(t), \dot{x}^\alpha(t)] . \tag{2.8b}$$

L is the classical Lagrangian of the system and the integrand is associated with a classical trajectory of total energy E passing through the space-time points $(R_0^\alpha, x_0^\alpha, t_0)$ and $(R_1^\beta, x_1^\beta, t_1)$. F_1 is the classical generating function which describes the change of coordinates (R_1^α, x_1^α) to (R_1^β, x_1^β) at time t_1 [12b]. The partial derivative $\partial p^\alpha_{x_0} / \partial x_1^\beta$ (in eq. (2.7)) involving the momentum canonically conjugate to x^α at time t_0 implies that R_0^α, R_1^β, x_0^α, t_0, and t_1 are the variables which remain constant. A derivation of eq. (2.7) is given in the Appendix.

Let us now perform the integrations indicated in eq. (2.4). It is convenient to express the Lagrangian in (2.8b) as

$$L(R^\alpha, \dot{R}^\alpha, x^\alpha, \dot{x}^\alpha) = p_R^\alpha \dot{R}^\alpha + p_x^\alpha \dot{x}^\alpha - H(R^\alpha, p_R^\alpha, x^\alpha, p_x^\alpha) \tag{2.9}$$

where H is the classical Hamiltonian and p_R^α and p_x^α are functions of $R^\alpha, \dot{R}^\alpha$ and $x^\alpha, \dot{x}^\alpha$. We rewrite eq. (2.8b) with the aid of eq. (2.9) (assuming that H is time-independent) as

$$\Phi^{sc}_{\alpha\alpha} = \int_{t_0}^{t_1} dt [p_R^\alpha(t) \dot{R}^\alpha(t) + p_x^\alpha(t) \dot{x}^\alpha(t)] - E(t_1 - t_0)$$

and define a new quantity $\phi^{sc}_{\beta\alpha}$ by

$$\phi^{sc}_{\beta\alpha} = \int_{t_0}^{t_1} dt [p_R^\alpha(t) \dot{R}^\alpha(t) + p_x^\alpha(t) \dot{x}^\alpha(t)] + F_1(R_1^\beta, x_1^\beta, R_1^\alpha, x_1^\alpha)\delta_{\beta\alpha} . \tag{2.10}$$

Eq. (2.8a) then becomes

$$\Phi^{sc}_{\beta\alpha} = \phi^{sc}_{\beta\alpha} - E(t_1 - t_0)$$
$$= \phi^{sc}_{\beta\alpha} - [\,(E(m^\beta) + E^\beta_{m\beta})t_1 - (E(n^\alpha) + E^\alpha_{n\alpha})t_0\,] \quad . \tag{2.11}$$

The semi-classical wavefunctions $\eta^{sc}_{n\alpha}$ and $\eta^{sc}_{m\beta}$ of eq. (2.3) can be written as

$$\eta^{sc}_{n\alpha}(x_0^\alpha, t_0) = \psi^{sc}_{n\alpha}(x_0^\alpha)\exp[\,-i\,E(n^\alpha)t_0/\hbar\,]$$
$$\eta^{sc}_{m\beta}(x_1^\beta, t_1) = \psi^{sc}_{m\beta}(x_1^\beta)\exp[\,-i\,E(m^\beta)t_1/\hbar\,] \quad , \tag{2.12}$$

where $\psi^{sc}_{n\alpha}(x_0^\alpha)$ and $\psi^{sc}_{m\beta}(x_1^\beta)$ are the JWKB wavefunctions given by eq. (2.15) below. The quantum numbers n^α and m^β specify the vibrational state of the diatom before and after collision respectively and $E(n^\alpha)$ and $E(m^\beta)$ are the corresponding semi-classical energy eigenvalues [17]. The total energy of the system E can be written as

$$E = E(n^\alpha) + E^\alpha_{n\alpha} = E(m^\beta) + E^\beta_{m\beta} \quad .$$

Inserting eqs. (2.5), (2.6), (2.7), and (2.12) into eq. (2.4) we obtain

$$S^{sc}_{m^\beta n^\alpha} = \lim_{\ell\to\infty} \int_{R_1^\beta}^{R_1^\beta+\ell} dR^\beta \int_{x^\beta_{min}}^{x^\beta_{max}} dx_1^\beta \int_{x^\alpha_{min}}^{x^\alpha_{max}} dx_0^\alpha \int_{R_0^\alpha}^{R_0^\alpha+\ell} dR^{\alpha\prime}$$
$$\ell^{-1}\exp[i(p^\beta_{R_1} - P^\beta_R)R^\beta/\hbar]\,\psi^{*sc}_{m^\beta}(x_1^\beta)(2\pi i\hbar)^{-\frac{1}{2}}$$
$$\times\,[\partial p^\alpha_{x_0}/\partial x_1^\beta]^{\frac{1}{2}}\exp[i\phi^{sc}_{\beta\alpha}(R_1^\beta, x_1^\beta, t_1; R_0^\alpha, x_0^\alpha, t_0)/\hbar]\,\psi^{sc}_{n^\beta}(x_0^\alpha)$$
$$\times\,\ell^{-1}\exp[i(P^{\alpha\prime}_R - p^\alpha_{R_0})R^{\alpha\prime}/\hbar]\exp\{i[(E^\beta_m - E^\beta_k)\,t + (E^\alpha_k - E^\alpha_n)t']/\hbar\}$$
$$\exp[i(p^\alpha_{R_0}R_0^\alpha - p^\beta_{R_1}R_1^\beta)/\hbar] \quad . \tag{2.13}$$

As described previously, the quantity $\phi^{sc}_{\beta\alpha}$ in this equation is determined by a trajectory of energy E which passes through the space-time points $(R_0^\alpha, x_0^\alpha, t_0)$ and $(R_1^\beta, x_1^\beta, t_1)$. Only four independent variables are needed to specify a trajectory for a two-dimensional configuration space. They can be chosen as R_0^α, x_0^α, R_1^β and x_1^β. Alternatively, the total energy E and the three variables R_0^α, x_0^α and R_1^β can be used. The elapsed time $t_1 - t_0$ is determined from these conditions and will not be taken as an independent variable. The functions $p_R^\alpha(t)$, $p_x^\alpha(t)$, $p_R^\beta(t)$ and $p_x^\beta(t)$ (the momentum canonically conjugate to $x^\beta(t)$) are also determined by the same conditions, and therefore so are $p^\alpha_{R_0}$, $p^\alpha_{x_0}$, $p^\beta_{R_1}$ and $p^\beta_{x_1}$.

It is convenient to replace the set of variables E, R_0^α, x_0^α and R_1^β used to specify a trajectory by the equivalent set E, R_0^α, $p^\alpha_{R_0}$ and $p^\beta_{R_1}$ and to choose the latter two variables according to a criterion suggested by eq. (2.13). We see that the integral of $\ell^{-1}\exp[\,i(P^\alpha_{R_0} - p_R^{\alpha\prime})R^{\alpha\prime}/\hbar\,]$ over $R^{\alpha\prime}$ appearing in that equation is equal to unity if $p^\alpha_{R_0} = P_R^{\alpha\prime}$ and zero otherwise. Similarly if $p^\beta_{R_1} = P_R^\beta$ the analogous integral over R^β is equal to unity but it is zero otherwise. Thus, we require that

$$p^\alpha_{R_0} = P_R^{\alpha\prime} \tag{2.14a}$$

and

$$p^\beta_{R_1} = P_R^\beta \quad . \tag{2.14b}$$

The set of variables E, R_0^α, $p^\alpha_{R_0} = P_R^{\alpha\prime}$, $p^\beta_{R_1} = P_R^\beta$ is then the one to determine the trajectory (or trajectories) for which the $\phi^{sc}_{\beta\alpha}$ of eq. (2.8) is calculated.

We now focus attention on the integrations over x_0^α and x_1^β remaining in eq. (2.13) and examine the consequences of conditions (2.14). To do this we note that $\psi^{sc}_{n\alpha}(x_0^\alpha)$ and $\psi^{sc}_{m\beta}(x_1^\beta)$ are given in general by [1a, 17]

$$\psi^{sc}_{n^\alpha}(x_0^\alpha) = (2\pi i\hbar)^{-\frac{1}{2}} \left[\frac{\partial^2 F_2(x_0^\alpha, n^\alpha)}{\partial x_0^\alpha \partial n^\alpha}\right]^{\frac{1}{2}} \exp[iF_2(x_0^\alpha, n^\alpha)/\hbar]$$

$$\psi^{sc}_{m^\beta}(x_1^\beta) = (2\pi i\hbar)^{-\frac{1}{2}} \left[\frac{\partial^2 F_2(x_1^\beta, m^\beta)}{\partial x_1^\beta \partial m^\beta}\right]^{\frac{1}{2}} \exp[iF_2(x_1^\beta, m^\beta)/\hbar] \qquad (2.15)$$

where $F_2(x_0^\alpha, n^\alpha)$ and $F_2(x_1^\beta, m^\beta)$ are generating functions which in this case are solutions to the time-independent Hamilton-Jacobi equation [12c] for the motion of the isolated diatom. These functions have the following important property:

$$\frac{\partial F_2(x_0^\alpha, n^\alpha)}{\partial x_0^\alpha} = P^\alpha_{x_0} \qquad (2.16a)$$

$$\frac{\partial F_2(x_1^\beta, m^\beta)}{\partial x_1^\beta} = P^\beta_{x_1} \qquad (2.16b)$$

where $P^\alpha_{x_0}$ is the internal momentum of the isolated diatom, which depends on the latter's vibrational quantum number n^α (or energy $E(n^\alpha)$) and internal coordinate x_0^α. For example, if x_0^α is the angle variable q_0^α then $F_2(q_0^\alpha, n^\alpha) = q_0^\alpha n^\alpha \hbar$ and $P^\alpha_{x_0}$ becomes independent of q_0^α and equal to the action variable $n^\alpha\hbar$. $p^\alpha_{x_0}$, as yet unspecified, is some value of the momentum variable and is related to $\phi^{sc}_{\beta\alpha}$ according to

$$\frac{\partial \phi^{sc}_{\beta\alpha}}{\partial x_0^\alpha} = -p^\alpha_{x_0} \cdot \qquad (2.17)$$

However, condition (2.14a) coupled with the conservation of energy equation requires that

$$p^{\alpha}_{x_0} = \pm P^{\alpha}_{x_0} \quad . \tag{2.18}$$

For example, if x_0^{α} is the diatom internuclear distance r_0^{α}, and μ^{α} and μ^{α} are respectively the reduced mass of the atom-diatom system and the reduced mass of the diatom we have

$$\frac{(p^{\alpha}_{R_0})^2}{2\mu^{\alpha}} + \frac{(p^{\alpha}_{r_0})^2}{2\mu_{\alpha}} + V^{\alpha}(r_0^{\alpha}) = \frac{(P^{\alpha\prime}_{R})^2}{2\mu^{\alpha}} + \frac{(P^{\alpha}_{r_0})^2}{2\mu_{\alpha}} + V^{\alpha}(r_0^{\alpha}) = E$$

which together with eq. (2.14a) yield eq. (2.18). If x_0^{α} is the diatom internal coordinate q_0^{α} it can be shown that eq. (2.18) holds with the positive sign on the right-hand side only. For the case in which both signs are permitted, we will exercise our limited remaining freedom of choice of $p^{\alpha}_{x_0}$ by picking the positive sign. The reason is that for this choice we get from eqs. (2.16a), (2.17) and (2.18)

$$\frac{\partial[\phi^{sc}_{\beta\alpha}(R_1^{\beta}, x_1^{\beta}, t_1; R_0^{\alpha}, x_0^{\alpha}, t_0) + F_2(x_0^{\alpha}, n^{\alpha})]}{\partial x_0^{\alpha}} = 0 \ , \tag{2.19}$$

which is the condition for being able to evaluate the x_0^{α} integral in eq. (2.13) by the method of stationary phase [18]. Doing this, and for the moment deferring the performance of the integration over R^{β} we obtain

$$S_{m^{\beta}n^{\alpha}} = \lim_{\ell\to\infty} \int_{R_1^{\beta}}^{R_1^{\beta}+\ell} dR^{\beta} \int_{x^{\beta}_{min}}^{x^{\beta}_{max}} dx_1^{\beta}\, \ell^{-1} \exp[i(p^{\beta}_{R_1} - P^{\beta}_{R})R^{\beta}/\hbar]\psi^{*sc}_{m^{\beta}}(x_1^{\beta})(2\pi i\hbar)^{-\frac{1}{2}}$$

$$\times [\partial q_0^{\alpha}/\partial x_1^{\beta}]^{\frac{1}{2}} \exp\{i[F_2(\overline{x_0^{\alpha}}, n^{\alpha}) + \phi^{sc}_{\beta\alpha}(R_1^{\beta}x_1^{\beta}, t_1; R_0^{\alpha}, \overline{x_0^{\alpha}}, t_0)]/\hbar\}$$

$$\times \exp[i(P^{\alpha\prime}_{R}R_0^{\alpha} - p^{\beta}_{R_1}R_1^{\beta})/\hbar] \exp[-i(E^{\beta}_{k} - E^{\beta}_{m\beta})t/\hbar] \quad , \tag{2.20}$$

where $\overline{x_0^\alpha}$ is the value of x_0^α which satisfies eq. (2.19). It is obviously a function of x_1^β and the other independent variables appearing in that equation. The quantity $[\partial q_0^\alpha/\partial x_1^\beta]^{\frac{1}{2}}$ in (2.20) results from the product $[\partial p_{x_0}^\alpha/\partial x_1^\beta]^{\frac{1}{2}} \cdot [\partial q_0^\alpha/\partial x_0^\alpha]^{\frac{1}{2}} \cdot [\partial x_0^\alpha/\partial p_{x_0}^\alpha]^{\frac{1}{2}}$ and the fact that [12b]

$$\frac{\partial F_2(x_0^\alpha, n^\alpha)}{\partial n^\alpha} = q_0^\alpha(x_0^\alpha, n^\alpha).$$

As stated previously, the set of variables E, R_0^α, $P_R^{\alpha\prime}$, P_R^β determine the trajectory or trajectories we wish to consider. One way of finding these trajectories is to pick R_0^α subject to the conditions given after eq. (2.3), $P_R^{\alpha\prime}$ to give the desired initial relative translational energy, x_0^α anywhere in the range x_{min}^α to x_{max}^α and $P_{x_0}^\alpha$ to yield the desired total energy. We then solve the classical equations of motion for the trajectory corresponding to these initial conditions. Then, at the time for which $R^\beta = R_1^\beta$ (where R_1^β is chosen according to the conditions given after eq. (2.3)), we verify whether or not eq. (2.14b) is satisfied. The entire allowed range of x_0^α is scanned with several possible kinds of results.

Case a. There may be a continuous range of values $\overline{x_0^\alpha}$, from $x_{0\ell}^\alpha$ to x_{0u}^α, which furnish trajectories satisfying the above conditions. Let the corresponding range of x_1^β have lower and upper limits $x_{1\ell}^\beta$ and x_{1u}^β, respectively. These can replace the lower and upper limit of the integration range of x_1^β in eq. (2.20) which then becomes, after the integral over R_1^β is performed (according to the remarks in the paragraph following eq. (2.14b))

$$S_{m^{\beta}n^{\alpha}} = \int_{x_{1\ell}^{\beta}}^{x_{1u}^{\beta}} dx_1^{\beta} \psi_{m^{\beta}}^{*sc}(x_1^{\beta})(2\pi i\hbar)^{-\frac{1}{2}}$$

$$[\partial q_0^{\alpha}/\partial x_1^{\beta}]^{\frac{1}{2}} \exp[i\delta^{sc}(R_1^{\beta}, x_1^{\beta}, t_1; R_0^{\alpha}, \overline{x_0^{\alpha}}, t_0)/\hbar] , \qquad (2.21)$$

where

$$\delta^{sc}(R_1^{\beta}, x_1^{\beta}, t_1; R_0^{\alpha}, \overline{x_0^{\alpha}}, t_0) = \phi_{\beta\alpha}^{sc}(R_1^{\beta}, x_1^{\beta}, t_1; R_0^{\alpha}, \overline{x_0^{\alpha}}, t_0)$$

$$+ F_2(\overline{x_0^{\alpha}}, x^{\alpha}) + P_R^{\alpha\prime} R_0^{\alpha} - P_R^{\beta} R_1^{\beta} \quad .$$

Since x_1^{β} can be considered a function of $\overline{x_0^{\alpha}}$ which is a function of q_0^{α}, we may change the integration variable in eq. (2.21) to q_0^{α}. We get the following expression for the semi-classical S matrix in terms of the initial angle variable.

$$S_{m^{\beta}n^{\alpha}} = \int_{q_{0\ell}^{\alpha}}^{q_{0u}^{\alpha}} dq_0^{\alpha} \psi_{m^{\beta}}^{*sc}(x_1^{\beta})(2\pi i\hbar)^{-\frac{1}{2}} [\partial x_1^{\beta}/\partial q_0^{\alpha}]^{\frac{1}{2}} \exp[i\delta^{sc}/\hbar] \quad . \qquad (2.22)$$

In practice, the conditions for this case are expected to be met rarely if at all. However, we have found situations for which a large number of values of $\overline{x_0^{\alpha}}$ (as opposed to a continuous range of such values) exist which furnish trajectories satisfying all of the required conditions mentioned above [7, 9]. For such situations, eq. (2.22) may be a useful approximation.

Case b. There are two trajectories which satisfy the required conditions. In this case we proceed to evaluate the integral over x_1^{β} in eq. (2.20) by stationary phase in a fashion analogous to the procedure carried out for the x_0^{α} integration. The points of stationary phase are simply those values $\overline{x_1^{\beta}}$ of x_1^{β} such that $p_{R_1}^{\beta} = P_R^{\beta}$. At this point we should notice that if only two trajectories exist which satisfy the required conditions, then there are only

two allowed values of x_0^α and correspondingly two allowed values of x_1^β. Under these conditions, what do the integrals over these variables mean? What is really implied is that we are considering an infinitesimal range of values of $p_{R_0}^\alpha$ around $P_R^{\alpha\prime}$, as well as a similar "shell" of $p_{R_1}^\beta$ around P_R^β. These shells result in continuous infinitesimal ranges of x_0^α and x_1^β around the $\bar{x}_0^\alpha$ and $\bar{x}_1^\beta$. Since these are points of stationary phase for the integrals over x_0^α and x_1^β, we are justified in using this technique to obtain these integrals. The most general stationary phase technique that can be applied in this case (two points of stationary phase which may or may not be coalescent) is the uniform method [1b, 1c, 2a, 2b]. This technique consists of expanding the phase of integrand about the stationary phase point to third order in the integration variable. The expression given by Miller [1b, 1c] can be applied here with the result that

$$S^{USC}_{m^\beta n^\alpha} = \exp\{i[\Delta_1+\Delta_2+(e_1+e_2)\pi/4]/2\}\pi^{\frac{1}{2}}z^{\frac{1}{4}}\{p_1[A_i(-z)+ie_0B_i(-z) + p_2[A_i(-z)-ie_0B_i(-z)]\}\ , \qquad (2.23)$$

where

$$\Delta_j = [\phi^{sc}_{\beta\alpha}(R_1^\beta, \bar{x}_1^\beta, t_1; R_0^\alpha, \bar{x}_0^\alpha, t_0) + F_2(\bar{x}_0^\alpha, n^\alpha) - F_2(\bar{x}_1^\beta, m^\beta) + P_R^{\alpha\prime}R_0^\alpha - P_R^\beta R_1^\beta]/\hbar\ , \qquad (2.24)$$

$$p_j = [2\pi\hbar\,|\partial m^\beta/\partial q_0^\alpha|_{q_{0j}^\alpha}]^{-\frac{1}{2}}\ , \qquad (2.25)$$

$$e_0 = \text{sign}(\Delta_1-\Delta_2)$$

$$e_j = \text{sign}[(\partial m^\beta/\partial q_0^\alpha)_{q_{0j}^\alpha}],\qquad j=1,2$$

and

$$z = \left[\tfrac{3}{4}\,\left|\Delta_1 - \Delta_2\right|\right]^{\frac{2}{3}} \quad .$$

$A_i(-z)$ and $B_i(-z)$ are respectively the regular and irregular Airy functions [19]. The q_{0j}^{α} (j = 1, 2) are the two values of the initial angle variable which give rise to the two acceptable trajectories. $\bar{x}_1^{\beta}$ and $\bar{x}_0^{\alpha}$ are the corresponding values of x_1^{β} and x_0^{α}. The square of the absolute value of $S^{USC}_{m\beta_n\alpha}$ yields the following uniform semi-classical (USC) expression for the transition probability

$$P^{USC}_{m\beta_n\alpha} = (p_1+p_2)^2\pi z^{\frac{1}{2}}A_i^2(-z) + (p_1-p_2)^2\pi z^{\frac{1}{2}}B_i^2(-z) \quad . \tag{2.26}$$

In the asymptotic limit of $\left|\Delta_1 - \Delta_2\right| \gg 1$ the USC expression for the scattering matrix becomes the "primitive" one, i.e.,

$$S^{PSC}_{m\beta_n\alpha} = p_1 \exp[i(\Delta_1 + e_1\pi/4)] + p_2 \exp[i(\Delta_2 + e_2\pi/4)] \quad . \tag{2.27}$$

This expression can also be obtained from eq. (2.22) by using the usual primitive stationary phase approximation [18]. From eq. (2.27) we obtain the primitive semi-classical (PSC) transition probability

$$P^{PSC}_{m\beta_n\alpha} = p_1^2+p_2^2 + 2(p_1p_2)^{\frac{1}{2}}\cos[(\Delta_1 + e_1\pi/4) - (\Delta_2 + e_2\pi/4)] \quad . \tag{2.28}$$

A classical semi-classical (CSC) expression for the transition probability results if the "interference term" $2(p_1p_2)^{\frac{1}{2}}\cos[(\Delta_1 + e_1\pi/4) - (\Delta_2 + e_2\pi/4)]$ is omitted:

$$P^{CSC}_{m\beta_n\alpha} = p_1^2 + p_2^2 \quad . \tag{2.29}$$

In effect by employing the method of stationary phase we have constructed a semi-classical S matrix on the quantum number shells $dn^{\alpha}dm^{\beta}$ in

accordance with the unitarity conditions [1a, 20]

$$\int dn^{\alpha} S^{*}_{m^{\beta} n^{\alpha}} S_{\bar{m}^{\beta} n^{\alpha}} = \delta(m^{\beta} - \bar{m}^{\beta})$$

$$\int dm^{\beta} S^{*}_{m^{\beta} n^{\alpha}} S_{m^{\beta} \bar{n}^{\alpha}} = \delta(n^{\alpha} - \bar{n}^{\alpha}) \quad .$$

In summary, to obtain $S^{sc}_{m^{\beta} n^{\alpha}}$ at a given total energy E for given initial and final quantum numbers n^{α} and m^{β}, we go through the following steps:

1. We choose R_0^{α} and R_1^{β} according to the criteria given after eq. (2.3)
2. We calculate the semi-classical energy eigenvalue $E(n^{\alpha})$, and from it and E the initial relative momentum $P_R^{\alpha'}$.
3. We pick a value q_0^{α} between 0 and 2π, obtain the corresponding x_0^{α} [12a], and from it the potential energy $V^{\alpha}(x_0^{\alpha})$. Then using energy conservation, we obtain the initial internal momentum $P_{x_0}^{\alpha}$ (there can be two of these).
4. We integrate the classical equations of motion for initial conditions R_0^{α}, $p_{R_0}^{\alpha} = P_R^{\alpha'}$, x_0^{α} and $p_{x_0}^{\alpha} = P_{x_0}^{\alpha}$.
5. At the time for which $R^{\beta} = R_1^{\beta}$ we calculate the final internal energy of the diatom and from it the corresponding (not necessarily integral) action variable M^{β}.
6. Using the above procedure we allow q_0^{α} to scan the entire range 0 to 2π and obtain the function $M^{\beta}(q_0^{\alpha})$ and determine the value(s) q_{0j}^{α} of q_0^{α} for which M^{β} equals the integer m^{β}. If two such values (j = 1, 2) exist and if $M^{\beta}(q_0^{\alpha})$ is continuous and differentiable at these values we calculate p_j according to eq. (2.25).
7. We calculate $\phi^{sc}_{\beta\alpha}$ from eqs. (2.8) and F_2 as indicated after eq. (2.15). From these and eq. (2.24) we calculate A_j.

At this point we have all the information needed to calculate the semi-classical scattering matrix elements according to the several expressions given.

Case c. There is one trajectory satisfying the required conditions. In this case we have only primitive and classical semi-classical expressions for the transition probabilities; both given by

$$P^{PSC}_{m^\beta n^\alpha} = P^{CSC}_{m^\beta n^\alpha} = p_1^2 \quad .$$

Case d. There are no trajectories which satisfy eqs. (2.14). In this case the transition $n^\alpha \rightarrow m^\beta$ has been termed "classically forbidden" (in the semi-classical sense) and the semi-classical S matrix vanishes according to the remarks made before eqs. (2.14). We prefer to call the transition "dynamically inaccessible." Since we are dealing with reactive and non-reactive collisions it is important to distinguish between two subcases here. One occurs when there are no trajectories starting in arrangement channel 1(2) and ending in arrangement channel 2(1). The other occurs when there are such trajectories but none for which the initial and final quantum numbers have the desired integral values. Relatively simple analytical continuation techniques have been developed to deal with the latter case [1b, 1d, 2a, 2b]. These techniques involve finding complex root(s) q_0^α to the equation $m^\beta = M^\beta(q_0^\alpha)$, where m^β is integral, by analytically continuing the function $M^\beta(q_0^\alpha)$ by means of a Taylor series or Fourier series expansion into the complex plane. Such analytical continuation is expected to be valid if the complex roots are not "too far" from the real axis, i.e., the transition is not "very forbidden". They have recently been applied to the $F+H_2 \rightarrow FH+H$ and $F+D_2 \rightarrow FD+D$ reactions [10]. In the event that the transition of interest is highly forbidden

or to deal with the former case Miller and George [22a] and Stine and Marcus [23] have developed techniques to integrate the classical equations of motion in complex space. These techniques have been applied to model inelastic collisions [23, 24] and to the $H + H_2$ exchange reaction [22b, 25]. Throughout the present treatment we have implicitly assumed that the classical trajectories were real-valued. The inclusion of complex-valued trajectories is, however, totally consistent with our treatment of the semi-classical S matrix.

Returning now to the expressions (2.22), (2.24), and (2.26) we consider possible choices for the variables x_1^β and x_0^α. As pointed out by Rankin and Miller [6] the choice $r^{\alpha(\beta)}$ in the reactive case leads to some simplification in the expression for $\phi^{sc}_{\beta\alpha}$ since $F_1(R_1^\beta, r_1^\beta, R_1^\alpha, r_1^\alpha,)$ (see eq. (2.8a)) is identically zero. This follows from the fact that the transformation from the (R^α, r^α) system of coordinates to the (R^β, r^β) one is a point transformation [12b]. As a result of this simplification and also because of computational convenience we have done all our calculations with $x^{\alpha(\beta)}$ equal to $r^{\alpha(\beta)}$. The $r^{\alpha(\beta)}$-dependent quantities in eqs. (2.24) and (2.26) are given by

$$\phi^{sc}_{\beta\alpha}(R_1^\beta, r_1^\beta, t_1; R_0^\alpha, r_0^\alpha, t_0) = \int_{t_0}^{t_1} dt\,[p_R^\alpha(t)\dot{R}^\alpha(t) + p_r^\alpha(t)\dot{r}^\alpha(t)]$$

$$= \int_{t_0}^{t_1} dt\,[p_R^\beta(t)\dot{R}^\beta(t) + p_r^\beta(t)\dot{r}^\beta(t)]\ ,$$

$$F_2(n^\alpha, r_0^\alpha) = \text{sign}[P_r^\alpha(r_0^\alpha)] \int_{r^\alpha_{min}}^{r_0^\alpha} dr^\alpha \{2\mu_\alpha [E(n^\alpha) - V^\alpha(r^\alpha)]\}^{\frac{1}{2}}$$

$$F_2(m^\beta, r_1^\beta) = \text{sign}[P_r^\beta(r_1^\beta)] \int_{r^\beta_{min}}^{r_1^\beta} dr^\beta \{2\mu_\beta [E(m^\beta) - V^\beta(r^\beta)]\}^{\frac{1}{2}}$$

where $\mu_{\alpha(\beta)}$ and $V^{\alpha(\beta)}$ are respectively the diatom's reduced mass and internal potential function in arrangement channel $\alpha(\beta)$.

Δ_j given above in the (R^α, r^α), (R^β, r^β) coordinate systems contains spurious discontinuities due to the fact that the functions sign $[P_r^\alpha(r_2^\alpha)]$ and sign $[P_r^\beta(r_1^\beta)]$ contained in the F_2 generating functions given above are discontinuous functions of r_0^α and r_1^β, respectively.
The value of the jump at the discontinuity is equal to $2F_2(r^\alpha_{max}, n^\alpha)$ which equals $(2n^\alpha+1)\pi\hbar$. Thus, the effect of the jump is equivalent to one extra vibration of the molecule. We can obviate this discontinuous behavior if Δ_j is modified as follows:

$$\Delta_j = \int_{t_0}^{t_1} dt[p_R^\alpha(t)\dot{R}^\alpha(t) + p_r^\alpha(t)\dot{r}^\alpha(t)] + F_2[r_0^\alpha(q_{0j}^\alpha), n^\alpha]$$
$$- \{\text{sign}[P_r^\alpha(r_0^\alpha)] - 1\}(n^\alpha + \tfrac{1}{2})\pi\hbar - F_2[r_1^\beta(q_{0j}^\alpha), m^\beta]$$
$$+ \{\text{sign}[P_r^\beta(r_1^\beta)] - 1\}(m^\beta + \tfrac{1}{2})\pi\hbar + P_R^{\alpha\prime}R_0^\alpha - P_R^\beta R_1^\beta \quad . \qquad (2.30)$$

Comparison with previous results

The USC, PSC and CSC expressions for the transition probabilities given by eqs. (2.24), (2.26) and (2.27), respectively, had been given previously by Miller [1b, 1c] for non-reactive collisions for which $x^\alpha = q^\alpha$. Their applicability to reactive collisions had also been established [1a, 6]. The integral representation of the semi-classical S matrix given by eq. (2.22) bears a close resemblance to the ones given by Miller [1b] and Marcus and co-workers [2a, 2b]. There are significant differences, however. In addition to being derived for reactive as well as non-reactive collisions, our representation is valid for any choice x^α of the internal diatom coordinate, be it the internuclear

distance r^{α}, the angle variable q^{α}, etc. Furthermore our representation is valid so long as every trajectory emanating from within the range $q_{o\ell}^{\alpha}$ to q_{ou}^{α} satisfies eq. (2.14b) (in addition to eq. (2.14a)). The previously given expressions carry no such stipulation. However, Marcus and co-workers note that their integral expression is R^{β}-dependent unless eq. (2.14b) is satisfied. Johnson and Levine have also given an approximate integral expression for the semi-classical S matrix [3] but it is substantially different from ours. Their expression does not contain the factor $[\partial x_1^{\beta} / \partial q_o^{\alpha}]^{\frac{1}{2}}$ and eq. (2.14b) is not explicitly required in their treatment.

In summary, we have rederived the uniform, primitive, and classical semi-classical expressions for transition probabilities in reactive and non-reactive collisions of an atom with a diatomic molecule. Our derivation and resulting expressions have been given in terms of a general internal diatom coordinate. In addition to offering additional insight into this semi-classical theory the new derivation has unified the treatment of reactive and non-reactive collisions. A new integral representation of the semi-classical S matrix, of limited applicability, has also resulted from the present derivation.

With a semi-classical S matrix theory available it remains to extensively test it against exact quantum and quasi-classical trajectory calculations. For reactive collisions such tests have been done for the collinear $H + H_2$ [7, 8, 9] and $F + H_2(D_2)$ [10] reactions.

Appendix

The classical limit of the propagator $K(R_1^\beta, x_1^\beta, t_1; R_0^\alpha, x_0^\alpha, t_0)$

The usual derivation of the classical limit of the propagator $K(R_1^\beta, x_1^\beta, t_1; R_0^\alpha, x_0^\alpha, t_0)$ starts from the Feynman path integral representation of K [14a]. Since the representation given by eq. (A1) below is more familiar, we derive in the present appendix the classical limit of the propagator from this representation.

First consider the non-reactive case, i.e., $\alpha = \beta$. The propagator is given by [13b, 14c]

$$K(R_1^\alpha, x_1^\alpha, t_1; R_0^\alpha, x_0^\alpha, t_0) = \sum_n \theta_n(R_1^\alpha, x_1^\alpha)\theta_n^*(R_0^\alpha, x_0^\alpha)\exp[-iE(t_1-t_0)/\hbar] \quad . \quad (A1)$$

The θ_n are the exact eigenfunctions of the total Hamiltonian of the system and the E_n are the corresponding energy eigenvalues which may be discrete and continuous. (The summation actually designates a summation over the discrete values of n and an integration over the continuous values of n.) We can clearly obtain a semi-classical expression for $K(R_1^\alpha, x_1^\alpha, t_1; R_0^\alpha, x_0^\alpha, t_0)$ by replacing the θ_n and E_n by their well-known (JWKB) classical limits [1a, 17]. For a collision in which E is only continuous we have

$$K^{SC}(R_1^\alpha, x_1^\alpha, t_1; R_0^\alpha, x_0^\alpha, t_0) = \int dE\, \theta_E^{SC}(R_1^\alpha, x_1^\alpha)\theta^{*SC}(R_0^\alpha, x_0^\alpha)\exp[-iE(t_1-t_0)/\hbar]. \quad (A2)$$

The θ_E^{SC} are given, without normalization, by [17]

$$\theta_E^{SC}(R^\alpha, x^\alpha) \sim \exp[i\eta_E(R^\alpha, x^\alpha)/\hbar] \quad (A3)$$

where the phase η_E is a real quantity which is a solution of the time-independent Hamilton-Jacobi equation [12c]. Defining the quantity $S_E(R^\alpha, x^\alpha, t)$ by

$$S_E(R^\alpha, x^\alpha, t) = \eta_E(R^\alpha, x^\alpha) - Et$$

we see that

$$K^{sc}(R_1^\alpha, x_1^\alpha, t_1; R_0^\alpha, x_0^\alpha t_0) \sim \int dE \exp\{i[S_E(R_1^\alpha, x_1^\alpha, t_1) - S_E(R_0^\alpha, x_0^\alpha, t_0)]/\hbar\}. \quad (A4)$$

$S(R^\alpha, x^\alpha, t)$, which is a solution of the time dependent Hamilton-Jacobi equation, is given by [12c]

$$S_E(R^\alpha, x^\alpha, t) = \int_0^t d\bar{t}\, L[\dot{R}^\alpha(\bar{t}), \dot{x}^\alpha(\bar{t}), \bar{t}] \quad ,$$

where L is the Lagrangian for the system. The integration is taken over a classical trajectory passing through $R^\alpha(t)$ and $x^\alpha(t)$. Thus, we have

$$S_E(R_1^\alpha, x_1^\alpha, t_1) - S_E(R_0^\alpha, x_0^\alpha, t_0) = \int_{t_0}^{t_1} d\bar{t}\, L[\dot{R}^\alpha(\bar{t}), \dot{x}^\alpha(\bar{t}), \bar{t}]$$

$$\equiv \Phi^{sc}_{\alpha\alpha}(R_1^\alpha, x_1^\alpha, t_1; R_0^\alpha, x_0^\alpha, t_0) \quad .$$

With this result we can rewrite eq. (A4) as follows:

$$K^{sc}(R_1^\alpha, x_1^\alpha, t_1; R_0^\alpha, x_0^\alpha, t_0) \sim \int dE \exp[i\Phi^{sc}_{\alpha\alpha}(R_1^\alpha, x_1^\alpha, t_1; R_0^\alpha, x_0^\alpha, t_0)/\hbar] \quad . \quad (A5)$$

Given the space time points $(R_0^\alpha, x_0^\alpha, t_0)$ and $(R_1^\alpha, x_1^\alpha, t_1)$ there may or may not be a classical trajectory which connects them. If no trajectory exists $K^{sc} = 0$; however, if such a trajectory exists, there is one value of the total energy E associated with it. Thus, the integrand in eq. (A5) is non-zero only on the energy shell E to E + dE with the result that

$$K^{sc}(R_1^\alpha; x_1^\alpha, t_1; R_0^\alpha, x_0^\alpha, t_0) \sim \exp[i\,\Phi^{sc}_{\alpha\alpha}(R_1^\alpha, x_1^\alpha, t_1; R_0^\alpha, x_0^\alpha, t_0)/\hbar] \quad . \quad (A6)$$

This result is identical to the well-known expression for the classical limit of the propagator [14a]. In our application of the semi-classical propagator, R_0^{α} and R_1^{α} are fixed and x_0^{α} and x_1^{α} are the quantities which vary. The normalization factor for K^{SC} can be found from a method given by Miller [1a] (also see reference [26]) wherein the following is required:

$$\int dx_0^{\alpha} K^{SC*}(R_1^{\alpha},x_1^{\alpha\prime}, t_1;R_0^{\alpha}, x_0^{\alpha}, t_0)K^{SC}(R_1^{\alpha}, x_1^{\alpha}, t_1;R_0^{\alpha}, x_0^{\alpha}, t_0) = \delta(x_1^{\alpha\prime} - x_1^{\alpha}) \qquad (A7a)$$

$$\int dx_1^{\alpha} K^{SC*}(R_1^{\alpha}, x_1^{\alpha}, t_1;R_0^{\alpha}, x_0^{\alpha\prime}, t_0)K^{SC}(R_1^{\alpha}, x_1^{\alpha}, t_1;R_0^{\alpha}, x_0^{\alpha}, t_0) = \delta(x_0^{\alpha\prime} - x_0^{\alpha}) . \qquad (A7b)$$

The result is, as given previously [1a]

$$K^{SC}(R_1^{\alpha}, x_1^{\alpha}, t_1;R_0^{\alpha}, x_0^{\alpha}, t_0) = \left[\frac{1}{2\pi i\hbar} \frac{\partial^2 \Phi_{\alpha\alpha}^{SC}(R_1^{\alpha}, x_1^{\alpha}, t_1;R_0^{\alpha}, x_0^{\alpha}, t_0)}{\partial x_1^{\alpha} \partial x_0^{\alpha}}\right]^{\frac{1}{2}}$$

$$\times \exp[i \Phi_{\alpha\alpha}^{SC}(R_1^{\alpha}, x_1^{\alpha}, t_1;R_0^{\alpha}, x_0^{\alpha}, t_0)/\hbar] . \qquad (A8)$$

Given this expression for the semi-classical propagator for non-reactive collisions the semi-classical propagator for reactive collisions can be derived directly. For the moment let α and β denote different arrangement channels. The propagator describing the reactive collision $K(R_1^{\beta}, x_1^{\beta}, t_1;R_0^{\alpha}, x_0^{\alpha}, t_0)$ can be written symbolically as

$$\langle R_1^{\beta}, x_1^{\beta} | \hat{K}(t_1, t_0) | R_0^{\alpha}, x_0^{\alpha} \rangle \quad , \qquad (A9)$$

where $\hat{K}(t_1, t_0)$ is the time-evolution operator. Inserting the identity operator

$$\hat{I} = \iint dR_1^{\alpha} dx_1^{\alpha} | R_1^{\alpha}, x_1^{\alpha} \rangle \langle R_1^{\alpha}, x_1^{\alpha} |$$

into eq. (A9) we obtain

$$K(R_1^\beta, x_1^\beta, t_1; R_0^\alpha, x_0^\alpha, t_0) = \iint dR_1^\alpha \, dx_1^\alpha \langle R_1^\beta, x_1^\beta | R_0^\alpha, x_0^\alpha \rangle \times \langle R_1^\alpha, x_1^\alpha | \hat{K}(t_1, t_0 | R_0^\alpha, x_0^\alpha \rangle \quad . \tag{A10}$$

The classical limit of this expression can be found once the classical limit of the transformation matrix element $\langle R_1^\beta, x_1^\beta | R_0^\alpha x_0^\alpha \rangle$ is known. Using the powerful tools developed previously we have that [26, 1a]

$$\langle R_1^\beta x_1^\beta | R_0^\alpha x_0^\alpha \rangle \sim \exp[iF_1(R_1^\beta, x_1^\beta, R_1^\alpha, x_1^\alpha)/\hbar] \tag{A11}$$

where F_1 is the classical generating function associated with the change in coordinates (R_1^α, x_1^α) to (R_1^β, x_1^β) [12b]. Thus, performing the integrals in eq. (A10) by stationary phase and applying the unitarity conditions analogous to the ones given by eqs. (A7a) and (A7b) we obtain

$$K^{sc}(R_1^\beta, x_1^\beta, t_1; R_0^\alpha, x_0^\alpha, t_0) = \left[\frac{1}{2\pi i\hbar} \frac{\partial^2 \Phi^{sc}_{\alpha\beta}(R_1^\beta, x_1^\beta, t_1; R_0^\alpha, x_0^\alpha, t_0)}{\partial x_1^\beta \partial x_0^\alpha} \right]^{\frac{1}{2}} \times \exp[i \Phi^{sc}_{\beta\alpha}(R_1^\beta, x_1^\beta, t_1; R_0^\alpha, x_0^\alpha, t_0)/\hbar] \quad , \tag{A12}$$

where

$$\Phi^{sc}_{\beta\alpha}(R_1^\beta, x_1^\beta, t_1; R_0^\alpha, x_0^\alpha, t_0) = \Phi^{sc}_{\alpha\alpha}(R_1^\alpha, x_1^\alpha, t_1; R_0^\alpha, x_0^\alpha, t_0) + F_1(R_1^\beta, x_1^\beta, R_1^\alpha, x_1^\alpha) \quad . \tag{A13}$$

If we now let $\alpha = 1, 2$ and $\beta = 1, 2$ as done in the text, eq. (A12) becomes the expression for the semi-classical propagator for reactive and non-reactive collisions once we rewrite eq. (A13) as

$$\Phi^{sc}_{\beta\alpha}(R_1^\beta, x_1^\beta, t_1; R_0^\alpha, x_0^\alpha, t_0) = \Phi^{sc}_{\alpha\alpha}(R_1^\alpha, x_1^\alpha, t_1; R_0^\alpha, x_0^\alpha, t_0) + F_1(R_1^\beta, x_1^\beta, R_1^\alpha, x_1^\alpha)\delta_{\beta\alpha} \quad . \tag{A14}$$

Combining eqs. (A10) and (A12) and noting that [12b]

$$\frac{\partial^2 \Phi^{sc}_{\alpha\beta}}{\partial x_1^\beta \partial x_0^\alpha} = \frac{\partial p^\alpha_{x_0}}{\partial x_1^\beta}$$

we have the expression for the semi-classical propagator for reactive and non-reactive collision given by eq. (2.7) in the text.

References

[1] (a) W. H. Miller, J. Chem. Phys. 53 (1970) 1949; (b) ibid., 53 (1970) 3578; (c) ibid., 54 (1971) 5386; (d) Chem. Phys. Letters, 7 (1970) 431.

[2] (a) R. A. Marcus, J. Chem. Phys. 54 (1971) 3965; (b) J. N. L. Connor and R. A. Marcus, J. Chem. Phys. 55 (1971) 5636; (c) W. H. Wong and R. A. Marcus, J. Chem. Phys. 55 (1971) 5663.

[3] R. D. Levine and B. R. Johnson, Chem. Phys. Letters 7 (1970) 404.

[4] B. C. Eu, J. Chem. Phys. 57 (1972) 2531.

[5] (a) P. Pechukas, Phys. Rev. 181 (1969) 174; (b) P. Pechukas and J. P. Davis, J. Chem. Phys. 56 (1972) 4970.

[6] C. C. Rankin and W. H. Miller, J. Chem. Phys. 55 (1971) 3150.

[7] J. M. Bowman and A. Kuppermann, Chem. Phys. Letters 19 (1973) 166.

[8] S.-F. Wu and R. D. Levine, to be published.

[9] J. M. Bowman and A. Kuppermann, to be published.

[10] G. C. Schatz, J. M. Bowman and A. Kuppermann (a) Abstracts of Papers VIII ICPEAC (1973); (b) ibid., to be published.

[11] D. Secrest and B. R. Johnson, J. Chem. Phys. 45 (1966) 4556.

[12] H. Goldstein, Classical mechanics (Addison-Wesley, Reading Mass., 1950) (a) section 9-5; (b) section 8-1; (c) section 9-1; (d) section 8-1.

[13] L. I. Schiff, Quantum mechanics (McGraw-Hill, New York, New York, 1968, 3rd Ed.) (a) p. 308; (b) p. 53 and p. 300.

[14] R. P. Feynman and A. R. Hibbs, Quantum mechanics and path integrals (McGraw-Hill, New York, New York, 1965) (a) chapters 2 and 7; (b) section 3-1; (c) p. 88.

[15] P. Pechukas, Phys. Rev. 181 (1969) 166.

[16] M. C. Gutzwiller, J. Math. Phys. 8 (1967) 1979.

[17] A. Davydov, Quantum mechanics (Addison-Wesley, Reading, Mass., 1965) chapter III.

[18] G. F. Carrier, M. Crook and C. E. Pearson, Functions of a complex variable (McGraw-Hill, New York, New York, 1966) section 6-4.

[19] M. Abramowitz and I. A. Stegun Eds., Handbook of mathematical functions (U.S. Govt. Printing Office, Washington, D.C., 1964) pp. 446-452.

[20] W. H. Miller and T. F. George, J. Chem. Phys. 56 (1972) 5637.

[21] W. H. Miller, Chem. Phys. Letters 7 (1970) 431.

[22] (a) W. H. Miller and T. F. George, J. Chem. Phys. 56 (1972) 5668; (b) T. F. George and W. H. Miller, J. Chem. Phys. 57 (1972) 2458.

[23] J. Stine and R. A. Marcus, Chem. Phys. Letters 15 (1972) 536.

[24] J. D. Doll and W. H. Miller, J. Chem. Phys. 57 (1972) 5019.

[25] J. D. Doll, T. F. George and W. H. Miller, J. Chem. Phys. 58 (1973) 1343.

[26] J. H. Van Vleck, Proc. Natl. Acad. Sci. U.S. 14 (1928) 178.

I.4 COMPARISON OF SEMI-CLASSICAL, QUASI-CLASSICAL AND EXACT QUANTUM TRANSITION PROBABILITIES FOR THE COLLINEAR H + H_2 EXCHANGE REACTION.*

* This paper appeared in the Journal of Chemical Physics 59, 6524 (1973).

Comparison of Semi-Classical, Quasi-Classical and Exact Quantum Transition Probabilities for the Collinear H + H_2 Exchange Reaction*

JOEL M. BOWMAN** AND ARON KUPPERMANN

A. A. Noyes Laboratory of Chemical Physics†

California Institute of Technology, Pasadena, California 91109

(Received)

Using the classical (CSC), primitive (PSC) and uniform (USC) semi-classical expressions for transition probabilities given by Miller and co-workers, we have calculated the reactive and non-reactive $0 \rightarrow 0$ and $0 \rightarrow 1$ transition probabilities for the collinear H + H_2 exchange reaction. Comparison with previously calculated exact quantum and quasi-classical results for the reactive and non-reactive $0 \rightarrow 0$ transitions reveals that the semi-classical approximations are not very good, expecially the CSC and PSC ones. All three semi-classical probabilities for the reactive $0 \rightarrow 0$ transition exceed unity in the collision energy range from 0.0 to 0.2 eV above the quasi-classical reaction threshold. This feature coupled with the failure of any of the semi-classical approximations to produce the marked quantum effects present in this transition causes these results to be less accurate than the corresponding quasi-classical ones. For the reactive and non-reactive $0 \rightarrow 1$ transitions the USC results are in qualitative agreement with the exact quantum ones and are better than the standard quasi-classical results. However, the reverse quasi-classical results are almost as good as the USC ones for these transitions. A probable reason for the inability of the USC expression to produce the strong oscillations

observed in the exact quantum results is that the latter are due to interference between direct and resonant (i. e., compound state) processes whereas the present formulation of the semi-classical method does not encompass such phenomena. A comparison of the total reaction probabilities obtained by the USC and quasi-classical methods with the exact quantum one indicates that the USC result is more accurate than the quasi-classical one, except at collision energies less than 0.50 eV. This improved accuracy is due to a partial cancellation of errors in the contributing $0 \rightarrow 0$ and $0 \rightarrow 1$ USC reactive transition probabilities.

1. INTRODUCTION

There has recently been much progress in the development of a semi-classical theory of reactive and non-reactive atom-molecule scattering.[1-6] The central theme of this theory is derived from the superposition principle of quantum mechanics. One assumes that "quantum effects" in heavy particle (e.g., atom-molecule) systems are due primarily, if not solely, to the interference of scattering amplitudes. It has been shown that the classical limit of the scattering matrix is obtained from information contained in the exact classical trajectories describing the atom-molecule scattering. The phases of the $\underset{\sim}{S}$ matrix elements are given by the action accrued along trajectories whose boundary conditions correctly describe the scattering process of interest and the absolute values of those elements are obtainable from the phases.[1a]

In a numerical application of his theory, Miller[1b] computed the transition probabilities for the translational to vibrational energy transfer

in collinear collisions of an atom (He) with a harmonic oscillator (H_2). He found, typically, two classical trajectories satisfying the correct boundary conditions. This feature gave rise to "uniform" (USC) and "primitive" (PSC) semi-classical expressions for the transition probabilities. A "classical" (CSC) semi-classical expression also resulted by ignoring the interference term in the primitive semi-classical expressions. The agreement between the CSC and PSC results and the exact quantum ones of Secrest and Johnson[7] was not very good. However, the USC results gave excellent agreement. Furthermore, a "rainbow" phenomenon caused the CSC and PSC results to diverge at certain energies, whereas the corresponding USC results were well-behaved. Rankin and Miller[1e] studied the collinear $H + Cl_2 \rightarrow HCl + Cl$ reaction semi-classically. They found that the final quantum number of the product molecule was an anomalously random function of the initial phase angle of the reagent molecule, and this precluded the use of the USC, PSC, and CSC expressions. Miller and co-workers[1f, 1g, 1h] have treated the collinear and three-dimensional $H + H_2$ exchange reaction at collision energies below the quasi-classical reaction threshold by employing complex-valued classical trajectories. They compared their collinear results with two different "exact" quantum calculations.[8, 9] In one[8] a Porter-Karplus[10] potential energy surface was used, whereas in the other[9] a harmonic-type approximation to this surface was employed. These exact quantum calculations differed from one another by a factor of two or more over the energy range of interest and therefore the most appropriate comparison is with the former calculation.[11]

No extensive comparison between semi-classical, exact quantum and quasi-classical transition probabilities for a chemical reaction has yet been made. In this paper we present such a comparison for the reactive

and non-reactive transition probabilities for the collinear $H + H_2$ exchange reaction. The quantum results we compare with are those of Truhler and Kuppermann[12] and Schatz and Kuppermann[13] and the quasi-classical ones are those of Bowman and Kuppermann.[14] The potential energy surface used in all these calculations was a Wall-Porter fit[15] to a scaled SSMK surface[16] and is described in detail elsewhere.[12] The range of total energies considered, 0 to 1.30 eV, includes energies for which vibrationally excited reagent and/or product H_2 are present. Some of the results of the present paper were presented in a preliminary form previously.[17]

2. CALCULATIONAL PROCEDURES

2.1 Semi-classical Expressions

The theoretical basis for the semi-classical method is described in detail elsewhere.[1a, 1b, 1e, 6] We summarize here the procedure followed in our calculations.

Let us consider the collinear $A+BC \rightarrow AB+C$ reaction. We define $R^{\alpha(\beta)}$ to be the distance from the atom to the center of mass of the diatom in arrangement channel $\alpha(\beta)$, where $\alpha, \beta = 1, 2$. Arrangement channels 1 and 2 are $A+BC$ and $AB+C$, respectively. $AC+B$ is excluded by the collinear nature of the reaction. The break-up arrangement $A+B+C$ is also excluded. The relative momentum variable conjugate to $R^{\alpha(\beta)}$ is $P_R^{\alpha(\beta)}$. The internal diatom angle variable is $q^{\alpha(\beta)}$ and its conjugate momentum is $M^{\alpha(\beta)}$. The diatom internuclear distance coordinate and momentum are respectively $r^{\alpha(\beta)}$ and $P_r^{\alpha(\beta)}$. Consider a reactive or non-reactive transition from the reagent state $M^{\alpha} = n^{\alpha}$ to the product state $M^{\beta} = m^{\beta}$, where n^{α} and m^{β} are given integers. To investigate this

transition semi-classically at a given total energy E a search of classical trajectories is carried out as follows. At time t_0 the initial atom-molecule separation is fixed at some large value, R_0^{α}, such that the interaction energy is negligibly small. P_R^{α} is obtained from the relative collision energy $E_{n\alpha}^{\alpha}$ through the usual expression

$$P_{R_0}^{\alpha} = -[2\mu_{\alpha} E_{n\alpha}^{\alpha}]^{\frac{1}{2}} \quad ,$$

where μ_{α} is the reduced mass of the atom-diatom system in the α arrangement channel. E is equal to $E_{n\alpha}^{\alpha} + E(n^{\alpha})$, where $E(n^{\alpha})$ is the semi-classical diatom energy eigenvalue. The initial value of the angle variable q_0^{α} is made to scan uniformly the range 0 to 2π and the corresponding initial value r_0^{α} of r^{α} is obtained from the relationship[18a]

$$\frac{\partial F_2(n^{\alpha}, r_0^{\alpha})}{\partial n^{\alpha}} = q_0^{\alpha} \quad .$$

For a Morse oscillator an exact analytical expression for the function $r_0^{\alpha} = r_0^{\alpha}(q_0^{\alpha})$ is available[1e] and was used in our calculations. $F_2(n^{\alpha}, r^{\alpha})$ is the classical generating function which is the solution to the time-independent Hamilton-Jacobi Equation.[18b] The initial momentum $P_{r_0}^{\alpha}$ can be obtained from n^{α}, q_0^{α}, and r_0^{α} using the expression[18a]

$$\frac{\partial F_2(n^{\alpha}, r^{\alpha})}{\partial r_0^{\alpha}} = P_{r_0}^{\alpha} \quad ,$$

from which one obtains

$$P_{r_0}^{\alpha} = \text{sign}(\pi - q_0^{\alpha})\{2\mu^{\alpha}[E(n^{\alpha}) - V^{\alpha}(r_0^{\alpha})]\}^{\frac{1}{2}} ,$$

where μ^{α} is the reduced mass of the diatom and V^{α} is its internal potential energy function. The quantities R_0^{α}, $P_{R_0}^{\alpha}$, r_0^{α} and $P_{r_0}^{\alpha}$ thus chosen furnish the initial conditions needed to integrate Hamilton's equations of motion. This integration is performed and the variables $R^{\beta(\alpha)}$, $P_R^{\beta(\alpha)}$, $r^{\beta(\alpha)}$ and $P_r^{\beta(\alpha)}$ are obtained as a function of time. At time t_1, when $R^{\beta(\alpha)}$ is equal to some large value $R_1^{\beta(\alpha)}$, the quantity $M^{\beta} = M^{\beta}(q_0^{\alpha};n^{\alpha}, E)$ is calculated (for fixed values of n^{α} and E) and root(s) to the equation

$$M^{\beta}(q_0^{\alpha};n^{\alpha}, E) = m^{\beta} \tag{1}$$

are sought for. Several possible outcomes exist.

The usual outcome is that there are two isolated, though perhaps coalescent, roots to Eq. (1). The uniform semi-classical (USC) expression for the reaction probability to form product AB in the m^{th} vibrational state from reagent BC in the n^{th} vibrational state is given by[1b, 1e, 2b, 6]

$$P^{USC}_{m^{\beta}\,n^{\alpha}} = [p_1^{\frac{1}{2}} + p_2^{\frac{1}{2}}]^2 \pi z^{\frac{1}{2}} A_i^2(-z) + (p_1^{\frac{1}{2}} - p_2^{\frac{1}{2}})^2 \pi z^{\frac{1}{2}} B_i^2(-z) \ , \tag{2}$$

where

$$p_j = \left[2\pi\hbar \left| \frac{\partial M^{\beta}(q_0^{\alpha};n^{\alpha}, E)}{\partial q_0^{\alpha}} \right|_{q_{0_j}^{\alpha}} \right]^{-1} , \qquad j = 1, 2$$

and

$$z = \left[\tfrac{3}{4} |\Delta_1 - \Delta_2| \right]^{\frac{2}{3}} .$$

The subscript j labels the two values of q_0^{α} which give rise to the two trajectories such that $M^{\beta} = m^{\beta}$. The Δ_j are calculated from the corresponding trajectories by[1e, 6]

$$\Delta_j = \frac{1}{\hbar}\left\{\int_{t_0}^{t_1} dt\left[P_R^{\alpha}(t)\frac{dR^{\alpha}(t)}{dt} + P_r^{\alpha}(t)\frac{dr^{\alpha}(t)}{dt}\right] \text{(calculated along the } j^{th} \text{ trajectory)} + F_2(r_j^{\alpha}(t_0), n^{\alpha}) + P_R^{\alpha}(t_0)R^{\alpha}(t_0) - F_2(r_j^{\beta}(t_1), m^{\beta}) - P_R^{\beta}(t_1)R^{\beta}(t_1)\right\} \quad . \tag{3}$$

$A_i(-z)$ and $B_i(-z)$ are respectively the regular and irregular Airy functions.[19] This Δ_j given by Eq. (3) is a discontinuous function of q_0^{α} since the function $\text{sign}[P_r^{\alpha}(r_0^{\alpha}(q_0^{\alpha}))]$ contained in the F_2 generating function is a discontinuous function. The spurious discontinuities introduced by this feature can be eliminated in several ways. The one we adopted is to modify Δ_j as follows:[6]

$$\Delta_j = \frac{1}{\hbar}\left\{\int_{t_0}^{t_1} dt\left[P_R^{\alpha}(t)\frac{dR^{\alpha}(t)}{dt} + P_r^{\alpha}(t)\frac{dr^{\alpha}(t)}{dt}\right] + P_R^{\alpha}(t_0)R^{\alpha}(t_0) - P_R^{\beta}(t_1)R^{\beta}(t_1) + F_2(r^{\alpha}(t_0), n^{\alpha}) - [\text{sign}(P_r^{\alpha}(r_0^{\alpha})) - 1](n^{\alpha} + \tfrac{1}{2})\pi\hbar - F_2(r^{\beta}(t_1), m^{\beta}) + [\text{sign}(P_r^{\beta}(r_1{}^{\beta}) - 1)](m^{\beta} + \tfrac{1}{2})\pi\hbar\right\} \quad . \tag{4}$$

In the limit of $|\Delta_1 - \Delta_2| \gg 1$, Eq. (2) becomes asymptotically equal to the primitive semi-classical (PSC) expression given by

$$P^{PSC}_{m^{\beta}\, n^{\alpha}} = \bar{p}_1 + \bar{p}_2 + 2(\bar{p}_1\bar{p}_2)^{\frac{1}{2}}\sin(\Delta_1 - \Delta_2) \quad . \tag{5}$$

By omitting the "interference" term $2(p_1p_2)^{\frac{1}{2}}\sin(\Delta_1 - \Delta_2)$ in Eq. (5) the classical semi-classical (CSC) expression results, viz.,

$$P^{CSC}_{m^{\beta}\, n^{\alpha}} = p_1 + p_2 \quad . \tag{6}$$

In another case, only one trajectory may yield a root to Eq. (1). As a consequence the USC, PSC and CSC expressions all become equal to

$$P^{SC}_{m\beta n\alpha} = p_1 \quad . \tag{7}$$

A third possibility is that no (real-valued) classical trajectory yields the desired root. In this case, in the absence of analytical continuation techniques[1b,1c, 2b] or the inclusion of complex-valued trajectories[1f, 1g, 1h, 2f] it is found that

$$P^{SC}_{m\beta n\alpha} \equiv 0 \quad .$$

In the calculations we report in section 3, no attempt to analytically continue by power series techniques or by employing complex-valued trajectories was made.

A fourth and very rare case is one in which a continuous range of values $q^{\alpha}_{o\ell}$ to q^{α}_{ou} yields roots to Eq. (1). In this case we have shown that the semi-classical $\underset{\approx}{S}$ matrix element is given by[6]

$$S^{SC}_{m\beta n\alpha} = \int_{q^{\alpha}_{o\ell}}^{q^{\alpha}_{ou}} dq_o^{\alpha} \psi^{*sc}_{m\beta}(r_1^{\beta})(2\pi i\hbar)^{-\frac{1}{2}} [\partial r_1^{\beta}/\partial q_o^{\alpha}]^{\frac{1}{2}} \exp[i\delta/\hbar] \quad , \tag{8}$$

where

$$\delta = \int_{t_o}^{t_1} dt \left[P_R^{\alpha}(t) \frac{dR^{\alpha}(t)}{dt} + P_r^{\alpha}(t) \frac{dr^{\alpha}(t)}{dt}\right] + F_2(r_o^{\alpha}(q_o^{\alpha}), n^{\alpha})$$

$$+ P_R^{\alpha}(t_o)R^{\alpha}(t_o) - P_R^{\beta}(t_1)R^{\beta}(t_1) \quad .$$

$\psi^{sc}_{m\beta}(r_1^{\beta})$ is the JWKB wavefunction for the diatom in arrangement channel β. The reaction probability is then

$$P^{SC}_{m\beta n\alpha} = \left|S^{SC}_{m\beta n\alpha}\right|^2 \quad .$$

No calculations of reaction probabilities based on Eq. (8) are reported in the present paper, although we shall see a situation where it approximately applies.

In reporting our results of calculations we adopt the following convention:

$$P^R_{nm} \equiv P_{m\beta n\alpha} \qquad \alpha \neq \beta$$

$$P^V_{nm} \equiv P_{m\beta n\alpha} \qquad \alpha = \beta \quad .$$

2.2 Numerical Methods

CSC, PSC, and USC P^R_{00}, P^V_{00}, P^R_{01}, and P^V_{01} transition probabilities were calculated as a function of energy for the collinear $H + H_2 \rightarrow H_2 + H$ reaction using the same potential energy surface employed in the exact quantum and quasi-classical calculations.[12, 13, 14]

The classical trajectories needed for the semi-classical calculations described in section 2.1 were computed as follows. An initial atom-molecule separation R_0 of 4.6 bohr was chosen, for which the corresponding interaction energy vanishes. Typically 100 values of q_0 uniformly spaced in the interval 0 to 2π were chosen, thereby generating 100 trajectories per energy. The integration of Hamilton's equations was performed using a fourth order Runge-Kutta-Gill initiator and an Adams-Moulton fourth order predictor, fifth order corrector.[20] The associated action Δ_j (see Eq. (4)) was checked by testing its invariance with respect to the initial and final integration times t_0 and t_1. The same results to within a few parts in 10^4 were obtained using either the reagent or product coordinate system. This, coupled with the general result that action differences $|\Delta_1 - \Delta_2|$ for two

trajectories were generally less than unity resulted in transition probabilities precise to ± 0.01. Computational time for one trajectory and its associated action in double precision arithmetic was 3 to 4 seconds on an IBM 370/155.

2.3 Behavior of Action Difference as a Function of Initial Phase

In order to illustrate the differences between Δ given by Eq. (4) and Δ given by Eq. (3) we have plotted these two Δs as a function of q_0 for a total energy E of 1.053 eV in Fig. 1. There, and more quantitatively in Table I, the continuity of Δ given by Eq. (4) and the discontinuous behavior of Δ given by Eq. (3) is demonstrated. We always used Eq. (4) to calculate Δ.

3. RESULTS

3.1 General Features of the Semi-Classical Transition Probabilities

As discussed in section 2 the location of root(s) to Eq. (1) of section 2.1 necessary in order to compute the CSC, PSC, and USC transition probabilities requires a scan of the final action number m of the product versus the initial angle variable q_0 of the reagent. (For simplicity in presentation we have omitted the superscripts on the variables m and q_0 and will use lower case m in place of upper case M.) A typical result of such a scan is shown in Fig. 2 for trajectories computed at a total energy E of 1.253 eV and for the reagent in its ground vibrational state. Several important features may be noted. Firstly, the reactive branch (solid curve) and the non-reactive branch (dashed curve) each have two roots to the equation m = 1, i.e., two trajectories leading to a final H_2 with internal energy E(1). Secondly, we note that there are no reactive tra-

jectories for which m = 0 in spite of the fact that this state is energetically accessible. In this case the semi-classical CSC, PSC, and USC reaction probabilities are set equal to zero, as stated in section 2, and the corresponding transition is usually termed "classically forbidden"[1b, 2a] at this particular energy. The non-reactive transition $0 \rightarrow 0$ is "allowed," however, since there are two trajectories corresponding to it. Another feature of interest is the fact that these curves almost reach the value m = 2. The reactive and non-reactive transition $0 \rightarrow 2$ are strictly forbidden for lack of sufficient energy. Thus, we prefer to term the $0 \rightarrow 0$ reactive transition dynamically inaccessible and the transition $0 \rightarrow f$ ($f \geq 2$) energetically inaccessible to stress the fact that the corresponding transition probabilities vanish for different reasons.

3.2 Comparison of Semi-Classical, Quantum, and Quasi-Classical Transition Probabilities

For the quasi-classical trajectories we define the vibrational quantum number of the final H_2 molecule as follows.[21] Let $\Delta E(n) = E(n+1) - E(n)$ and E^v_{Cl} be the continuous classical vibrational energy of that molecule. If $E(n) \leq E^v_{Cl} < E(n) + \frac{1}{2}\Delta E(n)$ or $E(n) + \frac{1}{2}\Delta E(n) \leq E^v_{Cl} < E(n+1)$ we set $v = n$ or $v = n+1$, respectively. If $E^v_{Cl} \leq E(0)$, we set $v = 0$. The quasi-classical transition probability to state v is then defined as the fraction of the trajectories leading to H_2 in that state.

Fig. 3 shows the USC, exact quantum, and quasi-classical P^R_{00} transition probabilities as a function of the total energy E and the initial translational energy E_0. The arrows on the lower abscissa designate the

total energies at which excited vibrational states v = 1, 2 become energetically accessible. The quasi-classical results have been compared to the exact quantum ones in some detail elsewhere.[14] The USC values are a better approximation at total energies greater than 1.0 eV, but deviate rapidly from the exact quantum ones as the energy decreases below 0.85 eV. Further, the strong oscillation occurring around E = 0.95 eV in the exact quantum curve is barely perceptible in the USC one. In addition, the dramatically sharp behavior in the quantum reaction probability at E = 1.27 eV is not produced by the USC result. (This quantum effect was not present in the quantum results used in our preliminary comparison.[17]) No USC results are given for total energies less than 0.78 eV because the m versus q_0 curve was nearly horizontal at these lower energies and hence preclude the use of the USC, as well as the CSC and PSC, expressions. This feature is illustrated in Fig. 4 where a plot of the final action number m versus initial phase angle q_0 is shown for E = 0.553 eV. m is seen to deviate only slightly from zero for both the reactive and non-reactive curves. Thus, practically every trajectory yields a root for the $0 \rightarrow 0$ transition and hence contributes about equally to the corresponding transition probability. As a result, the assumptions which lead to the USC, PSC, and CSC expressions[1b, 6] are violated and these expressions cannot be used. The behavior of $m(q_0)$ shown in Fig. 4 is approximately like the one for which the integral representation of the S matrix given by Eq. (8) of section 2 is valid. Hence, this may be the only valid expression of usefulness. By contrast, at this energy the quasi-classical result is in good agreement with the exact quantum result. In Fig. 5 we give the CSC and PSC results for the P_{00}^{R} transition probability along with the exact quantum ones. We note a divergent behavior in the CSC and PSC results at total energies around 1.25 eV. This behavior is easily

understood by inspection of Fig. 2 from which it can be surmised that at an energy slightly less than 1.253 eV the reactive m versus q_0 curve is tangent to the line m = 0 and hence $\left|\partial q_0/\partial m\right|_{m=0} \to \infty$. This fact causes the PSC and CSC results to diverge. The USC result, however, is well-behaved and in fact is in reasonable agreement with the exact quantum result. This rainbow phenomenon has been observed and discussed by Miller.[1b]

In Figs. 6 and 7 we give the USC, exact quantum, quasi-classical and CSC, PSC, and exact quantum P^V_{oo} transition probabilities, respectively. The highly oscillatory nature of the quantum curve is not reproduced by the USC curve which in addition deviates from it rapidly as the energy decreases below 0.58 eV. The USC results do, however, show an increase with energy for E >0.85 eV in agreement with the average trend of the exact results. This behavior is also exhibited by the quasi-classical results which in addition are well-behaved at low energies. The CSC and PSC curves are even worse approximations to the exact result than the USC one.

The USC, exact quantum, and quasi-classical P^R_{o1} transition probabilities are plotted in Fig. 8. The overall structure of the quantum curve is qualitatively reproduced by the USC one but not by the quasi-classical one. A difference of approximately 0.08 eV (1.9 kcal/mole) in the effective threshold energies of the quantum and USC results can be seen. The quasi-classical curve exhibits an unreasonable threshold behavior, i.e., non-zero, P^R_{o1} at total energies less than E(1) (0.7945 eV). This results from the definition of the quasi-classical transition probability we have used, for which the energy at which v = 1 becomes accessible is $E(1) - \frac{1}{2}[E(1) - E(0)]$. This unreasonable threshold behavior of the quasi-classical P^R_{o1} transition probability can be removed by introducing the quasi-classical P^R_{1o} transition probability which we can consider as the reverse P^R_{o1} transition probability. Since the

quasi-classical P^R_{01} and P^R_{10} transition probabilities are not equal, whereas the semi-classical and exact quantum ones are (see next section) we have investigated the quasi-classical P^R_{10} transition probability also. As seen in Fig. 8 this transition probability gives results in substantially better agreement with the exact P^R_{01} ones than the quasi-classical P^R_{01} transition probability. Indeed, the P^R_{10} quasi-classical results are only slightly worse than the USC P^R_{01} ones.

Fig. 9 shows the USC, exact quantum, and quasi-classical P^V_{01} transition probabilities. Here again, substantial qualitative agreement is found between the USC and the quantum results. As expected, the quasi-classical curve shows the correct average behavior but none of the structure of the quantum one, and shows improper threshold behavior. A difference in threshold energies of approximately 0.08 eV is again observed between the USC and exact results. We have also plotted the reverse P^V_{01} (i.e., the P^V_{10} transition probability) transition probability and note that although the threshold behavior of the P^V_{10} result is more reasonable than the P^V_{01} result with respect to proper threshold behavior, its spikey behavior is grossly incorrect.

The total reaction probability P^R_0 which is simply the sum $\sum_f P^R_{0f}$ is displayed in Fig. 10 where we compare the USC, the quasi-classical, and the exact quantum results. While the quasi-classical curve looks much like an averaged quantum one, the USC curve bears some resemblance to the exact one for total energies exceeding the v = 1 threshold. This latter behavior is surprising since the strong oscillation present in the exact P^R_{00} transition probability at energies slightly above the v = 1 threshold is not apparent in the corresponding USC one. Nevertheless the oscillation in the exact quantum total reaction probability at energies around 0.90 eV

appears in the USC result even though not in the quasi-classical one. This seems to be due to a fortuitous cancellation of errors in the uniform $0 \rightarrow 0$ and $0 \rightarrow 1$ reaction probabilities.

3.3 Microscopic Reversibility and Conservation of Flux

The semi-classical CSC, PSC, and USC transition probabilities all obey microscopic reversibility.[22] The exact quantum ones do also, of course, but the quasi-classical ones do not. We illustrate this property numerically in Table II where the quasi-classical and USC results are given for two energies.

The semi-classical collision probabilities in general do not sum up to unity and may differ from it by as much as 25%. In Fig. 11 we have plotted the sum of the USC collision probabilities over the total energy range 0.68 eV to 1.28 eV. In some of this energy range this sum is less than unity. This correlates partly with the fact that for certain energies one or more contributing transition probabilities is zero since the corresponding transition is dynamically forbidden. For example, in the energy range 0.85 eV to 0.91 eV the reactive and non-reactive $0 \rightarrow 1$ transitions are dynamically forbidden. If the corresponding transition probabilities were calculated by the use of complex trajectories or analytical continuation one might guess that, in analogy with the present reaction threshold behavior, they would increase montonically with increasing energies for energies in the above range. This expectation is consistent with the observed monotonic decrease in the present calculations, since we have not included such methods in the present calculations. For E between .91 eV and

.953 eV the rapid rise of the USC sum to a maximum of 1.34 is due to the abruptness with which these $0 \rightarrow 1$ transitions become dynamically allowed. The quasi-classical total reaction probabilities are automatically normalized and the quantum results are always within 2% of unity or better.

4. DISCUSSION

4.1 The Reaction Threshold Region

The threshold behavior of the reactive $0 \rightarrow 0$ transition, important for thermal rate constants, is not described properly by any of the semi-classical expressions used. In section 3 it was shown that at total energies around 0.55 eV the USC, PSC, and CSC expressions for the P^R_{00} transition probability did not apply. However, a possibly more serious shortcoming of the form of the semi-classical theory used in the present paper is that it furnishes a zero reaction probability at any energy for which no quasi-classical reactive trajectory exists. This is certainly the case in the $H + H_2$ surface here considered for total energies less 0.424 eV--the energy of the saddle point. At these energies the reaction proceeds totally by tunneling. Recently Miller and George[1f, 1g] have formulated an approach to this kind of tunneling and applied it to the collinear $H + H_2$ reaction at energies below the classical threshold for the Porter-Karplus surface.[1f, 1g] Stine and Marcus[2f] have applied complex-valued trajectories to a model collinear inelastic scattering calculation. These approaches make use of complex-valued trajectories. Freed[23] has shown that tunneling can be described semi-classically by transforming the classical propagator in space-time variables into a space-energy representation involving an integration over time which

is allowed to be complex. In our calculations no attempt was made to deal with such non-classical trajectories. Thus, the USC, PSC, and CSC P^R_{00} probabilities were also set equal to zero for total energies between 0.424 eV and 0.52 eV. Similarly, the semi-classical P^V_{00} transition probabilities vanish in the total energy range 0.6 eV to 0.7 eV since no non-reactive quasi-classical trajectories were found in this range.

The extension of semi-classical theory, such as the one made by George and Miller, to include non-classical trajectories is necessary if the reaction threshold behavior is to be better described. In order to acertain the accuracy of their approach, we have compared their results for the collinear $H + H_2$ exchange reaction[1g] with the quantum ones for the Porter-Karplus surface. (Whereas all other calculations presented so far were done with Wall-Porter fit to SSMK surface.[12]) In Fig. 12 we have plotted the ratio of the complex-trajectory semi-classical reaction probabilities P^R_{SC} to the accurate quantum ones[11] P^R_{EQ} as a function of translational energy E_0. It can be seen that over the energy range of 0.02 to 0.2 eV, of importance for tunneling process, the semi-classical reaction probabilities equal in average 71% of the accurate ones, indicating that for this collinear system the complex-trajectory method used[1g] underestimates the effect of tunneling. The steep rise in the P^R_{SC}/P^R_{EQ} ratio above $E_0 = 0.2$ eV shown in Fig. 12 may be indicative of the same kind of divergent behavior as the one shown in Fig. 3 by the USC P^R_{00} curve.

We have also calculated the collinear rate constants corresponding to the P^R_{SC} and P^R_{EQ} above by a numerical integration of the appropriate expression.[12] The corresponding rate constant ratio $k_{SC}(T)/k_{EQ}(T)$ is plotted in Fig. 13 as a function of 1/T. It can be seen that in the temperature range from 100 to 300 K this ratio varies from about 0.65 to about 0.73. This is a significant improvement over the corresponding quasi-classical ratio calculated from the same collinear reaction on a slightly different potential

energy surface.[14] The fact that these ratios are less than unity is a manifestation of the fact that this complex-trajectory semi-classical method underestimates tunneling, as just pointed out.

4.2 The Reactive and Non-Reactive 0 → 0 Transitions Above the Reaction Threshold Region

It has been noted in section 3 that the reactive 0 → 0 transition becomes dynamically inaccessible at total energies greater than 1.25 eV. In this case, there are no real roots of the equation m = 0, and therefore Eqs. (2), (5), and (6) of section 2 are not applicable. Hence the USC, PSC, and CSC P_{00}^{R} transition probabilities are equal to zero for these energies, as stated in section 2 and depicted in Figs. 2 and 4. In fact, this result is not a bad approximation to the exact quantum values, which at energies between 1.3 eV and 1.5 eV have an average value of about 0.08. At total energies slightly below 1.25 eV the PSC and CSC P_{00}^{R} transition probabilities diverge for the reason given in section 4.2, whereas the USC curve shows a behavior quite similar tothat of the exact quantum one. This is a manifestation of the improvement obtained in going to the uniform approximation.

The oscillations in the exact quantum curves are not well reproduced by the semi-classical ones especially for the P_{00}^{V} transition probabilities, as indicated in Figs. 5 and 6. The USC results, however, are in much better average agreement with the exact ones than are the PSC and CSC results. Clearly the attempt by the present semi-classical theory to introduce the quantum effects present in these transitions for this collinear reaction has not succeeded. Apparently such quantum effects are not of a simple interference nature. Indeed, recent life-time calculations done on the same potential energy surface[24] indicate that the marked quantum oscillations

at total energies of 0.90 eV and 1.28 eV are due to the interference of resonant (compound state) and direct parts of the pertinent $\underset{\approx}{S}$ matrix elements. We might say that the present semi-classical theory is aimed at approximating the direct part of the exact $\underset{\approx}{S}$ matrix. If this is the case, an illuminating comparison would be one between the present semi-classical transition probabilities and quantum transition probabilities modified so as to exclude (approximately) the effects of the resonant component of the $\underset{\approx}{S}$ matrix elements. We expect that the result of such a comparison would show better agreement between the USC and such modified quantum transition probabilities. A composite theory including an approximate treatment of the resonant component and a semi-classical treatment of the direct component of the scattering matrix may be expected to yield a significant improvement.

4.3 The Reactive and Non-Reactive 0 → 1 Transitions

The USC threshold energies for the 0 → 1 reactive and non-reactive transition probabilities are about 0.08 eV higher than those for the exact quantum calculations but show a similar steep rise as the energy increases above threshold.

The oscillatory behavior of the exact quantum curves is qualitatively displayed by the USC curves especially for the reactive transition, except at E = 1.28 eV where a sharp resonance occurs. There is much better overall agreement between the USC and exact quantum results than was the case for the 0 → 0 transition.

Whereas for the 0 → 0 transitions, the quasi-classical results were in better agreement with exact quantum one than the USC results (especially for the reactive case), the reverse is true for the 0 → 1 transitions. This

is particularly so in the threshold region, due to the arbitrariness of the quasi-classical definition of the final state quantum number, as mentioned towards the end of section 4. The reverse P_{10}^{R} quasi-classical results do not suffer from this defect, which partially explains the significant improvement in using this quantity as an approximation to the accurate quantum P_{01}^{R}. However, this does not explain why the P_{10}^{R} QC results are better than the P_{01}^{R} ones substantially away from threshold.

5. CONCLUSION

The uniform, primitive, and classical semi-classical reactive and non-reactive $0 \rightarrow 0$ and $0 \rightarrow 1$ transition probabilities for the collinear $H + H_2 \rightarrow H_2 + H$ reaction do not in general agree closely with the exact quantum results. As expected, the USC approximation is better than the PSC and CSC ones. The low energy divergent behavior of the reactive and non-reactive $0 \rightarrow 0$ USC, PSC, and CSC transition probabilities is greatly in error. By contrast, the corresponding quasi-classical trajectory results are generally in much better agreement with the exact quantum ones.

Agreement between the USC and exact quantum results for the $0 \rightarrow 1$ transitions is much better than for the $0 \rightarrow 0$ ones. The $0 \rightarrow 1$ USC threshold energies are about 0.08 eV greater than the correct ones, but as the energy increases above the respective thresholds the USC and exact quantum curves show a similar steep rise. In addition there is qualitative agreement between the USC and exact results. The standard quasi-classical results are in poor agreement with the exact ones and as a result the USC results give substantial improvement over the former ones. However, the reverse

quasi-classical results also give significant improvement over the usual quasi-classical ones and in fact are not much worse than the USC ones.

A possible explanation for the inability of the semi-classical results reported herein to produce the pronounced quantum effects in this reaction lies in the importance of resonant processes for this reaction. These processes were found to be present in the exact quantum results and the present semi-classical theory does not take such phenomena into account.

TABLE I. Action difference Δ and final action number m versus initial phase angle q_0 in vicinity of discontinuities.[a]

q_0	Type of Collision	m	Δ[b, c]	Δ[b, d]
0.07359	Reactive	1.057	-10.88	-20.66
0.07372	Reactive	1.056	-20.68	-20.68
3.15995	Reactive	1.141	-17.52	-17.52
3.16300	Reactive	1.142	- 7.17	-17.49
4.01125	Non-Reactive	0.9012	-15.75	-24.56
4.01251	Non-Reactive	0.8994	-24.58	-24.58
6.21810	Non-Reactive	1.021	-21.26	-21.26
6.23562	Non-Reactive	1.022	-11.69	-21.25

[a] The total energy E is 1.053 eV.

[b] The action difference Δ is in units of $\hbar$.

[c] Δ given by Eq. (3).

[d] Δ given by Eq. (4).

TABLE II. Microscopic Reversibility of Semi-Classical Transition Probabilities

	E = 0.953 eV	E = 1.033 eV
P_{01}^{R} (USC)	0.40	0.37
P_{10}^{R} (USC)	0.41	0.37
P_{01}^{R} (quasi-classical)	0.18	0.21
P_{10}^{R} (quasi-classical)	0.38	0.45
P_{01}^{V} (USC)	0.30	0.19
P_{10}^{V} (USC)	0.31	0.18
P_{01}^{V} (quasi-classical)	0.10	0.17
P_{10}^{V} (quasi-classical)	0.08	0.07

REFERENCES

*This work was supported in part by the United States Atomic Energy Commission, Report Code No. CALT-767P4-125.

**Work performed in partial fulfillment of the requirements for the Ph.D. degree in Chemistry at the California Institute of Technology.

†Contribution No. 4744

[1](a) W.H. Miller, J. Chem. Phys. 53, 1949 (1970); (b) ibid. 53, 3578 (1970); (c) W.H. Miller, Chem. Phys. Letters 7, 431 (1970); (d) W.H. Miller, J. Chem. Phys. 54, 5386 (1971); (e) C.C. Rankin and W.H. Miller, ibid. 55, 3150 (1971); (f) W.H. Miller and T.F. George, ibid. 56, 5668 (1972); (g) ibid. 57, 2458 (1972); (h) J.D. Doll, T.F. George, and W.H. Miller, ibid. 58, 1343 (1973).

[2](a) R.A. Marcus, J. Chem. Phys. 54, 3965 (1971); (b) J.N.L. Connor and R.A. Marcus, ibid. 55, 5636 (1971); (c) W.H. Wong and R.A. Marcus, ibid. 55, 5663 (1971); (d) R.A. Marcus, ibid. 56, 311 (1972); (e) ibid. 56, 3548 (1972); (f) J. Stine and R.A. Marcus, Chem. Phys. Letters 15, 536 (1972).

[3]R.D. Levine and B.R. Johnson, Chem. Phys. Letters 7, 404 (1970).

[4](a) P. Pechukas, Phys. Rev. 181, 174 (1969); (b) P. Pechukas and J.P. Davis, J. Chem. Phys. 56, 4970 (1972).

[5]B.C. Eu, J. Chem. Phys. 57, 2531 (1972).

[6]J.M. Bowman and Aron Kuppermann, Chem. Phys. 1, 000 (1973).

[7]D. Secrest and B.R. Johnson, J. Chem. Phys. 45, 4556 (1966).

[8]D.J. Diestler, J. Chem. Phys. 54, 4547 (1971).

[9]S.-F. Wu and R.D. Levine, Mol. Phys. 22, 881 (1971).

[10]R. N. Porter and M. Karplus, J. Chem. Phys., 40, 1105 (1964).

[11]G. C. Schatz and Aron Kuppermann (private communication) have repeated the exact quantum calculations on the Porter-Karplus surface using a fully converged close coupling method and obtained reaction probabilities in agreement with those of Ref. 8. A comparison between these accurate quantum results and the complex-trajectory semiclassical ones is given in Section 4.1 of the present paper.

[12]D. G. Truhlar and Aron Kuppermann, J. Chem. Phys. 56, 2232 (1972).

[13]G. C. Schatz and Aron Kuppermann, to be published.

[14]J. M. Bowman and Aron Kuppermann, Chem. Phys. Letters, 12, 1 (1972).

[15]F. T. Wall and R. N. Porter, J. Chem. Phys. 36, 3256 (1962).

[16]I. Shavitt, R. M. Stevens, F. L. Minn, and M. Karplus, J. Chem. Phys., 48, 2700 (1968).

[17]J. M. Bowman and Aron Kuppermann, Chem. Phys. Letters, 19, 166 (1973).

[18]H. Goldstein, Classical Mechanics (Addison-Wesley, Reading, Mass., 1950) (a) p. 241; (b) section 9-1.

[19]M. Abramowitz and I. Stegum Eds., Handbook of Mathematical Functions (U.S. Govt. Printing Office, Washington, D.C., 1964), pp 446-452.

[20]B. Carnahan, H. A. Luther, and J. O. Wilkes, Applied Numerical Methods (John Wiley and Sons, New York, 1969), pp. 361,386.

[21]In reference 14 the phrase "we assign to this diatom the quantum number $v = n$ if $E(n) \leq E^{v}_{Cl} < \frac{1}{2}\Delta E(n)$" should have read "we assign to this diatom the quantum number $v = n$ if $E(n) \leq E^{v}_{Cl} < E(n) + \frac{1}{2}\Delta E(n)$."

[22]To show that the semi-classical expressions obey microscopic reversibility it suffices to demonstrate that $\Delta_2-\Delta_1 = \Delta_1-\Delta_2$ and that $|\partial m^\beta/\partial q_0^\alpha|^{-1} = |\partial n^\alpha/\partial q_1^\beta|^{-1}$ (see Eqs. 2, 5, 6 and 7). From Eq. 4 it is clear that upon time-reversal $\Delta_j \rightarrow -\Delta_j$ and hence $\Delta_2-\Delta_1 = \Delta_1-\Delta_2$. It has been shown previously[1a] that the Jacobian factor $|\partial m^\beta/\partial q_0^\alpha|^{-1}$ is equal to $|\partial^2\phi(m^\beta,n^\alpha)/\partial m^\beta \partial n^\alpha|$. The phase function $\phi(m^\beta, n^\alpha)$ can be differentiated with respect to n^α or m^β in either order. This fact coupled with the properties that $|\partial\phi(m^\beta, n^\alpha)/\partial n^\alpha| = q_0^\alpha$ and $|\partial\phi(m^\beta, n^\alpha)/\partial m^\beta| = q_1^\beta$ gives the desired equality between $|\partial m^\beta/\partial q_0^\alpha|^{-1}$ and $|\partial n^\alpha/\partial q_1^\beta|^{-1}$.

[23]K. F. Freed, J. Chem. Phys., 56, 692 (1972).

[24]G. C. Schatz and Aron Kuppermann, J. Chem. Phys. 59, 000 (1973).

FIGURE CAPTIONS

Fig. 1. Corrected (circles; Eq. (4)) and uncorrected (squares; Eq (3)) action Δ as a function of the initial phase angle q_0 for reactive (R) and non-reactive (V) trajectories. The total energy is 1.053 eV. For initial phases for which only circles are indicated, Eqs. (4) and (3) furnish the same value of Δ.

Fig. 2. Reactive (solid curve) and non-reactive (dashed curve) final action number, m, as a function of initial phase angle, q_0. The total energy is 1.253 eV.

Fig. 3. Uniform semi-classical (solid curve), exact quantum (dashed curve), and quasi-classical (dashed-dotted curve) P_{00}^{R} transition probabilities as a function of total energy, E, and initial translational energy, E_0.

Fig. 4. Reactive (solid curve) and non-reactive (dashed-curve) final action number, m, as a function of initial phase angle, q_0. The total energy is 0.558 eV.

Fig. 5. Classical semi-classical (solid curve), primitive semi-classical (dashed-dotted curve), and exact quantum (dashed curve) P_{00}^{R} transition probabilities as a function of total energy, E, and initial translational energy, E_0.

Fig. 6. Uniform semi-classical (solid curve), exact quantum (dashed curve), and quasi-classical (dashed-dotted curve) P_{00}^{V} transition probabilities as a function of total energy, E, and initial translational energy, E_0.

Fig. 7. Classical semi-classical (solid curve), primitive semi-classical (dashed-dotted curve) and exact quantum (dashed curve) P^V_{00} transition probabilities as a function of total energy, E, and initial translational energy, E_0.

Fig. 8. Uniform semi-classical (solid curve), exact quantum (dashed curve), quasi-classical (dashed-dotted curve) P^R_{01} transition probabilities and quasi-classical (dotted curve), P^R_{10} transition probability as a function of total energy E and initial translational energy E_0.

Fig. 9. Uniform semi-classical (solid curve), exact quantum (dashed curve), and quasi-classical (dashed-dotted curve) P^V_{01} transition probabilities as a function of total energy E and initial translational energy E_0.

Fig. 10. Uniform semi-classical (solid curve), exact quantum (dashed curve), and quasi-classical (dashed-dotted curve) total reaction probability P^R_0 as a function of total energy E and initial translational energy E_0.

Fig. 11. Total uniform semi-classical collision probabilities as a function of the total energy, E.

Fig. 12. Ratio of complex-trajectory semi-classical reaction probability P^R_{SC} (taken from Ref. 1g) to exact quantum reaction probability P^R_{QM} (taken from Ref. 11) for very low initial translational energies E_0.

Fig. 13. Ratio of complex-trajectory semi-classical rate constant $k_{SC}(T)$ to exact quantum rate constant $k_{EQ}(T)$ as a function of 1/T (lower abcissa) and T (upper abscissa).

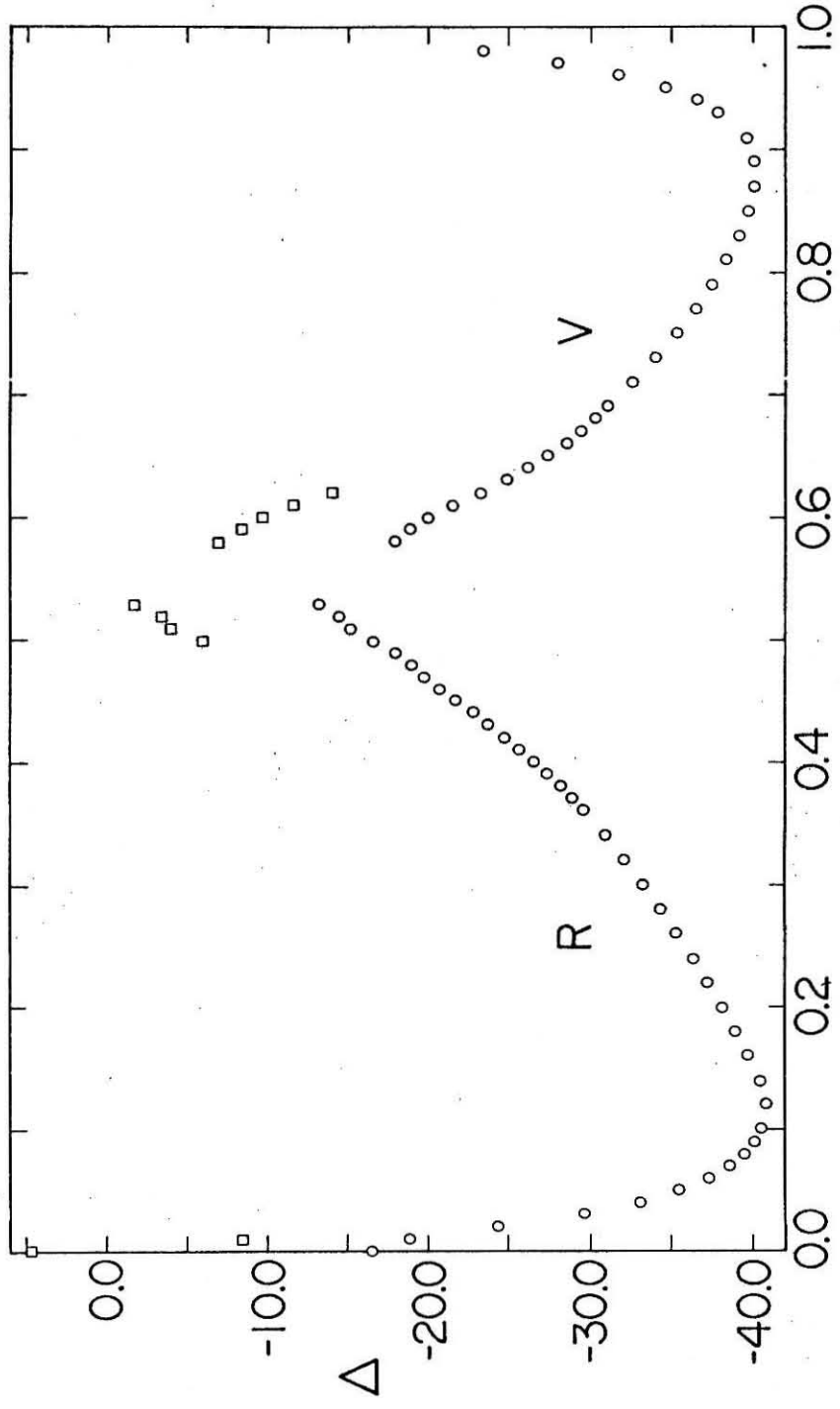

Figure 1

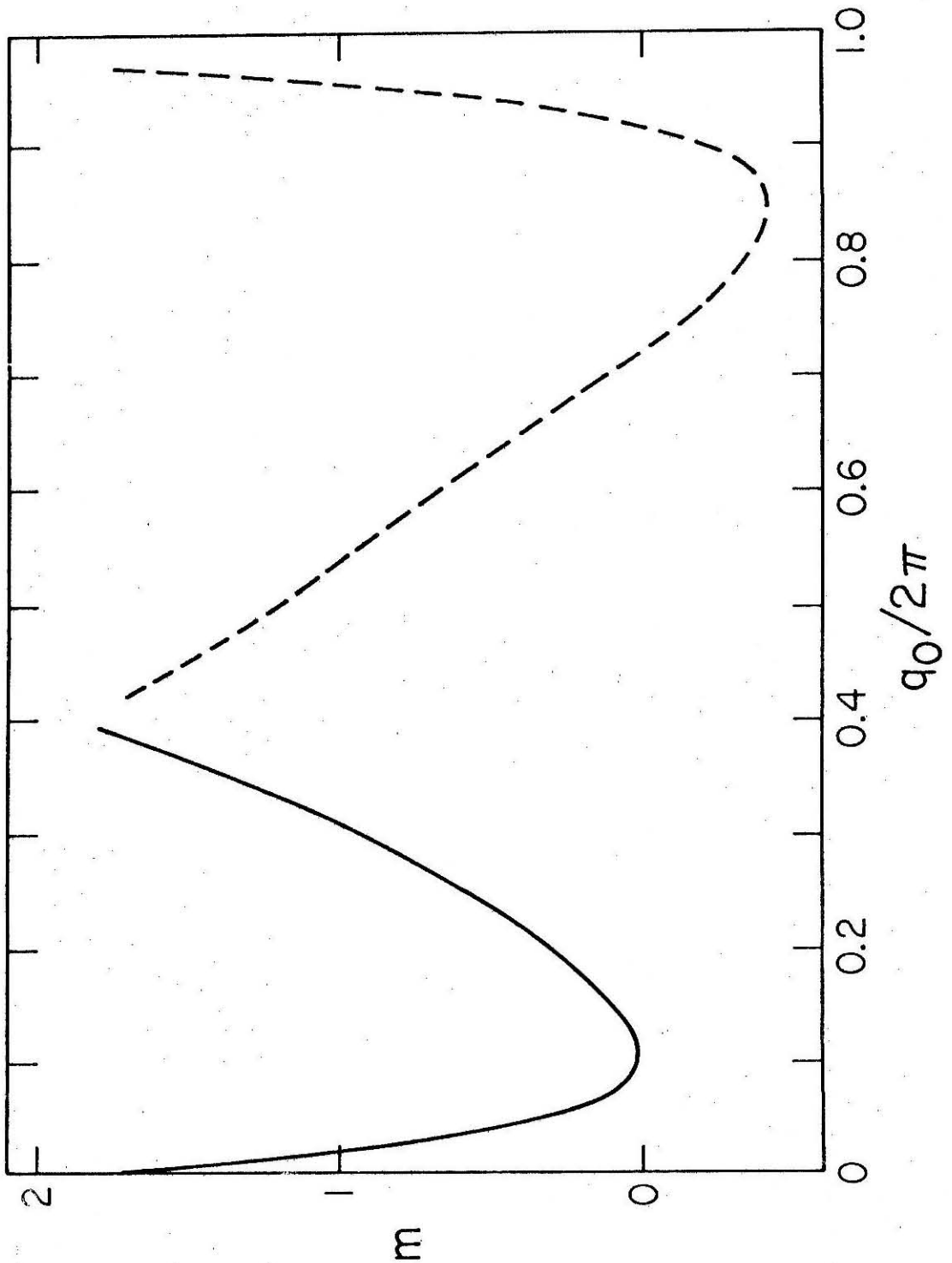

Figure 2

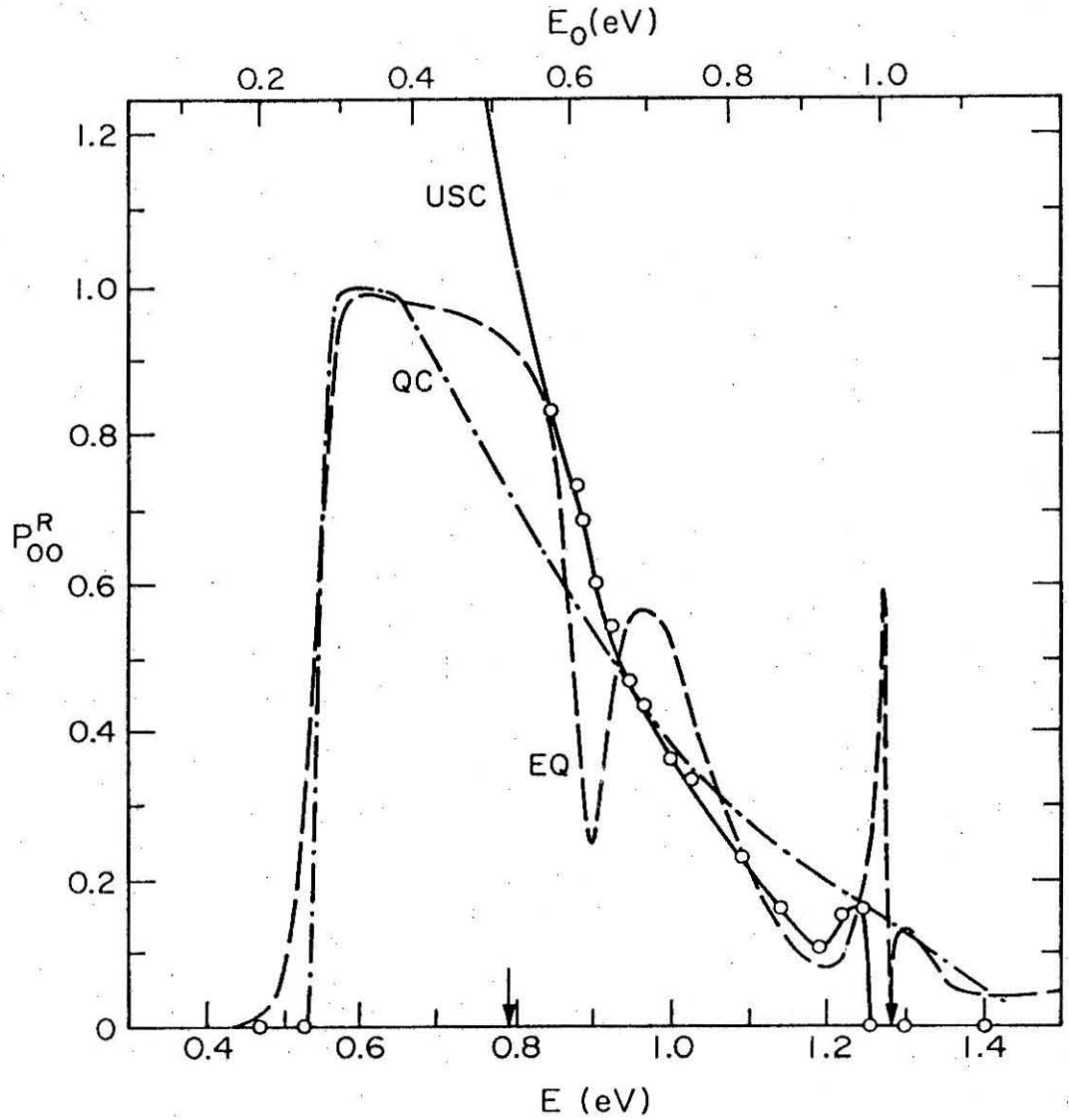
E0(eV)
0.2
0.4
0.6
0.8
1.0
1.2
USC
QC
EQ
P00R
0
0.2
0.4
0.6
0.8
1.0
0.4
0.6
0.8
1.0
1.2
1.4
E (eV)

Figure 3

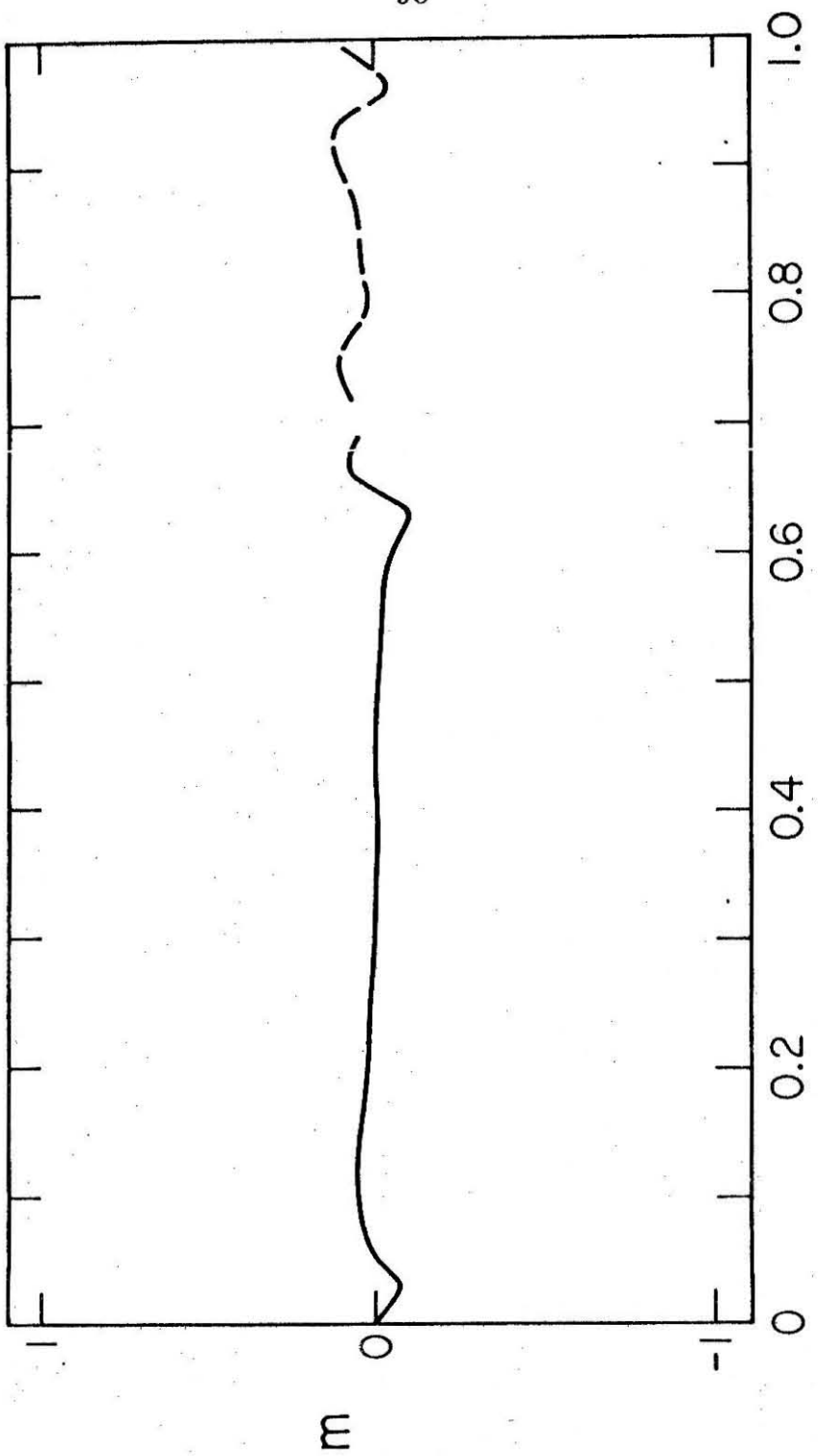

Figure 4

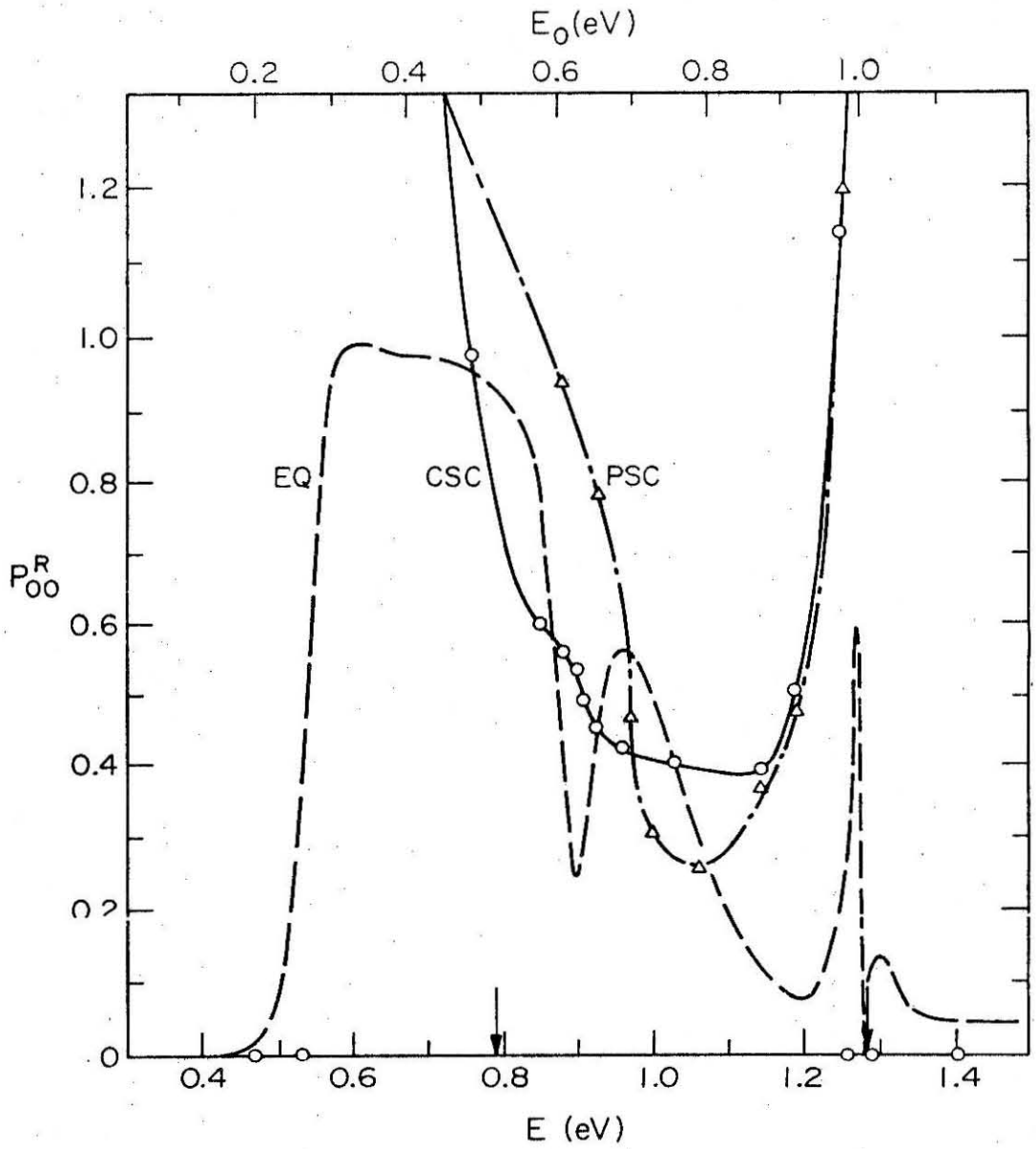
E0(eV)
0.2
0.4
0.6
0.8
1.0
1.2
1.0
0.8
0.6
0.4
0.2
0
EQ
CSC
PSC
P00R
0.4
0.6
0.8
1.0
1.2
1.4
E (eV)

Figure 5

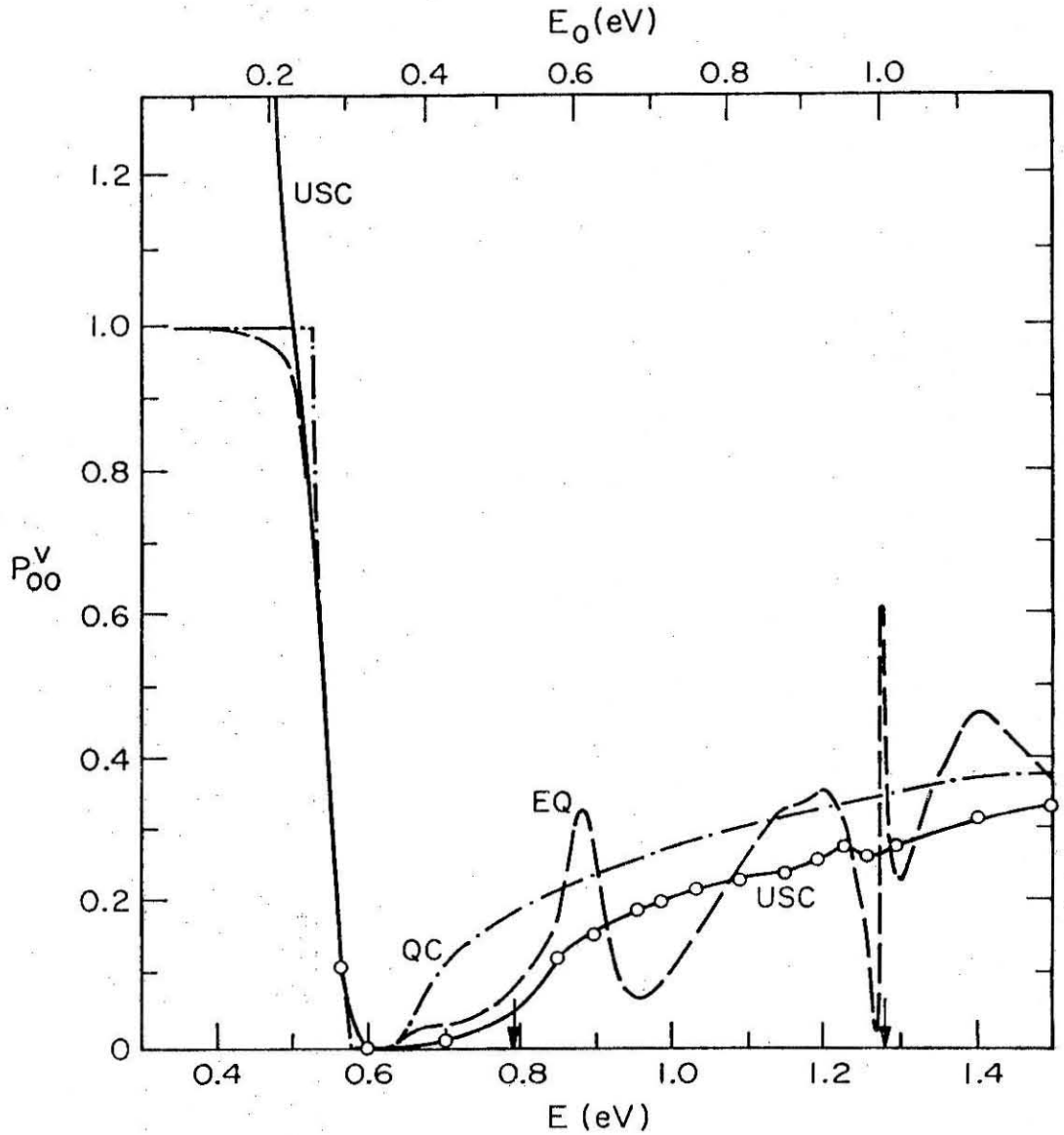
E0(eV)
0.2
0.4
0.6
0.8
1.0
1.2
USC
1.0
0.8
P00V
0.6
0.4
EQ
0.2
QC
USC
0
0.4
0.6
0.8
1.0
1.2
1.4
E (eV)

Figure 6

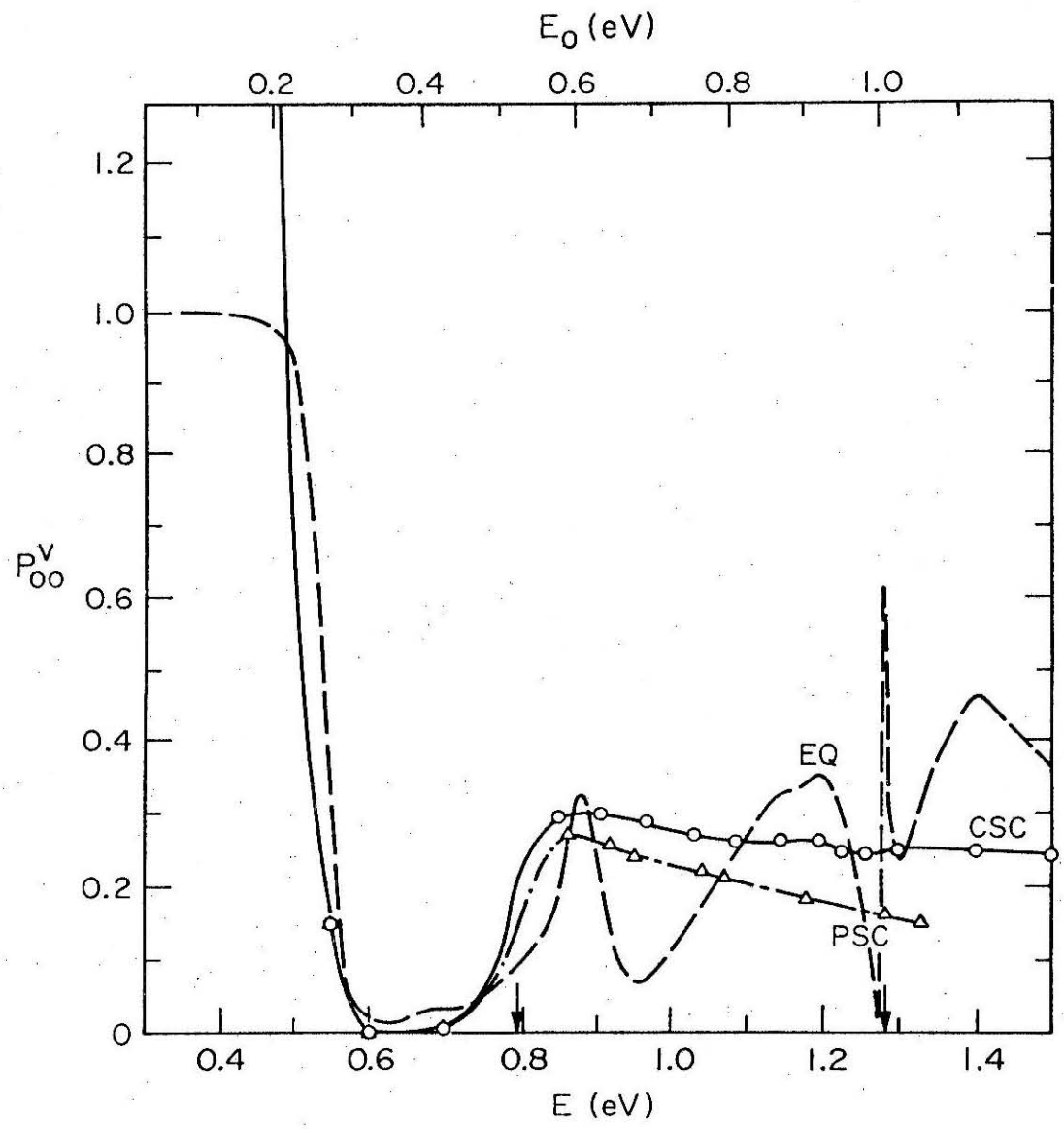
E0 (eV)
0.2
0.4
0.6
0.8
1.0
1.2
1.0
0.8
0.6
0.4
0.2
0
P00V
EQ
CSC
PSC
0.4
0.6
0.8
1.0
1.2
1.4
E (eV)

Figure 7

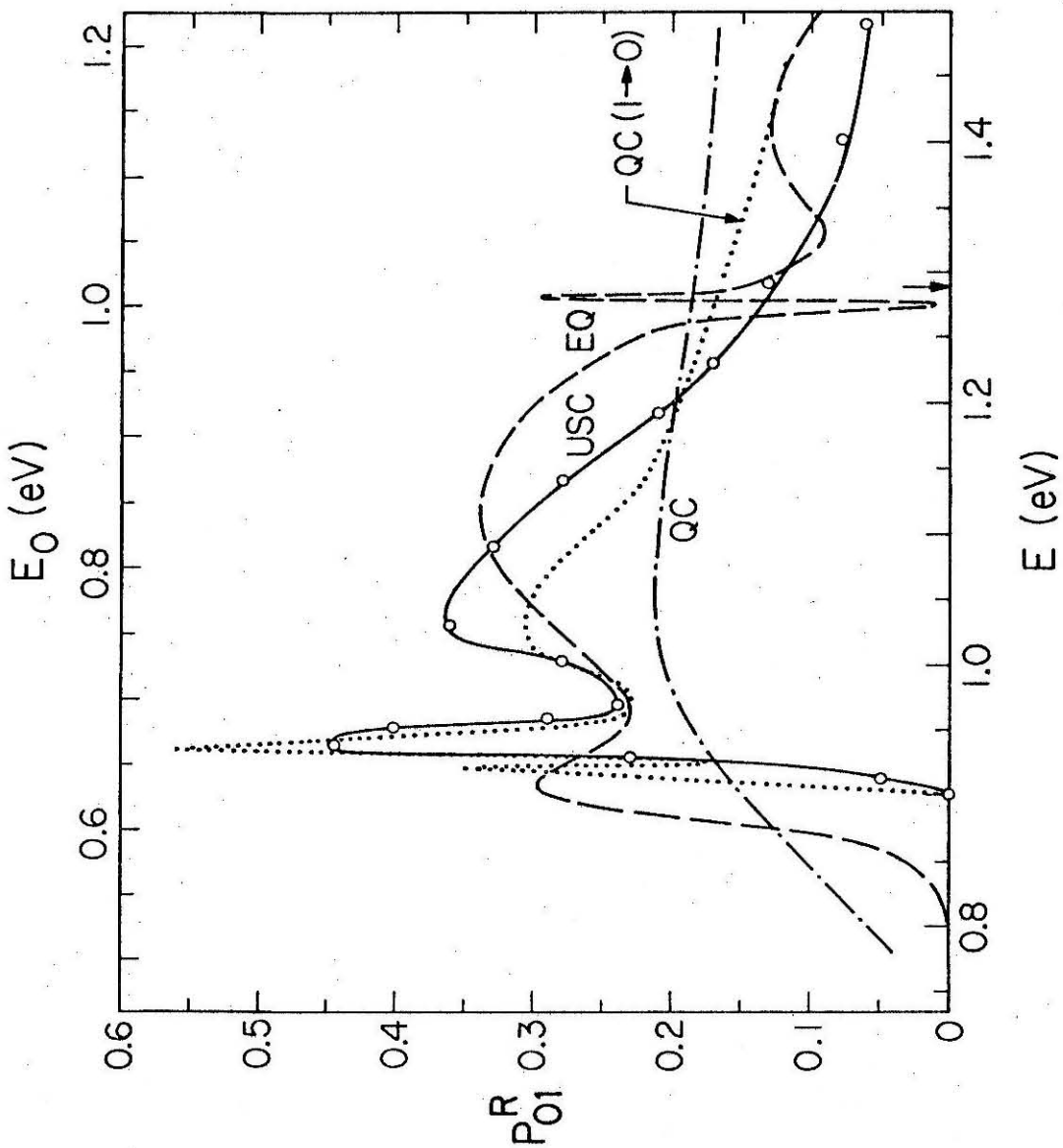
E0 (eV)
1.2
1.0
0.8
0.6
0.6
0.5
0.4
0.3
0.2
0.1
0
P01R
E (eV)
1.4
1.2
1.0
0.8
QC (I→O)
EQ
USC
QC

Figure 8

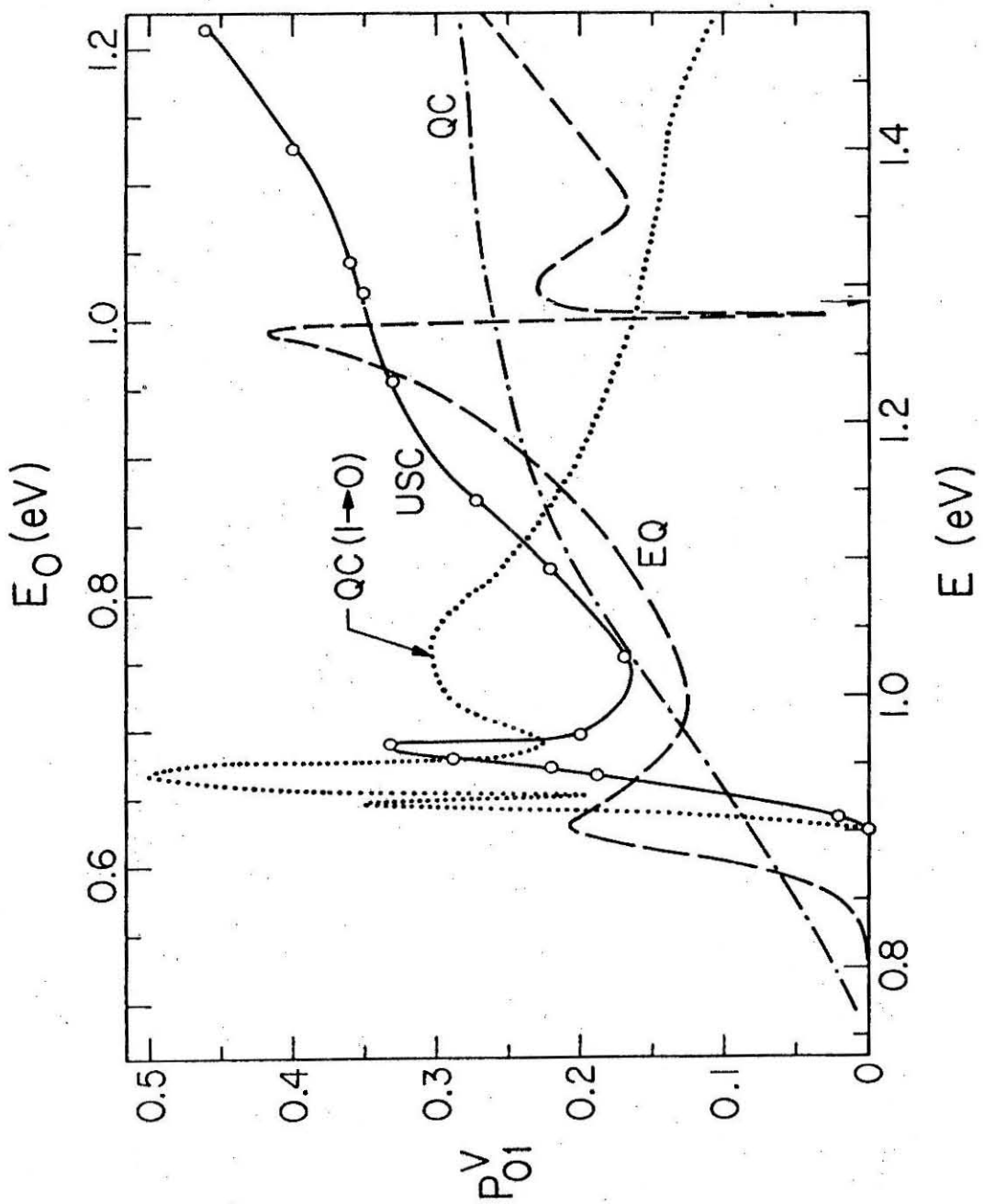

Figure 9

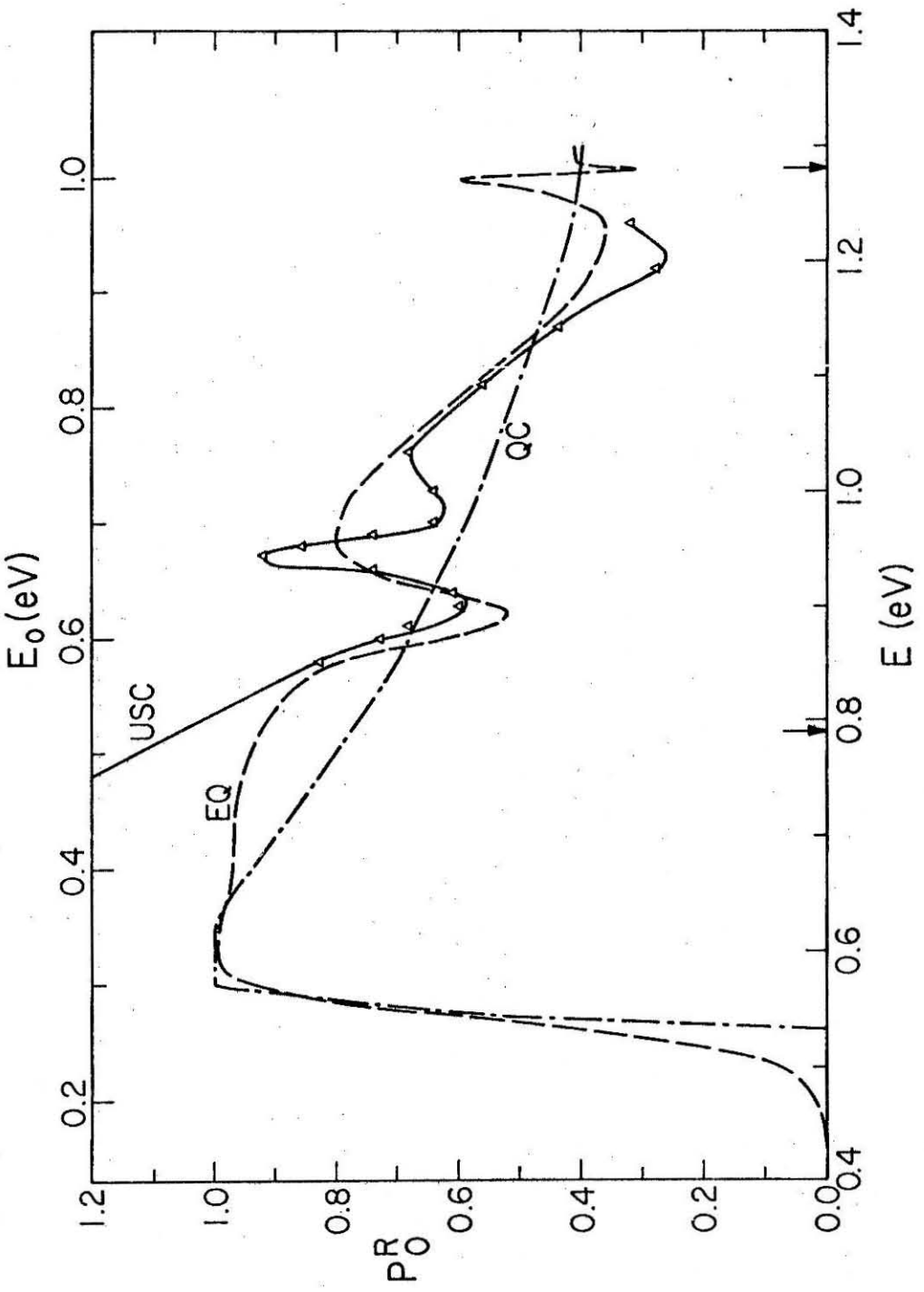

Figure 10

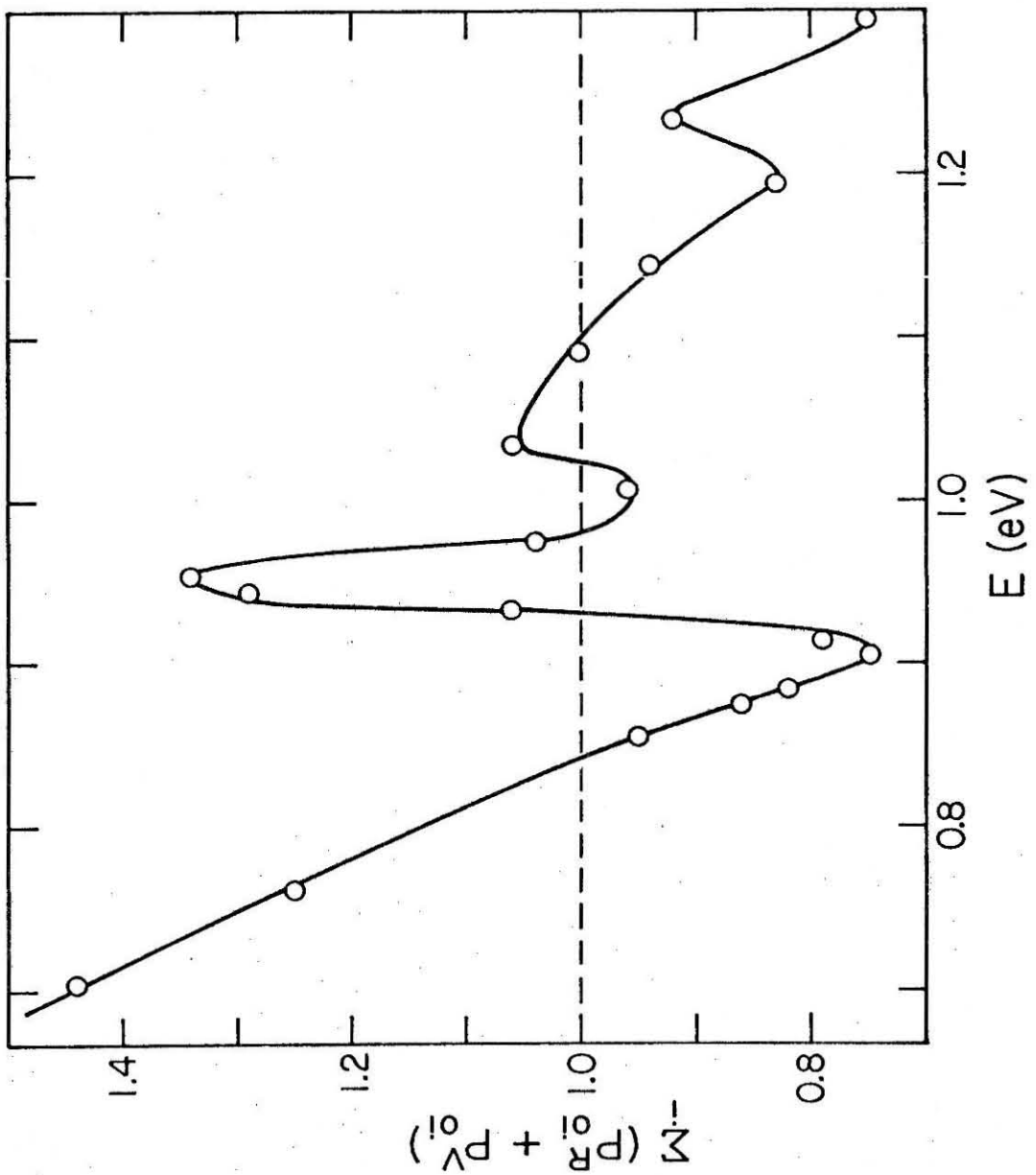

Figure 11

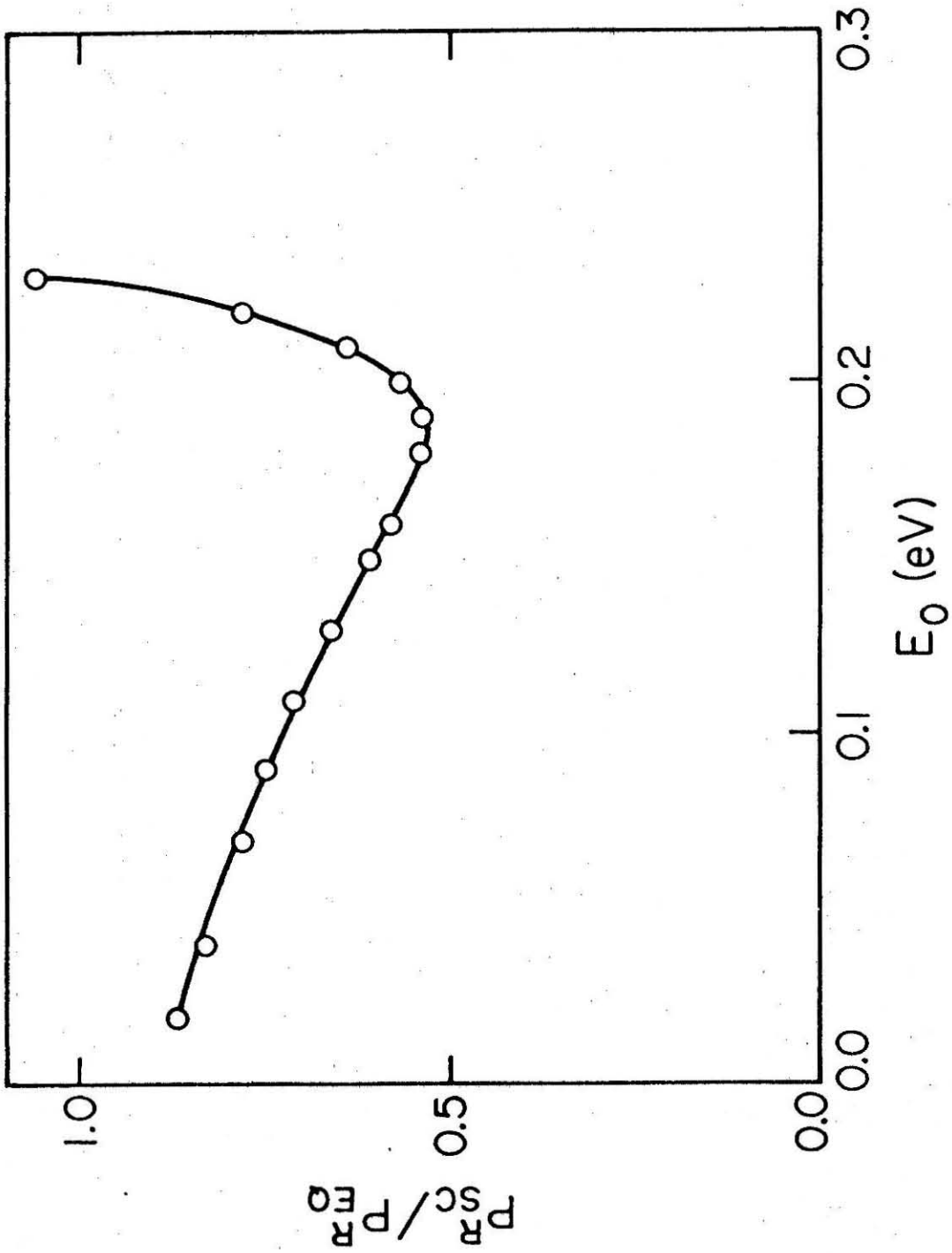

Figure 12

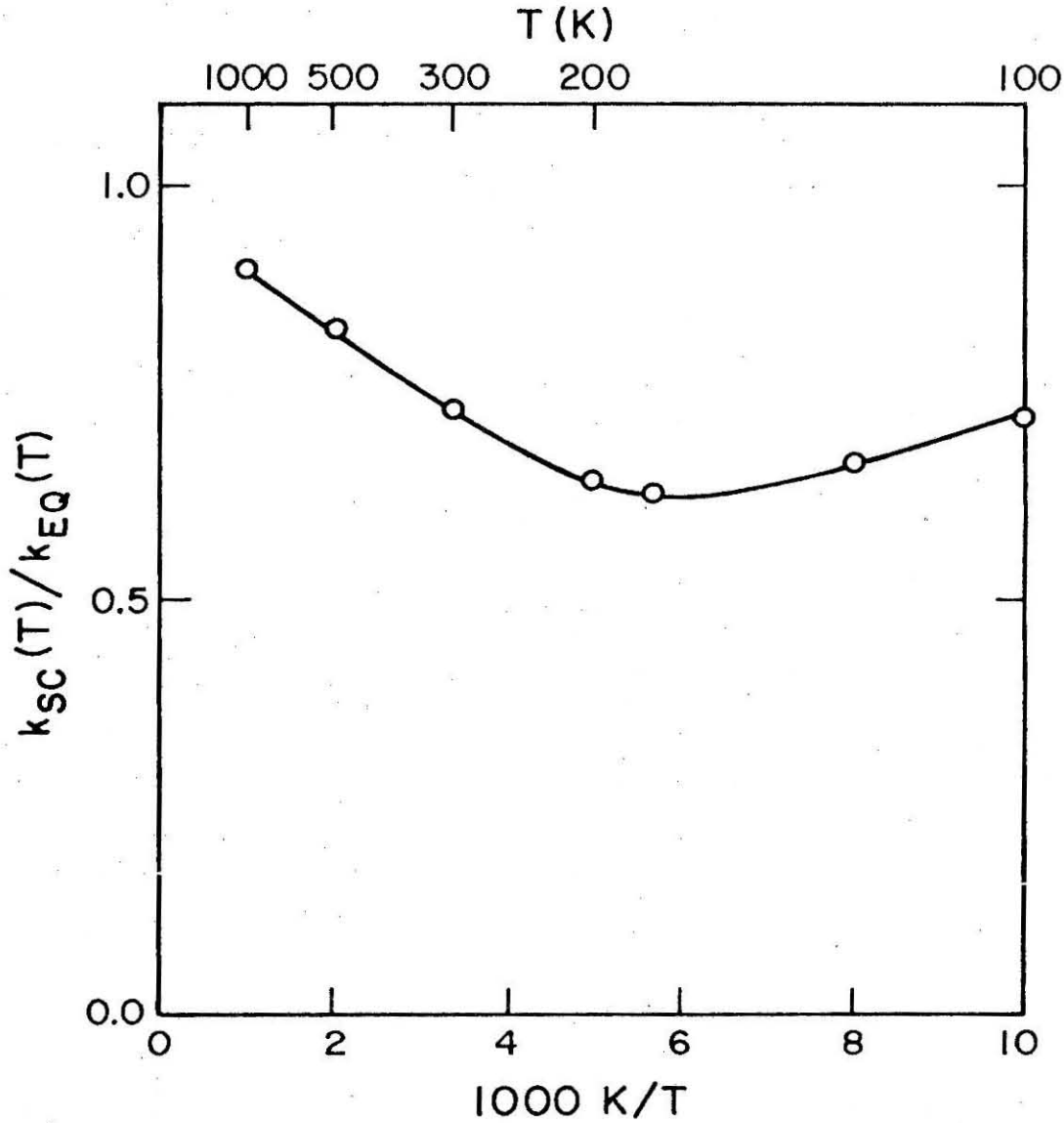

Figure 13

I. 5 COMPARISON OF QUASI-CLASSICAL AND QUANTUM PROBABILITY CURRENT DENSITIES, STREAMLINES, AND CURRENT DENSITY PROFILES FOR THE COLLINEAR $H + H_2$ REACTION.

COMPARISON OF QUASI-CLASSICAL AND QUANTUM PROBABILITY CURRENT DENSITIES, STREAMLINES, AND CURRENT DENSITY PROFILES FOR THE COLLINEAR H + H_2 REACTION.

1. Introduction

Classical and quantal calculations of reactive scattering usually focus on quantities which can (at least in principle) be observed experimentally, e.g. cross-sections, transition rates, branching ratios, rate constants, etc. These are "asymptotic" quantities, that is they are the results of the chemical reaction after it has occurred. The information content of these "asymptotic observables" is only a part of the total information that, in principle, is available. The complete characterization of a chemical reaction, which includes the asymptotic observables as well as information about the transition region, is contained in a classical or quantal calculation of the chemical reaction. However, only a small number of such calculations has made use of all of the available information. Mortensen and Pitzer[1] in their classic paper on the collinear H + H_2 reaction presented figures of the probability density obtained from the wavefunction describing the reaction at the total energy of 10 kcal/mole. Dion et al.[2] in a model collinear quantum calculation computed the probability density and the current density for the reaction at one energy. In a time-dependent treatment of the collinear H + H_2 reaction, McCullough and Wyatt[3] presented classical and quantal time-dependent probability densities and current densities at several values of the time variable for one energy.

In that study, the classical calculation was very different from the one we shall describe below. There a quantal wavepacket was integrated in time using the classical equations of motion. Although such a hybrid classical-quantum technique may yield interesting results, it is of questionable validity.[4]

In the study reported here, we compare time-independent quantal[5] and quasi-classical current densities, streamlines, and current density profiles for the collinear $H + H_2$ reaction with reagent H_2 initially in the ground vibrational state. The quantum reaction probabilities have been reported previously[6] as has a comparison with quasi-classical calculations.[7] The potential energy surface employed in all the classical and quantum calculations is a Wall-Porter[8] fit to the scaled SSMK surface[9] and is described elsewhere.[6]

2. Classical and Quantum Probability Current Densities

The generation of the quantum probability current density, $\underset{\sim}{j}$, follows directly from the wavefunction, ψ, according to the well-known expression,[10]

$$\underset{\sim}{j} = \frac{\hbar}{2mi} \left[\psi^* \underset{\sim}{\nabla} \psi - \psi (\underset{\sim}{\nabla} \psi)^* \right] .$$

However, the expression for the classical probability current density is not well known. Therefore, we shall develop the appropriate expression for the classical probability current density.

Let x_2 and x_3 be coordinates defined as follows:

$$x_2 = r_{BC} \quad ; \quad x_3 = \left(\frac{\mu_{A,BC}}{\mu_{BC}}\right)^{\frac{1}{2}} \left[r_{AB} + \frac{m_B}{m_B + m_C} \, r_{BC} \right], \quad (1)$$

where r_{BC} and r_{AB} are the internuclear distances of the A + BC collinear configuration. In terms of the coordinates x_2 and x_3 and their conjugate momenta, the classical Hamiltonian of the A + BC system is given by

$$H = \frac{P_{x_2}^2 + P_{x_3}^2}{2\mu_{BC}} + V(x_2, x_3) \, . \quad (2)$$

The reduced masses, μ_{BC} and $\mu_{A,BC}$, are the usual ones, namely

$$\mu_{BC} = \frac{m_B m_C}{m_B + m_C} \quad ; \quad \mu_{A,BC} = \frac{m_A(m_B + m_C)}{m_A + m_B + m_C} \, .$$

V is the Born-Oppenheimer potential energy function which describes the classical and quantum motion of the A + BC system. The choice of coordinates given by eq. (1) was made so that the Hamiltonian (eq. (2)) would involve a single mass. Hence, we can describe the A + BC motion by a single mass point (of mass μ_{BC}). This is important in the concept of the probability current density which by definition describes the motion of a single mass point in configuration space.

Suppose that the entire configuration space encompassing the A + BC reaction zone is specified by dimensions

$$x_{2o} \leq x_2 \leq x_{2f} \quad ; \quad x_{3o} \leq x_3 \leq x_{3f} \, . \quad (3)$$

(These dimensions define the area over which the interaction potential, $V_I \equiv V(x_2, x_3) - V(x_2, \infty) = V(x_2, x_3) - V(\infty, x_3)$, is not vanishingly small.)

In the ensemble-averaged sense (to be described in detail below) let $\rho(x_2, x_3)$ be the probability density of finding the mass point in the interval x_2 to $x_2 + dx_2$ and x_3 to $x_3 + dx_3$, where x_2 and x_3 are restricted according to eq. (3). We now introduce a time-independent, ensemble-averaged, velocity vector written symbolically as

$$\underset{\sim}{v}(x_2, x_3) \equiv v_{x_2}(x_2, x_3)\,\hat{x}_2 + v_{x_3}(x_2, x_3)\,\hat{x}_3 \quad , \tag{4}$$

where $\hat{x}_2$ and $\hat{x}_3$ are two unit vectors which span the configuration space. Then, in terms of ρ and $\underset{\sim}{v}$, the classical probability current density vector is defined as

$$\underset{\sim}{j}(x_2, x_3) = \rho(x_2, x_3)\,\underset{\sim}{v}(x_2, x_3) \quad . \tag{5}$$

As an example of the utility and meaning of eq. (5) consider the motion of an A + BC system governed by a zero interaction potential. In this case $V(x_2, x_3)$ can be written as

$$V(x_2, x_3) = V^0(x_2), \tag{6}$$

where $V^0(x_2)$ is the diatom potential function describing the internal motion of AB. $V^0(x_2)$ can be a harmonic potential or the Morse potential, for example. As a consequence of eq. (6) the x_2 and x_3 motions are uncoupled and we have that

$$\rho(x_2, x_3) = \rho^0(x_2)\,\rho^I(x_3), \tag{7a}$$

and

$$v_{x_2} = v_{x_2}(x_2) \quad ; \quad v_{x_3} = v_{x_3}(x_3) \quad . \tag{7b}$$

Since the x_3 motion is "free," i.e. it is subject to zero force, the

probability of finding the coordinate x_3 with some particular value must be a constant independent of x_3. Hence eq. (7a) can be written as

$$\rho(x_2, x_3) = \rho^0(x_2) \quad . \tag{8}$$

The density $\rho^0(x_2)$ describes the distribution of values of x_2 of a harmonic, Morse, etc. oscillator. Thus, from eqs. (5), (7), and (8) for this example,

$$\underset{\sim}{j} = \rho^0(x_2)\, \nu_{x_2}(x_2)\, \hat{x}_2 + \rho^0(x_2)\, \nu_{x_3}(x_3)\, \hat{x}_3 , \tag{9a}$$

$$= j_{x_2} \hat{x}_2 + j_{x_3} \hat{x}_3 \quad . \tag{9b}$$

Let us now examine the components of $\underset{\sim}{j}$, j_{x_2} and j_{x_3}, separately. First, we demonstrate that j_{x_2} is identically zero. To do this we stress that the distribution function $\rho^0(x_2)$ is a non-negative function (single-valued of course) of x_2 only. Thus, the scalar function $\nu_2(x_2)$ must be identically zero if the assertion that j_{x_2} is zero is correct. That $\nu_{x_2}(x_2)$ is zero is trivially true if the definition of ν_{x_2} is made clear. For the internal motion of molecule AB an ensemble of classical trajectories (at a given total energy) can be generated as follows. The range of classically allowed coordinates is sampled according to the distribution function $\rho^0(x_2)$. Then the magnitude of the momentum, P_{x_2}, is determined by the energy equation and its sign is chosen to be plus or minus. With x_2 and P_{x_2} so determined the classical trajectory is uniquely specified. In this way an ensemble of classical trajectories (for the isolated AB molecule) is generated. In scanning the set of

initial conditions it is clear that P_{X_2} and hence ψ_{X_2} is a double-valued function of x_2. That is, for each value of x_2 there exists two values of $P_{X_2}(\psi_{X_2})$, namely $P_{X_2}(\psi_{X_2})$ and $-P_{X_2}(\psi_{X_2})$. Furthermore, it must be true that at any and all times the ensemble of classical trajectories produces a distribution of coordinates identical to the initial one.[4] This is due to the periodic motion of the AB molecule. Thus, the ensemble-averaged value of $\psi_{X_2}(x_2)$ will be the same as it was initially. (This is of course implied by the fact that ψ_{X_2} is time-independent.) We have already seen that at a given value of x_2, ψ_{X_2} takes on two values, ψ_{X_2} and $-\psi_{X_2}$. Hence, their average is identically zero; true for all x_2. Thus, we have demonstrated that j_{X_2} is identically zero and hence

$$\underset{\sim}{j}(x_2, x_3) = j_{X_3}\hat{x}_3 \quad . \tag{10}$$

Finally, since $\psi_{X_3}(x_3)$ is a constant (due to the force free motion of the x_3 coordinate) we have the following simple expression for the classical probability current density:

$$\underset{\sim}{j}(x_2, x_3) = \rho^0(x_2)\psi_{X_3}\hat{x}_3 \quad . \tag{11}$$

Several interesting things are to be noted about eq. (11). First it indicates that the bound motion of the AB molecule contributes no vector component to the total current density. This is in complete agreement with the general rigorous quantum result. Second, the form of eq. (11) is identical to the quantum result, if the classical probability density function, $\rho^0(x_2)$, is replaced by the corresponding quantum probability density function. Third, the probability current density

given by eq. (11) obeys a conservation principle. Stated briefly the conservation principle requires that the following be true for the classical and quantum probability current densities. For any closed contour, C, which encircles the reaction zone, $\underset{\sim}{j}$ must satisfy the following expression:[5]

$$\oint_C \underset{\sim}{j}(x_2, x_3) \cdot d\underset{\sim}{\ell} \equiv 0 \quad . \tag{12}$$

It is straightforward to show that for chemical reactions for which the break-up channel is energetically closed, eq. (12) implies, for a certain class of lines (examples of such lines will be given in Section 4), the quantity

$$\int \underset{\sim}{j}(x_2, x_3) \cdot \hat{n} d\ell \tag{13}$$

is a constant, independent of the particular line.[5] Furthermore, the quantity given by (13) is proportional to the total reaction probability.[5] If the expression for $\underset{\sim}{j}$ given by eq. (11) is substituted into (13) it is easily shown that the result is indeed a constant, equal to v_{x_3}, for any line (satisfying a criterion to be specified in Section 4).

In summary, we have shown, somewhat sketchily, that our definition of the classical probability current density (given by eq. (5)) makes physical sense and obeys a conservation theorem for the example of an A + BC collision with no interaction. We shall use the fact that the classical probability current density for a chemical reaction obeys the same conservation condition, expressed by eq. (12), to check the accuracy of our numerical results given in Section 4.

3. Numerical Methods and Convergence Tests

The calculation of the quantum current density is described in detail elsewhere.[5] The calculation of the classical probability current density, according to eq. (5), requires the computation of the classical probability density, ρ, and the ensemble-averaged velocity vector, $\underset{\sim}{v}$. The methods used to calculate these quantities and some convergence tests of the results are given below.

The region of (x_2, x_3) space of interest is given by eq. (3). In our calculations

$$x_{3f} = 5.456 \text{ bohr}; \; x_{30} = 0.0 \text{ bohr},$$
$$x_{2f} = 4.2 \text{ bohr}; \; x_{20} = 0.0 \text{ bohr} \quad .$$

This region of configuration space is divided into a grid of n rectangles (n is typically 55), each with dimensions

$$\Delta x_3 = (x_{3f} - x_{30})/n; \quad \Delta x_2 = (x_{2f} - x_{20})/n \quad .$$

The calculation of ρ and $\underset{\sim}{v}$ at the center coordinates of each rectangle is performed as follows. An ensemble of classical trajectories (consisting of typically 500 trajectories) is generated by sampling the complete set of initial conditions for a chemical reaction (cf. reference 4). A large number of points, N, in the (x_2, x_3) configuration space is thereby generated with the time step Δt a constant. Typically, $N \approx 10^5$. A trajectory is "followed" as long as it remains within the boundaries of the region of configuration space defined by eq. (3). Thus, for the jth rectangle, with center coordinates (x_{3j}, x_{2j}), $\rho(x_{3j}, x_{2j})$ is given by

$$\rho(x_{3j}, x_{2j}) = N_j/N \quad , \tag{14}$$

where N_j is the number of points located within the jth rectangle. Associated with each of the N_j points is a velocity vector $\underset{\sim}{v}_{ji}$ with components $v_{x_{2ji}}$ and $v_{x_{3ji}}$. The ensemble-averaged velocity at coordinates (x_{2j}, x_{3j}) is given by

$$v_{x_2}(x_{3j}, x_{2j}) = \frac{1}{N_j} \sum_{i=1}^{N_j} v_{x_{2ji}} \quad , \tag{15a}$$

$$v_{x_3}(x_{3j}, x_{2j}) = \frac{1}{N_j} \sum_{i=1}^{N_j} v_{x_{3ji}} \quad , \tag{15b}$$

and

$$\underset{\sim}{v}(x_{3j}, x_{2j}) = v_{x_2}(x_{3j}, x_{2j})\hat{x}_2 + v_{x_3}(x_{3j}, x_{2j})\hat{x}_3 \quad . \tag{16}$$

Thus from eq. (5) the classical probability current density is given by

$$\underset{\sim}{j}(x_{3j}, x_{2j}) = \rho(x_{3j}, x_{2j})\underset{\sim}{v}(x_{3j}, x_{2j}),$$

where ρ and $\underset{\sim}{v}$ are given by eqs. (14) and (16) respectively.

In order to achieve an accurate, converged result for $\underset{\sim}{j}$ two limits must be approached. First, the grid dimensionality, $n \times n$, must be made quite large (in principle it must be $\infty \times \infty$ to yield exact results). However, that is obviously not sufficient to give a converged $\underset{\sim}{j}$. In order to get accurate results the number of classical trajectories must increase concomitantly with the increase in dimensions of the grid. In our calculations a finite grid was used, of course, and the number of trajectories performed yielded a probability current density which had converged to within 10% or better.

Clearly, a coarse grid requires fewer trajectories to reach a 10% level of convergence. However, coarse grids tend to average results more and interesting details in the actual $\underset{\sim}{j}$ (which we are approximating) become "washed out."

In Table 1 we give some indication of the nature of the convergence properties for the probability density $\rho(x_2, x_3)$ for batches of 100, 200, and 300 trajectories for an initial translational energy E_0 of 0.28 eV. It is seen that with 300 trajectories ρ changes by 10% or less of the ρ calculated with 200 trajectories. The grid dimensions, 30×30, are somewhat coarse, however.

A study of the convergence of ρ for three grids, 20×20, 40×40, and 80×80 is made in Table 2 at $E_0 = 0.28$ eV. As expected the coarsest grid, the 20×20 one, shows the best convergence followed by the 40×40 and the 80×80 grids.

The convergence of the current density at $E_0 = 0.28$ eV is investigated in Table 3 for a 30×30 grid and with ensembles consisting of 200 and 300 trajectories. As can be seen the results change by 10% or less in going from 200 to 300 trajectories.

Thus, the convergence studies given above indicate that 300 trajectories should yield probability current densities and probability densities which are converged to within 10% of the the accurate result for 30×30 and 40×40 grids (corresponding to $\Delta x_3 \approx 0.1 - 0.2$ bohr and $\Delta x_2 \approx 0.05 - 0.1$ bohr). In Section 4 where the results are presented, we will comment on the extent of the averaging out of the details of the classical probability current density.

For most of the calculations reported in the next section 300 - 500 classical trajectories were performed in calculating the classical probability current density, and grid dimensions were either 40×40 or 55×55. Also, a simple five-point bivariate interpolation scheme was devised in order to generate the classical current density for all values of x_2 and x_3. A description of this scheme is given below.

Let $j_{X_2}(j_{X_3})$ evaluated at the five points depicted below be denoted by $j_{X_2-1,0}$, $j_{X_20,-1}$, $j_{X_20,1}$, $j_{X_21,0}$, and $j_{X_20,0}$, and let h and k be the separation distances as indicated. Then $j_{X_2}(x_0 + ph, y_0 + qk)$, where

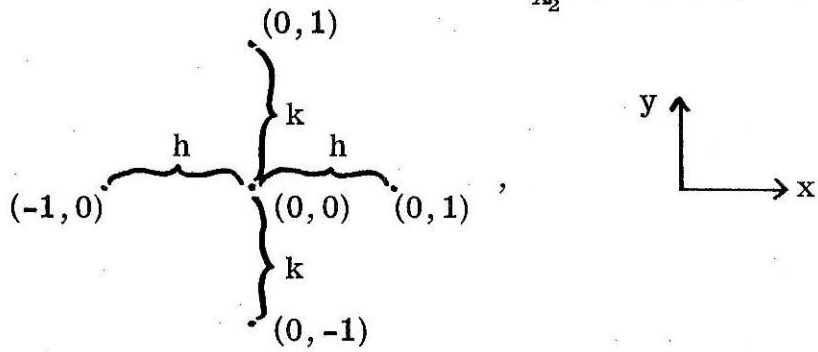

p and q have values between 1 and -1, is given by

$$j_{X_2}(x_0 + ph, y_0 + qk) = (1-p)(1-q)(1+p)(1+q)j_{X_20,0} + \frac{p(1-q)(1+p)(1+q)}{2} j_{X_21,0}$$
$$+ \frac{q(1-p)(1+p)(1+q)}{2} j_{X_20,1} - \frac{(1-q)(1+q)(1-p)p}{2} j_{X_2-1,0}$$
$$- \frac{(1+p)(1-p)(1-q)q}{2} j_{X_20,-1} .$$

In our calculations, the components of $j(x_2, x_3)$ were interpolated directly from the components determined at the appropriate five sets of center coordinates.

4. Results and Discussion

There are, in addition to probability current densities, two other quantities which we have calculated and which yield some insight into the details of chemical reaction. They are streamlines and current density profiles. Both quantities are derivable from the probability current density. Streamlines, which are used in studies of fluid flow are defined as lines which are tangent to the direction of the fluid current density vector.[11] They are useful in visualization of the "flow" of the system. A detailed discussion of the relationship of streamlines to the probability current density vector will be given elsewhere.[5] The second quantity, current density profiles, are defined by the expression below. For a given line ℓ in (x_2, x_3) space, the current density profile, J_n, along the line is given by

$$J_n = \hat{n} \cdot \underset{\sim}{j}(x_2, x_3) \quad . \tag{17}$$

The unit vector n is normal to line ℓ and is oriented to the left of the line. A plot of J along a series of lines can reveal a great deal of information about the distribution of the probability current density vector field. In addition if the end points of the line are deeply embedded in classically forbidden regions of space then the total flux, $\mathcal{J}$, given by

$$\mathcal{J} = \int_{\ell} d\ell \, J_n \tag{18}$$

is a constant, independent of the location of the line. This is a consequence of the statement that probability (or fluid) is neither created nor

destroyed in the chemical reaction. The nature of these lines is made clear in the figures.

Calculations of classical probability current densities, streamlines, and current density profiles have been performed at total energies, E, of 0.5719 eV, 0.62 eV, 0.7540 eV, and 0.8978 eV. Classical current density profiles for the total energy of 1.0331 eV have also been calculated. The results are shown in a series of figures with the corresponding quantum results displayed for comparison.

In Figures 1a and 1b are exhibited the classical and quantum probability current densities respectively, for E = 0.5719 eV. Also, shown are some H_3 potential energy contours. In contrast to the smooth quantum result, the classical result is oscillatory and turbulent. Especially striking in the classical result is the "pinching" of the classical $\underset{\sim}{j}$ in the region near the saddle point (denoted by the plus sign in the Figures). At this energy the classical and quantum reaction probabilities are 1.0 and 0.94 respectively. The contour lines labeled E are the boundaries defining the classically allowed region of configuration space. As can be seen the classical results do remain confined to this area as they should. However, the quantum results are not restricted to this classically allowed region of space, and indeed a significant amount of tunneling is present where the quantum $\underset{\sim}{j}$ is "cutting the corner." A detailed discussion of this type of quantum tunneling is presented elsewhere.[5] In Figures 2a and 2b the corresponding classical and quantum streamlines are displayed. Very similar information about the classical and quantum flow as seen in

Figure 1 is seen here. The classical and quantum current density profiles are given respectively in Figures 3a and 3b for five lines which are normal to the minimum energy path. Here the great contrast in the shapes of the classical and quantum profiles indicates that different regions of configuration space are sampled by the two sets of results.

In Figures 4a and 4b the classical and quantum probability current densities are given, respectively, for E = 0.62 eV. At this energy the classical and quantum reaction probabilities are both unity. The "pinching" in the classical result is still present and, as in the E = 0.5719 eV result, the "flow" rate through this region of pinching is high, as evidenced by the length of the classical probability current density vectors. This is a consequence of the conservation principle given by expression (18). The same features are also seen in Figures 5a and 5b. The differences in the classical and quantum results at E = 0.62 eV are striking, and perhaps somewhat surprising since both calculations give a unit reaction probability. This means that the areas under all of the classical and quantum current density profiles, given in Figures 6a and 6b respectively, are the same. Yet, as seen from those figures, the distribution of the current density profiles are very different.

Focussing on Figure 6a, the classical current density profile along the line x_3 = 5.46 bohr is seen to have a shape very similar to the classical probability distribution function for a harmonic oscillator.[12] Indeed it should (or more precisely it should for a Morse oscillator),

since for unit reaction probability the current density in the reagent asymptotic region (x_3 = 5.46 bohr is in this region) is given rigorously by eq. (11). Furthermore, the "sharpness" of the numerical result gives an indication that the grid we have used in these calculations (55 × 55) is not "washing" out important details of the classical current density.

For E = 0.7540 eV the classical and quantum probability current densities are given in Figures 7a and 7b respectively. As previously (cf. Figures 1a and 4a) the classical result exhibits a pinching effect, however, it is seen to occur in the product side of the saddle point. This contrasts with the classical result at E = 0.5719 eV where the effect occurs in the reagent side of the saddle point. At E = 0.62 eV the classical pinching occurs essentially at the saddle point (displaced somewhat towards the plateau region).

The corresponding classical and quantum streamlines are given in Figures 8a and 8b respectively. There the oscillatory structure of the classical "flow" is clearly seen. The structure in the reagent channel is due to inelastic scattering which, of course, changes the vibrational energy of reagent H_2 by a continuous amount. No such inelastic scattering is possible in the quantum case since the v = 1 state of H_2 is not energetically accessible for E less than 0.7945 eV.

The classical and quantum current density profiles, given in Figures 9a and 9b respectively, show structure which becomes much more pronounced at higher energies. The classical results for the lines passing through and in the reagent side of the saddle point reveal

that some normal components of the probability current density point toward the regeant arrangement channel. This phenomenon is an indication of vortices in the probability current density. This behavior is also seen (though greatly attenuated) in the quantum result given in Figure 9b for the profile along the line passing through the saddle point.

In Figures 10 - 12 classical and quantum probability current densities, streamlines, and current density profiles are given for $E = 0.8978$ eV. At this energy vibrational excitation of reagent and product H_2 is possible. For this reason, apparently, the classical and quantum probability current densities show some similarities, as can be seen in Figures 10a, 10b and especially well in 11a and 11b. In Figure 10a a vortex in the classical probability current density has been included. This vortex is not accessible to any current density vector (or streamline) which originates in the asymptotic region of configuration space. That this vortex is present in the classical result can be deduced from Figure 12a. There it is seen that the current density profile along the line passing through the saddle point reveals a circulation of the probability current density vector field. Also, we note the similarity in the quasi-classical and quantum current density profiles given in Figures 12a and 12b especially for those lines in the product channel. The changing position of the peaks of the classical and quantum profiles suggests that the probability flow is "sloshing" through the product arrangement channel.

Classical and quantum current density profiles are presented in Figures 13a and 13b, respectively, for $E = 1.0331$ eV. As can be

seen from these figures vortices are present in both the classical and quantum results. As previously found for E = 0.8978 eV, the classical and quantum results show similarities for the lines which pass through and toward the product side of the saddle point. Of particular interest are the results for the line passing through the saddle point. In sharp contrast to the quantum and classical results at low energies, e.g., E = 0.5719 eV and E = 0.62 eV, the peak of the profiles is shifted towards the hard wall of the potential surface. Previously the peaks were located towards the plateau region. Evidently at the high total energy of 1.0331 eV the quasi-classical and quantum probability current densities are "bob-sledding" high on the repulsive wall.

The quantum probability current density and streamlines for E = 1.0331 eV are presented in Figures 14 and 15 respectively. There the vortex in these results is prominently displayed.

In summary, the comparison of classical and quantum probability current densities, streamlines, and current density profiles reveals great differences between the two sets of results for energies below the threshold for vibrational excitation of product (and reagent) H_2. Classically such excitation can occur at any energy. This obvious defect, inherent in the quasi-classical calculations, seems chiefly responsible for the striking differences mentioned above. Substantiation for this conclusion is provided by the higher energy comparisons. There, the quasi-classical and quantum results show some similarities in overall oscillatory structure of the probability current density vector fields. Such structure is apparently due to the vibrational excitation of the

product (and reagent) H_2.

The high energy quasi-classical and quantum results contain vortices in the probability current density vector field. Although the significance of these vortices, if any, is at present unclear, the fact that they appear in both the classical and quantum results has been established. Perhaps it can be said that these vortices create turbulence in the probability current densities, impeding flow and hence that they are responsible for the decline in the total reaction probability (quasi-classically and quantum mechanically) at the higher energies.

Table 1. Convergence of classical probability density.[a]

x_2(bohr)	x_3(bohr)	$\rho(100)$[b]	$\rho(200)$	$\rho(300)$
1.19	5.456	0.6163(-2)[c]	0.6625(-2)	0.6730(-2)
1.33	5.456	0.5821(-2)	0.6017(-2)	0.6738(-2)
1.47	5.456	0.6527(-2)	0.7431(-2)	0.7705(-2)
1.61	5.456	0.1637(-1)	0.1552(-1)	0.1449(-1)
1.19	4.001	0.1000(-1)	0.8892(-2)	0.8216(-2)
1.33	4.001	0.7800(-2)	0.8097(-2)	0.7634(-2)
1.47	4.001	0.5958(-2)	0.6894(-2)	0.7383(-2)
1.61	4.001	0.1426(-1)	0.1400(-1)	0.1363(-1)
1.75	4.001	0.1585(-1)	0.1630(-1)	0.1511(-1)
3.43	4.001	0 4548(-4)	0.2804(-3)	0.2752(-3)
3.57	4.001	0.3866(-3)	0.6778(-3)	0.6920(-3)
3.71	4.001	0.1796(-2)	0.1776(-2)	0.1627(-2)
3.85	4.001	0.3343(-2)	0.2734(-2)	0.2595(-2)
3.99	4.001	0.3525(-2)	0.3809(-2)	0.3609(-2)
4.13	4.001	0.3752(-2)	0.4276(-2)	0.4521(-2)
1.47	2.7886	0.4753(-2)	0.4837(-2)	0.4379(-2)
1.75	2.7886	0.2008(-1)	0.2206(-1)	0.2550(-1)
2.03	2.7886	0.2706(-2)	0.2524(-2)	0.2052(-2)
2.31	2.7886	0.1978(-2)	0.2162(-2)	0.1879(-2)
2.59	2.7886	0.1137(-3)	0.7011(-4)	0.6290(-4)

[a]Initial relative kinetic energy is 0.28 eV. The grid is 30×30.

[b]The numbers in parentheses are the total number of trajectories used in calculating ρ.

[c]The numbers in parentheses are powers of ten which multiply the preceding number.

Table 2. Convergence of classical probability density for three grids.[a]

x_2(bohr)	x_3(bohr)	$\rho(100)$[b]	$\rho(200)$	$\rho(300)$
		20×20		
3.5	3.522	0.788(-2)[c]	0.912(-2)	0.101(-1)
3.5	4.215	0.148(-3)	0.759(-4)	0.509(-4)
2.9	3.406	0.826(-2)	0.913(-2)	0.917(-2)
2.9	3.868	0.337(-2)	0.378(-2)	0.340(-2)
1.5	3.291	0.128(-1)	0.129(-1)	0.130(-1)
1.5	4.446	0.196(-1)	0.197(-1)	0.191(-1)
		40×40		
x_2(bohr)	x_3(bohr)	$\rho(100)$	$\rho(200)$	$\rho(300)$
3.5	3.522	0.692(-3)	0.913(-3)	0.953(-3)
3.5	4.215	0.840(-2)	0.862(-2)	0.820(-2)
2.9	3.406	0.180(-1)	0.168(-1)	0.158(-1)
2.9	3.868	0.180(-1)	0.202(-1)	0.206(-1)
1.5	3.291	0.619(-3)	0.261(-3)	0.381(-3)
1.5	4.446	0.626(-2)	0.487(-2)	0.422(-2)

[a] The initial translational energy is 0.28 eV

[b] The numbers in parentheses are the total number of classical trajectories used in calculating ρ.

[c] The numbers in parentheses are powers of ten which multiply the preceding numbers.

Table 2. (Cont.)

80 × 80				
x_2(bohr)	x_3(bohr)	ρ(100)	ρ(200)	ρ(300)
3.5	3.522	0.424(-4)	0.976(-4)	0.153(-3)
3.5	4.215	0.339(-3)	0.401(-3)	0.277(-3)
2.9	3.406	0.614(-3)	0.629(-3)	0.634(-3)
2.9	3.868	0.256(-2)	0.193(-2)	0.500(-2)
1.5	3.291	0.466(-3)	0.488(-3)	0.574(-3)
1.5	4.446	0.176(-2)	0.150(-2)	0.138(-2)

Table 3. Convergence of the classical probability current density for a 30 × 30 grid.[a]

x_2(bohr)	x_3(bohr)	$j_{x_2}(200)$[b]	$j_{x_2}(300)$	$j_{x_3}(200)$	$j_{x_3}(300)$
1.19	5.456	-0.128(-3)[c]	-0.3638(-3)	-0.412(-2)	-0.424(-2)
1.33	5.456	0.598(-3)	0.532(-3)	-0.357(-2)	-0.419(-2)
1.61	5.456	-0.183(-2)	-0.149(-2)	-0.634(-2)	-0.596(-2)
1.19	4.729	0.133(-2)	0.105(-2)	-0.396(-2)	-0.399(-2)
1.33	4.729	0.274(-2)	0.238(-2)	-0.383(-2)	-0.340(-2)
1.61	4.729	0.222(-3)	0.625(-3)	-0.822(-2)	-0.861(-2)
1.19	4.001	0.259(-4)	0.112(-4)	-0.151(-2)	-0.138(-2)
1.33	4.001	-0.260(-3)	-0.801(-3)	-0.544(-2)	-0.595(-2)
1.61	4.001	-0.334(-2)	-0.298(-2)	-0.564(-2)	-0.524(-2)
3.57	4.001	0.626(-3)	0.653(-3)	0.403(-3)	0.384(-3)
3.99	4.001	0.209(-2)	0.198(-2)	0.454(-2)	0.427(-2)

[a]The initial translational energy is 0.28 eV.

[b]See Table 2.

[c]See Table 2.

References

1. E. Mortensen and K. S. Pitzer, The Transition State, Chem. Soc. (London), Special Publication 16, 57 (1962).
2. D. R. Dion, M. B. Milleur, and J. O. Hirschfelder, J. Chem. Phys. 52, 3179 (1970).
3. E. A McCullough and R. E. Wyatt, J. Chem. Phys. 54, 3578 (1971).
4. J. M. Bowman, A. Kuppermann, and G. C. Schatz, Chem. Phys. Letters 19, 21 (1973).
5. A. Kuppermann, to be published.
6. D. G. Truhlar and A. Kuppermann, J. Chem. Phys. 56, 2232 (1972).
7. J. M Bowman and A. Kuppermann, Chem. Phys. Letters 12, 1 (1971).
8. F. T. Wall and R. N. Porter, J. Chem. Phys. 36, 3256 (1962).
9. I. Shavitt, R. M. Stevens, F. L. Minn, and M. Karplus, J. Chem. Phys. 48, 2700 (1968).
10. E. Merzbacher, Quantum Mechanics, (Wiley, New York, 1961), 2nd ed., p. 37.
11. L. M. Milne-Thomson, Theoretical Hydrodynamics, (MacMillan, New York, 1968), 5th ed., p. 5.
12. L. Pauling and E. B. Wilson, Introduction to Quantum Mechanics, (McGraw-Hill, New York, 1935), p. 76.

FIGURE CAPTIONS

Figure 1a: Quasi-classical probability current density for total energy E = 0.5719 eV (initial translational energy E_0 = 0.2991 eV) for the collinear H + H_2 reaction. Minimum energy path is indicated by a long-dashed curve and the plus sign gives the location of the potential surface saddle point. Equipotential energy contours are given (in eV); contour labeled E is one of value equal to the total energy E. The coordinates x_2 and x_3 are defined in the text.

Figure 1b: Quantum probability current density for the total energy E = 0.5719 eV. See caption of Figure 1a for explanation of other symbols used.

Figure 2a: Quasi-classical streamlines for total energy E = 0.5719 eV. See caption of Figure 1a for explanation of other symbols used.

Figure 2b: Quantum streamlines for total energy E = 0.5719 eV. See caption of Figure 1a for explanation of other symbols used.

Figure 3a: Quasi-classical current density profiles along five lines which are normal to the minimum energy path. The total energy E is 0.5719 eV. See caption of Figure 1a for explanation of other symbols used.

Figure 3b: Quantum current density profiles along five lines which are normal to the minimum energy path. The total energy E is 0.5719 eV. See caption of Figure 1a for explanation of other symbols used.

Figure 4a: Quasi-classical probability current density for total energy E = 0.62 eV. See caption of Figure 1a for explanation of other symbols used.

Figure 4b: Quantum probability current density for the total energy E = 0.62 eV. See caption of Figure 1a for explanation of other symbols used.

Figure 5a: Quasi-classical streamlines for total energy E = 0.62 eV. See caption of Figure 1a for explanation of other symbols used.

Figure 5b: Quantum streamlines for total energy E = 0.62 eV. See caption of Figure 1a for explanation of other symbols used.

Figure 6a: Quasi-classical current density profiles along five lines which are normal to the minimum energy path. The total energy E is 0.62 eV. See caption of Figure 1a for explanation of other symbols used.

Figure 6b: Quantum current density profiles along five lines which are normal to the minimum energy path. The total energy E is 0.62 eV. See caption of Figure 1a for explanation of other symbols used.

Figure 7a: Quasi-classical probability current density for total energy E = 0.7540 eV. See caption of Figure 1a for explanation of other symbols used.

Figure 7b: Quantum probability current density for the total energy E = 0.7540 eV. See caption of Figure 1a for explanation of other symbols used.

Figure 8a: Quasi-classical streamlines for total energy E = 0.7540 eV. See caption of Figure 1a for explanation of other symbols used.

Figure 8b: Quantum streamlines for total energy E = 0.7540 eV. See caption of Figure 1a for explanation of other symbols used.

Figure 9a: Quasi-classical current density profiles along five lines which are normal to the minimum energy path. The total energy E is 0.7540 eV. See caption of Figure 1a for explanation of other symbols used.

Figure 9b: Quantum current density profiles along five lines which are normal to the minimum energy path. The total energy E is 0.7540 eV. See caption of Figure 1a for explanation of other symbols used.

Figure 10a: Quasi-classical probability current density for total energy E = 0.8978 eV. A vortex is also shown. See caption of Figure 1a for explanation of other symbols used.

Figure 10b: Quantum probability current density for the total energy E = 0.8978 eV. See caption of Figure 1a for explanation of other symbols used.

Figure 11a: Quasi-classical streamlines for total energy E = 0.8978 eV. See caption of Figure 1a for explanation of other symbols used.

Figure 11b: Quantum streamlines for total energy E = 0.8978 eV. See caption of Figure 1a for explanation of other symbols used.

Figure 12a: Quasi-classical current density profiles along five lines which are normal to the minimum energy path. The total energy E Is 0.8978 eV. See caption of Figure 1a for explanation of other symbols used.

Figure 12b: Quantum current density profiles along five lines which are normal to the minimum energy path. The total energy E is 0.8978 eV. See caption of Figure 1a for explanation of other symbols used.

Figure 13a: Quasi-classical current density profiles along five lines which are normal to the minimum energy path. The total energy E is 1.0331 eV. See caption of Figure 1a for explanation of other symbols used.

Figure 13b: Quantum current density profiles along five lines which are normal to the minimum energy path. The total energy E is 1.0331 eV. See caption of Figure 1a for explanation of other symbols used.

Figure 14: Quantum probability current density for the total energy E = 1.0331 eV. See caption of Figure 1a for explanation of other symbols used.

Figure 15: Quantum streamlines for total energy E = 1.0331 eV. See caption of Figure 1a for explanation of other symbols used.

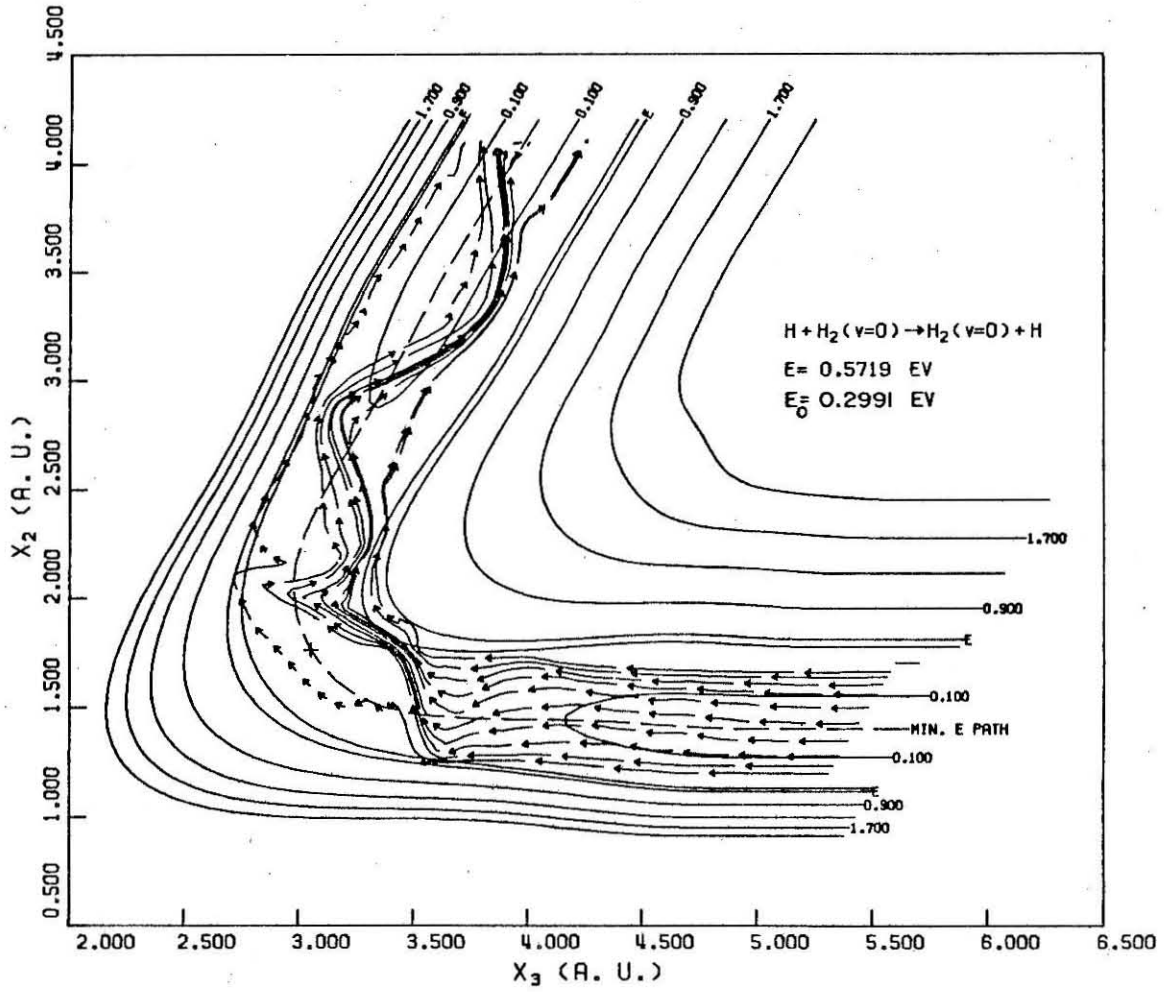
H + H2 (v=0) → H2 (v=0) + H
E= 0.5719 EV
E0= 0.2991 EV
1.700
0.900
E
0.100
MIN. E PATH
0.100
E
0.900
1.700
X2 (A. U.)
X3 (A. U.)
0.500
1.000
1.500
2.000
2.500
3.000
3.500
4.000
4.500
2.000
2.500
3.000
3.500
4.000
4.500
5.000
5.500
6.000
6.500

Figure 1a

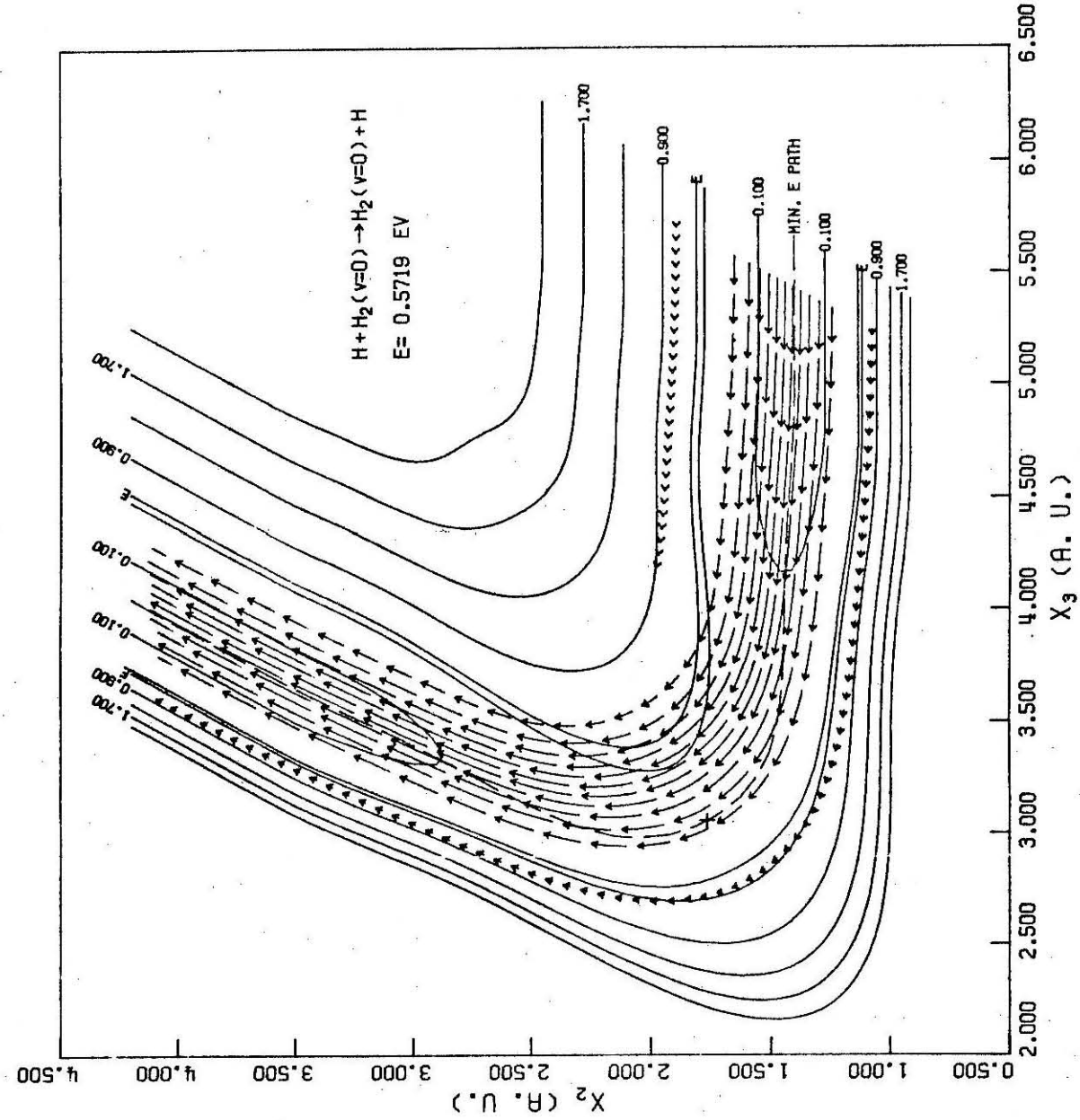
H+H2(v=0)→H2(v=0)+H
E= 0.5719 EV
1.700
0.900
0.100
MIN. E PATH
0.100
0.900
1.700
X3 (A. U.)
X2 (A. U.)
0.500
1.000
1.500
2.000
2.500
3.000
3.500
4.000
4.500
5.000
5.500
6.000
6.500

Figure 1b

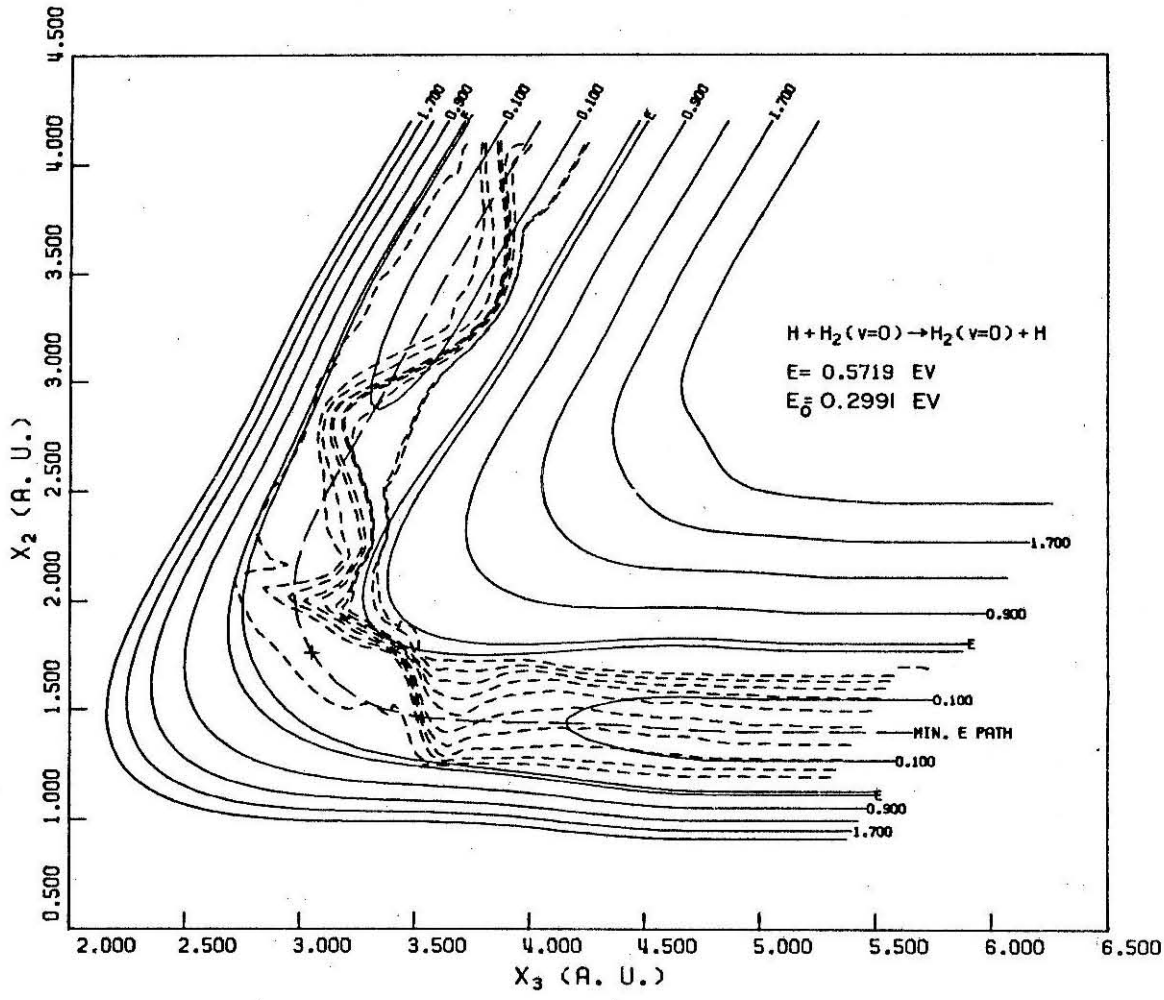
H + H2 (v=0) → H2 (v=0) + H
E= 0.5719 EV
E0= 0.2991 EV
1.700
0.900
E
0.100
MIN. E PATH
0.100
E
0.900
1.700
X2 (A. U.)
X3 (A. U.)
0.500
1.000
1.500
2.000
2.500
3.000
3.500
4.000
4.500
2.000
2.500
3.000
3.500
4.000
4.500
5.000
5.500
6.000
6.500

Figure 2a

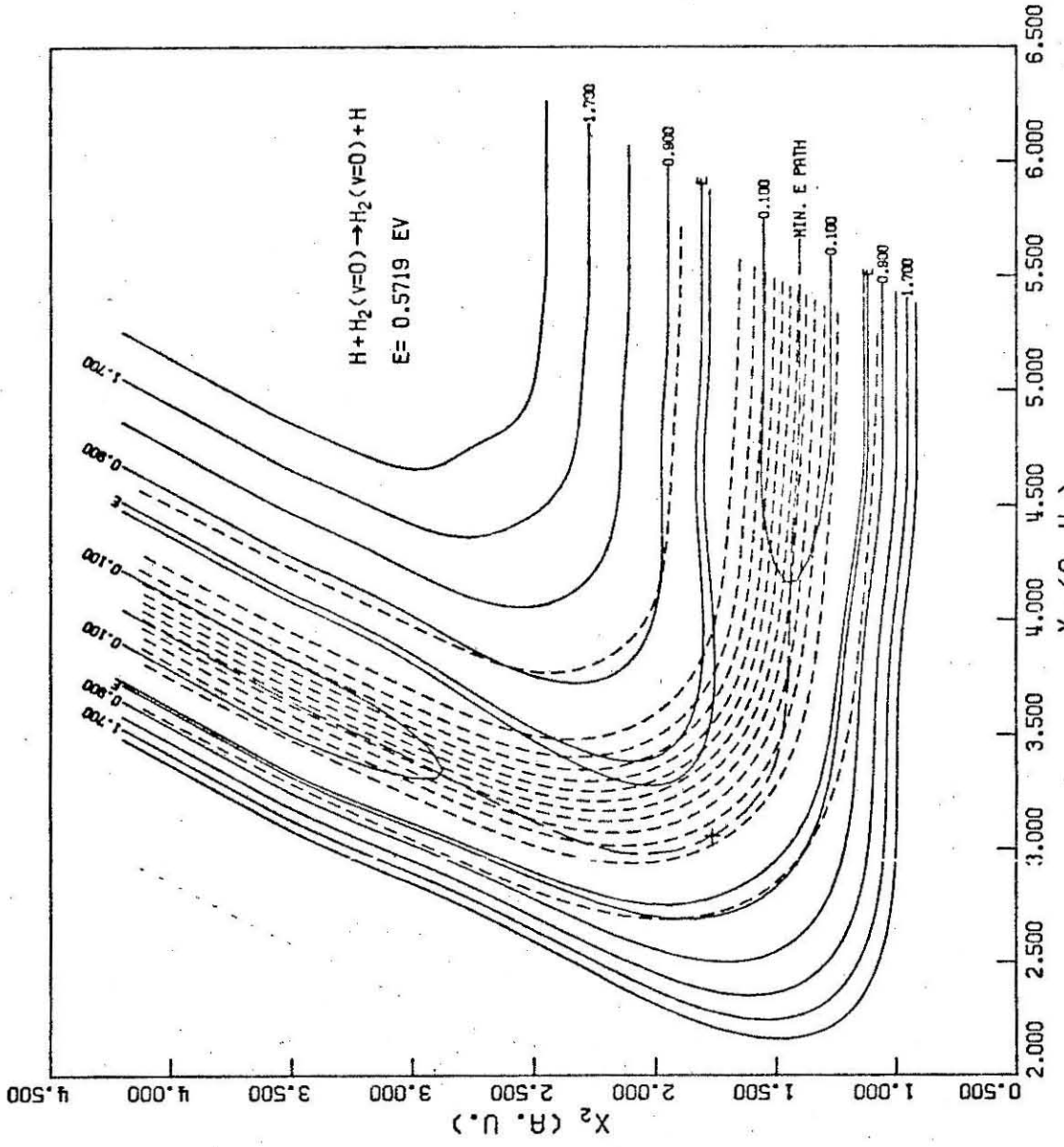
H+H2(v=0)→H2(v=0)+H
E= 0.5719 EV
MIN. E PATH
1.700
0.900
0.100
0.100
0.900
1.700
X2 (A. U.)
X3 (A. U.)

Figure 2b

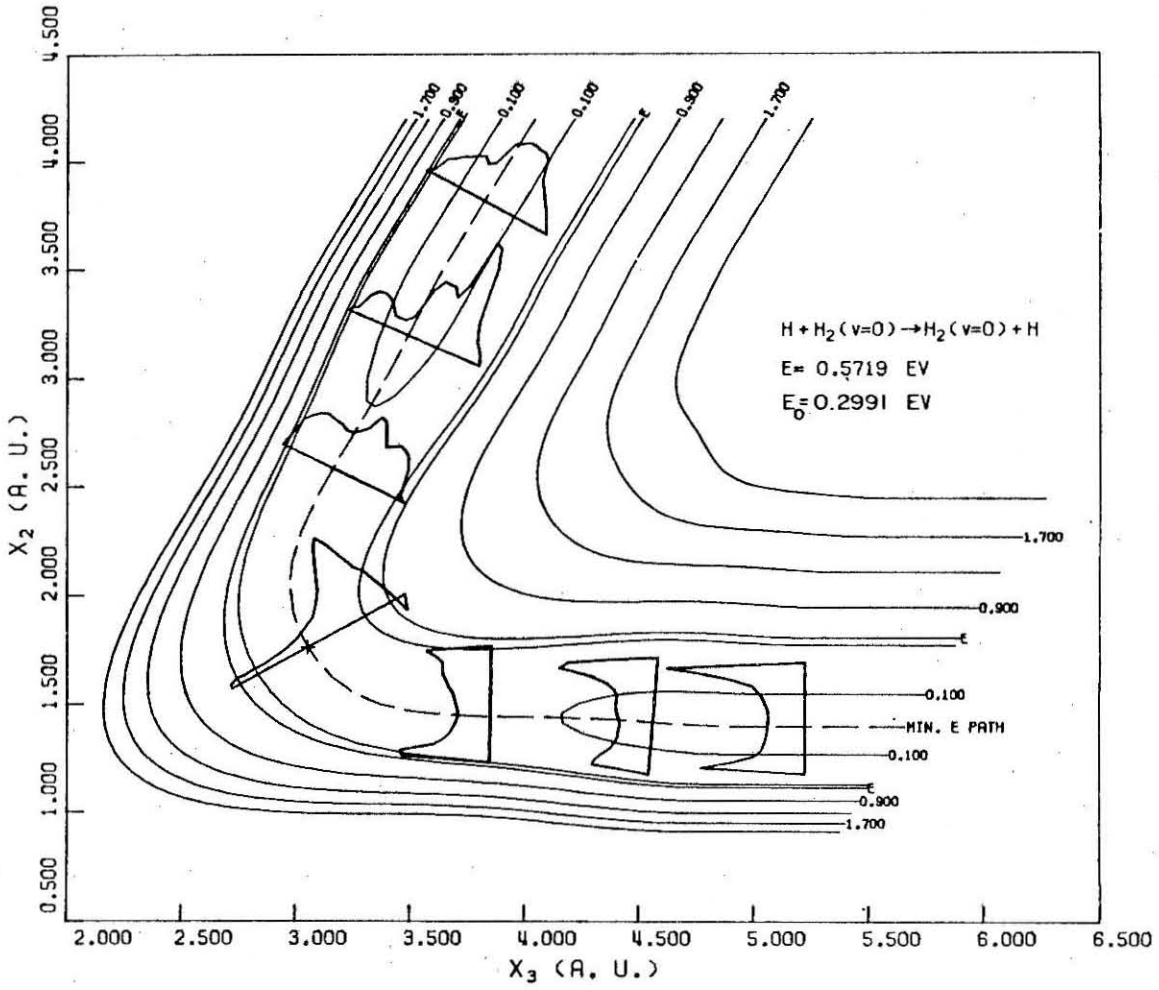
H + H2 (v=0) → H2 (v=0) + H
E= 0.5719 EV
E0= 0.2991 EV
1.700
0.900
E
0.100
MIN. E PATH
0.100
E
0.900
1.700
X2 (A. U.)
X3 (A. U.)
0.500
1.000
1.500
2.000
2.500
3.000
3.500
4.000
4.500
2.000
2.500
3.000
3.500
4.000
4.500
5.000
5.500
6.000
6.500

Figure 3a

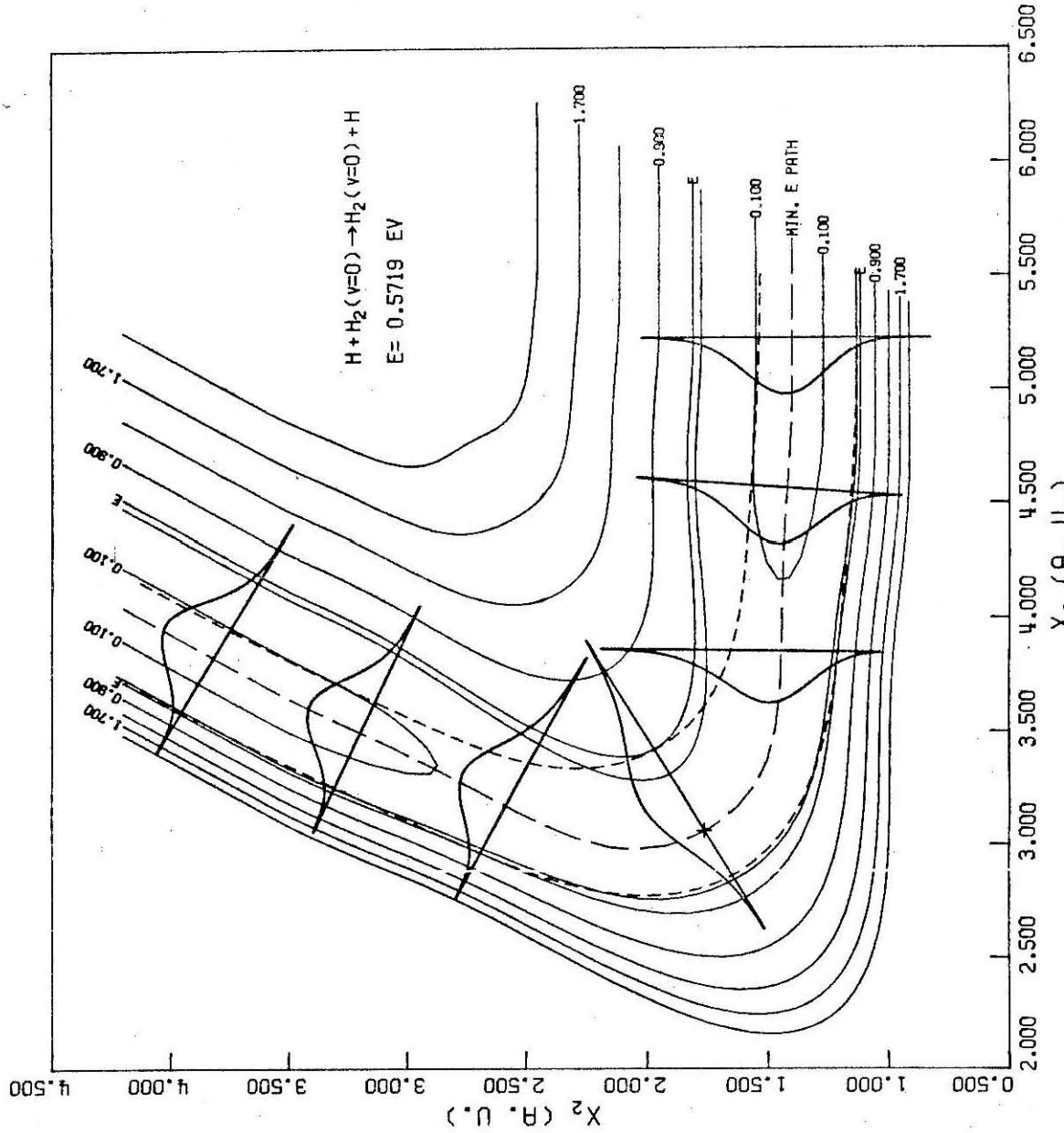
H + H2(v=0) → H2(v=0) + H
E= 0.5719 EV
MIN. E PATH
1.700
0.900
0.100
0.800
X2 (A. U.)
X3 (A. U.)

Figure 3b

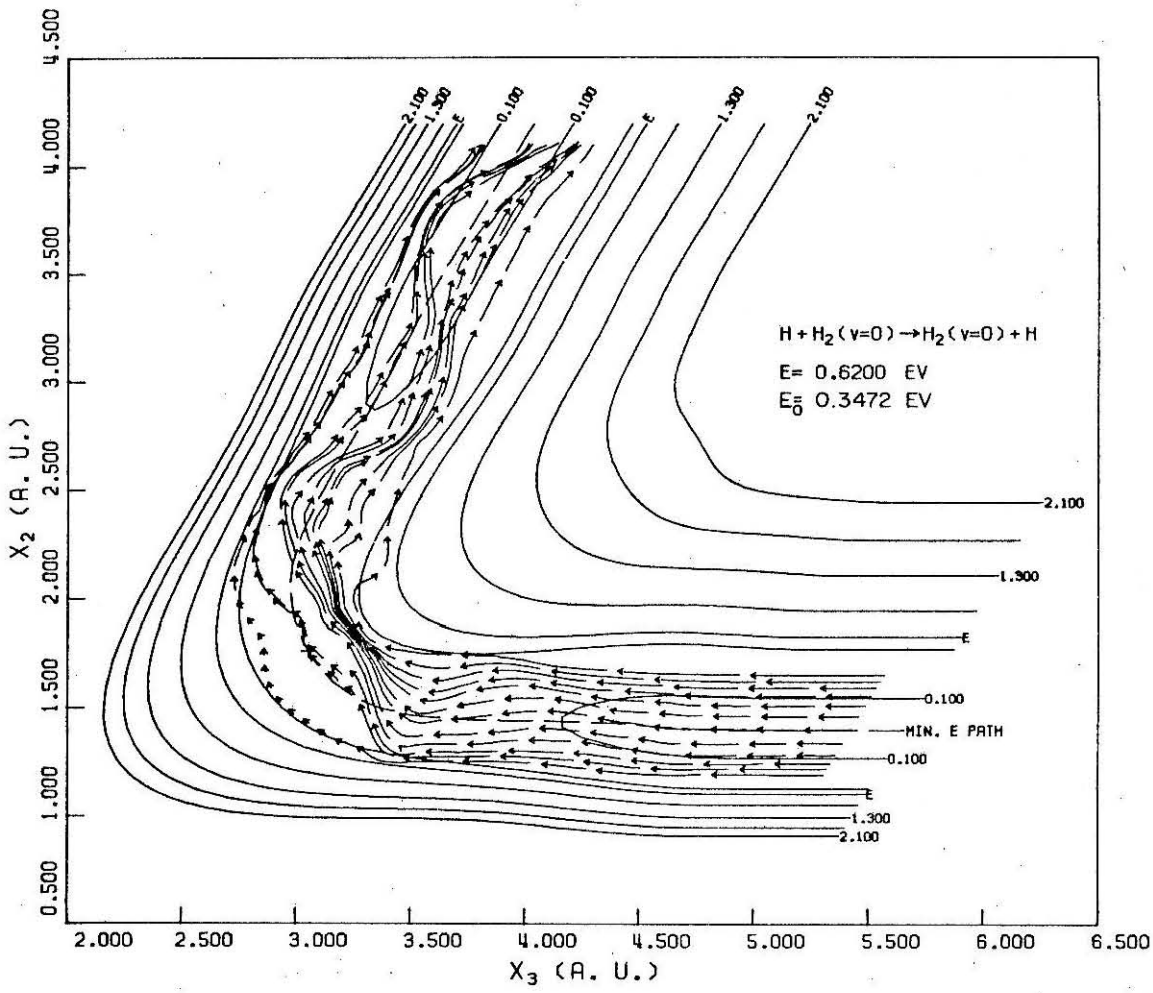
H + H2 (v=0) → H2 (v=0) + H
E= 0.6200 EV
E0= 0.3472 EV
2.100
1.300
E
0.100
MIN. E PATH
0.100
E
1.300
2.100
X2 (A. U.)
X3 (A. U.)
0.500
1.000
1.500
2.000
2.500
3.000
3.500
4.000
4.500
2.000
2.500
3.000
3.500
4.000
4.500
5.000
5.500
6.000
6.500

Figure 4a

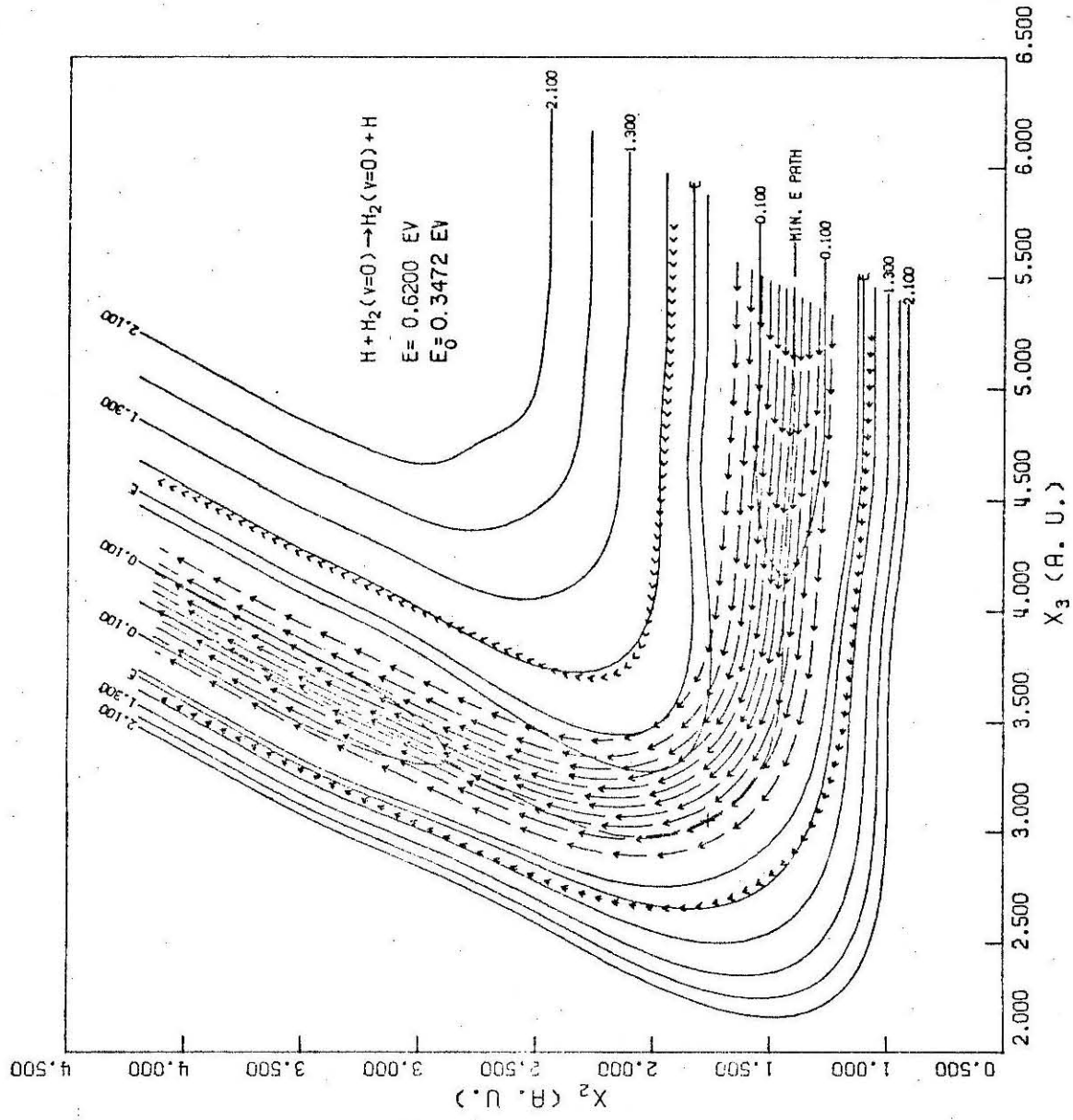
H + H2 (v=0) → H2 (v=0) + H
E= 0.6200 EV
E0= 0.3472 EV
2.100
1.300
0.100
MIN. E PATH
X3 (A. U.)
X2 (A. U.)

Figure 4b

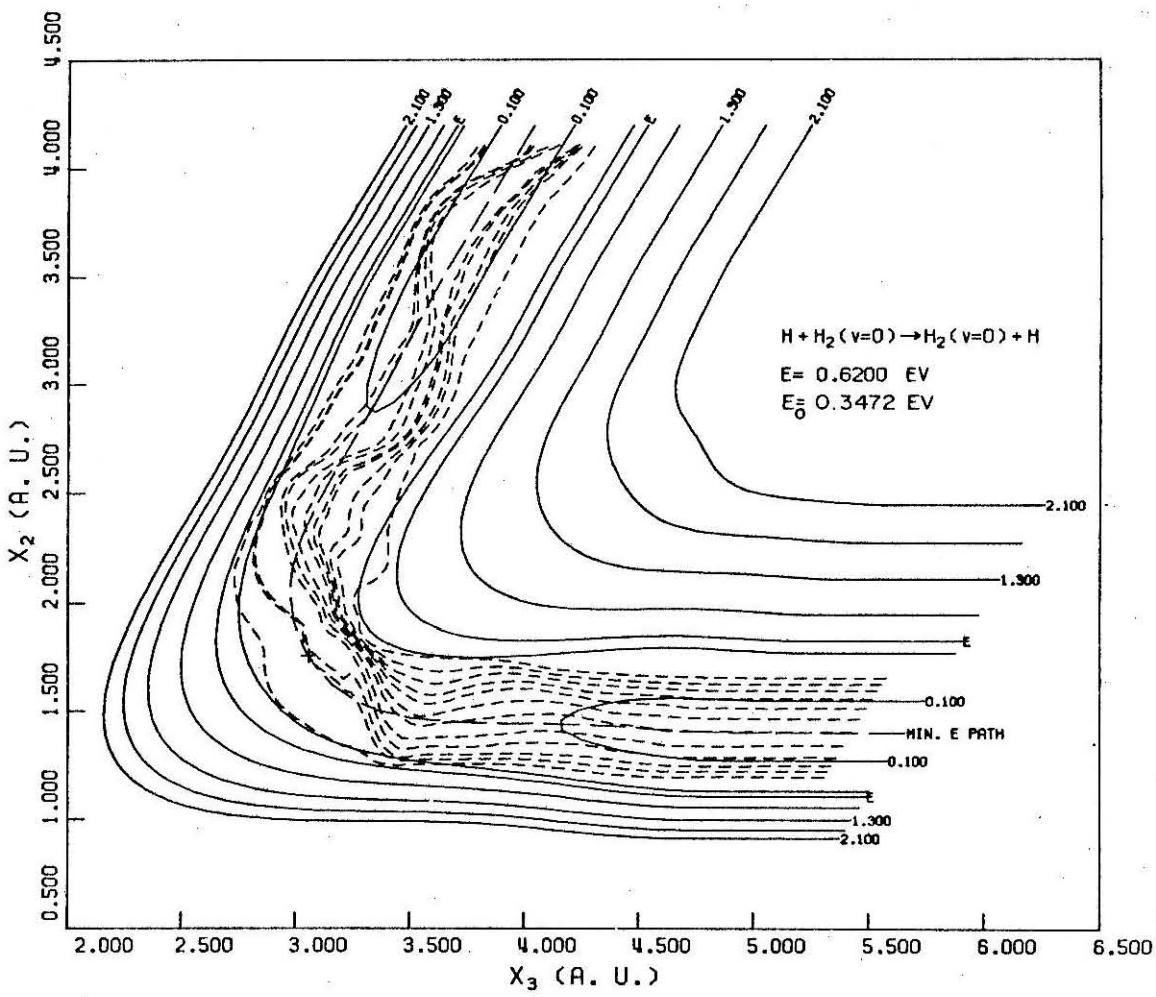
H + H2 (v=0) → H2 (v=0) + H
E= 0.6200 EV
E0= 0.3472 EV
2.100
1.300
E
0.100
MIN. E PATH
0.100
E
1.300
2.100
X2 (A. U.)
X3 (A. U.)
0.500
1.000
1.500
2.000
2.500
3.000
3.500
4.000
4.500
2.000
2.500
3.000
3.500
4.000
4.500
5.000
5.500
6.000
6.500

Figure 5a

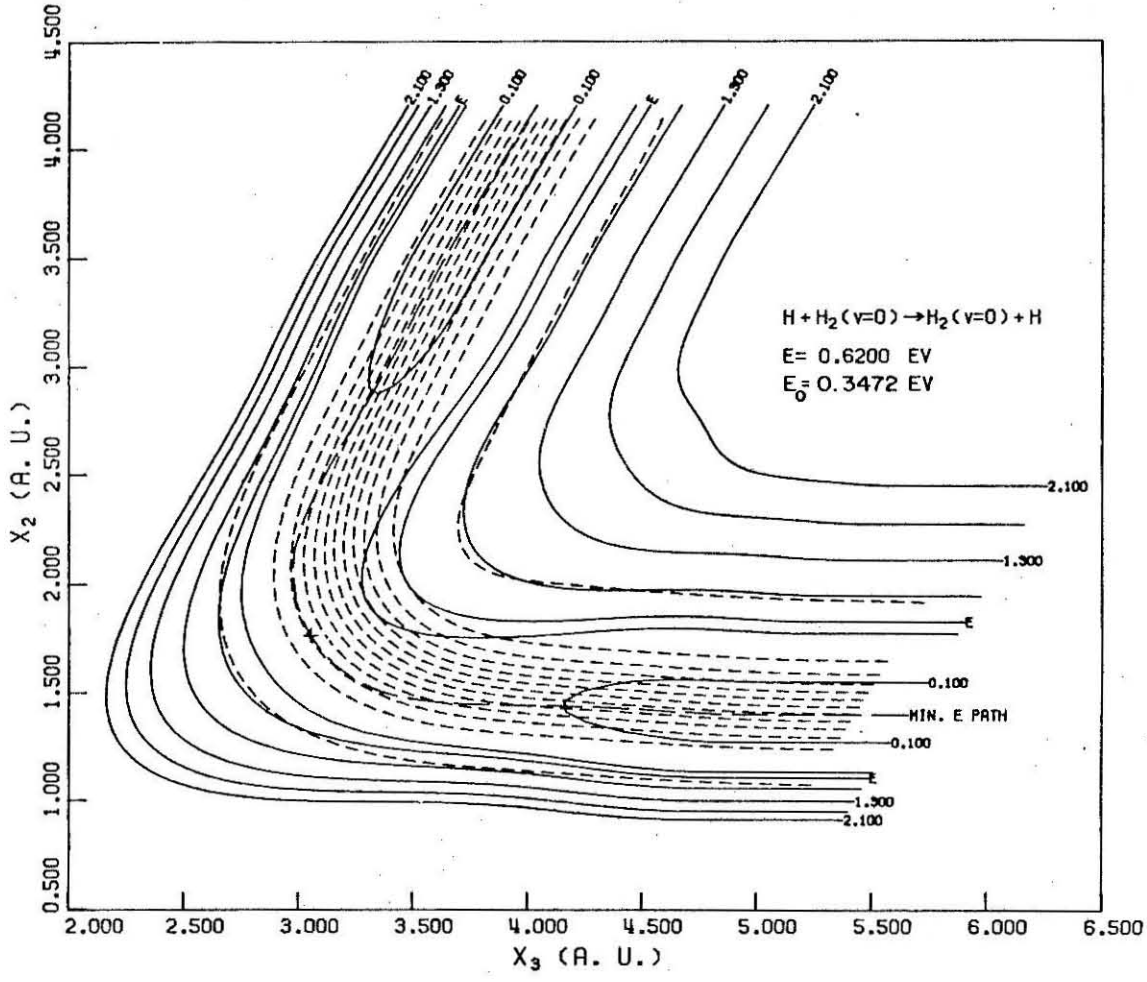
H + H2 (v=0) → H2 (v=0) + H
E= 0.6200 EV
E0= 0.3472 EV
2.100
1.300
E
0.100
MIN. E PATH
X2 (A. U.)
X3 (A. U.)
0.500
1.000
1.500
2.000
2.500
3.000
3.500
4.000
4.500
5.000
5.500
6.000
6.500

Figure 5b

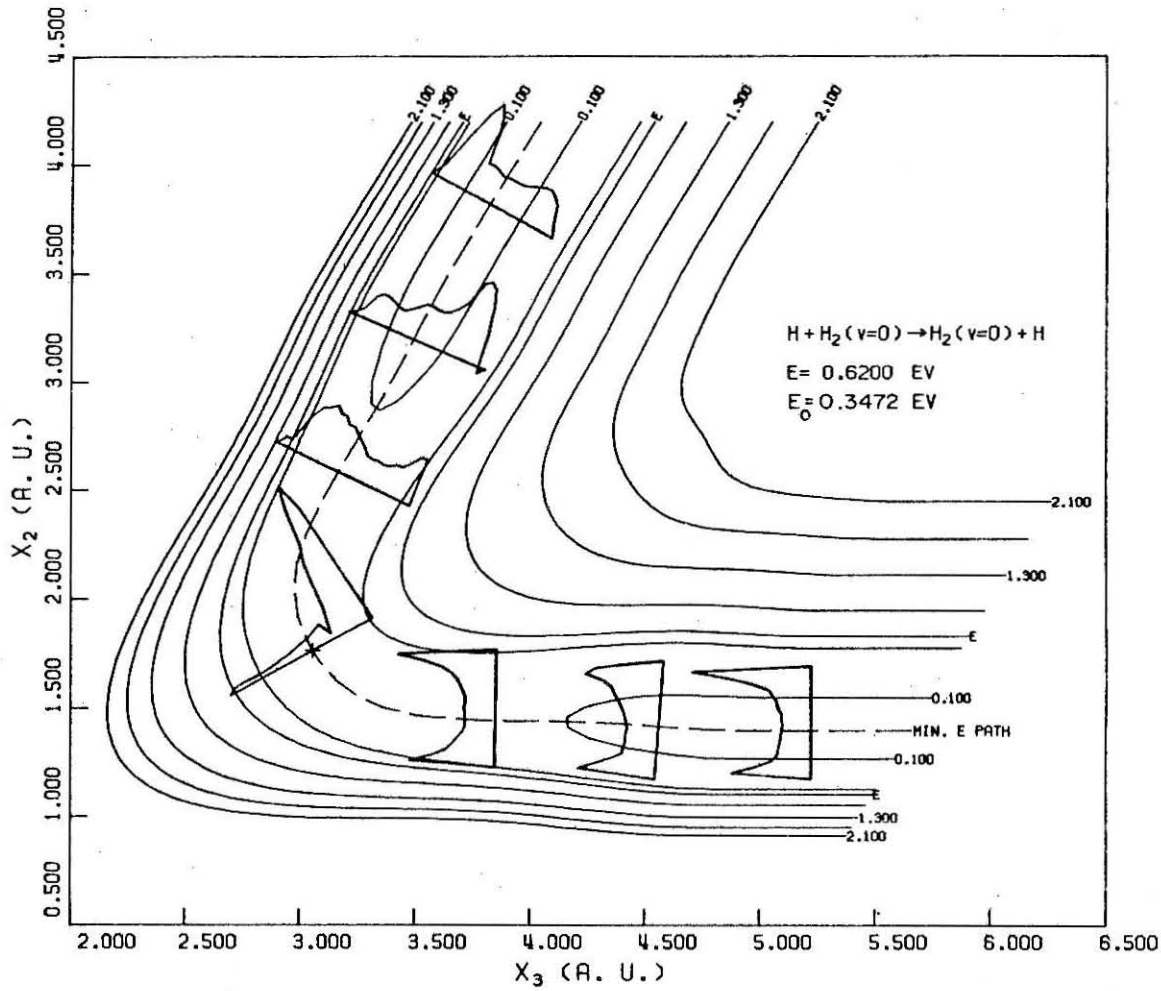
H + H2 (v=0) → H2 (v=0) + H
E= 0.6200 EV
Eo= 0.3472 EV
2.100
1.300
E
0.100
MIN. E PATH
0.100
E
1.300
2.100
X2 (A. U.)
X3 (A. U.)
0.500
1.000
1.500
2.000
2.500
3.000
3.500
4.000
4.500
2.000
2.500
3.000
3.500
4.000
4.500
5.000
5.500
6.000
6.500

Figure 6a

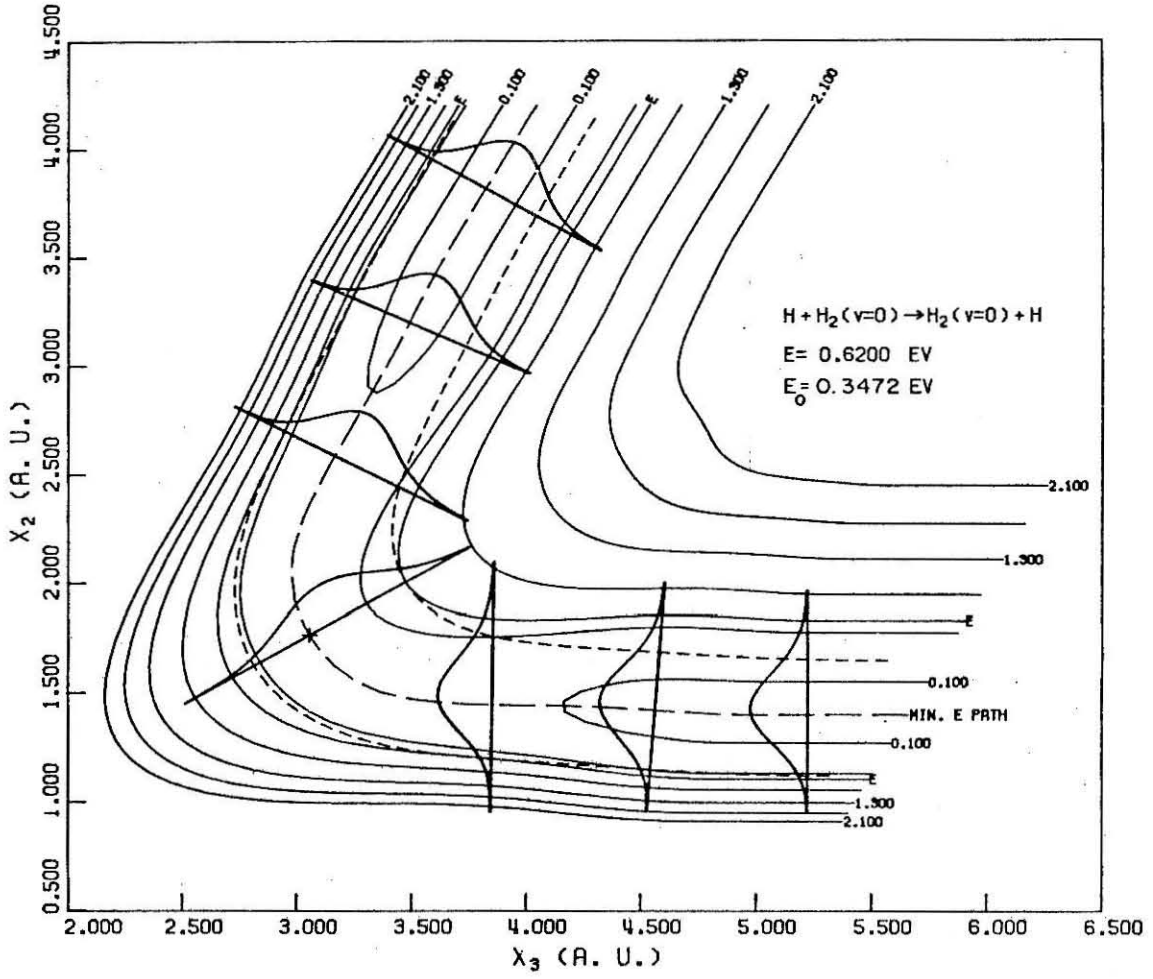
H + H2(v=0) → H2(v=0) + H
E= 0.6200 EV
Eo= 0.3472 EV
2.100
1.300
E
0.100
MIN. E PATH
0.100
E
1.300
2.100
X2 (A. U.)
X3 (A. U.)
0.500
1.000
1.500
2.000
2.500
3.000
3.500
4.000
4.500
2.000
2.500
3.000
3.500
4.000
4.500
5.000
5.500
6.000
6.500

Figure 6b

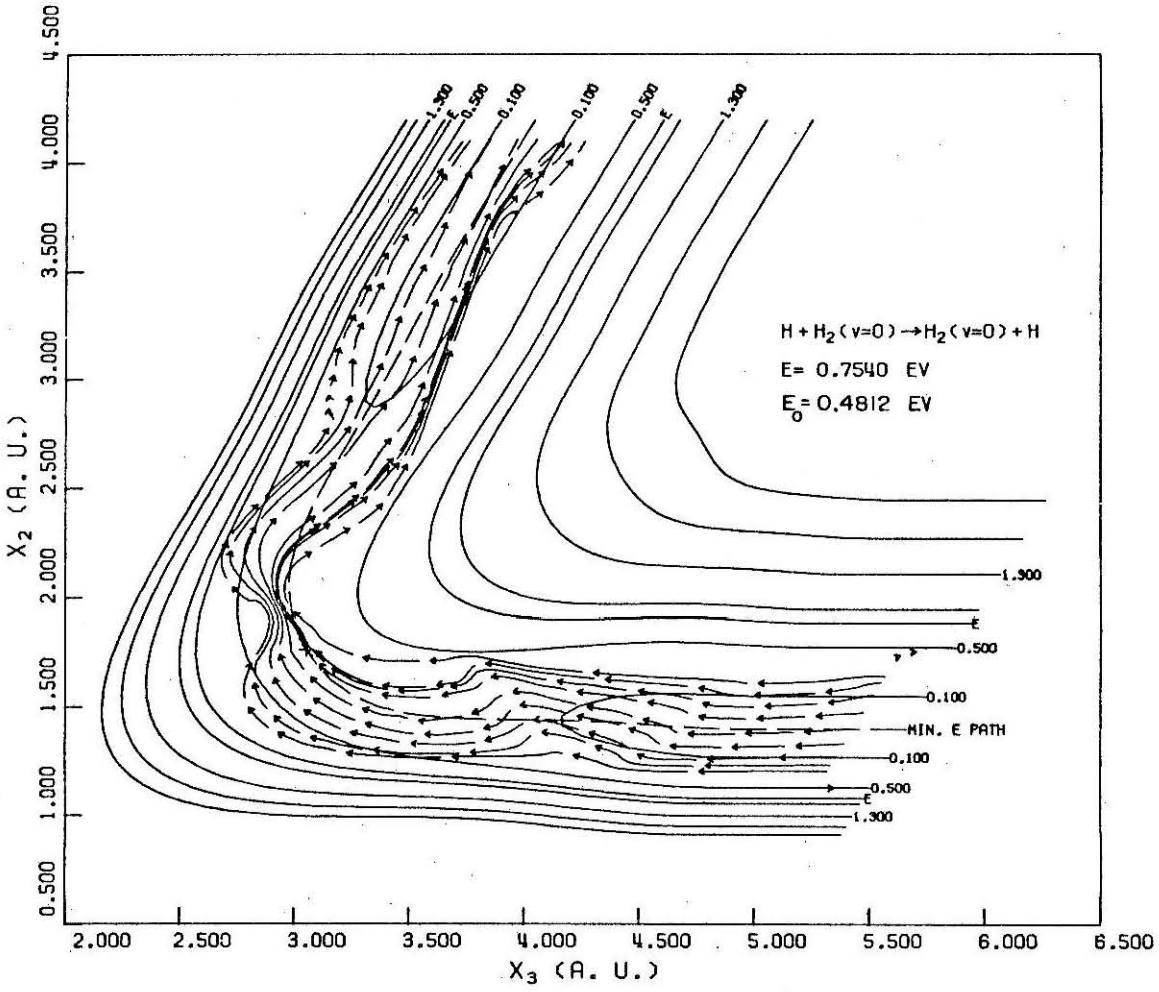
H + H2 (v=0) → H2 (v=0) + H
E= 0.7540 EV
E0= 0.4812 EV
1.300
E
0.500
0.100
MIN. E PATH
0.100
0.500
E
1.300
X2 (A. U.)
X3 (A. U.)
0.500
1.000
1.500
2.000
2.500
3.000
3.500
4.000
4.500
2.000
2.500
3.000
3.500
4.000
4.500
5.000
5.500
6.000
6.500

Figure 7a

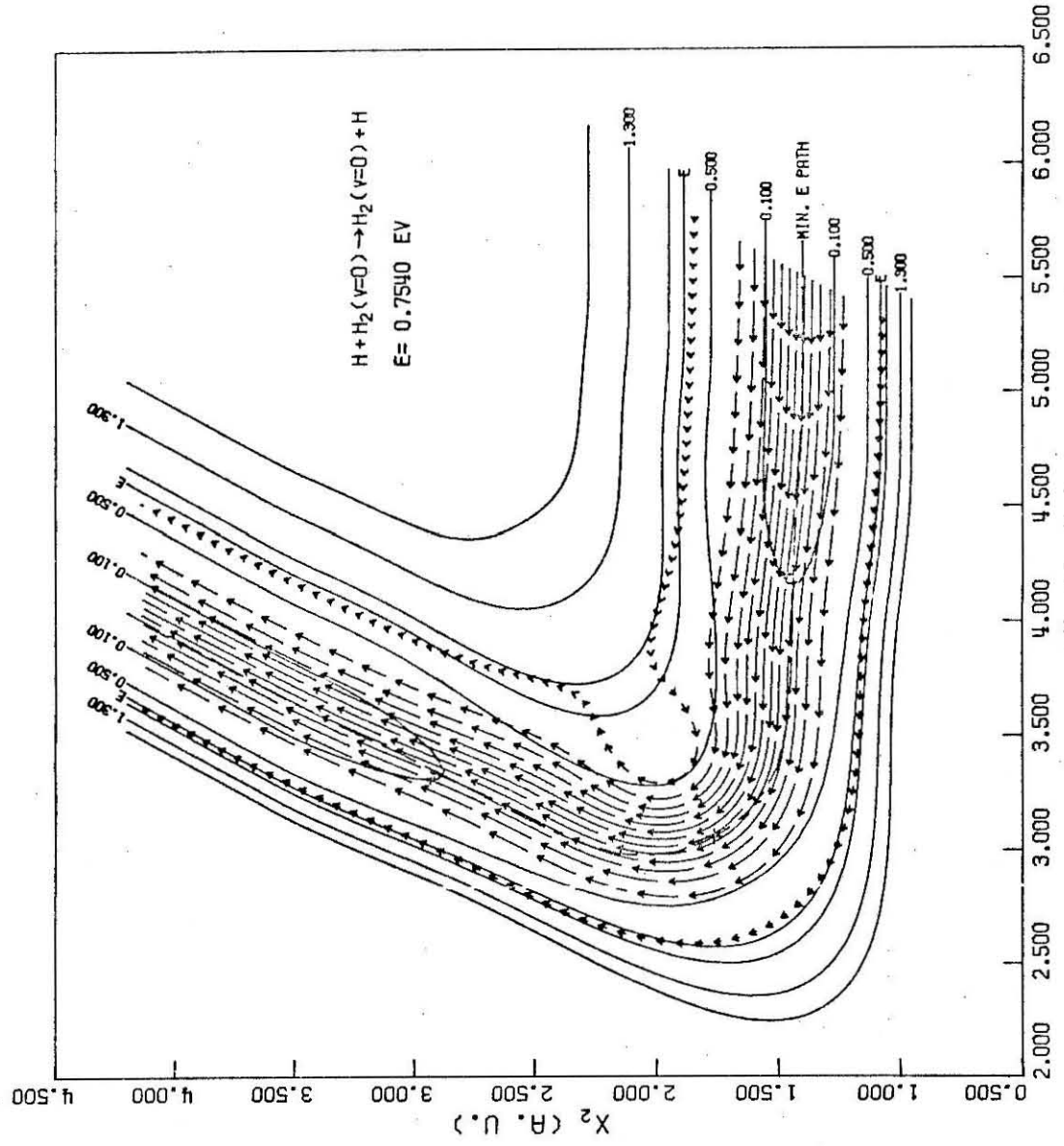
H+H2(v=0)→H2(v=0)+H
E= 0.7540 EV
1.300
E
0.500
0.100
MIN. E PATH
0.100
0.500
E
1.900
X3 (A. U.)
X2 (A. U.)

Figure 7b

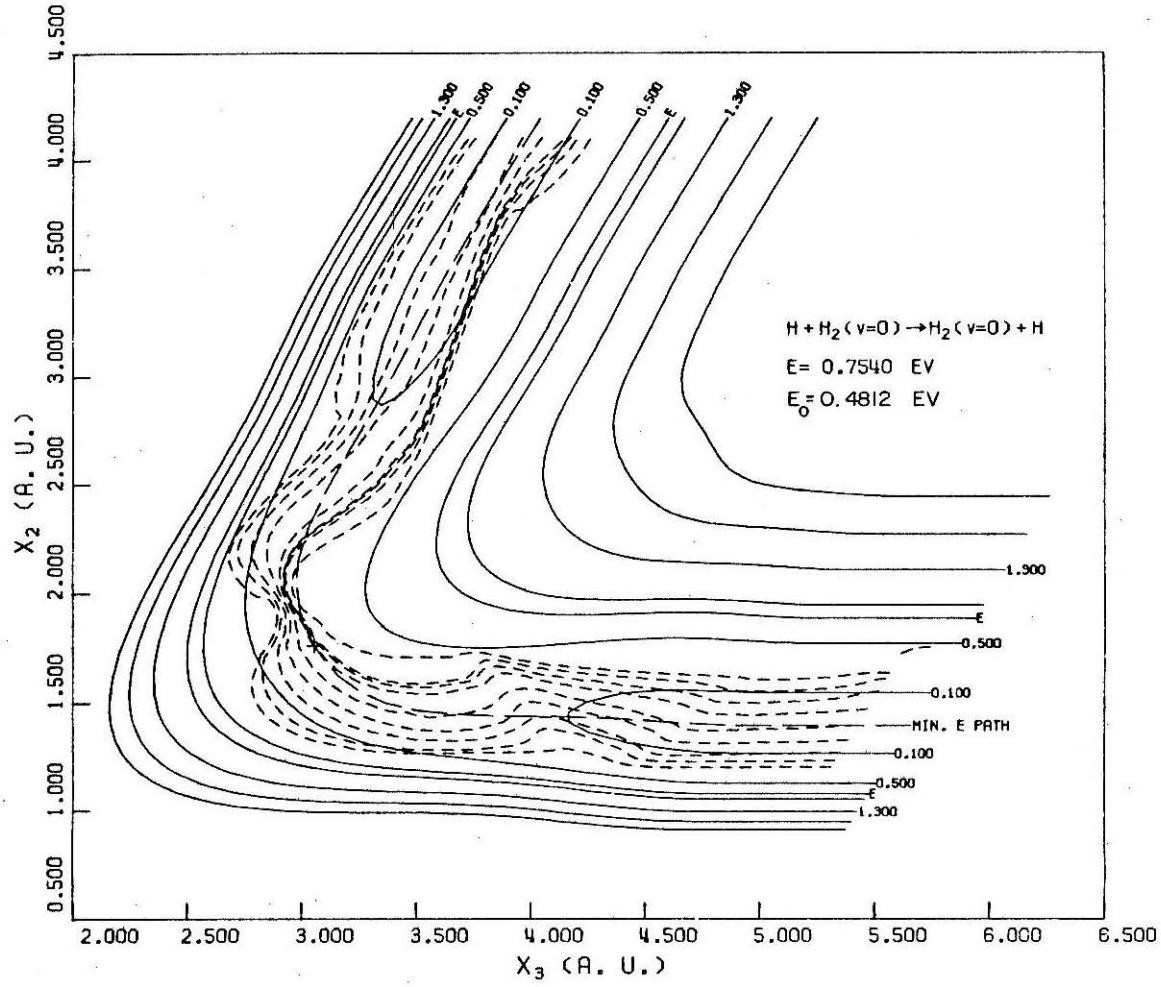
H + H2 (v=0) → H2 (v=0) + H
E= 0.7540 EV
E0= 0.4812 EV
1.300
E
0.500
0.100
MIN. E PATH
0.100
0.500
E
1.300
X2 (A. U.)
X3 (A. U.)
0.500
1.000
1.500
2.000
2.500
3.000
3.500
4.000
4.500
2.000
2.500
3.000
3.500
4.000
4.500
5.000
5.500
6.000
6.500

Figure 8a

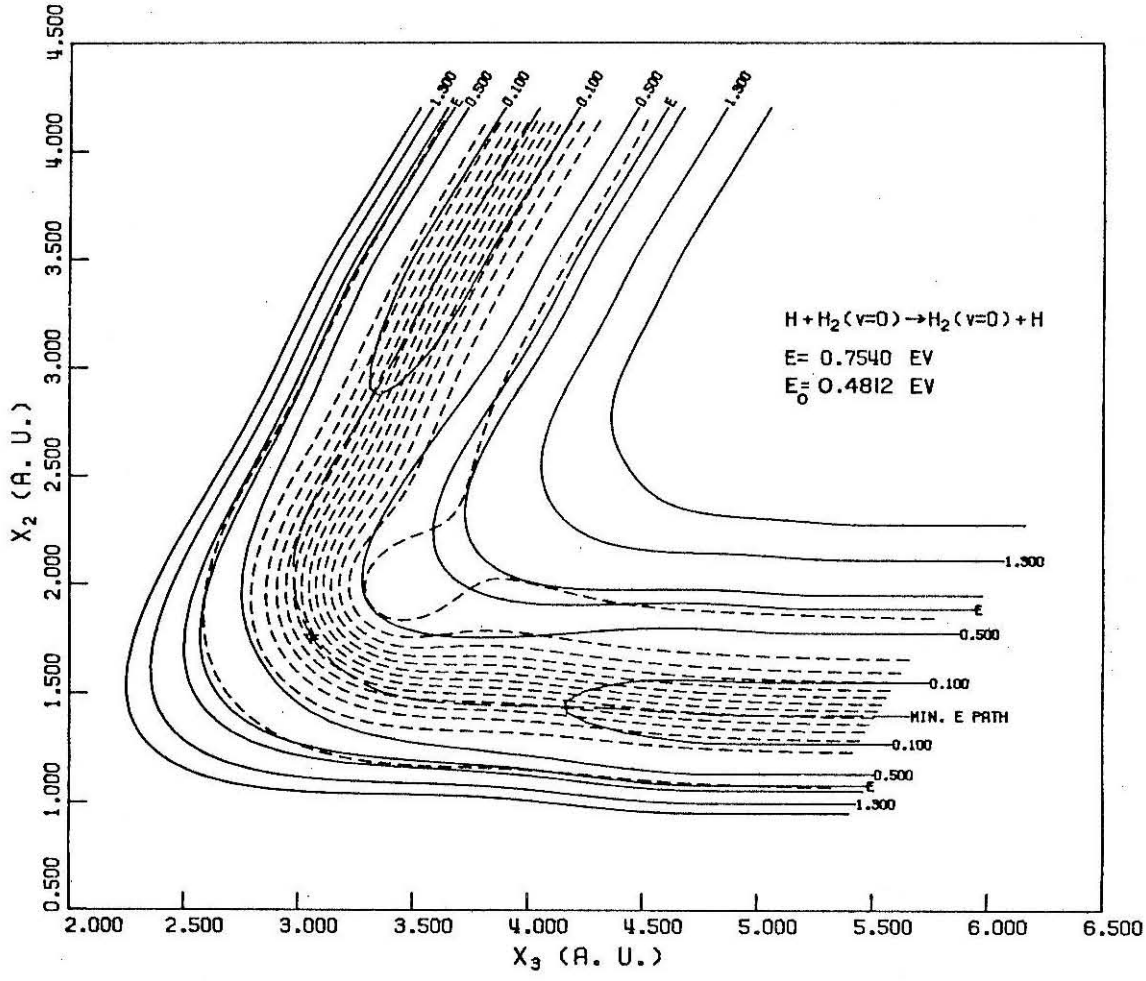
H + H2 (v=0) → H2 (v=0) + H
E= 0.7540 EV
E0= 0.4812 EV
1.300
ε
0.500
0.100
MIN. E PATH
0.100
0.500
ε
1.300
X2 (A. U.)
X3 (A. U.)
0.500
1.000
1.500
2.000
2.500
3.000
3.500
4.000
4.500
2.000
2.500
3.000
3.500
4.000
4.500
5.000
5.500
6.000
6.500

Figure 8b

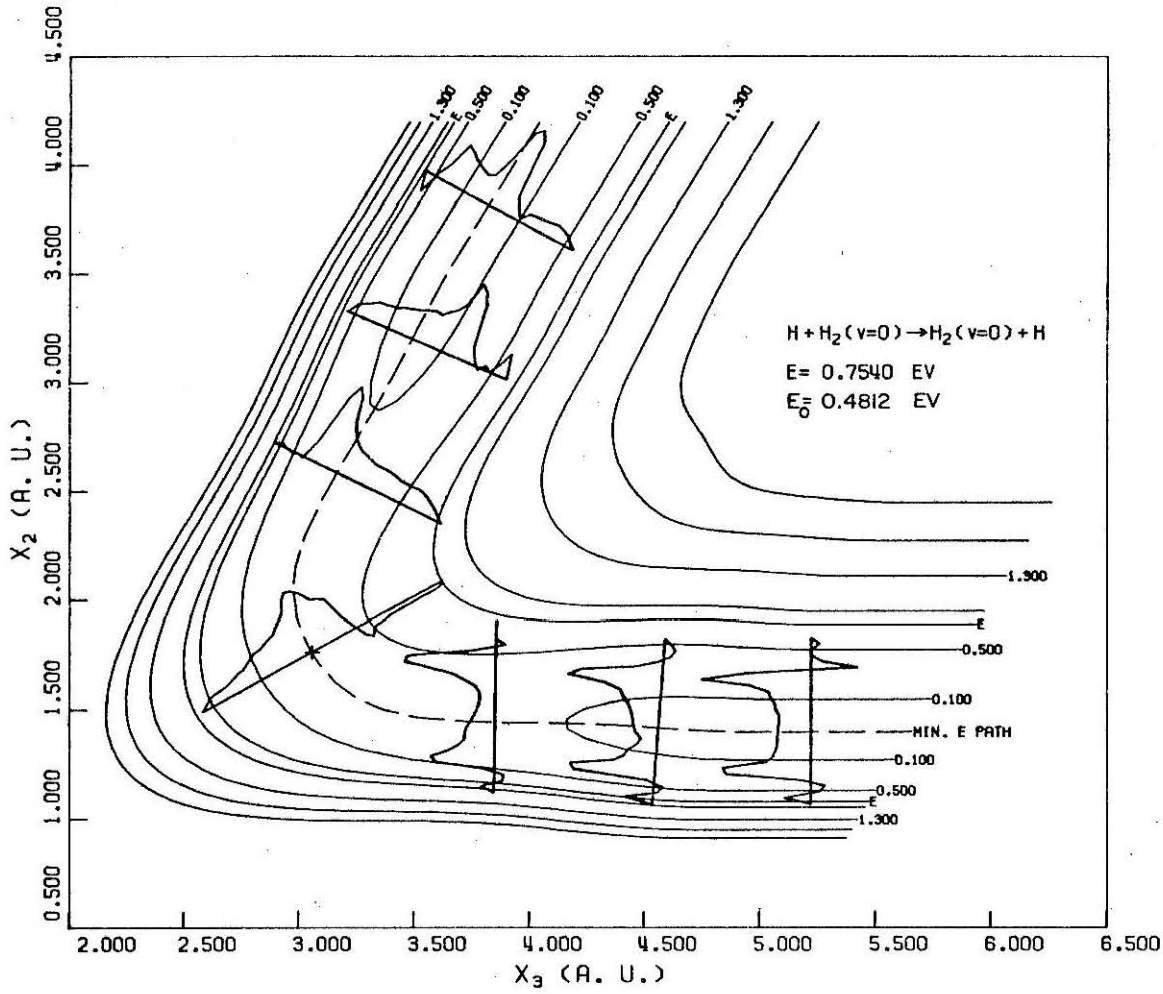
H + H2 (v=0) → H2 (v=0) + H
E= 0.7540 EV
Eo= 0.4812 EV
1.300
E
0.500
0.100
MIN. E PATH
0.100
0.500
E
1.300
X2 (A. U.)
X3 (A. U.)
0.500
1.000
1.500
2.000
2.500
3.000
3.500
4.000
4.500
2.000
2.500
3.000
3.500
4.000
4.500
5.000
5.500
6.000
6.500

Figure 9a

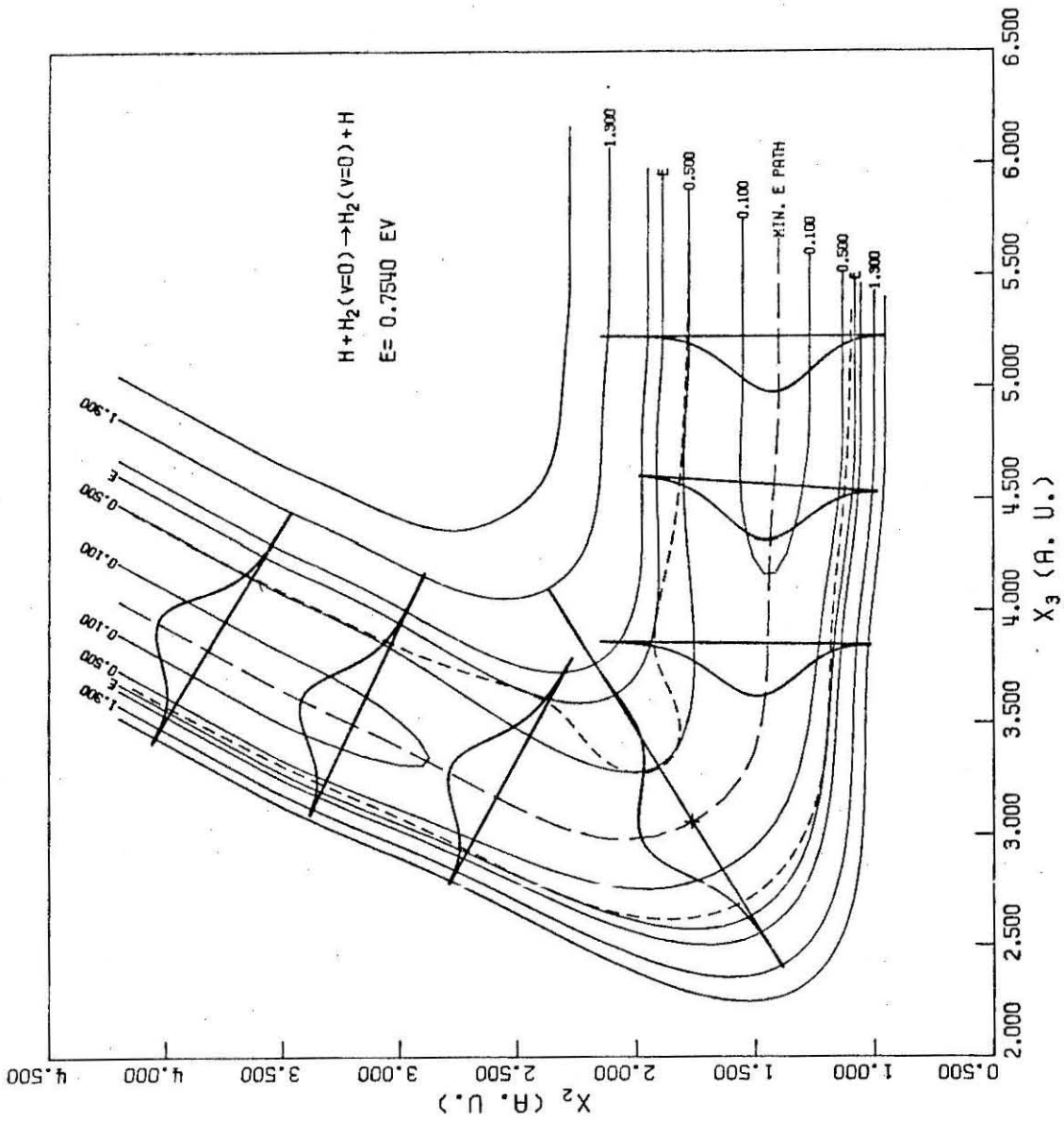
H + H2(v=0) → H2(v=0) + H
E= 0.7540 EV
1.300
E
0.500
0.100
MIN. E PATH
0.100
0.500
E
1.300
X3 (A. U.)
X2 (A. U.)

Figure 9b

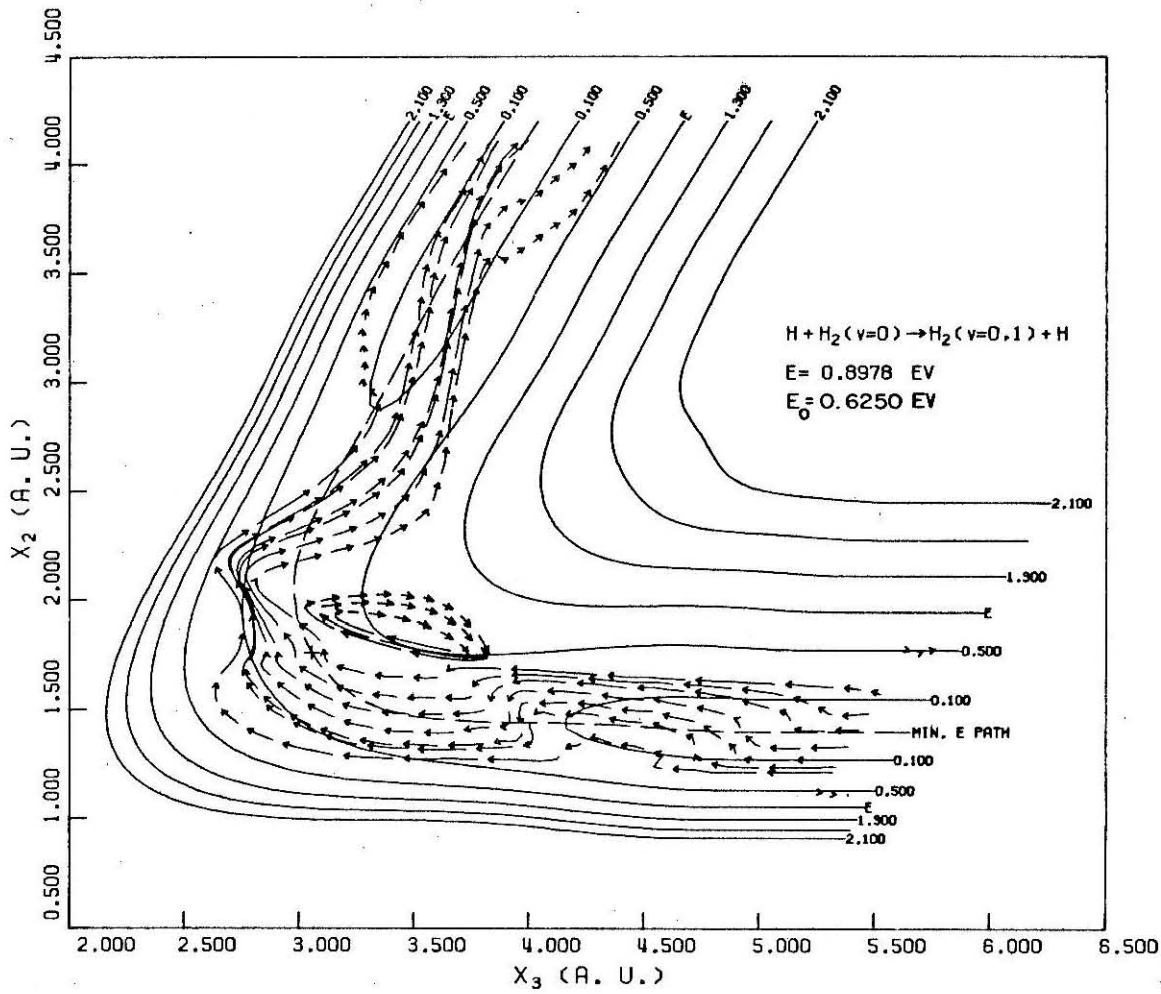
H + H2 (v=0) → H2 (v=0,1) + H
E= 0.8978 EV
E0= 0.6250 EV
2.100
1.900
E
0.500
0.100
MIN. E PATH
0.100
0.500
E
1.900
2.100
X2 (A. U.)
X3 (A. U.)
0.500
1.000
1.500
2.000
2.500
3.000
3.500
4.000
4.500
2.000
2.500
3.000
3.500
4.000
4.500
5.000
5.500
6.000
6.500

Figure 10a

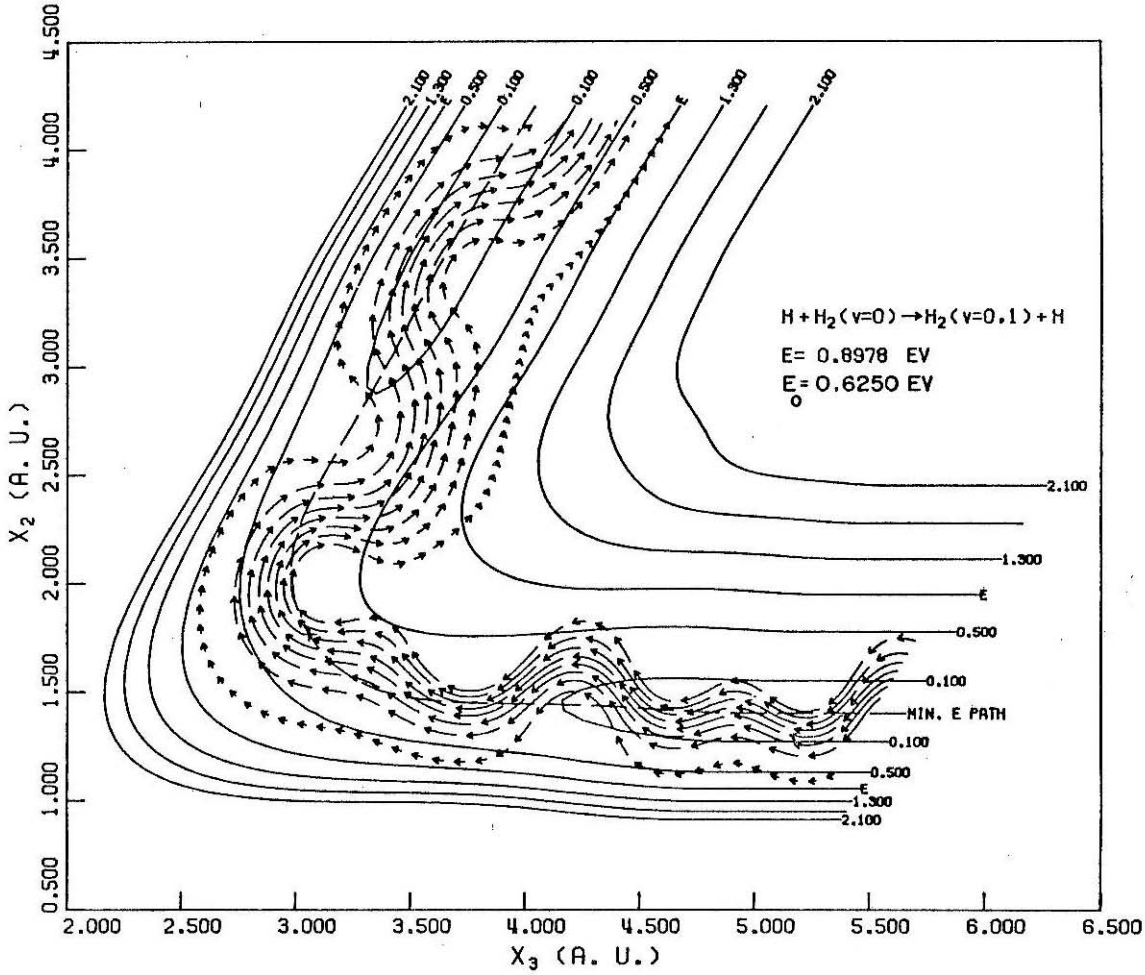
H + H2 (v=0) → H2 (v=0.1) + H
E= 0.8978 EV
Eo= 0.6250 EV
2.100
1.300
E
0.500
0.100
MIN. E PATH
0.100
0.500
E
1.300
2.100
X2 (A. U.)
X3 (A. U.)
0.500
1.000
1.500
2.000
2.500
3.000
3.500
4.000
4.500
2.000
2.500
3.000
3.500
4.000
4.500
5.000
5.500
6.000
6.500

Figure 10b

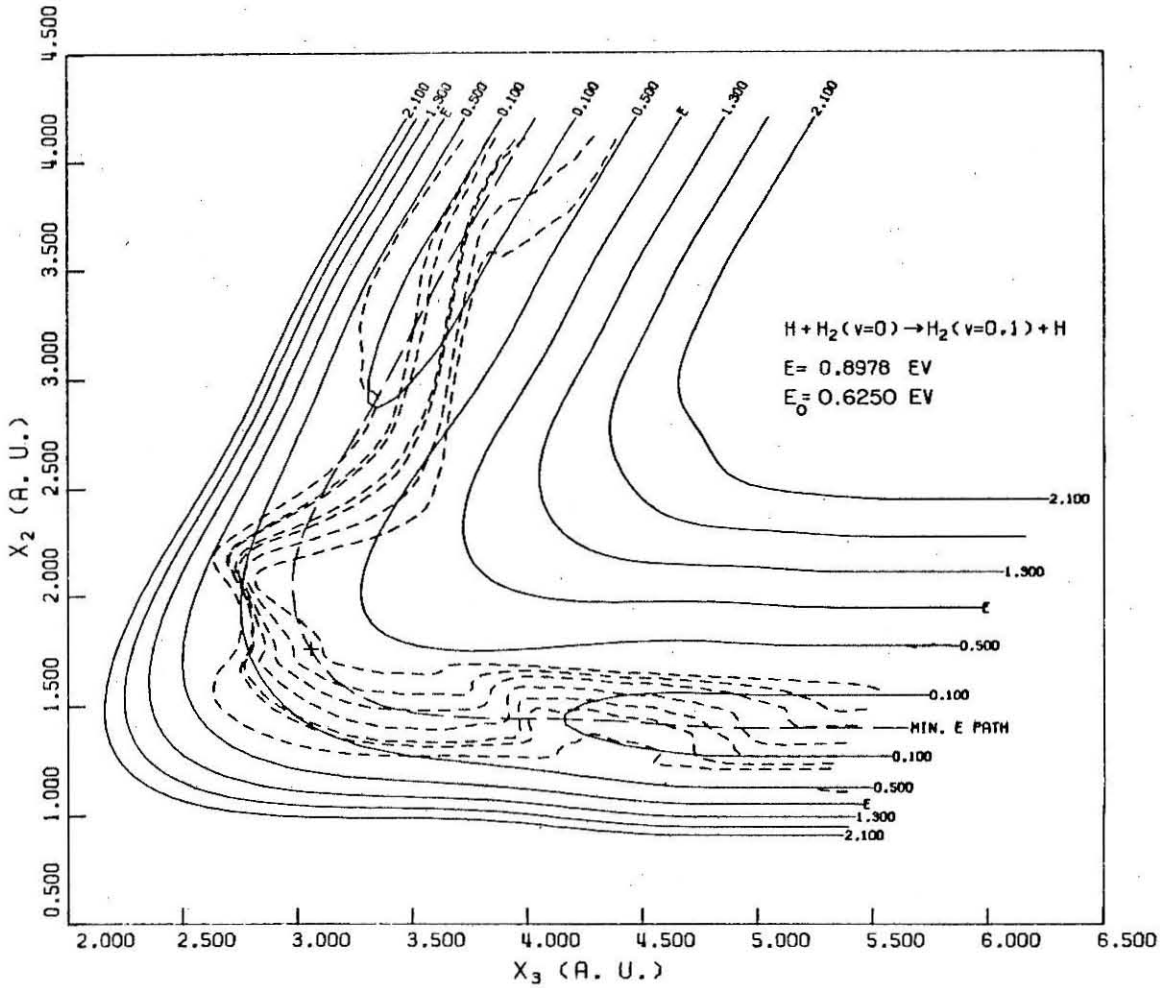
H + H2 (v=0) → H2 (v=0,1) + H
E= 0.8978 EV
E0= 0.6250 EV
2.100
1.300
ε
0.500
0.100
MIN. E PATH
0.100
0.500
ε
1.300
2.100
X2 (A. U.)
X3 (A. U.)
0.500
1.000
1.500
2.000
2.500
3.000
3.500
4.000
4.500
2.000
2.500
3.000
3.500
4.000
4.500
5.000
5.500
6.000
6.500

Figure 11a

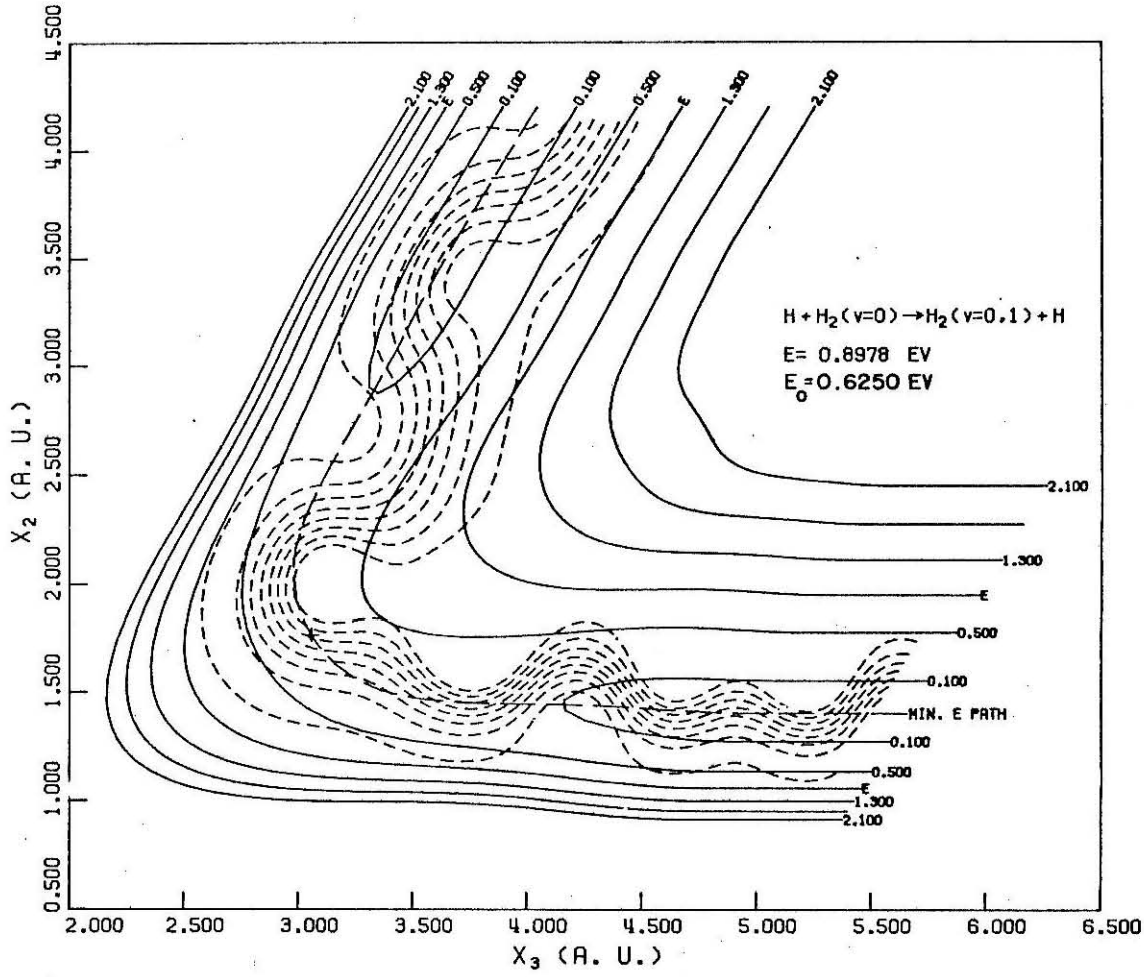
H + H2(v=0) → H2(v=0,1) + H
E= 0.8978 EV
E0=0.6250 EV
2.100
1.300
E
0.500
0.100
MIN. E PATH
0.100
0.500
E
1.300
2.100
X2 (A. U.)
X3 (A. U.)
0.500
1.000
1.500
2.000
2.500
3.000
3.500
4.000
4.500
2.000
2.500
3.000
3.500
4.000
4.500
5.000
5.500
6.000
6.500

Figure 11b

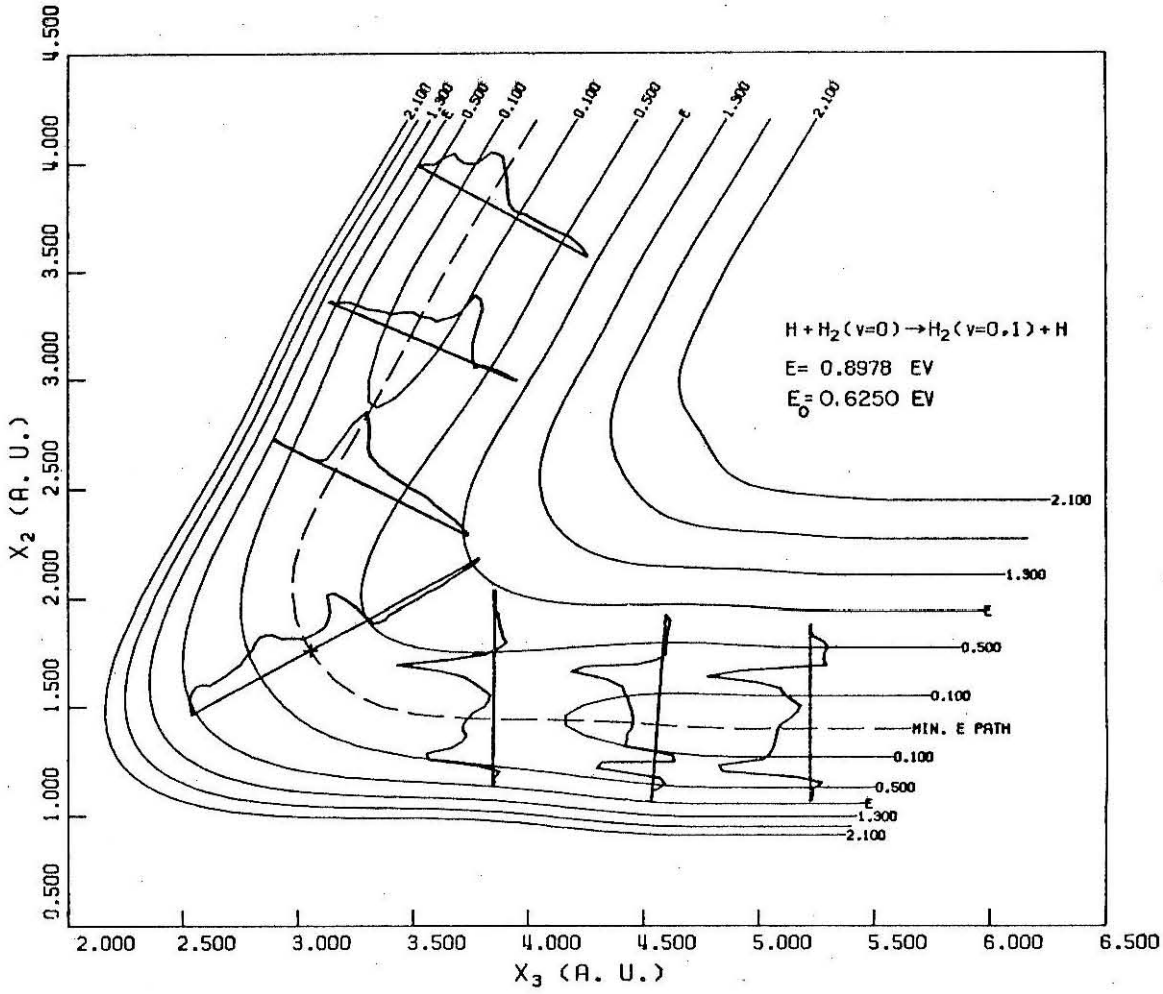
H + H2 (v=0) → H2 (v=0.1) + H
E= 0.8978 EV
E0= 0.6250 EV
2.100
1.900
ε
0.500
0.100
MIN. E PATH
0.100
0.500
ε
1.300
2.100
X2 (A. U.)
X3 (A. U.)
0.500
1.000
1.500
2.000
2.500
3.000
3.500
4.000
4.500
2.000
2.500
3.000
3.500
4.000
4.500
5.000
5.500
6.000
6.500

Figure 12a

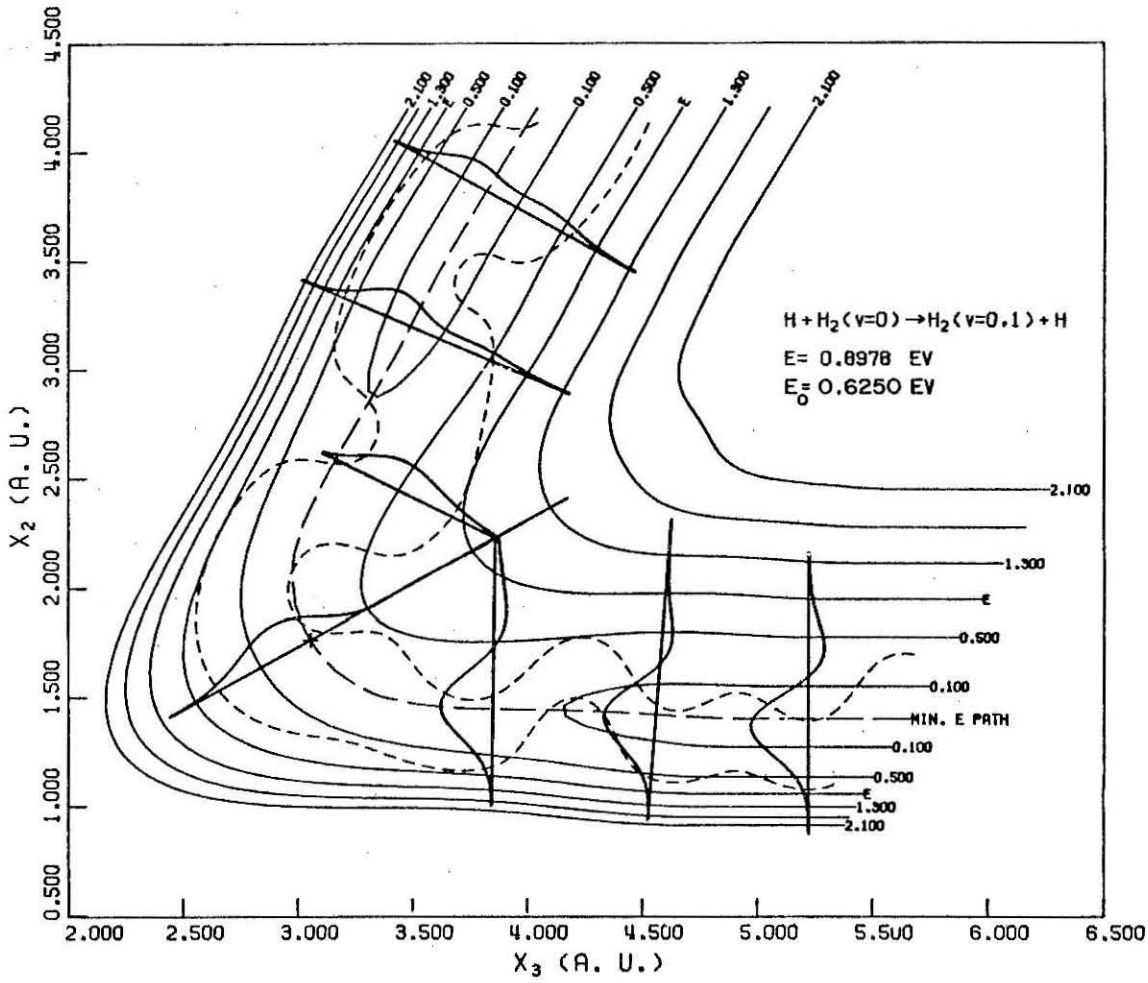
H + H2 (v=0) → H2 (v=0,1) + H
E= 0.8978 EV
E0= 0.6250 EV
2.100
1.300
ε
0.500
0.100
MIN. E PATH
0.100
0.500
ε
1.300
2.100
X2 (A. U.)
X3 (A. U.)
0.500
1.000
1.500
2.000
2.500
3.000
3.500
4.000
4.500
2.000
2.500
3.000
3.500
4.000
4.500
5.000
5.500
6.000
6.500

Figure 12b

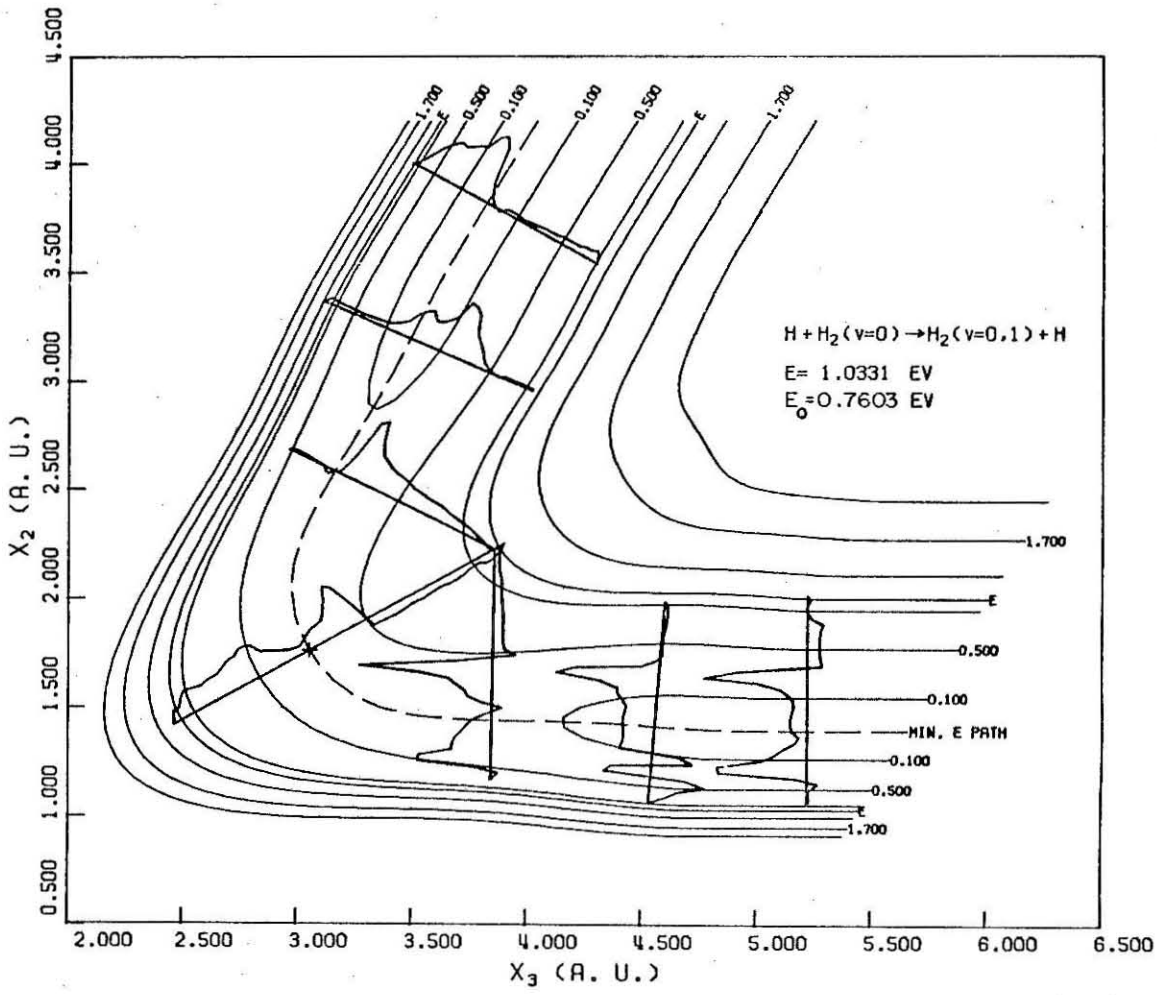
H + H2 (v=0) → H2 (v=0,1) + H
E= 1.0331 EV
E0=0.7603 EV
1.700
E
0.500
0.100
MIN. E PATH
0.100
0.500
E
1.700
X2 (A. U.)
X3 (A. U.)
0.500
1.000
1.500
2.000
2.500
3.000
3.500
4.000
4.500
2.000
2.500
3.000
3.500
4.000
4.500
5.000
5.500
6.000
6.500

Figure 13a

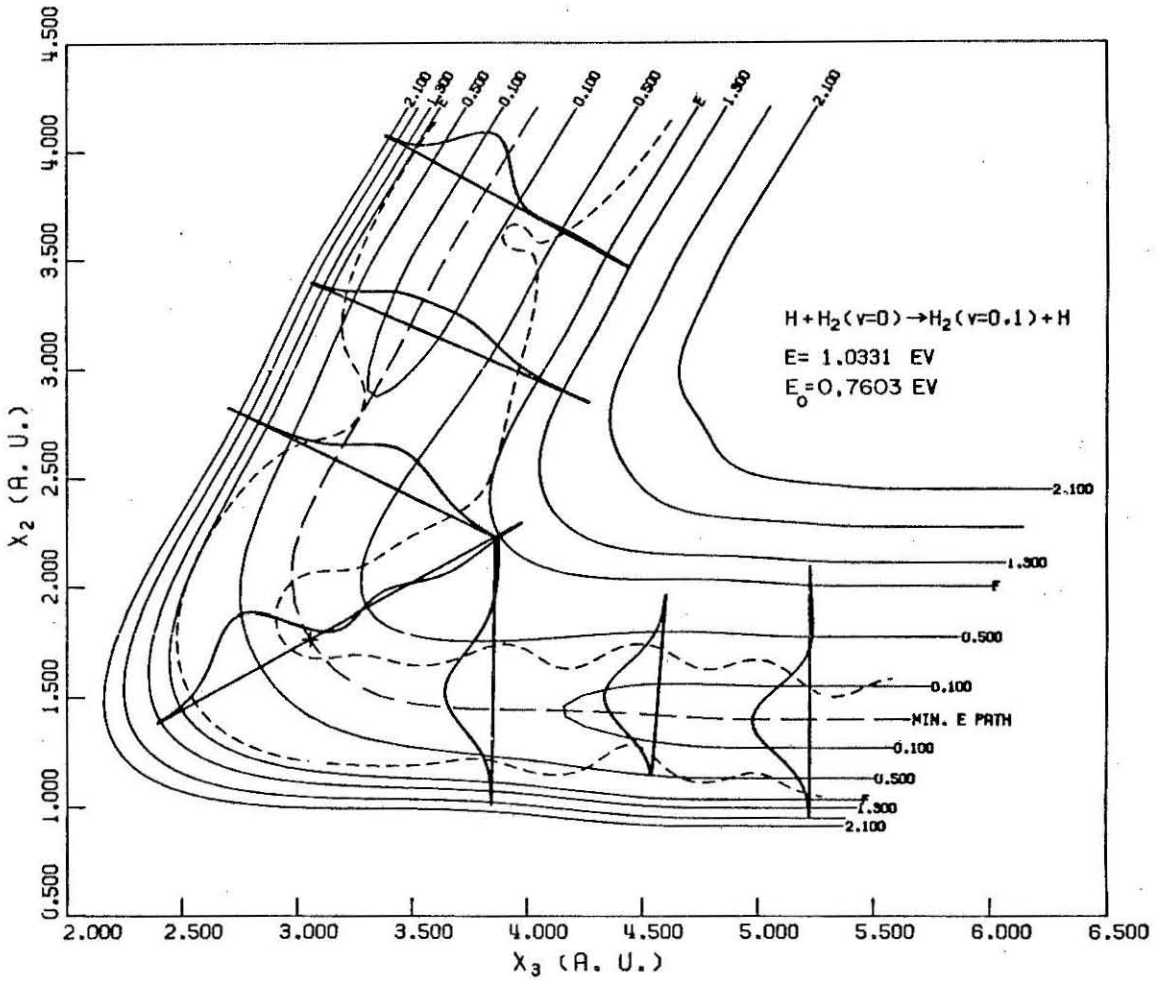
H + H2(v=0) → H2(v=0,1) + H
E= 1.0331 EV
Eo=0,7603 EV
2.100
1.500
E
0.500
0.100
MIN. E PATH
0.100
0.500
1.500
2.100
X2 (A. U.)
X3 (A. U.)
0.500
1.000
1.500
2.000
2.500
3.000
3.500
4.000
4.500
2.000
2.500
3.000
3.500
4.000
4.500
5.000
5.500
6.000
6.500

Figure 13b

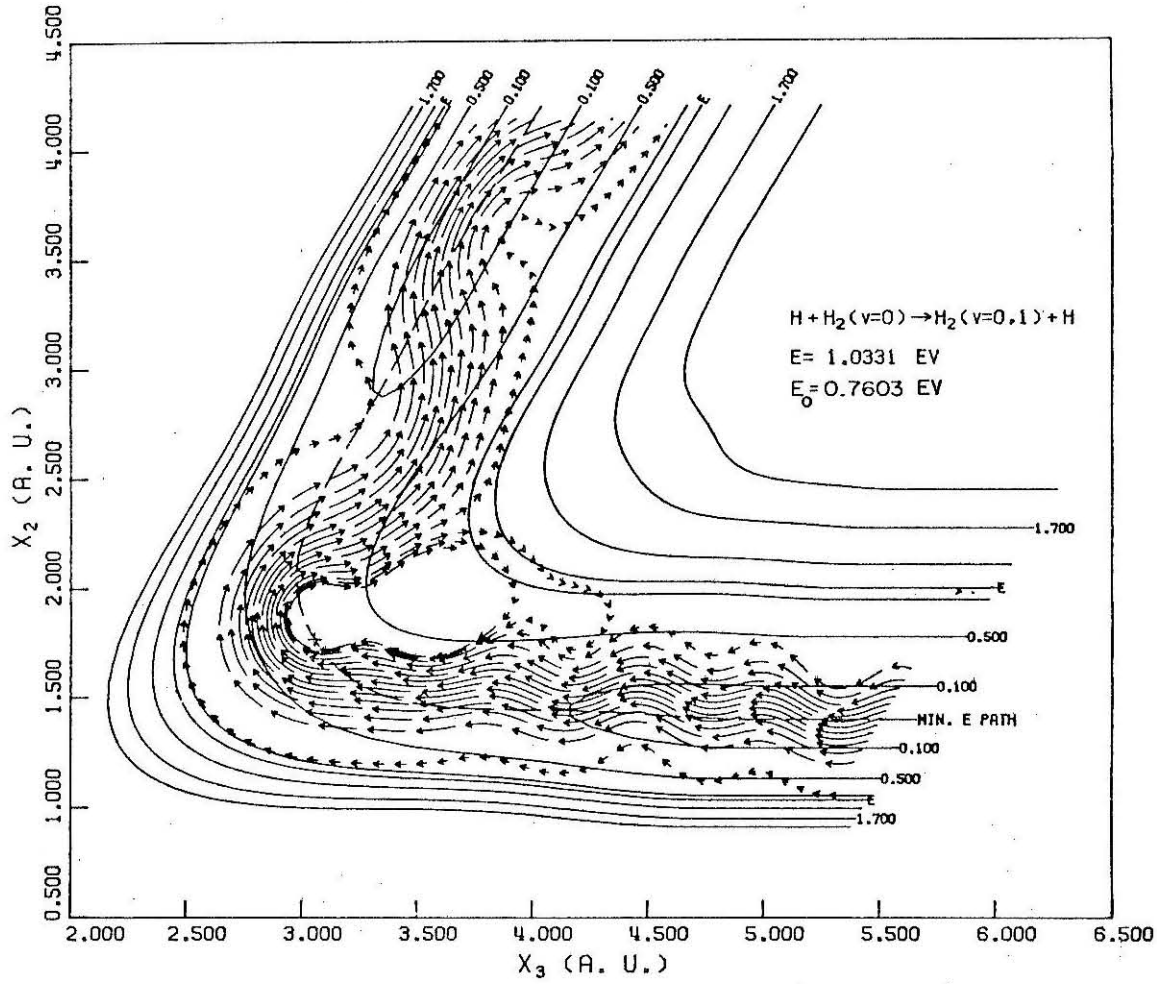
H + H2(v=0) → H2(v=0,1) + H
E= 1.0331 EV
E0= 0.7603 EV
1.700
E
0.500
0.100
MIN. E PATH
X2 (A. U.)
X3 (A. U.)
0.500
1.000
1.500
2.000
2.500
3.000
3.500
4.000
4.500
2.000
2.500
3.000
3.500
4.000
4.500
5.000
5.500
6.000
6.500

Figure 14

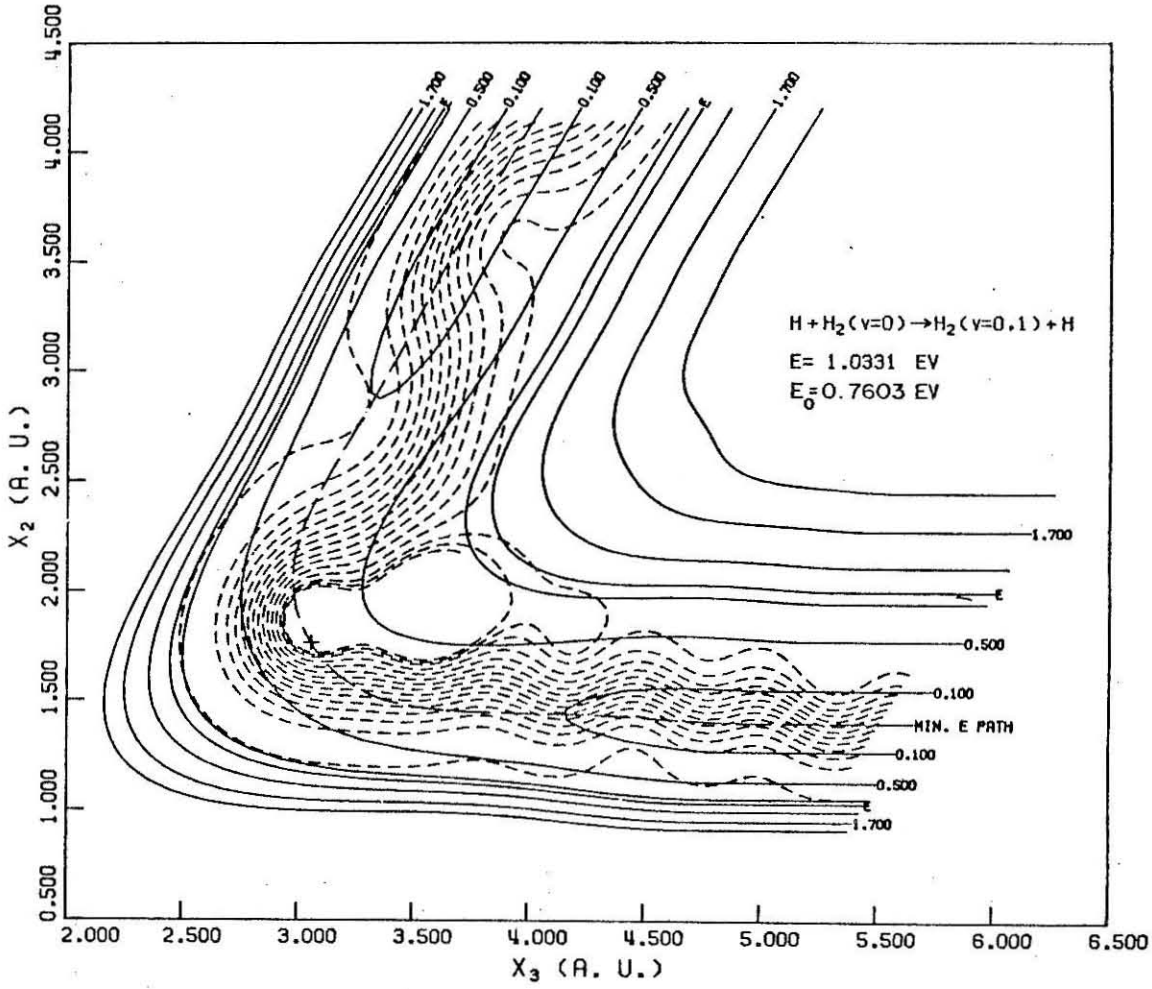
H + H2 (v=0) → H2 (v=0,1) + H
E= 1.0331 EV
E0=0.7603 EV
1.700
E
0.500
0.100
MIN. E PATH
0.100
0.500
E
1.700
X2 (A. U.)
X3 (A. U.)
0.500
1.000
1.500
2.000
2.500
3.000
3.500
4.000
4.500
2.000
2.500
3.000
3.500
4.000
4.500
5.000
5.500
6.000
6.500

Figure 15

I.6 EXACT QUANTUM, QUASI-CLASSICAL AND SEMI-CLASSICAL REACTION PROBABILITIES FOR THE COLLINEAR $F + H_2 \rightarrow FH + H$ REACTION.

Exact Quantum, Quasi-Classical and Semi-Classical Reaction Probabilities for the Collinear $F + H_2 \rightarrow FH + H$ Reaction.*

George C. Schatz,† Joel M. Bowman† and Aron Kuppermann
Arthur Amos Noyes Laboratory of Chemical Physics**
California Institute of Technology, Pasadena, California 91109

(Received

Exact quantum, quasi-classical and semi-classical reaction probabilities and rate constants for the collinear reaction $F + H_2 \rightarrow FH + H$ are presented and compared. The exact quantum results indicate a large degree of population inversion in the FH product with P_{02}^R and P_{03}^R being the dominant reaction probabilities. The energy dependence of these two probabilities at low translational energies are quite different. P_{02}^R shows an effective threshold of 0.005eV which can largely be interpreted as resulting from tunnelling through a vibrationally adiabatic barrier. P_{03}^R has a much larger effective threshold (0.045eV) apparently resulting from dynamical effects. Quasi-classical probabilities for the collinear $F + H_2$ reaction were calculated by both the forward (initial conditions chosen for reagent $F + H_2$) and reverse (initial conditions for product $H + FH$) trajectory

---

*Work supported in part by the United States Air Force Office of Scientific Research.

†Work performed in partial fulfullment of the requirements for the Ph. D. degree in Chemistry at the California Institute of Technology.

**Contribution No.

methods. The results of both calculations correctly indicate that P_{03}^{R} and P_{02}^{R} should be the dominant reaction probabilities. However, the threshold behavior of the quasi-classical forward P_{03}^{R} disagrees strongly with the corresponding exact quantum threshold energy dependence. By contrast, there is good agreement between the reversed trajectory results and the exact quantum ones. The uniform semi-classical results also agree well with the corresponding exact quantum ones indicating that the quasi-classical reverse and the semi-classical methods are preferable to the quasi-classical forward method for this reaction. The important differences between the threshold behavior of the exact quantum and quasi-classical forward reaction probabilities are manifested in the corresponding rate constants primarily as large differences in their activation energies. Additional exact quantum results at higher total energies indicate that threshold effects are no longer important for reactions with vibrationally excited H_2. Resonances play an important role in certain reaction probabilities primarily at higher relative translational energies.

1. Introduction

The reactions $F + H_2$ (D_2, DH) $\rightarrow$ FH (FD) + H (D) have recently been the subject of several experimental studies in which very detailed rate constants and cross sections for these reactions have been measured. Relative rate constants into specific vibrational (and sometimes vibrational-rotational) states of the products have been measured by both infrared chemiluminescence[1] and chemical laser[2] techniques and, quite recently, both methods have been used to study the temperature dependences of these relative rates.[1f, 2e] Angular distributions for specific product vibrational states of the $F + D_2$ reaction have been studied at several incident energies by a crossed molecular beam apparatus.[3] In addition, there exist several (usually indirect) determinations of the overall bulk rate constants for the $F + H_2$ reaction[4] and more recently studies of isotope effects for the $F + H_2$, $F + D_2$, F + HD and F + DH series.[5] A very important application of these reactions has been to the fluorine-hydrogen chemical lasers[2a,6], where $F + H_2 \rightarrow FH + H$ serves as the main pumping reaction.

Complementing these experimental studies have been several quasi-classical trajectory studies on $F + H_2$[7,8,9], $F + D_2$[7,10,11] and F + DH (HD)[7, 9] and one recent semi-classical study on collinear $F + D_2$.[12] The results of the quasi-classical studies have generally been in reasonably good agreement with the detailed rate constants obtained by infrared chemiluminescence and chemical laser experiments but in much poorer agreement with the angular distributions obtained by the molecular beam experiments. There also exists some

disagreement between experiment and the classical calculations on the rotational distribution of the detailed rate constants,[7b] and on isotope effects.[5] Additional theoretical developments have been the characterization of the product state distributions by temperature-like parameters,[13] and the establishment of a relationship between these parameters and certain details of the potential energy surface.[14] All of the classical theoretical studies have employed semi empirical potential energy surfaces.[7-11] An ab initio potential energy surface has also been calculated[15] and the semi-empirical surfaces are in reasonable agreement with it.

Aside from possible defects in the potential energy surface used, the most important sources of disagreement between the quasi-classical trajectory calculations and experiment are: (a) electronically non-adiabatic effects, and (b) quantum dynamical effects. The first problem has been discussed by various investigators[16,17,18] but its importance is not completely understood at present and we shall not consider it here.

In this paper, we study the importance of quantum dynamical effects in the $F + H_2 \rightarrow FH + H$ reaction by comparing the results of accurate quantum mechanical solutions to the Schrödinger equation for the collinear collisions to the results of the corresponding quasi-classical and semi-classical calculations. In the following paper (hereafter referred to as II), we make the analogous study for the $F + D_2$ reaction and also examine exact quantum results for F + HD(DH). Results of our preliminary studies[19,20] indicated that quantum effects were quite important in the collinear $F + H_2$ reaction[19] and, in fact,

the disagreement between the quasi-classical and exact quantum reaction probabilities at low reagent relative translational energies was quite large. In the present paper, we give a more detailed analysis of the reaction probabilities for $F + H_2$ as calculated by four different methods: an exact quantum mechanical solution, the quasi-classical forward and quasi-classical reverse trajectory methods and the uniform semi-classical method. We also present and compare the corresponding rate constants obtained from the results of these four methods. In addition, we examine resonances, tunnelling and energy partitioning in this reaction, and examine the results of exact quantum calculations at total energies for which two vibrational states of the reagent H_2 are accessible.

In all cases, we restrict our considerations to collinear collisions of a fluorine atom with a hydrogen molecule where the two hydrogen atoms are considered to be distinguishable. The resulting cross sections are in the form of dimensionless probabilities of reaction between specific vibrational states of the reagents to form products in specific states and are not directly comparable with experiment (although certain other quantities such as final state distributions can, with caution, be subject to such a comparison. Our justification for studying collinear dynamics lies mainly in its use as a predictive model for the energy release behavior in actual three dimensional collisions[21] and as a testing ground for approximate theories of chemical dynamics.[22] Exact quantum dynamics is currently feasible for many types of collinear reactions and thus the importance of quantum effects in chemical reactions can readily be

established within the collinear restriction. How these quantum effects will be modified in two or three dimensional systems has not yet been fully established but some progress has been made towards obtaining exact quantum solutions to these problems[23] and better converged results will soon be available[24] for the $H + H_2$ coplanar exchange reaction.

In section 2 the potential energy surface used in our calculations is described. In section 3 we compare the quantum, quasi-classical and semi-classical reaction probabilities for $F + H_2$ and in section 4 we compare the corresponding rate constants. Reaction probabilities for $F + H_2$ in the higher total energy range where two reagent vibrational states are open are discussed in section 5 and in section 6 is a short summary.

2. Potential Energy Surface

We used the semi-empirical LEPS potential energy surface of Muckerman[25] (his surface 5). This surface is intermediate in character between his surfaces 2 and 3 of reference 7b and was chosen to optimize agreement between his three dimensional trajectory results and experiment.[7b] Using Muckerman's notation, the parameters describing the extended LEPS surface are D_e (HF) = 6.1229eV, β_e (HF) = 2.2187 Å^{-1}, R_e (HF) = .9170 Å, Δ (HF) = 0.167, D_e (H_2) = 4.7462eV, β_e (H_2) = 1.9420 Å^{-1}, R_e (H_2) = 0.749 Å and Δ (H_2) = 0.106. The exothermicity is 1.3767eV (31.76 kcal/mole) and the barrier height 0.0461eV (1.06 kcal/mole). Figure 1 shows an equipotential contour plot of the collinear surface along with the minimum energy path. The coordinate system for the plot (and for all calculations) is chosen to diagonalize the kinetic energy with a single reduced mass and is defined by:[26]

$$x_1' = \left(\frac{\mu_{F\,HH}}{\mu_{HF}}\right)^{\frac{1}{4}} \left(r_{HF} + \frac{\mu_{HH}}{m_H} r_{HH}\right)$$

$$x_2' = \left(\frac{\mu_{HH}}{\mu_{F,HH}}\right)^{\frac{1}{4}} \left(r_{HH}\right)$$

where r_{HF} is the shorter of the two HF bond distances in the H - H - F linear geometry. The analogous coordinate system appropriate for the product arrangement channel (FH + H) is:

$$z_1' = \left(\frac{\mu_{H,FH}}{\mu_{HF}}\right)^{\frac{1}{4}} \left(r_{HH} + \frac{\mu_{HF}}{m_H}\right)$$

$$z_2' = \left(\frac{\mu_{HF}}{\mu_{H,FH}}\right)^{\frac{1}{4}} \left(r_{HF}\right)$$

These coordinate systems have the advantage over others[27] in that the transformation between the (x_1', x_2') coordinate system appropriate for reagents and the (z_1', z_2') system appropriate for the products, is orthogonal.

Since the vibrational spacing in H_2 is about 12 kcal/mole and that in HF is 11 kcal/mole, four vibrational states of HF are normally accessible for thermal distributions of reagent H_2 due to the exothermicity of the reaction.

3. Quantum, Quasi-Classical and Semi-Classical Reaction Probabilities and Rate Constants for Collinear $F + H_2 \rightarrow FH + H$

3. 1 Exact Quantum Reaction Probabilities

3. 1. 1 Numerical Method

We used the close coupling propagation method of Kuppermann[28] to solve the Schrödinger equation for the collinear system $F + H_2$. The method involves dividing the configuration space depicted in Fig. 1 into different regions and then propagating though a given region in a coordinate system appropriate to that region. In particular, rectangular coordinates were used in the near asymptotic regions appropriate to reagents and products and polar coordinates in the strong interaction region with the origin of the coordinate system chosen in the classically inaccessible plateau area corresponding to dissociation. A basis set of pseudo vibrational eigenfunctions describing motion transverse to the direction of propagation was used for expanding the wave functions. These eigenfunctions were calculated by a finite difference procedure,[29] and the basis set was changed often during the propagation to insure an efficient representation of the wave function. Contributions from continuum vibrational channels are not included in this method. The integration of the coupled Schrödinger equation was done with an Adams-Moulton 4th order predictor -- 4th order corrector method (with a 4th order Runge-Kutta-Gill initiator). The procedure for extracting the probability matrices from the asymptotic solutions is similar to that used by Truhlar and Kuppermann.[22] Convergence of the final reaction probabilities was carefully checked by observing the effect of varying the location of the origin of the polar coordinate

system, location of the end point of the integration,[30] number of closed vibrational channels, number of integration steps, and number of grid points in the finite difference eigenfunction determination. Using 12 to 15 vibrational channels throughout the integration, we obtained a scattering matrix for which unitarity and symmetry were deemed adequate (flux conservation to 0.5% and symmetry to 5% or better) in the reagent translational energy range (relative to $\nu = 0$) $E_0 = 0.0$ to 1.10eV. The computation time for a 13 channel calculation on an IBM 370-158 computer was approximately 32 min. for the initial calculation in which a large amount of energy independent information was stored on disk for subsequent use and 5 min. per energy thereafter.

3. 1. 2. Results

We define the probability of reaction from an initial state ν (of the reagent H_2) to a final state ν' (of the product HF) by the symbol $P^R_{\nu\nu'}$. (This symbol will also be used as a shorthand notation for the phrase "$\nu \rightarrow \nu'$ reactive collision.") The total reaction probability P^R_ν from a given incident state ν is the sum of $P^R_{\nu\nu'}$ over all accessible ν'. The exact quantum (EQ) reaction probabilities P^R_{02}, P^R_{03} and P^R_0 for $F + H_2$ in the translational energy range $E_0 = 0.0$ to 0.4eV are presented in Fig. 2. The reaction probabilities for the transitions P^R_{00} and P^R_{01}, which are also allowed in this E_0 range, are plotted in Fig. 3. We see that P^R_{00} and P^R_{01} have an energy dependence very similar to P^R_{02}, but with much smaller values ($P^R_{00} \simeq 6\times10^{-5}\, P^R_{02}$, $P^R_{01} \simeq 1\times10^{-2}\, P^R_{02}$). As a result, only P^R_{02} and P^R_{03} contribute appreciably to P^R_0 in the energy range con-

sidered. As was pointed out previously,[19] P^R_{02} and P^R_{03} have remarkably different threshold behaviors. We shall define the effective threshold energy E_T for the $v \rightarrow v'$ transition as the difference between the (lowest) energy for which the corresponding $P^R_{vv'}$ is equal to, say, 1% of the maximum value attained by this quantity and the energy at which the $v \rightarrow v'$ process becomes energetically possible. With this definition, P^R_{02} has an effective threshold of 0.005eV while for P^R_{03} (which is energetically forbidden until E_0=0.013eV) E_T is 0.045. Note that while the barrier height is 0.0461eV, the zero point energy of H_2 is 0.268eV, so the transition P^R_{02} is classically allowed even at zero translational energy. Likewise the 0→3 reactive transition is classically allowed as the HF (3) channel opens up at E_0 = 0.013eV. One possible explanation for why the effective threshold of P^R_{02} is greater than zero is that the exchange of energy between motion transverse to the reaction coordinate and that along the reaction coordinate is not efficient (at least in the entrance channel region of configuration space where the saddle point lies). Truhlar and Kuppermann have shown[22] that a more realistic estimate of the effective barrier height in H + H_2 is obtained from vibrationally adiabatic theory. The vibrationally adiabatic barrier (for zero curvature and using the harmonic approximation) for F + H_2 is 0.26eV which is still appreciably larger than the effective quantum threshold energy for P^R_{02} (0.005eV) although it is quite close to the P^R_{02} quasi-classical threshold energy (.025eV) (see section 3.2.2). This difference between the quantum and quasi-classical threshold energies could in part be due to tunnelling through the one dimensional adiabatic barrier, within the framework of an adiabatic description of the quantum dynamics in the neighbor-

hood of the saddle point. In II we shall see that the results for $F + D_2$, F+ HD and F + DH support this conclusion. The high threshold energy for P_{03}^R is not easily explained as resulting from one dimensional adiabatic barrier tunnelling and is probably due to a dynamical effect as will be discussed in section 3. 2. 2.

The sharp spike in the P_{02}^R curve at energies slightly above threshhold is reminiscent of the Feshbach type internal excitation resonances observed in the collinear $H + H_2$ reaction.[31] A discussion of other resonances in the $F + H_2$ reaction is presented in section 5.

Simultaneously with the reactive transition probabilities, we have calculated the nonreactive ones corresponding to the collisions $F + H_2(0) \rightarrow F + H_2(0)$ and $FH(\nu) + H \rightarrow FH(\nu') + H$. The probabilities for the first of these non-reactive processes are simply the difference between unity and the total reaction probability P_0^R (as long as $\nu = 1$ of H_2 is closed). The transition probabilities for the $H + HF(\nu')$ inelastic ($\nu' \neq \nu$) processes are all quite small (generally less than 0.01) up to $E_0 = 0.4$eV and vary relatively slowly with energy. Unitarity of the scattering matrix then forces the elastic probabilities for $H + HF(\nu)$ collisions to be roughly equal to the difference between unity and the probability for the $F + H_2(0) \rightarrow FH(\nu) + H$ reactive process. The behavior of the inelastic transition probabilities for nonreactive H + HF collisions contrasts strongly with the corresponding inelastic transition probabilities for collinear H + FH collisions.[32] In the latter case we find that the probability of an inelastic collision is comparable in magnitude to the elastic transition

probabilities and, in addition, the probabilities of multiquantum jump transitions are often greater than the probabilities of single quantum jump transitions. A more complete discussion of the results for collinear H + FH will be given in ref. 32.

3. 2 Quasi-Classical Reaction Probabilities

3. 2. 1 Method

The classical trajectory calculations were carried out in the same way as in a previous H + H_2 study.[33, 34] The initial phase angle variable for the vibration of the ground state of H_2 was varied uniformly over a grid of typically 100 points in the interval 0 to 2π. The final action number of the product HF was computed for each reactive trajectory and assigned a quantum number by rounding off the action number to the nearest integer. Thus, the transition probability $P^{R}_{0\nu'}$ was defined as the fraction of reactive trajectories with final quantum number ν'.

When this procedure is carried out in the direction F + H_2 (ν=0)→ FH (ν') + H we term the quasi-classical transition probabilities "Quasi-Classical Forward" (QCF). For the reverse reaction the quasi-classical transition probabilities are termed "Quasi-Classical Reverse" (QCR). Quantum mechanically, the forward and reverse probabilities are rigorously equal at the same total energy, but quasi-classically they are not.[20] Therefore, either of the two quasi-classical results, QCF or QCR, could be used to represent the probabilities for the (forward) reactive collisions. Since there is presently no a priori way of deciding which of these two procedures will give results closer to the EQ ones, we have used them both and corresponding results are presented below.

3. 2. 2 Results

In Fig. 4 we plot the QCF and EQ reaction probabilities P_{02}^R, P_{03}^R and P_0^R versus the translational energy E_0, as well as the corresponding exact quantum ones given in Fig. 2. Out of the 100 trajectories, none yielded HF with $\nu = 0$ or 1 (i.e., $P_{01}^R = P_{00}^R = 0$ probably to within 0.01 or less). There are two important points to be noted in comparing the EQ and QCF results. First, both the exact quantum and the quasi-classical results predict roughly the same amount of vibrational excitation in the HF product on the average. Indeed, if we define f_v as the fraction of the total energy which ends up as vibrational energy in the product HF, then in Fig. 5 we see that f_v is roughly 0.81 and nearly independent of E_0 in the QCF results, and fluctuates between 0.66 and 0.89 with an average value of 0.79 in the EQ results. From this, we conclude that the quantum and quasi-classical dynamics agree (on the average) with respect to partitioning of product energy between translational and vibrational degrees of freedom. Second, despite this average agreement, there are very significant differences between the EQ and QCF reaction probabilities particularly with respect to the P_{03}^R threshold and the P_{03}^R / P_{02}^R ratio. In Fig. 6 this ratio is displayed as a function of E_0 for both the EQ and QCF results. As has been pointed out previously,[19] the lack of agreement between the individual transition probabilities P_{02}^R and P_{03}^R can be partially explained as arising from the reasonable but nevertheless arbitrary way of assigning a discrete quantum number to a continuous product vibrational energy. However, the large differences in the energy

dependences of the EQ and QCF $P_{0\nu}^{R}$ (ν=2, 3) suggests that this is probably not the whole explanation and that other significant differences exist between the classical and quantum dynamics in this system. In addition, this arbitrariness in the definition of a product quantum number is not present in the total reaction probabilities P_0^R, yet the differences in magnitude and energy dependence of the EQ and QCF results are still very significant.

In Fig. 7 are plotted the QCR and EQ reaction probabilities P_{02}^{R}, P_{03}^{R} and P_0^R versus E_0. The transition probability P_{02}^{R} is non-zero at zero reagent translational energies. This can occur because of the convention of rounding classical vibrational quantum numbers to the nearest integer.[20, 33, 34]

The QCR results in Fig. 7 are in much better agreement with the quantum probabilities than are the QCF results in Fig. 4. This is true not only of the total reaction probabilities P_0^R, but also of the individual transition probabilities especially P_{03}^{R}. The fact that the threshold behavior of the P_{03}^{R} transition can be described correctly by a quasi-classical method suggests that the 0.045eV effective threshold energy in P_{03}^{R}(EQ) is a dynamical effect related to motion through classically accessible regions of configuration space. The fact that the reverse rather than the forward trajectory method produces the best agreement with the exact quantum results must be regarded as an empirical observation at present. It would be interesting to further analyze the quasi-classical results from the viewpoint of what regions of configuration space are being sampled by the QCR and QCF trajectories and with what velocities, and how

well the current density fields derived from these trajectories agree with the corresponding exact quantum current densities.[35] The good agreement between the QCR and EQ results suggests that the QCR procedure should be applied to a three dimensional trajectory calculation. If the differences between the one dimensional QCR and QCF results are also found in three dimensional calculations, this could be indicative of the presence of important quantum dynamical effects in the three dimensional reaction. Wilkins[36] has completed a three dimensional QCF study of the reaction FH (ν) + H $\rightarrow$ H_2(ν') + F (ν varying from 1 through 6). His results can be considered to be QCR calculations for the reaction F + H_2 (ν') $\rightarrow$ FH (ν) + H. He has also published QCF rate constant calculations[9a] for the latter reaction with $\nu' = 0$. It would be very interesting to compare the corresponding (QCR and QCF) cross sections. Perry et al[37] have recently published a three dimensional comparison of the QCR and QCF cross sections for the endothermic I + H_2 $\rightarrow$ HI + I reaction at one total energy. They found that microscopic reversibility was approximately obeyed at this energy but made no detailed study of the energy dependence of the cross sections and did not investigate threshold effects.

3. 3 Semi-Classical Reaction Probabilities

3. 3. 1 Method

For most energies, uniform semi-classical reaction probabilities were calculated according to the procedure described in reference 34. However, for translational energies E_0 greater than 0.10eV the transition P_{02}^R was computed by a simple analytical continuation technique,[38] similar in spirit to that of Miller.[39] This was necessary in order to obtain a non-vanishing value of this transition probability since in the above energy range, although energetically allowed, it is dynamically forbidden.[34, 39] In addition, it was found that P_{03}^R was ill-determined near threshhold in that a plot of final FH vibrational action number m_f versus initial H_2 vibrational phase angle (q_0) revealed discontinuous behavior for m_f near the value 3.[40, 41] We managed to overcome this difficulty at several energies by doing the semi-classical analysis for the reverse reaction, i.e. $H + HF\ (v = 3) \rightarrow H_2\ (v = 0) + F$.[42] For this reaction, the results were considerable less "ragged" for m_f approximately equal to 0 than they were for the forward reaction at $m_f = 3$. A more complete discussion of this procedure is given in paper II for the $F + D_2$ reaction.

3. 3. 2 Results

The semi-classical reaction probabilities P_{02}^{R} and P_{03}^{R} for $F + H_2$ are presented in Fig. 8 along with the corresponding exact quantum probabilities. In the absence of considering complex-valued trajectories (in complex phase space at complex times), vanishing quasi-classical reaction probabilities implies that the corresponding semi-classical ones also vanish. Therefore, P_{01}^{R} (USC) = P_{00}^{R} (USC) = 0. From the appearance of the reaction probabilities in Fig. 8, we see that the qualitative agreement between the EQ and USC results is quite good. There are large differences between the magnitudes of the USC and EQ probabilities at certain energies, but such differences are not usually too important for the resulting collinear rate constants (see section 4). Of more serious consequence for such rate constants is the small difference between the threshold energies of the P_{02}^{R} curves. As pointed out in section 3. 2. 1., this threshold difference of about 0.020eV could be partly due to an adiabatic tunnelling effect and it may be possible to improve the agreement between the EQ and USC results by using complex trajectories.[43, 44]

3.4 Comparison of EQ, QCF, QCR, and USC Reaction Probabilities

In Figs. 9 and 10 we compare the exact quantum, quasi-classical forward, quasi-classical reverse and semi-classical reaction probabilities P_{02}^R, P_{03}^R and P_0^R for $F + H_2$ as a function of the reagent translational energy. Note that the QCR results resemble the USC ones much more than the QCF results do. Obviously, the USC threshold energy must be larger than or equal to both the QCF and QCR threshold energies. However, we cannot presently put forward an a priori reason that would have permitted us to predict which of the latter two energies is greater nor which of the quasi-classical reaction probabilities should be closer to the USC ones. It is also very interesting to note that the QCR results resemble the EQ ones more than the USC ones do. One should, however, be cautious not to generalize this observation. As shown in paper II, the reverse behavior is found for the $F + D_2$ reaction.

4. EQ, QCF, QCR and USC Rate Constants for $F + H_2$

The detailed $v \rightarrow v'$ rate constant for a one-dimensional bimolecular reaction such as $F + H_2\ (v) \rightarrow FH\ (v') + H$ is defined as

$$k^R_{vv'}\ (T) = \langle\, V_v\ P^R_{vv'}\ (V_v)\,\rangle_T$$
$$= \int_0^\infty f_T\,(V_v)\ V_v\ P^R_{vv'}\ (V_v)\ dV_v\ ,$$

where V_v is the initial relative velocity of the reagents $F + H_2$ (v) and $f_T\ (V_v)$ is the one-dimensional Boltzmann relative velocity distribution function. Changing the integration variable from V_v to the initial relative reagent translational energy E_v this expression becomes[22]

$$k^R_{v\,v'}(T) = \frac{1}{(2\pi\mu_{F,HH}kT)^{\frac{1}{2}}}\left[\int_0^\infty P^R_{vv'}\ (E_v)\ e^{-E_v/RT}\,dE_v\right].$$

Note that for one-dimensional systems, number densities are expressed in molecule/cm so that a bimolecular rate constant has the units cm/(molecule · sec.).

Using the reaction probabilities presented in Fig. 7, we have calculated the rate constants k_{03}^R and k_{02}^R from the EQ, QCF, QCR and USC reaction probabilities. Arrhenius plots of these rate constants are presented in Fig. 11. We see that for k_{03}^R all plots are nearly linear at high temperatures. Because of the extremely small effective threshold energies of P_{02}^R, the Arrhenius plots of k_{02}^R are only linear at low temperature (< 500 K). At high temperature, the temperature dependence of k_{02}^R approaches $T^{\frac{1}{2}}$ which is characteristic of a reaction with zero activation energy. Arrhenius activation energies E_a^{02} and E_a^{03} and pre-exponential factors A_{02} and A_{03}, which were determined by a least squares fit to the 200-400 K results and to the 900-1200 K results, are given in Table I. It is clear from Fig. 11 and Table I that k_{03}^R (QCF) has an activation energy which is significantly lower than the activation energies of k_{03}^R (EQ, QCR or USC). This is an obvious consequence of the different effective threshold energies of the reaction probabilities (Fig. 9) and illustrates how these threshold differences can affect the detailed rate constants. As might be expected from Fig. 9, k_{03}^R (QCR) and k_{03}^R (USC) are in quite good agreement with k_{03}^R (EQ).

The relative agreement among the corresponding three k_{02}^R rate constants is much less satisfactory at low temperatures, the

difference between k_{02}^R (EQ) and k_{02}^R (USC) is mainly determined by the 0.02 eV difference in the threshold energies of the P_{02}^R reaction probabilities. Since P_{02}^R (QCR) has its effective threshold at zero translational energy, k_{02}^R (QCR) has a smaller activation energy than k_{02}^R (EQ) which in turn has a smaller activation energy than k_{02}^R (QCF or USC). The total rate constant k_0^R which is essentially due to the contributions of k_{03}^R and k_{02}^R does not exhibit simple Arrhenius behavior because it is the sum of two Arrhenius expressions which are of equal magnitude near T = 1000 K, but which have quite different activation energies. Note that the experimental activation energy (which is 1.71 kcal/mole)[45] seems to represent an average of the present EQ values of E_a^{02} and E_a^{03}.

In Fig. 10 we plot the ratio k_{03}^R / k_{02}^R as a function of temperature. The large difference between the temperature variation of the QCF ratio and that of the EQ, QCR or USC ratios is again a consequence of the difference in the reaction probabilities in Fig. 9. It is interesting to note that the three dimensional quasi-classical forward trajectory method yields a rate constant ratio which is nearly independent of temperature,[9a] in agreement with the one dimensional QCF results presented here. An experimental measurement of the temperature dependence of k_{03}^R / k_{02}^R[2e] seems to agree reasonably well with the three dimensional QCF result[9a] and consequently disagrees with our EQ result. This may indicate that the strong difference between the activation energies of k_{03}^R and k_{02}^R observed here are largely averaged out in three dimensions. On the other hand, for the $F + D_2$ reaction, the agreement between experiment and the quasi-

classical results is not as consistent as it is for $F + H_2$ (to be discussed in paper II), so it is possible that the averaging process in three dimensions does not completely destroy the important differences between the results of quantum and classical mechanics as reported in this paper.

In contrast to the k_{03}^R / k_{02}^R ratio, k_{02}^R (EQ) / k_{01}^R (EQ) is nearly constant in the temperature range considered here. This agrees with the temperature variations of both the experimental[2e] and three dimensional QCF[9a] results, although the absolute magnitudes of the ratios are quite different (~ 90 for 1-D versus $\sim$ for 3-D). We also found that k_{01}^R (EQ) / k_{00}^R (EQ) is nearly independent of temperature with a value of roughly 210. Therefore k_{01}^R (EQ) and k_{00}^R (EQ) are respectively about 2 and 4 orders of magnitude smaller than k_{02}^R (EQ).

5. Exact Quantum Reaction Probabilities for Vibrationally Excited Reagents

In order to observe the effect of vibrational excitation of the reagent H_2 on the resulting reaction probabilities, we extended the range of our exact quantum calculations to total energies of 1.4 eV. In Fig. 13 we plot P_{02}^R, P_{03}^R and P_{14}^R, the three largest reaction probabilities for $F + H_2$ in this energy range, as a function of energy. There are several important points to note about this figure.

First, the transition P_{14}^R has virtually zero effective threshold energy but otherwise has a similar translational energy dependence to that of P_{03}^R (which has the same $v' - v$ value as P_{14}^R). The absence of a significant threshold energy in P_{14}^R indicates that the dynamical effects responsible for the appearance of a significant effective energy threshold in P_{03}^R are no longer significant in P_{14}^R. This will lead to lower activation energies and higher rates of reaction for reagents which are initially vibrationally excited. The similarity between P_{14}^R and P_{03}^R implies that for the most significant reaction probabilities, an increase in the vibrational energy of the reagent results in a corresponding increase in the vibrational energy of the product. This agrees with experimental observations for $F + D_2$.[1f]

Second, the reaction probabilities P_{03}^R and P_{14}^R have sharp peaks at $E_0 = 0.425$eV and 0.823eV respectively. An analysis of the energy dependence of the scattering matrix elements corresponding to similarly shaped reaction probability curves in the $H + H_2$ collinear reaction[31, 46] showed that narrow peaks (or dips) in the reaction probabilities were the result of the presence of internal excitation

(Feshbach) resonances. These resonances are associated with excitations of virtual states of the intermediate triatomic complex (FHH in the present case). From Fig. 13 we see that the contributions of the direct processes seem to be rather small in regions of energy where the resonance processes are important. This results in only small interference effects between direct and compound state contributions to the scattering amplitude and the resulting reaction probabilities have nearly symmetrical peaks as a function of energy near the resonance energies. The resonance widths are about .01eV and only one non-negligible transition probability seems to show resonant behavior at either of the two resonance energies. There seems to be a correlation between the appearance of an internal excitation resonance and the opening of a specific vibrational state of the product (as in the resonance at 0.823eV, which is close to the opening of the $\nu = 5$ channel in HF at 0.839eV). This indicates a correlation of the resonance state with the reaction products rather than with the reagents or with the transition state. We shall analyze this phenomenon further in paper II when we examine the high energy $F + D_2$ reaction probabilities.

Although the total E in Figure 13 extends to 1.16eV only, we have done calculations up to E = 1.4eV but found all reaction probabilities in this higher energy range to be less than 0.01. This behavior seems to be related to "centrifugal" effects associated to the angle between the x'_1, and z'_1 axes (i.e., the skew angle between the asymptotic portions of the minimum energy path for the potential of Fig. 1) and will be further discussed in paper II.

6. Summary

Many of the dynamical effects presented in this paper will be further examined in paper II to where we will relegate a more extensive summary of quantum effects in the $F + H_2$ reaction. In this paper we have seen that there are very serious differences between the results of quantum and standard quasi-classical mechanics for collinear $F + H_2$, most notably in the energy dependence of the reaction probability P_{03}^{R} near threshold. These differences in the behavior of the reaction probabilities result in important differences in the detailed thermal rate constants. The fact that the quasi-classical forward reaction probabilities and rate constants disagree quite strongly with the exact quantum results is of great significance since nearly all the trajectory studies done to date on this reaction have been of the quasi-classical forward type. For the present reaction, both the quasi-classical methods provide us with more accurate ways of approximating the exact quantum results. This suggests that it might be of interest to use these methods in three dimensions. Indeed, it may be possible to use the results of collinear calculations such as the ones presented here as a guide line when choosing an approximate method for doing three dimensional calculations.

Additional exact quantum results for $F + H_2$ show that threshold effects are no longer important when the reagent H_2 is initially vibrationally excited. The dominant transitions appear to be those which channel additional vibrational energy in the reagents into additional vibrational energy in the products. Internal excitation resonances are found to play an important role in the reaction prob-

abilities at certain translational energies. There seems to be a one to one correspondence between the energy at which a resonance occurs and the energy at which a related product vibrational channel opens.

Acknowledgement

We thank Ambassador College for the use of their computational facilities in most of the work reported here.

TABLE I. Arrhenius Rate Constant Parameters for $F + H_2 \rightarrow FH + H$[(a)]

	Temp. Range	EQ	QCF	QCR	USC
E_a^{02}	200-400 K	.411	.791	.230	.766
E_a^{02}	200-400	2.279	.853	2.596	2.495
A_{02}	200-400	1.620×10^4	2.424×10^4	1.669×10^4	1.486×10^4
A_{03}	200-400	2.667×10^4	2.492×10^4	3.377×10^4	4.621×10^4
E_a^{02}	900-1200	.223	.750	.086	.390
E_a^{03}	900-1200	2.628	1.444	2.869	2.368
A_{02}	900-1200	1.459×10^4	2.558×10^4	1.628×10^4	1.182×10^4
A_{03}	900-1200	4.433×10^4	4.464×10^2	4.689×10^4	4.499×10^4

(a) $k_{oi}(T) = A_{oi} \exp(-E_a^{oi} / RT)$ where E_a^{oi} is in kcal/mole and A_{oi} is in cm/ (molec · sec).

REFERENCES

1. (a) J.C. Polanyi and D.C. Tardy, J. Chem. Phys. 51, 5717 (1969); (b) K.G. Anlauf, P.E. Charters, D.S. Horne, R.G. MacDonald, D.H. Maylotte, J. Polanyi, W.J. Skrlac, D.C. Tardy and K.B. Woodall, J. Chem. Phys. 53, 4091 (1970); (c) N. Jonathan, C.M. Melliar-Smith and D.H. Slater, Mol. Phys. 20, 93 (1971); (d) N. Jonathan, C.M. Melliar-Smith, D. Timlin, and D.H. Slater, Appl. Optics 10, 1821 (1971); (e) N. Jonathan, C.M. Melliar-Smith, S. Okuda, D.H. Slater and D. Timlin, Mol. Phys. 22, 561 (1971); (f) J.C. Polanyi and K.B. Woodhall, J. Chem. Phys. 58, 2298 (1973); (g) H.W. Chang, and D.W. Setser, J. Chem. Phys. 58, 2298 (1973).

2. (a) K.L. Kompa and G.C. Pimentel, J. Chem. Phys. 47, 857 (1967); (b) K.L. Kompa, J.H. Parker and G.C. Pimentel, J. Chem. Phys. 51, 91 (1969); (d) O.D. Krogh and G.C. Pimentel, J. Chem. Phys. 51, 5717 (1969); (e) R.D. Coombe and G.C. Pimentel, J. Chem. Phys. 59, 251 (1973); (f) W.H. Green and M.C. Lin, J. Chem. Phys. 54, 3222 (1971); (g) M.J. Berry, J. Chem. Phys. 59, 6229 (2973).

3. (a) T.P. Schaefer, P.E. Siska, J.M. Parson, F.P. Tully, Y.C. Wong and Y.T. Lee, J. Chem. Phys. 53, 3385 (1970); (b) Y.T. Lee, invited talk at the VII International Conference on the Physics of Electronic and Atomic Collisions, Amsterdam, 1971.

4. See compilations by N. Cohen, Report No. TR-0073(3430)-9, The Aerospace Corporation, El Segundo, Calif. (1972) and Report No. TR-0074(4530)-9, The Aerospace Corporation, El Segundo, Calif. (1974).

5. A. Persky, J. Chem. Phys. 59, 5578 (1973).

6. (a) D.J. Spencer, T.A. Jacobs, H. Mirels and R.W. F. Gross, Int. J. Chem. Kinetics 1, 493 (1969); (b) T.F. Deutsch, Appl. Phys. Lett, 10, 234 (1967); (c) S.N. Suchard, R.L. Kerber, G. Emanuel and J.S. Whittier, J. Chem. Phys. 57, 5065 (1972) and references therein.

7. (a) J.T. Muckerman, J. Chem. Phys. 54, 1155 (1971); (b) ibid., 56, 2997 (1972).

8. (a) R.L. Jaffe and J.B. Anderson, J. Chem. Phys. 54, 2224 (1971); (b) ibid., 56, 682 (1972), (c) R.L. Jaffe, J.M. Henry and J.B. Anderson, J. Chem. Phys. 59, 1128 (1973).

9. (a) R.L. Wilkins, J.Chem. Phys. 56, 912 (1972); (b) R.L. Wilkins, J. Phys. Chem. 77, 3081 (1973).

10. N.C. Blais and D. G. Truhlar, J. Chem. Phys. 58, 1090 (1973).

11. A. Ding, L. Kirsch, D. Perry, J. Polanyi, J. Schreiber, Disc. Far. Soc., in press.

12. P.A. Whitlock and J.T. Muckerman, to be published.

13. (a) A. Ben-Shaul, R.D. Levine, and R.B. Bernstein, Chem. Phys. Lett. 15, 160 (1972); (b) A. Ben-Shaul, R.D. Levine, R.B. Bernstein, J. Chem. Phys. 57, 5427 (1972);

(c) A. Ben-Shaul, G. L. Hofacker, and K. L. Kompa, J. Chem. Phys. 59, 4664 (1973).

14. G. L. Hofacker and R. D. Levine, Chem. Phys. Lett. 15, 165 (1972), also unpublished results.

15. (a) C. F. Bender, S. V. O'Neil, P. K. Pearson and H. F. Schaefer III, Science, 176, 1412 (1972); (b) C. F. Bender, P. K. Pearson, S. V. O'Neil and H. F. Schaefer III, J. Chem. Phys. 56, 4626 (1972).

16. D. G. Truhlar, J. Chem. Phys. 56, 3189 (1972).

17. J. T. Muckerman and M. D. Newton, J. Chem. Phys. 56, 3191 (1972)

18 J. C. Tully, J. Chem. Phys. 60, 3042 (1974).

19. G. C. Schatz, J. M. Bowman and A. Kuppermann, J. Chem. Phys. 58, 4023 (1973).

20. J. M. Bowman, G. C. Schatz, A. Kuppermann, Chem. Phys. Lett. 24, 378 (1974).

21. (a) P. J. Kuntz, E. M. Nemeth, J. C. Polanyi, S. D. Rosner, and C. E. Young, J. Chem. Phys. 44, 1168 (1966); (b) J. C. Polanyi and W. H. Wong, J. Chem. Phys. 51, 1439 (1969).

22. D. Truhlar and A. Kuppermann, J. Chem. Phys. 56, 2232 (1972).

23. (a) R. Saxon and J. Light, J. Chem. Phys. 56, 3874 (1972); (b) ibid., 56, 3885 (1972); (c) G. Wolken and M. Karplus, Abstracts of Papers, VII International Conference on the Physics of Electronic and Atomic Collisions, Amsterdam (1974).

24. A. Kuppermann, G. Schatz and M. Baer, to be published.

25. J.T. Muckerman (private communication).

26. L.M. Delves, Nuclear Phys. 20, 275 (1960).

27. G. Glasstone, K. Laidler and H. Eyring, Theory of Reaction Rates, McGraw Hill, 1941, p. 101; M. Karplus and K. Tang, J. Chem. Phys. 50, 1119 (1970).

28. (a) A. Kuppermann, Potential Energy Surfaces in Chemistry, ed. W.A. Lester (University of California at Santa Cruz, August 1970) pp. 121-129; (b) Abstracts of papers, VII International Conference on the Physics of Electronic and Atomic Collisions, Amsterdam, 1971.

29. D.G. Truhlar, J. Comp. Phys. 10, 123 (1972).

30. The reaction probabilities were found to be independent of the location of the endpoints of the integrations in each arrangement channel before the potential had completely reached its asymptotic value. However, the translational energies computed at the points of termination of the integrations were slightly smaller than their correct asymptotic values. The results reported here have been corrected by the difference (less than .0002eV).

31. G.C. Schatz and A. Kuppermann, J. Chem. Phys. 59, 964 (1973).

32. G.C. Schatz and A. Kuppermann, to be published.

33. J.M. Bowman and Aron Kuppermann, Chem Phys. Lett. 12, 1 (1972).

34. J.M. Bowman and Aron Kuppermann, J. Chem. Phys. 59, 6524 (1973).

35. A. Kuppermann, J.T. Adams and D.G. Truhlar, Abstracts of Papers, Eighth International Conference on the Physics of Electronic and Atomic Collisions, edited by B.C. Cobic and M.V. Kurepa, Belgrade (1973) p. 149.

36. R.L. Wilkins, J. Chem. Phys. 58, 3038 (1973).

37. D.S. Perry, J.C. Polanyi and C.W. Wilson, Chem. Phys. Lett. 24, 484 (1974).

38. J.M. Bowman, unpublished Ph.D. Thesis, California Institute of Technology, 1974.

39. W.H. Miller, Chem. Phys. Lett. 4, 431 (1970); J. Chem Phys. 53, 3578 (1970).

40. C.C. Rankin and W.H. Miller, J. Chem. Phys. 55, 3150 (1971).

41. J.T. Muckerman (private communication) has also found similar statistical behavior for the F + D_2 reaction.

42. This procedure is obviously valid if the function $m_f(q_o)$ is differentiable for both the forward and reverse trajectories since under these conditions, semi-classical reaction probabilities (contrarily to quasi-classical ones) rigorously obey microscopic reversibility.[32] As a result, when one of these $m_f(q_o)$ is differentiable and the other not, it is reasonable to associate the semi-classical reaction probability of both the forward and reverse reactions to the differentiable $m_f(q_o)$.

43. W.H. Miller and T.F. George, J. Chem. Phys. 56, 5668 (1972); J. Chem. Phys. 57, 2458 (1972).

44. For the $H + H_2$ reaction, the complex trajectory method yields reaction probabilities differing by less than 30% from the exact quantum results for energies less than the barrier (ref. 32).

45. G.C. Fettis, J.H. Knox and A.F. Trotman-Dickenson, J. Chem. Soc. 1064 (1960).

46. R.D. Levine and S.F. Wu, Chem. Phys. Lett. 11, 557 (1971).

Figure Captions

1. Equipotential contour plot of the FH_2 collinear potential energy surface used in all calculations reported here. Energies given are relative to the minimum in the H_2 diatomic potential curve. Coordinate system is defined in text. Heavy line denotes the minimum energy path with saddle point indicated by a cross.

2. Exact quantum reaction probabilities for collinear $F + H_2$ as a function of relative translational energy E_0 and total energy E (relative to minimum in H_2 diatomic potential energy curve). (a) Total reaction probability P_0^R from $v = 0$ of H_2 (b) Reaction probabilities P_{02}^R and P_{03}^R (defined in text). Vertical arrow in abscissa indicates the energy at which $v = 3$ of HF becomes accessible.

3. Exact quantum reaction probabilities P_{01}^R and P_{00}^R (similar to Fig. 2).

4. Quasi-classical forward and exact quantum reaction probabilities for $F + H_2$: (a) P_0^R, (b) P_{02}^R and P_{03}^R. Dashed line indicates QCF results with their associated statistical errors indicated by vertical bars. Solid line indicates EQ results (as in Fig. 2).

5. Fraction (f_v) of the total reagent energy (in excess of product zero point energy) which ends up as vibrational energy in the product HF as a function of the reagent translational energy E_0 and total energy E. Solid line indicates EQ results and dashed line QCF results. Other notation analogous to Fig. 2.

6. Ratio of reaction probabilities P_{03}^R / P_{02}^R versus translational energy E_0 and total energy E. Solid line indicates EQ results and dashed line QCF results. Other notation analogous to Fig. 2.

7. Quasi-classical reverse and exact quantum reaction probabilities for F + H_2: (a) P_0^R, (b) P_{02}^R and P_{03}^R. Dashed line indicates QCR results with their associated statistical errors indicated by vertical bars. Solid line indicates EQ results (as in Fig. 2).

8. Uniform semi-classical and exact quantum reaction probabilities for F + H_2: (a) P_0^R, (b) P_{02}^R and P_{03}^R. Dashed line indicates USC results, solid line EQ results as in Fig. 2.

9. EQ (solid), QCF (short dash), QCR (dash dot) and USC (long dash) reaction probabilities P_{03}^R (a) and P_{02}^R (b) for F + H_2 (from Figs. 2, 4, 7-8).

10. EQ (solid), QCF (short dash), QCR (dash dot) and USC (long dash) total reaction probability P_0^R for F + H_2 (from Figs. 2, 4, 7-8).

11. Arrhenius plot of EQ (solid), QCF (short dash), QCR (dash dot) and USC (long dash) rate constants for F + H_2: (a) k_{02}^R, (b) k_{03}^R.

12. Ratios of rate constants k_{03}^R / k_{02}^R for F + H_2 as a function of temperature. EQ (solid), QCF (short dash), QCR (dash dot), and USC (long dash).

13. Exact quantum reaction probabilities P_{02}^R, P_{03}^R and P_{14}^R for F + H_2 at translational energies higher than those in Fig. 2. Arrows near E_0 = 0.44eV and 0.84eV indicate the opening of ν = 4 and 5 respectively of HF while that at 0.51eV indicates the energy E_0 at which ν = 1 of H_2 becomes accessible.

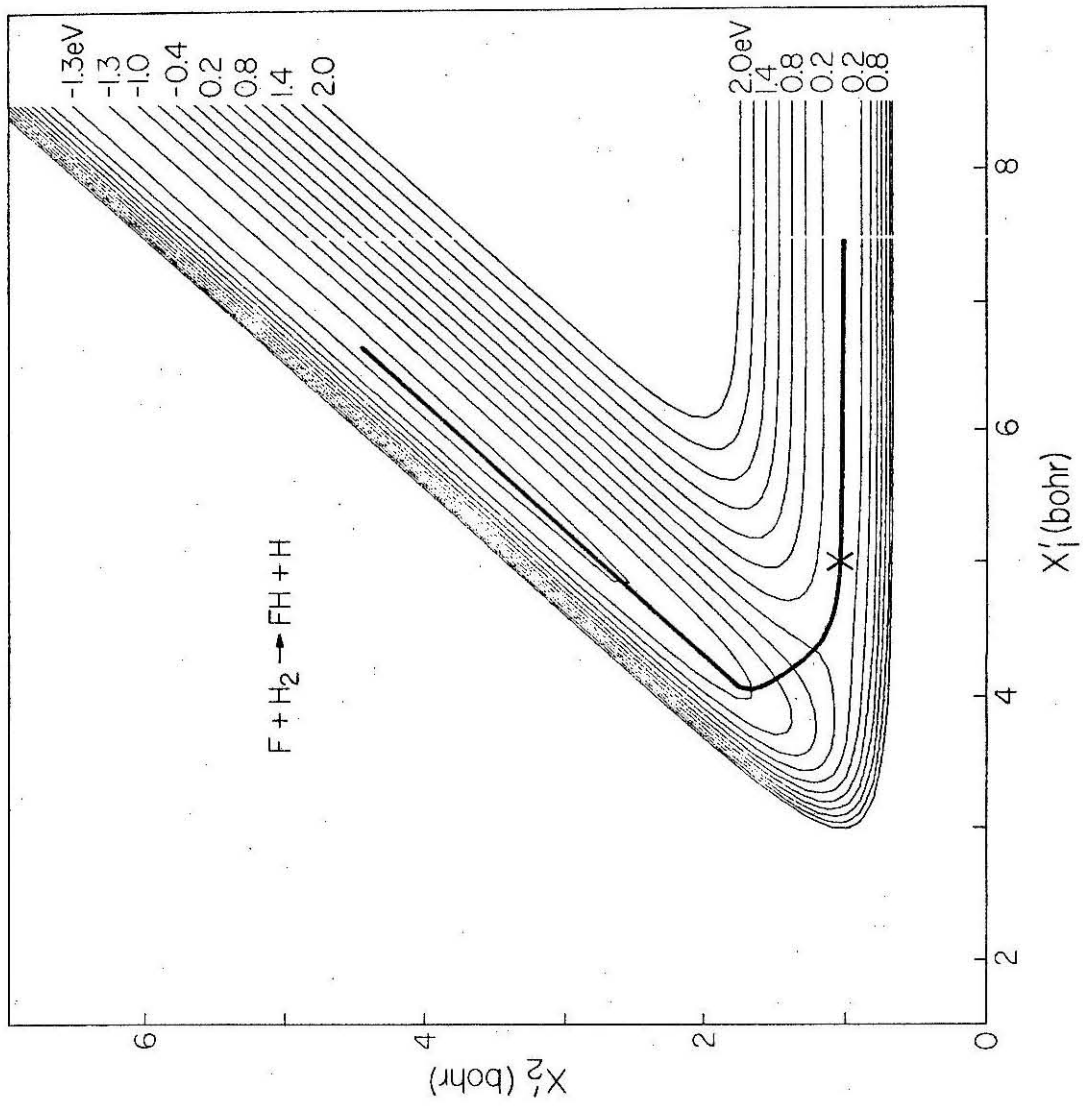
-1.3eV
-1.3
-1.0
-0.4
0.2
0.8
1.4
2.0
2.0eV
1.4
0.8
0.2
0.2
0.8
F + H2 → FH + H
X'2 (bohr)
X'1 (bohr)
0
2
4
6
8

Figure 1

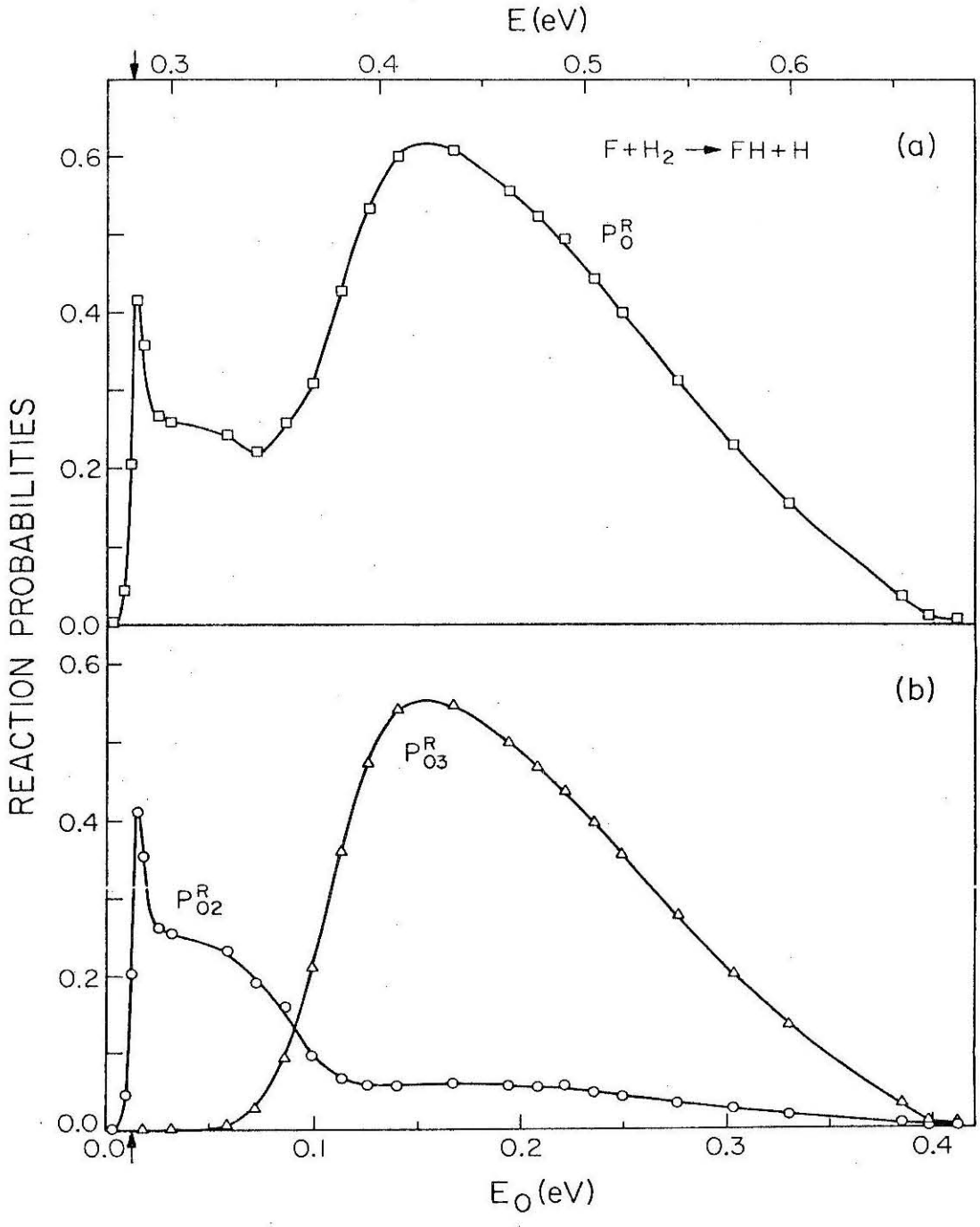
E (eV)
0.3
0.4
0.5
0.6
F + H2 → FH + H
(a)
P0R
REACTION PROBABILITIES
0.6
0.4
0.2
0.0
(b)
P03R
P02R
0.0
0.1
0.2
0.3
0.4
E0 (eV)

Figure 2

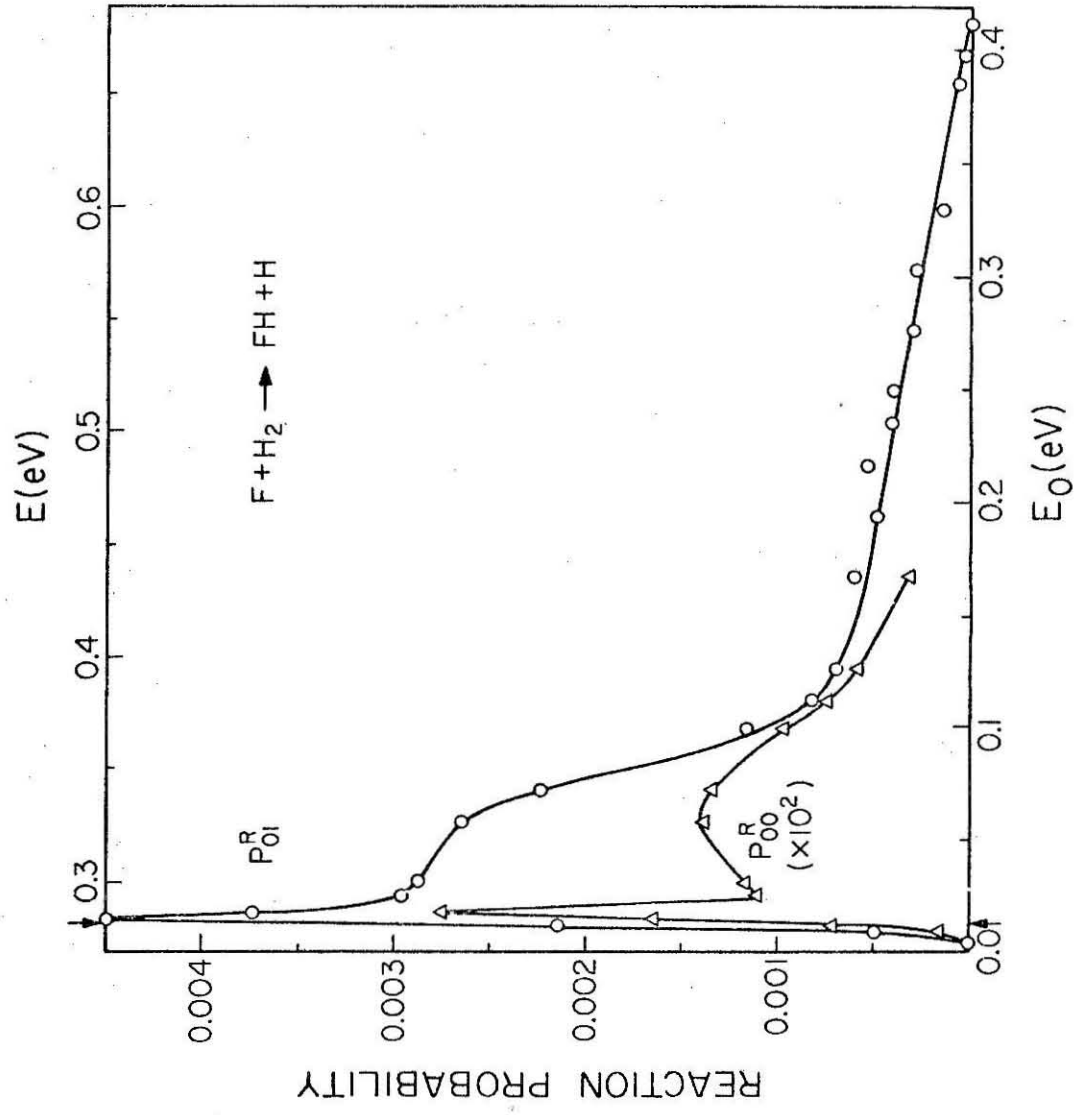
E(eV)
0.3
0.4
0.5
0.6
F+H2 → FH+H
P^R_01
P^R_00 (×10^2)
0.004
0.003
0.002
0.001
0.0
REACTION PROBABILITY
0.1
0.2
0.3
0.4
E0(eV)

Figure 3

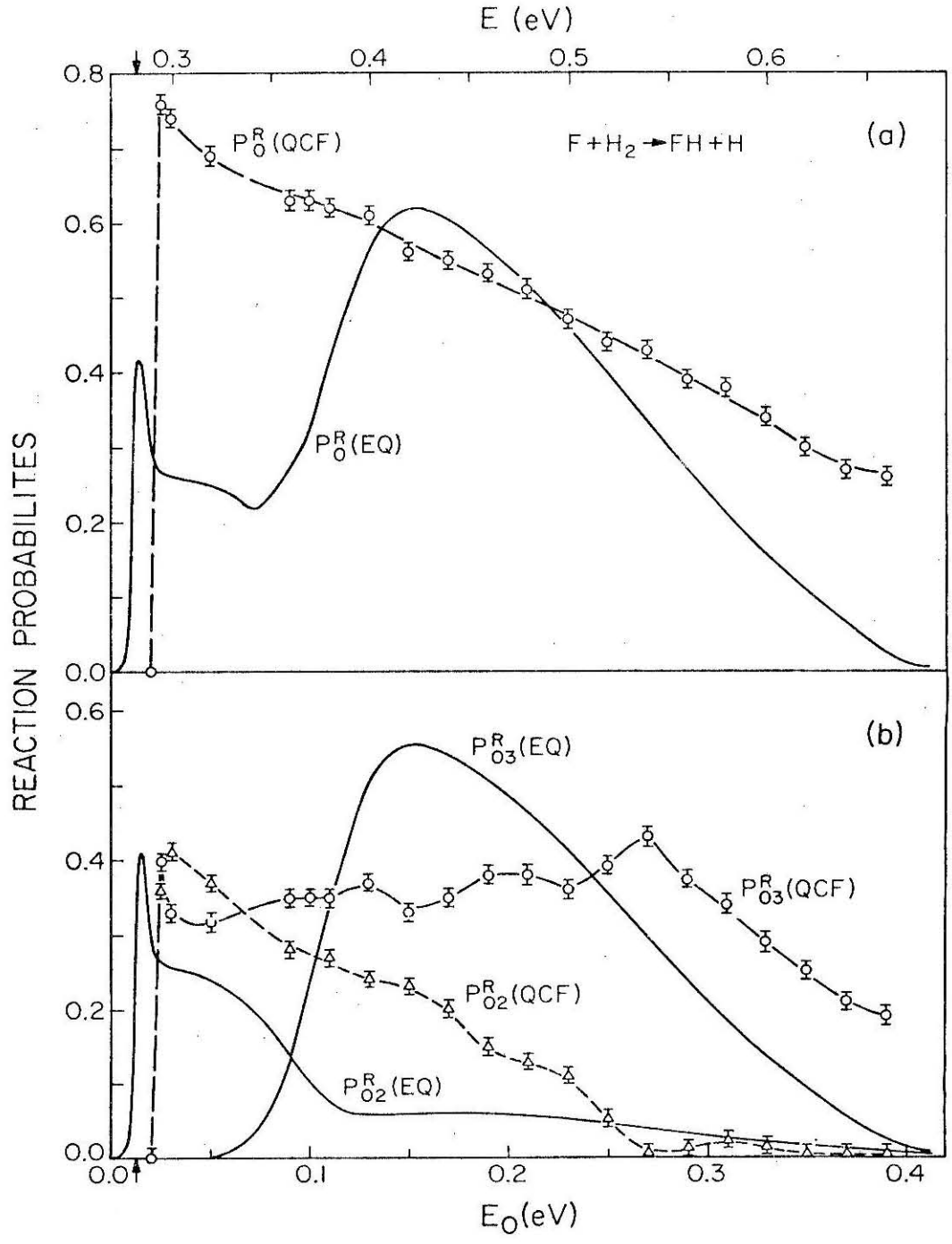
E (eV)
0.3
0.4
0.5
0.6
REACTION PROBABILITIES
P_0^R(QCF)
F+H$_2$→FH+H
(a)
P_0^R(EQ)
(b)
P_{03}^R(EQ)
P_{03}^R(QCF)
P_{02}^R(QCF)
P_{02}^R(EQ)
E_0(eV)

Figure 4

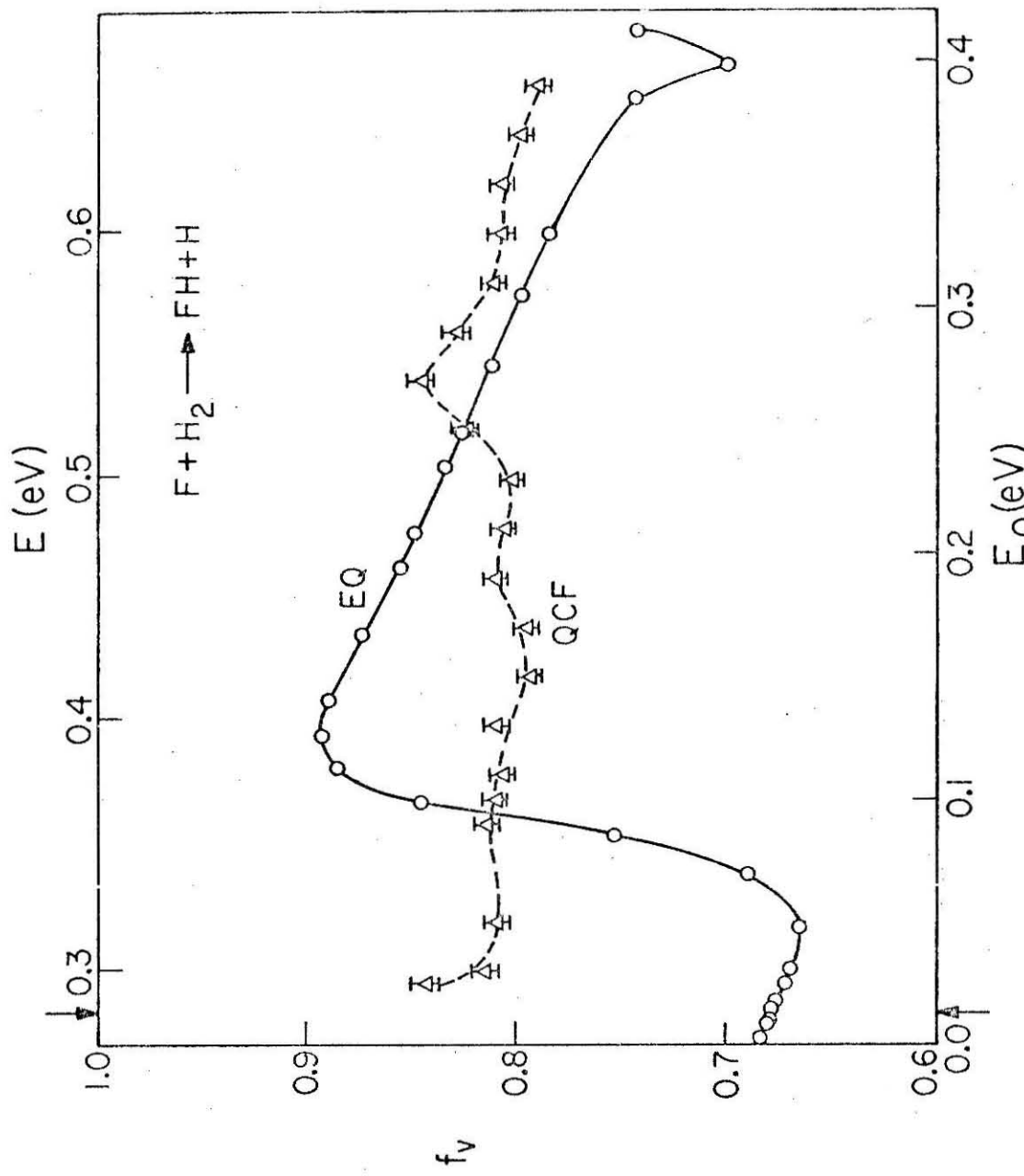

Figure 5

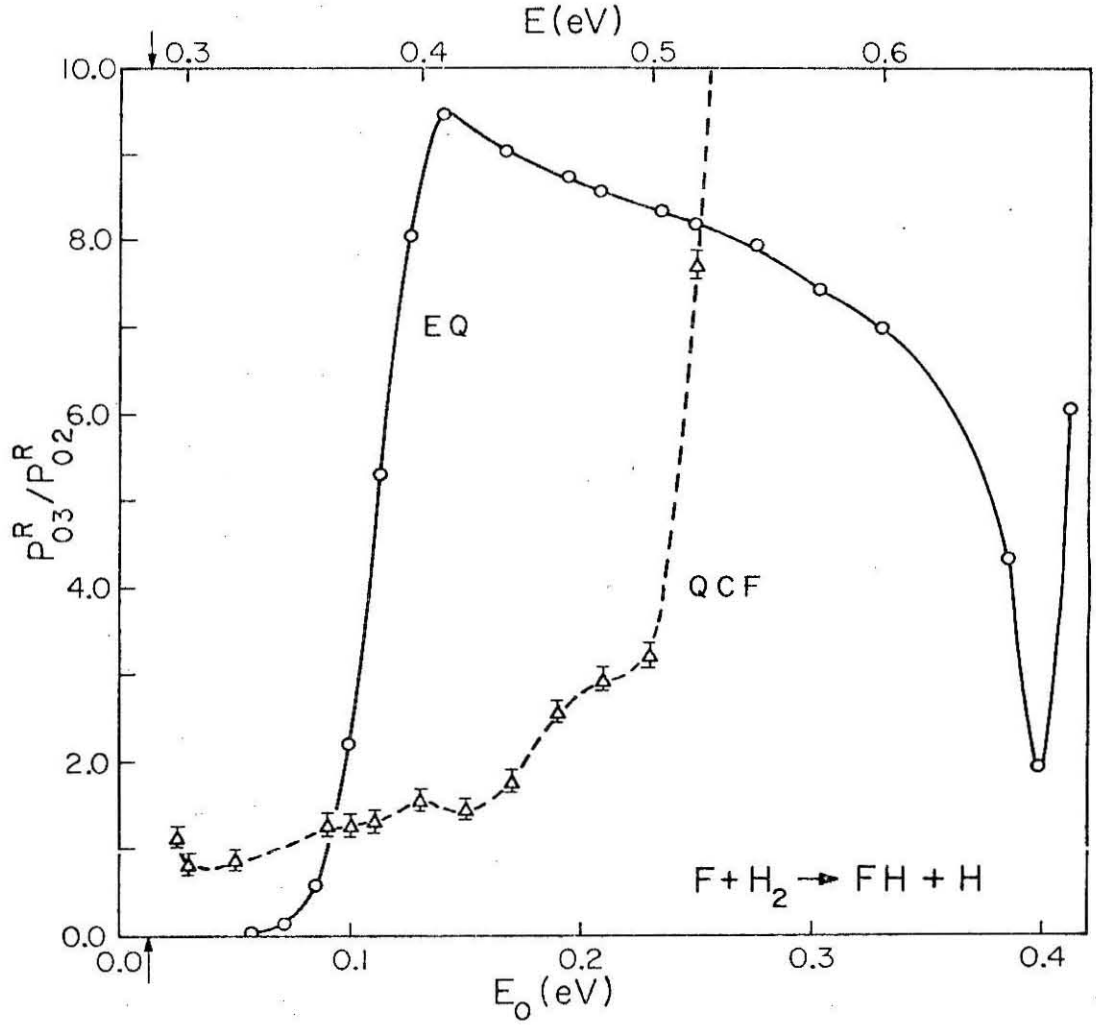
E(eV)
0.3
0.4
0.5
0.6
10.0
8.0
6.0
4.0
2.0
0.0
P^R_{03}/P^R_{02}
EQ
QCF
$F + H_2 \rightarrow FH + H$
0.0
0.1
0.2
0.3
0.4
E_0 (eV)

Figure 6

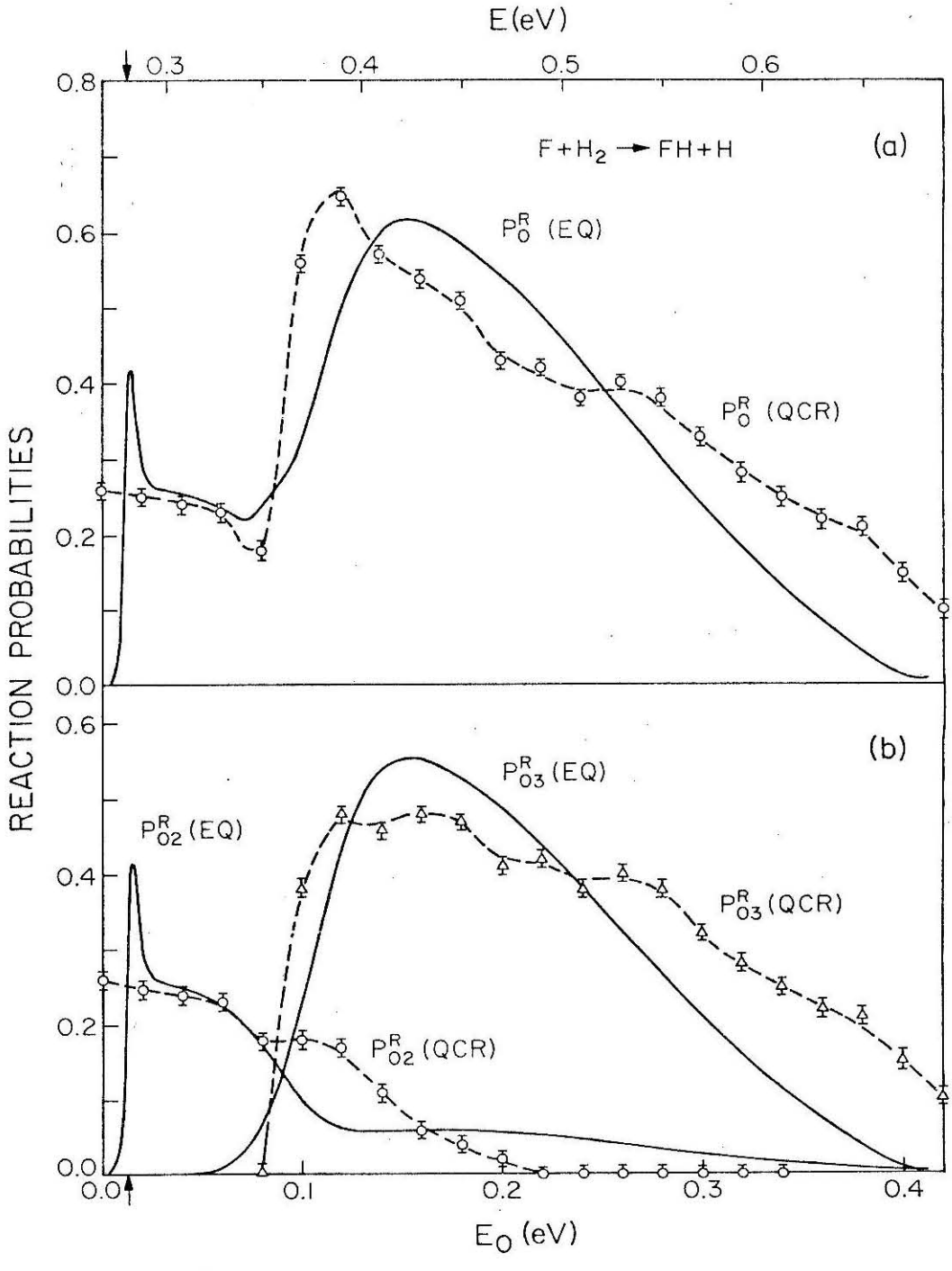
E(eV)
0.3
0.4
0.5
0.6
F+H2 → FH+H
(a)
P0R (EQ)
P0R (QCR)
REACTION PROBABILITIES
(b)
P03R (EQ)
P02R (EQ)
P03R (QCR)
P02R (QCR)
0.0
0.1
0.2
0.3
0.4
E0 (eV)

Figure 7

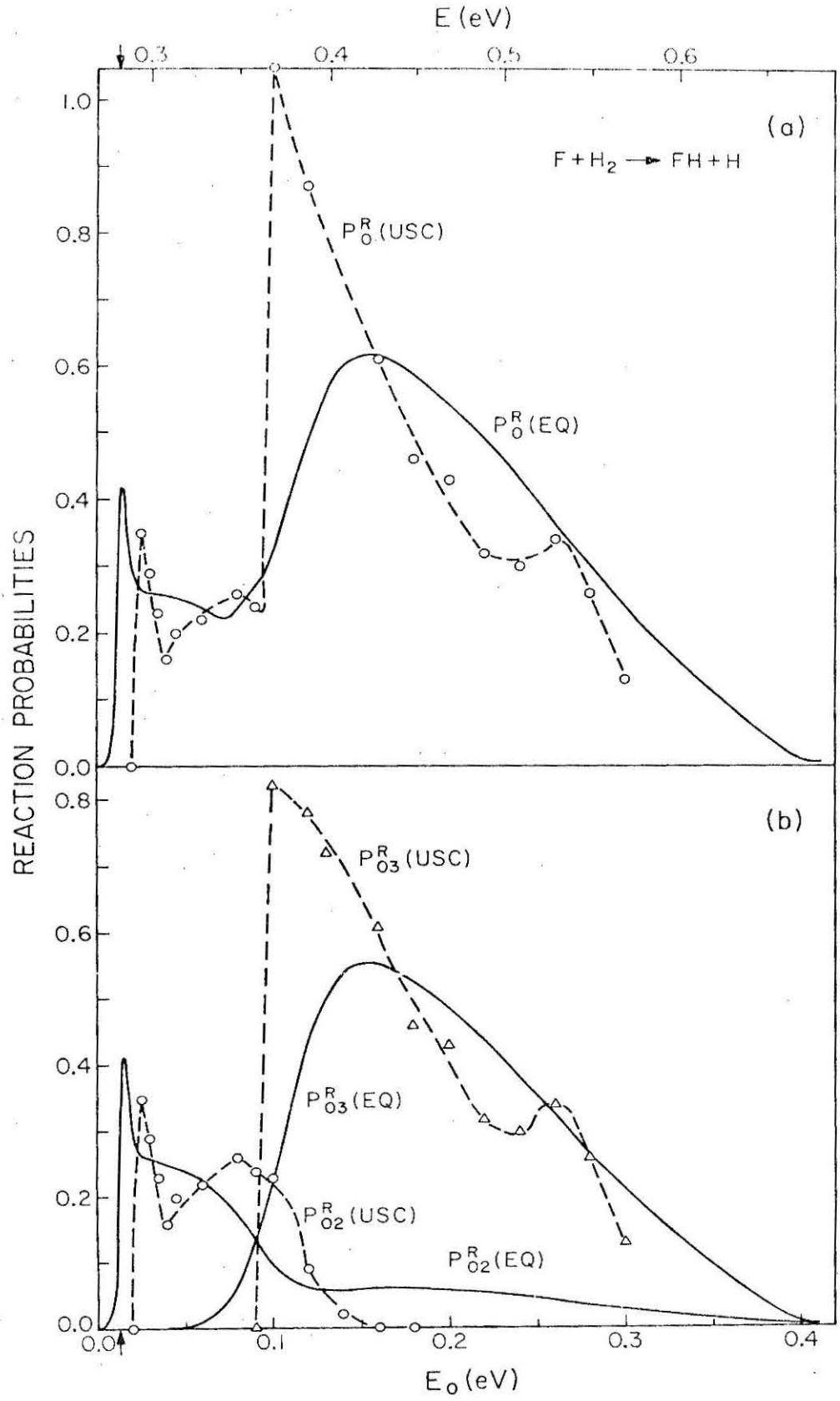
E (eV)
0.3
0.4
0.5
0.6
(a)
F + H2 → FH + H
P0R(USC)
P0R(EQ)
REACTION PROBABILITIES
(b)
P03R(USC)
P03R(EQ)
P02R(USC)
P02R(EQ)
0.0
0.1
0.2
0.3
0.4
E0 (eV)

Figure 8

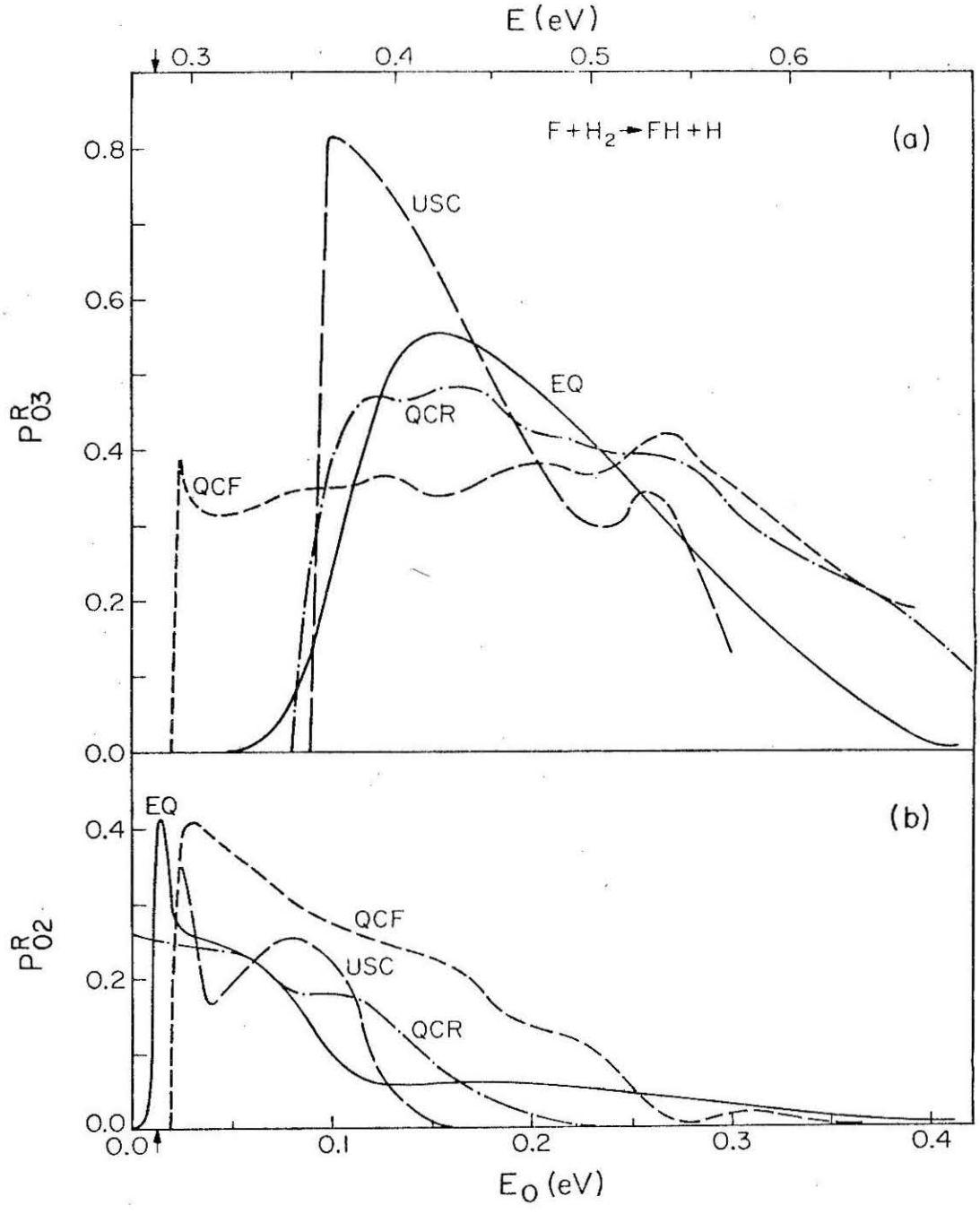
E (eV)
0.3
0.4
0.5
0.6
F+H2→FH+H
(a)
USC
EQ
QCR
QCF
P03R
0.0
0.2
0.4
0.6
0.8
(b)
EQ
QCF
USC
QCR
P02R
0.0
0.1
0.2
0.3
0.4
E0 (eV)

Figure 9

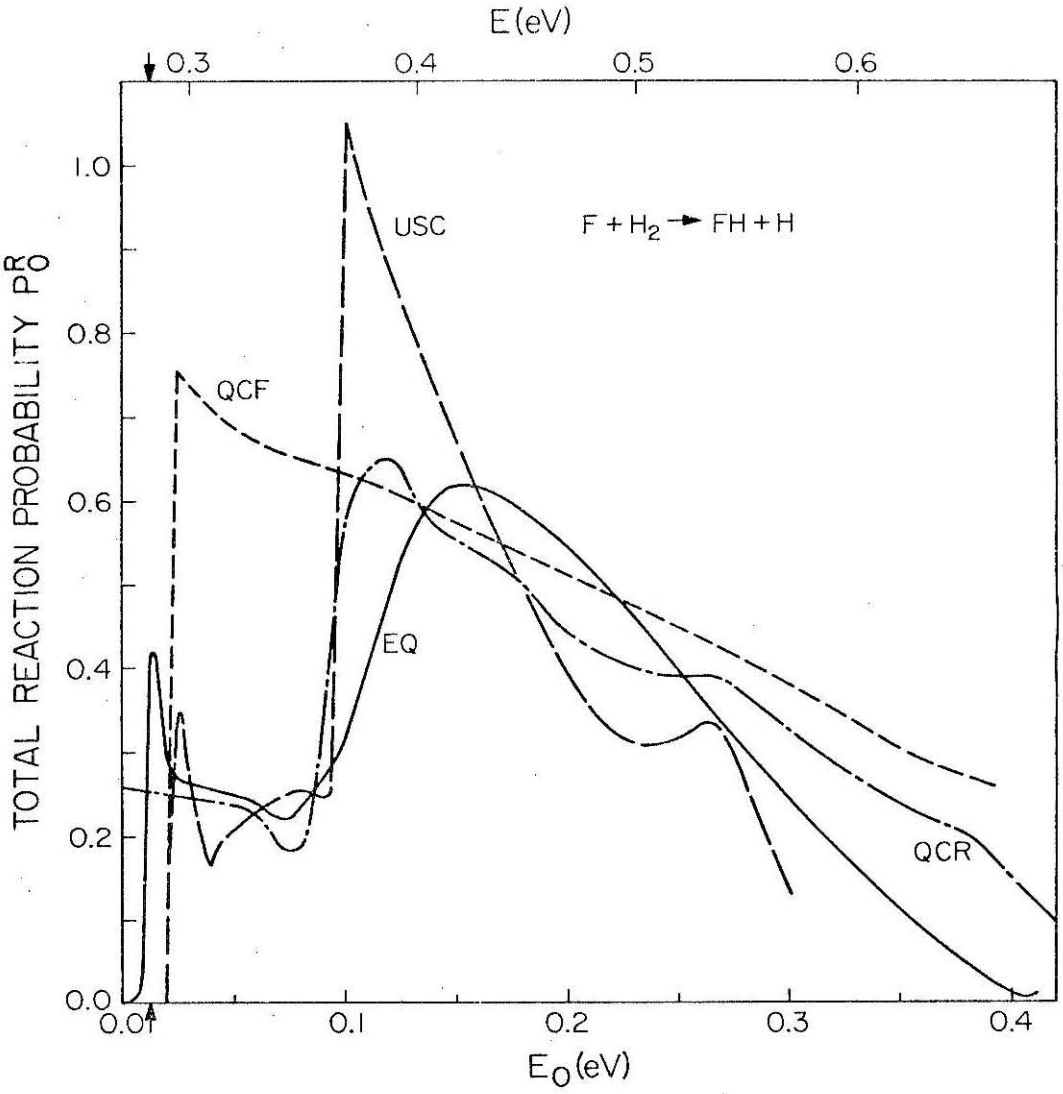
E(eV)
0.3
0.4
0.5
0.6
1.0
0.8
0.6
0.4
0.2
0.0
TOTAL REACTION PROBABILITY P_O^R
USC
$F + H_2 \rightarrow FH + H$
QCF
EQ
QCR
0.01
0.1
0.2
0.3
0.4
E_O(eV)

Figure 10

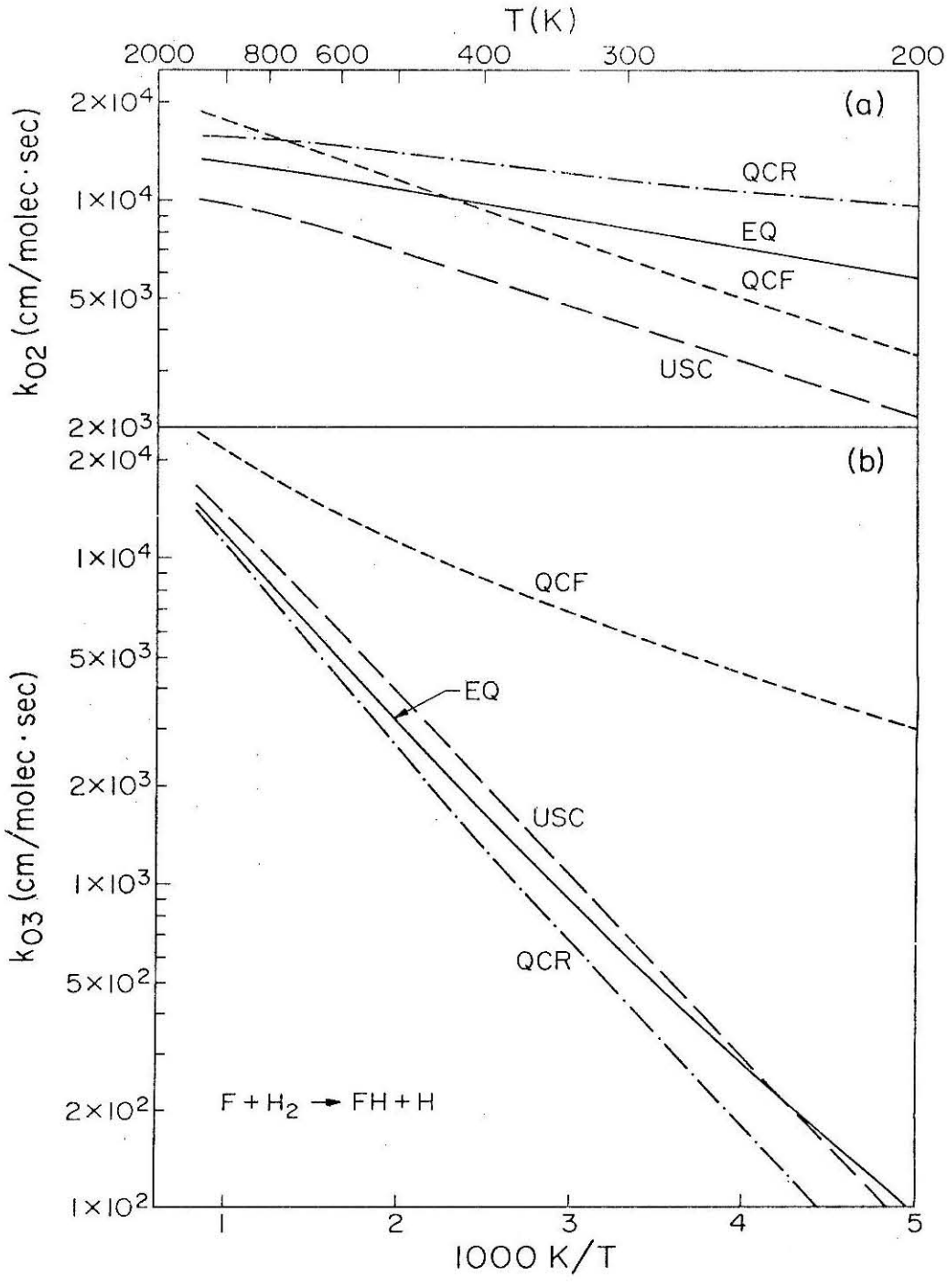
T(K)
2000
800
600
400
300
200
(a)
QCR
EQ
QCF
USC
k_{02} (cm/molec·sec)
2×10^4
1×10^4
5×10^3
2×10^3
(b)
QCF
EQ
USC
QCR
k_{03} (cm/molec·sec)
2×10^4
1×10^4
5×10^3
2×10^3
1×10^3
5×10^2
2×10^2
1×10^2
$F + H_2 \rightarrow FH + H$
1
2
3
4
5
1000 K/T

Figure 11

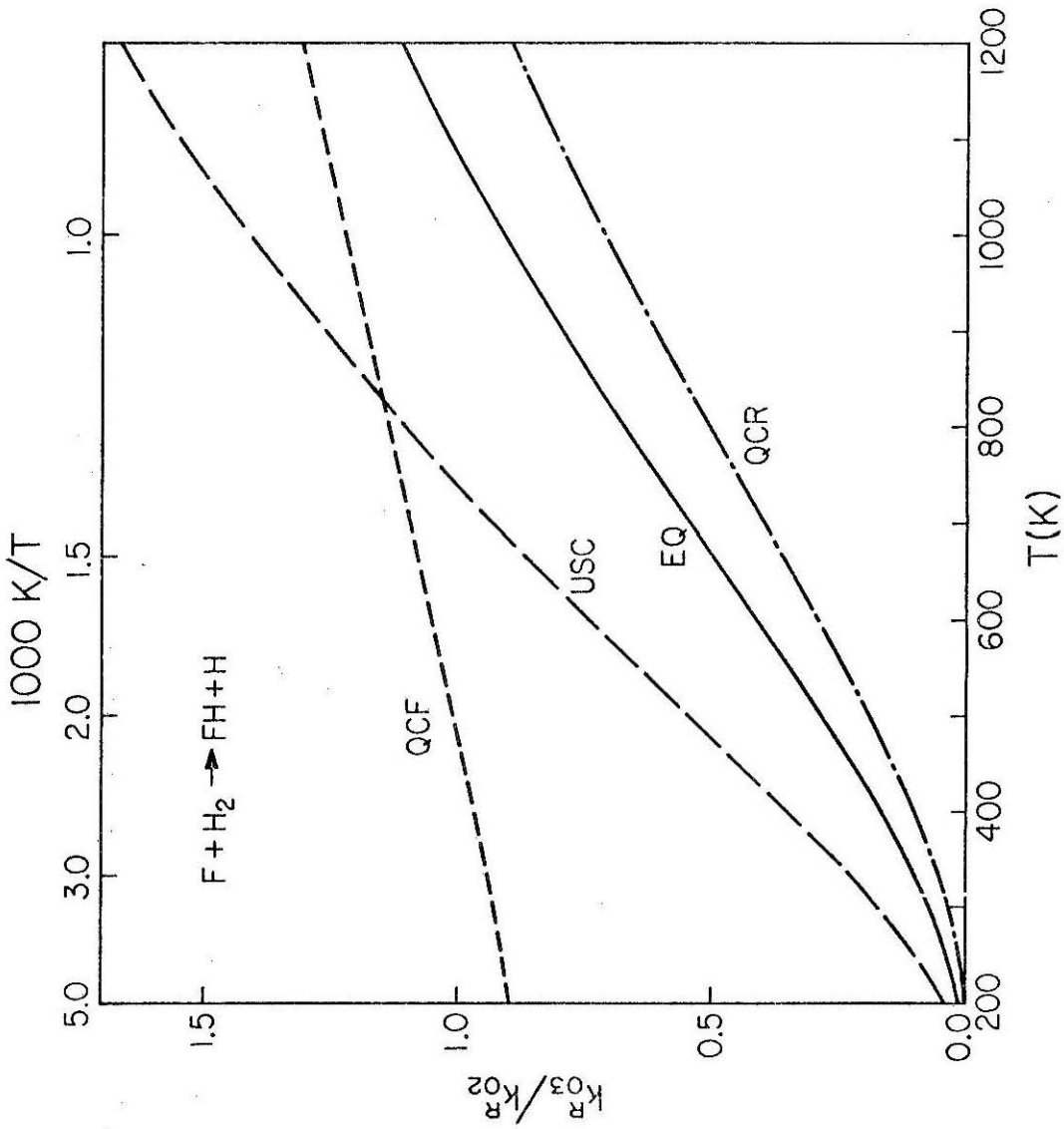
1000 K/T
1.0
1.5
2.0
3.0
5.0
T(K)
200
400
600
800
1000
1200
0.0
0.5
1.0
1.5
k_{03}^R/k_{02}^R
F + H2 → FH + H
QCF
USC
EQ
QCR

Figure 12

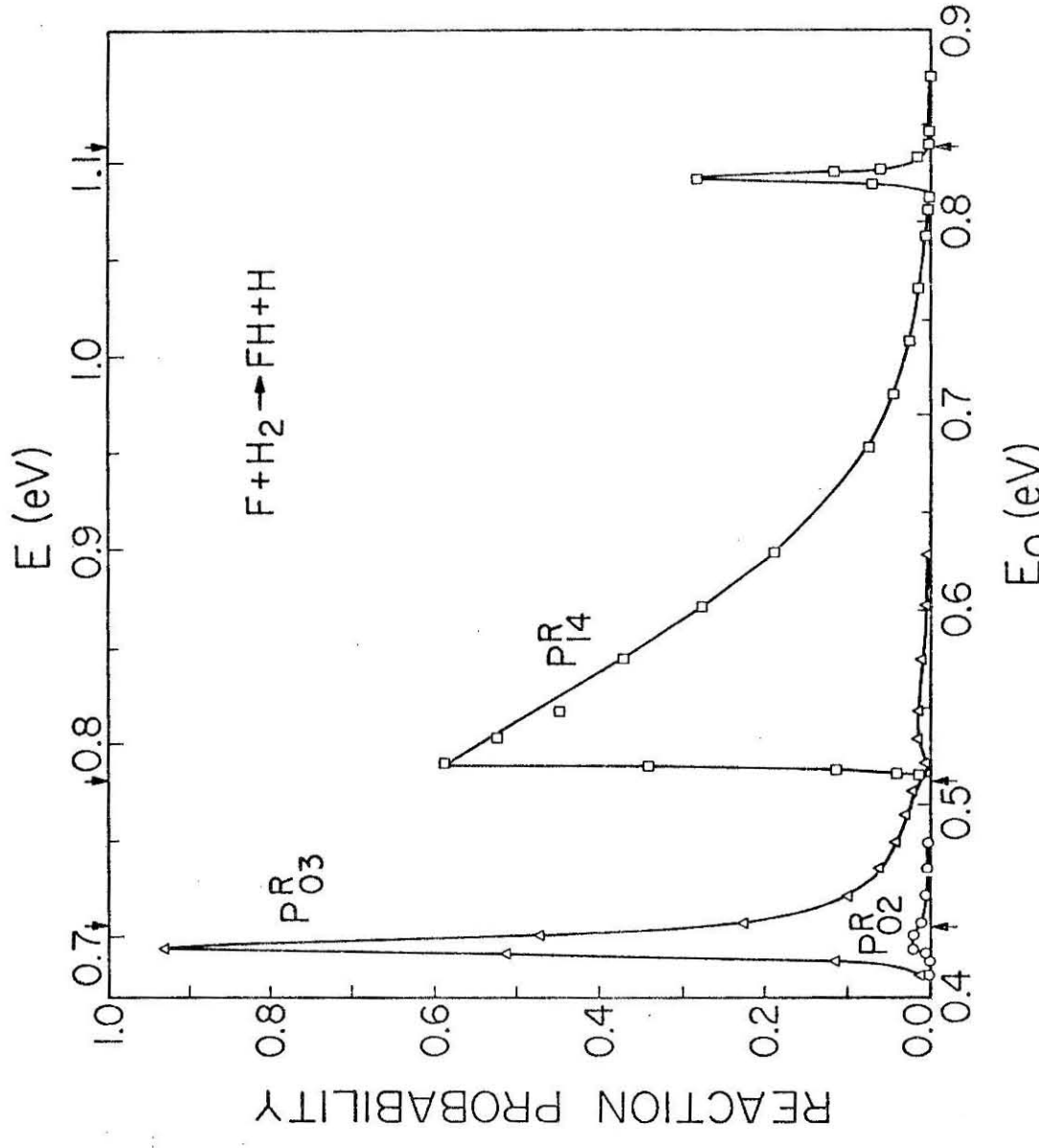
REACTION PROBABILITY
E (eV)
E_0 (eV)
$F+H_2 \rightarrow FH+H$
P^R_{03}
P^R_{14}
P^R_{02}
1.0
0.8
0.6
0.4
0.2
0.0
0.7
0.8
0.9
1.0
1.1
0.4
0.5
0.6
0.7
0.8
0.9

Figure 13

I.7 EXACT QUANTUM SEMI-CLASSICAL AND QUASI-CLASSICAL REACTION PROBABILITIES FOR THE COLLINEAR $F + D_2 \rightarrow$ REACTION.

EXACT QUANTUM SEMI-CLASSICAL AND QUASI-CLASSICAL REACTION PROBABILITIES FOR THE COLLINEAR $F + D_2 \rightarrow FD + D$ REACTION*

George C. Schatz†, Joel M. Bowman† and Aron Kuppermann

Arthur Amos Noyes Laboratory of Chemical Physics**

California Institute of Technology

Pasadena, California 91109

(Received)

Exact quantum, quasi-classical and semi-classical reaction probabilities and rate constants for the collinear reaction $F + D_2 \rightarrow FD + D$ are presented. In all calculations, a high degree of population inversion is predicted with P_{03}^R and P_{04}^R being the dominant reaction probabilities. In analogy with the $F + H_2$ reaction (ref. 1, preceding paper), the exact quantum $0 \rightarrow 3$ and $0 \rightarrow 4$ probabilities show markedly different energy dependence with P_{03}^R having a much smaller effective threshhold energy ($E_T = 0.014$ eV) than P_{04}^R (0.055 eV). The corresponding quasi-classical forward probabilities P_{03}^R and P_{04}^R are in poor agreement with the exact quantum ones, while their quasi-classical reverse and semi-classical counterparts provide much better approximations to the exact results. Similar

* Work supported in part by the United States Air Force Office of Scientific Research.

† Work performed in partial fulfillment of the requirements for the Ph. D. degree in Chemistry at the California Institute of Technology.

** Contribution No.

comparisons are also made in the analysis of the corresponding EQ, QCF, QCR and USC rate constants. Additional quantum results at higher energies are presented and discussed in terms of threshold behavior and resonances. Exact quantum reaction probabilities for the related F + HD $\rightarrow$FD + H reactions are given and an attempt to explain the observed isotope effects is made.

1. Introduction

In the preceding paper[1] (hereafter referred to as I) we compared the exact quantum (EQ), quasi-classical forward (QCF), quasi-classical reverse (QCR) and uniform semi-classical (USC) reaction probabilities for the collinear $F + H_2 \rightarrow FH + H$ reaction. The results of all four methods agreed in their prediction of a high degree of population inversion in the products of this exothermic reaction. However, the QCF probabilities were found to differ substantially from the corresponding EQ results in threshold behavior and energy dependence. This could have important consequences regarding the validity of the standard three-dimensional quasi-classical method which has been used on $F + H_2$ (D_2) and which is the three-dimensional version of the QCF method. We found much better agreement between the exact quantum probabilities and both the quasi-classical reverse and the uniform semi-classical results thus indicating that either of the last two methods might be preferred to the quasi-classical forward one in three-dimensional calculations.

In this paper we present the analogous EQ, QCF, QCR and USC results for the collinear $F + D_2$ reaction over roughly the same range of translational energies as was used in I. In addition, exact quantum probabilities for the reactions F + HD (DH) $\rightarrow$ FH (FD) + H (D) are given. We also study the importance of tunnelling and resonances in $F + D_2$, F + HD and F + DH. These calculations were done in order to assess the effect of isotopic substitution on the magnitude of the quantum effects and on the validity of the approximate methods.

The potential energy surface used in these calculations is identical to that described in I.[2] In addition, most of the numerical techniques are the same as was used in I and will not be described again here except to note changes made.

In Section 2 we discuss the EQ, QCF, QCR and USC reaction probabilities for $F + D_2$ and the corresponding collinear rate constants are presented in Section 3. Section 4 contains a study of the behavior of the reaction probabilities at energies sufficiently high to excite the first two vibrational states of reagent D_2. In addition, we discuss resonances in this reaction, giving specific comparisons between the results of the exact quantum, and approximate methods in the vicinity of these resonances. Section 5 contains a description of the EQ reaction probabilities for F + HD (DH) and in Section 6 we present a summary of conclusions.

2. Quantum, Quasi-Classical and Semi-Classical Reaction Probabilities for Collinear $F + D_2 \rightarrow FD + D$

2.1 Exact quantum reaction probabilities

Since the vibrational spacing in D_2 is roughly 9 kcal/mole and that in FD is about 8 kcal/mole, and the reaction is exothermic by 32 kcal/mole approximately, at least five vibrational levels of DF are accessible when D_2 has an initial quantum number $\nu = 0$. By coincidence, the $\nu = 3$ and 4 vibrational levels of DF have nearly the same total energies as the $\nu = 2$ and 3 vibrational levels of HF, respectively. This results in remarkable similarities between these two reactions despite the significant difference in the corresponding

reduced masses ($\mu_{F,H_2}/\mu_{F,D_2} = 0.548$). As in I, we will designate by $P^R_{\nu\nu'}$ the reaction probability for a reagent initially in state ν to form product in state ν', and by P^R_ν the total reaction probability from initial state ν (i.e., $\sum_{\nu'} P^R_{\nu\nu'}$). In Figure 1 we present the exact quantum reaction probabilities P^R_{04}, P^R_{03} and P^R_0 for F + D_2 at relative translational energies (E_0) in the range 0.0 to 0.25 eV. The corresponding probabilities P^R_{02}, P^R_{01} and P^R_{00} are plotted in Figure 2. It is apparent from these figures that P^R_{04} and P^R_{03} are the most significant contributors to P^R_0 in this E_0 range. The P^R_{02}, P^R_{01} and P^R_{00} curves are all very similar in appearance to the P^R_{03} one, but with greatly reduced magnitudes ($P^R_{02} \sim 6.8 \times 10^{-2} P^R_{03}$, $P^R_{01} \sim 5 \times 10^{-4} P^R_{03}$, $P^R_{00} \sim 6 \times 10^{-6} P^R_{03}$). There is a very significant difference between the threshold behavior of P^R_{03} and that of P^R_{04} quite analogous to what was observed in I for the reaction probabilities P^R_{02} and P^R_{03} of F + H_2. As in I, it is convenient to define an effective threshold energy E_T for the $\nu \rightarrow \nu'$ reaction as the difference between the (lowest) energy for which the corresponding $P^R_{\nu\nu'}$ is equal, say, to 1% of the maximum value attained by this quantity and the energy at which the $\nu \rightarrow \nu'$ process becomes energetically possible. Table I contains the values of E_T for several important reaction probabilities for the reactions of F with H_2, D_2, HD and DH as well as the corresponding vibrationally adiabatic zero curvature barrier heights E_{VAZC} (described in I). From it we see that for F + D_2 the value of E_T for $P^R_{03}(EQ)$, 0.014 eV, is appreciably lower than the E_{VAZC} value of 0.032 eV. This can be interpreted as an indication of the extent of

vibrationally adiabatic one-dimensional tunnelling (see paper I) in this system. The value of E_T for P_{03}^R (QCF) of 0.030 eV is very close to E_{VAZC}. This suggests that the chemical motion for this system is nearly vibrationally adiabatic in the approach coordinate in the sense that the local action number for the motion transverse to the reaction coordinate should vary relatively little between the separated reagent region and the saddle point region. The corresponding values of E_T and E_{VAZC} for P_{02}^R (EQ) of F + H_2 are 0.005 eV and 0.026 eV, indicating somewhat more tunnelling in this system than in the F + D_2, as expected. The effective threshold energy of P_{04}^R (F + D_2) E_T = 0.055 eV is similar to that of P_{03}^R (F + H_2) (0.045 eV). The near coincidence in energy between the v = 3 and 4 vibrational levels of FD and v = 2 and 3 of FH is probably responsible for the very similar appearance of the corresponding EQ reaction probabilities. (Compare Figure 2 of I with Figure 1 of the present paper.) There are, however, differences in the maximum values of certain analogous reaction probabilities especially P_{03}^R(F + D_2) and P_{02}^R (F + H_2) (which have maximum values of 0.66 and 0.44 respectively). We shall see in Section 4 that the differences between analogous reaction probabilities for the two reactions become even more important for $E_0 > 0.25$ eV.

2.2 Quasi-classical reaction probabilities

In Figure 3 are plotted the QCF and EQ reaction probabilities P_{03}^R, P_{04}^R and P_0^R for F + D_2. No reactive trajectories yield DF with v' = 0 or 1 but there is a small probability of reaction to v' = 2 (always

< 0.1 and vanishing for $E_0 > 0.12$ eV). The corresponding QCR reaction probabilities for the same energy range ($0.0 < E_0 < 0.12$ eV). are plotted in Figure 4. In Figure 3 we see that there is a very large difference between the threshold behavior of P_{04}^R (EQ) and P_{04}^R (QCF). In analogy with the F + H_2 P_{03}^R behavior,[1] we find that the quasi-classical reverse P_{04}^R of F + D_2 (Figure 4) has a threshold behavior which is much closer to the exact quantum one than is the QCF threshold. Unlike P_{02}^R (F + H_2), the energy dependence of P_{03}^R (F + D_2) is predicted somewhat more accurately by the QCF method than by the QCR method. The EQ and QCF total reaction probabilities P_0^R (Figure 3) are in somewhat better average agreement than are the EQ and QCF total reaction probabilities in F + H_2 (Figure 4 of I). This seems to indicate that the differences between quantum and classical dynamics are less severe for F + D_2 than for F + H_2. However, at least for collinear reactions, these differences are still quite significant.

In Figure 5 we plot as a function of E_0 the fraction f_v of the total energy which appears as vibrational energy of the DF product for the EQ and QCF calculations. It can be seen that f_v(QCF) is nearly independent of E_0 and has an average value of 0.79. The corresponding EQ curve has a more pronounced E_0 dependence but about the same average value over the E_0 range considered. We find that the average value of f_v is almost the same for both F + H_2 and F + D_2. This independence of isotopic substitution agrees with the corresponding experimental result[2] and with the predictions of

three-dimensional trajectory calculations[4] although our value of f_v (0.79) which ignores rotational degrees of freedom is somewhat higher than the experimental result (0.66)[3]. This general average agreement between the EQ and QCF f_v versus E_0 curves indicates that the dynamic processes governing the average energy disposal between vibrational and translational degrees of freedom of the products can be well approximated by the classical trajectory method. However, one should keep in mind that this is not so for the distribution of this vibrational energy among the available vibrational states, i.e., that large differences between product state population ratios obtained from the EQ and QCF methods do exist, as indicated in Figure 6.

2.3 Semi-classical reaction probabilities

Figure 7 shows the uniform semi-classical reaction probabilities P_{03}^R and P_{04}^R along with the corresponding EQ results. It was noted in paper I (Section 3.3) that "raggedness" in the final action number function $m(q_0;\nu, E)$ as a function of initial vibrational phase q_0 caused difficulties in calculating USC transition probabilities at the threshold of the $F + H_2(0) \rightarrow FH(3) + (H)$ reaction. The same problem occurred for the $0 \rightarrow 4$ transition in the $F + D_2$ reaction. We were able to overcome this difficulty by using the reverse final action number function, $n(q_0;m, E)$, which was found to be smooth for the values $n = 0$ and $m = 4$. The justification for using this procedure was given in I. The curves for the forward and reverse values of m for this $0 \rightarrow 4$ transition at an energy $E = 0.3107$ eV ($E_0 = 0.12$ eV)

are given in Figure 8. When all the relevant semi-classical quantities are well-behaved ("non-ragged") functions of q_0, the USC transition probabilities obey microscopic reversibility[5] and it is not necessary to calculate both the forward and reverse results. However, as the example above demonstrates, when "raggedness" exists, it is advisable to consider the forward and the reverse results. In our example, the reverse results are the preferred ones since there is no raggedness in the region corresponding to $D + DF(4) \rightarrow D_2(0) + F$. These were the ones used in calculating P_{04}^R (and P_{03}^R for the $F + H_2$ reaction) in its threshold region. The USC P_{04}^R transition probabilities at $E_0 = 0.08$ eV and 0.085 eV were calculated in the statistical approximation.[6] At these energies the reverse reaction showed that the $4 \rightarrow 0$ transition was dynamically forbidden. However, since statistical (i.e., ragged) behavior was evident in the forward reaction we did calculate a non-zero value for P_{04}^R at the two energies just mentioned.

The USC probabilities in Figure 7 are in much better agreement with the corresponding EQ results than are the quasi-classical ones. As was the case with the QCF P_{03}^R threshold, there is a small difference between the P_{03}^R (USC) and P_{03}^R (EQ) threshold energies, but the USC result may be improved by using complex trajectories.[7] The oscillations in P_{03} (USC) in the E_0 range 0.10 eV - 0.25 eV do not have any analog in the quantum results. One might expect that the raggedness in the plot of final action versus initial phase (see Figure 8a) could be an indication of resonant behavior in this energy

range, but the quantum results of Figure 1 do not substantiate this. In Section 4 we discuss the possible relationship between resonances in the EQ results and "raggedness" in the USC ones.

One significant aspect of the comparison between the USC and EQ results in Figure 7 is that the maximum values of the EQ and USC reaction probabilities P_{03}^R and P_{04}^R are nearly identical. This contrasts with the results of both the QCF and QCR calculations which generally tend to underestimate the maximum values of the probabilities (Figures 3 and 4). The significant improvement in the quality of the results obtained in going from the quasi-classical to the semi-classical approximation suggests that an equivalent improvement may occur for the three-dimensional $F + D_2$ reaction and that the semi-classical results may be quite reliable for this case. However, we must stress that the utilization of uniform rather than primitive semi-classical techniques is essential to the success of this method for the collinear reaction and thus it seems likely that an analogous uniform procedure will be required in the three-dimensional problem.[8]

2.4 Comparison of EQ, QCF, QCR and USC reaction probabilities

In Figure 9 we compare the reaction probabilities P_{03}^R and P_{04}^R of $F + D_2$ as calculated by all four methods EQ, QCF, QCR and USC. Figure 10 presents the analogous comparison for the total reaction probability P_0^R. It is apparent from both figures that the USC method gives the best agreement with the EQ reaction probabilities for this reaction.

3. EQ, QCF, QCR and USC Rate Constants for $F + D_2$

The rate constants k_{03}^R and k_{04}^R obtained from the EQ, QCF, QCR and USC reaction probabilities P_{03}^R and P_{04}^R for $F + D_2$ are plotted in Figure 11. The expression for these rate constants is the same as the one given in I.[1] The corresponding Arrhenius parameters obtained from fits to the rate constants in the 200 to 400 K and 900to 1200 K temperature ranges are listed in Table II. The difference between k_{04}^R (QCF) and k_{04}^R (EQ) (which results from the different threshold properties of the P_{04}^R's in Figure 9) is quite noticeable and leads to a 0.8 kcal difference between the corresponding high temperature activation energies in Table II. In analogy with our $F + H_2$ study,[1] the QCR and USC rate constants k_{04}^R and corresponding activation energies E_{04}^a agree with the EQ ones better than do the QCF quantities. The similar comparison for the rate constants k_{03}^R is much less satisfactory. The low temperature differences between the various k_{03}^R's are determined to a large extent by the different threshold energies of the corresponding reaction probabilities P_{03}^R. The transition probability P_{03}^R (QCR) has zero threshold energy and thus the largest rate constant at low temperatures, while the EQ, USC and QCF P_{03}^R's have successively higher threshold energies and therefore successively lower rate constants. (See Figure 9b.) This illustrates that the low energy (< 0.03 eV) behavior of the reaction probabilities (or cross sections) can be exceedingly important in determining the low temperature (< 300 K) behavior of the corresponding rate constants for these reactions.

The ratios k_{04}^R/k_{03}^R are plotted as a function of temperature in Figure 12. We see that the QCF ratio is nearly temperature independent while the EQ, QCR and USC ratios increase monotonically with increasing temperature, approaching the QCF ratio at high temperatures. These k_{04}^R/k_{03}^R ratios are quite similar in appearance to the k_{03}^R/k_{02}^R ratios for the F + H_2 reaction given in Figure 12 of I, but the F + D_2 ratios actually increase somewhat more slowly with temperature than do the F + H_2 ones.

The QCF ratio k_{04}^R/k_{03}^R is 0.63 at 300 K in approximate agreement with the experimental value[9] of 0.66. The results of three-dimensional classical trajectory calculations indicate that this ratio is not strongly temperature dependent.[10] If this is also true experimentally then, in analogy with F + H_2, we would have evidence that the collinear model overestimates the effects of threshold differences on reaction rates to different product vibrational states. We might note, however, that Lee and coworkers[10,11] have measured the ratio of cross sections σ_{04}/σ_{03} at three different energies and they find that it increases rapidly with increasing energy from 0.75 at E_0 = 0.034 eV to 3.5 at E_0 = 0.11 eV. If we consider the analogous collinear ratio P_{04}^R/P_{03}^R (Figure 6) we find that it also increases rapidly with increasing energy (much more rapidly than Lee's cross section ratio) from near zero at zero translational energy to roughly a value of 4.3 for $E_0 \sim 0.12$ eV. The ratios of cross sections from three-dimensional QCF trajectory calculations over a family of several potential energy surfaces do not reproduce this energy dependence

(Ref. 10, Table VI). This may indicate that the differences between quantum and quasi-classical results are still significant in three dimensions and, indeed, are observable in experiments which are at least partially state selected such as cross section measurements.

4. Higher Energy Reaction Probabilities for $F + D_2$

Figure 13 shows the higher energy exact quantum reaction probabilities P_{03}^R, P_{04}^R, P_{05}^R, P_{14}^R and P_{15}^R for $F + D_2$ in the translational energy range $E_0 = 0.25$ to 0.70 eV. Those transition probabilities not plotted are all small (usually < 0.02). P_{04}^R (QCR) is also plotted in Figure 13 in the energy range 0.25 to 0.42 eV for reasons to be discussed in detail below. This figure is analogous in many ways to Figure 13 of I, although the close correlation between the reaction probabilities of $F + H_2$ and the related $F + D_2$ ones (see end of Section 2.1) becomes less important as the energy is increased. Nevertheless, many of our remarks concerning the $F + H_2$ reaction probabilities described in I are also applicable here. We note that the transition probabilities P_{15}^R in Figure 13 and P_{04}^R in Figure 1 have similar translational energy dependences except near threshold. This confirms our statement in I that reaction probabilities for reagents initially in $\nu = 1$ are virtually insensitive to the presence of a barrier in the $F + H_2$ (D_2) reagent channel. In addition, P_{15}^R is significantly larger than the other $P_{1\nu'}^R$ with $\nu' < 5$ over the energy range considered. This implies that the additional vibrational energy in the reagents is being predominantly channelled into additional vibrational energy in the products.[12]

The transition probability P_{05}^{R} exhibits a rather unusual energy dependence. As shown in Figure 11, it remains quite small (< 0.01), even though energetically allowed, until the total energy becomes high enough to excite $v = 1$ of D_2 at which point it rises suddenly to a peak value of 0.34 before finally levelling off at about 0.13. It is not obvious how simple resonance or threshold theories can explain this unusual behavior since the effective threshold is apparently related to the opening of a vibrational state not involved in the transition asymptotically. One possible explanation for the influence of the $v = 1$ state of D_2 on this transition probability can be formulated by observing that the inelastic $0 \rightarrow 1$ transition probability for $F + D_2$ is quite appreciable[13] (0.10 to 0.25) and, as noted above, P_{15}^{R} is quite large. This suggests that the $0 \rightarrow 5$ reactive transition occurs almost exclusively with $v = 1$ as an intermediate state. It is also significant that it is not sufficient for this state to be accessible via virtual transitions but rather it must be open asymptotically. This seems to indicate that a high degree of vibrational excitation must be maintained over a considerable region in configuration space. This would only be possible if the $v = 1$ vibrational state is open and hence there is no enhancement of P_{05}^{R} when the state is closed.

For the transitions P_{04}^{R} at $E_0 = 0.327$ eV and P_{15}^{R} at $E_0 = 0.599$ eV we see peaks in the reaction probabilities suggestive of internal excitation resonances.[14] In contrast to the resonances observed in I in $F + H_2$, the direct processes in $F + D_2$ still seem to be quite important in the vicinity of the resonances. The resultant interference between

the direct and resonant contributions to the scattering amplitude leads to characteristic oscillations in the reaction probabilities in the vicinities of the resonance energies quite similar to what was observed in the H + H_2 reaction.[14,15] As in the F + H_2 reaction, we see an approximate correspondence between the appearance of a resonance and the opening of a specific vibrational state of the product DF ($\nu = 5$ at $E_0 = 0.29$ eV and $\nu = 6$ at $E_0 = 0.59$ eV). This implies that the virtual states of the triatomic complex may have energy levels resembling product states more than reagent states. The relation is probably complicated, however, since the correspondence between the resonance energy and the energy of the associated product vibrational level is not always in the same direction (i.e., the resonance energy is sometimes greater and sometimes smaller than the corresponding vibrational energy as can be seen in Figure 13 of I and Figure 13 in the present paper).

It is interesting to note that the QCR reaction probability P_{04}^R depicted in Figure 13 seems to "average out" the quantum oscillations in P_{04}^R (EQ) in the vicinity of the 0.327 eV resonance. It is also of interest to examine the semi-classical results at this energy. Rankin and Miller have reported extensive statistical behavior in the final action number function, m_f, for the H + Cl_2 collision.[6] From this behavior, they inferred that a converged quantum treatment of that reaction would yield internal excitation resonances. However, as Figure 14 shows, m_f, at the resonance energy, is a smooth function of q_0 with about the same degree of "raggedness" as seen previously

away from resonance in Figure 8b. We have also observed non-statistical behavior of m_f [16] at the energy of the sharp 1.28 eV resonance for the collinear H + H_2 reaction.[14] Thus, we can conclude that statistical behavior of m_f is at best a sufficient but not necessary condition for the presence of quantum mechanical internal excitation resonances. This conclusion is in qualitative agreement with the one reached by Duff and Truhlar[17] who found no evidence from their semi-classical study of the H + H_2 reaction of the resonant behavior present in exact quantum calculations.

5. Exact Quantum Reaction Probabilities for the Reactions F + HD → FH + D and F + DH → FD + H

We have also calculated the exact quantum reaction probabilities for F + HD → FH + D and F + DH → FD + H hereafter designated F + HD and F + DH respectively. In three dimensions, these two reactions represent different product arrangement channels of the same collision system. In collinear collisions, however, they must be considered entirely separately. This implies that coupling between these two product arrangement channels is ignored in our collinear calculations.

The largest reaction probabilities for the two reactions are plotted in Figure 15[18] as a function of the reagent translational energy E_0 (relative to $v = 0$ of HD) in the range 0 to 0.25 eV. For F + HD, the only reaction probability greater than 0.025 in the energy range studied is P_{02}^R while P_{04}^R, P_{03}^R and P_{02}^R are the major contributors to the total reaction probability in F + DH (P_{02}^R is always less than

0.10). From Figure 15 it is apparent that the reaction probabilities P_{04}^R and P_{03}^R of F + DH are very similar in shape to the corresponding probabilities P_{04}^R and P_{03}^R of F + D_2 (Figure 10), although the sharp differences between the threshold energies of P_{04}^R and P_{03}^R (F + D_2) are reduced considerably for P_{04}^R and P_{03}^R (F + DH). In contrast, the results for F + HD do not show a strong resemblance to those for F + H_2 (Figure 2 of I). Instead, we see that P_{02}^R (Figure 15) consists of one very sharp (width ~ 0.0005 eV) spike near 0.012 eV and then remains quite small (< 0.02) for the remainder of the energy range studied. P_{03}^R, which is energetically forbidden until $E_0 = 0.039$ eV is quite small throughout the energy range considered here. The rather dramatic differences between the results for F + HD and F + DH can probably be explained as resulting from the difference in the mass of the atom being exchanged in the collinear triatomic collision system. The small mass of the H atom in F + HD in comparison with that of the D atom in F + DH results in much more important pseudo-centrifugal barriers in "turning the corner" in the former reaction than in the latter. That this should be the case is apparent from a comparison of the skew angles (defined in I) for these two systems. For F + HD, this angle is 37.3° while for F + DH it is 56.7°, thus indicating that the curvature along the reaction path should be much larger for F + HD than for F + DH. Only at low translational energies do the centrifugal effects become small enough to render F + HD dynamically allowed. For F + DH, on the other hand, the centrifugal effects are not important in the energy range studied and

thus we observed very large reaction probabilities throughout that energy range.

From Figure 15, we can also conclude that the rate constant for formation of DF is predicted to be greater than that for formation of HF (except at very low temperatures ($< 150°$) where the slightly smaller effective threshold of F + HD becomes important). This disagrees with the experimental result[19] that the rate of H atom transfer is a factor of 1.45 faster than that for D atom transfer at 298 K. The disagreement can probably be explained by noting that the distance of the H atom from the center of mass of HD is about twice that of the D atom from the same center of mass. This means that H sweeps through a larger volume of space than D when HD rotates and thus is more "visible" to the attacking F atom. Since the barrier height is quite low at most orientations of the reagents[10], one would expect that H should be preferentially abstracted. For collinear reactions, this three-dimensional effect is ignored and we find, instead, that dynamical effects such as pseudo-centrifugal barriers are important in the reaction. These centrifugal effects favor reaction with the D atom and thus explain why the collinear results differ from the experimental ones. A similar argument has been used to explain the J dependence of three-dimensional quasi-classical cross sections for the same reactions[4a]. One might add that for a reaction with a high barrier, which simultaneously favors reaction through collinear geometries, the three dimensional effect should be less important and the collinear results should be more

representative of the experimental results. This has indeed been observed for the Cl + HD (DH) reactions.[20]

6. Discussion

We shall now summarize the differences between the results of the exact quantum, quasi-classical and semi-classical methods for studying the F + H_2 (paper I) and F + D_2 reactions. The most important of these differences may be categorized into three divisions: vibrationally adiabatic tunnelling, resonances and threshold dynamical effects. These effects may, however, be coupled to one another to a lesser or greater extent.

Vibrationally adiabatic tunnelling seems to be most significant at very low energies especially for F + H_2 and for those transitions for which at threshold there are no strongly restrictive dynamical effects (of the type occurring in P_{03}^{R} for F + H_2). Such tunnelling appears to be responsible for important differences between EQ and QCF rate constants at low temperatures (Figures 11a in I and also 11a in this paper). The semi-classical complex trajectory method (which was not studied here) may be able to describe tunnelling quantitatively.[5,7] Excitation resonances seem to be very important at higher translational energies and will therefore not be significant in thermal experiments. They may be important in beam and hot atom experiments if these resonance effects carry over without strong attenuation into three dimensions. The current semi-classical theories do not seem to furnish a computationally practical description of the interference effects associated with these resonances.[18] Threshold dynamical effects are very significant

for collinear F + H_2 and F + D_2 and this leads to important differences between exact quantum and quasi-classical reaction probabilities and rate constants for thermal distributions of reagents. These threshold effects are partially classical in nature since we found that the QCR method was capable of describing roughly the proper threshold behavior within a completely classical framework. An important result of this paper was the demonstration that the uniform semi-classical method provides a greatly improved description of threshold behavior of the quantum results in comparison with the QCF method. How important these threshold effects will be in three dimensions is not entirely clear from an analysis of existing experimental and theoretical studies, but it appears that the effects are at least partially attenuated by the averaging that inevitably occurs in experimental measurements. They may, however, still be important for experiments which are sufficiently state selected.

Acknowledgements

We thank J. T. Muckerman, with whom we have exchanged results on the USC calculations, for useful discussions.

We also thank Ambassador College for the use of their computational facilities in most of the work reported here.

Table I. Effective threshold energies (E_T) for the most significant reaction probabilities in the F + H_2, F + D_2, F + DH and F + HD reactions.[a]

	F + H_2	F + HD
$E_T(P_{02}^R(EQ))$	0.005	0.010
$E_T(P_{02}^R(QCF))$	0.025	N.C.[b]
$E_T(P_{03}^R(EQ))$	0.045	0.071
$E_T(P_{03}^R(QCF))$	0.012	N.C.[b]
E_{VAZC}	0.026	0.028
	F + D_2	F + DH
$E_T(P_{03}^R(EQ))$	0.014	0.011
$E_T(P_{03}^R(QCF))$	0.030	N.C.[b]
$E_T(P_{04}^R(EQ))$	0.055	0.022
$E_T(P_{04}^R(QCF))$	0.030	N.C.[b]
E_{VAZC}	0.032	0.028

[a] All energies are in eV.

[b] No QCF calculations were done for this transition.

Table II. Arrhenius rate constant parameters for $F + D_2 \rightarrow FD + D$.[a]

	Temp. Range	EQ	QCF	QCR	USC
E_a^{o3}	200 - 400 K	0.676	0.935	0.266	0.852
E_a^{o4}	200 - 400	2.167	0.990	2.576	2.471
A_{o3}	200 - 400	2.551×10^{-4}	2.443×10^{-4}	1.884×10^{-4}	2.340×10^{-4}
A_{o4}	200 - 400	2.775×10^{-4}	1.686×10^{-4}	2.502×10^{-4}	3.269×10^{-4}
E_a^{o3}	900 - 1200	0.361	0.912	0.416	0.611
E_a^{o4}	900 - 1200	2.108	1.343	2.742	2.344
A_{o3}	900 - 1200	2.104×10^{-4}	2.674×10^{-4}	2.402×10^{-4}	2.082×10^{-4}
A_{o4}	900 - 1200	3.240×10^{-4}	2.604×10^{-4}	3.261×10^{-4}	3.365×10^{-4}

[a] E_a^{oi} is in kcal/mole and A_{oi} is in cm/(molec·sec).

References

1. G. C. Schatz, J. M. Bowman, and A. Kuppermann, preceding paper.
2. J. T. Muckerman (private communication).
3. J. C. Polanyi and K. B. Woodhall, J. Chem. Phys. 58, 2298 (1973).
4. (a) J. T. Muckerman, J. Chem. Phys. 54, 1155 (1971); (b) ibid. 56, 2997 (1972).
5. J. M. Bowman and A. Kuppermann, J. Chem. Phys. 59, 6524 (1973).
6. C. C. Rankin and W. H. Miller, J. Chem. Phys. 55, 3150 (1971).
7. W. H. Miller and T. F. George, J. Chem. Phys. 56, 5668 (1972); J. D. Doll, T. F. George, and W. H. Miller, J. Chem. Phys. 58, 1343 (1973); J. Stine and R. A. Marcus, Chem. Phys. Lett. 15, 536 (1972).
8. W. H. Miller, J. Chem. Phys. 54, 5386 (1971); R. A. Marcus, J. Chem. Phys. 57, 4903 (1972); J. D. Doll and W. H. Miller, J. Chem. Phys. 57, 5019 (1972); J. N. L. Connor, Mol. Phys. 25, 181 (1973).
9. M. J. Berry, J. Chem. Phys. 59, 6229 (1973).
10. N. C. Blais and D. G. Truhlar, J. Chem. Phys. 58, 1090 (1973).
11. T. P. Schaefer, P. E. Siska, J. M. Parson, F. P. Tully, Y. C. Wong and Y. T. Lee, J. Chem. Phys. 53, 3385 (1970). See also reference 10.
12. A. Ding, L. Kirsch, D. Perry, J. Polanyi, and J. Schreiber, Disc. Far. Soc. 55, 252 (1973).
13. G. C. Schatz and A. Kuppermann, unpublished calculations.

14. G. C. Schatz and A. Kuppermann, J. Chem. Phys. 59, 964 (1973).

15. R. D. Levine and S.-F. Wu, Chem. Phys. Lett. 11, 557 (1971).

16. J. M. Bowman and A. Kuppermann, unpublished results.

17. J. D. Duff and D. G. Truhlar, Chem. Phys., to be published.

18. Note that for these calculations, a slightly different value of β (HF) was used (2.2087 Å^{-1}) than in I (2.2187 Å^{-1}).

19. A. Persky, J. Chem. Phys. 59, 5578 (1973).

20. M. Baer, U. Halavee and A. Persky, to be published.

Figure Captions

Figure 1: Exact quantum reaction probabilities for $F + D_2$ as a function of relative translational energy E_0 and total energy E (relative to minimum in D_2 diatomic potential curve). (a) Total reaction probability P_0^R and (b) Reaction probabilities P_{03}^R and P_{04}^R.

Figure 2: Exact quantum reaction probabilities P_{02}^R, P_{01}^R and P_{00}^R for $F + D_2$ (similar to Figure 1).

Figure 3: Quasi-classical forward (dashed curve) and exact quantum (solid curve) reaction probabilities for $F + D_2$: (a) P_0^R, (b) P_{03}^R and P_{04}^R.

Figure 4: Quasi-classical reverse (dashed curve) and exact quantum (solid curve) reaction probabilities for $F + D_2$: (a) P_0^R, (b) P_{03}^R and P_{04}^R.

Figure 5: Fraction (f_v) of the total reagent energy (exclusive of product zero point energy) which ends up as vibrational energy in the product DF plotted as a function of the reagent translational energy E_0 and total energy E. Solid line indicates EQ results and dashed line QCF ones. Other notation analogous to Figure 1.

Figure 6: Ratio of reaction probabilities P_{04}^R/P_{03}^R versus translational energy E_0 and total energy E. Solid line indicates EQ results and dashed line QCF ones. Other notation analogous to Figure 1.

Figure 7: Uniform semi-classical (dashed curve) and exact quantum (solid curve) reaction probabilities for $F + D_2$: (a) P_0^R, (b) P_{03}^R and P_{04}^R.

Figure 8: (a) m_f versus q_0 for the forward reaction $F + D_2(0) \rightarrow FD(m_f) + D$, total energy E is 0.3107 eV; (b) m_f versus q_0 for the reverse reaction $D + DF(4) \rightarrow D_2(m_f) + F$, total energy E is 0.3107 eV.

Figure 9: EQ(solid), QCF (short dash), QCR (dash dot) and USC (long dash) reaction probabilities P_{04}^R (a) and P_{03}^R(b). (From Figures 1, 3-5.)

Figure 10: EQ(solid), QCF (short dash), QCR (dash dot) and USC (long dash) total reaction probabilities P_0^R for $F + D_2$. (From Figures 1, 3-5.)

Figure 11: Arrhenius plot of EQ (solid), QCF (short dash), QCR (dash dot) and USC (long dash) rate constants for $F + D_2$: (a) k_{03}^R, (b) k_{04}^R.

Figure 12: Ratios of rate constants k_{04}^R/k_{03}^R for $F + D_2$; EQ (solid), QCF (short dash), QCR (dash dot), USC (long dash).

Figure 13: Exact quantum reaction probabilities at translational energies higher than those in Figure 1. (a) P_{03}^{R}, P_{04}^{R} and P_{05}^{R} (b) P_{14}^{R} and P_{15}^{R}. Also shown in (a) is the QCR P_{04}^{R} curve (dashed). Arrows near $E_0 = 0.29$ eV and 0.59 eV indicate the opening of $\nu = 5$ and 6 respectively of DF while that at 0.37 eV indicates the energy E_0 at which $\nu = 1$ of D_2 becomes accessible.

Figure 14: m_f versus q_0 for the reverse reaction $D + DF(4) \rightarrow D_2(m_f) + F$ at the resonance energy 0.5107 eV (corresponding to $E_0 = 0.32$ eV).

Figure 15: Exact quantum reaction probabilities P_{02}^{R} for F + HD, and P_{03}^{R} and P_{04}^{R} for F + DH as a function of relative translational energy E_0 and total energy E (relative to minimum in HD diatomic potential curve). Arrow near 0.04 eV indicates the energy at which $\nu = 3$ of HF becomes accessible.

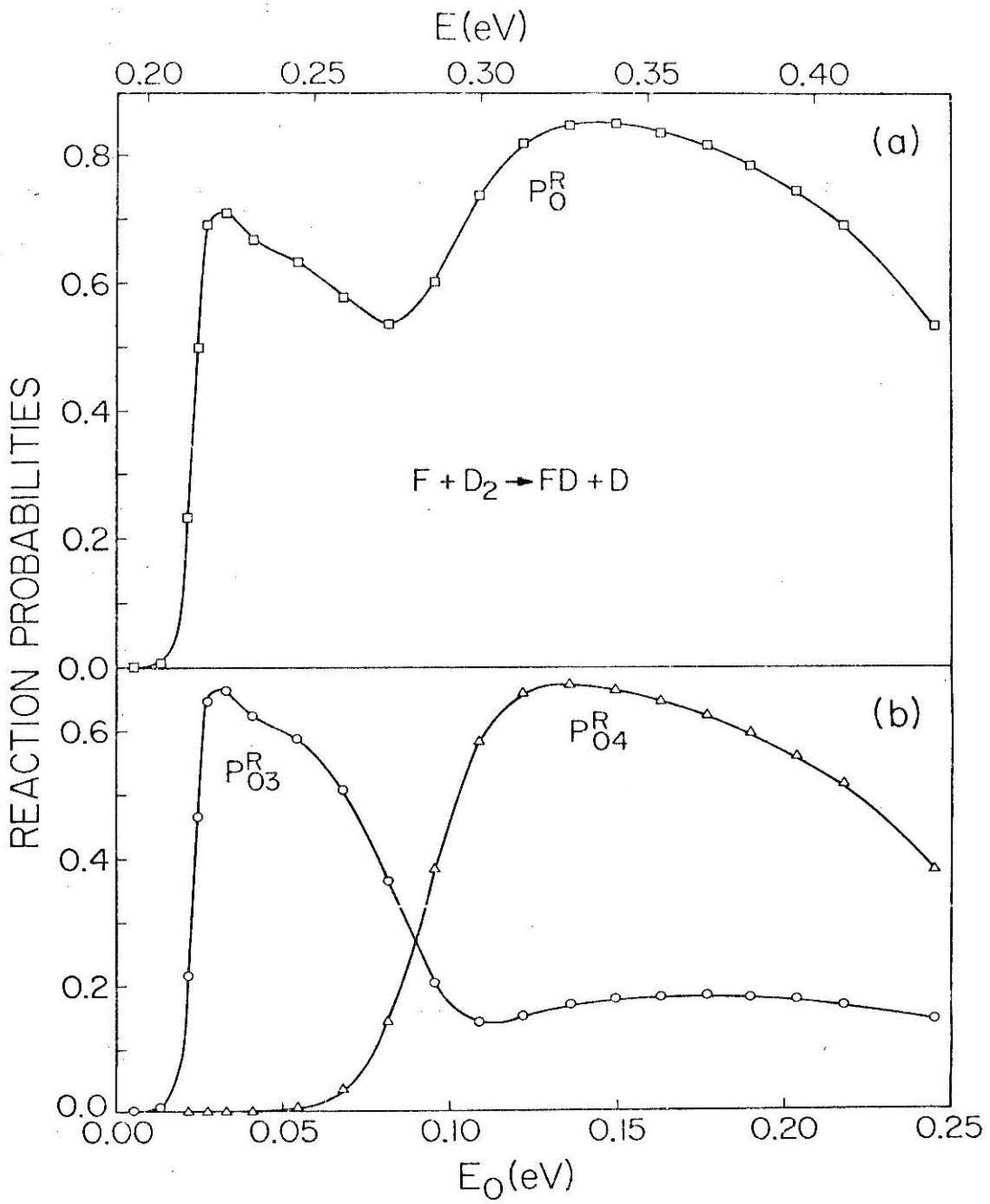
E(eV)
0.20
0.25
0.30
0.35
0.40
(a)
P_0^R
F + D_2 → FD + D
(b)
P_{03}^R
P_{04}^R
REACTION PROBABILITIES
0.0
0.2
0.4
0.6
0.8
0.00
0.05
0.10
0.15
0.20
0.25
E_0(eV)

Figure 1

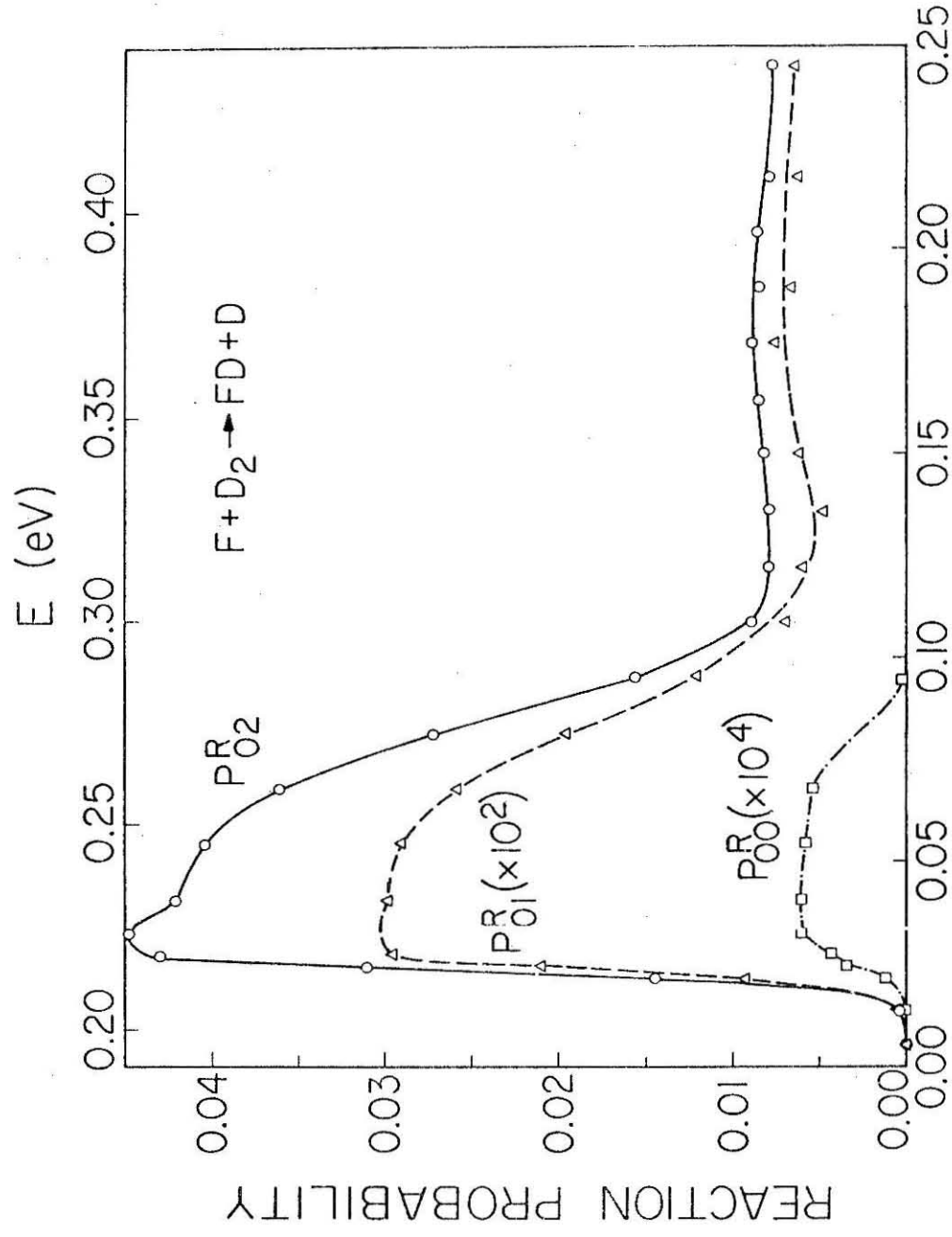
E (eV)
0.20
0.25
0.30
0.35
0.40
F+D2→FD+D
P02R
P01R(x102)
P00R(x104)
REACTION PROBABILITY
0.00
0.01
0.02
0.03
0.04
0.00
0.05
0.10
0.15
0.20
0.25
E0 (eV)

Figure 2

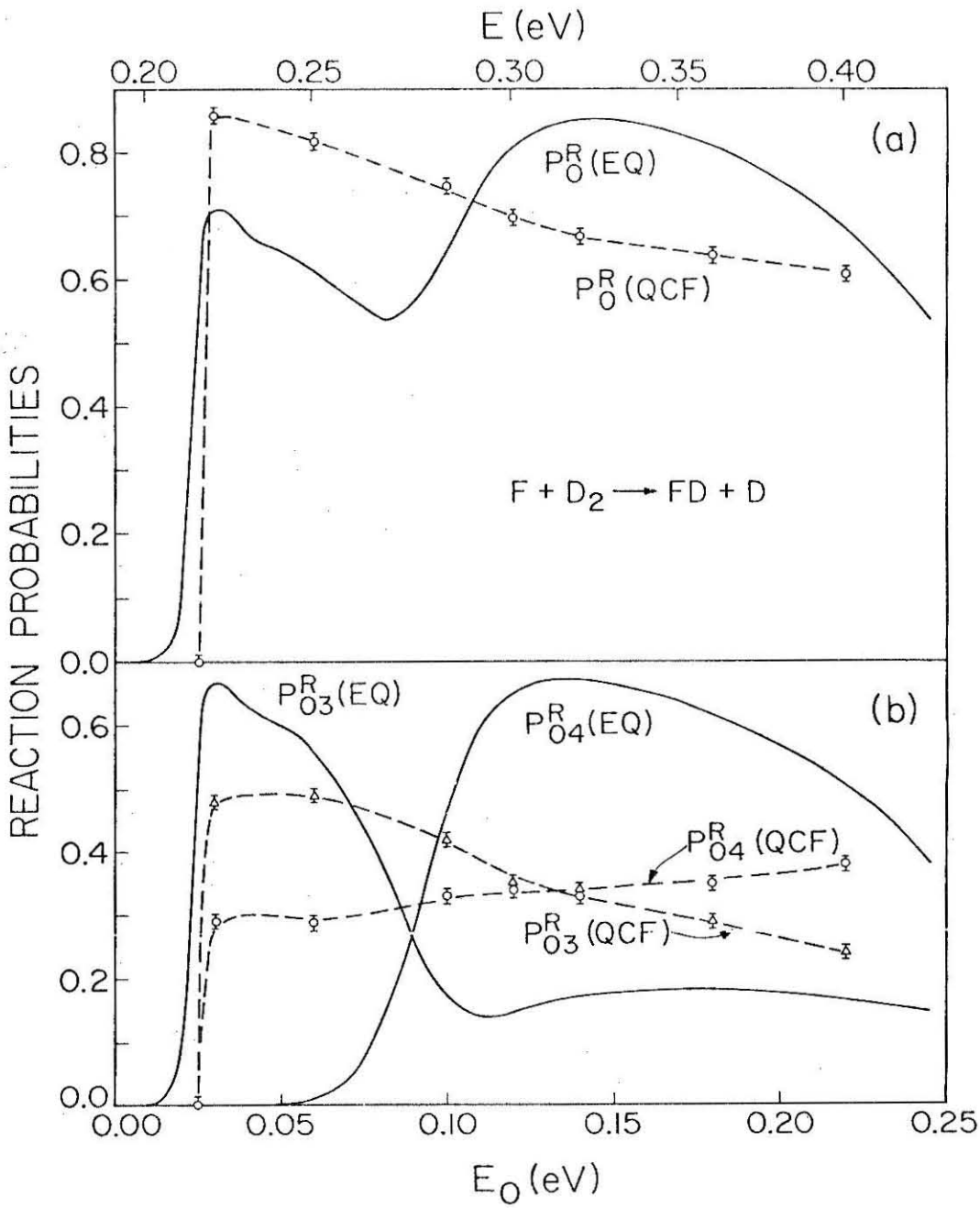
E (eV)
0.20
0.25
0.30
0.35
0.40
(a)
P_0^R(EQ)
P_0^R(QCF)
F + D_2 → FD + D
REACTION PROBABILITIES
0.0
0.2
0.4
0.6
0.8
(b)
P_{03}^R(EQ)
P_{04}^R(EQ)
P_{04}^R(QCF)
P_{03}^R(QCF)
0.00
0.05
0.10
0.15
0.20
0.25
E_0 (eV)

Figure 3

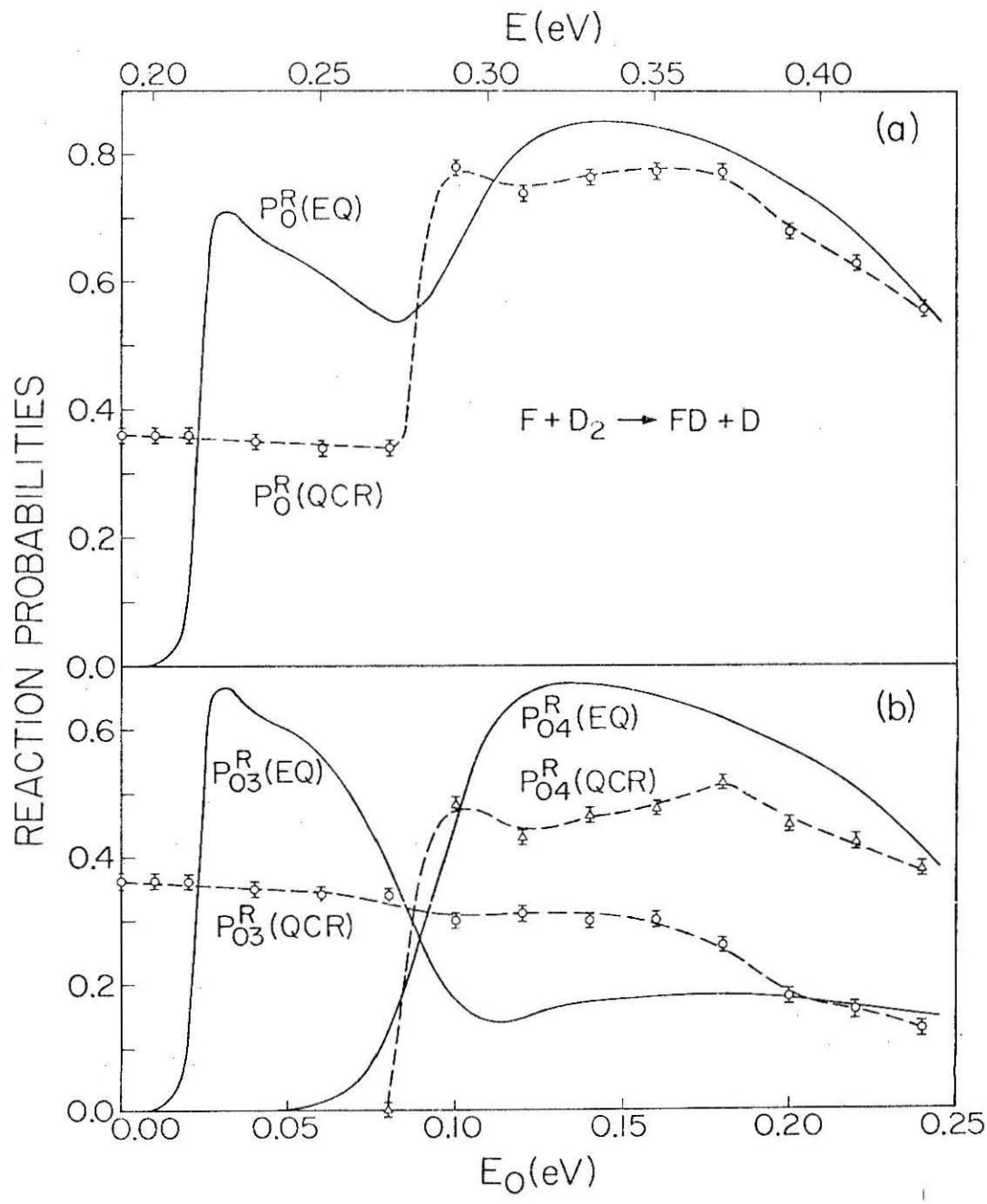
E(eV)
0.20
0.25
0.30
0.35
0.40
(a)
$P_0^R(EQ)$
$P_0^R(QCR)$
$F + D_2 \rightarrow FD + D$
REACTION PROBABILITIES
0.0
0.2
0.4
0.6
0.8
(b)
$P_{03}^R(EQ)$
$P_{03}^R(QCR)$
$P_{04}^R(EQ)$
$P_{04}^R(QCR)$
0.00
0.05
0.10
0.15
0.20
0.25
$E_0(eV)$

Figure 4

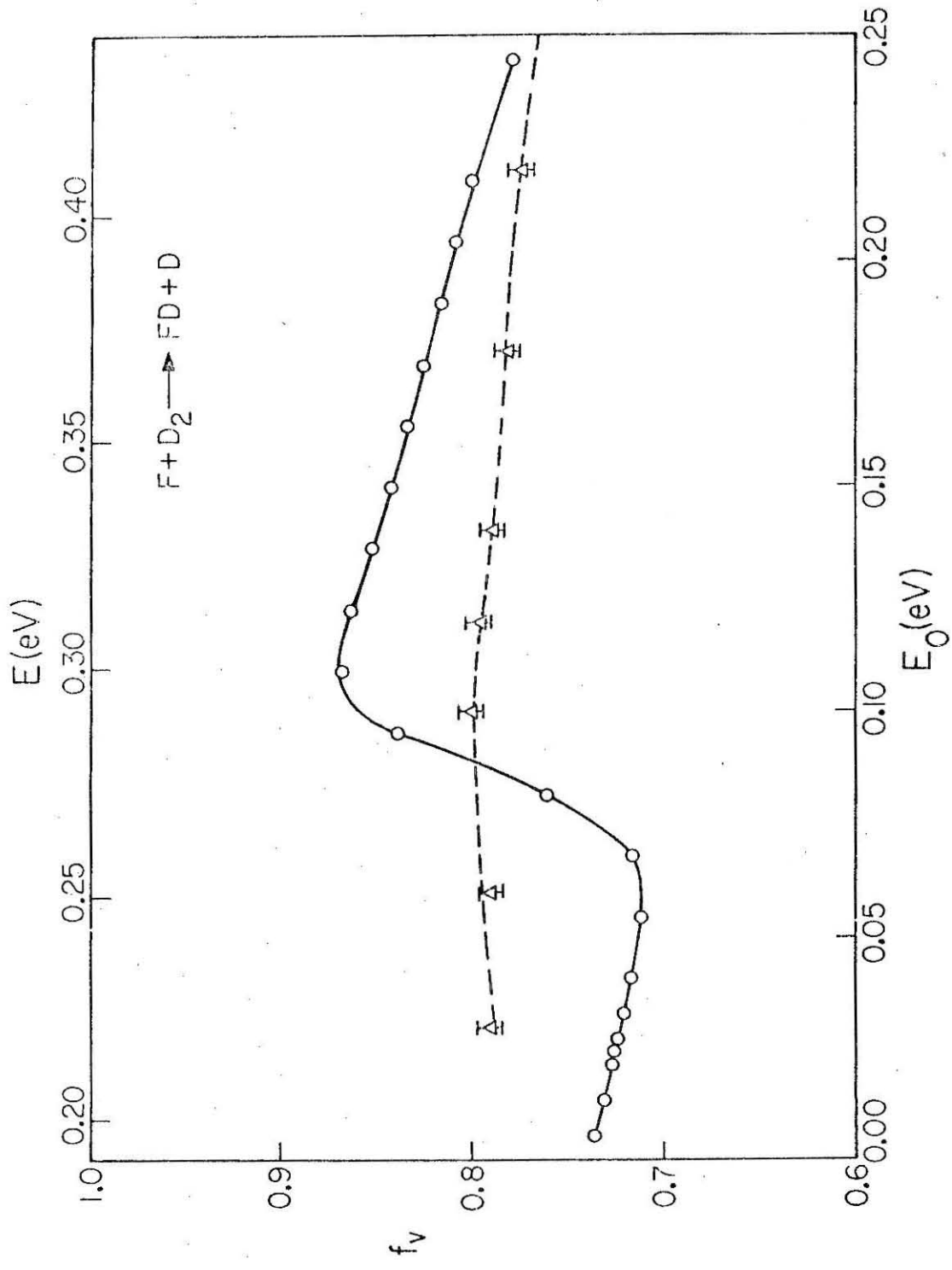
F + D2 ⟶ FD + D
E(eV)
0.40
0.35
0.30
0.25
0.20
1.0
0.9
0.8
0.7
0.6
fv
0.00
0.05
0.10
0.15
0.20
0.25
E0(eV)

Figure 5

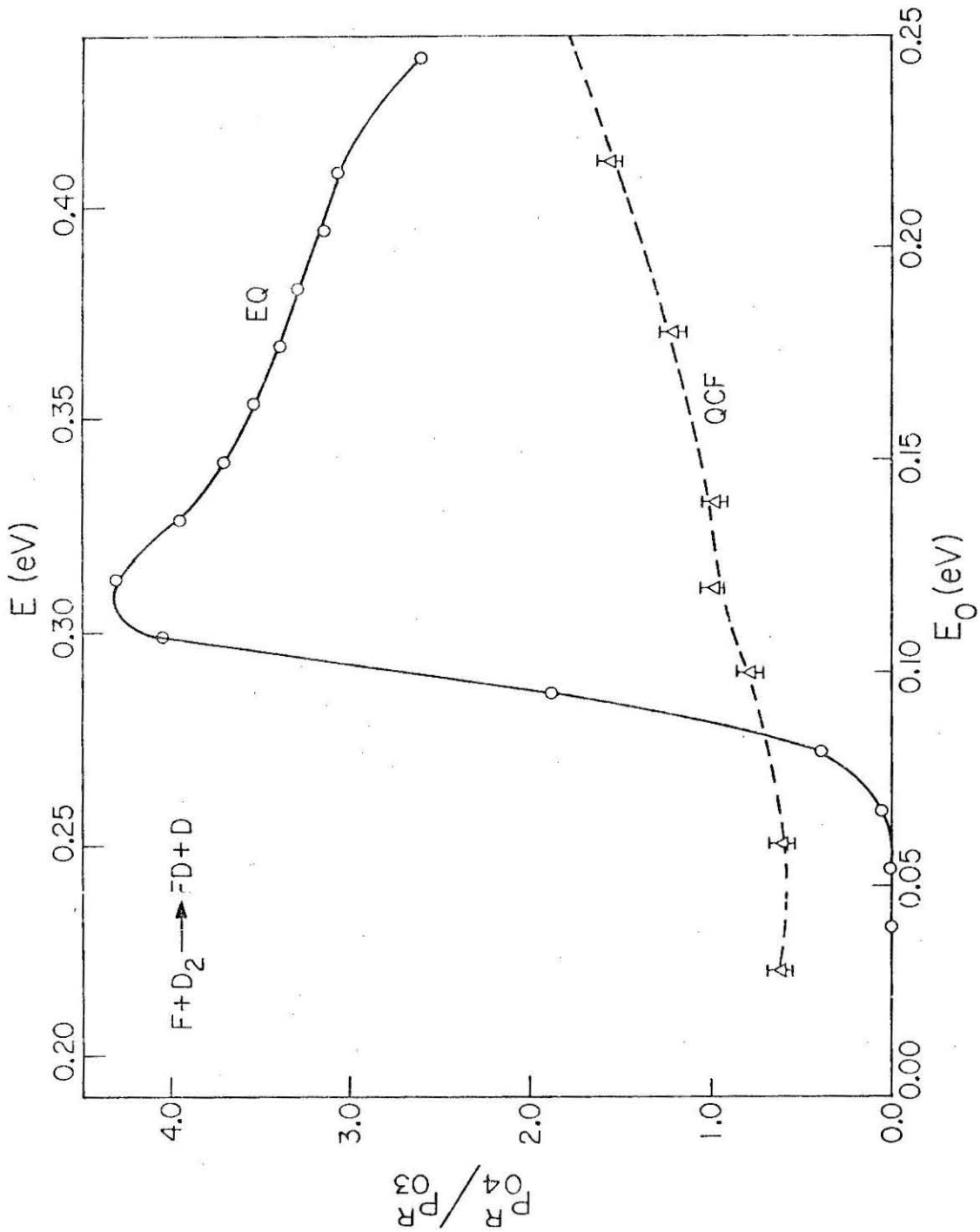
E (eV)
0.20
0.25
0.30
0.35
0.40
EQ
QCF
F+D2 → FD+D
4.0
3.0
2.0
1.0
0.0
0.00
0.05
0.10
0.15
0.20
0.25
E0 (eV)

Figure 6

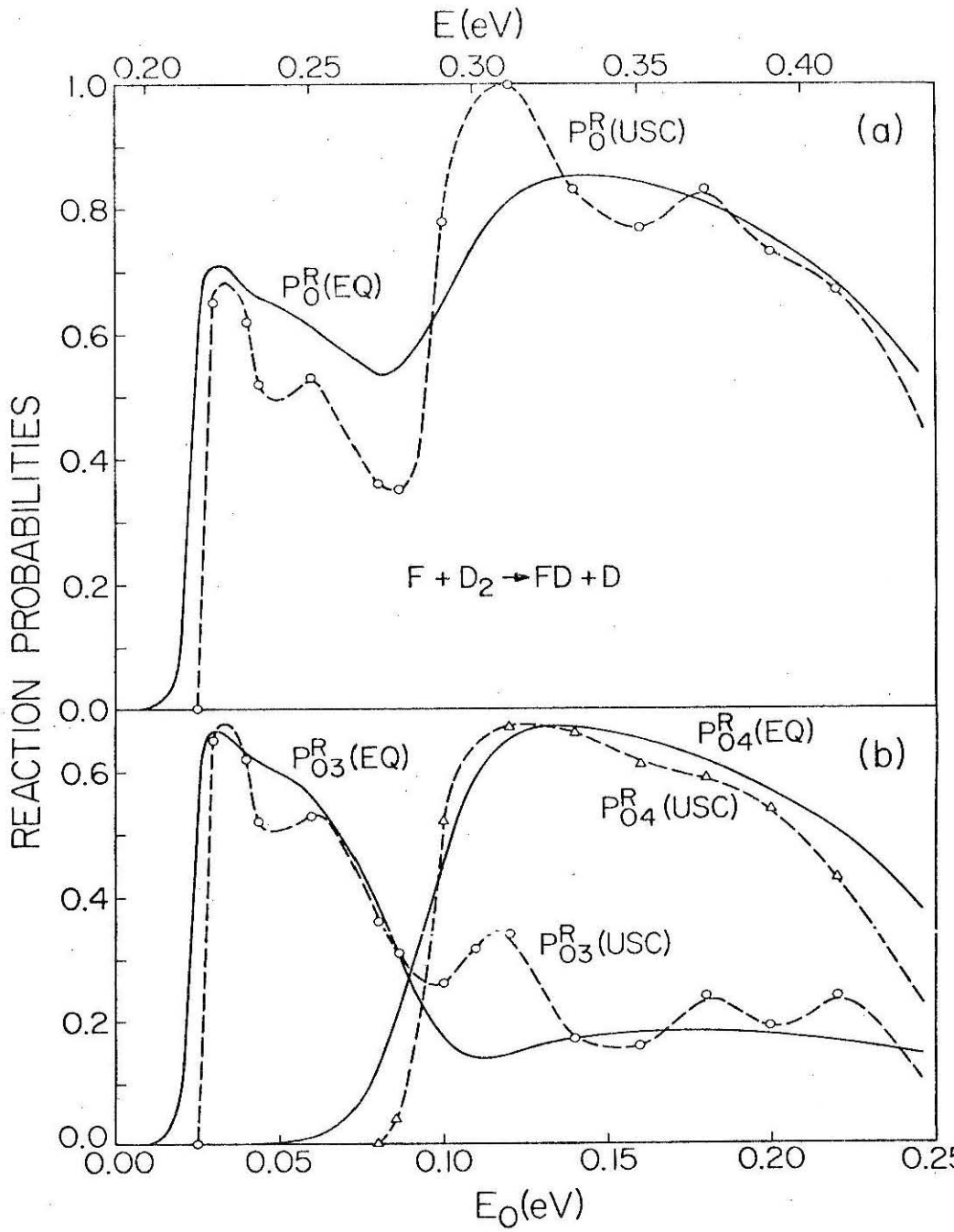
E(eV)
0.20
0.25
0.30
0.35
0.40
1.0
0.8
0.6
0.4
0.2
0.0
P_0^R(USC)
(a)
P_0^R(EQ)
F + D_2 → FD + D
REACTION PROBABILITIES
P_{03}^R(EQ)
P_{04}^R(EQ)
(b)
P_{04}^R(USC)
P_{03}^R(USC)
0.00
0.05
0.10
0.15
0.20
0.25
E_0(eV)

Figure 7

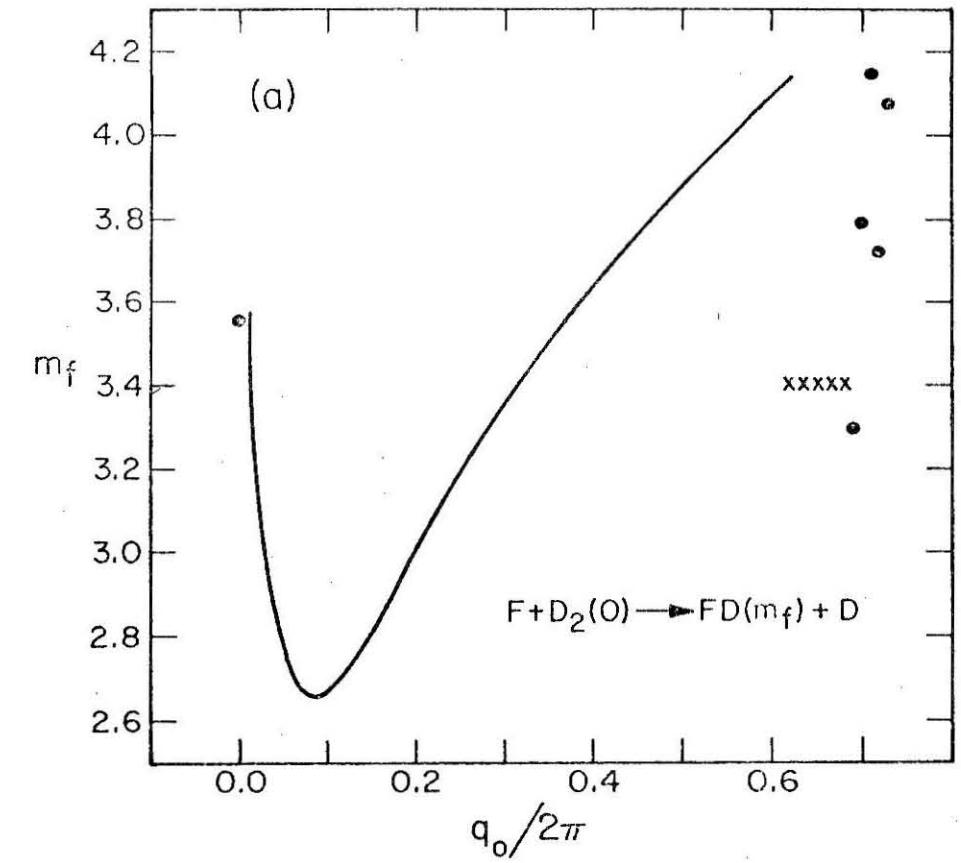
(a)
4.2
4.0
3.8
3.6
3.4
3.2
3.0
2.8
2.6
m_f
xxxxx
$F+D_2(0) \rightarrow FD(m_f)+D$
0.0
0.2
0.4
0.6
$q_o/2\pi$

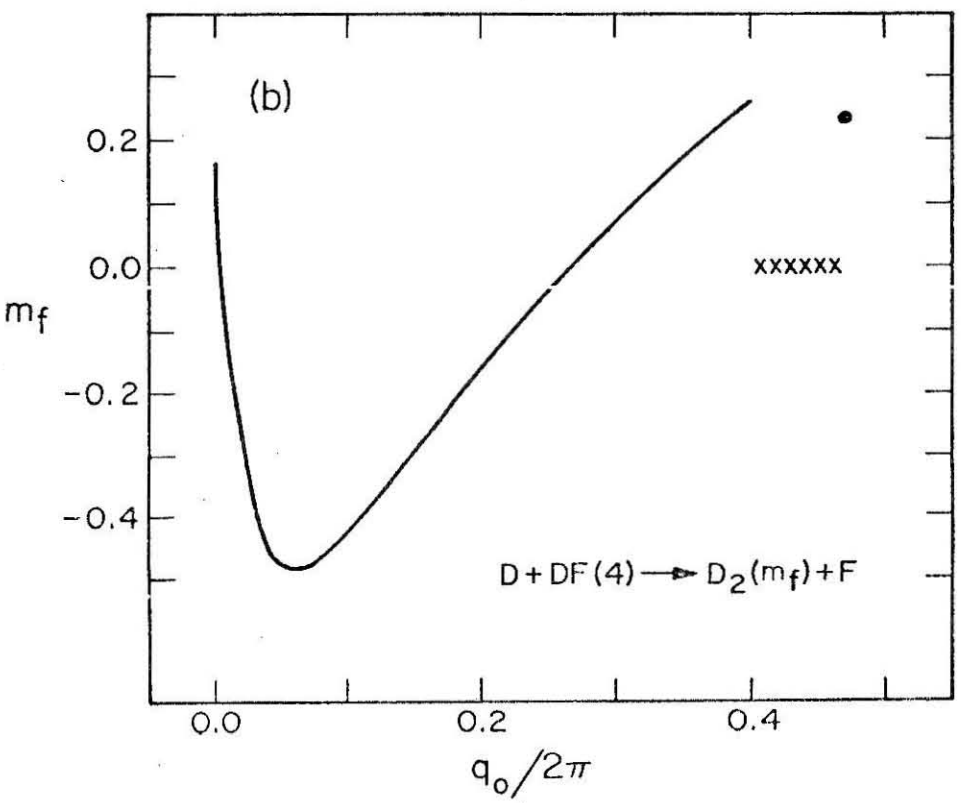
(b)
0.2
0.0
-0.2
-0.4
m_f
xxxxxx
$D+DF(4) \rightarrow D_2(m_f)+F$
0.0
0.2
0.4
$q_o/2\pi$

Figure 8

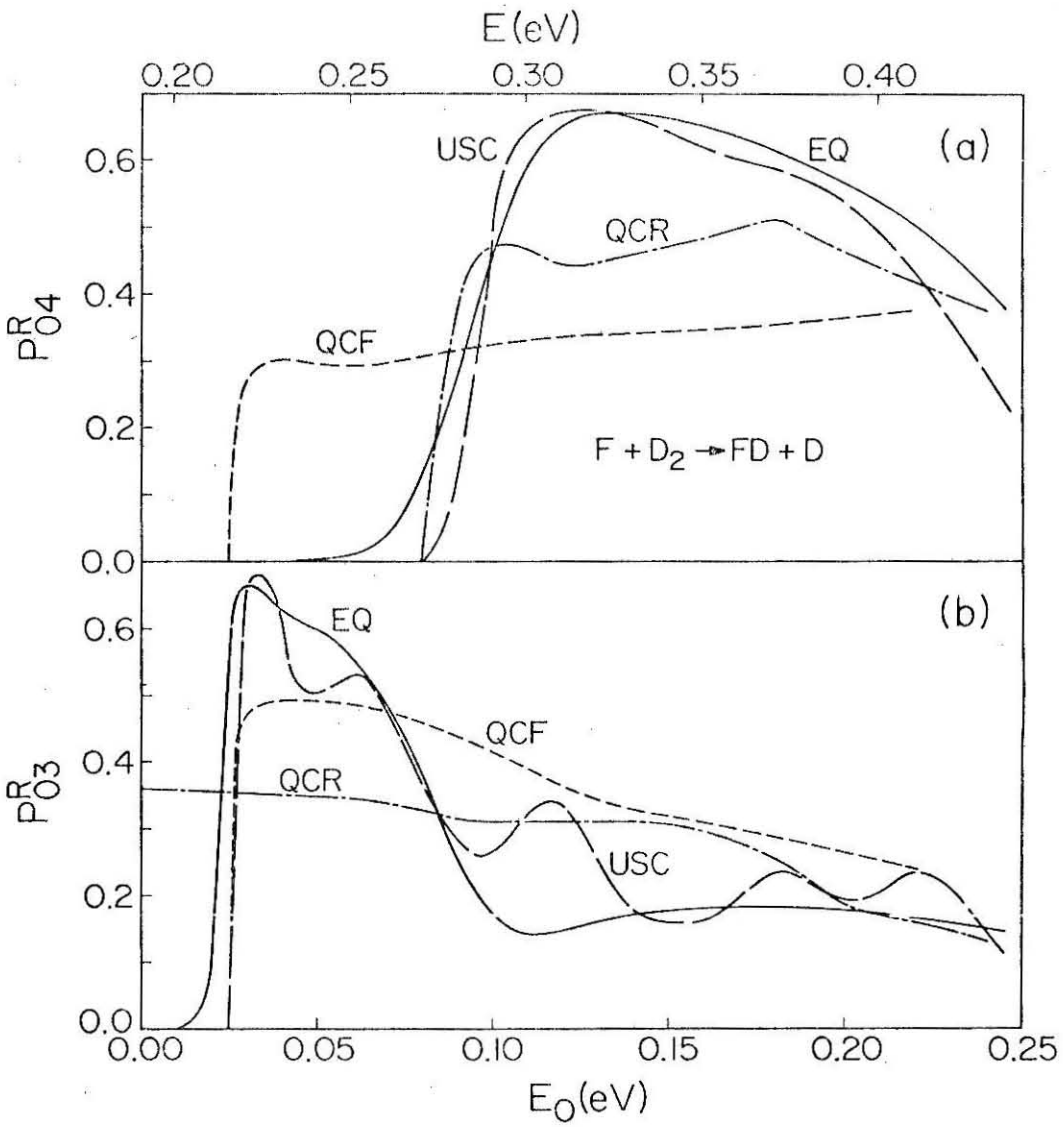
E(eV)
0.20
0.25
0.30
0.35
0.40
USC
EQ
(a)
QCR
QCF
P^R_{04}
0.6
0.4
0.2
0.0
F + D_2 → FD + D
(b)
EQ
QCF
QCR
USC
P^R_{03}
0.6
0.4
0.2
0.0
0.00
0.05
0.10
0.15
0.20
0.25
E_0(eV)

Figure 9

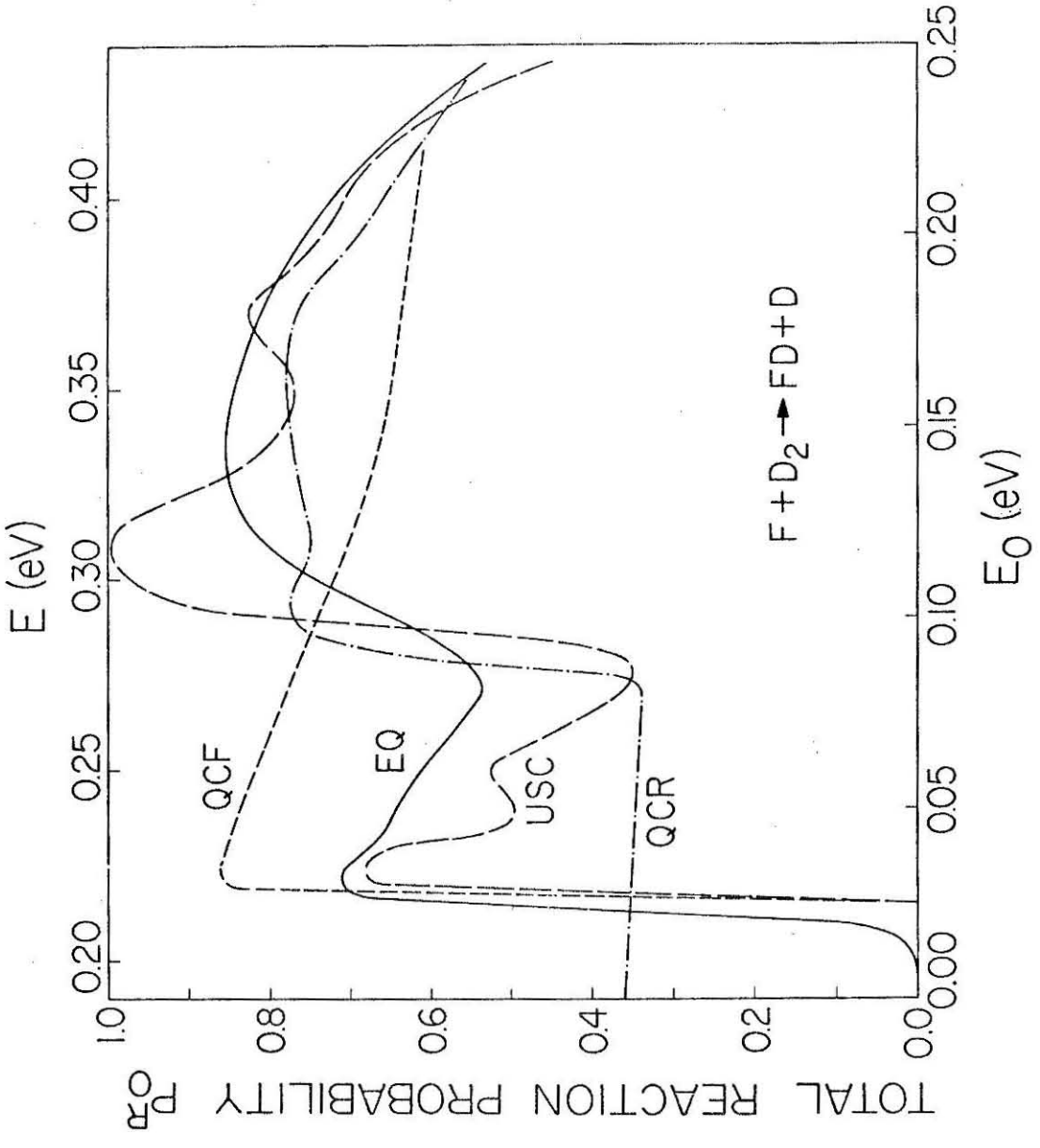
TOTAL REACTION PROBABILITY P_{OR}
1.0
0.8
0.6
0.4
0.2
0.0
0.20
0.25
0.30
0.35
0.40
E (eV)
0.00
0.05
0.10
0.15
0.20
0.25
E_O (eV)
F + D_2 → FD + D
QCF
EQ
USC
QCR

Figure 10

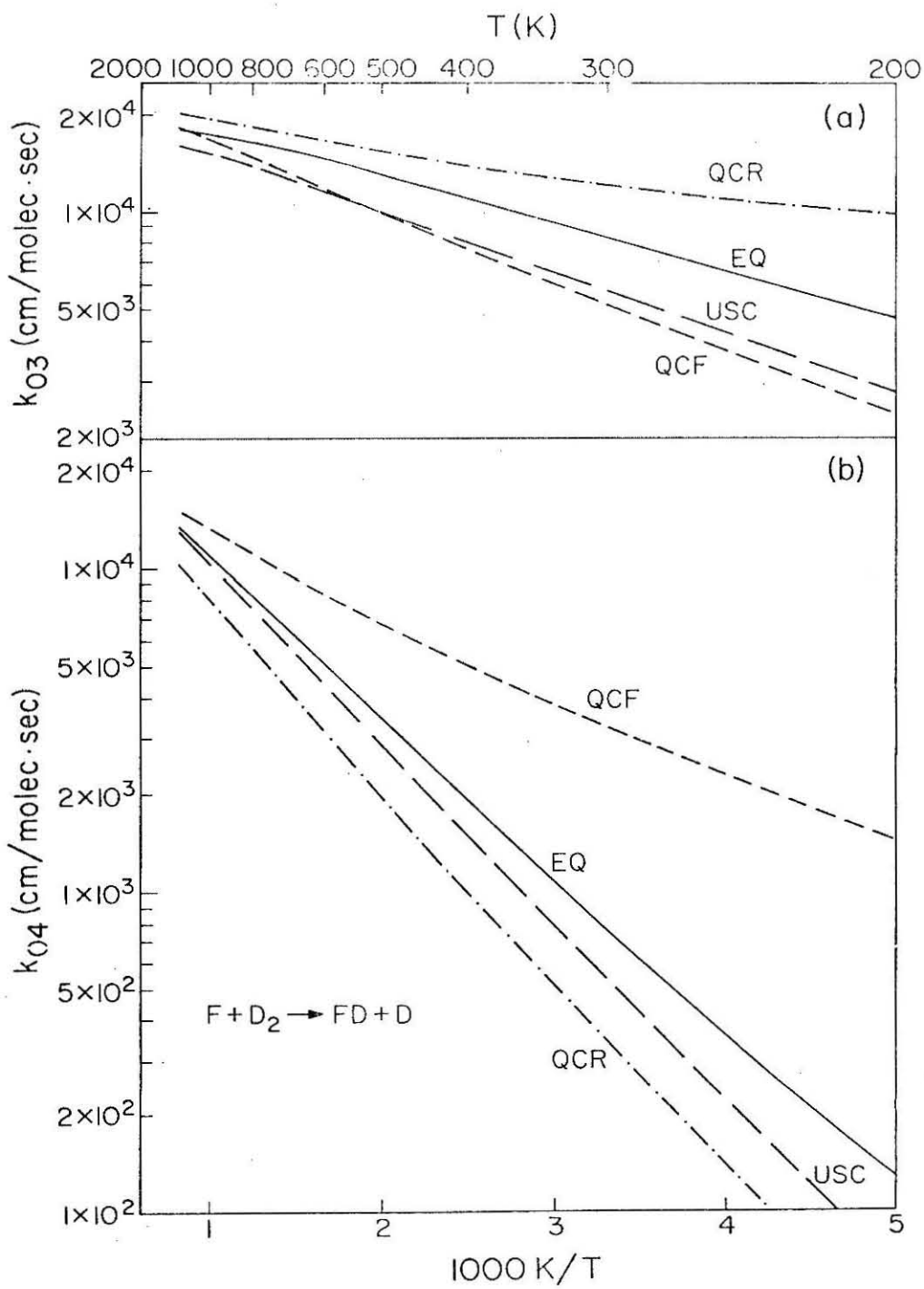
T(K)
2000 1000 800 600 500 400 300 200
(a)
QCR
EQ
USC
QCF
k_{03} (cm/molec·sec)
2×10^4
1×10^4
5×10^3
2×10^3
(b)
QCF
EQ
QCR
USC
F + D_2 → FD + D
k_{04} (cm/molec·sec)
2×10^4
1×10^4
5×10^3
2×10^3
1×10^3
5×10^2
2×10^2
1×10^2
1
2
3
4
5
1000 K/T

Figure 11

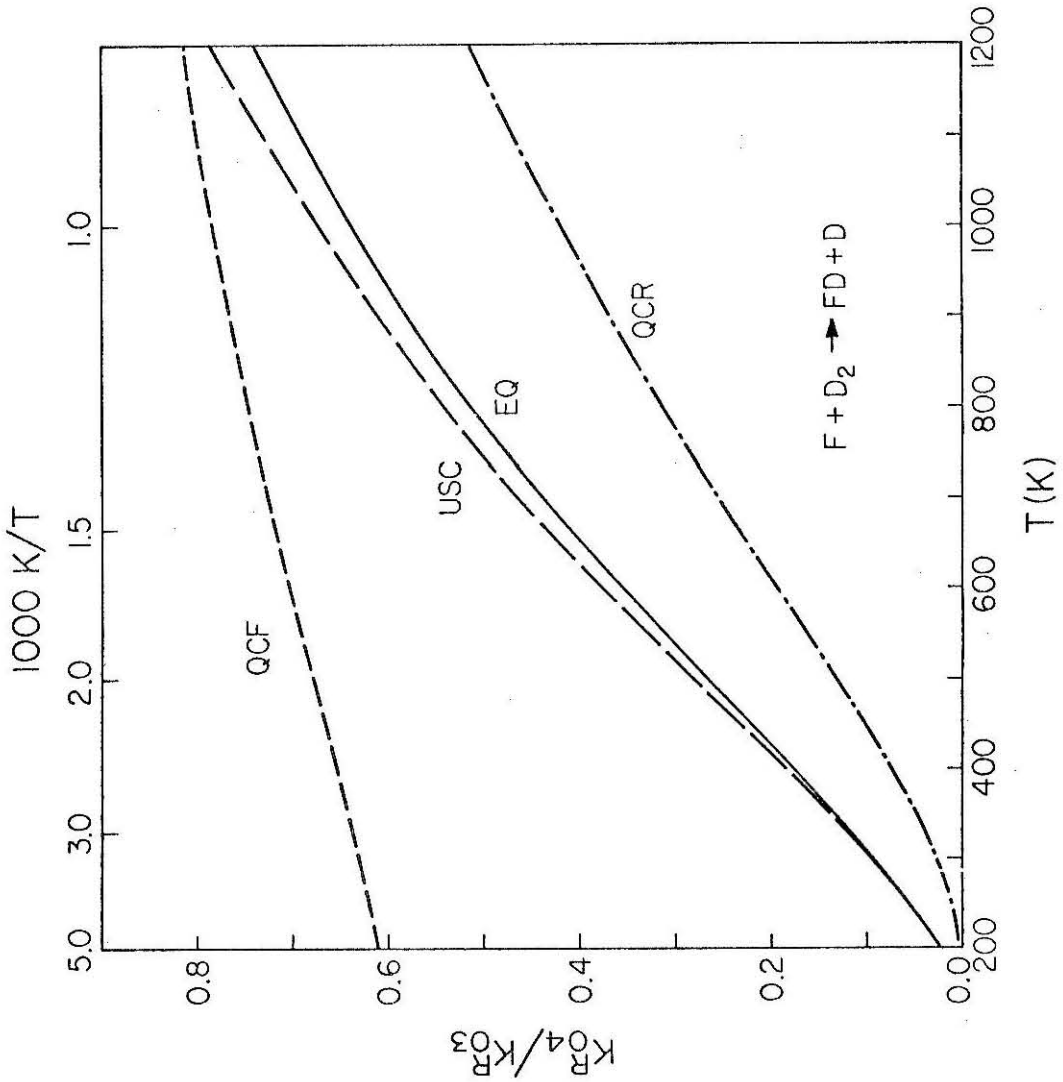
1000 K/T
5.0
3.0
2.0
1.5
1.0
T (K)
200
400
600
800
1000
1200
0.0
0.2
0.4
0.6
0.8
K_{O4}^{R}/K_{O3}^{R}
QCF
USC
EQ
QCR
F + D2 → FD + D

Figure 12

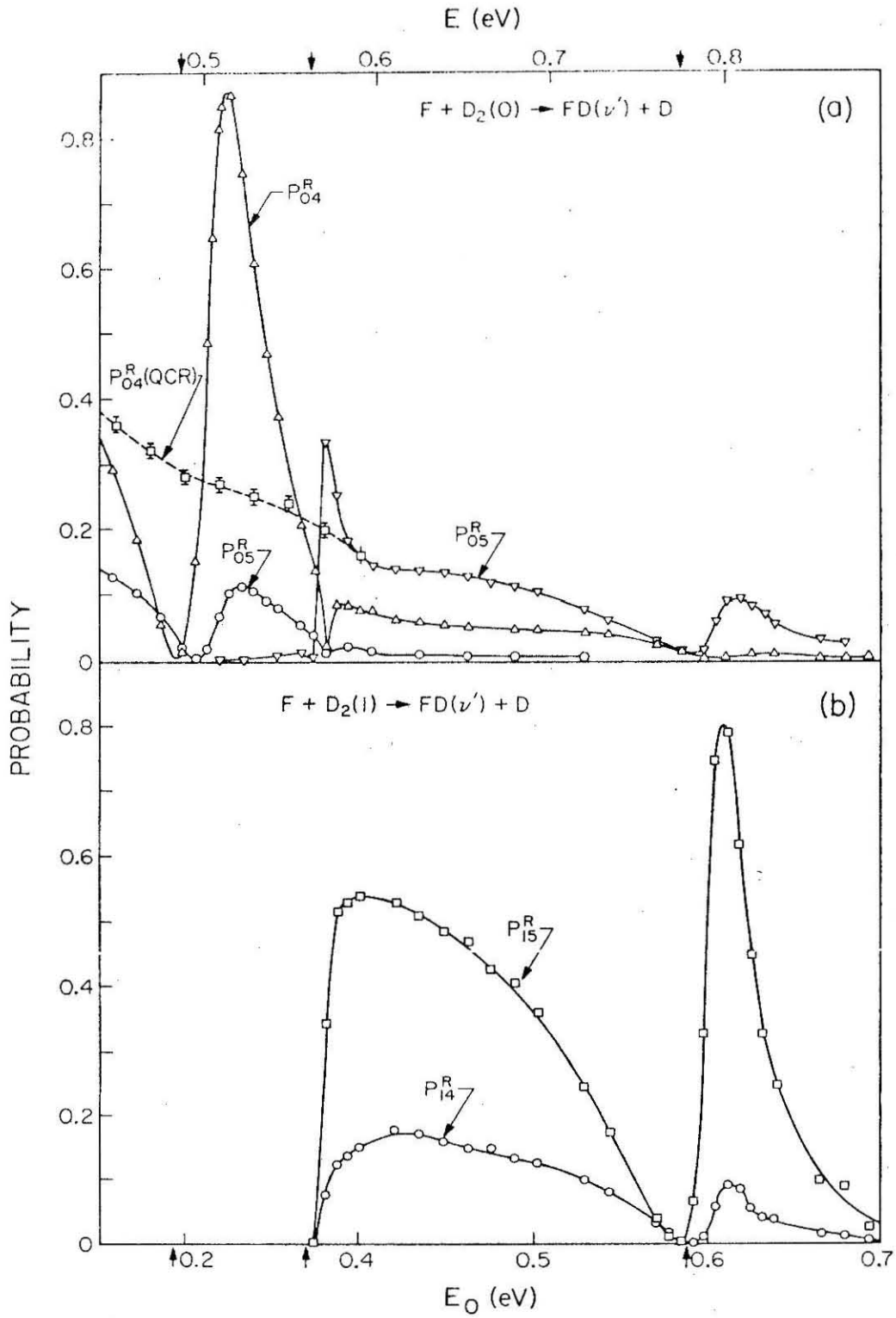
E (eV)
0.5
0.6
0.7
0.8
F + D2(0) → FD(ν') + D
(a)
P04R
P04R(QCR)
P05R
P05R
F + D2(1) → FD(ν') + D
(b)
P15R
P14R
PROBABILITY
0.2
0.4
0.5
0.6
0.7
E0 (eV)

Figure 13

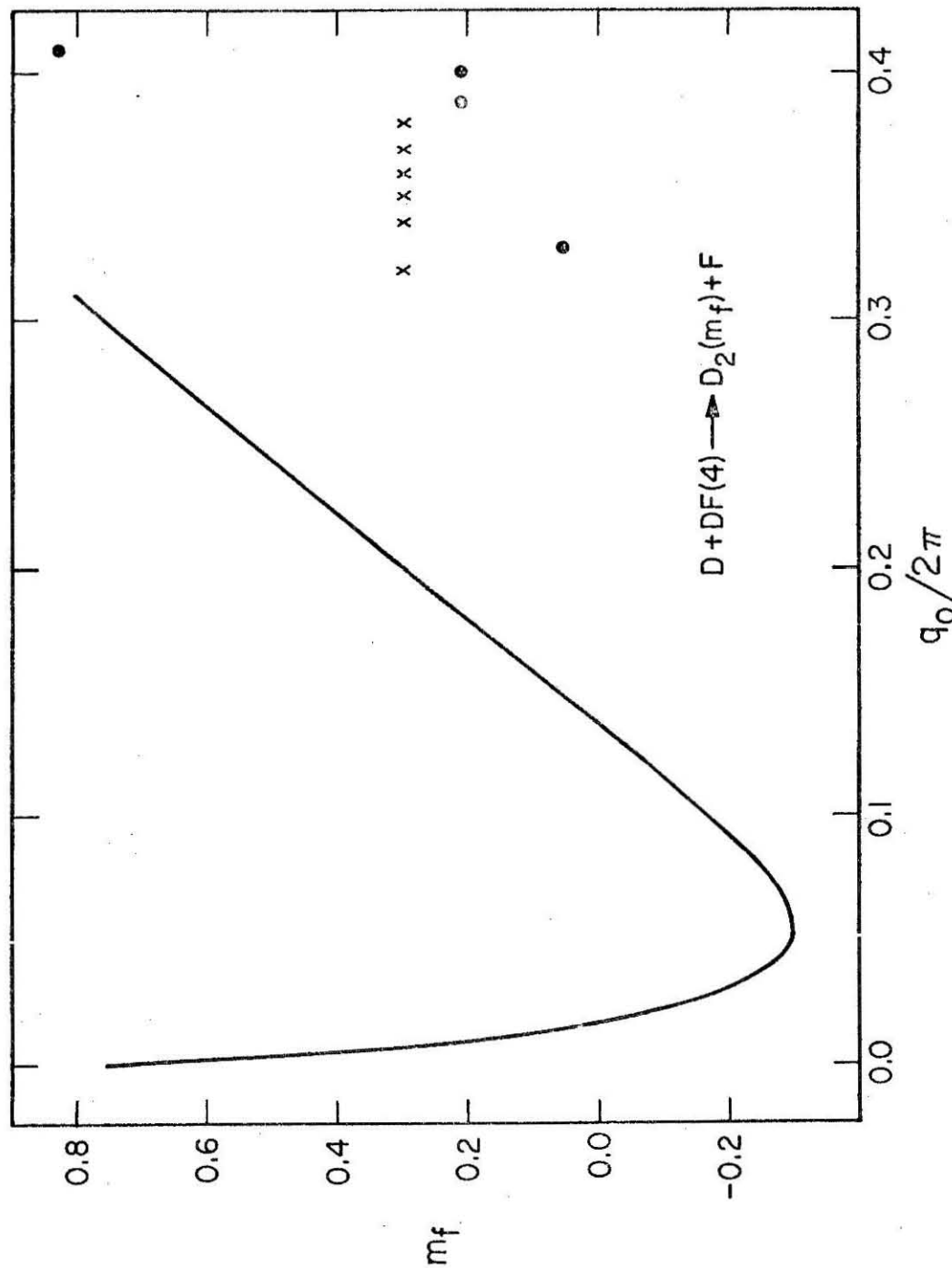

Figure 14

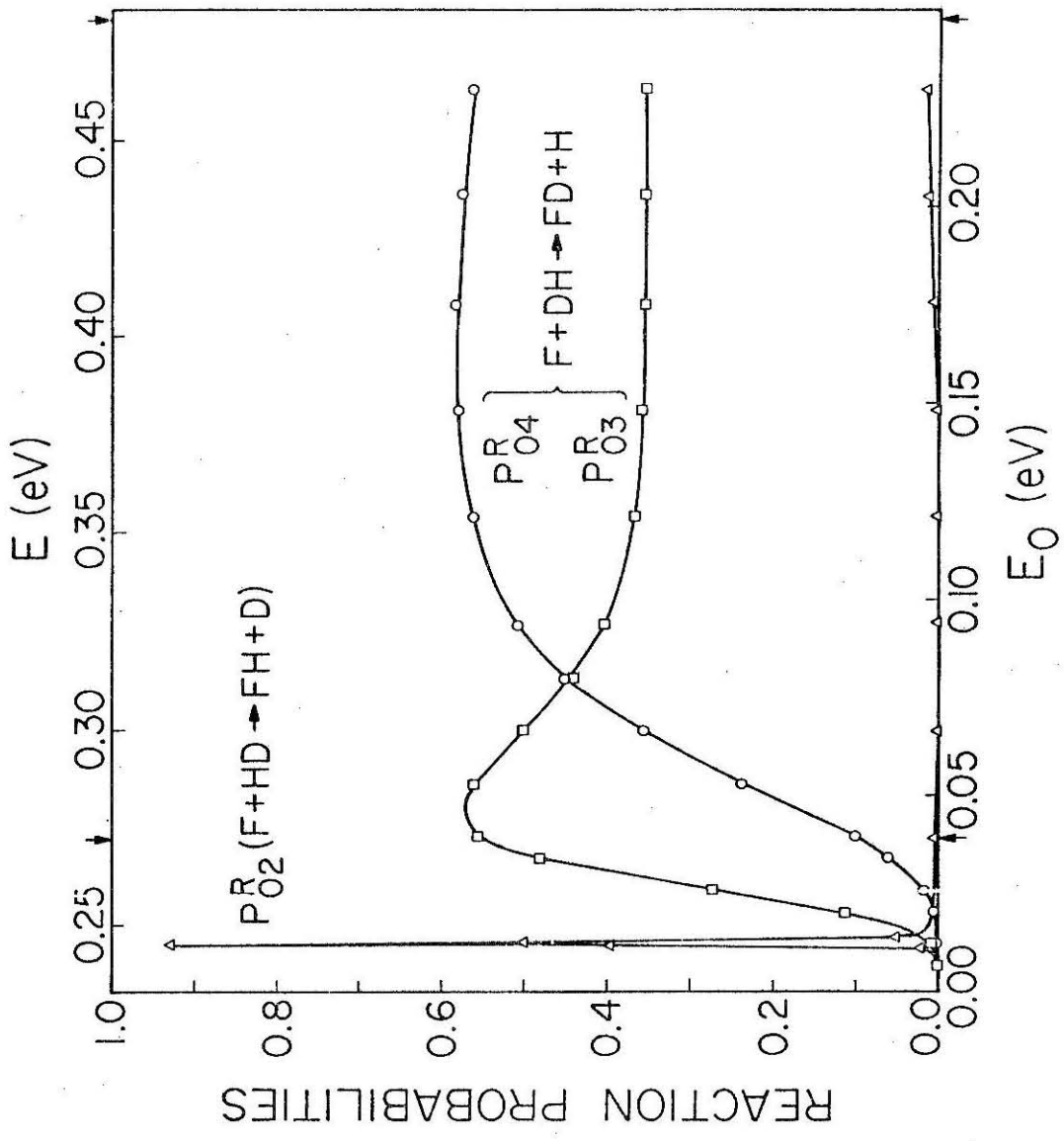
E (eV)
0.25
0.30
0.35
0.40
0.45
P^R_{02}(F+HD→FH+D)
P^R_{04}
P^R_{03}
F+DH→FD+H
1.0
0.8
0.6
0.4
0.2
0.0
REACTION PROBABILITIES
0.00
0.05
0.10
0.15
0.20
E_0 (eV)

Figure 15

SUMMARY

SUMMARY

The comparisons between standard forward quasi-classical calculations and the exact quantum ones for the $H + H_2$ and $F + H_2 (D_2)$ reactions reveal several important areas of disagreement. Low energy tunneling, especially in the $H + H_2$ reaction, is of course not reproduced by the classical calculations. This failure of the quasi-classical method is responsible for the factor of twenty-five difference in the corresponding thermal rate constants at 200°K (with the classical result less than the quantum one, of course). Another significant difference between the two sets of results is in the energy dependences of the reaction probabilities. The classical ones tend to be smooth and, in general, monotonic functions of the energy. The quantum ones, however, oscillate markedly about the corresponding classical ones as a function of the energy. In fact, the quasi-classical forward results resemble the averaged quantal ones. The arbitrary way of assigning final "quantum" states in the quasi-classical method results, in several cases, in gross disagreement with quantal results at energies in the vicinity of the energetic threshold for a given transition.

The attempt to reproduce quantum oscillations with the semi-classical expressions for transition probabilities was largely unsuccessful. The semi-classical interpretation of quantum oscillations as simple interference effects apparently does not apply to the reactions considered. It has recently been shown that most of the quantum

oscillations are due to resonant scattering which interferes with direct scattering. Thus, we conclude that the semi-classical theory used is capable of treating the direct scattering but at best it offers only an averaged description of resonant scattering.

The semi-classical theory does provide a unique and logically consistent way of quantizing initial and final states of the reactants and products, respectively. Evidently, this is responsible for the fact that the semi-classical transition probabilities are in qualitative agreement (at least) with the quantum ones near the threshold energies. This is a significant improvement over the quasi-classical forward results. An extension of semi-classical utilizing complex-valued trajectories in complex time was not incorporated in our calculations. Hence, the semi-classical results do not show any improvement over the quasi-classical ones with regard to collision processes which proceed by tunneling in classically forbidden regions of configuration space.

The investigation of reverse quasi-classical results revealed many interesting, if not totally understood, results. First, it was found that the differences between forward and reverse results could be substantial, especially for energies in the vicinity of energetic thresholds for certain transitions. Second, one of the two sets of quasi-classical results was in much better agreement with the exact ones than the other. The implications of this result for three-dimensional trajectory calculations could be very significant. A comparison of the quasi-classical reverse and forward results for the $F + H_2$

reaction suggests strongly that the three-dimensional forward trajectory calculations are not as accurate as the reverse ones might be.

The investigation of the possibility of using the quantum probability distribution function to phase-average classical trajectories proved that the procedure is illogical. It was shown that such a sampling technique resulted in transition probabilities which were (symmetric) functions of the initial atom-molecule separation distance.

A comparison of exact quantum and quasi-classical current densities, streamlines, and current density profiles revealed some interesting differences and similarities between the two sets of results. Due, apparently, to the fact that classically the H_2 molecule can be vibrationally excited at any collision energy, the classical current densities exhibit an oscillatory pattern. In contrast to the classical behavior, the quantum current densities are non-oscillatory for total energies below the threshold for vibrational excitation of H_2. For total energies above this threshold the classical and quantum results do show some similarities in structure as well as in the regions of configuration space sampled by the respective current densities. An interesting and striking difference between the classical and quantum current densities is seen at a total energy at which both the classical and quantum reaction probabilities are equal to unity. The classical result shows a sharp "pinching" near the saddle point of the potential surface whereas the quantal results shows no such effect.

APPENDIX 1.

Appendix 1: Symmetry Properties of the "Quantum" Total Reaction Probability, $P_Q(R)$

In paper I.2 it was noted that the "quantum" total reaction probability, $P_Q(R)$, is a symmetric function of R (the initial atom-molecule separation) with respect to some value of R, denoted by $\bar{R}$. It was noted that this symmetry resulted from the fact that the quantum distribution function, $F_Q(q)$, is symmetric about the point $q = \pi$. We prove this property in this appendix.

We wish to prove the following theorem. If the quantum distribution function, $F_Q(q)$, is symmetric about $q = \pi$, i.e.,

$$F_Q(\pi + q) = F_Q(\pi - q), \tag{1}$$

then for some value of R, denoted by $\bar{R}$, P_Q satisfies the following:

$$P_Q(\bar{R} + a) = P_Q(\bar{R} - a), \tag{2}$$

where a is some arbitrary displacement from $\bar{R}$. Without loss in generality, let us assume that for a given value of R, R_0, there corresponds an interval in q-space, $q_2 - q_1$, such that every trajectory with the initial conditions $R = R_0$ and $q_1 \leq q \leq q_2$ is a reactive one. In general, the midpoint of this interval, $(q_1 + q_2)/2$, does not equal π but differs from it by an amount δ, given by

$$\delta = \pi - (q_1 + q_2)/2. \tag{3}$$

Let us now displace the interval $q_2 - q_1$ by the amount δ. A new interval, $q_2' - q_1'$, results with the property that

$$(q_1' + q_2')2 = \pi. \tag{4}$$

This new interval has a corresponding R, denoted by $\bar{R}$, and given by

$$\bar{R} = R_0 + v\delta/\omega, \tag{5}$$

where v is the initial relative velocity of the atom-diatom system, ω is the angular frequency of the periodic motion of the isolated diatom (with a given internal energy initially). Equation (5) results from the fact that asymptotically q(t) and R(t) are given by

$$q(t) = q_0 + \omega t$$
$$R(t) = R_0 + vt$$

and hence

$$\Delta q/\omega = \Delta t$$

and thus

$$\Delta R = v\Delta q/\omega,$$

which is a general statement of eq. (5). We now show that $\bar{R}$ given by eq. (5) is the point of symmetry of the function $P_Q(R)$. By definition P_Q, in q-space, is given by (see eq. (1) of paper I.2)

$$P_Q = \left[\int_0^{\pi} dq\, K^+(q)\, F_Q(q) + \int_{\pi}^{2\pi} dq\, K^-(q)\, F_Q(q)\right]/2\pi\,.$$

At $R = R_0$ this expression becomes

$$P_Q(R_0) = \int_{q_1}^{q_2} dq\, F_Q(q)/2\pi,$$

and for $R = \bar{R}$ it becomes

$$P_Q(\bar{R}) = \int_{q_1'}^{q_2'} dq\ F_Q(q)/2\pi. \tag{6}$$

Consider now arbitrary displacements from $\bar{R}$ by amount $\pm a$. This corresponds to displacing the interval $q_2' - q_1'$ by amounts $\pm\Delta$, where

$$\Delta = a\omega/v.$$

Thus, to prove that $P_Q(\bar{R} + a) + P_Q(\bar{R} - a)$ it suffices to show, according to eq. (6), that

$$\int_{q_1'+\Delta}^{q_2'+\Delta} dq\ F_Q(q)/2\pi = \int_{q_1'-\Delta}^{q_2'-\Delta} dq\ F_Q(q)/2\pi\ . \tag{7}$$

To prove the validity of eq. (7), we note that the following integrals have integration ranges placed symmetrically about $q = \pi$:

$$\int_{q_1'-\Delta}^{q_2'+\Delta} dq\ F_Q(q), \qquad \int_{q_1'+\Delta}^{q_2'-\Delta} dq\ F_Q(q), \tag{8}$$

and thus

$$\int_{q_1'-\Delta}^{\pi} dq\ F_Q(q)/2\pi = \int_{\pi}^{q_2'+\Delta} dq\ F_Q(q)/2\pi \tag{9}$$

and

$$\int_{q_1'+\Delta}^{\pi} dq\ F_Q(q)/2\pi = \int_{\pi}^{q_2'-\Delta} dq\ F_Q(q)/2\pi. \tag{10}$$

Note that we have made use of the symmetry of the integration range of the integrals given by eq. (8) and the fact that $F_Q(q)$ is symmetric

about π to arrive at eqs. (9) and (10). Let us now add the left hand side of eq. (10) to the right hand side of eq. (9) and similarly add the right and left hand sides of eqs. (10) and (9) respectively to obtain:

$$\int_{q_1'+\Delta}^{q_2'+\Delta} dq\ F_Q(q)/2\pi = \int_{q_1'-\Delta}^{q_2'-\Delta} dq\ F_Q(q)/2\pi\ . \tag{11}$$

This equation is identical to eq. (7) and hence we have proved that $P_Q(R)$ is a symmetric function of R with respect to some value of R, $\bar{R}$. Indeed, in paper I.2 (Figure 1) the symmetry of $P_Q(R)$ was demonstrated numerically.

APPENDIX 2

Appendix 2: Analytical Continuation of the Semi-Classical S Matrix

In this appendix we describe the analytical continutaion method used to calculate certain semi-classical S-matrix elements for the $F + H_2$ and $F + D_2$ reactions described in the preceding papers.

As discussed in the preceding papers (especially see paper I.3 the roots to the transcendental equation

$$m^{\beta} = m^{\beta}(q_o^{\alpha}; n^{\alpha}, E) \tag{1}$$

are sought in the semi-classical analysis. That is, at fixed values of n^{α} (the action number of the molecule initially) and E (the total energy) roots, $q_o^{\alpha}i$, are sought; m^{β} (the action number of the molecule in arrangement channel β finally) is a specified integer. An interesting situation arises when there are no real roots to eq. (1) at some particular E. As discussed in paper I. 3 the semi-classical S-matrix element $S_{m^{\beta}n^{\alpha}}$ is apparently zero. However, a more interesting and fruitful alternative is to seek complex roots to eq. (1). This approach was first developed by Miller and co-workers[1] and Marcus and co-workers.[2] In its simplest form, the idea is to make use of the properties of the function $m^{\beta}(q_o^{\alpha})$ (we suppress the n^{α} and E variables hereafter) on the real q_o^{α} axis. If there is some value $\overline{m}^{\beta} = m^{\beta}(\overline{q}_o^{\alpha})$ which differs from the desired value by a "small" amount then the complex root(s) is expected to lie "close" to the real q_o^{α} axis. If that is the case, then this complex root can be found by simply analytically continuing the function $m(q_o^{\alpha})$ into the complex q_o^{α}-plane by means of

a power series representation. Note that even if the complex root(s) lies "far" from the real q_0^{α} axis it may be found in general by an analytic continuation of $m(q_0^{\alpha})$ (if indeed one exists). We shall not pursue this more general approach which has recently been considered by George and Miller[1d, 1e] and Stine and Marcus[2b].

In Figure 1 we show examples of typical behavior of the function $m(q_0^{\alpha})$ at energies for which no real roots are found (for the $F + H_2$ and $F + D_2$ reactions). There it is seen that the values $m^{\beta} = 2$ and $m^{\beta} = 3$ for the respective reactions are dynamically forbidden.

We now develop the theory for the analytical continuation of the semi-classical S-matrix. The expression for the S-matrix for a dynamically allowed transition is given by[1a, 2a]

$$S_{m^{\beta}n^{\alpha}} = \frac{1}{2\pi i\hbar} \left| \frac{\partial q_0^{\alpha}}{\partial m^{\beta}} \right|^{\frac{1}{2}} \exp[\, i\Delta(m^{\beta};n^{\alpha})/\hbar\,] \,. \qquad (2)$$

Thus, the analytical continuation of $S_{m^{\beta}n^{\alpha}}$ is accomplished by continuing the amplitude and phase of $S_{m^{\beta}n^{\alpha}}$ into the complex plane.

First we consider the analytic properties of a function of a complex variable near the real axis. Let f(z) be analytic in a neighborhood of $z = z_0$. Then we may write:

$$f(z) = f(z_0) + f'(z_0)(z-z_0) + f''(z_0)(z-z_0)^2/2\,! + \ldots$$

where, as usual

$$f'(z_0) = \lim_{z \to z_0} [f(z) - f(z_0)]/(z - z_0).$$

If we take $z \to z_0$ along the imaginary axis we have that

$$f'(z_0) = u_y(z_0) + i v_y(z_0)$$

where $u(z)$ and $v(z)$ are respectively the real and imaginary parts of $f(z)$ and where y denotes the imaginary axis. Taking $z \to z_0$ along the real axis we have that

$$f'(z_0) = u_x(z_0) + i v_x(z_0)$$

Now, we wish to consider the difference $z - z_0$ to be along the imaginary axis, i.e., $z - z_0 = i(y - y_0)$. Using the latter expression for $f'(z_0)$ (and the obvious extension to higher derivatives) we have

$$f(z) = f(z_0) + [u_x(z_0) + i v_x(z_0)]i(y-y_0) + [u_{xx}(z_0) + i v_{xx}(z_0)]i^2(y-y_0)^2/2$$
$$+ [u_{xxx}(z_0) + i v_{xxx}(z_0)]i^3(y-y_0)^3/6 + \ldots \quad .$$

Equating real and imaginary parts of the right and left hand sides of this equation, we have

$$u(z) = u(z_0) - v_x(z_0)(y - y_0) - u_{xx}(z_0)(y - y_0)^2/2 + v_{xxx}(z_0)(y - y_0)^3/6 + \ldots$$
$$v(z) = v(z_0) + u_x(z_0)(y - y_0) - v_{xx}(z_0)(y - y_0)^2/2 - u_{xxx}(z_0)(y - y_0)^3/6 + \ldots$$

Now, consider the equation

$$f(z) = m \ , \qquad (3)$$

where m is real and where we stipulate that $f(z_0)$ is a real number, n. Thus, $v(z) \equiv 0$ and, in addition, we see that $u_x(z_0) = 0$ (to second order in $y - y_0$). Thus, from the above equation for $u(z)$, we have the following for the first non-vanishing contribution to $f(z)$:

$$f(z) = m = \mathcal{U}(z_0) - \mathcal{U}_{xx}(z_0)(y - y_0)^2/2.$$

Hence, the imaginary part of the root to eq. (3) can be found trivially. Letting $\tau = y - y_0$ we have that

$$f(z) - f(z_0) = m - n = -\mathcal{U}_{xx}\tau^2/2$$

and thus,

$$\tau = \pm[2(m - n)/-\mathcal{U}_{xx}]^{\frac{1}{2}} . \qquad (4)$$

Let us now consider if what we have done makes sense for our later applications. First, the point z_0 is to lie on the real axis. Thus, $y_0 = 0$. The condition $\mathcal{U}_x(z_0) = 0$ is seen to be satisfied by our final action number function (cf. Figure 1). Also if $\mathcal{U}_x = 0$ occurs at a minimum then $\mathcal{U}_{xx} > 0$ and clearly $m - n < 0$ and if $\mathcal{U}_x = 0$ occurs at a maximum, then $\mathcal{U}_{xx} < 0$ and $m - n > 0$. Thus, eq. (4) is guaranteed to make mathematical sense. We see further that there really are two roots to eq. (3); they are complex conjugates of each other given by

$$z = x_0 + i\tau \text{ and } z^* = x_0 - i\tau .$$

This is a consequence of the Schwarz Reflection Principle.[3]

Let us now apply these results to the analytical continuation of $S_{m^\beta n^\alpha}$. Let m^β of eq. (1) be f(z), and let m be its desired value. Further, let n be the minimum value of the function m^β which occurs for $q_0^\alpha = \overline{q_0^\alpha}$. From eq. (4) we have

$$\tau = \pm[2(m - n)/-m^\beta qq(\overline{q_0^\alpha})]^{\frac{1}{2}} . \qquad (5)$$

Thus, according to eq. (2) and the above equation, the amplitude of $S_{m^{\beta}n^{\alpha}}$, $J_{m^{\beta}n^{\alpha}}$, is given by

$$J_{m^{\beta}n^{\alpha}} = [2\pi i\hbar\, m^{\beta}\, qq(\bar{q}_o^{\alpha})\tau]^{-\frac{1}{2}} . \qquad (6)$$

Note that $J_{m^{\beta}n^{\alpha}}$ is the same for each of the two roots $q_o^{\alpha} = \bar{q}_o^{\alpha} \pm \tau$.

To analytically continue the phase of $S_{m^{\beta}n^{\alpha}}$, $\Delta(m^{\beta}, n^{\alpha})$, we note that Δ will in general be complex in the complex q-plane (of course Δ is real on the real q_o^{α}-axis). Making use of the previous results, in particular the expansions of $\mathcal{U}(z)$ and $\mathcal{V}(z)$ just before eq. (2), we have

$$\mathrm{Re}\Delta\,(m^{\beta}(\bar{q}_o^{\alpha} \pm i\tau), n^{\alpha}) = \Delta\,(\bar{q}_o^{\alpha}) - \Delta qq(\bar{q}_o^{\alpha})\,\tau^2/2 \qquad (7a)$$

$$\mathrm{Im}\Delta(m^{\beta}(\bar{q}_o^{\alpha} \pm i\tau), n^{\alpha}) = -\Delta\, qqq\, \tau^3/3! \quad . \qquad (7b)$$

Note we have made use of the fact that $\Delta\, q(\bar{q}_o^{\alpha}) = 0$. Thus, we have established the analytical continuation of the amplitude and phase of $S_{m^{\beta}n^{\alpha}}$ up to order τ^2. This is expected to be adequate for $\tau \ll 1$. For $\tau > 1$ the power series expansion approach becomes inaccurate and a more direct method of analytical continuation is required.[1c, 1d, 1e, 2b]

To proceed from $S_{m^{\beta}n^{\alpha}}$ to the corresponding transition probability we make use of the "uniform" semi-classical expression (for classically allowed transitions)[1b, 4, 5] given by

$$P^{USC}_{m^{\beta}n^{\alpha}} = (J_1 + J_2)^2\, \pi\, |x|^{\frac{1}{2}}\, Ai^2(-x) + (J_1 - J_2)^2\, \pi\, |x|^{\frac{1}{2}} Bi^2(-x) \quad . \qquad (8)$$

J_1 and J_2 are the amplitudes of $S_{m^{\beta}n^{\alpha}}$ corresponding to the two roots, Ai(x) and Bi(x) are respectively the regular and irregular Airy functions[10]

and x is given by

$$x = [\tfrac{3}{4}(\Delta_1 - \Delta_2)]^{\frac{2}{3}},$$

where Δ_1 and Δ_2 are the phases of $S_{m^{\beta}n^{\alpha}}$ for the two roots. As shown previously, J_1 equals J_2 and $\Delta_1 - \Delta_2 = 2i\,\mathrm{Im}\,\Delta_1 = 2i\,\mathrm{Im}\,\Delta_2$. Thus,

$$x = [\tfrac{3}{2}\,\mathrm{Im}\,\Delta_1]^{\frac{2}{3}}\, i^{\frac{2}{3}}$$
$$= -[\tfrac{3}{2}\,\mathrm{Im}\,\Delta_1]^{\frac{2}{3}} .$$

Thus, eq. (8)

$$P^{USC}_{m^{\beta}n^{\alpha}} = 4J_{m^{\beta}n^{\alpha}}\,\pi\,|x|^{\frac{1}{2}}\,Ai^2(|x|) . \tag{9}$$

Note, in the limit $|x| \to \infty$,[6]

$$Ai(|x|) \underset{|x|\to\infty}{\sim} \frac{1}{2}\,\frac{1}{\pi^{\frac{1}{2}}}\,\frac{1}{|x|^{\frac{1}{4}}}\,\exp[-\tfrac{2}{3}\,x^{3/2}]$$
$$= \frac{1}{2\pi^{\frac{1}{2}}|x|^{\frac{1}{4}}}\,\exp[-\mathrm{Im}\,\Delta_1],$$

and from this we obtain the "primitive" semi-classical expression for the transition probability,

$$P^{PSC}_{m^{\beta}n^{\alpha}} = J_{m^{\beta}n^{\alpha}}\exp[-2\mathrm{Im}\Delta_1] . \tag{10}$$

In our calculations the functions $m^{\beta}(q_o^{\alpha})$ and $\Delta(q_o^{\alpha})$ were determined in the neighborhood of an approximate $\bar{q}_o^{\alpha}$ at ten or twenty points. These "data" points were then fit by a cubic spline curves. These curves were then used to determine the location of the "true"

$\bar{q}_o^{\alpha}$ and the quantities $m_{qq}(\bar{q}_o^{\alpha})$ and $\Delta_{qqq}(\bar{q}_o^{\alpha})$.

In the table below (Table 1) we give the values for the pertinent quantities contained in eqs. (9) and (10) for the energies and reactions indicated. From that table we see that the PSC and USC transition probabilities differ significantly when $\mathrm{Im}\,\Delta < 1$, however, they are equal (within error limits) for $\mathrm{Im}\Delta > 1$.

Table 1. Numerical values of quantities pertinent to the analytic continuation of semi-classical transition probabilities for the $F+H_2$ and $F+D_2$ reactions.

	$F+H_2(0) \rightarrow FH(2)+H$, E=0.378eV	$F+D_2(0) \rightarrow FD(3)+D$, E=0.411eV
$\bar{q}_0^{\alpha}$	3.41711	2.2571
$m^{\beta}(\bar{q}_0^{\alpha})$	2.01638	3.0166
τ	0.0896	0.0989
$m_{qq}(\bar{q}_0^{\alpha})$	4.08 ± 0.04	3.40 ± 0.03
$\Delta_{qqq}(\bar{q}_0^{\alpha})$	14530 ± 3000	938 ± 100
$J_{m^{\beta}n^{\alpha}}$	0.660	0.688
$Im\Delta$	1.74 ± 0.40	0.14 ± 0.01
$P^{PSC}_{m^{\beta}n^{\alpha}}$	0.02 ± 0.01	0.51 ± 0.02
$P^{USC}_{m^{\beta}n^{\alpha}}$	0.02 ± 0.01	0.25 ± 0.01

References

1. (a) W. H. Miller, J. Chem. Phys. 53, 3578 (1970); (b) W. H. Miller, Chem. Phys. Lett. 7, 431 (1970); (c) W. H. Miller and T. F. George, J. Chem. Phys. 56, 5668 (1972); (d) T. F. George and W. H. Miller, J. Chem. Phys. 57, 2458 (1972); (e) J. D. Doll, T. F. George and W. H. Miller, J. Chem. Phys. 58, 1343 (1973).
2. (a) R. A. Marcus, J. Chem. Phys. 54, 3965 (1971); (b) J. Stine and R. A. Marcus, Chem. Phys. Lett. 15, 536 (1972).
3. E. C. Titchmarsh, The Theory of Functions (Oxford Univ. Press, London, 1939), pp. 155-157.
4. J. N. L. Connor and R. A. Marcus, J. Chem. Phys. 55, 5636 (1971).
5. J. M. Bowman and A. Kuppermann, Chem. Phys. 2, 158 (1973).
6. M. Abramowitz and I. Stegun, Eds., Handbook of Mathematical Functions (U.S. Govt. Printing Office, Washington, D.C., 1964), pp. 446-452.

Figure Caption

Figure 1: Final action number m_f versus initial phase angle q_o for the $F + H_2$ reaction (a) and the $F + D_2$ reaction (b) for total energies E of 0.378 eV and 0.411 eV respectively.

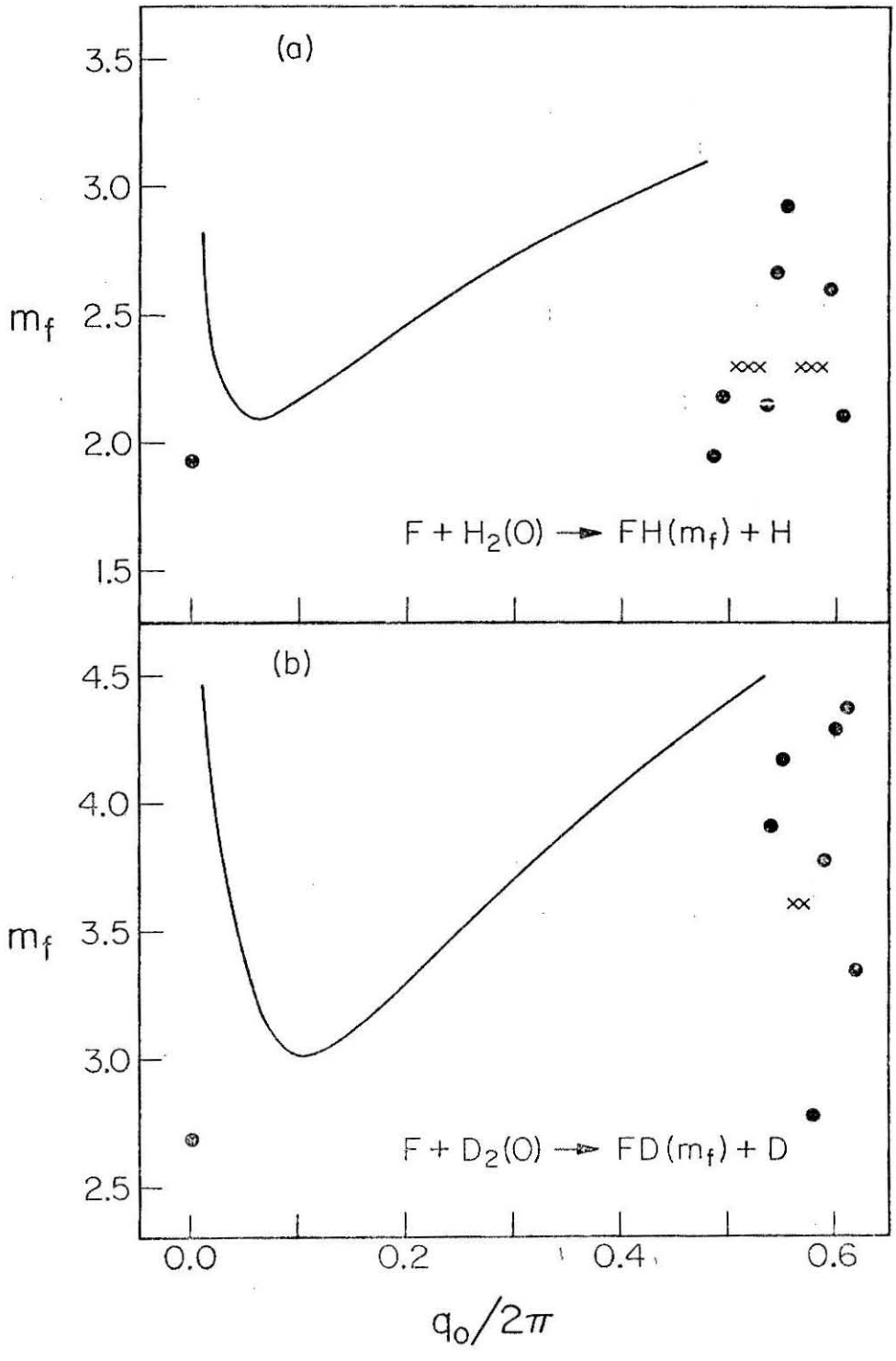
(a)
3.5
3.0
2.5
2.0
1.5
m_f
$F + H_2(0) \rightarrow FH(m_f) + H$
(b)
4.5
4.0
3.5
3.0
2.5
m_f
$F + D_2(0) \rightarrow FD(m_f) + D$
0.0
0.2
0.4
0.6
$q_o/2\pi$

Figure 1

PART II

A DIRECT TEST OF THE VIBRATIONALLY ADIABATIC THEORY OF CHEMICAL REACTIONS

INTRODUCTION

INTRODUCTION

The primary source of the great difficulty in solving the Schrödinger equation for collinear, coplanar, and three-dimensional chemical reactions is the multidimensional nature of the partial differential equation to be solved. For the collinear case, the Schrödinger equation is a two-mathematical dimensional partial differential equation. A great simplification in this equation results if the two independent variables, i.e., two nuclear coordinates can be decoupled from each other. If such a decoupling exists then the partial differential equation can be rewritten as two uncoupled ordinary differential equations. These equations can be solved with comparative ease. Unfortunately such a decoupling does not rigorously exist. However, with the introduction of so-called natural collision coordinates, R. A. Marcus formulated reactive scattering in a manner suitable to approximate uncoupling of the two degrees of freedom (in collinear collisions).

The resulting theory borrowed much from the simple ideas of Hirschfelder and Wigner on vibrationally adiabaticity in chemical reactions. This approximate theory has been cast into two forms; one is termed the vibrationally adiabatic zero-curvature theory and the other is the vibrationally adiabatic theory.

In paper II. 1 the vibrationally adiabatic zero-curvature theory is tested by making use of exact scattering wavefunctions describing the collinear $H+H_2$ exchange reaction. An energy scan of the results

is made to ascertain the range of validity (if any) of the approximate theory. In addition, the test is performed in several regions of configuration space to determine where the theory is reliable. Also, the factors which contribute to the failure of the theory are investigated. The work reported in this paper was carried out in collaboration with Dr. John T. Adams, Professor Donald G. Truhlar (and of course Professor Aron Kuppermann).

A test of the vibrationally adiabatic theory including curvature is presented in paper II. 2 for the symmetric stretch motion of the transition state of H_3. The results are compared with the zero-curvature ones given in paper II. 1. A numerical difficulty inherent in the adiabatic theory including curvature is pointed out and is shown to detract significantly from the potential usefulness of this theory. As previously the test makes use of exact scattering wavefunctions for the $H+H_2$ reaction. The results are presented as a function of the collision energy for reagent H_2 in its ground and first excited vibrational state.

II.1 A DIRECT TEST OF THE VIBRATIONALLY ADIABATIC (ZERO-CURVATURE) THEORY OF CHEMICAL REACTIONS

A DIRECT TEST OF THE VIBRATIONALLY ADIABATIC (ZERO-CURVATURE) THEORY OF CHEMICAL REACTIONS.

1. Introduction

Numerical techniques have recently been developed to calculate exact quantum scattering wavefunctions describing collinear atom-molecule reactions. With the availability of such wavefunctions it is possible to rigorously test old approximate theories of chemical reactions and to stimulate the development of new ones. One approximate theory that has received much attention is the historically important vibrationally adiabatic (VA) theory of chemical reactions. The idea of vibrational adiabaticity in chemical reactions was first introduced in 1939 by Hirschfelder and Wigner.[1] In both the classical and quantum versions of this theory, it is assumed that the motion of an atom-molecule system could be described by two separable degrees of freedom (for the collinear case) referenced to a "reaction path." Motion transverse to this path was assumed to adjust instantaneously so as to maintain its quantum state (or in the classical case to maintain its constant of the motion) as the reaction proceeded along this path. In the separated reagent and product limits this transverse motion is simply the vibration of the corresponding molecule. More recently, this idea was quantified by Marcus[2] who introduced "natural-collision coordinates" and expressed the quantum and classical hamiltonians in terms of these variables. Actual calculations of reaction probabilities and cross sections based on the vibrationally adiabatic theory have been performed by Child,[3] Wyatt,[4] Truhlar and Kuppermann,[5] and

Diestler and Karplus.[6] In the latter two calculations the vibrationally adiabatic zero-curvature (VAZC) results were compared with exact quantum ones for the collinear $H + H_2 \rightarrow H_2 + H$ reaction. Wu and Levine[7] also examined the validity of the VA theory in exact quantum calculations using a model potential energy surface. Comparisons between exact classical trajectory and classical vibrationally adiabatic theory calculations have also been done by Marcus and co-workers[8] and Tweedale and Laidler.[9] McCullough and Wyatt in a time-dependent wave packet treatment of the collinear $H + H_2$ reaction made a time-dependent test of the VAZC theory at one energy.[10] In addition to its historical significance the VA theory of chemical reactions is closely connected with transition state theory.[11,1] It has been shown that the validity of VA theory is a sufficient condition for the validity of transition state theory.[12] In a more modern context the suitability of a VA or VAZC basis set in performing exact quantum reactive scattering calculations using close-coupling techniques is also of interest.

A direct test of the VAZC theory is made in the present paper. We use exact scattering wavefunctions calculated previously[5] for the collinear $H + H_2 \rightarrow H_2 + H$ reaction to determine the extent of adiabaticity in the reagent, strong interaction, and product regions of configuration space. The total energy range considered, 0.2778 eV to 1.0331 eV, allows for ground and first excited vibrational states of the reagent and product H_2. A preliminary account of some of these results has already been reported.[13]

2. Theory

Natural-collision coordinates[2-4] (s, x) are defined with respect to a curve C which passes smoothly from the reagent configuration, through the strong interaction region, and to the product configuration. The two-dimensional configuration space in which C is defined can be chosen in a variety of ways. As previously[5a,13] we have chosen the transition state normal-mode coordinate space with coordinates[14,15]

$$p = \sqrt{3}/2\ (r_{AB} + r_{BC} - 2r_o),$$

$$q = (1/2)(r_{BC} - r_{AB}),$$

where r_{AB} and r_{BC} are internuclear distances in the collinear A-B-C system and $r_{AB} = r_{BC} = r_o$ is the location of the saddle point of the potential energy surface. The potential energy surface employed in our calculations is a Wall-Porter[16] fit to the SSMK surface[17] with a scaled barrier height of 0.424 eV.[15] The curve C is the minimum energy path in the (p, q) coordinate system, i.e., it is the path of steepest descent from the saddle point p = q = 0 to the reagent and product regions of space. The coordinate s is defined as the distance from an origin on C to a point Q on C and x is the shortest distance from any point to Q. The origin is chosen at the saddle point with the negative sense for s in the reagent region and the positive sense in the product region. For all points lying between the point $r_{AB} = r_{BC} = 0$ and C the x coordinate is positive and negative otherwise. (As usual $0 \leq r_{AB(BC)} < \infty$.)

In terms of the variables (s, x) the collinear Schrödinger equation

for a total energy E is given by [2a, 4]

$$\frac{-\hbar^2}{2\mu}\left[\frac{1}{\eta}\frac{\partial}{\partial s}\left(\frac{1}{\eta}\frac{\partial}{\partial s}\right) + \frac{1}{\eta}\frac{\partial}{\partial x}\left(\eta\frac{\partial}{\partial x}\right) + V(s,x) - E\right]\Psi(x,s) = 0. \quad (1)$$

The quantity $\eta(s,x)$ is given by

$$\eta(x,s) = 1 + \kappa(s)x,$$

where $\kappa(s)$ is the curvature of C at the point $(0,s)$. The reduced mass μ is equal to $2/3\,M_H$ in the p, q coordinate system for the $H + H_2$ reaction. The collinear potential energy function $V(s,x)$ is conveniently decomposed as follows[2a, 4]

$$V(x,s) = V_1(s) + V_2(x,s), \quad V_2(0,s) = 0$$

As previously[2a, 4] $\Psi(x,s)$ is assumed to have the form

$$\Psi(x,s) = \psi(s)\phi(x;s) \quad . \quad (2)$$

Substituting (2) into (1), separating the variable x and s, neglecting terms which couple these variable and setting the curvature $\kappa(s)$ equal to zero the following VAZC translational and vibrational equations are obtained:[2a, 4]

$$\left[\frac{-\hbar^2}{2\mu}\frac{d^2}{ds^2} + V_1(s) + \varepsilon_i(s) - E\right]\psi(s) = 0 \quad (3)$$

$$\left[\frac{-\hbar^2}{2\mu}\frac{d^2}{dx^2} + V(x,s) - \varepsilon_i(s)\right]\phi(x;s) = 0 \quad . \quad (4)$$

In the translational equation (Eq. (3)) E is the total energy of the system and $\varepsilon_i(s)$ is the local vibrational energy eigenvalue determined by the

vibrational equation (Eq. (4)). For $s \rightarrow -\infty$ ε_i is the vibrational energy corresponding to the ith vibrational state of the reagent. The approximate VAZC reaction probabilities as a function of E are obtained from the solution to Eq. (3). For the collinear $H + H_2(v=0) \rightarrow H_2(v=0) + H$ reaction such approximate reaction probabilities have been computed and compared with exact results.[5,6]

In the present paper we present a direct and detailed test of the VAZC theory by focussing on the validity of Eq. (4). According to that equation for any value of s the exact scattering wavefunction $\psi^{exact}(x, s)$ is proportional to $\phi_i(x;s)$. Without any approximation, however, we may express ψ_I^{exact} as follows:[18]

$$\psi_I^{exact}(x, s) = \sum_{i=0}^{\infty} C_{iI}(s)\phi_i(x;s) \quad . \tag{5}$$

The superscript I references the exact scattering wavefunction to a given initial vibrational state of H_2, namely the Ith vibrational state. Considering s as a parameter (according to Eq. (4)) and according to the definitions of s and x we can consider Eq. (5) to be a representation of ψ_I^{exact} along cuts transverse to the minimum energy path. Along these cuts it is convenient to normalize ψ_I^{exact} and to introduce the real quantities a_{iI} by

$$a_{iI}(s) = |C_{iI}(s)|^2 / \sum_{i=0}^{\infty} |C_{iI}(s)|^2 \quad . \tag{6}$$

Thus, as a consequence of Eq. (5) the VAZC theory predicts that

$$a_{iI}^{VAZC}(s) = \delta_{iI}\,, \quad i = 0,\ 1,\ 2\ldots \tag{7}$$

for all values of s. By making use of previously calculated exact scattering wavefunctions for the collinear H + H_2 reaction we can compare the exactly calculated a_{iI}, given by Eq. (6), against the a_{iI}^{VAZC}, given by Eq. (7), at different values of s and the total energy E. The results of this comparison constitute our test of VAZC theory. Preliminary results for the cut defined by s = 0 (the symmetric stretch motion of the transition state) have already been reported.[13] A test of the VA theory including the curvature terms is given in paper II.2.

3. Numerical Methods and Tests

The eigenfunctions and eigenvalues of Eq. (4) were computed by a finite difference boundary value method (FDBVM).[19] Essentially this amounts to replacing the second derivative of ϕ_i, $\frac{d^2}{dx^2}\phi_i$, of Eq. (4) by its finite difference approximation and requiring the resulting algebraic equation to be satisfied at each of a grid of points which span the physically allowed domain of the variable x. This set of algebraic equations plus appropriate bound state boundary conditions transform Eq. (4) into a matrix eigenvalue-eigenvector equation. The eigenvalues and eigenvectors of this matrix equation are the approximate eigenvalues and eigenfunctions of Eq. (4). In our calculations a 75 point grid which corresponded to a step size of 0.05 bohr was used. This step size was shown previously to yield eigenvalues accurate to within less than 0.5 percent for a very similar kind of problem.[20]

The lines labeled by -0.15, +0.15, and the p axis all penetrate

deeply into classically forbidden regions of space and as a result the expansion of ψ_I^{exact} given by Eq. (5) is well-defined since ψ_I^{exact} and the basis functions $\phi_i(x;s)$ satisfy the same boundary conditions. However, the lines labeled by -1.60, +1.60, -2.50 and +2.50 would not penetrate deeply into classically forbidden regions of space before passing through classically allowed regions of reagent and product space. This feature is inconsistent with the spirit of VA theory. As a result these lines were truncated at points in the classically forbidden regions of the plateau where the potential along these lines was a maximum. As seen from Figure 1 the potential energy is greater than 2.0 eV at the end points of these as well as the other lines. In Table 1 some results for these truncated lines will be compared with the corresponding untruncated ones.

As a numerical test of the expansion of ψ_I^{exact} given by Eq. (5) we used the fact that for a complete set of orthonormal functions

$$\langle \Psi_I^{exact} | \Psi_I^{exact} \rangle = \sum_{i=0}^{\infty} |C_{iI}|^2 . \tag{8}$$

The integration is performed along a given line and for regions of the line where Ψ_I^{exact} is non-negligible. For a finite number of functions $\phi_i(x;s)$, N, we have that

$$\langle \Psi_I^{exact} | \Psi_I^{exact} \rangle \gtrsim \sum_{i=1}^{N} |C_{iI}|^2 . \tag{9}$$

That is, the expansion given by the right hand side of Eq. (5) converges (in the mean-square sense) from below its limit. In Table 1 the conver-

gence of the expansion given by Eq. (5) for ψ_0^{exact} is examined for the lines labeled by -1.60, -0.15, p-axis, +0.15, +1.60 for total energies E of 0.5080 eV and 0.8978 eV. There it can be seen that the convergence property given by Eq. (9) is indeed obeyed and that for N = 7 convergence better than 5 parts in 10^5 has been achieved. Also in Table 1 we have compared results for the truncated and untruncated lines labeled by s = -1.60 and s = +1.60. There it can be seen that there are very small differences between the two sets of results.

4. Results and Discussion

The test of VAZC theory performed consists of an examination of the energy dependence of the $a_{iI}(s)$ coefficients given by Eq. (6). These coefficients are calculated for five lines corresponding to five values of s which pass through the reagent, strong interaction, and product regions of configuration space. The exactly computed coefficients $a_{iI}(s)$ are then compared with the $a_{iI}^{VAZC}(s)$ ones (given by Eq. (7)) and the results give a test of VAZC theory as a function of the collision energy and the distance along the minimum energy path, s. The lines labeled by -2.50 and +2.50 have been included in Figure 1 to indicate the asymptotic regions of the (p, q) configuration space. The a_{iI} coefficients were not calculated for these lines since necessarily for $E < \epsilon_1 = 0.79$ eV VAZC theory is rigorously (and trivially) correct. For $E > 0.7945$ eV the exact a_{iI} coefficients for these lines can be calculated from the corresponding transition probabilities and S-matrix elements.

Figures 2 - 6 present results for reagent H_2 in the ground

vibrational state. In Figure 2 the coefficients a_{00} and a_{10} are given for the cut at s = -1.60 bohr as a function of the total energy E (lower abscissa) and initial relative kinetic energy E_0 (upper abscissa). All other a_i coefficients are less than 5×10^{-3} and hence are not included in the figure. The (inner) arrows labeled T_0, T_1, and E_b designate respectively the total energies equal to the ground and first excited vibrational energy levels of H_2 and the classical barrier height. The (outer) arrows labeled T_0^S and T_1^S designate respectively the total energies equal to the ground and first excited vibrational energy levels of the potential energy surface along the cut indicated (measured with respect to the energy of the separated reagents). As can be seen for this cut there is excellent agreement with VAZC theory for E less than T_1. This is not too surprising since this cut is near the reagent asymptotic region and as noted above VAZC is rigorously correct in the asymptotic region for E less than T_1.

The energy dependence of the coefficients a_{00}, a_{10}, a_{20}, and a_{30} is depicted in Figure 3 for the cut at s = -0.15 bohr. The label V(s) indicates the value of the potential energy surface at the point V(0, s). The coefficient a_{00} is seen to be greater than 0.8 for E less than 0.73 eV. This compares reasonably well with the VAZC coefficient $a_{00}^{VAZC} = 1.0$. At total energies greater than 0.8 eV, however, the VAZC theory is greatly in error. Considerably more non-adiabaticity is present in these results for all energies than was found in Figure 1 for s = -1.60 bohr. This is expected since the s = -0.15 bohr cut is located in the strong interaction region.

In Figure 4 the extent of adiabaticity is examined for the symmetric stretch motion of the transition state corresponding to the cut at s = 0.0 bohr. Here the results show less agreement with VAZC theory than the results shown in Figures 2 and 3. However, for E between 0.46 eV and 0.75 eV the a_{00} coefficient is greater than or equal to 0.8. As E decreases from the value V(s) (the classical barrier height) the extent of non-adiabaticity increases. This fact seems to correlate with probability current density calculations[21] which reveal that in this energy range a substantial amount of tunneling occurs as the current density vector field "cuts the corner." "Cutting the corner" clearly requires several vibrational functions $\phi_i(0,x)$ in the expansion of $\psi_0^{exact}(o,x)$ as seen from the results in Figure 4.

Figure 5 shows substantial non-adiabaticity in the results for s = +0.15 bohr especially for E less than the classical barrier height E_b and for E greater than T_1^s. Here as in the three previous figures four coefficients at most (at any given energy) contribute substantially to the summation

$$\sum_{i=1}^{\infty} a_{iI} = 1.$$

The energy dependence of the coefficients a_{00} and a_{10} is given in Figure 6 for the cut at s = +1.60 bohr. The essentially exact adiabaticity exhibited by a_{00} for E less than T_1^s confirms the expectation that in the near asymptotic regions of configuration space the H_3 system propagates with nearly zero interaction.

In Figures 7 and 8 coefficients a_{i1} are presented as a function

of energy along five cuts. Here reagent H_2 is initially in the v = 1 vibrational state. Although the coefficient a_{11} is the dominant one for all cuts, a substantial amount of non-adiabaticity is present. For the cuts at ± 1.60 bohr the a_{01} coefficient is the only significant one in addition to the a_{11} coeffieicnt. However, in the strong interaction region the coefficients a_{21}, a_{31}, and a_{41} are non-negligible indicating that $\psi_1^{exact}(x, s)$ has a significant overlap with the $\phi_2(x;s)$, $\phi_3(x;s)$, and $\phi_4(x;s)$ vibrational eigenfunctions for the cuts at ± 0.15 bohr and 0.0 bohr.

5. Summary and Conclusions

The vibrationally adiabatic (zero-curvature) theory of chemical reactions has been tested for the collinear H + H_2 exchange reaction. The theory is shown to be qualitatively valid in the sense that the coefficients a_{00} and a_{11} (corresponding to H_2 initially in the v = 0 and v = 1 states respectively) are the dominant ones for most energies considered. However, at low initial translational energies, where tunneling is significant, a substantial amount of non-adiabaticity is found. Also, at energies for which vibrationally excited products can be formed the adiabatic theory expectedly breaks down.

The expansion of the exact scattering wavefunctions $\psi_0^{exact}(x, s)$ and $\psi_1^{exact}(x, s)$ in terms of "vibrational" eigenfunctions along any of five cuts transverse to the reaction path is converged to better than 1 part in 10^5 for a seven term expansion and to better than 1 part in 10^2 for a four term expansion. This suggests that the VAZC vibrational

eigenfunctions might form a good basis set for describing the collinear $H + H_2$ reaction.

Table 1. Convergence of expansion of $\psi_0^{exact}(x, s)$ along five lines (labeled by their point of intersection with the minimum energy path) for initial relative kinetic energies E_0 of 0.2352 eV and 0.6250 eV.

E_0 = 0.2352 eV								
s(bohr)	N=1[a]	N=2	N=3	N=4	N=5	N=6	N=7	$\langle\psi_0^{exact}\|\psi_0^{exact}\rangle$
-1.60[t]	2.71605	2.71643	2.71642	2.71643	2.71643	2.71644	2.71644	2.71657
-1.60[u]	2.71600	2.71621	2.71633	2.71635	2.71635	2.71636	2.71626	2.71650
-0.15	0.94871	0.99611	0.99678	0.99701	0.99704	0.99705	0.99706	0.99707
0.0	0.69224	0.76425	0.76933	0.76948	0.76948	0.76948	0.76948	0.76949
+0.15	0.55665	0.64736	0.66778	0.67054	0.67054	0.67094	0.67107	0 67112
+1.60[t]	0.099505	0.099527	0 099530	0.099530	0.099530	0.099530	0.099530	0.099537
+1.60[u]	0.099498	0.099520	0.099524	0.099525	0.099608	0.099614	0.099612	0.099656

[a] N is the number of terms in the partial sum $\sum_{i=1}^{N} |C_{io}|^2$.

[t] Truncated.

[u] Untruncated.

Table 1. Continued

E_0 = 0.6250 eV								
s(bohr)	N=1[a]	N=2	N=3	N=4	N=5	N=6	N=7	$\langle\psi_0^{exact}\|\psi_0^{exact}\rangle$
-1.60[t]	0.84366	1.17832	1.17886	1.17887	1.17887	1.17887	1.17887	1.17894
-1.60[u]	0.84219	1.17716	1.17721	1.17722	1.17829	1.17830	1.17834	1.17928
-0.15	1.95106	3.53820	3.78277	3.81480	3.82448	3.82623	3.82682	3.82722
0.0	0.47208	3.42887	3.60105	3.62612	3.62814	3.62817	3.62818	3.62825
+0.15	0.16487	4.30638	4.39090	4.41546	4.42155	4.42160	4.42430	4.42491
+1.60[t]	0.22599	0.75710	0.75716	0.75717	0.75717	0.75717	0.75717	0.75720
+1.60[u]	0.22626	0.75578	0.75581	0.75584	0.75631	0.75634	0.75635	0.75646

[a] N is the number of terms in the partial sum $\sum_{i=1}^{N} |C_{io}|^2$.

[t] Truncated.

[u] Untruncated.

References

1. J. O. Hirschfelder and E. Wigner, J. Chem. Phys. 7, 616 (1939).
2. (a) R. A. Marcus, J. Chem. Phys. 45, 4495 (1966); (b) R. A. Marcus, ibid., 46, 959 (1967); (c) R. A. Marcus, Discussion Faraday Soc. 44, 90 (1968).
3. M. S. Child, Discussion Faraday Soc. 44, 68 (1968).
4. R. E. Wyatt, J. Chem. Phys. 51, 3489 (1969).
5. (a) D. G. Truhlar and A. Kuppermann, J. Amer. Chem. Soc. 93, 1840 (1971); (b) D. G. Truhlar and A. Kuppermann, J. Chem. Phys. 56, 2232 (1972).
6. D. J. Diestler and M. Karplus, J. Chem. Phys. 55, 5832 (1971).
7. S.-F. Wu and R. S. Levine, Mol. Phys. 22, 881 (1971).
8. (a) S.-F. Wu and R. A. Marcus, J. Chem. Phys. 53, 4026 (1970); (b) M. Attermeyer and R. A. Marcus, ibid., 52, 393 (1970).
9. A. Tweedale and K. J. Laidler, J. Chem. Phys. 53, 2045 (1970).
10. E. A. McCullough and R. E. Wyatt, J. Chem. Phys. 54, 3592 (1971).
11. (a) M. A. Eliason and J. O. Hirschfelder, J. Chem. Phys. 30, 1426 (1959); (b) R. A. Marcus, J. Chem. Phys. 35, 4493 (1966); (c) D. G. Truhlar, J. Chem. Phys. 53, 2041 (1970).
12. A. Kuppermann, to be published.
13. J. M. Bowman, A. Kuppermann, J. T. Adams, and D. G. Truhlar, Chem. Phys. Letters 20, 229 (1973).
14. H. S. Johnston, Gas Phase Reaction Rate Theory (Ronald, New York, 1966) Chapt. 5, Appendix C.
15. I. Shavitt, J. Chem. Phys. 49, 4048 (1968).

16. F. T. Wall and R. N Porter, J. Chem. Phys. 36, 3256 (1962).

17. I. Shavitt, R. M. Stevens, F. L. Minn, and M. Karplus, J. Chem. Phys. 48, 2700 (1968).

18. In practice the summation in Eq. (5) is truncated after a desired accuracy is achieved.

19. (a) D. G. Truhlar, J. Comp. Phys. 10, 123 (1972); (b) D. J. Diestler and V. McKoy, J. Chem. Phys. 47, 45 (1967); N. Winter, D. J. Diestler, and V. McKoy, J. Chem. Phys. 48, 16 (1968).

20. D. G. Truhlar, Ph.D. Thesis, California Institute of Technology, Pasadena, California (1970), Part I, Appendix 4.

21. J. T. Adams, D. G. Truhlar, and A. Kuppermann, unpublished results.

Figure 1: Potential energy contours (solid curves) in normal-mode coordinate space p, q of the Wall-Porter fit to the scaled SSMK surface. Minimum energy path (thicker solid curve) and six normal cuts (long-dashed lines) are also shown. The corresponding values of s, in bohr, ranging from -2.50 to +2.50 are indicated. The p-axis (s = 0) is an additional normal cut. r_{AB} and r_{BC} are internuclear distances in the linear A-B-C triatomic system.

Figure 2: Coefficients a_{io} for the cut at s = -1.60 bohr as a function of the total energy E and initial relative kinetic energy E_o. See text for definition of other symbols used in this figure.

Figure 3: Coefficients a_{io} for the cut at s = -0.15 bohr as a function of the total energy E and initial relative kinetic energy E_o. See text for definition of other symbols used in this figure.

Figure 4: Coefficients a_{io} for the cut at s = 0.0 bohr as a function of the total energy E and initial relative kinetic energy E_o. See text for definition of other symbols used in this figure.

Figure 5: Coefficients a_{io} for the cut at s = +0.15 bohr as a function of the total energy E and initial relative kinetic energy E_o. See text for definition of other symbols used in this figure.

Figure 6: Coefficients a_{i_0} for the cut at s = + 1.60 bohr as a function of the total energy E and initial relative kinetic energy E_0. See text for definition of other symbols used in this figure.

Figure 7: Coefficients a_{i_1} for the cuts at (a) s = 0.0 bohr, (b) s = -0.15 bohr, and (c) s = -1.60 bohr as a function of the total energy E and the initial relative kinetic energy E_1.

Figure 8: Coefficients a_{i_1} for the cuts at (a) s = + 1.60 bohr, and (b) s = + 0.15 bohr as a function of the total energy E and the initial relative kinetic energy E_1.

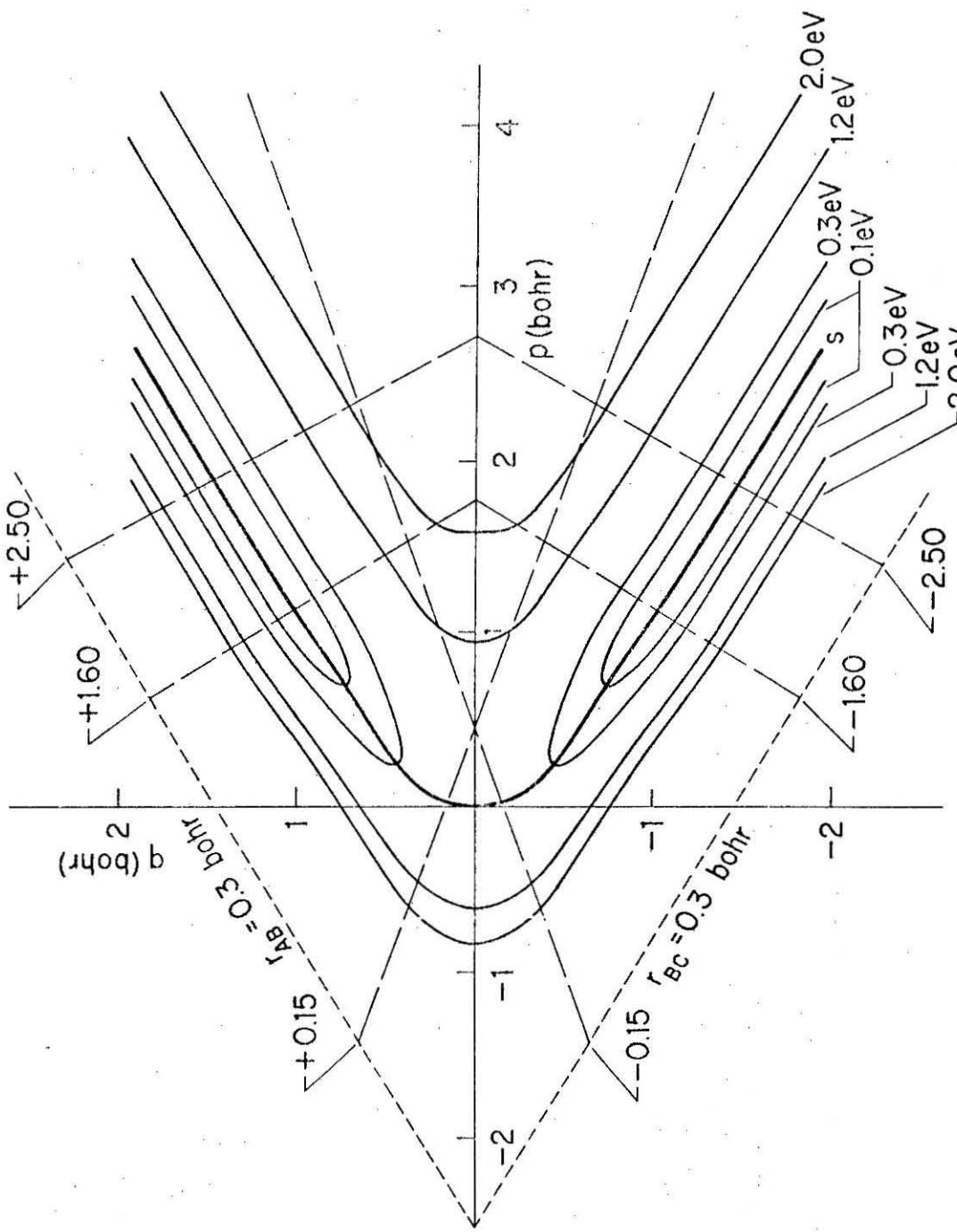
2.0eV
1.2eV
0.3eV
0.1eV
s
0.3eV
1.2eV
2.0eV
4
3
p (bohr)
2
+2.50
+1.60
+0.15
−0.15
−1.60
−2.50
2
1
−1
−2
q (bohr)
r_{AB} =0.3 bohr
r_{BC} =0.3 bohr

Figure 1

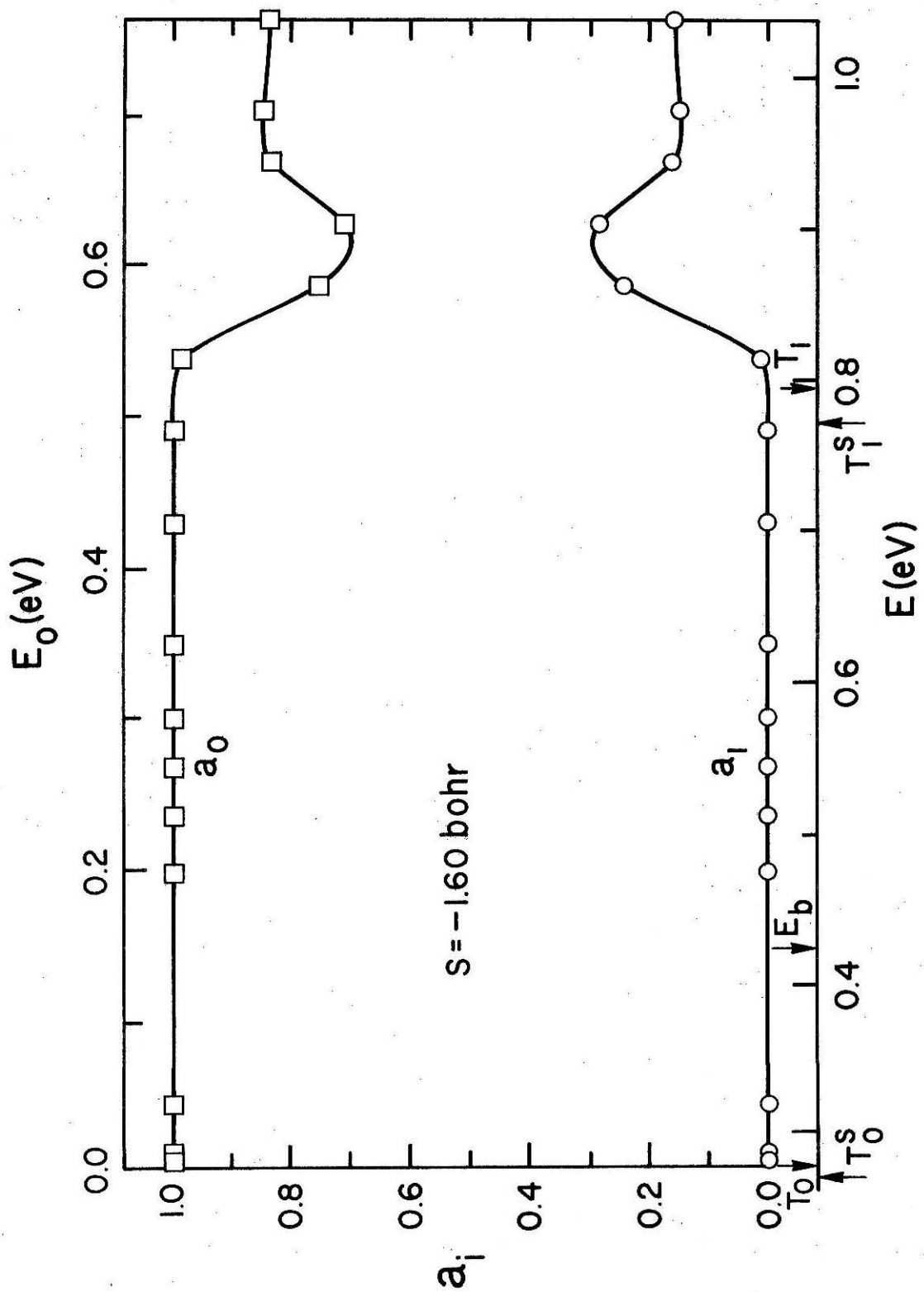
E_0(eV)
0.0
0.2
0.4
0.6
a_0
S=−1.60 bohr
a_1
E_b
T_1
T_1^s
0.8
1.0
E(eV)
0.6
0.4
T_0^s
T_0
0.0
0.2
0.4
0.6
0.8
1.0
a_i

Figure 2

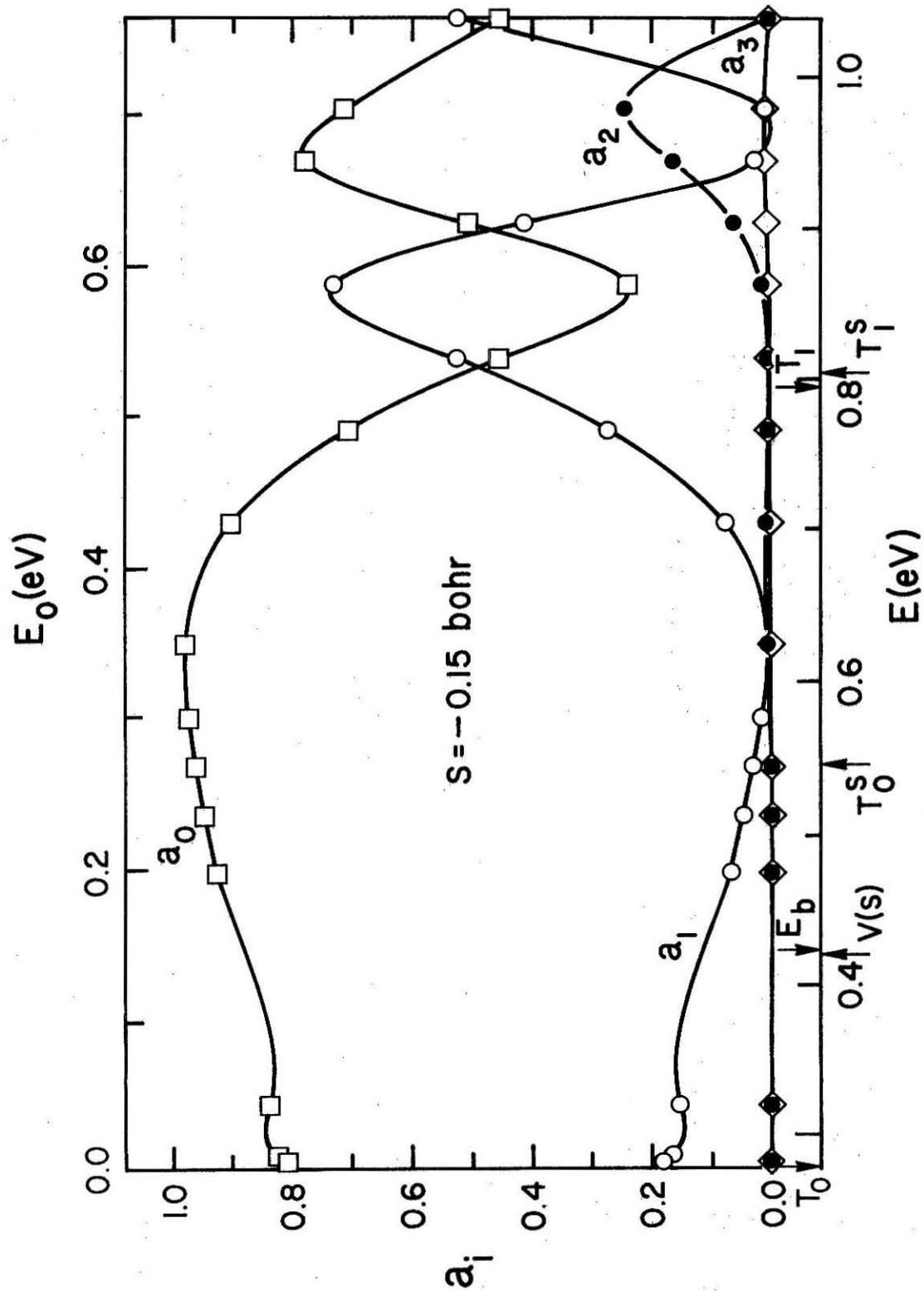
E_0(eV)
0.0
0.2
0.4
0.6
a_i
1.0
0.8
0.6
0.4
0.2
0.0
a_0
a_1
a_2
a_3
S = −0.15 bohr
T_0
E_b
V(s)
T_0^S
T_1
T_1^S
0.4
0.6
0.8
1.0
E(eV)

Figure 3

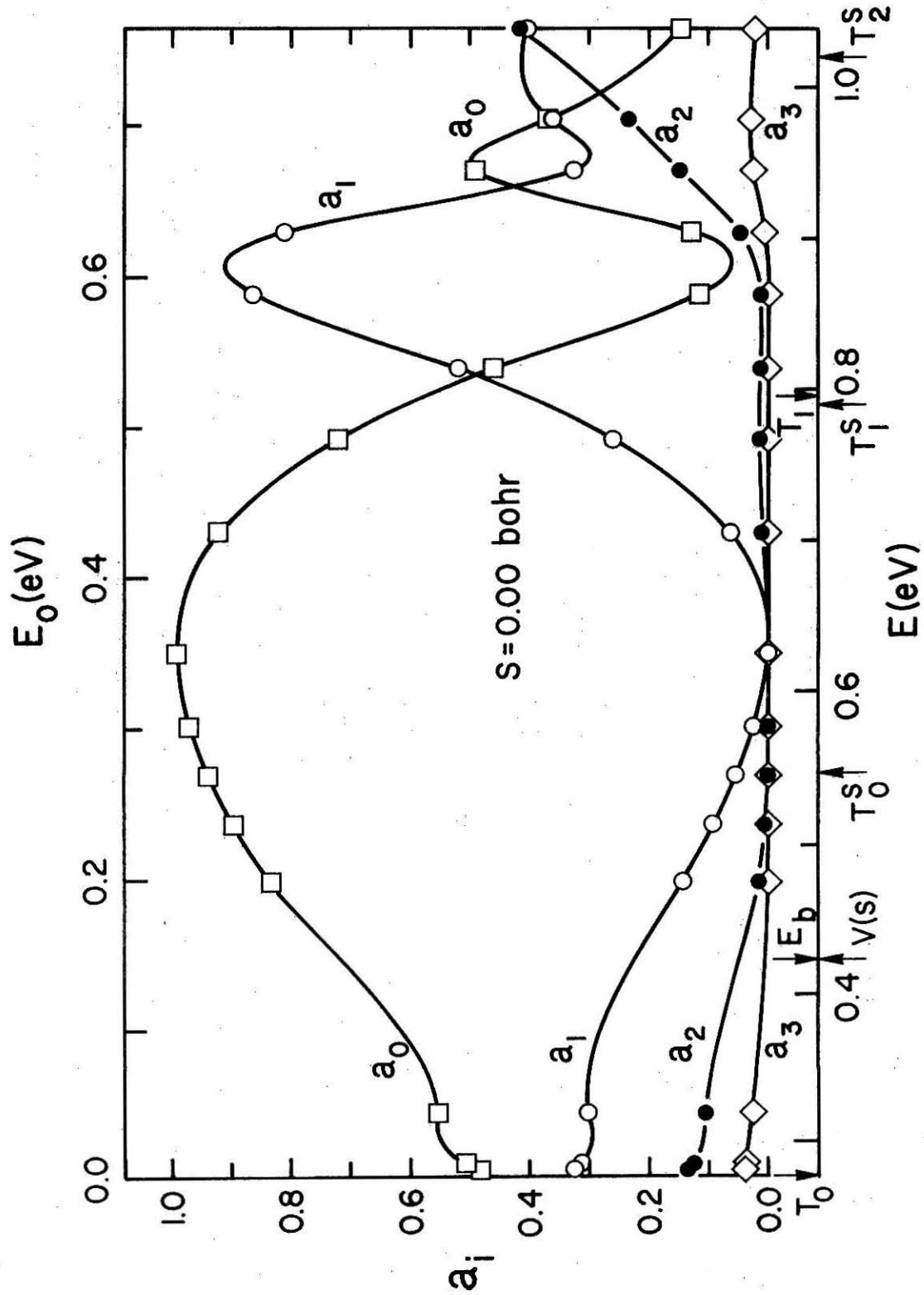
E_0(eV)
0.0
0.2
0.4
0.6
a_i
0.0
0.2
0.4
0.6
0.8
1.0
a_0
a_1
a_2
a_3
S=0.00 bohr
T_0
E_b
V(s)
T_0^S
T_1^S
T_2^S
E(eV)
0.4
0.6
0.8
1.0

Figure 4

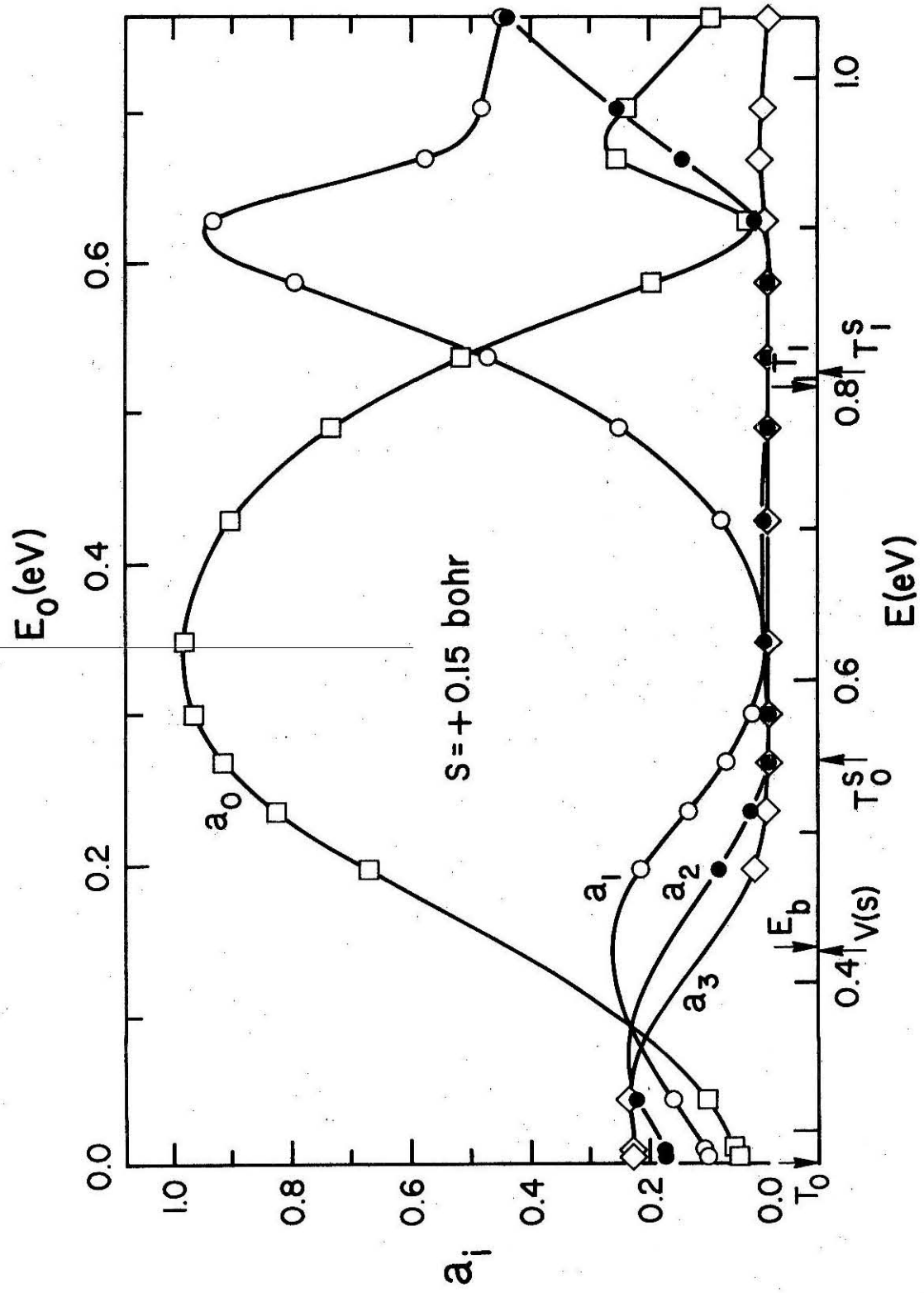
E_0(eV)
0.0
0.2
0.4
0.6
S=+0.15 bohr
a_0
a_1
a_2
a_3
a_i
1.0
0.8
0.6
0.4
0.2
0.0
T_0
E_b
V(s)
T_0^S
T_1
T_1^S
E(eV)
0.4
0.6
0.8
1.0

Figure 5

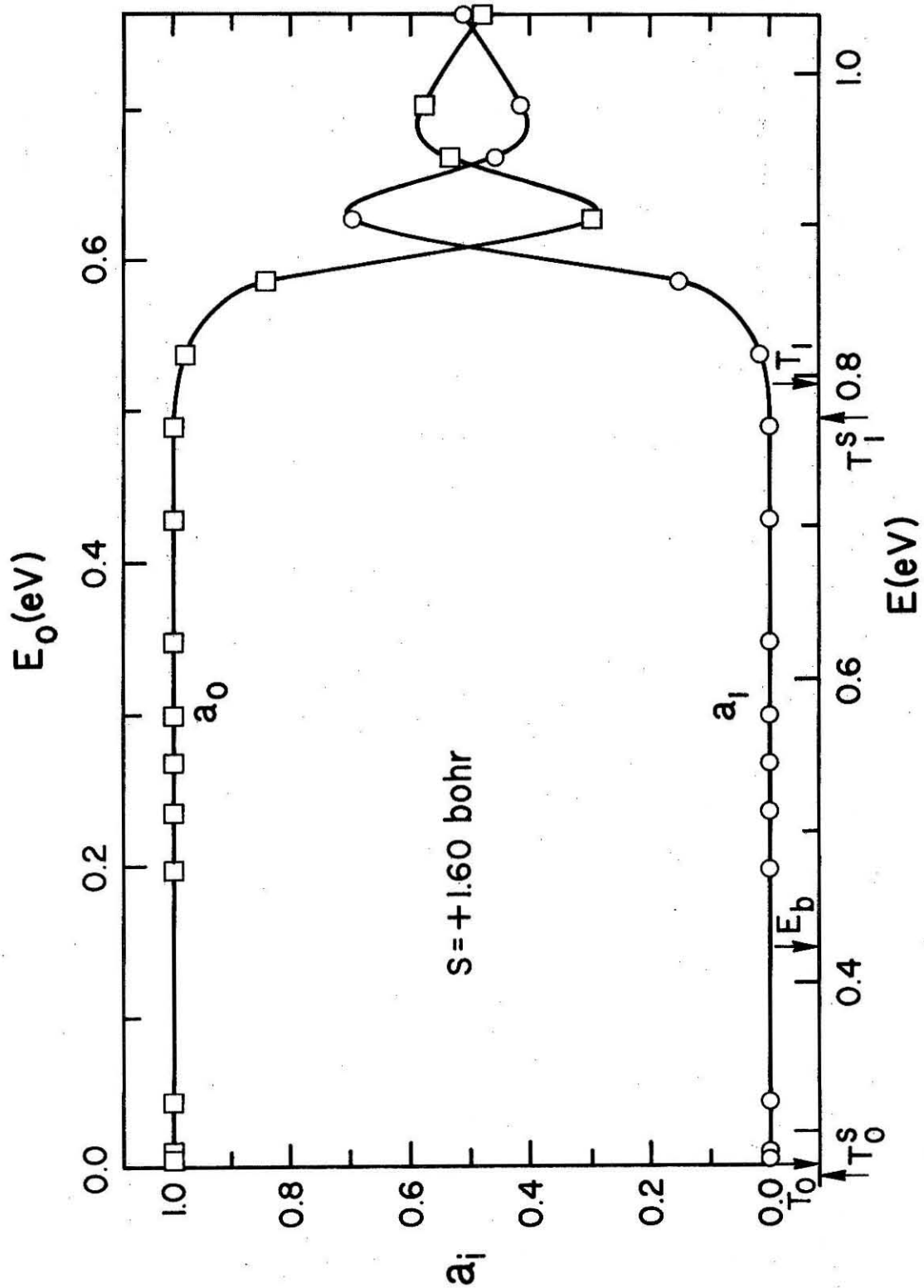
E₀(eV)
0.0
0.2
0.4
0.6
a₀
a₁
S=+1.60 bohr
E_b
T₀
T₁
T₀ˢ
T₁ˢ
E(eV)
0.4
0.6
0.8
1.0
1.0
0.8
0.6
0.4
0.2
0.0
aᵢ

Figure 6

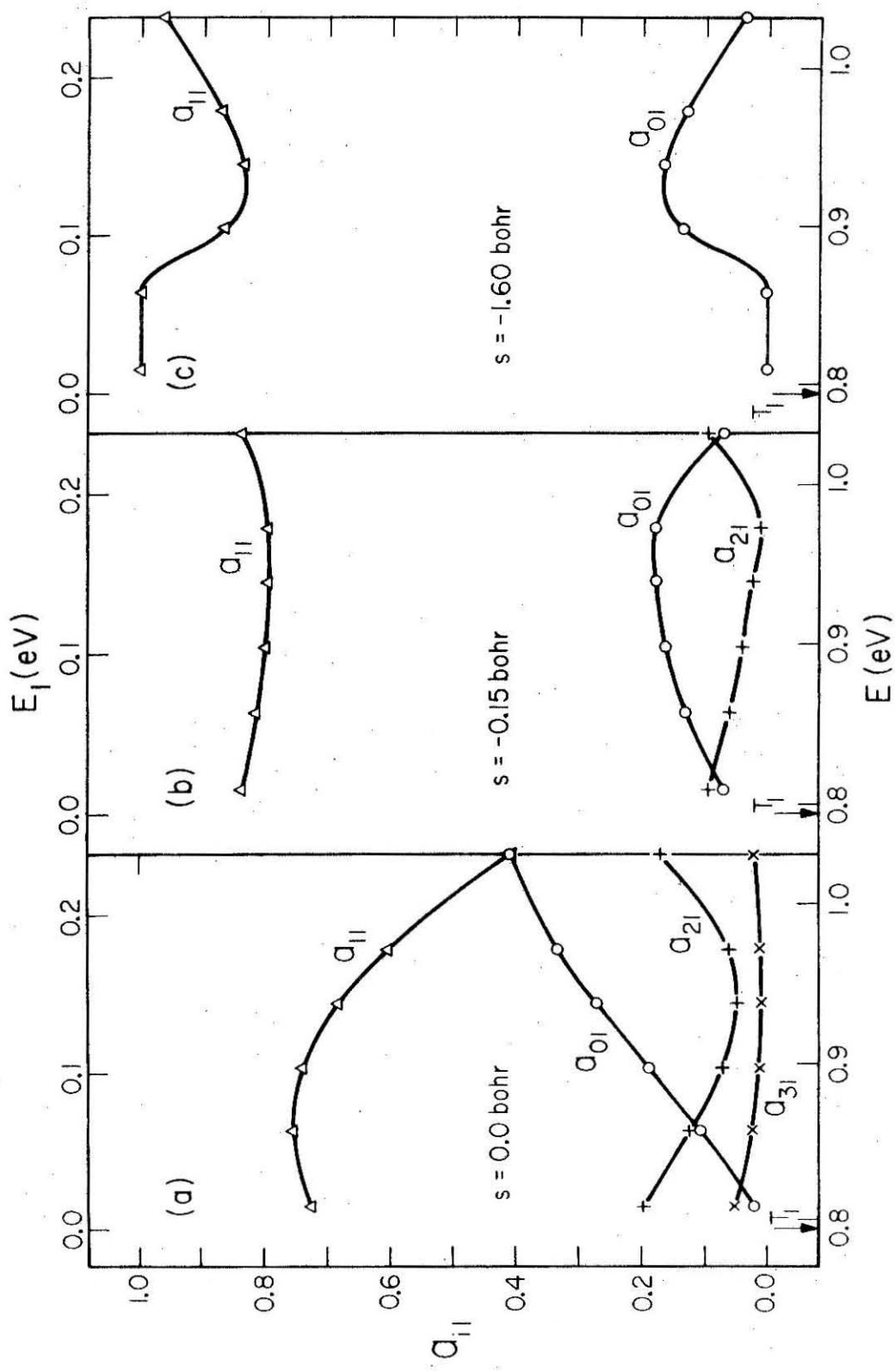
(a)
(b)
(c)
s = 0.0 bohr
s = -0.15 bohr
s = -1.60 bohr
a_{11}
a_{01}
a_{21}
a_{31}
T_1
E_1 (eV)
E (eV)
a_{i1}

Figure 7

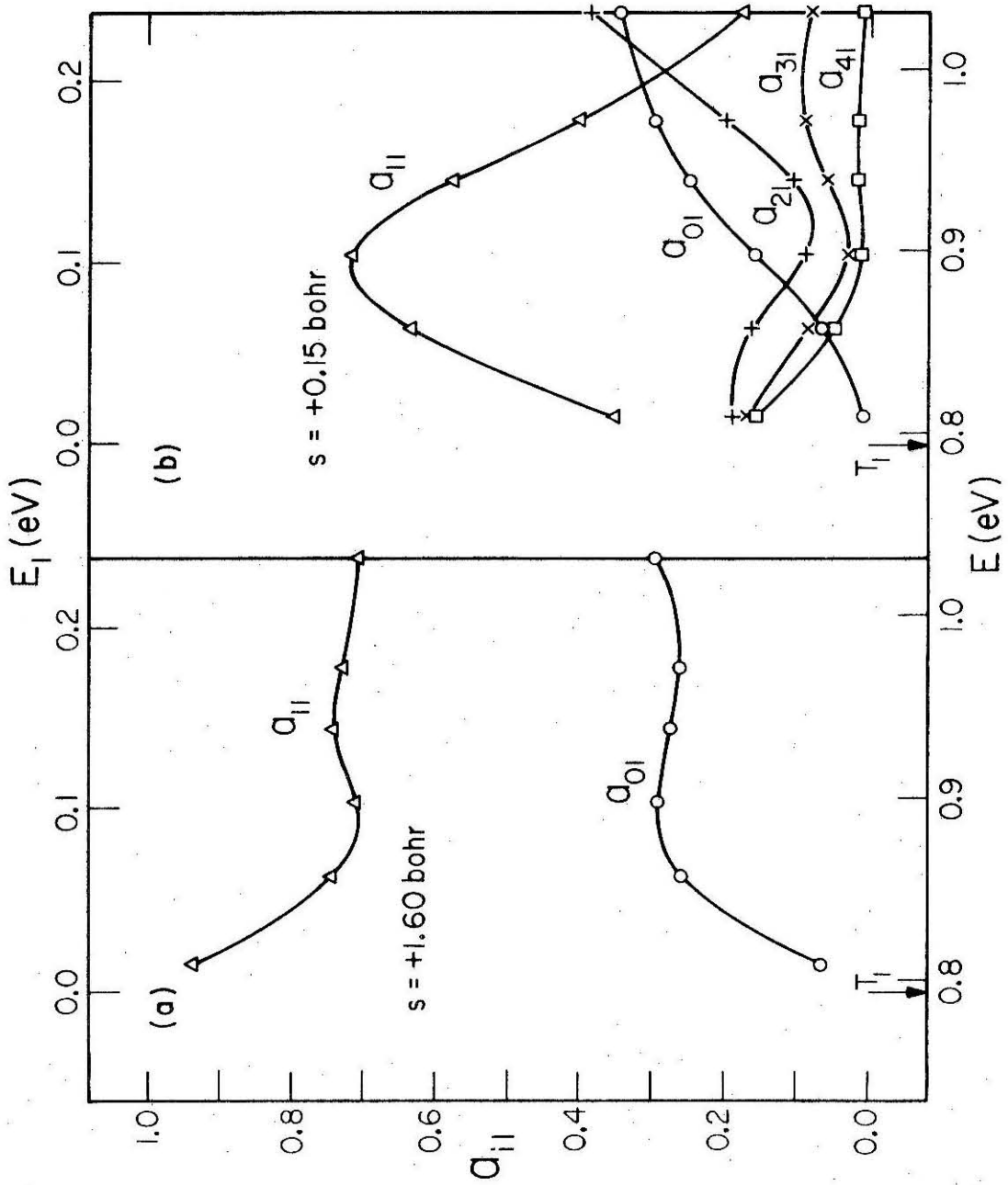
(a)
s = +1.60 bohr
(b)
s = +0.15 bohr
a_{11}
a_{01}
a_{21}
a_{31}
a_{41}
T_1
E_1 (eV)
E (eV)
a_{i1}
0.0
0.1
0.2
0.8
0.9
1.0
0.2
0.4
0.6
0.8
1.0

Figure 8

II.2 THE EFFECT OF THE CURVATURE CORRECTION ON THE VIBRATIONALLY ADIABATIC THEORY OF CHEMICAL REACTIONS .

THE EFFECT OF THE CURVATURE CORRECTION ON THE VIBRATIONALLY ADIABATIC THEORY OF CHEMICAL REACTIONS.

1. Introduction

In a previous paper, a direct test of the vibrationally adiabatic theory of chemical reactions in the zero-curvature approximation (VAZC) was made for the collinear H + H_2 reaction.[1] In addition to this test, comparisons between exact quantum and VAZC reactive transition probabilities have been carried out for the collinear H + H_2 reaction.[2,3] A VAZC analysis was also performed on a time-dependent quantal treatment of this reaction.[4]

Much less information is available on the value of the vibrationally adiabatic theory including curvature (VA).[4,5] This theory is internally consistent, making no ad hoc assumptions about the curvature of the reaction path as the VAZC theory does. It is clear that the assumption of zero curvature has been made for computational convenience only. Indeed non-zero curvature is an essential feature of the theory of chemical reactions. A calculation of reaction probabilities and reaction cross sections within the VA approximation has been performed by Wyatt.[5] This represents the only attempt to use the VA theory in a calculation of reaction probabilities.

In the present paper we make use of exact quantum scattering wavefunctions calculated previously[2] for the collinear H + H_2 reaction to test the VA theory and to compare VA and VAZC results. The test and comparison are made for the symmetric stretch motion of the H_3

transition state.

In Section 2 a review of VA theory is presented and the relevant equations are given and discussed. Also, the details of the test of the theory are given. The numerical methods employed in our calculations, and a numerical examination of the VA vibrational potential are given in Section 3. The results and discussion are given in Section 4 and conclusions are presented in Section 5.

2. Theory

2.1 The adiabatic equations

In terms of the natural-collision coordinates (x, s) introduced by Marcus[4] and indicated in Figure 1 and defined in the corresponding figure caption, the collinear Schrödinger equation is given by

$$\frac{-\hbar^2}{2\mu}\left[\frac{1}{\eta_1}\frac{\partial}{\partial s}\left(\frac{1}{\eta_1}\frac{\partial}{\partial s}\right)+\frac{1}{\eta_1}\frac{\partial}{\partial x}\left(\eta_1\frac{\partial}{\partial x}\right)+V(x,s)-E\right]\Psi(x,s)=0. \qquad (1)$$

V(x, s) is the Born-Oppenheimer potential energy surface for the collinear configuration, μ is the reduced mass of the three particle system and E is the total energy. The quantity η_1 is related to the curvature κ through the equation

$$\eta_1 = 1 + \kappa(s)x. \qquad (2)$$

The coordinates (x, s) are referenced with respect to a curve C (as shown in Figure 1) constructed in some orthogonal coordinate space. The coordinate x is the shortest distance from any point P to a point Q on the curve C (with the sign convention given in Figure 1) and s is the distance from an origin on C to Q (with the sign convention given in Figure 1).

The origin of C is taken at the saddle point of the potential surface. As previously,[1,2,6] we have chosen the normal-mode coordinate space (p, q) defined[7,8]

$$p = (\sqrt{3}/2)(r_{AB} + r_{BC} - 2r_0),$$

$$q = (1/2)(r_{BC} - r_{AB}),$$

$$\mu = (2/3)\, M_A$$

for a collinear A + BC → AB + C reaction.

It is convenient to decompose the potential energy function as follows[4,5]

$$V(x, s) = V_1(s) + V_2(x, s), \tag{3}$$

$$V_2(0, s) = 0,$$

and to write $\Psi(x, s)$ as

$$\Psi(x, s) = \psi(s)\Phi(x, s) \quad . \tag{4}$$

Upon substitution of eqs. (3) and (4) into eq. (1) and separating the variables the following equations are obtained:

$$\left[\frac{-\hbar^2}{2\mu}\frac{d^2}{ds^2} + V_1(s) - \frac{\hbar^2\kappa^2}{8\mu} - \epsilon(s)\right]\psi(s) = 0,$$

$$\left[\frac{-\hbar^2}{2\mu}\frac{1}{\eta}\frac{\partial}{\partial x}\left(\eta\frac{\partial}{\partial x}\right) + \frac{\epsilon(s) + \hbar^2\kappa^2/8\mu - V_1(s)}{(1+\kappa x)^2} + V(x, s) - E\right]\Phi(x, s)$$

$$= S(x, s)\,\Phi(x, s).$$

S is the operator which couples the s and x motion and hence is respon-

sible for non-adiabaticity in this formulation. It is given by[4, 5]

$$S = \frac{\hbar^2}{\partial \mu \eta^2} \left(\frac{\partial}{\partial s} + 2\frac{\partial \ln \psi}{\partial s} - \frac{\partial \ln \eta}{\partial s} \right) \frac{\partial}{\partial s} - \frac{\partial \ln \psi}{\partial s} \frac{\partial \ln \eta}{\partial s} \quad .$$

By setting S equal to zero we obtain the general adiabatic equations (which include the curvature term).

$$\left[\frac{-\hbar^2}{2\mu} \frac{d^2}{ds^2} + V_1(s) - \frac{\hbar^2 \kappa^2}{8\mu} - \epsilon(s) \right] \psi(s) = 0, \tag{5}$$

$$\left[\frac{-\hbar^2}{2\mu} \frac{1}{\eta} \frac{d}{dx} \left(\eta \frac{d}{dx} \right) + \frac{\epsilon(s) + \frac{\hbar^2 \kappa^2}{8\mu} - V_1(s)}{(1 + \kappa x)^2} + V(x, s) - E \right] \Phi_i = 0. \tag{6}$$

The quantity $\epsilon(s)$ (the "local translational energy"[5]) which appears in eqs. (5) and (6) is a separation constant and enters the theory as a parameter upon which the vibrational energy eigenvalue depends (when the curvature $\kappa(s) \neq 0$). To see this explicitly the function $\mathcal{U}(x, s)$ is introduced;[4, 5] it is defined as

$$\mathcal{U}(x, s) = V(x, s) + [\epsilon(s) - V_1(s)]/(1 + \kappa x)^2 \quad .$$

Also, let x_0 be the minimum of $\mathcal{U}(x, s)$. Then adding and subtracting $\mathcal{U}(x_0, s)$ to eq. (6) we obtain for the vibrational equation

$$\left[\frac{-\hbar^2}{2\mu} \frac{1}{\eta} \frac{\partial}{\partial x} \left(\eta \frac{\partial}{\partial x} \right) + \mathcal{U}(x, s) - \mathcal{U}(x_0, s) - E_v^i(s) \right] \Phi_i = 0, \tag{7}$$

where $E_v^i(s)$ is the ith local vibrational energy eigenvalue and the total energy is given by

$$E = E_v^i(s) + \mathcal{U}(x_0, s). \tag{8}$$

Thus, by inspection of eq. (7) it is evident that this equation contains

$\epsilon(s)$ as a parameter when $\kappa(s) \neq 0$.

Before proceeding with further manipulation of eq. (7) we note that in the asymptotic limits, defined by $s \rightarrow \pm \infty$,

$$\kappa = 0, \; x_0 = 0,$$

and

$$\mathcal{U}(x, s) = V_2(x, s) - \epsilon(s).$$

As a result of this, eq. (7) becomes

$$\left[\frac{-\hbar^2}{2\mu}\frac{d^2}{dx^2} + V_2(x, s) - V_2(x_0, s) - E_v^i(s)\right] = 0 \tag{9}$$

eq. (5) becomes

$$\left[\frac{-\hbar^2}{2\mu}\frac{d^2}{ds^2} + V_1(s) - \epsilon(s)\right]\psi(s) = 0, \tag{10}$$

and the total energy is given by

$$E = E_v^i(s) + \epsilon(s).$$

Eqs. (8) and (9) are the zero-curvature vibrational and translational equations, respectively. The assumption that they are valid for all values of s is made in the VAZC theory.

Returning to the solution of eq. (7) we note that this eigenvalue equation can be put into standard Sturm-Liouville form[9] by multiplying it by $-2\mu\eta/\hbar^2$. The function $\eta(x, s)$ can be identified as the weight function and it is assumed to be positive.[10] With this assumption we define the function ϕ_i by

$$\Phi_i = (\eta)^{-\frac{1}{2}} \phi_i \tag{11}$$

and then eq. (7) becomes

$$\left[\frac{-\hbar^2}{2\mu}\frac{d^2}{dx^2} + \mathcal{U}(x, s) - \mathcal{U}(x_o, s) - E_v^i(s)\right] \phi_i(x, s) = 0. \tag{12}$$

The real-valued functions ϕ_i and Φ_i satisfy the following orthonormality conditions:

$$\int_{-[\kappa(s)]^{-1}}^{\infty} dx\, \phi_i(x, s)\, \phi_j(x, s) = \delta_{ij}, \tag{13a}$$

$$\int_{-[\kappa(s)]^{-1}}^{\infty} dx\, \Phi_i(x, s)\, \Phi_j(x, s)\, \eta(x, s) = \delta_{ij}, \tag{13b}$$

where δ_{ij} is the standard Kronecker delta function. The lower limit of integration $-[\kappa(s)]^{-1}$ is imposed by the requirement that the weight function $\eta(x, s)$ be greater than or equal to zero in the range of integration. From eq. (2) this range is seen to be $-[\kappa(s)]^{-1} \leq x \leq \infty$. In practice the upper limit of the above integrals is some value of x, x_u, such that $V(x_u, s)$ is much greater than the total energy of the H_3 system. We examine the choice for x_u in more detail below. The functions Φ_i (and hence ϕ_i) form a complete orthonormal set of functions over the integration range given above.

To find the eigenvalues and eigenfunctions of eq. (12) for a given value of the total energy E requires a numerical search procedure. This is so because the function $\epsilon(s)$ occurs both in the eigenvalue equation (eq. 12) and in the total energy equation (eq. (8)). In the

following section a description of the search procedure is given.

2.2 Projection coefficients and the test of vibrational adiabaticity

According to our assumptions about the completeness of the vibrational eigenfunctions $\Phi_i(x, s=0)$ (and $\phi_i(x, s=0)$ we assert that the exact scattering wavefunction $\psi_I^{exact}(x, s=0)$ can be represented as

$$\psi_I^{exact}(x, s=0) = \sum_{i=1}^{\infty} C_{iI}\, \Phi_i(x, s=0). \tag{14}$$

The subscript I indicates the initial vibrational state of reagent H_2, e.g. for reagent H_2 initially in the v = 0 vibrational state I = 0. The coefficients C_{iI} are determined in the standard way, namely

$$C_{iI} = \int_{[-\kappa(s=0)]^{-1}}^{x_u} dx\, \psi_I^{exact}(x, s=0)\, \eta(x, s=0)\, \Phi_i(x, s=0). \tag{15}$$

Making use of eq. (11) we also have that

$$C_{iI} = \int_{[-\kappa(s=0)]^{-1}}^{x_u} dx\, \psi_I^{exact}(x, s=0)\, \eta^{\frac{1}{2}}(x, s=0)\, \phi_i(x, s=0). \tag{16}$$

Expression (16) is the one employed in our calculations. We then define the coefficients a_{iI} as follows:

$$a_{iI} = |C_{iI}|^2 / (\psi_I^{exact},\ \eta\, \psi_I^{exact}). \tag{17}$$

According to the vibrationally adiabatic theory outlined in Section 2.1

$$\psi_I = C_{II}\, \Phi_I(x, s) \tag{18}$$

and hence

$$a_{iI}^{VA} = \delta_{iI} \quad . \tag{19}$$

The test we have carried out consists of calculating the exact coefficients a_{iI} (eq. (17)) from the exact scattering wavefunctions and comparing the results to the VA prediction given by eq. (19) as a function of the collision energy. In addition, we compare the coefficients given by eq. (17) which have the curvature term properly included in the VA Schrödinger equation to those calculated in the zero-curvature approximation.[1]

3. Numerical Methods

3.1 Solution of the vibrational eigenvalue problem

To solve the vibrational eigenvalue equation (eq. (12)) for a given total energy E requires an iterative search procedure. The value of $\epsilon(s=0)$ is changed with each iteration until the total energy equation, eq. (8), is satisfied. As mentioned previously this iteration procedure is necessary since the parameter $\epsilon(s=0)$ is contained in both the eigenvalue equation and the energy equation through the potential $U(x, s)$. Typically six iterations were done to find the value of $\epsilon(s=0)$ which yielded equality of eq. (8) to several parts in 10^4.

The eigenvalues and eigenfunctions were solved for by a finite difference boundary-value method. This method is described briefly in paper II.1 and in greater detail elsewhere.[11]

3.2 The potential $\mathcal{U}(s,x)$

By definition

$$\mathcal{U}(x,s) = V(x,s) + [\epsilon(s) - V_1(s)]/(1 + \kappa x)^2 \quad .$$

This function has a second order pole at

$$x = -[\kappa]^{-1}$$

and the singularity is positive if $\epsilon(s) > V_1(s)$ and negative if $\epsilon(s) < V_1(s)$.

Consider first the case when $\epsilon(s) > V_1(s)$ and as a relevant example let $s = 0$. In Figure 2 the potential $\mathcal{U}(x,0)$ is given for the H_3 potential surface used in our calculations. This surface, $V(x,s)$, is a Wall-Porter fit[12] to the scaled SSMK surface[13] with a barrier height of 0.424 eV.[8] It is described in detail elsewhere.[2] Several values of $\epsilon(s=0)$ are considered to indicate the nature of the singularity. The total energies which correspond to the values of $\epsilon(s=0)$ in Figure 2 are included in Table 1. As seen $\mathcal{U}(x,0)$ becomes very large as $x \rightarrow -[\kappa(s=0)]^{-1}$ and $x > 1.0$ bohr . The value of x_u chosen for our calculations was $x_u = 2.07$ bohr. Thus, the boundary conditions

$$\phi_i(x=x_u, s=0) = 0, \tag{20a}$$

$$\phi_i(x=-[\kappa(s=0)]^{-1}, s=0) = 0 \tag{20b}$$

which were imposed in solving the eigenvalue equation (eq. 12) are seen to make physical sense for $\epsilon(s) > V_1(s)$.

For $\epsilon(s=0) = V_1(s=0)$ $\mathcal{U}(x, s=0)$ is equal to $V(x, s=0)$. This case is also shown in Figure 2. From Table 1 it is seen that for $\epsilon(s=0) = V_1(s=0) = 0.424$ eV the corresponding total energy E is 0.549 eV. For $x = x_u$ and $\epsilon(s=0) > V_1(s=0)$ $\mathcal{U}(x_u, s=0)$ is substantially greater than the corresponding total energies. However, for $\epsilon(s=0) = V_1(s=0)$ $\mathcal{U}(x=-[\kappa(s)]^{-1}, 0) = 0.892$ eV which is not much greater than the corresponding E. Hence, the boundary condition given by eq. (20b) is only marginally correct for this case. We see no way to overcome this numerical difficulty without choosing for the curve C a path different from the minimum energy path.

The approximate nature of the boundary condition given by eq. (20b) mentioned above becomes a serious problem for $\epsilon(s=0) < V_1(s=0)$ as seen in Figure 3. Clearly, the boundary condition given by eq. (20b) seems incorrect. However, as seen from Figure 3 for $\epsilon(s=0)$ greater than 0.35 eV the negative singularity is quite sharp and the potential $\mathcal{U}(x, s=0)$ rises rapidly to a large positive value relative to the total energy. This situation suggests that the correct eigenfunctions oscillate rapidly in the vicinity of the singular point $x = [-\kappa(s=0)]^{-1}$ and then decay exponentially to zero for $x = [-\kappa(s=0)]^{-1} - \delta$ for δ less than 0.15 bohr. Thus there is some justification for eq. (20b) for total energies greater than around 0.50 eV. This procedure as well as a more detailed justification for it is given in Appendix A of reference 5. As implied above, this procedure is expected to be a reasonable one for $|\epsilon(s) - V_1(s)|$ not very large.

4. Results and Discussion

As discussed in Section 2 one boundary condition on $\phi_i(x, s=0)$ was that it equal zero for $x = -[\kappa(s=0)]^{-1}$. In our calculations $\kappa(s=0) = 1.76$ bohr^{-1}. Thus, $x = -0.568$ bohr and the corresponding values for r_{AB} and r_{BC} are 2.167 bohr ($r_{AB} = r_{BC}$ for the s=0 cut for H_3). To investigate the consequences of this imposed boundary condition on the completeness of the basis set $\{\phi_i(x, s=0)\}$ (and hence $\{\Phi_i(x, s=0)\}$) the convergence of the expansion given by eq. (14) was examined for all energies considered in our calculations. Some representative results are given in Table 2 for total energies E of 0.572 eV and 0.852 eV and for reagent H_2 initially in the v = 0 vibrational state. There it can be seen that although the summation

$$\sum_{i=1}^{N} |C_{io}|^2$$

has essentially converged for N = 10 the representation of ψ_o^{exact} by the expansion given in eq. (14) is not very good. Evidently ψ_o^{exact} is non-negligible for $r_{AB}(r_{BC})$ greater than 2.167 bohr. Thus, the eigenfunctions $\{\Phi_i\}$ do not form a complete set of functions over the space spanned by ψ_o^{exact}. This is in sharp contrast to the result found for the VAZC eigenfunctions which were seen in Paper II.1 to give an excellent representation of ψ_o^{exact}. The definition of a_{iI} given by eq. (17) in terms of (ψ_I^{exact}, $\eta\,\psi_I^{exact}$) anticipated the differences seen above between ψ_I^{exact} and its representation given by eq. (14). Thus, the fact that the expansion of ψ_I^{exact} is incomplete is manifested

in the fact that the summation of a_{iI} converges to a number less than one. (At some energies the summation of a_{iI} exceeds unity.)

In Figure 4 the VA and VAZC coefficients a_{oo} are given as a function of the total energy E (lower abscissa) and initial relative kinetic energy E_o (upper abscissa). The T_o^s, T_1^s, and V(s) arrows indicate the values of the ground and first excited vibrational states of the symmetric stretch motion and the value of the potential energy along the minimum energy path respectively. The T_o, T_1, and E_o arrows correspond to the values of the ground and first excited vibrational states of H_2 and the classical barrier height respectively. For E less than 0.6 eV the present VA results and the VAZC ones are quite similar in magnitude and energy dependence. As mentioned in Section 3.2 the procedure used for handling the negative singularity in the potential $U(x, s=0)$ was justified for total energies greater than 0.5 eV. As seen in Figure 2 calculations have been made for E below 0.5 eV. There is no real justification for this other than to offer some comparison with the VAZC results. For E greater than 0.6 eV, however, the VA result shows significant improvement over the VAZC result. This seems to indicate that some of the non-adiabaticity present in the VAZC calculations can be accounted for by the inclusion of the curvature term in the correct VA Hamiltonian. That this is reasonable can be argued from inspection of Figure 2 where the potential $U(x, s=0)$ is plotted for several values of $\epsilon(s=0)$. As $\epsilon(s=0)$ increases and hence as E increases (cf. Table 1) the minimum of $U(x, s=0)$ is seen to shift to smaller values of $r_{AB}(r_{BC})$. Thus, the VA eigenfunction $\phi_o(x, s=0)$ has its peak shifted

in that direction. Thus, the VA description of the scattering wavefunction shows that as the energy increases the wavefunction increasingly samples the hard wall of the potential surface. This description is the quantum version of the "bob sled" effect and is borne out by calculations of the quantum probability current density vector.[14] (The VAZC theory, however, is a "static" one in the sense that the VAZC vibrational eigenfunctions do not change with the total energy.) Indeed, as seen in Figure 3 the location of the negative singularity in $\mathcal{U}(x, s=0)$ for E less than 0.54 eV suggests that the correct VA eigenfunction would "cut the corner" as the exact scattering function does in this energy range. The fact that the VA result is worse than the VAZC one in this energy range may be due to the manner in which we handled this negative singularity.

The VA and VAZC coefficients a_{11} are compared in Figure 5 as a function of the total energy E and the initial translational energy E_1. The VAZC result shows greater adiabaticity than does the VA one. This may be in part due to the fact that the representation of ψ_1^{exact} given by eq. (15) is significantly in error as seen from Table 3 where the convergence and completeness of the expansion of ψ_1^{exact} is examined for $E_1 = 0.063$ eV and 0.144 eV. A comparison of Tables 2 and 3 reveals that the representation of ψ_1^{exact} in the basis $\{\Phi_i\}$ is worse than it is for ψ_0^{exact}. This is due to the imposed boundary condition given by eq. (20b). The wavefunction ψ_1^{exact} is probably more diffuse in the (p, q) coordinate space than ψ_0^{exact} is and hence it is expected that the representation in the basis set $\{\Phi_i\}$ of the former wavefunction would be worse than the

latter one. Thus, although the coefficient C_{11} might be the dominant one in the expansion given by eq. (14) the VA a_{11} could still be small compared to unity according to its definition and the above discussion.

5. Conclusions

The attempt to improve upon results of a previous test of VAZC theory by including the curvature term in the VA vibrational Hamiltonian has been mainly unsuccessful. This is due primarily to several numerical difficulties present in the VA theory. A negative singularity in the VA potential occurring for total energies E less than 0.549 eV make the calculation of exact VA vibrational eigenfunctions impossible. In addition the boundary condition that $\phi_i([-\kappa(s=0)]^{-1}, s=0) = 0$ causes these VA vibrational eigenfunctions to be an incomplete basis for expansion of the exact scattering wavefunction ψ_I^{exact}. This incompleteness is more serious for ψ_1^{exact} than it is for ψ_0^{exact}.

The adiabatic potential which includes the curvature term is energy dependent due to the parameter $\epsilon(s)$. This energy dependence which enters through the curvature term causes the VA wavefunction to shift towards the hard wall with increasing energy in qualitative accord with the exact quantum result.[14]

A possible way to improve the present VA results might be to choose a reaction path with less curvature at the saddle point than the minimum energy path chosen in this study. This would help to remove the incompleteness of the VA vibrational basis set.

Table 1. Relationship between the total energy E and the "local kinetic energy" ϵ for s = 0.0 bohr[a] for reagent $H_2(v = 0)$.

ϵ(eV)	E(eV)
0.424	0.549
0.439	0.572
0.476	0.620
0.555	0.700
0.623	0.762
0.682	0.762
0.682	0.808
0.797	0.898
0.857	0.939
0.907	0.973
1.001	1.033

[a] This cut corresponds to the symmetric stretch motion of H_3.

Table 2. Convergence and completeness of expansion of $\psi_0^{\text{exact}}(x, s=0)$ for initial relative kinetic energies E_0 of 0.30 eV and 0.58 eV.

E_0(eV)	N=1[a]	N=4	N=7	N=10	$(\psi_0^{\text{exact}}, \eta\psi_0^{\text{exact}})$
0.299	2.3907	2.4544	2.4569	2.4580	2.6977
0.579	2.0905	2.6873	2.8893	2.9690	3.2692

[a] N is the number of terms in the partial sum $\sum_{i=1}^{N} |C_{i_0}|^2$.

Table 3. Convergence and completeness of expansion of $\psi_1^{exact}(x, s=0)$ for initial relative kinetic energies E_1 of 0.065 eV and 0.144 eV.

E_1(eV)	N=1[a]	N=4	N=7	N=10	$(\psi_1^{exact}, \eta\psi_1^{exact})$
0.062	0.04569	0.09997	0.1411	0.1631	0.3549
0.144	0.1994	0.8657	0.8784	0.8829	1.1649

[a] N is the number of terms in the partial sum $\sum_{i=1}^{N} |C_{i1}|^2$.

References

1. J. M. Bowman, J. T. Adams, A. Kuppermann, and D. G. Truhlar, Chem. Phys. Letters 20, 229 (1973).
2. D. G. Truhlar and A. Kuppermann, J. Chem. Phys. 56, 2232 (1972).
3. D. J. Diestler and M. Karplus, J. Chem. Phys. 55, 5832 (1971).
4. R. A. Marcus, J. Chem. Phys. 45, 4493 (1966).
5. R. E. Wyatt, J. Chem. Phys. 51, 3489 (1969).
6. D. G. Truhlar and A. Kuppermann, J. Amer. Chem. Soc. 93, 1840 (1971).
7. H. S. Johnston, Gas Phase Reaction Rate Theory (Ronald, New York, 1966) Chapt. 5, Appendix C.
8. I. Shavitt, J. Chem. Phys. 49, 4048 (1968).
9. G. Birkhoff and G.-C. Rota, Ordinary Differential Equations (Blaisdell, Waltham, Mass., 1969) Chapt. 10.
10. Reference 9, p. 279.
11. (a) D. G. Truhlar, J. Comp. Phys. 10, 123 (1972); (b) D. J. Diestler and V. McKoy, J. Chem. Phys. 47, 45 (1967); (c) N. Winter, D. J. Diestler, and V. McKoy, J. Chem. Phys. 48, 16 (1968); (d) D. G. Truhlar, Ph.D. Thesis, California Institute of Technology, Pasadena, California (1970).
12. F. T. Wall and R. N. Porter, J. Chem. Phys. 36, 3256 (1962).
13. I. Shavitt, R. M. Stevens, F. L. Minn, and M. Karplus, J. Chem. Phys. 48, 2700 (1968).
14. J. T. Adams, D. G. Truhlar, and A. Kuppermann, unpublished results.

Figure 1: Reaction path, C, for the Wall-Porter fit to the scaled SSMK H_3 potential surface in normal-mode coordinate space (p, q). Also shown are the natural collision coordinates (x, s).

Figure 2: Potential $U(x, 0)$ for four values of the local translational energy ϵ as a function of x and one internuclear distance R. For s = 0 $R_1 = R_2$. Note the positive singularities for these values of ϵ.

Figure 3: Potential $U(x, 0)$ for four values of the local translational energy ϵ as a function of x and one internuclear distance R. For s = 0 $R_1 = R_2$. Note the negative singularities for these values of ϵ.

Figure 4: Curvature and zero-curvature coefficients a_{00} for s = 0.0 as a function of the total energy E and the initial translational energy E_0. The significance of the arrows on the lower abscissa is given in the text.

Figure 5: Curvature and zero-curvature coefficients a_{11} for s = 0.0 as a function of the total energy E and the initial translational energy E_1.

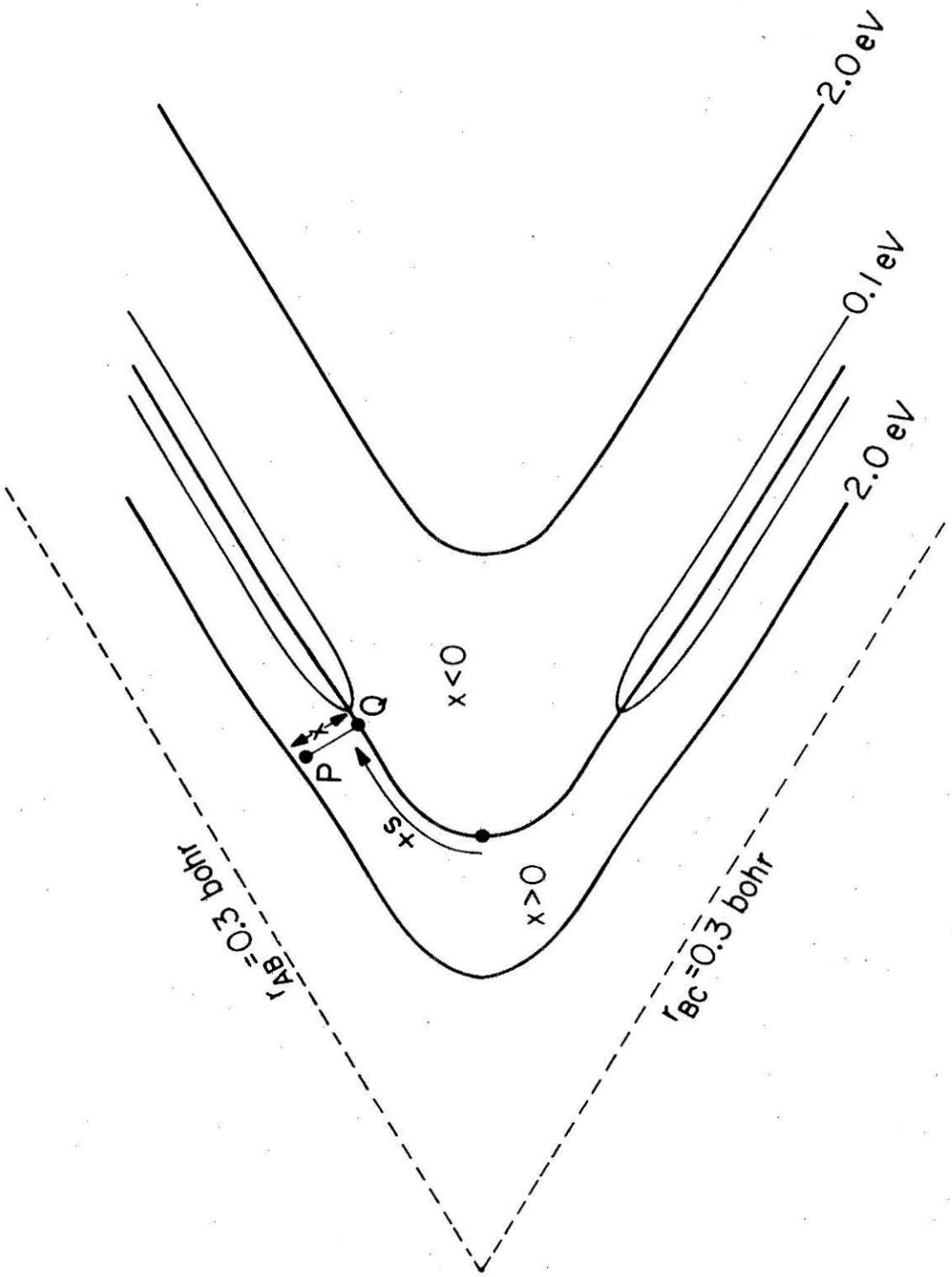

Figure 1

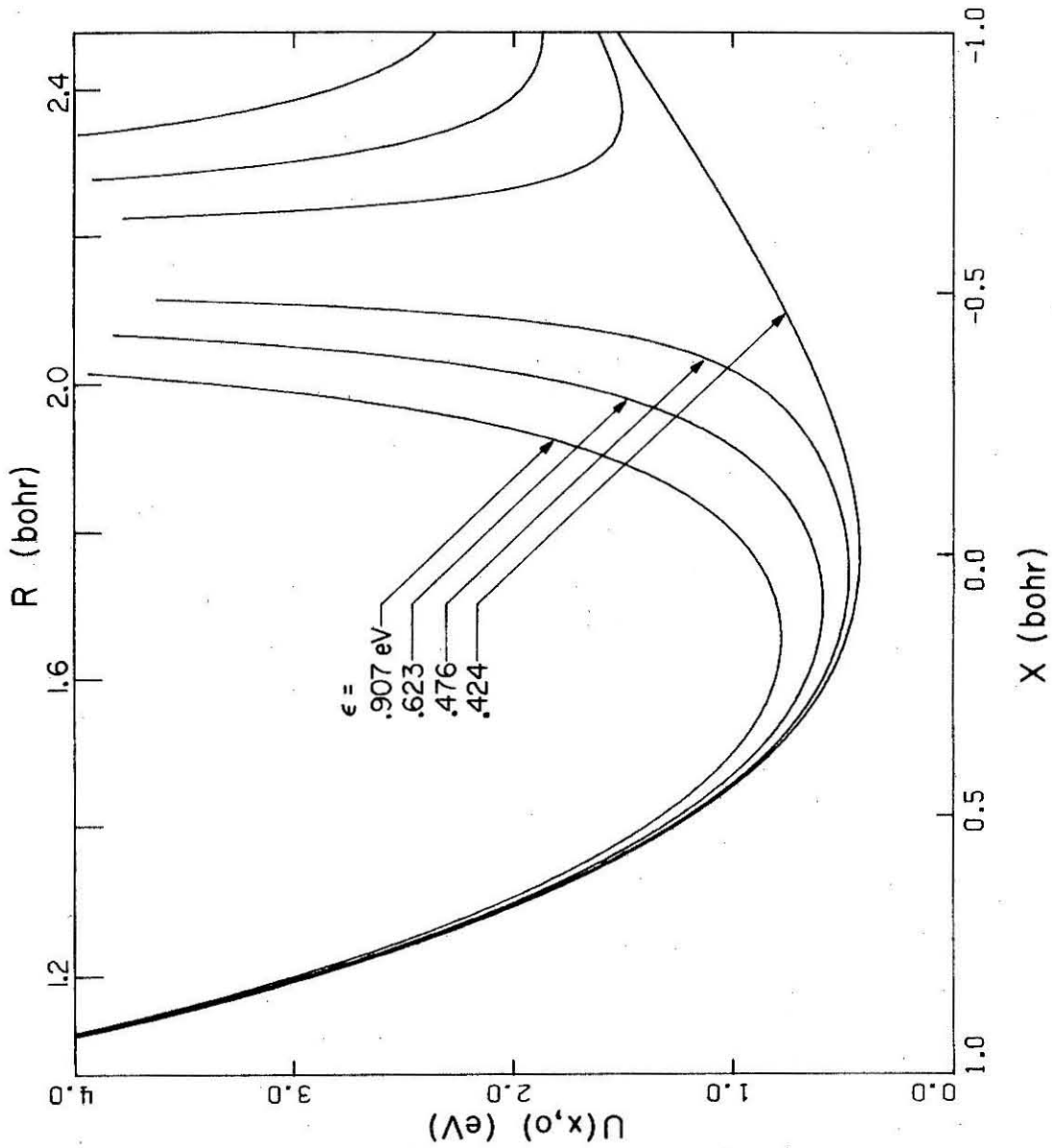
R (bohr)
X (bohr)
U(x,o) (eV)
ϵ =
.907 eV
.623
.476
.424
1.2
1.6
2.0
2.4
-1.0
-0.5
0.0
0.5
1.0
0.0
1.0
2.0
3.0
4.0

Figure 2

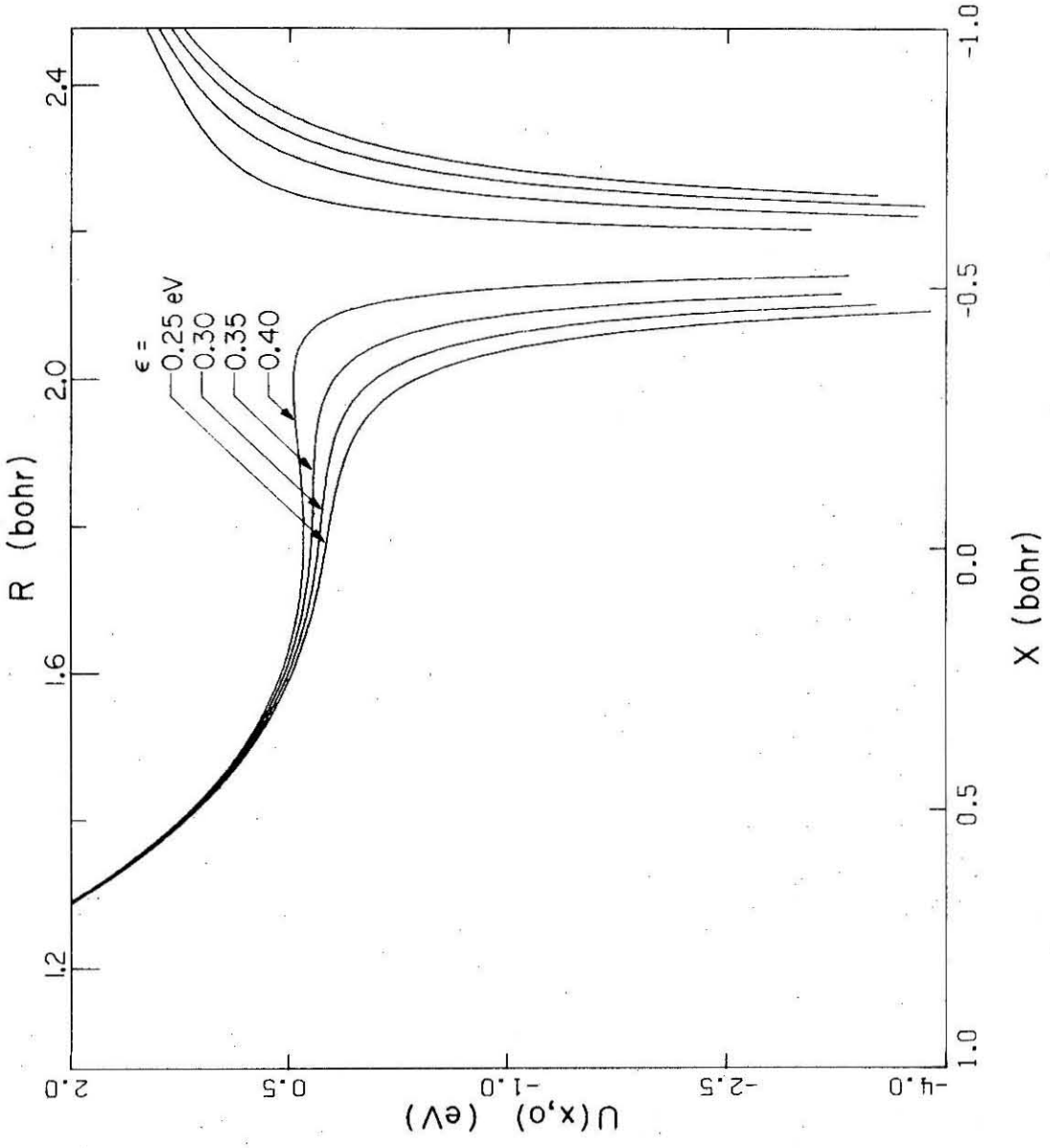
R (bohr)
X (bohr)
U(x,o) (eV)
ε =
0.25 eV
0.30
0.35
0.40
2.4
2.0
1.6
1.2
-1.0
-0.5
0.0
0.5
1.0
2.0
0.5
-1.0
-2.5
-4.0

Figure 3

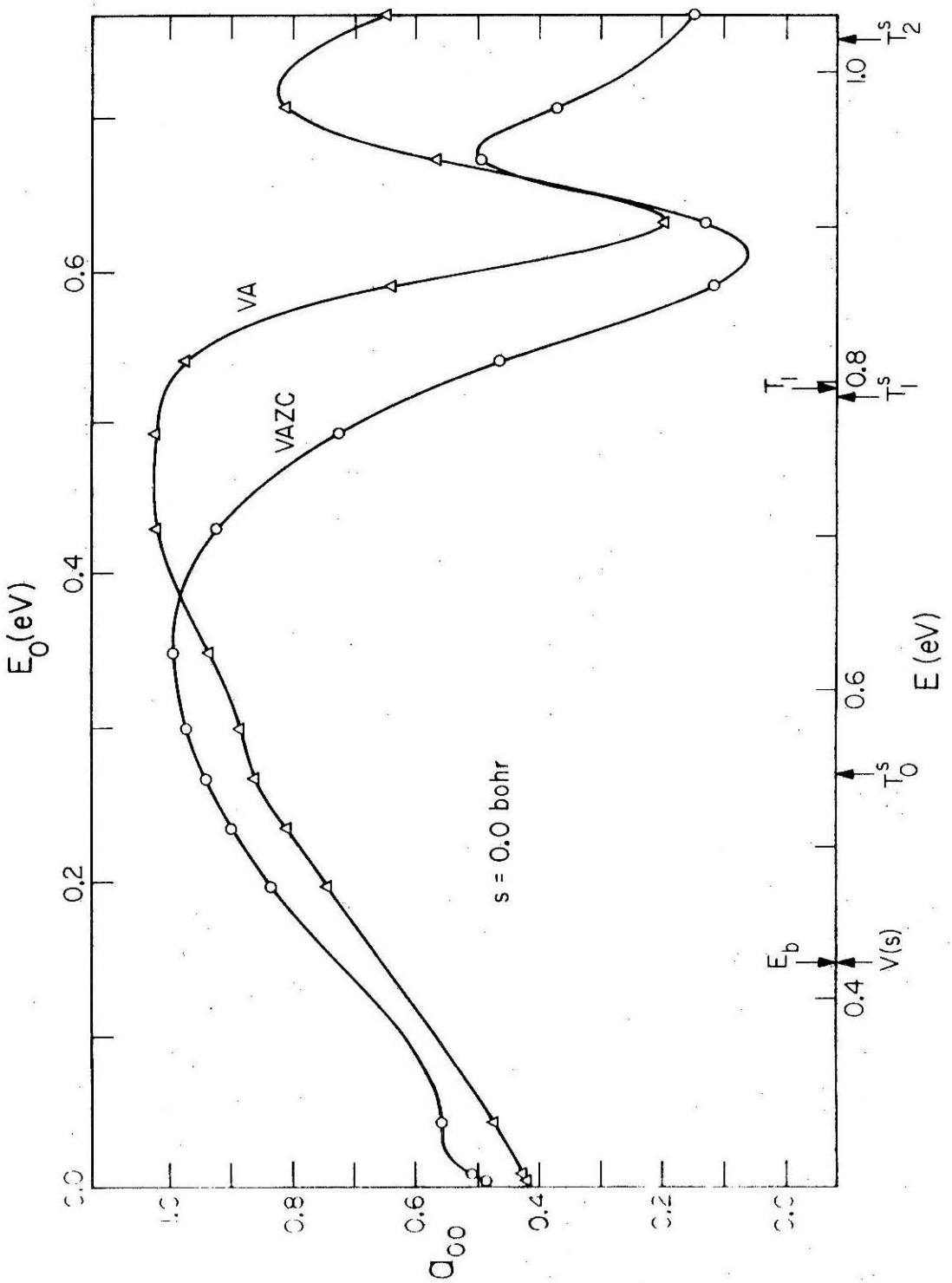
E_0(eV)
0.0
0.2
0.4
0.6
VA
VAZC
s = 0.0 bohr
a_{00}
0.0
0.2
0.4
0.6
0.8
1.0
E_b
V(s)
T_0^s
T_1
T_1^s
T_2^s
0.4
0.6
0.8
1.0
E (eV)

Figure 4

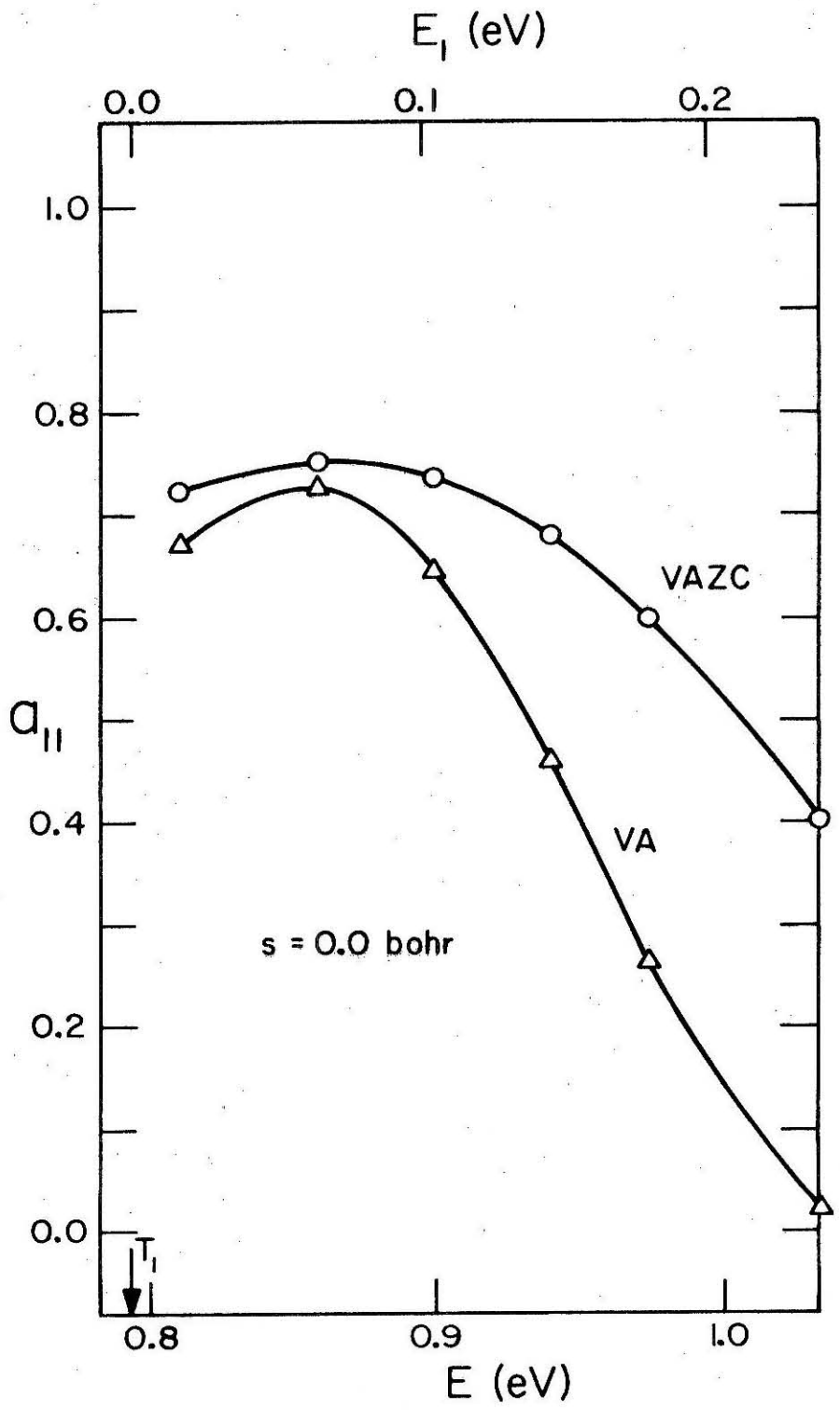

Figure 5

SUMMARY

SUMMARY

The results of the test of the vibrationally adiabatic zero-curvature theory presented in paper II. 1 revealed that the theory is in qualitative agreement with exact quantum results over a limited range of collision energies. For total energies below the energetic threshold for vibrational excitation of H_2 it was found that the reaction is vibrationally adiabatic in the near asymptotic regions of space. In the strong interaction region significant non-adiabaticity was found, especially at the very low collision energies where tunneling is substantial. Thus, we concluded that tunneling is non-adiabatic. For energies above the energetic threshold for vibrational excitation the adiabatic theory expectedly breaks down.

An investigation of the use of vibrationally adiabatic zero-curvature basis sets to represent the scattering wavefunctions along five cuts was performed. It was found that convergence of the representation was rapid at all the energies considered.

In paper II. 2 the attempt to improve the zero-curvature results of II. 1 by including curvature in the calculations was mainly unsuccessful. The chief reason for this seemed to be due to numerical difficulties inherent in the curvature treatment. Depending on the value of the total energy the potential function has a positive or negative singularity at the local radius of curvature. In addition to presenting some numerical difficulties in the calculation of the vibrationally adiabatic basis

sets (especially for the negative singularity) the domain of the independent variable was restricted. This restriction caused the vibrationally adiabatic basis sets to be incomplete over the domain of configuration space spanned by the exact scattering wavefunction. This contributed to the inability of the curvature correction to improve the zero-curvature results. In addition, the representation of the exact wavefunction by the vibrationally adiabatic basis sets (including curvature) was not very good. At higher collision energies, the accuracy of this representation was found to deteriorate substantially over the lower energy results.

PART III

THEORETICAL STUDIES OF ELECTRONICALLY NON-ADIABATIC CHEMICAL REACTION DYNAMICS

ELECTRONICALLY NON-ADIABATIC REACTION DYNAMICS

1. Introduction

The field of electronically non-adiabatic (ENA) reaction dynamics is a rapidly developing one.[1] An example of an ENA chemical reaction which has been studied extensively experimentally is[2-6]

$$H^+ + D_2(x^1\Sigma_g^+) \rightarrow HD^+(x^2\Sigma_g^+) + D(^1S) \quad .$$

Many other reactions, expecially chemiluminescent ones, are known to be of the ENA type. In particular, reactions with barium atoms such as

$$Ba(^1S) + NO_2 \rightarrow BaO(A^1\Sigma^+) + N_2(x^1\Sigma_g^+)$$

$$Ba(^1S) + Cl_2 \rightarrow BaCl_2 + \text{photon}$$

have recently been studied under single collision conditions.[7-9] Many oxygen atom reactions may well be of the ENA type. Indeed, it has been speculated that the reactions

$$O(^3P) + Br_2 \rightarrow OBr^* + Br$$

$$O_2(^3P) + Ba \rightarrow BaO^* + O$$

may involve a singlet as well as the triplet surface.[10,11,12]

Theoretically, although much interest is developing towards describing ENA reactions, not very much has been done. A classical trajectory surface-hopping technique based on semi-classical atom-atom theory has been developed and applied to the $H^+ + D_2$ reaction.[13,14] An elegant semi-classical theory of ENA chemical reactions has also

been developed[15,16] and recently applied to the $H^+ + D_2$ reaction.[17,18] In addition the possible role of several potential surfaces in the $F + H_2$ reaction has been questioned[19] and explored within an approximate classical trajectory surface-hopping method.[20]

The fact that ENA reactions are receiving increasing interest has stimulated us to perform exact quantum studies of some model collinear ENA chemical reactions. In addition it is quite likely that insight gained in studies of ENA reactions will be applicable to the subject of radiationless transitions and unimolecular decay from an excited electronic state.[21]

In the next six sections the general quantum theory of ENA reactions is presented. Following that are manuscripts describing our calculations. The first manuscript presents some results we have obtained for the collinear $H^+ + H_2 \rightarrow H_2 + H^+$ reaction in which only the ground state surface was considered. The results are of sufficient interest to merit their presentation even though the study involves only a single potential surface. The second manuscript gives results on model (fictitious) $H + H_2$ studies on two potential energy surfaces coupled by a third "spin-orbit" surface. The third manuscript contains results for our study of the reaction.

$$Ba(^1S) + ON_2(x\,^1\Sigma) \longrightarrow \begin{cases} BaO^* + N_2 \\ \searrow\ BaO + N_2 \end{cases}$$

This reaction is of current interest as a possible candidate for an electronic transition chemical laser. Details of the relevant two-state differential equations for the collinear reactions as well as the

scattering analysis are given in several Appendices.

2. The Adiabatic Representation of Electronically Non-Adiabatic Chemical Reactions

In the fully quantum treatment of the electronic and nuclear motion (described by sets of coordinates $\underset{\sim}{r}$ and $\underset{\sim}{R}$ respectively) the complete wavefunction Ψ is written as follows:

$$\Psi(\underset{\sim}{R}, \underset{\sim}{r}) = \sum_i \chi_i(\underset{\sim}{r};\underset{\sim}{R})\psi_i(\underset{\sim}{R}) \quad . \tag{1}$$

This expansion assumes that for each value of $\underset{\sim}{R}$ the $\chi_i(\underset{\sim}{r};\underset{\sim}{R})$ form a complete set of functions over the space spanned by the wavefunction Ψ. The ψ_i can be thought of as expansion coefficients at a fixed $\underset{\sim}{R}$ in the expansion of Ψ. As $\underset{\sim}{R}$ changes these expansion coefficients change, hence ψ_i becomes a function of $\underset{\sim}{R}$. Indeed, the assumption that a complete orthonormal set of electronic functions exists for each $\underset{\sim}{R}$ is a non-trivial one. However, if such sets exist then they must be related to each other by a unitary transformation. The so-called adiabatic $\chi_i(\underset{\sim}{r};R)$ are a particular set of electronic wavefunctions which satisfy an eigenvalue equation specified below. The nuclear wavefunctions $\psi_i(\underset{\sim}{R})$ describe the scattering properties of the system from a given initial quantum state to all possible final quantum states. Since our interest is centered on chemical reactions in which the electron motion is always bound, only electronic wavefunctions which describe such motion are included in expansion (1). This condition further assumes that virtual electronic continuum states can be ignored. In this section we focus on electronic eigenfunctions χ_i^a which are

the molecular wavefunctions obtained in the Born-Oppenheimer[22] approximation and they satisfy the following eigenvalue equation:

$$H^{el}(r;R)\,\chi_i^{a}(\underset{\sim}{r};\underset{\sim}{R}) = E_i(\underset{\sim}{R})\,\chi_i^{a}(\underset{\sim}{r};\underset{\sim}{R}) \quad . \tag{2}$$

The Hamiltonian H^{el} is the piece of the total electronic and nuclear Hamiltonian which describes the electronic motion for "clamped" nuclei. H^{el} depends parametrically on the nuclear coordinates $\underset{\sim}{R}$ (in most cases on R only) due to the nature of the usual electron-nuclear interactions. In addition, H^{el} is required to contain all of the electron interactions to be considered in the problem, e.g., spin-orbit interactions. In a later section the possibility of excluding such interactions in H^{el} but including them in the total Hamiltonian will be considered.

The χ_i^{a} defined by eq. (2) adjust to the nuclear motion (for infinitely slow nuclear motion) and hence are termed adiabatic states. Furthermore the eigenvalues $E_i(\underset{\sim}{R})$ form a family of adiabatic potential energy hypersurfaces which govern the nuclear motion (cf. below) and obey the "non-crossing" rule.[23] Thus, the representation of Ψ given by (1) for the χ_i set of functions is termed the adiabatic representation.

To examine some of the consequences of this adiabatic representation on the equations describing $\psi_i(\underset{\sim}{R})$ we write the full electron nuclear Hamiltonian H in terms of the nuclear kinetic energy operator T_N and H^{el} as

$$H = T_N + H^{el} \tag{3}$$

and note the Ψ must satisfy the Schrödinger equation for a total energy E

$$(H - E)\,\Psi(\underset{\sim}{R}, \underset{\sim}{r}) = 0. \tag{4}$$

Then, inserting expansion (1) for Ψ into (4) and making use of (2) we have that

$$\sum_i [\,\hat{T}_N + E_i(\underset{\sim}{R}) - E]\,\chi_i^{a}(\underset{\sim}{r};\underset{\sim}{R})\,\psi_i(\underset{\sim}{R}) = 0. \tag{5}$$

To develop coupled equations for the ψ_i we multiply (5) by $\chi_j^{a^*}$ and integrate with respect to $\underset{\sim}{r}$. Making use of the fact that the χ_i can be taken as orthonormal (since H_{el} is Hermitian) eq. (5) becomes [24]

$$\sum_i \{\langle \chi_j^{a} | \hat{T}_N | \chi_i^{a} \rangle_{el} + [E_i(R) - E]\,\delta_{ji}\,\psi_i(\underset{\sim}{R}) = 0. \tag{6}$$

If $\hat{T}_N$ is written as

$$\hat{T}_N = (2M)^{-1}\hat{\underset{\sim}{P}} \cdot \hat{\underset{\sim}{P}} \tag{7}$$

where $\hat{\underset{\sim}{P}}$ denotes the sum of nuclear momentum operators and where M denotes a collective mass (a coordinate system $\underset{\sim}{R}$ such that (7) is valid can constructed), then (6) becomes

$$\sum_i \{(2M)^{-1}\langle \chi_j | \hat{P}^2 | \chi_i \rangle_{el} + M^{-1}\langle \chi_j | \hat{\underset{\sim}{P}} | \chi_i \rangle_{el} \cdot \hat{\underset{\sim}{P}} + \delta_{ji}(2M)^{-1}\hat{P}^2]\,\psi_i(\underset{\sim}{R})$$
$$+ [E_i(R) - E]\,\delta_{ji}\}\,\psi_i(\underset{\sim}{R}) = 0. \tag{8}$$

The first two terms of eq. (8) involving matrix elements of $\hat{\underset{\sim}{P}}$ and $\hat{P}^2$ are responsible for coupling the $\psi_i(\underset{\sim}{R})$. These quantities are called

the Born-Oppenheimer (BO) coupling terms. In the example below their explicit form is given.

A very important point to note is that the BO coupling terms are Hermitian with respect to their operation on the nuclear coordinates. Since this is not obvious from their form we shall demonstrate this in the example given below.

Consider now a collinear reactive collision of an atom with a diatomic molecule, $A + BC \rightarrow AB + C$. In the Delves mass-weighted coordinate system[25] the two nuclear coordinates describing the A, BC arrangement channel are denoted by x_1 and x_2 and their conjugate momenta are designated by $\hat{P}_{x_1}$ and $\hat{P}_{x_2}$. In terms of the internuclear distances r_{AB} and r_{BC} and the nuclear mass M_A, M_B, and M_C these coordinates are given by

$$x_1 = \left(\frac{\mu_{A,BC}}{\mu_{BC}}\right)^{\frac{1}{4}} \left[r_{AB} + \frac{M_B}{M_B + M_C}\, r_{BC}\right] ,$$

$$x_2 = \left(\frac{\mu_{BC}}{\mu_{A,BC}}\right)^{\frac{1}{4}} r_{BC}$$

where

$$\mu_{A,BC} = M_A(M_B + M_C)/(M_A + M_B + M_C) ,$$

and

$$\mu_{BC} = M_B M_C/(M_B + M_C) .$$

For the product arrangement channel a pair of coordinates, denoted by z_1 and z_2, are analogously defined. In terms of the variables x_1, x_2

and their conjugate momenta eq. (8) becomes

$$\sum_i \{[(2\mu)^{-1} \langle \chi_j^a | -\hbar^2 (\frac{\partial^2}{\partial x_1^2} + \frac{\partial^2}{\partial x_2^2}) | \chi_i^a \rangle_{el} + \mu^{-1} \langle \chi_j^a | -i\hbar (\frac{\partial}{\partial x_1} \hat{x}_1 + \frac{\partial}{\partial x_2} \hat{x}_2) | \chi_i^a \rangle_{el}$$

$$\cdot -i\hbar (\frac{\partial}{\partial x_1} \hat{x}_1 + \frac{\partial}{\partial x_2} \hat{x}_2)] \psi_i(x_1, x_2) + \delta_{ji} [-\frac{\hbar^2}{2\mu} (\frac{\partial^2}{\partial x_1^2} + \frac{\partial^2}{\partial x_2^2}) + E_i(x_1, x_2) - E]$$

$$\cdot \psi_i(x_1, x_2) = 0. \qquad (9)$$

Consider now the two-state approximation to eq. (9). That is, the summation over i is restricted to two terms. Within this approximation eq. (9) can be written explicitly as

$$[-\frac{\hbar^2}{2\mu} (\frac{\partial^2}{\partial x_1^2} + \frac{\partial^2}{\partial x_2^2}) + T_{11}''(x_1, x_2) + E_1(x_1, x_2) - E] \psi_1(x_1, x_2)$$

$$= -(T_{12}' + T_{12}'') \psi_2(x_1, x_2) \qquad (10a)$$

$$[-\frac{\hbar^2}{2\mu} (\frac{\partial^2}{\partial x_1^2} + \frac{\partial^2}{\partial x_2^2}) + T_{22}''(x_1, x_2) + E_2(x_1, x_2) - E] \psi_2(x_1, x_2)$$

$$= -(T_{21}' + T_{21}'') \psi_1(x_1, x_2) \quad , \qquad (10b)$$

where in notation introduced previously [26]

$$T_{ij}' = -\frac{\hbar^2}{\mu} \langle \chi_i | \frac{\partial}{\partial x_1} \hat{x}_1 + \frac{\partial}{\partial x_2} \hat{x}_2 | \chi_j \rangle_{el} \cdot (\frac{\partial}{\partial x_1} \hat{x}_1 + \frac{\partial}{\partial x_2} \hat{x}_2)$$

and

$$T_{ij}'' = -\frac{\hbar^2}{2\mu} \langle \chi_i | \frac{\partial^2}{\partial x_1^2} + \frac{\partial^2}{\partial x_2^2} | \chi_j \rangle_{el}, \quad i, j = 1, 2 \quad .$$

The diagonal terms T_{11}' and T_{22}' are absent from eqs. (10a) and (10b) since they are rigorously zero. To see that, consider the identity

$$\frac{\partial}{\partial x_1} \langle \chi_i | \chi_i \rangle_{el} = 0$$

which leads to the result that

$$\langle \chi_i | \frac{\partial}{\partial x_1} | \chi_i \rangle_{el} = 0.$$

Equations (9), (10a), and (10b) are well known, however, few calculations have actually been carried out with them. This may be due in part to the difficulty in obtaining the BO coupling terms T_{ij}' and T_{ij}'' for atomic and molecular systems by ab initio methods. Accurate ab initio bound state calculations of the vibrational motion of H_2^+ and H_2 have been carried out utilizing equations analogous to eqs. (10a) and (10b);[27-29] however, to our knowledge no scattering calculation has been performed which makes use of these equations. Many scattering calculations have been done in the spirit of these equations but making semi-classical approximations to them.

The Hermiticity of the BO coupling terms is undoubtedly known, especially by those who have used the above formalism in bound state problems. However, since this property is not self-evident we prove it for the above collinear example. Consider first the identity

$$0 = \frac{\partial}{\partial x_1} \langle \chi_1 | \chi_2 \rangle_{el} .$$

This implies that

$$\langle \chi_2 | \frac{\partial}{\partial x_1} | \chi_1 \rangle^* = - \langle \chi_1 | \frac{\partial}{\partial x_1} | \chi_2 \rangle_{el} \qquad (11a)$$

and similarly

$$\langle \chi_2 | \frac{\partial}{\partial x_2} | \chi_1 \rangle_{el}^{*} = - \langle \chi_1 | \frac{\partial}{\partial x_2} | \chi_2 \rangle_{el} . \tag{11b}$$

For future use it is convenient to define the quantities

$$F_{ij} \equiv \langle \chi_i | \frac{\partial}{\partial x_1} | \chi_j \rangle_{el}, \tag{12a}$$

$$G_{ij} \equiv \langle \chi_i | \frac{\partial}{\partial x_2} | \chi_j \rangle_{el}, \quad i,j = 1,2 . \tag{12b}$$

The assertion that the BO coupling terms are Hermitian is given by the equality

$$\langle \psi_1 | T_{12}' + T_{12}'' | \psi_2 \rangle_N = \langle \psi_2 | T_{21}' + T_{21}'' | \psi_1 \rangle_N^{*} , \tag{13}$$

where the integration is with respect to the variables x_1 and x_2. Consider first the integrals involving the operators T_{12}' ; $\langle \psi_1 | T_{12}' | \psi_2 \rangle_N$. By definition

$$\langle \psi_1 | T_{12}' | \psi_2 \rangle_N = - \frac{\hbar^2}{\mu} \langle \psi_1 | F_{12} \frac{\partial}{\partial x_1} + G_{12} \frac{\partial}{\partial x_2} | \psi_2 \rangle_N .$$

Examining the term $\langle \psi_1 | F_{12} \frac{\partial}{\partial x_1} | \psi_2 \rangle_N$ we have that

$$\langle \psi_1 | F_{12} \frac{\partial}{\partial x_1} | \psi_2 \rangle_N = \int dx_2 \int dx_1 \, \psi_1^{*}(x_1, x_2) \, F_{12}(x_1, x_2) \frac{\partial}{\partial x_1} \psi_2(x_1, x_2) .$$

Since the integrations over x_1 and x_2 are independent we can perform the x_1 integration by parts to obtain,

$$\int dx_1 \, \psi_1^{*}(x_1, x_2) \, F_{12}(x_1, x_2) \frac{\partial}{\partial x_1} \psi_2(x_1, x_2) = \psi_1^{*}(x_1, x_2) \, F_{12}(x_1, x_2) \, \psi_2(x_1, x_2) \Big|_{x_1}^{x_1^u}$$
$$- \int dx_1 \, \psi_2(x_1, x_2) \left[F_{12}(x_1, x_2) \frac{\partial}{\partial x_1} \psi_1^{*}(x_1, x_2) + \psi_1^{*}(x_1, x_2) \frac{\partial F_{12}}{\partial x_1} \right] .$$

The first term on the right hand side of the above equation vanishes since the BO coupling term F_{12} vanishes for large values of the

scattering coordinate x_1^u and for small values of the coordinate x_1^l either F_{12} or ψ_1 and ψ_2 or both vanish due to the repulsive nature of the potentials $E_1(x_1, x_2)$ and $E_2(x_1, x_2)$. Thus

$$\langle\psi_1 | F_{12} \frac{\partial}{\partial x_1} | \psi_2\rangle_N = - \langle\psi_2 | F_{12}^* \frac{\partial}{\partial x_1} | \psi_1\rangle_N^* - \langle\psi_2 | \frac{\partial F_{12}}{\partial x_1}^* | \psi_1\rangle_N^* \quad (14a)$$

and by similar reasoning

$$\langle\psi_1 | G_{12} \frac{\partial}{\partial x_2} | \psi_2\rangle_N = - \langle\psi_2 | G_{12}^* \frac{\partial}{\partial x_2} | \psi_1\rangle_N^* - \langle\psi_2 | \frac{\partial G_{12}}{\partial x_2}^* | \psi_1\rangle_N^* . \quad (14b)$$

Now making use of eqs. (11a) and (11b) eqs. (14a) and (14b) can be written as

$$\langle\psi_1 | F_{12} \frac{\partial}{\partial x_1} | \psi_2\rangle_N = \langle\psi_2 | F_{21} \frac{\partial}{\partial x_1} | \psi_1\rangle_N^* + \langle\psi_2 | \frac{\partial F_{21}}{\partial x_1} | \psi_1\rangle_N^*, \quad (15a)$$

and

$$\langle\psi_1 | G_{12} \frac{\partial}{\partial x_2} | \psi_2\rangle_N = \langle\psi_2 | G_{21} \frac{\partial}{\partial x_1} | \psi_1\rangle_N^* + \langle\psi_2 | \frac{\partial G_{21}}{\partial x_2} | \psi_1\rangle_N^* . \quad (15b)$$

Thus, we have the important result that

$$\langle\psi_1 | T_{12}' | \psi_2\rangle_N = \langle\psi_2 | T_{21}' | \psi_1\rangle_N^* - \frac{\hbar^2}{\mu} \langle\psi_2 | \frac{\partial F_{21}}{\partial x_1} + \frac{\partial G_{21}}{\partial x_2} | \psi_1\rangle_N^* , \quad (16)$$

and hence the operator T_{12}' is not Hermitian (unless $\partial F_{21}/\partial x_1$ and $\partial G_{21}/\partial x_2$ vanish).

From the definition of F_{21}

$$\frac{\partial F_{21}}{\partial x_1} = \frac{\partial}{\partial x_1} \langle\chi_2 | \frac{\partial}{\partial x_1} | \chi_1\rangle_{el}$$

$$= \langle\frac{\partial \chi_2}{\partial x_1} | \frac{\partial \chi_1}{\partial x_1}\rangle_{el} + \langle\chi_2 | \frac{\partial^2}{\partial x_2^2} | \chi_1\rangle_{el} \quad (17a)$$

and similarly

$$\frac{\partial G_{21}}{\partial x_2} = \langle \frac{\partial \chi_2}{\partial x_2} | \frac{\partial \chi_1}{\partial x_2} \rangle_{el} + \langle \chi_2 | \frac{\partial^2}{\partial x_1^2} | \chi_1 \rangle_{el} \quad . \tag{17b}$$

Thus, eq. (16) can be written as

$$\langle \psi_1 | T_{12}' | \psi_2 \rangle_N = \langle \psi_2 | T_{21}' | \psi_1 \rangle_N^* - \frac{\hbar^2}{\mu} \langle \psi_2 | [\langle \frac{\partial \chi_2}{\partial x_1} | \frac{\partial \chi_1}{\partial x_1} \rangle_{el} + \langle \frac{\partial \chi_2}{\partial x_2} | \frac{\partial \chi_1}{\partial x_2} \rangle_{el}$$

$$\langle \chi_2 | \frac{\partial^2}{\partial x_1^2} + \frac{\partial^2}{\partial x_2^2} | \chi_1 \rangle_{el}] | \psi_1 \rangle_N^* \quad . \tag{18}$$

To complete the proof of the Hermiticity of the BO coupling terms we make use of the following identity

$$\frac{\partial^2}{\partial x_1^2} \langle \chi_1 | \chi_2 \rangle_{el} = 0$$

to establish that

$$-\frac{\hbar^2}{2\mu} \langle \chi_1 | \frac{\partial^2}{\partial x_1^2} + \frac{\partial^2}{\partial x_2^2} | \chi_2 \rangle_{el} = \frac{\hbar^2}{\mu} [\langle \frac{\partial \chi_2}{\partial x_1} | \frac{\partial \chi_1}{\partial x_1} \rangle_{el}^* + \langle \frac{\partial \chi_2}{\partial x_2} | \frac{\partial \chi_1}{\partial x_2} \rangle_{el}^*]$$

$$+ \frac{\hbar^2}{2\mu} \langle \chi_2 | \frac{\partial^2}{\partial x_1^2} + \frac{\partial^2}{\partial x_2^2} | \chi_1 \rangle_{el}^* \quad . \tag{19}$$

Thus,

$$-\frac{\hbar^2}{2\mu} \langle \psi_1 | \langle \chi_1 | \frac{\partial^2}{\partial x_1^2} + \frac{\partial^2}{\partial x_2^2} | \chi_2 \rangle_{el} | \psi_2 \rangle_N = \frac{\hbar^2}{\mu} \langle \psi_2 | \langle \frac{\partial \chi_2}{\partial x_1} | \frac{\partial \chi_1}{\partial x_1} \rangle_{el}$$

$$+ \langle \frac{\partial \chi_2}{\partial x_2} | \frac{\partial \chi_1}{\partial x_2} \rangle_{el} | \psi_1 \rangle_N^* + \frac{\hbar^2}{2\mu} \langle \psi_2 | \langle \chi_2 | \frac{\partial^2}{\partial x_1^2} + \frac{\partial^2}{\partial x_2^2} | \chi_1 \rangle_{el} | \psi_1 \rangle_N^* \quad . \tag{20}$$

Now we add the left and right hand sides of eq. (20) to the left and right hand sides of eq. (18) respectively to secure

$$-\frac{\hbar^2}{2\mu}\langle\psi_1|\langle\chi_1|\frac{\partial^2}{\partial x_1^2}+\frac{\partial^2}{\partial x_2^2}|\chi_2\rangle_{el}|\psi_2\rangle_N+\langle\psi_1|T_{12}'|\psi_2\rangle_N=$$

$$\langle\psi_2|T_{21}'|\psi_1\rangle_N^*-\frac{\hbar^2}{2\mu}\langle\psi_2|\langle\chi_2|\frac{\partial^2}{\partial x_1^2}+\frac{\partial^2}{\partial x_2^2}|\chi_1\rangle_{el}|\psi_1\rangle_N^* \quad . \qquad (21)$$

This is the desired result which according to the definitions of T_{ij}'' given after eq. (10b) can be rewritten as

$$\langle\psi_1|T_{12}'+T_{12}''|\psi_2\rangle_N=\langle\psi_2|T_{21}'+T_{21}''|\psi_1\rangle_N^* \quad . \qquad (22)$$

Thus, we have shown that the BO coupling terms $T_{ij}'+T_{ij}''$ are Hermitian and that separately the quantities T_{ij}' and T_{ij}'' are not in general Hermitian. The latter point is very important for rigorous quantum calculations. In semi-classical descriptions of the two-state problem the T_{ij}'' term is absent in the formalism[30-32] and hence there may be a temptation to omit it in the rigorous quantum description.[33] However, unless its omission is carefully justified it may result in a non-Hermitian coupling which will produce a non-unitary scattering matrix.[34]

3. The Diabatic Representation of Electronically Non-Adiabatic Chemical Reactions

In the previous section the adiabatic representation of electronically non-adiabatic chemical reactions was presented. The crucial point which gave rise to this representation is expressed by Eq. (2). In other words the electronic wavefunctions χ_i^a were required to be eigenfunctions of the full and complete electronic Hamiltonian, H^{el} at all internuclear separations. Such eigenfunctions are also termed molecular wavefunctions.

If instead of using these exact solutions to eq. (2) a different set of electronic wavefunctions is employed in the expansion of $\Psi(\underset{\sim}{R}, \underset{\sim}{r})$ then the representation is termed diabatic[35] and these electronic wavefunctions are denoted by the symbol χ_i^d. Clearly, this description of the diabatic representation is quite vague and hence obviates the possibility of a unique diabatic representation. For example the χ_i^d might be chosen in the following ways. They might be eigenfunctions of H^{el} for the isolated atoms (and/or molecules) and then "frozen" at all other atomic (and/or molecular) internuclear distances. Such frozen orbitals would not satisfy eq. (2) in general. Another, more realistic possibility is that the χ_i^d are allowed to change somewhat as the nuclei are moved, however, not so as to be exact eigenfunctions of H^{el}.[36] This diabatic picture though not unique does produce a set of coupled equations for the diabatic nuclear wavefunctions $\psi_i^d(\underset{\sim}{R})$.[37] The procedure to develop these equations is identical to the one used in the previous section. However, eq. (2) can no longer be used. Thus, in place of eq. (6) we have the following set of coupled equations

$$\sum_i [\langle \chi_j^d | \hat{T}_N | \chi_i^d \rangle_{el} + H_{ji}^{el} - E] \psi_i^d = 0 \quad , \tag{22}$$

where

$$H_{ji}^{el} = \langle \chi_j^d | H^{el} | \chi_i^d \rangle_{el} .$$

The use of approximate electronic wavefunctions has resulted in additional coupling (through the matrix elements H_{ji}^{el}) in the coupled equation for the ψ_i^d when compared with the adiabatic representation

(cf. eq. (4)). At this point, without justification, we assume that

$$\langle \chi_j^d | \hat{T}_N | \chi_i^d \rangle_{el} = \delta_{ji} \hat{T}_N \tag{23}$$

and eq. (22) becomes simply

$$\sum_i [(\hat{T}_N - E)\delta_{ji} + H_{ji}^{el}] \psi_i^d = 0 \quad . \tag{24}$$

A justification of eq. (23) has not been made in the literature and the fact that this is even assumed (when it certainly is) is given only casual notice.[31, 32] A possible source of justification might be offered if the χ_i^d are frozen orbitals. By definition these atomic orbitals change little with R and hence derivatives of these functions with respect to R might be very small. These coupled equations are simpler in structure than are ones given by (4), since the coupling is of simpler and "cleaner" nature than the one in (4) which involves nuclear knietic energy and velocity operators. However, the simplicity of eq. (24) rests on the validity of eq. (23). Indeed it might be argued that in the presence of a complete expansion of the total wavefunction $\Psi(\underset{\sim}{R}, \underset{\sim}{r})$ in some diabatic representation by introducing some coupling through the H_{ji}^{el} matrix coupling $\langle \chi_j^d | \hat{T}_N | \chi_i^d \rangle_{el}$ might be reduced. In the time-dependent impact parameter approximation to (22) it is argued that the nuclear velocity coupling is negligible for high energy collision.[24] Further, eq. (23) may serve as a guiding principle in choosing a "good" diabatic representation χ_i^d. That is, one seeks the χ_i^d for which eq. (23) is best satisfied. In any event, it has recently been shown that a unique

diabatic representation can be found such that eq. (23) can be satisfied exactly.[38] We return to a consideration of this approach in the next section.

Let us consider again the example of a collinear A + BC → AB + C collision described in the previous section. In the two-state approximation eq. (24) becomes for this example the following

$$\left[-\frac{\hbar^2}{2\mu}\left(\frac{\partial^2}{\partial x_1^2}+\frac{\partial^2}{\partial x_2^2}\right)+H_{11}^{el}(x_1,x_2)-E\right]\psi_1^{d}(x_1,x_2)=H_{12}^{el}(x_1,x_2)\psi_2^{d}(x_1,x_2) \quad (25a)$$

$$\left[-\frac{\hbar^2}{2\mu}\left(\frac{\partial^2}{\partial x_1^2}+\frac{\partial^2}{\partial x_2^2}\right)+H_{22}^{el}(x_1,x_2)-E\right]\psi_2^{d}(x_1,x_2)=H_{21}^{el}(x_1,x_2)\psi_1^{d}(x_1,x_2). \quad (25b)$$

The functions H_{11}^{el} and H_{22}^{el} are called the diabatic potential curves (surfaces in the present example) and in many cases of interest these curves cross. This is not in violation of the non-crossing rule since the diabatic electronic wavefunctions λ_i^{d} are not eigenfunctions of H^{el}.

The Hermiticity of the coupling terms in eqs. (25a) and (25b) is practically self-evident. By definition

$$H_{12}^{el}=\langle\chi_1^{d}|H^{el}|\chi_2^{d}\rangle_{el}$$

and

$$H_{21}^{el}=\langle\chi_2^{d}|H^{el}|\chi_1^{d}\rangle_{el}$$

and since H^{el} is Hermitian we have that

$$H_{12}^{el}=H_{21}^{el\,*}\ .$$

Thus, the following matrix elements are equal

$$\langle \psi_1 | H_{12}^{el} | \psi_2 \rangle_N = \langle \psi_2 | H_{21}^{el} | \psi_1 \rangle_N^*$$

and thus, Hermiticity is established.

Another approach to a diabatic representation is to employ the adiabatic representations for those regions of space where the BO coupling terms T_{ij}' and T_{ij}'' are negligible. However, when these coupling terms are not small, i.e., in the vicinity of a pseudocrossing point the representation is changed via a unitary transformation to some diabatic representation (again perhaps one which best satisfies eq. (23)).[31]

In concluding this section we reiterate that the coupled diabatic equations given by eq. (24) are not rigorous since the approximation given by eq. (23) must be introduced in order to obtain the simple form for the coupled equations given by (24). Thus, the description given in this section of the diabatic representation has shown that the adiabatic and diabatic descriptions are not rigorously equivalent, with the adiabatic description being the exact one. In the next section we outline a recent attempt to develop equivalent diabatic and adiabatic formalisms.[38]

4. On the Equivalence of the Adiabatic and Diabatic Representations of Electronically Non-Adiabatic Chemical Reactions

In the previous section the non-uniqueness of the diabatic representation proposed was pointed out. Also, it was shown that in the absence of a justification of eq. (23) the diabatic formalism was not equivalent to the rigorous adiabatic one (outlined in Section 2).

However, recently it has been shown[38] that the two representations can be made equivalent by a procedure which uniquely determines a diabatic representation and in which eq. (23) is essentially satisfied. An outline of this procedure is given below.

Let us consider a compact notation for the coupled equations in an unspecified representation, i.e., adiabatic or diabatic. Let the matrix $\underline{\vec{P}}$ be defined as follows:[38]

$$(\underline{\vec{P}})_{jk} = \langle \chi_j | \vec{p}_N | \chi_k \rangle_{el}, \tag{26}$$

where $\vec{p}_N$ is the nuclear momentum operator and let $\underline{\vec{P}}$ be a generalized momentum matrix operator

$$\underline{\vec{P}} = \underline{\vec{P}} + \underline{I}\,\vec{p}_N \tag{27}$$

where $\underline{I}$ is the identity matrix. The dimensionality of these momentum matrix operators should be large enough to ensure the completeness of the set of functions χ_k. That is, for further manipulation it must be assumed that

$$\sum_k |\chi_k\rangle \langle \chi_k| = \hat{1} \tag{28}$$

where $\hat{1}$ is the identity operator. Finally, a potential matrix $\underline{U}$ is defined, which in our previous notation is given by

$$(\underline{U})_{jk} = \langle \chi_j | H^{el} | \chi_k \rangle_{el}. \tag{29}$$

Then in terms of $\underline{\vec{P}}$ and $\underline{U}$ and the total energy matrix $\underline{I}E$ the coupled equations can be written as

$$[(2M)^{-1}\vec{\underline{P}}\cdot\vec{\underline{P}} + \underline{U} - \underline{I}E]\psi = 0. \tag{30}$$

In view of eq. (27) the preceding equation can be re-written as

$$[\underline{I}\hat{T}_N + (2M)^{-1}(\vec{\underline{P}}\cdot\vec{\underline{P}} + \vec{p}_N\cdot\vec{\underline{P}}) + M^{-1}\vec{\underline{P}}\cdot\vec{p}_N + \underline{U} - \underline{I}E]\psi = 0. \tag{31}$$

ψ in eq. (30) and (31) represents a column vector consisting of the nuclear wavefunctions ψ_k. Equation (31) is the rigorous set of coupled equations that any diabatic or the adiabatic representation of the ψ_k must satisfy. In fact eq. (31) is identical to eq. (22). The matrix $\underline{I}\hat{T}_N$ is simply the diagonal nuclear kinetic energy operator matrix, $(2M)^{-1}\vec{\underline{P}}\cdot\vec{\underline{P}}$ is a diagonal matrix whose elements are given by

$$[(2M)^{-1}\vec{\underline{P}}\cdot\vec{\underline{P}}]_{jk} = \langle\chi_j|\hat{T}_N|\chi_k\rangle_{el}\delta_{jk},$$

and the coupling matrices $(2M)^{-1}\vec{p}_N\cdot\vec{\underline{P}}$ and $M^{-1}\vec{\underline{P}}\cdot\vec{p}_N$ are

$$[(2M)^{-1}\vec{p}_N\cdot\vec{\underline{P}}]_{jk} = \langle\chi_j|\hat{T}_N|\chi_k\rangle_{el} \qquad j \neq k$$
$$= 0 \qquad j = k$$

and

$$[M^{-1}\vec{\underline{P}}\cdot\vec{p}_N]_{jk} = (M)^{-1}\langle\chi_j|\vec{\underline{P}}|\chi_k\rangle_{el}\cdot\vec{p}_N \qquad j \neq k$$
$$= 0 \qquad j = k\ .$$

The form of the coupled equations given by (30) is very useful since it allows for a very transparent adiabatic or diabatic transformation. The requirement that the potential matrix $\underline{U}$ be diagonal for all internuclear distances leads directly and rigorously (as long as eq. (28) is satisfied) to the adiabatic representation. In this case

eq. (30) (or more clearly eq. (31)) becomes identical to eq. (8) of Section 2. If, however, the requirement that the $\underline{\vec{P}}$ matrix operator be diagonal for all internuclear distances is made then the $\underline{U}$ matrix will in general remain non-diagonal and the diabatic representation results from this procedure. Note that this procedure is somewhat less restrictive than eq. (23) which states that $\underline{\vec{P}}$ is identically zero. Thus, the coupling in the diabatic representation is solely through the potential matrix $\underline{U}$.

The above procedure clearly established that the adiabatic and diabatic representations are equivalent rigorous descriptions of electronically non-adiabatic collisions within the framework outlined above. In the following section we shall restrict the discussion to the two-state approximation and explore the relationship between the adiabatic and diabatic representations within this approximation. Specifically, the equivalence of the two methods is examined.

5. The Adiabatic and Diabatic Representations in the Two-State Approximation

For the sake of simplicity and with no loss in generality for our purpose consider a collinear atom-atom electronically non-adiabatic collision. We shall assume that two adiabatic electronic eigenfunctions yield a complete expansion for the electronic coordinates for all internuclear distances. The coupled equations for the adiabatic nuclear wavefunctions are given, according to eqs. (9), (10a), and (10b)

$$\left[-\frac{\hbar^2}{2\mu}\frac{d^2}{dx^2} + E_1(x) + T_{11}''(x) - E\right]\psi_1(x) = -(T_{12}' + T_{12}'')\psi_2(x) \quad (32a)$$

$$\left[-\frac{\hbar^2}{2\mu}\frac{d^2}{dx^2} + E_2(x) + T_{22}''(x) - E\right]\psi_2(x) = -(T_{21}' + T_{21}'')\psi_1(x) \quad (32b)$$

T_{ij}' and T_{ij}'' are the BO coupling terms defined in Section 2, E is the total energy, μ is the reduced mass of the system and x is the internuclear distance. Explicitly in the two-state approximation

$$T_{12}' = -\frac{\hbar^2}{\mu} F_{12}(x)\frac{d}{dx}, \quad (33a)$$

$$T_{21}' = \frac{\hbar^2}{\mu} F_{12}(x)\frac{d}{dx}, \quad (33b)$$

$$T_{12}'' = -\frac{\hbar^2}{2\mu}\frac{d}{dx} F_{12}(x), \quad (33c)$$

$$T_{21}'' = \frac{\hbar^2}{2\mu}\frac{d}{dx} F_{12}(x), \quad (33d)$$

and

$$T_{11}'' = T_{22}'' = \frac{\hbar^2}{2\mu} F_{12}^2(x). \quad (33e)$$

Eqs. (33c), (33d), and (33e) are valid only within the two-state approximation. They are derived in Appendix 1. Substituting eqs. (33a-33e) into eqs. (32a) and (32b) and multiplying the latter two equations by $-2\mu/\hbar^2$ we obtain the following two coupled equations

$$\left[\frac{d^2}{dx^2} - U_1(x) - F_{12}^2 + k^2\right]\psi_1(x) = \left[2F_{12}\frac{d}{dx} + \frac{dF_{12}}{dx}\right]\psi_2, \quad (34a)$$

$$\left[\frac{d^2}{dx^2} - U_2(x) - F_{12}^2 + k^2\right]\psi_2(x) = -\left[2F_{12}\frac{d}{dx} + \frac{dF_{12}}{dx}\right]\psi_1, \quad (34b)$$

where

$$U_i(x) = \frac{2\mu E_i(x)}{\hbar^2}, \quad i = 1,2$$

and

$$k^2 = -\frac{2\mu E}{\hbar^2} \quad .$$

The coupling operators which appear on the right hand sides of eqs. (34a) and (34b) are Hermitian. Their Hermiticity has already been established in Section 2 for a more general example, i.e., one for which eqs. (33c-33e) were not assumed. This Hermiticity can also be proved for this special example by the same methods employed in the general proof given in Section 2. In any event, eqs. (34a) and (34b) are the correct and rigorous (within the two state approximation) adiabatic equations.

Let us now consider the diabatic representation within the two-state approximation. As in the general discussion of Section 3 we assume that the generalized momentum $\vec{\underline{P}}$ is diagonal and in addition for this example it can be shown that a diabatic representation can be found in which $\vec{\underline{P}}$ vanishes for all internuclear distances.[38] Thus, the diabatic coupled equations are

$$\left[-\frac{\hbar^2}{2\mu}\frac{d^2}{dx^2} + H_{11}(x) - E\right]\psi_1^d = -H_{12}(x)\,\psi_2^d(x) \quad , \tag{35a}$$

$$\left[-\frac{\hbar^2}{2\mu}\frac{d^2}{dx^2} + H_{22}(x) - E\right]\psi_2^d = -H_{12}(x)\,\psi_1^d(x) \quad . \tag{35b}$$

According to the equivalence relationship established in Section 4 (for a complete expansion) diagonalization of the matrix

$$\underline{U}^d = \begin{bmatrix} H_{11} & H_{12} \\ H_{12} & H_{22} \end{bmatrix}$$

should yield the adiabatic equations (34a) and (34b). In fact it does; the details of this diagonalization as well as the explicit relationship between the $\underline{U}^d$ matrix and the BO coupling terms of eqs. (34a) and (34b) are given in Appendix 2.

6. Adiabatic and Diabatic Coupling Between Electronic States of Different Spin

In the absence of spin-orbit, spin-spin, etc. coupling the total electron spin of a molecular system is a good quantum number. Since the BO coupling terms contain no spin variables the quantities T_{ij}' and T_{ij}'' vanish identically when χ_i^a and χ_j^a correspond to different (orthonormal) spin-states. If the chemical reaction of interest involves a transition between these two states then the spin-orbit coupling must be introduced. If this coupling is small compared with the other terms in H^{el} then the rigorous quantum calculation may be easier to perform in the diabatic representation in the following sense. Ordinarily, to find the diabatic representation equivalent to the adiabatic one requires a knowledge of the BO coupling terms T_{ij}' and T_{ij}'' and then diagonalization of the $\vec{\underline{P}}$ matrix (according to the results of Sections 4 and 5). However, in the case of a small spin-orbit coupling V^{SO} it should be a good approximation to assume a diabatic representation generated by the χ_i^a which are eigenfunctions of H^{el} without the spin-orbit coupling. The diabatic potential $\underline{U}^d$ for a two-state expansion would have the general form

$$\underline{U}^d = \begin{bmatrix} H_{11} & V_{12}^{SO} \\ V_{12}^{SO} & H_{22} \end{bmatrix}$$

This direct approach might be particularly useful in chemical reactions since BO coupling terms are in general difficult to calculate ab initio as are exact spin-orbit eigenfunctions. Also, in studies of chemical reactions for which no ab initio information is available on the relevant electronic states it may be easier to approximate the coupling in the diabatic representation.

In our calculations described in papers III.2 and III.3 the diabatic representation was chosen for collinear reaction studies involving spin-orbit coupling between a singlet and triplet state. Such an approach has also recently been used in calculations of

$$F(^2P_{\frac{1}{2}}) + H^+ \rightarrow F(^2P_{\frac{3}{2}}) + H^+.$$ [39]

References

1. (a) T. Carrington, Chemiluminescence and Bioluminescence, edited by M. J. Cormier, D. M. Hercules, and J. Lee (Plenum, New York, 1973), Chapter 1; (b) D. R. Herschbach, ibid., Chapter 3.
2. J. R. Kernos and R. Wolfgang, J. Chem. Phys. 52, 5961 (1970).
3. M. G. Holliday, J. T. Muckerman, and L. Friedman, J. Chem. Phys. 54, 1058, 3858 (1971).
4. W. B. Maier, J. Chem. Phys. 57, 2732 (1971).
5. H. Udseth, C. F. Giese, and W. R. Gentry, Phys. Rev. A8, 2483 (1973). This reference is concerned with vibrational excitation in the collision $H^+ + D_2(\nu = 0) \rightarrow H^+ + D_2(\nu')$.
6. J. R. Kernos, R. K. Preston, R. Wolfgang, and J. C. Tully, J. Chem. Phys. 60, 1634 (1974).
7. (a) C. D. Jonah, R. N. Zare, and Ch. Ottinger, J. Chem. Phys. 56, 263 (1973).
8. C. D. Jonah and R. N. Zare, Chem. Phys. Letters 9, 65 (1971).
9. D. R. Yarkony, W. J. Hunt, and H. F. Schaefer, III, Mol. Phys. 26, 941 (1973), discuss an MO explanation of the Ba + Cl_2 results.
10. D. D. Parrish and D. R. Herschbach, J. Amer. Chem. Soc. 94, 6133 (1973).
11. D. A. Dixon, D. D. Parrish, and D. R. Herschbach, Disc. Faraday Soc. 55, 385 (1973).
12. C. F. Carter, M. R. Levy, K. B. Woodall, and R. Grice, Disc. Faraday Soc. 55, 381 (1973).

13. R. K. Preston and J. C. Tully, J. Chem. Phys. 54, 4297 (1971).

14. J. C. Tully and R. K. Preston, J. Chem. Phys. 55, 562 (1971).

15. W. H. Miller and T. F. George, J. Chem. Phys. 56, 5637 (1972).

16. T. F. George and Y.-W. Lin, J. Chem. Phys. 60, 2340 (1974).

17. Y.-W. Lin, T. F. George, and K. Morokuma, Chem. Phys. Lett. 22, 547 (1973).

18. Y.-W. Lin, T. F. George, and K. Morokuma, J. Chem. Phys. 60, 4311 (1974).

19. D. G. Truhlar, J. Chem. Phys. 56, 3189 (1972).

20. J. C. Tully, J. Chem. Phys. 59, 5122

21. E. C. Lim, Ed. Molecular Luminescence (W. A. Benjamin, New York, 1969).

22. M. Born and J. R. Oppenheimer, Ann. Phys. 84, 457 (1927).

23. E. Teller, J. Phys. Chem. 41, 109 (1937).

24. D. R. Bates, H. S. W. Massey, and A. L. Stewart, Proc. Roy. Soc. (London) A216, 437 (1953).

25. L. M. Delves, Nuclear Phys. 20, 275 (1960).

26. J. C. Tully, J. Chem. Phys. 59, 5122 (1973).

27. G. Hunter and H. O. Pritchard, J. Chem. Phys. 40, 2153 (1967).

28. (a) W. Kolos and L. Wolniewicz, J. Chem. Phys. 41, 3674 (1964); (b) G. A. Fisk and B. Kirtman, J. Chem. Phys. 41, 3517 (1964).

29. T. Orlikowski and L. Wolniewicz, Chem. Phys. Lett. 24, 461 (1974).

30. D. R. Bates and A. R. Holt, Proc. Roy. Soc. A292, 168 (1966).

31. D. R. Bates, Atomic and Molecular Processes, edited by

D. R. Bates (Academic, New York, 1962), Section 3.3.

32. E. E. Nikitin, Chemische Elementorprozesse, edited by H. Hartmann (Springer-Verlag, Berlin, 1968), p. 44.

33. H. Nakamura, Mol. Phys. 26, 673 (1973).

34. N. F. Mott and H. S. W. Massey, The Theory of Atomic Collisions (Oxford, London, 1965), p. 370.

35. W. Lichten, Phys. Rev. 131, 229 (1963).

36. W. Lichten, Phys. Rev. B9, A27 (1965); 164, 131 (1967).

37. Reference 34, Chapter XIII.

38. F. T. Smith, Phys. Rev. A179, 111 (1969).

39. F. H. Mies, Phys. Rev. A7, 957 (1973).

40. A. S. Davydov, Quantum Mechanics, (Addison-Wesley) Reading, Mass., 1965), Section 30.

III. 1 EXACT QUANTUM CALCULATIONS OF THE COLLINEAR $H^+ + H_2(X^1\Sigma_g^+) \rightarrow H_2(X^1\Sigma_g^+) + H^+$ REACTION.

III.1 EXACT QUANTUM CALCULATIONS OF THE COLLINEAR $H^+ + H_2(X^1\Sigma_g^+) \rightarrow H_2(X^1\Sigma_g^+) + H^+$ REACTION.

1. Introduction

Considerable effort has been expended on experimental [1-4] and theoretical[5,6] studies of the "simplest" chemical reaction, $H^+ + H_2(X^1\Sigma_g^+) \rightarrow H_2(X^1\Sigma_g^+) + H^+$. This reaction is of interest for a variety of reasons. First, since it is a two electron problem several ab initio potential energy surfaces have been calculated and are available for the collinear configuration.[7-9] These surfaces contain a well in the saddle point region corresponding to the stable H_3^+ molecule. The effect of this well on the reaction should be prominent in the experiments as well as the calculations. Second, the electronically non-adiabatic channel $H_2^+(X^2\Sigma_g^+) + H$ opens for collision energies greater than 1.83 eV relative to the ground state reaction. Future quantum studies will involve the excited state potential surface describing the $H_2^+ + H$ channel and the coupling to the ground state $H^+ + H_2$ channel. In addition the effect of this excited state surface on the ground state scattering when the former surface is energetically closed is of substantial interest. In order to assess this effect requires a calculation of the scattering on the ground state potential surface with and without the coupling to the virtual excited potential surface.

In the present study we have calculated the reactive and non-reactive transition probabilities for the ground state reaction $H^+ + H_2(\nu) \rightarrow H_2(\nu') + H^+$ over a range of initial translational energies

of 0.0 to 0.8 eV for one study and 0.0 to 1.2 eV for another one. The reactive transition probabilities are denoted by $P^R_{\nu\nu'}$. The potential surface used in some of our calculations is the semi-empirical DIM one of Preston and Tully.[10] This surface is depicted as a function of the two internuclear distances in Figure 1. The R_1 and R_2 saddle point is located at internuclear distance $R_1 = R_2 = 1.53$ bohr and the energy at this point is -3.391 eV. This very deep well supports thirteen symmetric stretch vibrational states. This potential surface was modified in a second study by adding to it a gaussian function of the form

$$D \exp\{-[\alpha(R_1 - R_0)^2 + (R_1 - R_0)^2]\} \quad .$$

The values chosen for D, α, and R_0 were respectively 2.391 eV, 0.5 bohr^{-2}, and 1.53 bohr. The resulting potential surface is depicted in Figure 2. A comparison of these potential surfaces is made for the line $R_1 = R_2$ and along the reaction coordinate s in Figures 3 and 4 respectively. A small barrier of around 0.12 eV is seen in the entrance and exit channels for the modified potential surface.

Exact quantum calculations were performed using the modified and unmodified potential surfaces. The close-coupling method of Kuppermann was used[6] and 20 to 25 expansions functions were required to obtain unitarity of the scattering matrix to better than 2% and symmetry to better than 5%.

The reaction probability P^R_{00} is displayed in Figure 5 as a function of the initial kinetic energy E_0 for the modified H_3^+ surface.

Several features are of interest. First, the effect of the 0.12 eV barrier in the entrance channel is undoubtedly responsible for the low energy threshold behavior. Second, the presence of two sharp resonances in the reaction probability at E_0 of 0.236 eV and 0.406 eV is striking. Since these resonances occur well below the threshold for excitation of vibrationally excited products, we speculate that these resonances are shape resonances[11] associated to the well in the potential surface. Finally, we note that P^R_{00} reaction probability is always greater than 0.8 in the energy range studied. This means of course that very little product is formed in a vibrationally excited state. This result may be of some interest for the coupled $H^+ + H_2$ reaction. Based on a trajectory surface hopping model Preston and Tully[6,10] concluded that vibrational excitation of the ground state products H_2 would be necessary to surface hop with a non-negligible probability. Our results indicate that H_2 is formed vibrationally unexcited. Since a relatively large cross section is found for the HD^+ product[1] it might be that the quantum mechanism for this non-adiabatic transition does not require vibrational excitation of the ground state products.

Results for the unmodified DIM H_3^+ surface are shown in Figure 6. There it can be seen that the P^R_{00} transition probability undergoes many resonances, only some of which are well-resolved. In all 153 energies were run in the range $0 < E_0 < 0.82$ eV. The threshold for this reaction is extremely steep. At the lowest translational energies considered, $E_0 = 0.004$ eV, the reaction probability is 0.921. A reasonably accurate characterization of the energy

dependence of reaction probability P_{00}^{R} would be to say that it exhibits resonant behavior superimposed on a background of unit probability. The behavior of the reaction probability is statistical[13,14] as a result of the many resonances. At higher translational energies, i.e., E_0 greater than 0.6 eV, the reaction probability P_{00}^{R} remains large in qualitative agreement with the results found for the modified H_3^+ surface.

The energy range around 0.05 eV has been expanded in Figure 7 where it can be seen that P_{00}^{R} exhibits very sharply resonant behavior. Here we may be seeing the effect of several overlapping resonances.

References

1. J. R. Krenos and R. Wolfgang, J. Chem. Phys. 52, 5961 (1970).
2. M. G. Holliday, J. T. Muckermann, and L. Friedman, J. Chem. Phys. 54, 1058, 3853 (1971).
3. W. B. Maier, J. Chem. Phys. 54, 2732 (1971).
4. J. R. Krenos, R. K. Preston, R. Wolfgang, and J. C. Tully, J. Chem. Phys. 60, 1634 (1974).

The experimental studies reported in references 1-4 involve the reaction $H^+ + D_2 \rightarrow HD + D^+$.

5. I. G. Csizmadia, J. C. Polanyi, A. C. Roach, and W. H. Wong, Can. J. Chem. 47, 4097 (1969).
6. J. C. Tully and R. K. Preston, J. Chem. Phys. 55, 562 (1971).
7. M. E. Schwartz and L. J. Schaad, J. Chem. Phys. 47, 5325 (1967).
8. H. Conroy, J. Chem. Phys. 51, 3979 (1969).
9. I. G. Csizmadia, R. E. Karl, J. C. Polanyi, A. C. Roach, and M. A. Robb, J. Chem. Phys. 52, 6205 (1970).
10. R. K. Preston and J. C. Tully, J. Chem. Phys. 54, 4297 (1971).
11. R. G. Newton, Scattering Theory of Waves and Particles (McGraw-Hill, New York, 1966), pp. 313-317.
13. B. C. Eu and J. Ross, J. Chem. Phys. 44, 2467 (1966).
14. W. H. Miller, J. Chem. Phys. 52, 543 (1970).

Figure Captions

Figure 1: Equipotential contours of the ground state H_3^+ DIM potential energy surface for the collinear configuration. R_1 and R_2 are the nearest neighbor internuclear distances.

Figure 2: Equipotential contours for the modified ground state H_3^+ potential energy surface for the collinear configuration.

Figure 3: Comparison of the modified ($\alpha = 0.5$ bohr^{-2}) and unmodified ($\alpha=0$) H_3^+ potential surfaces along the cut $R_1 = R_2$.

Figure 4: Comparison of the modified ($\alpha=0.5$ bohr^{-2}) and unmodified ($\alpha = 0$) H_3^+ potential surfaces along the (same) minimum energy path.

Figure 5: Reaction probability P_{00}^R as a function of initial relative translational energy E_0 for the modified H_3^+ potential surface. T_1 and T_2 indicate the values of E_0 for which the $\nu' = 1$ and $\nu' = 2$ vibrational levels of H_2 become energetically accessible.

Figure 6: Reaction probability P_{00}^R as a function of initial translational energy E_0 for the unmodified H_3^+ potential surface. T_1 is defined in Figure caption 5.

Figure 7: Reaction probability P_{oo}^{R} for the unmodified H_3^+ potential surface in the vicinity of $E_o = 0.04$ eV.

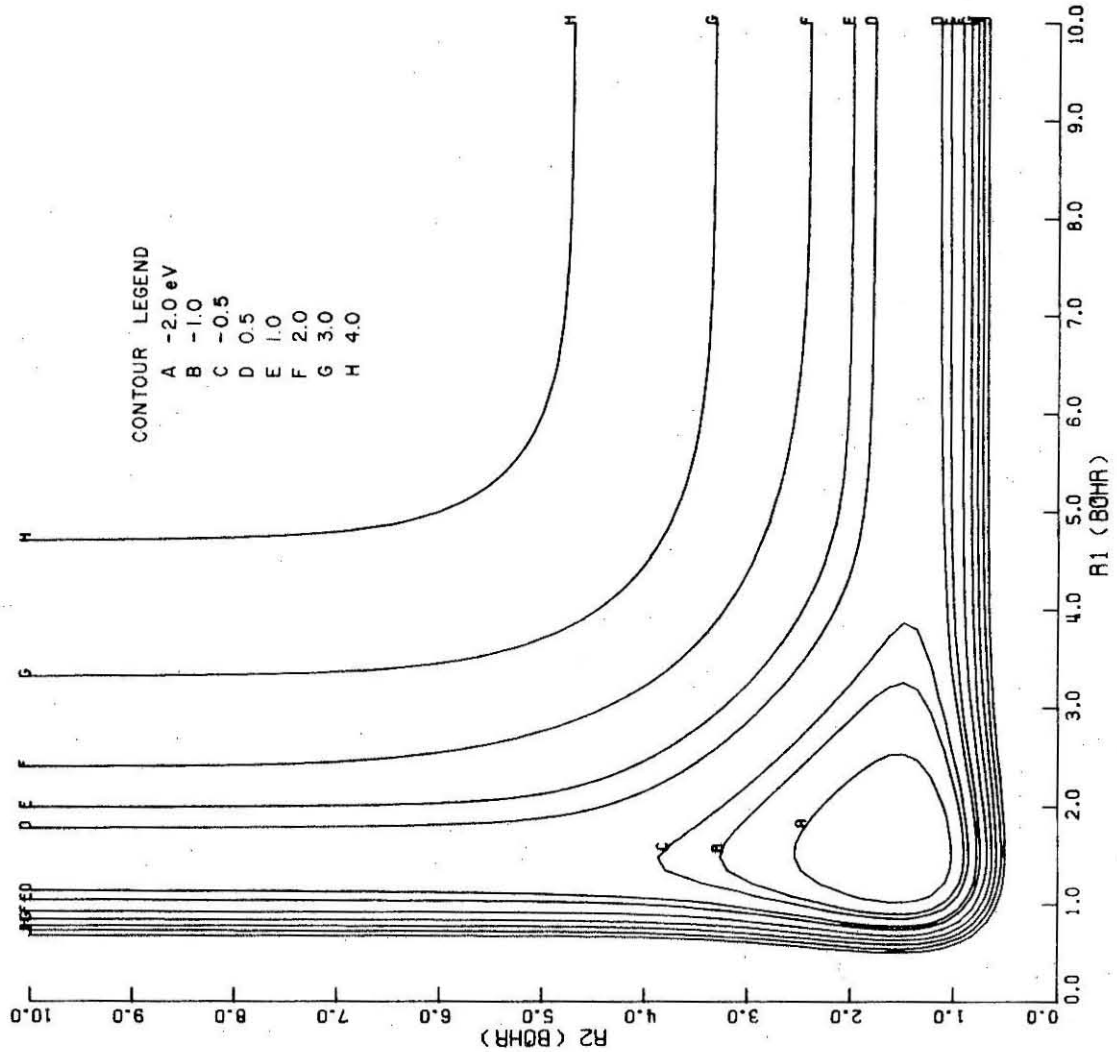
CONTOUR LEGEND
A -2.0 eV
B -1.0
C -0.5
D 0.5
E 1.0
F 2.0
G 3.0
H 4.0
R1 (BOHR)
R2 (BOHR)
0.0
1.0
2.0
3.0
4.0
5.0
6.0
7.0
8.0
9.0
10.0

Figure 1

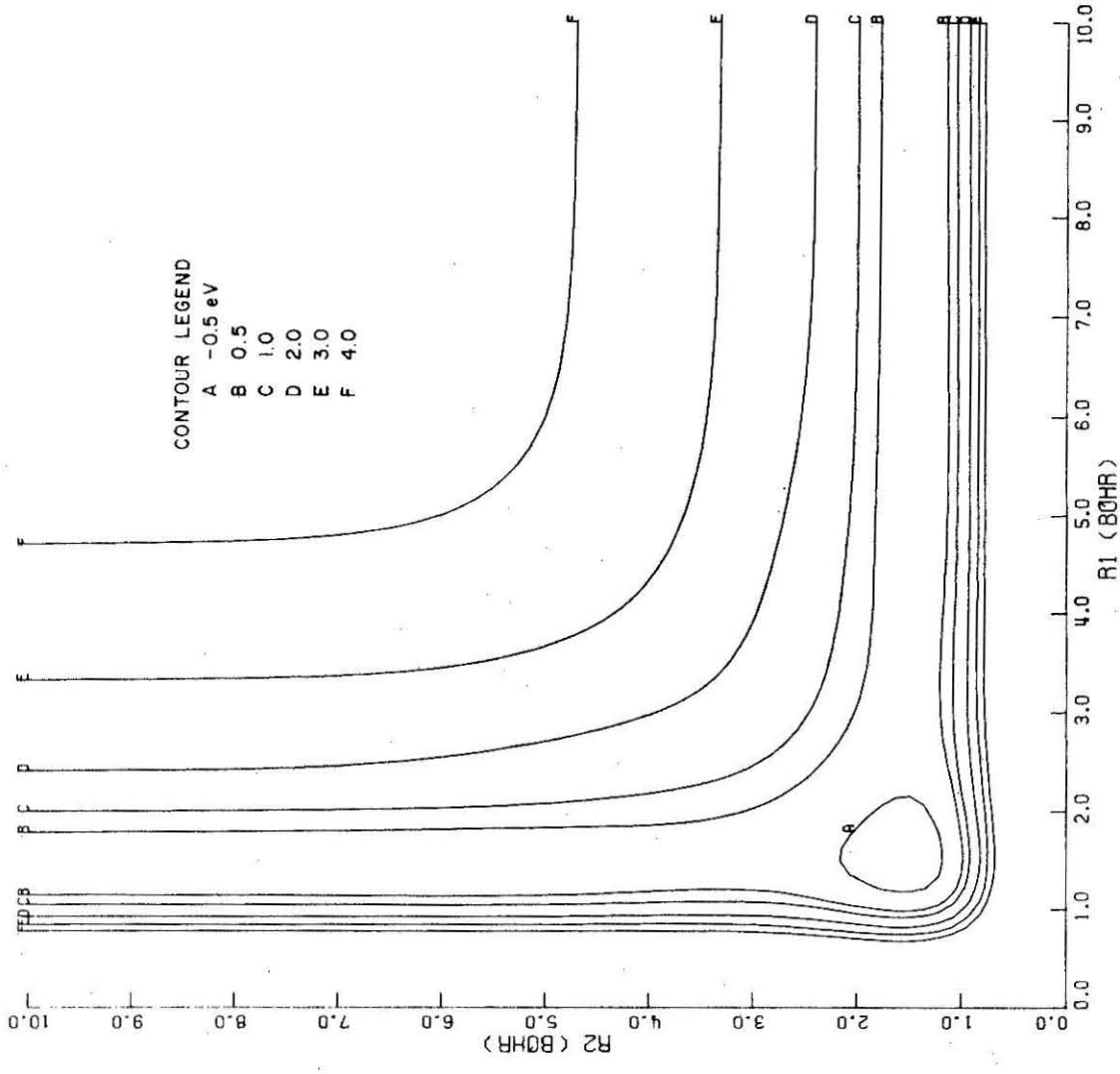
CONTOUR LEGEND
A -0.5 eV
B 0.5
C 1.0
D 2.0
E 3.0
F 4.0
R1 (BOHR)
R2 (BOHR)
0.0
1.0
2.0
3.0
4.0
5.0
6.0
7.0
8.0
9.0
10.0

Figure 2

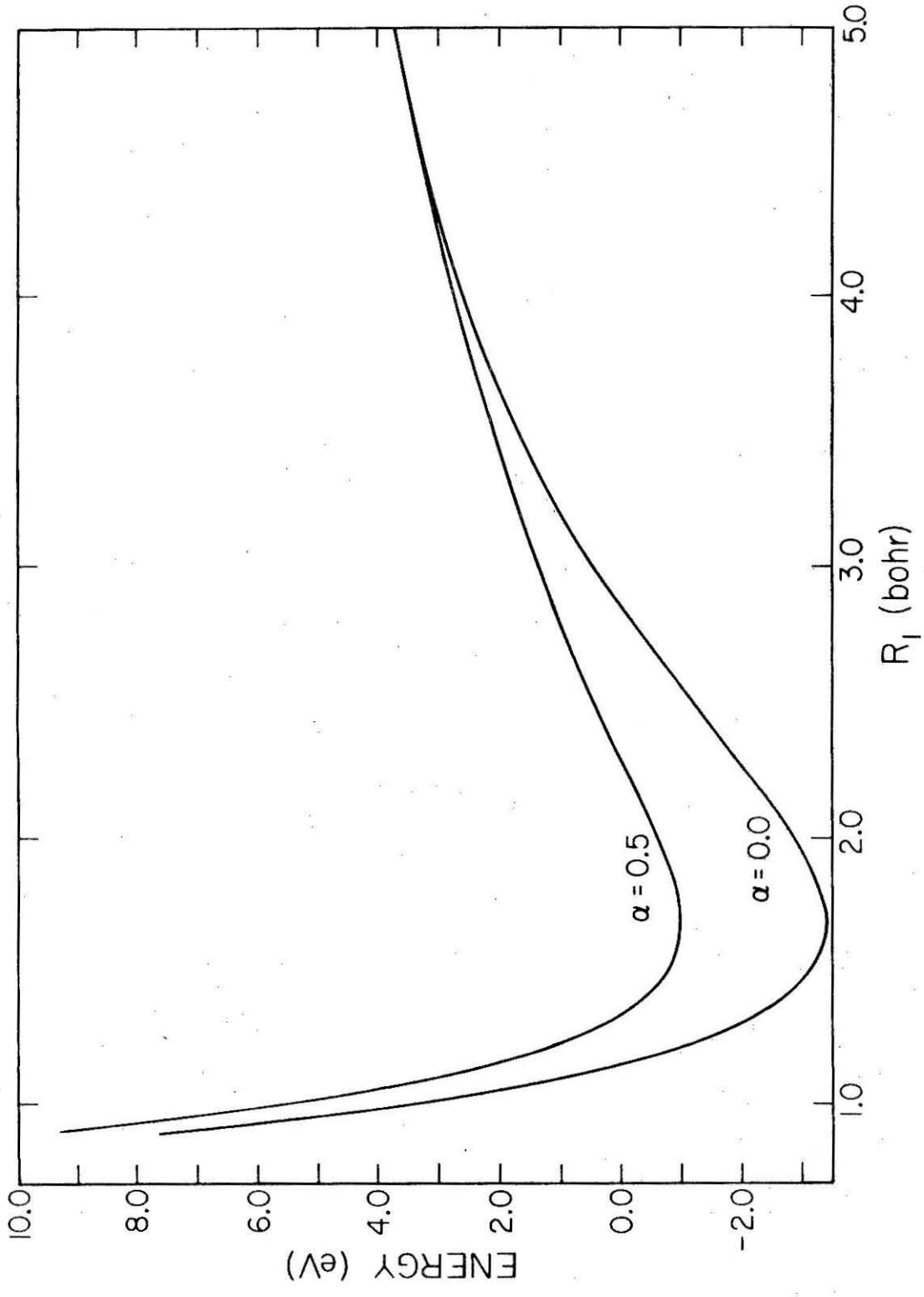

Figure 3

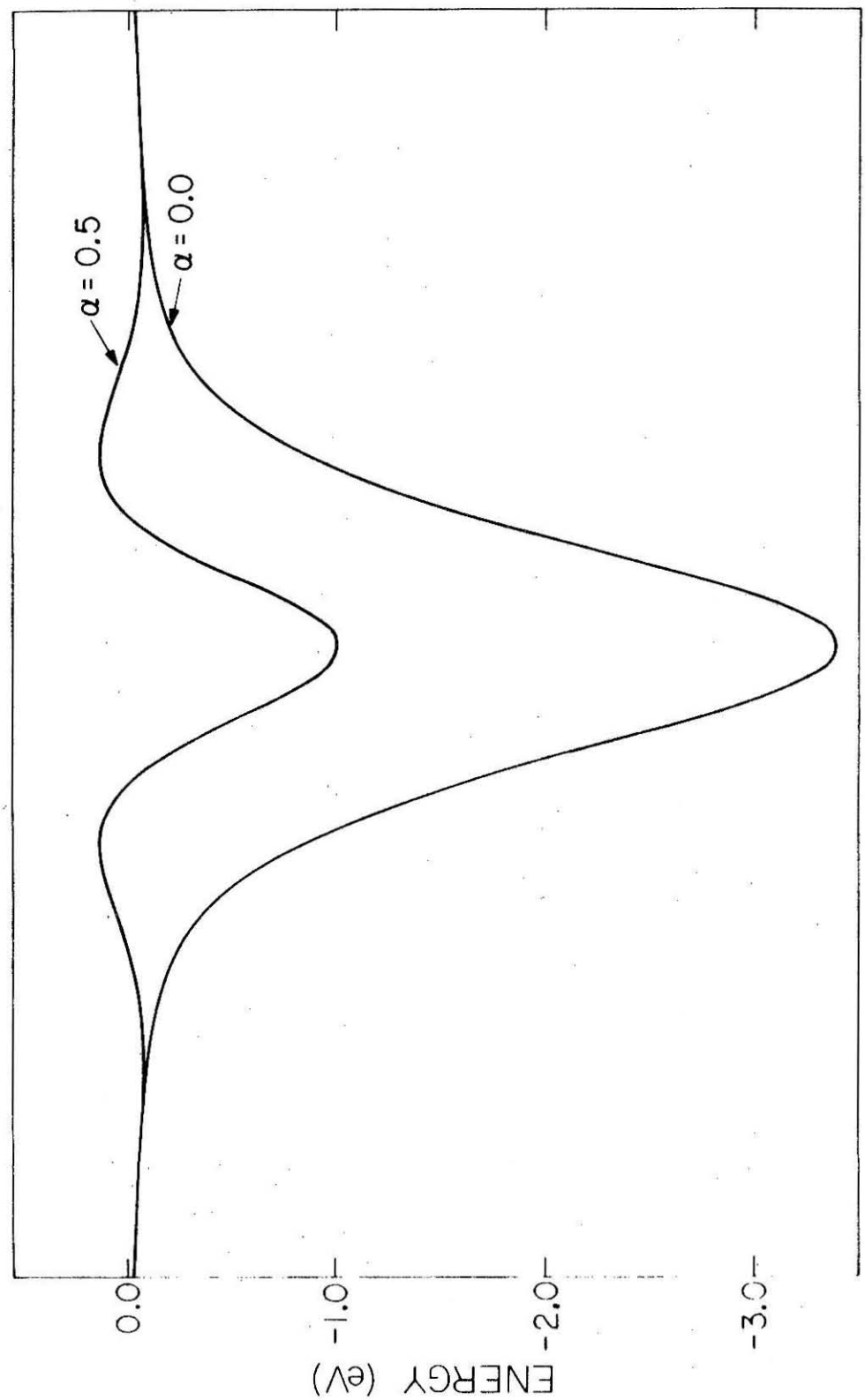
α = 0.5
α = 0.0
0.0
-1.0
-2.0
-3.0
ENERGY (eV)
DISTANCE ALONG MINIMUM ENERGY PATH

Figure 4

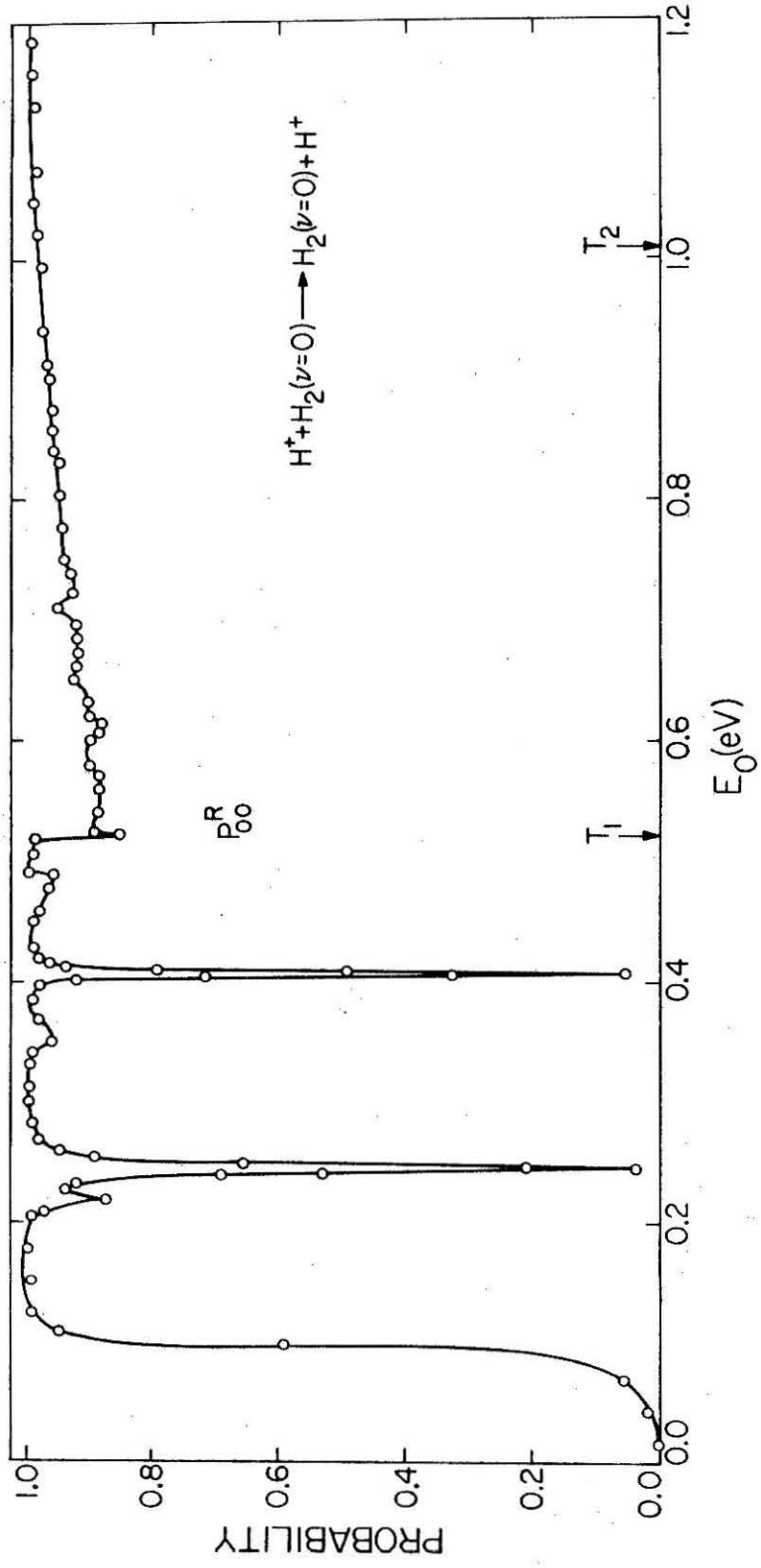
PROBABILITY
1.0
0.8
0.6
0.4
0.2
0.0
0.0
0.2
0.4
0.6
0.8
1.0
1.2
E_0(eV)
T_1
T_2
P_{00}^R
$H^+ + H_2(v=0) \longrightarrow H_2(v=0) + H^+$

Figure 5

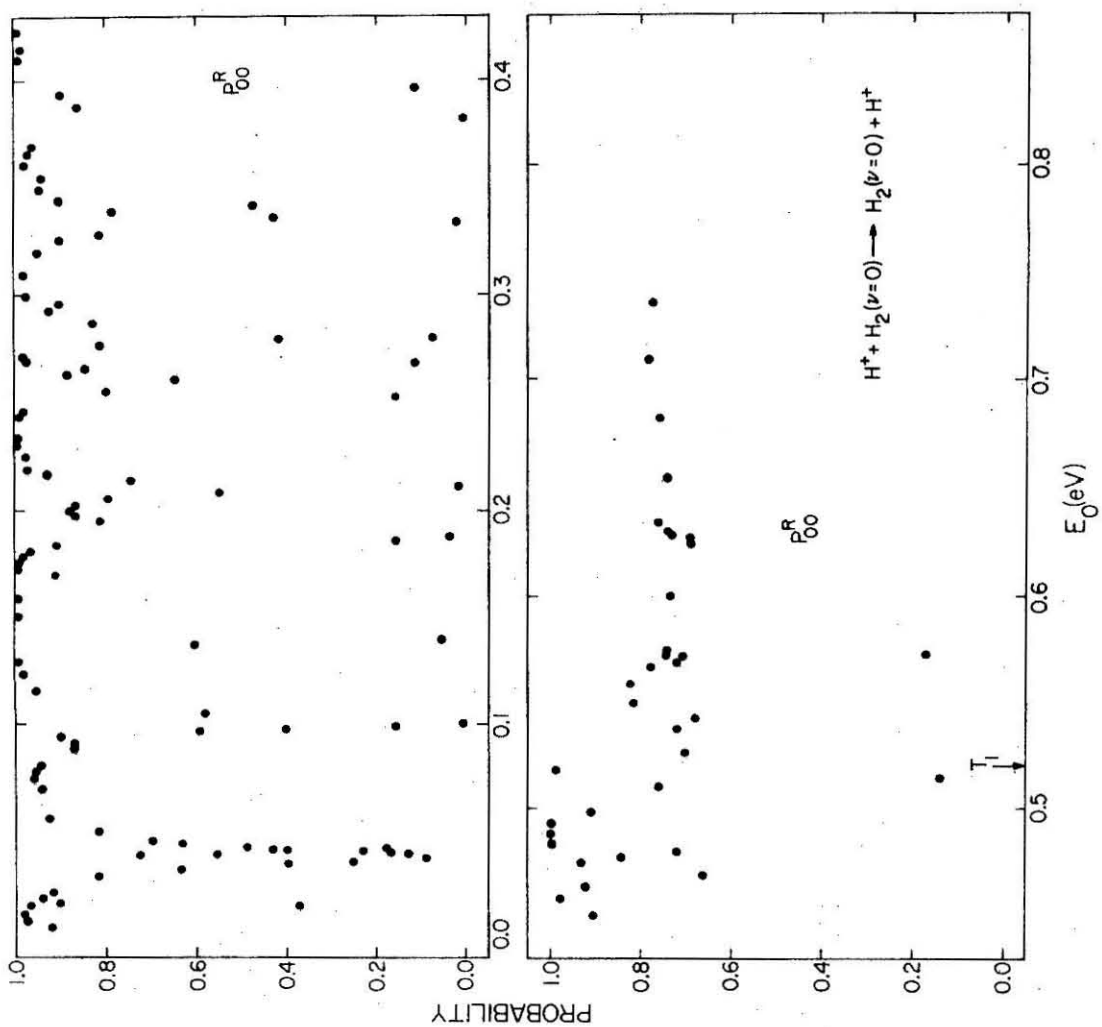

Figure 6

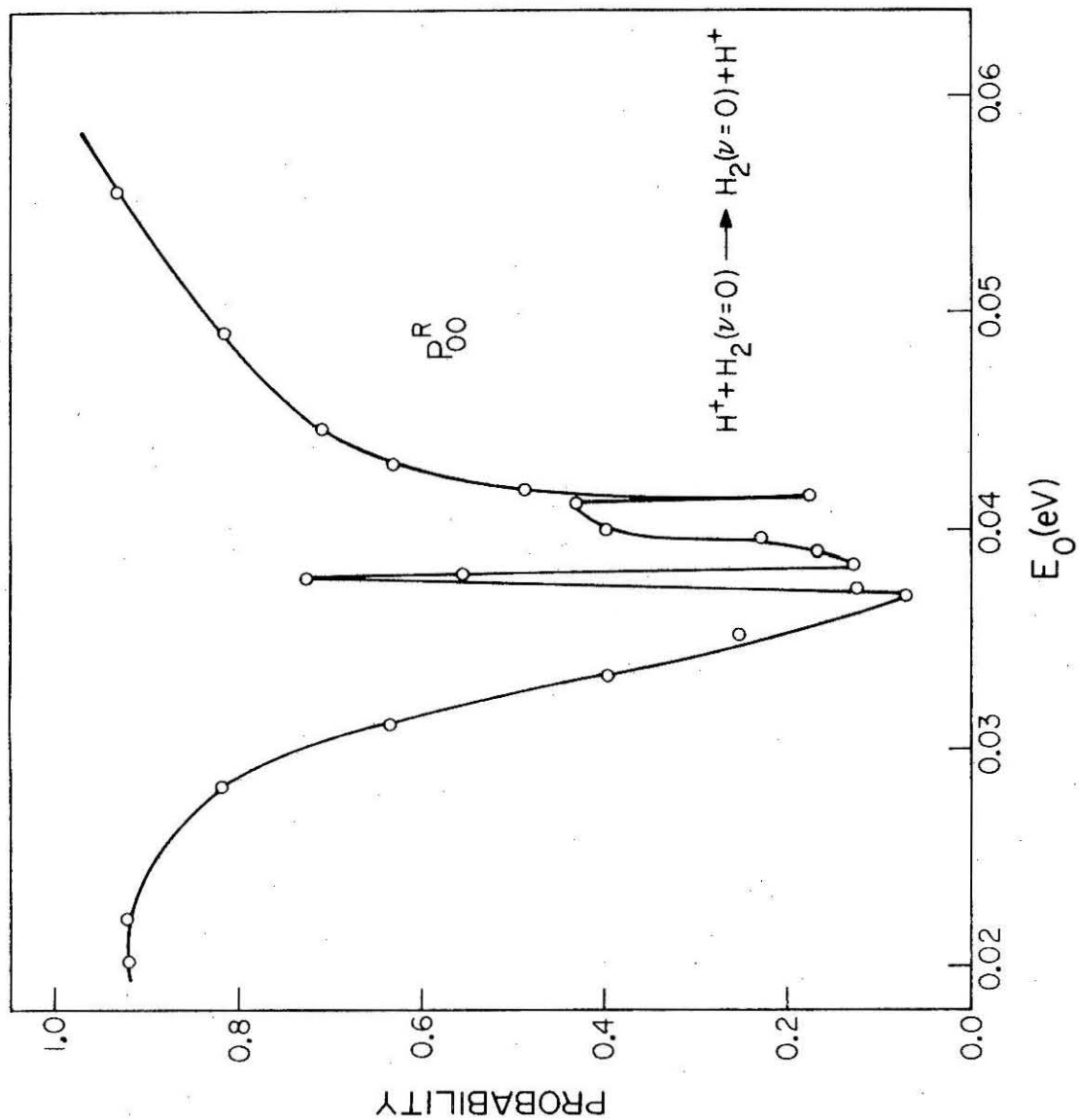
PROBABILITY
1.0
0.8
0.6
0.4
0.2
0.0
0.02
0.03
0.04
0.05
0.06
E_0(eV)
P_{00}^R
$H^+ + H_2(\nu=0) \longrightarrow H_2(\nu=0) + H^+$

Figure 7

III. 2 MODEL CALCULATIONS OF ELECTRONICALLY NON-ADIABATIC $H + H_2 \rightarrow H_2 + H$, $H_2^* + H_2$ REACTIONS.

III.2 MODEL CALCULATIONS OF ELECTRONICALLY NON-ADIABATIC $H + H_2 \rightarrow H_2 + H,\ H_2^* + H$ REACTIONS.

1. Introduction

The subject of electronically non-adiabatic (ENA) chemical reactions is very new and not well understood. There have been several trajectory surface hopping calculations on the reaction $H^+ + D_2 \rightarrow HD + D^+,\ HD^+ + D$ [1] as well as an attempt to perform difficult collinear semi-classical calculations on this system.[2] No quantum calculations of a chemical reaction involving more than one potential energy surface has been reported. The need for such calculations is becoming obvious in view of current experimental interest in ENA chemical reactions.[3]

In this paper we present some results of an exact quantum study of a model $H + H_2$ ENA chemical reaction. A diabatic representation[4] is employed and the coupling between the two intersecting potential surfaces is affected by a fictitious spin-orbit coupling surface. We examine the effect of the location and strength of the coupling surface on the various branching probabilities. These probabilities are defined as follows. ${}^1P^R_{\nu\nu'}$, is the probability for the reaction $H + H_2(\nu) \rightarrow H_2(\nu') + H$ and ${}^{1,2}P^R_{\nu\nu}$, is the probability for the ENA reaction $H + H_2(\nu) \rightarrow H_2^*(\nu') + H$ where H_2^* denotes the electronically excited H_2.

2. Theory and Calculations

In terms of the two mass-weighted Delves coordinates[5] x_1 and x_2 the two coupled Schrödinger equations describing the ENA reaction

are[6]

$$\left[-\frac{\hbar^2}{2\mu}\left(\frac{\partial^2}{\partial x_1^2}+\frac{\partial^2}{\partial x_2^2}\right)+V_1(x_1,x_2)-E\right]\psi_1(x_1,x_2)=-V_{12}^{SO}(x_1,x_2)\,\psi_2(x_1,x_2)$$

$$\left[-\frac{\hbar^2}{2\mu}\left(\frac{\partial^2}{\partial x_1^2}+\frac{\partial^2}{\partial x_2^2}\right)+V_2(x_1,x_2)-E\right]\psi_2(x_1,x_2)=-V_{12}^{SO}(x_1,x_2)\,\psi_1(x_1,x_2)\ ,$$

where V_1 and V_2 are respectively the ground and excited electronic potential energy surfaces, V_{12}^{SO} is the spin-orbit coupling surface, and E is the total energy. The equations are solved by an extension of the close-coupling method of Kuppermann[7,8] and the details are given elsewhere. The total number of expansion functions used in the close-coupling solution for ψ_1 and ψ_2 was 20 to 24. This number of functions was required to obtain unitarity of the S-matrix to better than 1% and symmetry to 5%. The model H + H_2 system was chosen in part because this number of expansion functions did not require an exorbitant amount of computer time. The first step in which potential matrix elements are generated and stored on disc required approximately 27 minutes of IBM 370/158 CPU time and thereafter in step 2 approximately 5 minutes of CPU time was required per energy. The initial translational energy range considered is $0.0 < E_0 < 1.0$ eV.

3. Potential Energy Surfaces

The potential energy surface V_1 is a Wall-Porter[9] fit to the scaled SSMK H_3 surface[10] and is described in detail elsewhere.[11] V_2 is in shape identical to V_1 with constant displacements of 0.2 bohr in the internuclear distances variables R_1 and R_2. Also, V_2 is displaced from V_1 in energy by 0.3 eV. The purpose of these displace-

ments is to produce two potential surfaces which intersect. Equipotential contours of these two surfaces are plotted in Figure 1 and 2. $H_3(x)$ denotes the ground state surface V_1 and $H_3(a)$ denotes the excited state surface V_2. The curve which crosses an equipotential line is the "seam" of intersection along which the two potential surfaces cross. From general theoretical considerations it is expected that spin-orbit coupling potential will be localized somewhat near this crossing seam.

The mathematical form of the coupling surface V_{12}^{SO} we have used is given by

$$V_{12}^{SO} = \begin{cases} \gamma \operatorname{sech}[\beta(R_{20} - R_2)] \exp[-\alpha(R_{10} - R_1)^2], & R_2 > R_{20} \\ 0, & R_2 < R_{20}, \end{cases}$$

$$\alpha = 8.0 \text{ bohr}^{-2}$$

$$\beta = 1.1 \text{ bohr}^{-1}$$

$$\gamma = 0.05 \text{ eV}$$

$$R_{10} = 1.704 \text{ bohr}.$$

In Figures 3 and 4 we present equipotential contour plots of V_{12}^{SO} for $R_{20} = 3.2$ bohr and $R_{20} = 2.2$ bohr respectively. As seen from these figures V_{12}^{SO} is localized near the crossing seam but in a limited region of configuration space. This choice for V_{12}^{SO} was made to mimic the form of a realistic coupling surface for chemical reactions which do have strongly interacting potential surfaces, e.g., $F + H_2 \rightarrow FH + H$, and $Ba + N_2O \rightarrow BaO + N_2$. The parameter R_{20} was given two values in order that the effect on ${}^{1,2}P_{\nu\nu'}^{R}$, of the location of the coupling

surface relative to the strong interaction region could be assessed.

Finally in Figure 5 we present a plot of the potential surfaces along a cut of constant R_1 showing the intersection of the ground and excited H_2 internal potential curves in the asymptotic region of space.

4. Results and Discussion

The zero-point energy of the ground and excited H_2 molecule is 0.2728 eV and 0.5728 eV respectively. Thus, relative to the energy of the ground state reagents the excited state channel is endothermic by 0.3 eV. Unless otherwise stated, the results presented below are for the coupling surface localized in the product exit channel.

In Figure 6 the total reaction probabilities ${}^{1,2}P_0^R$ and ${}^{1}P_0^R$ are plotted as a function of the total energy E and the initial translational energy E_0 for the coupling surface shown in Figure 3. It can be seen that ${}^{1,2}P_0^R$ rises rapidly from its energetic threshold denoted by the inner arrow labeled 0. The inner arrow labeled 1 denotes the energetic threshold for formation of product $H_2^*(\nu' = 1)$ and the outer arrows labeled 1 and 2 indicate the energetic thresholds for the formation of product $H_2(\nu' = 1)$ and $H_2(\nu' = 2)$ respectively. In addition it is seen that the magnitude of the ${}^{1,2}P_0^R$ transition probability is roughly one order of magnitude lower than the electronically adiabatic probability ${}^{1}P_0^R$.

In Figure 7 we present the total reaction probabilities ${}^{1,2}P_0^R$ and ${}^{1}P_0^R$ as a function of E and E_0 for the coupling surface shown in Figure 4. Here the ${}^{1,2}P_0^R$ reaction probability exhibits a striking

threshold delay. This is in sharp contrast to the results seen in Figure 6. Also in comparing these two figures we note that the value of ${}^{1,2}P_0^R$ in Figure 7 is on the average twice the value of ${}^{1,2}P_0^R$ in Figure 6. The differences in threshold behavior in the two ${}^{1,2}P_0^R$ results may be explained by a semi-classical, time-dependent mechanism for ENA transitions. The reagents $H + H_2$ approach on the ground electronic surface and begin to react, i.e., $R_1 \simeq R_2$. Suddenly the effect of the coupling potential is felt. Let us suppose that this effect is merely to cause a certain fraction of the reagents to "jump" from the ground state surface to the excited one. After this jump occurs the products exit on the excited surface. For the coupling given in Figure 3 it can be guessed that this jump occurs for R_2 greater than 3.2 bohr and less than say 4.0 bohr. An examination of Figure 2 reveals that the value of the potential function for the above region of configuration space is less 0.7 eV (in fact it is between 0.4 eV and 0.5 eV). This means that for this coupling the system jumps to a classically allowed region of configuration space at and above the energetic threshold of 0.573 eV. The results for the coupling surface given in Figure 4 show that this is obviously not the case. The energy in the region of the jump for that coupling is greater than or equal to 0.7 eV as seen from Figure 2. This energy does exceed the energetic threshold and hence the system must tunnel through a classically forbidden region of space to reach the $H_2^*(\nu' = 0)$ product channel. This is in accord with results of Figure 7.

Another interesting feature of these model two-state calcula-

tions which can be explained by the above semi-classical, time-dependent mechanism is seen in Figure 8. There two ENA transition probabilities ${}^{1,2}P^{R}_{00}$ and ${}^{1,2}P^{R}_{10}$ are plotted as a function of E and E_0. Here, the coupling surface (the one depicted in Figure 3) is located in the reagent arrangement channel. In particular we note that the ${}^{1,2}P^{R}_{00}$ curve has a delayed threshold. This can be accounted for by an explanation similar to the one given previously for the delayed threshold of the ${}^{1,2}P^{R}_{00}$ curve of Figure 8. Namely, the reagents jump to the excited surface, propagate in a classically allowed region of space until the system nears the saddle point region of the upper surface. There the energy is around 0.7 eV and the system must tunnel in order to form $H_2^*(\nu' = 0)$ product.

The transition probability ${}^{1,2}P^{R}_{10}$ exhibits a rapid rise from its energetic threshold. This is easily understood since the total energy available to the $H + H_2$ reagent at the threshold, 0.795 eV, permits the system to propagate in classically allowed regions of space on the upper surface to form $H_2^*(\nu = 0)$ product. As before we note that the reaction probabilities are never greater than 0.05.

In order to investigate the factors which influence the magnitude of the ENA transition probability we calculated ${}^{1,2}P^{R}_{00}$ for the coupling surface shown in Figure 3 as a function of the coupling strength γ at E = 0.898 eV. The results are shown in Figure 9. There it can be seen that as the value of γ is increased from 0.005 eV to 0.05 eV, ${}^{1,2}P^{R}_{00}$ increases by two orders of magnitude and that when γ increases from 0.05 eV to 0.15 eV, ${}^{1,2}P^{R}_{00}$ increases by almost one order of magnitude. This nearly quadratic dependence on γ indicates

the strong sensitivity of the magnitude of the ENA transition probability on the coupling strength. We speculate, based on these and other similar calculations on a very different system, that the relevant parameter with which γ correlates is the vibrational energy level spacing in the molecule. That is, in order for an ENA transition probability to be large, i.e., the same order of magnitude as an electronically adiabatic one , γ must be of the same order of magnitude as the vibrational energy level spacing of the molecule. For H_2 (and H_2^* of course) this energy spacing is 0.52 eV.

5. Summary and Conclusions

We have calculated electronically adiabatic and non-adiabatic reaction probabilities for a model fictitious $H + H_2 \rightarrow H_2 + H$, $H_2^* + H$ two state reaction. The location and strength of a fictitious spin-orbit coupling surface was varied to determine the effect on the magnitude and energy dependence of several reaction probabilities.

It was found that the threshold behavior of certain transition probabilities could be understood on the basis of a simple semi-classical, time-dependent picture of the electronically non-adiabatic process. Also, based on some limited calculations, it was speculated that the coupling strength has to be of the same order of magnitude as the vibrational energy level spacing of the product (or reagent) molecule in order for the electronically non-adiabatic transition probabilities to be of the same order of magnitude as the electronically adiabatic transition probabilities.

References

1. (a) J. C. Tully and R. K. Preston, J. Chem. Phys. 55, 562 (1971); (b) J. R. Krenos, R. K. Preston, R. Wolfgang, and J. C. Tully, J. Chem. Phys. 60, 1634 (1974).
2. (a) W. H. Miller and T. F. George, J. Chem. Phys. 56, 5637 (1972); (b) T. F. George and Y.-W. Lin, J. Chem. Phys. 60, 2340 (1974); (c) Y.-W. Lin, T. F. George, and K. Morokuma, Chem. Phys. Lett. 22, 547 (1973); (d) Y.-W. Lin, T. F. George, and K. Morokuma, J. Chem. Phys. 60, 4311 (1974).
3. Chemiluminescence and Bioluminescence edited by M. J. Cormier, D. M. Hercules, and J. Lee (Plenum, New York, 1973).
4. F. T. Smith, Phys. Rev. A179, 111 (1969).
5. L. M. Delves, Nuclear Phys. 20, 275 (1960).
6. J. M. Bowman, Ph.D. Thesis (California Institute of Technology, Pasadena, California, 1974).
7. A. Kuppermann, Electronic and Atomic Collisions, VIIth International Conference on the Physics of Electronic and Atomic Collisions, Abstract of Papers (North-Holland, Amsterdam, 1971), p. 3.
8. (a) G. C. Schatz, J. M. Bowman, and A. Kuppermann, J. Chem. Phys. 58, 4023 (1973); (b) G. C. Schatz and A. Kuppermann, J. Chem. Phys. 59, 964 (1973); (c) J. M. Bowman, G. C. Schatz, and A. Kuppermann, Chem. Phys. Lett. 24, 378 (1974).
9. F. T. Wall and R. N. Porter, J. Chem. Phys. 36, 3256 (1962).
10. I. Shavitt, R. M. Stevens, F. L. Minn, and M. Karplus, J. Chem. Phys. 48, 2700 (1968).
11. D. G. Truhlar and A. Kuppermann, J. Chem. Phys. 56, 2232 (1972).

Figure Captions

Figure 1: Equipotential contour plot of the collinear H_3 ground state potential energy surface as a function of the two internuclear distances R_1 and R_2. The curve which crosses the 0.7 eV contours is the seam of intersection of this surface with the excited state H_3 potential surface.

Figure 2: Equipotential contour plot of the collinear H_3 fictitious triplet excited state potential energy surface as a function of the two internuclear distances R_1 and R_2.

Figure 3: Equipotential contour plot of a model spin-orbit coupling potential as a function of R_1 and R_2.

Figure 4: Equipotential contour plot of a model spin-orbit coupling potential as a function of R_1 and R_2.

Figure 5: Ground and excited state H_2 potential curves as a function of the internuclear distance R.

Figure 6: Electronically adiabatic and non-adiabatic total reaction probabilities ${}^1P_0^R$ and ${}^{1',2}P_0^R$ as a function of the total energy E and the initial translational energy E_0. Calculations were done with the coupling surface shown in Figure 3 and located in the product exit channel.

Figure 7: Electronically adiabatic and non-adiabatic total reaction probabilities ${}^{1}P_{0}^{R}$ and ${}^{1',2}P_{0}^{R}$ as a function of E and E_0 for the coupling surface shown in Figure 4. This surface is located in the product exit channel.

Figure 8: Electronically non-adiabatic transition probabilities ${}^{1',2}P_{00}^{R}$ and ${}^{1',2}P_{10}^{R}$ as a function of E and E_0. Calculations were done with the coupling surface shown in Figure 3 and located in the reagent entrance channel.

Figure 9: Dependence of the electronically non-adiabatic transition probability ${}^{1',2}P_{00}^{R}$ on the coupling strength γ for $E = 0.898$ eV.

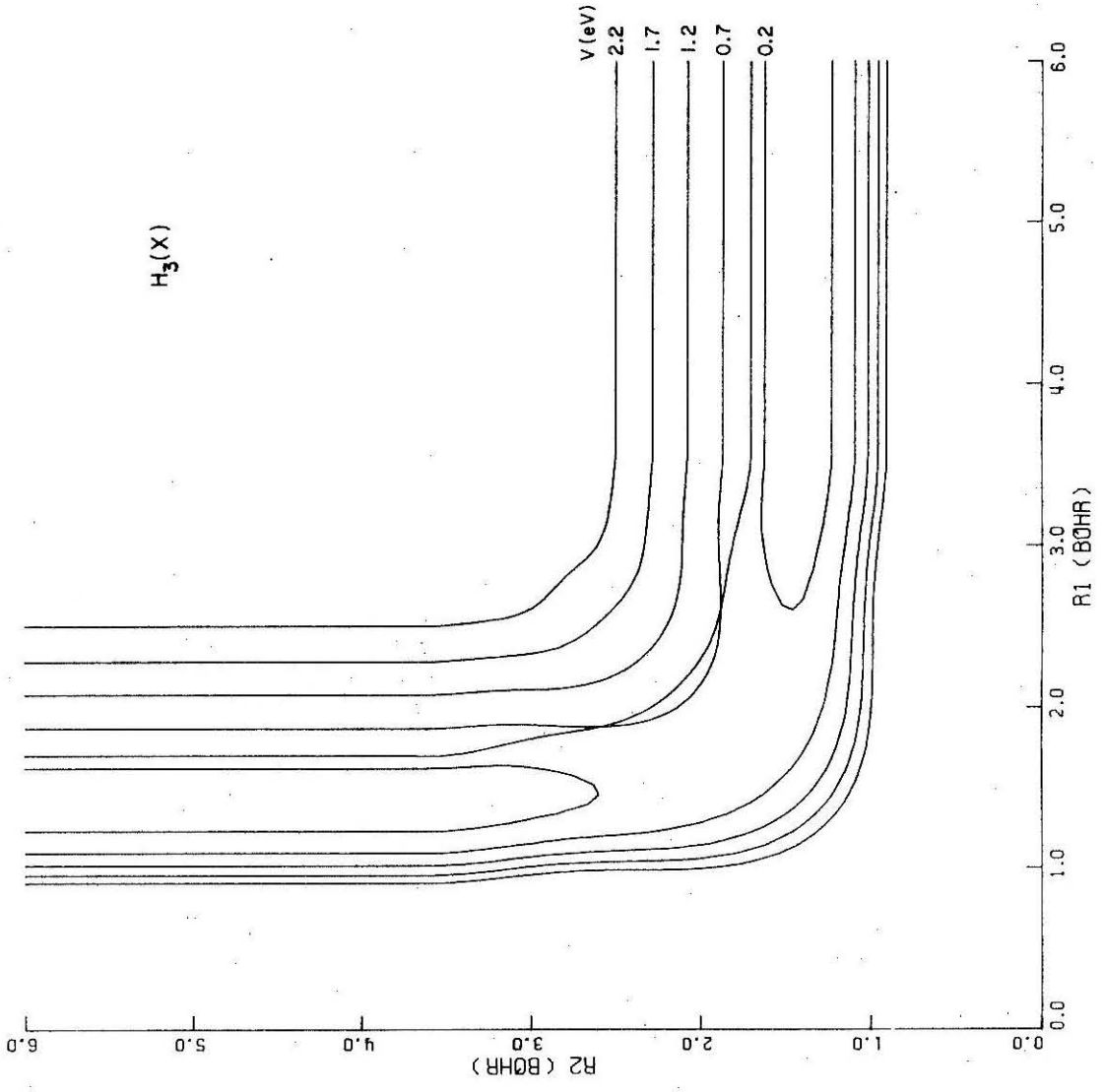

Figure 1

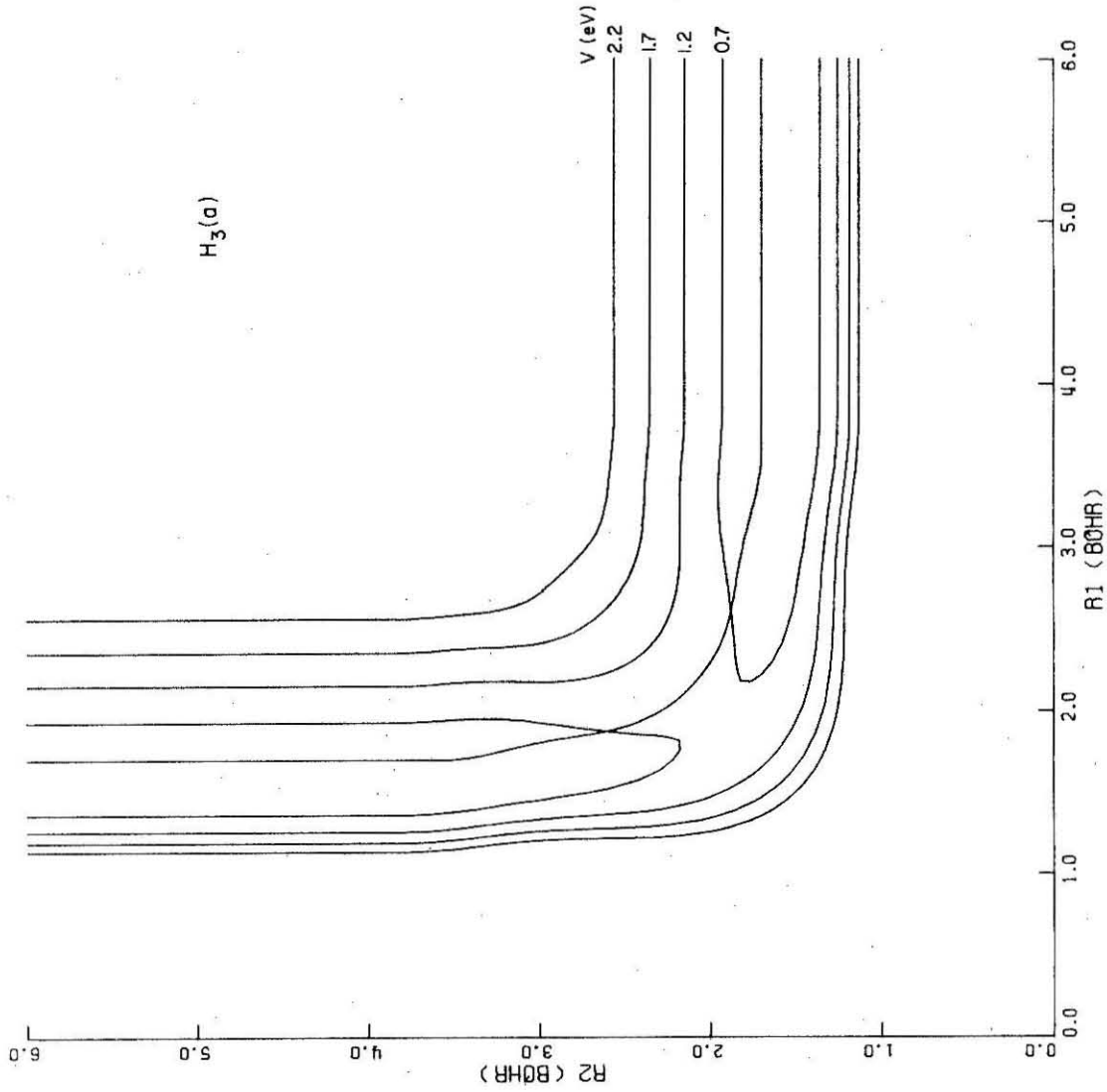
V (eV)
2.2
1.7
1.2
0.7
$H_3(a)$
0.0
1.0
2.0
3.0
4.0
5.0
6.0
R1 (BOHR)
0.0
1.0
2.0
3.0
4.0
5.0
6.0
R2 (BOHR)

Figure 2

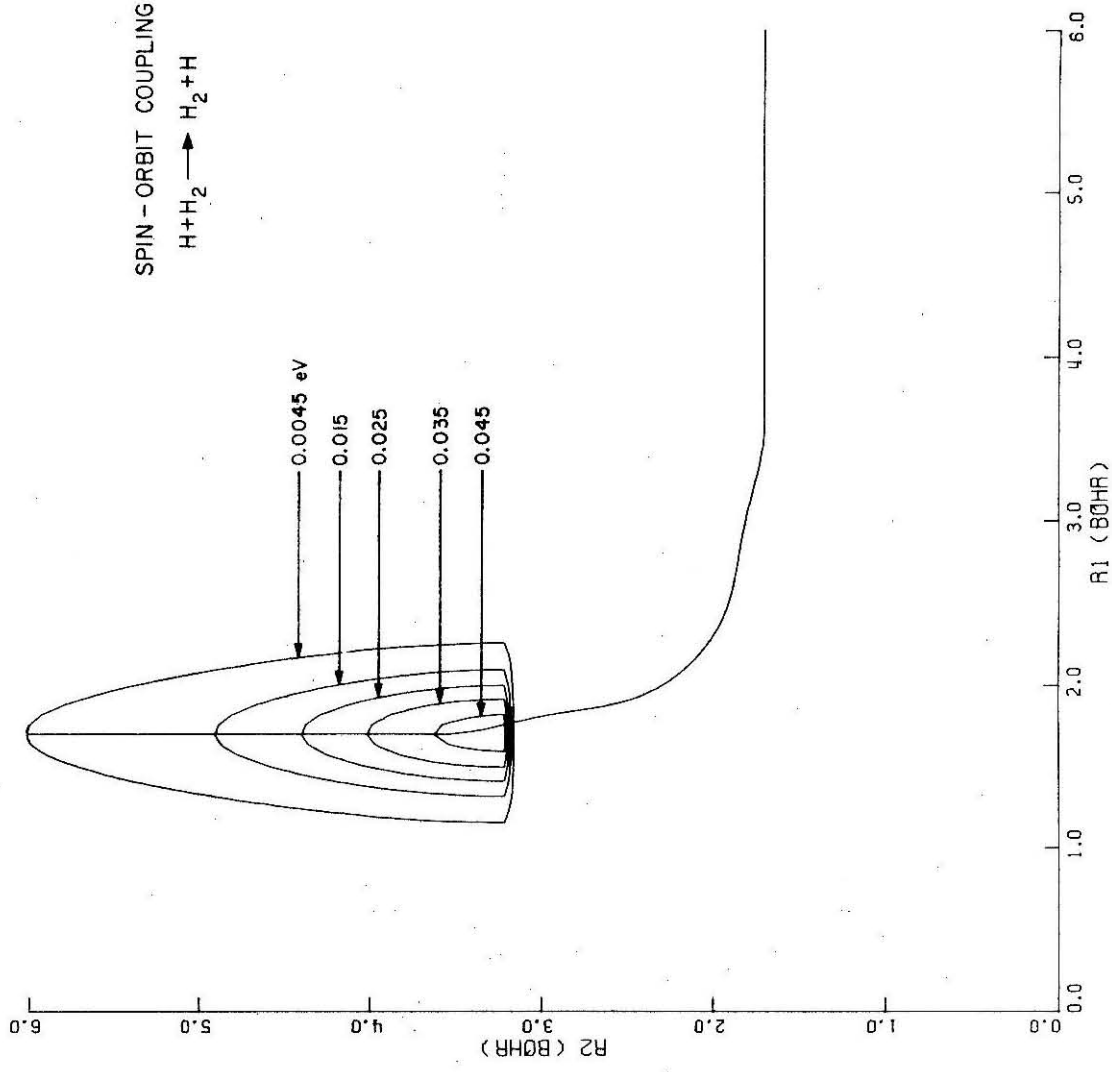
SPIN – ORBIT COUPLING
H+H2 ⟶ H2+H
0.0045 eV
0.015
0.025
0.035
0.045
R1 (BØHR)
R2 (BØHR)
0.0
1.0
2.0
3.0
4.0
5.0
6.0

Figure 3

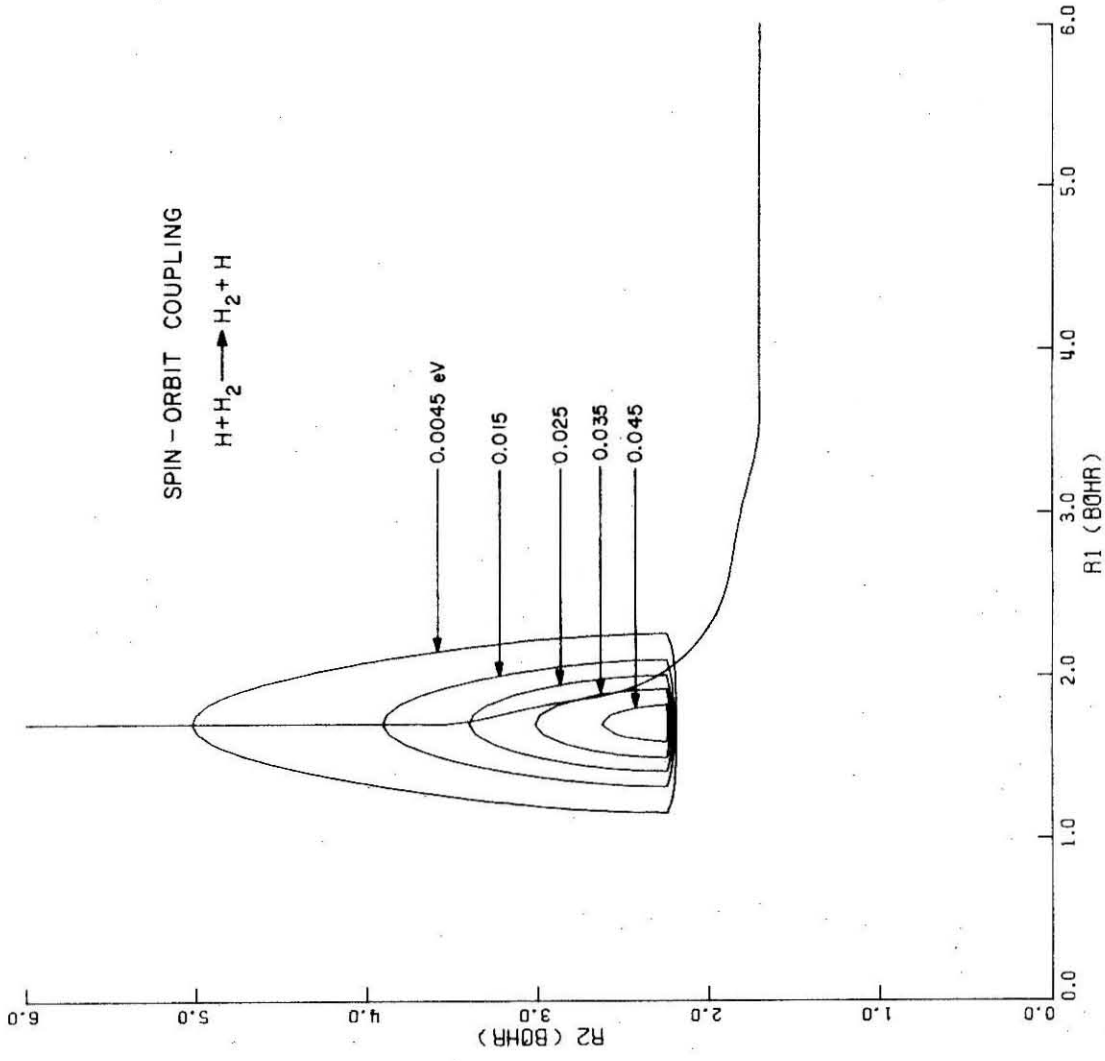
SPIN – ORBIT COUPLING
H+H2 ⟶ H2+H
0.0045 eV
0.015
0.025
0.035
0.045
R1 (BOHR)
R2 (BOHR)
0.0
1.0
2.0
3.0
4.0
5.0
6.0

Figure 4

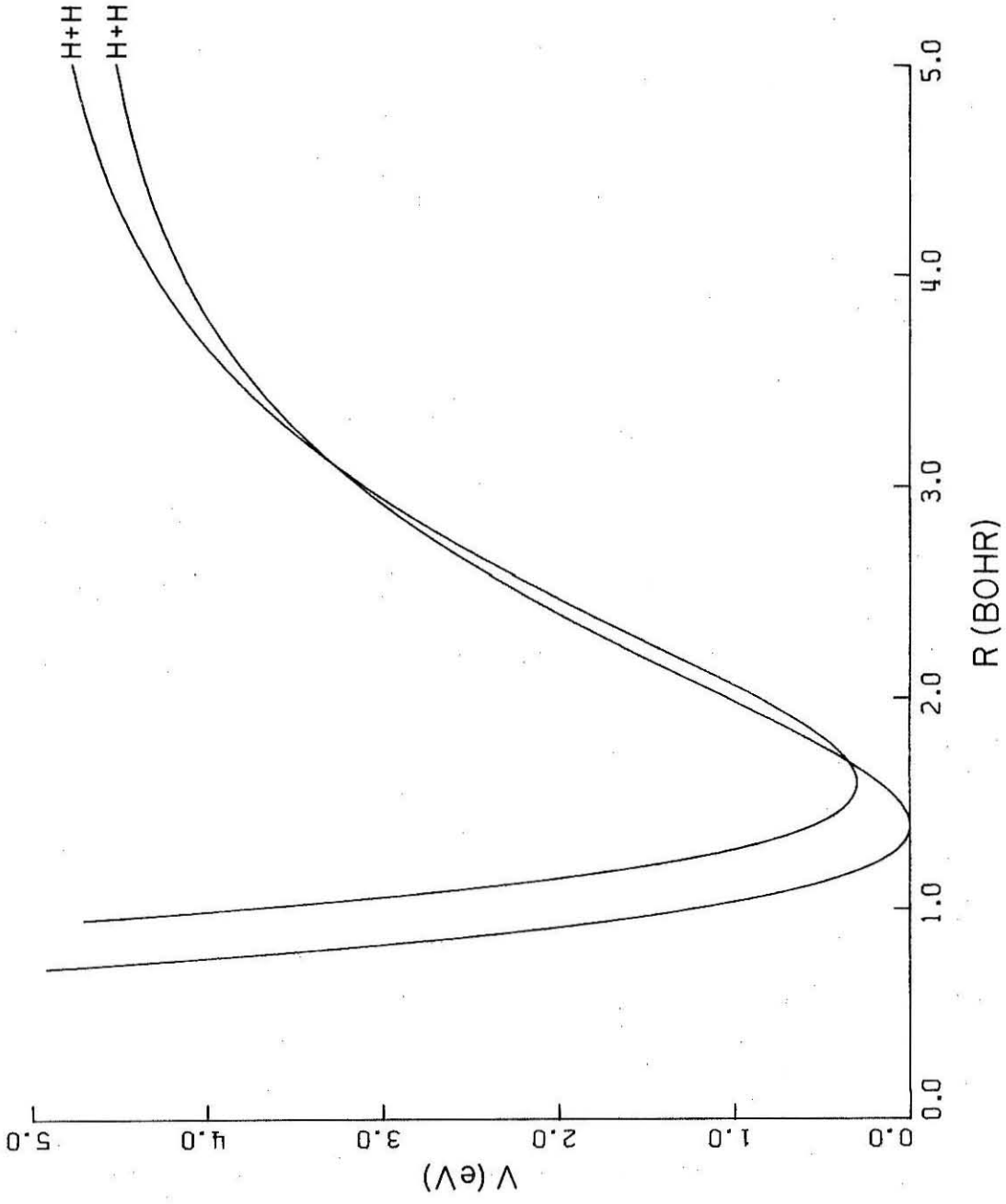

Figure 5

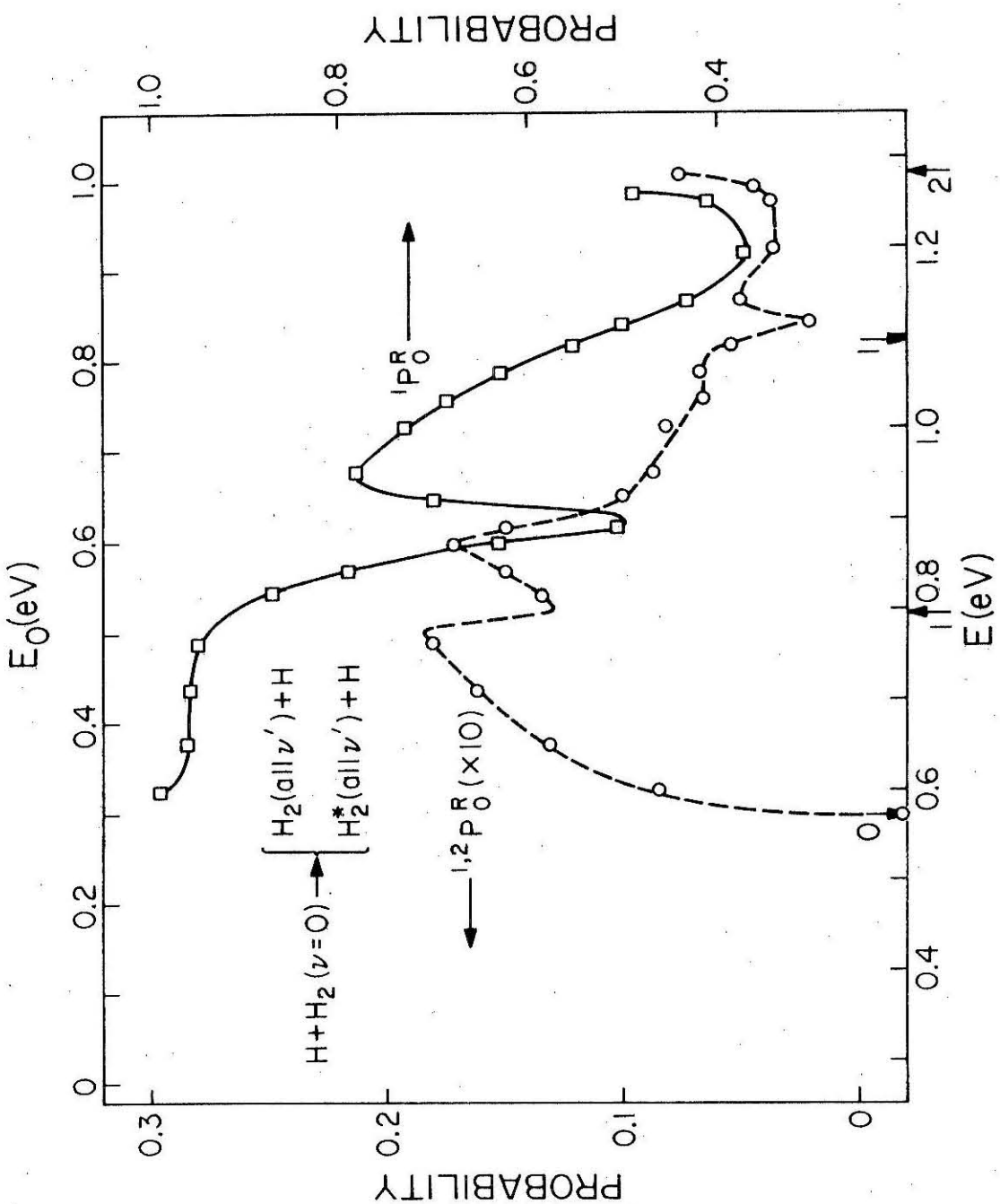
PROBABILITY
1.0
0.8
0.6
0.4
E_0(eV)
0
0.2
0.4
0.6
0.8
1.0
$^1P_0^R$
$H_2(all\ v')+H$
$H_2^*(all\ v')+H$
$H+H_2(v=0)$
$^{1,2}P_0^R(\times 10)$
0.3
0.2
0.1
0
PROBABILITY
E(eV)
1.2
2
1
0.8
0.6
0.4

Figure 6

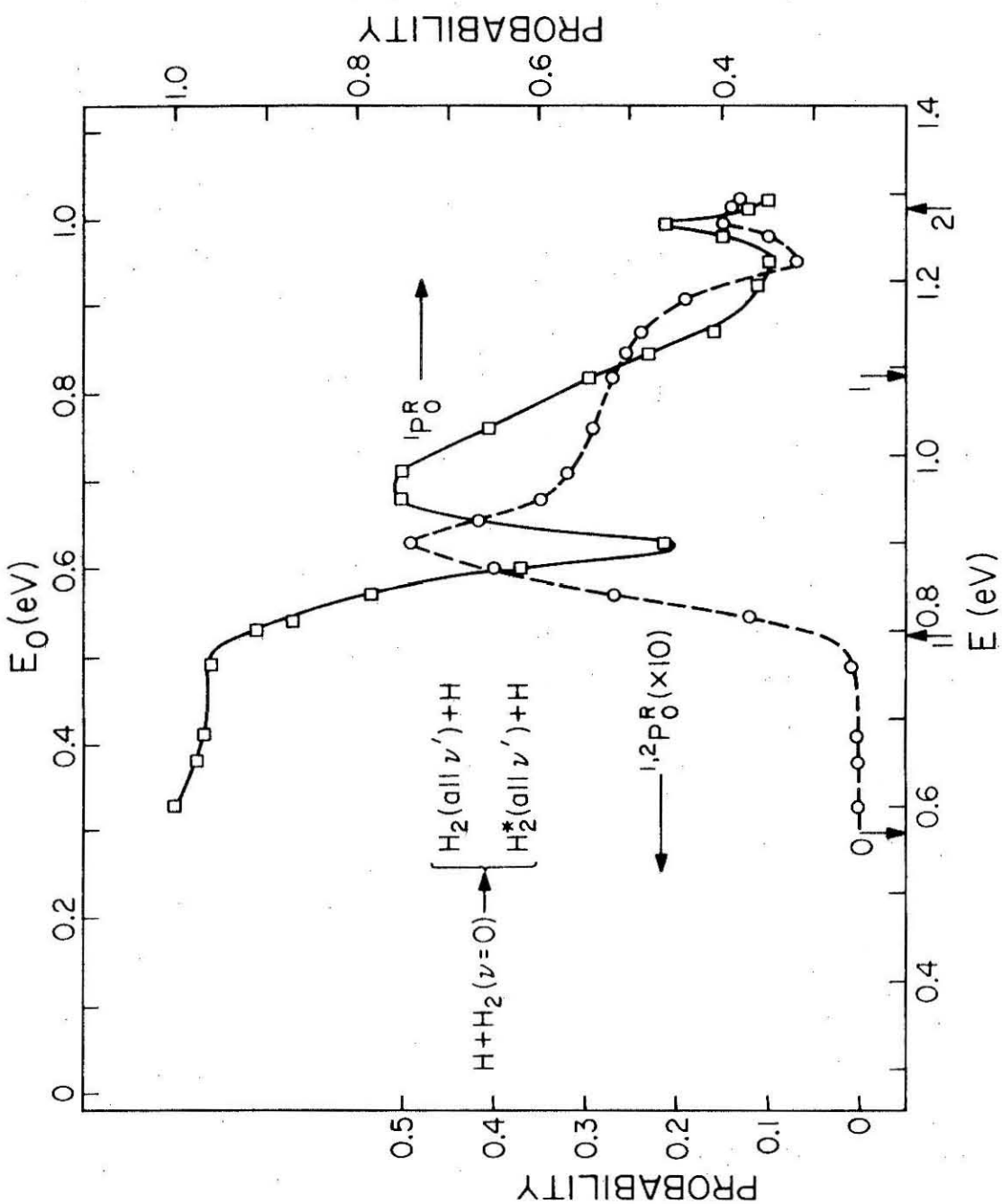
PROBABILITY
1.0
0.8
0.6
0.4
E_0(eV)
0
0.2
0.4
0.6
0.8
1.0
$^1P_0^R$
$^{1,2}P_0^R$(×10)
H_2(all ν')+H
H_2^*(all ν')+H
H+H_2(ν=0)
PROBABILITY
0.5
0.4
0.3
0.2
0.1
0
E (eV)
0.4
0.6
0.8
1.0
1.2
1.4
1
2

Figure 7

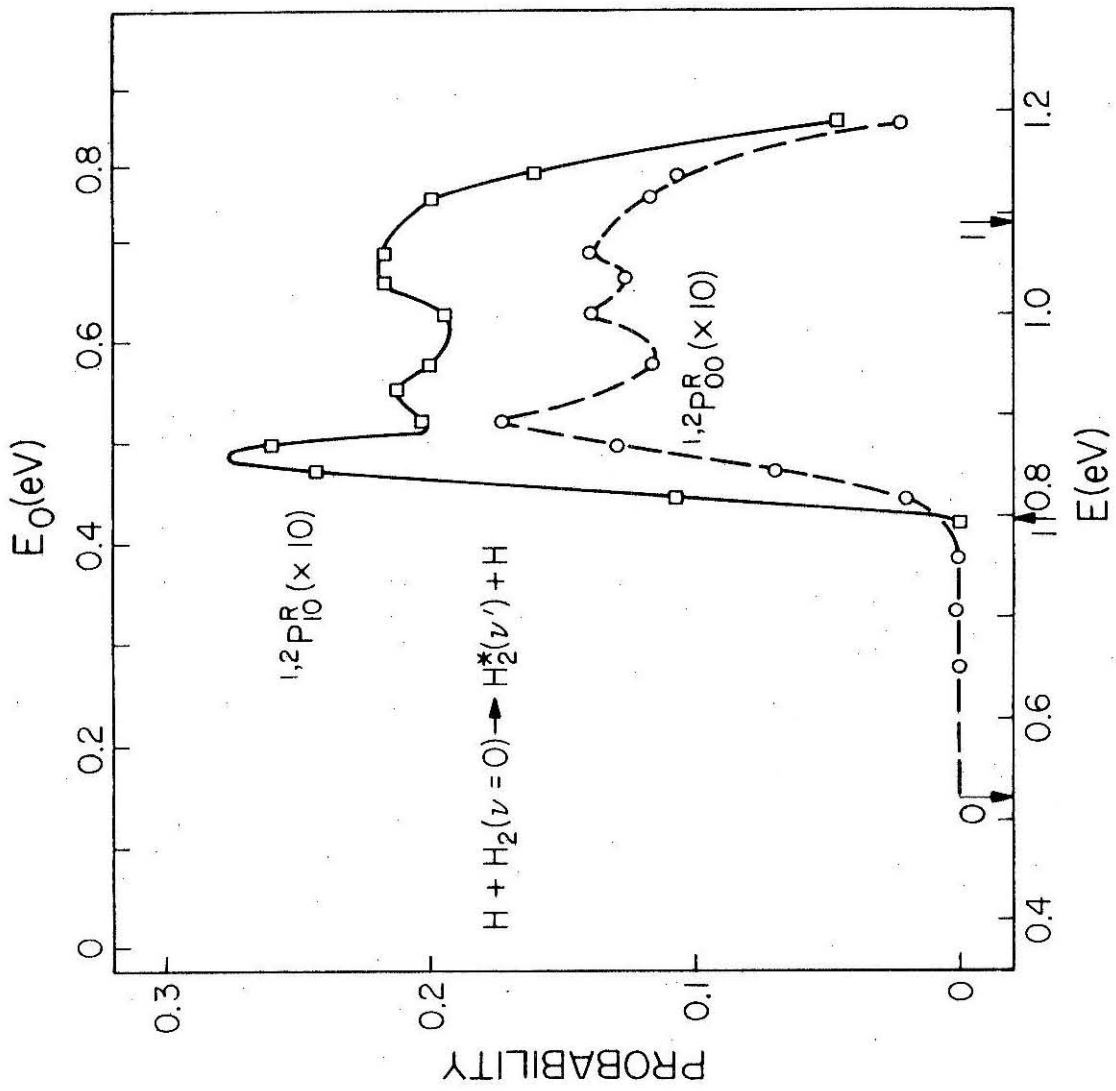
E_0(eV)
0
0.2
0.4
0.6
0.8
$^{1,2}P^R_{10}$(x 10)
H + H_2(v = 0) → H_2^*(v') + H
$^{1,2}P^R_{00}$(x 10)
0
0.1
0.2
0.3
PROBABILITY
0.4
0.6
0.8
1.0
1.2
E(eV)

Figure 8

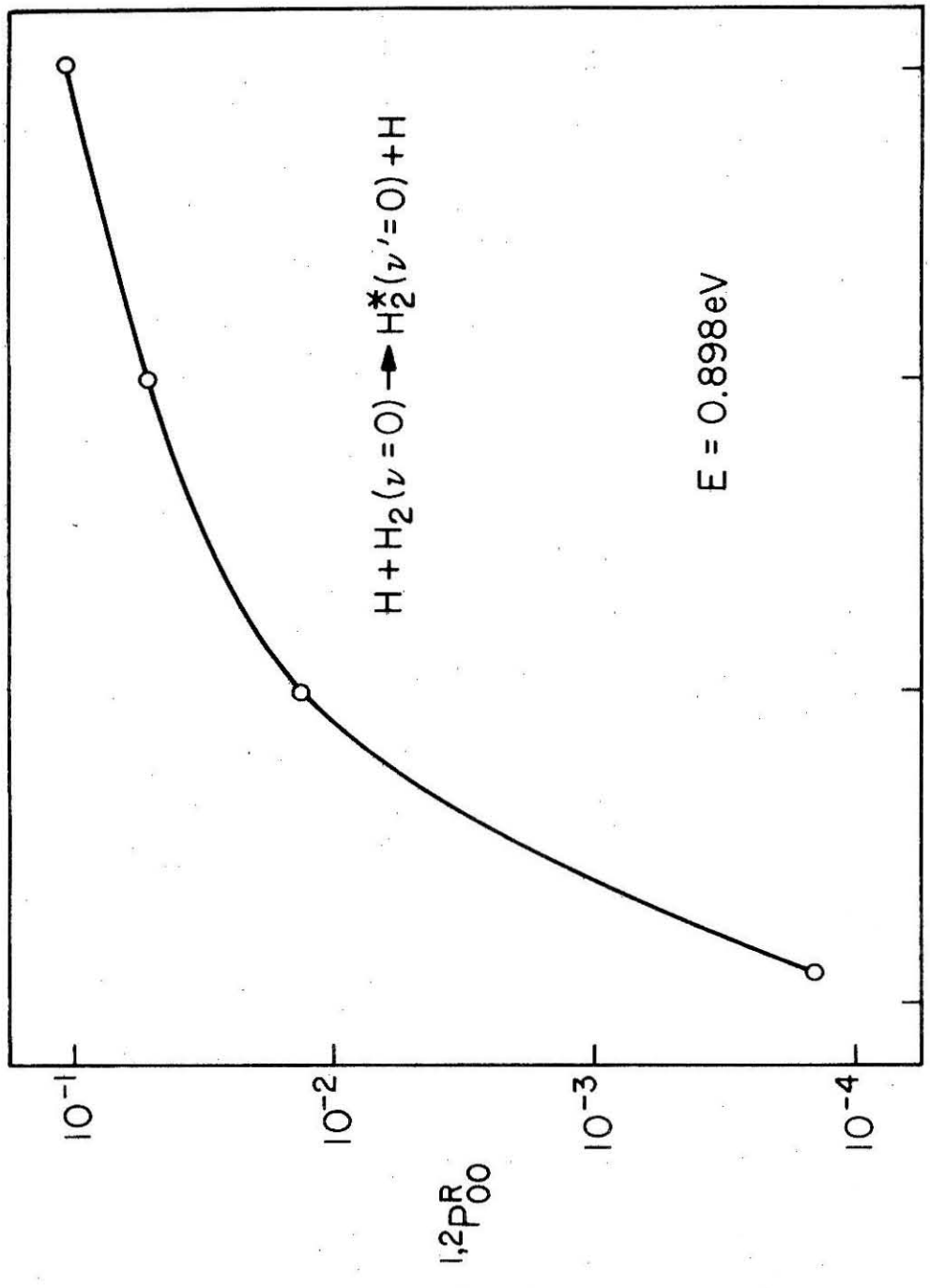

Figure 9

III. 3 QUANTUM CALCULATIONS OF THE ELECTRONICALLY NON-ADIABATIC REACTION $Ba + ON_2 \rightarrow BaO^* + N_2$, $BaO + N_2$.

III. 3 QUANTUM CALCULATIONS OF THE ELECTRONICALLY NON-ADIABATIC REACTION $Ba + ON_2 \rightarrow BaO^* + N_2$, $BaO + N_2$.

1. Introduction

The study of simple bimolecular chemiluminescent reactions has recently increased greatly both experimentally and theoretically.[1] Such reactions can be written schematically as follows:

(i) $A + BC \rightarrow AB^* + C$

(ii) $AB^* \rightarrow AB + h\nu$

(iii) $A + BC \rightarrow AB + C$.

In step (i) atom-molecule reactants A and BC undergo a chemical reaction in which an electronically excited molecule AB^* is formed (reactions yielding $AB + C^*$ are also well-known); in step (ii) the AB^* molecule relaxes to its ground electronic state by the emission of a photon. Step (iii) is included to stress the fact that there are channels which compete with step (i). Indeed, the competition between step (i) and other processes such as step (iii) is an important factor in the development of an electronic transition chemical laser driven by a suitable chemiluminescent chemical reaction. This possible development is at least partly responsible for the recent vigorous interest in chemiluminescent reactions.

The ab initio calculation of the reaction cross-sections for steps (i) and (iii) requires several independent efforts. First, the Born-Oppenheimer potential energy surfaces for these reaction channels must be known. Ab initio calculations of such surfaces are

a very time consuming and expensive task. Second, the quantities which couple these surfaces together must be calculated. These terms are also very difficult to calculate. Finally, the chemical dynamics calculations must be carried out in order to obtain the reaction cross-sections, rate constants, branching ratios, etc. However, ab initio calculations of cross-sections for such reactions, i.e., three-dimensional quantum reactive scattering calculations are not yet feasible and thus the need for approximate reliable methods to calculate the reaction dynamics is clear.

A classical trajectory surface hopping scheme has recently been developed and applied to the $H^+ + D_2 \rightarrow HD^+ + D$ reaction.[2,3] In addition a semi-classical description of electronically non-adiabatic reactions based on the Feynman propagator has been formulated.[4,5] It also has been applied to the $H^+ + D_2 \rightarrow HD^+ + D$ reaction.[6]

As a means of assessing the accuracy of these approximate methods a quantum scattering program has been developed to calculate transition probabilities for collinear electronically non-adiabatic reactions. Exact quantum calculations for collinear reactions can be compared with approximate collinear calculations. Thus, within this collinear framework a rigorous test of the approximate theories can be carried out.

We have performed exact quantum calculations of a model chemical reaction based on a reaction of much current interest,

$$Ba(^1S) + N_2O(x\,^1\Sigma^+) \begin{cases} \rightarrow BaO^* + N_2 \\ \rightarrow BaO + N_2 \end{cases} .$$

Unfortunately there is neither ab initio or accurate semi-empirical information about the relevant potential energy surfaces or the coupling surface. Thus, within the collinear restriction, our calculations are ab initio from the dynamics point of view but highly approximate otherwise. We have developed model potential surfaces and coupling for this reaction.

Chemiluminescence from the reaction of Ba + N_2O was first reported by Ottinger and Zare[7a] and Jonah, Zare, and Ottinger,[7b] who performed a crossed-beam experiment and assigned the emitted light to the electronic transition $BaO^*(A^1\Sigma^+) \rightarrow BaO(x^1\Sigma^+)$. However, the emission spectrum revealed an underlying complexity which was speculated to be caused by a triplet state emission of BaO^*.[7] Supportive evidence for this idea was presented by Jones and Broida[8] who monitored the chemiluminescent intensity and spectral characteristics as a function of the pressure of an inert carrier gas. The results were interpreted by Jones and Broida[8] and by Field, Jones, and Broida[9] who suggest the following mechanism for the reaction:

$$Ba(^1S) + N_2O(x^1\Sigma^+) \rightarrow BaO(a^3\pi) + N_2(x^1\Sigma_g^+) \quad (1)$$

$$BaO(a^3\pi) + M \rightarrow BaO(A^1\Sigma^+) + M \quad (2)$$

$$BaO(A^1\Sigma^+) \rightarrow BaO(x^1\Sigma^+) + h\nu \quad (3)$$

$$BaO(a^3\pi) \rightarrow BaO(x^1\Sigma^+) + h\nu' \quad . \quad (4)$$

This mechanism in addition to accounting for the complex emission spectrum also is consistent with the observed pressure dependence (on M) of this spectrum. In addition to reaction (1), the competing reaction

$$Ba(^1S) + N_2O(x^1\Sigma^+) \rightarrow BaO(x^1\Sigma^+) + N_2(x^1\Sigma_g^+)$$

must be considered in a theoretical investigation of this chemiluminescent reaction.

Very recently two groups have observed chemiluminescence from the Ba + N_2O reaction under low pressure conditions[10,11] and have concluded that the observed emission is from the $A^1\Sigma^+$ state. Thus, it appears as though the mechanism given by (1) - (4) may be somewhat oversimplified. Evidently $BaO(A^1\Sigma^+)$ is formed directly in the reaction along with $BaO(a^3\pi)$. Our quantum calculations are based on the two-surface reaction implied by the Field, Jones, and Broida mechanism

$$Ba(^1S) + ON_2(x^1\Sigma^+) \begin{cases} \rightarrow BaO(a^3\pi) + N_2(x^1\Sigma_g^+) \\ \rightarrow BaO(x^1\Sigma^+) + N_2(x^1\Sigma_g^+) \end{cases} .$$

In Section 2 we present and discuss the model potential surfaces and coupling surface used in our calculations. Section 3 contains a brief description of the two-state theory and equations as well as some details regarding the calculations. Results for the coupled two-state calculation are presented and compared with those for the uncoupled calculations which we have also carried out in Section 4. In addition an examination of the non-reactive processes

$$BaO(x^1\Sigma^+, \nu) + N_2 \rightarrow BaO(a^3\pi, \nu') + N_2$$

is made and discussed. In Section 5 a summary and conclusions are given.

2. Potential Surfaces and the Coupling Surface

2.1 The $x^1\Sigma^+$ and $a^3\pi$ potential surfaces

The ground state reaction $Ba(^1S) + N_2O(x\,^1\Sigma^+) \rightarrow BaO(x\,^1\Sigma^+) + N_2(x\,^1\Sigma_g^+)$ is exothermic by approximately 4 eV.[12] Due to the large reduced mass of BaO this means that at zero collision energy there are more than fifty vibrational states open. This many states make the present available close-coupling integration schemes unpractical even for collinear collisions. In order to achieve feasibility in the quantum calculations we have reduced the exothermicity of the reaction to 0.2 eV. Even with such a drastic reduction in the exothermicity there are four vibrational states open at zero initial translational energy and six open at 0.1 eV initial translational energy for the ground state reaction. Also, we treat the N_2 molecule as a mass-point (with mass of N_2). This seems reasonable since apparently N_2 plays a spectator role in the reaction.

An LEPS[13] surface was devised for the singlet ground state reaction in accord with the above criterion for exothermicity. The dissociation energy of $N_2O \rightarrow N_2(x^1\Sigma_g^+) + O(^1D)$ is 3.64 eV[14] and hence the dissociation energy of BaO (fictitious) is 3.84 eV. The r_e and β_e values of $BaO(x^1\Sigma^+)$ were chosen so that the curve crossing between the $x^1\Sigma^+$ state of BaO and the $a^3\pi$ state would resemble the one computed by ab initio methods.[15] We return to this point in the discussion of the $a^3\pi$ state. The construction of this ground state potential surface assumes that the ground state singlet state of $Ba(^1S) + N_2O(x^1\Sigma^+)$ correlates diabatically with the singlet ground state of $BaO(x\,^1\Sigma^+) + N_2(x^1\Sigma_g^+)$.[9] The LEPS parameters for this surface are given in Table 1.

A three-dimensional perspective plot of this surface is presented in Figure 1, however, we defer a discussion of this figure to the discussion of the $a^3\pi$ surface.

The $a^3\pi$ state of $BaO(a^3\pi) + N_2(x^1\Sigma_g^+)$ is assumed to correlate diabatically with the $a^3\pi$ state of $Ba(^1S) + N_2O(a^3\pi)$.[9] The r_e and β_e values of $BaO(a^3\pi)$ were estimated to be 2.50 Å and 1.55 $Å^{-1}$ respectively[15] and the dissociation energy was estimated to be 2.63 eV.[16] These estimates do not agree very well with the assignments made recently by Field [12] however, since our calculations are essentially of a model type we feel that this fact is of minor relevance to our purpose.

An LEPS surface was constructed for this $a^3\pi$ state and the parameters are given in Table 2. As seen from that table a fictitious $N_2O(a^3\pi)$ molecule with a dissociation energy of 1.0 eV is "created" by the surface. This was done for two reasons. First, it facilitated the construction of a facsimile of a non-reactive surface (using the LEPS expression). Second it was thought that with the scheme used to integrate the Schrödinger equation[17,18] on this surface would be more efficient than on a purely non-reactive one.

Three-dimensional perspective plots of these LEPS $x^1\Sigma^+$ and $a^3\pi$ potential surfaces are given as a function of the Ba - O and O - N_2 internuclear distances in Figures 1 and 2 respectively. The $a^3\pi$ surface is displaced in energy by 1.63 eV above the $x^1\Sigma^+$ surface. This was done to create a somewhat realistic curve crossing of the surfaces in the asymptotic limits of separated reagents and products. We return to this point later. These surfaces do cross along a seam. This seam is shown in Figures 3 and 4 where equipotential plots are

shown of the model $x^1\Sigma^+$ and $a^3\pi$ surfaces as a function of the O - N_2 internuclear distance R_1 and the Ba - O internuclear distance R_2. The points plotted along this seam indicate a 0.1 eV incremental increase in the value of the potential surfaces along the seam relative to the value at the crossing point in the BaO + N_2 asymptotic limit (0.03 eV). It can be seen that the potential energy remains essentially constant along the portion of the seam located in the product exit channel. The value of the potentials at the "corner" of the seam increases rapidly from approximately 0.23 eV to 0.53 eV. The total energy considered in our calculations does not exceed 0.16 eV, thus the portion of the seam extending from the "corner" to the Ba + ON_2 asymptotic limit is embedded in a classically forbidden region of configuration space. This fact is relevant to the form of the coupling surface chosen and described below. Finally, we note that the model $a^3\pi$ surface resembles a nonreactive surface (which it should rigorously be).

Plots of the $x^1\Sigma^+$ and $a^3\pi$ potential surfaces, hereafter referred to as V_1 and V_2 respectively, in the Ba + ON_2 and BaO + N_2 asymptotic limits are given in Figures 5 and 6 respectively. Both sets of curves cross and in a manner qualitatively similar to the correct ones.[13,14]

In Figure 7 a vibrational energy level diagram for the $x^1\Sigma^+$ and $a^3\pi$ states of BaO is presented. The zero of energy is referenced to the minimum of the potential surface V_1 in the Ba + N_2O asymptotic limit. At zero collision energy of the Ba + N_2O reactants the total energy is equal to the zero-point vibrational energy of the

molecule (according to the model surface V_1), 0.0496 eV. Thus, as seen from Figure 7, at this energy there are four open vibrational states for the $x\,^1\Sigma^+$ state of BaO and one open vibrational state for the $a^3\pi$ state.

Based on the fact that many more vibrational states are open in $BaO(x^1\Sigma^+)$ than in $BaO(a^3\pi)$ at all collision energies in the real system (and mimicked in our model system) we felt intuitively that reactions to produce $BaO(a^3\pi)$ efficiently would also produce vibrationally excited ground state products as well. Thus, we tried to make the V_1 surface of the "attractive" or "mixed energy-release type"[19] by a suitable variation of the Δ parameters in the LEPS expression for V_1. We did not succeed in doing this without also introducing spurious 0.05 eV to 0.1 eV hollows in the Ba + ON_2 entrance channel. Thus, as seen from Figure 1 the V_1 surface is of the "repulsive" type[19] and is not expected to produce vibrationally excited $BaO(x^1\Sigma^+)$ (for the uncoupled calculations).

2.2 The spin-orbit coupling surface

The coupling between the $x\,^1\Sigma^+$ and $a^3\pi$ states of the $BaON_2$ system is due to a spin-orbit interaction. As a reasonable form for the model spin-orbit coupling surface it was assumed (based on first order perturbation arguments) that this coupling should be relatively large near the crossing seam and that it should decay in the direction transverse to the seam. Also, we require that this coupling vanish in the reagent and product asymptotic limits. Although this is not rigorously true it is assumed for two reasons. First, the uncoupling of the scattering

equations is necessary if the usual chemical scattering analysis is to be carried out. Second, from a mechanistic point of view we assume that the chemical interaction of the reagents coupled with the spin-orbit interaction is primarily responsible for the formation of product $BaO(a^3\pi)$. Thus, in this sense it is the spin-orbit interaction in the region of chemical interaction that is of interest. Roughly speaking then we consider the spin-orbit coupling surface devised as an interaction coupling surface, e.g., the spin-orbit interaction produced by Ba - O - N_2 system minus the BaO spin-orbit interaction.

In Figure 8 we have plotted some equipotential contours of the spin-orbit coupling surface V^{SO} used in our calculations. It is given by the simple expression

$$V^{SO} = \begin{cases} \gamma \operatorname{sech}[\beta(R_2 - R_{20})] \exp[-\alpha(R_1 - R_{10})^2], & R_2 > R_{20} \\ 0 & R_2 \leq R_{20} \end{cases} \quad (1)$$

and the values of the parameters γ, β, x, R_{20}, and R_{10} are given in Table 3. As seen from Figure 8 this coupling surface does not follow the direction of the seam except in the product BaO exit channel. This was done for convenience and simplicity. However, as noted earlier, the seam penetrates into a classically forbidden region of space immediately after "turning the corner" and entering the reagent entrance channel. Thus, the coupling surface shown in Figure 8 is probably a reasonable representation of the effective spin-orbit coupling. A three-dimensional perspective plot of this surface is shown in Figure 9.

The value of γ chosen, 0.05 eV, is essentially a guess based on the strength of the spin-orbit coupling in BaO.[12] Furthermore, other studies indicate that in order for the surface coupling to be effective γ must be of the same order of magnitude as the vibrational energy spacing of the product molecule[20] (for our model BaO($x^1\Sigma^+$ or $a^3\pi$) this spacing is roughly 0.06 eV).

3. Theory and Calculations

3.1 The two-state coupled equations

The two-state coupled "Schrödinger" equations which govern the nuclear motion are given in the Delves coordinate system[21] by[22,23]

$$-\frac{\hbar^2}{2\mu}\left(\frac{\partial^2}{\partial x_1^2}+\frac{\partial^2}{\partial x_2^2}\right)+V_1(x_1,x_2)-E\Big]\psi_1(x_1,x_2)=-V^{SO}\psi_2(x_1,x_2)$$

$$\Big[-\frac{\hbar^2}{2\mu}\left(\frac{\partial^2}{\partial x_1^2}+\frac{\partial^2}{\partial x_2^2}\right)+V_2(x_1,x_2)-E\Big]\psi_2(x_1,x_2)=-V^{SO}\psi_1(x_1,x_2)$$

where

$$x_1=\left(\frac{\mu_{A,BC}}{\mu_{BC}}\right)^{\frac{1}{4}}\left(R_1+\frac{\mu_{BC}}{M_B}R_2\right),$$

$$x_2=\left(\frac{\mu_{BC}}{\mu_{A,BC}}\right)^{\frac{1}{4}}R_2,$$

and

$$\mu_{A,BC}=M_A(M_B+M_C)/(M_A+M_B+M_C),\quad \mu_{BC}=M_BM_C/(M_B+M_C)$$

for the A + BC arrangement channel. For the AB + C arrangement channel an analogous set of coordinates z_1 and z_2, is defined. The procedure used for solving these two coupled partial differential equations is an extension of the close-coupling propagation method of

Kuppermann.[17] Details regarding this extended method and the R-S scattering analysis are given elsewhere.[24]

3.2 Calculations

For the Ba + ON_2 calculations typically 16-18 pseudo-vibrational states were used in the expansion of $\psi_1(x_1, x_2)$ and 8-10 pseudo-vibrational states in the expansion of $\psi_2(x_1, x_2)$. The calculations were done on an IBM 370/155 computer in single precision arithmatic. The compute time for the first step in which energy independent matrix elements are calculated and stored on disc was typically 160 minutes. Thereafter the time per energy was typically 20 minutes. The results were deemed converged when the S-matrix was unitary to better than 2% and symmetric to within 5%.

Calculations were done on this system of coupled equations with V^{SO} given by (1) and with $V^{SO} \equiv 0$. Results for both sets of calculations are reported in the next section. The notation for a transition probability and the corresponding process are given as follows:

$$\text{Ba} + ON_2(\nu) \rightarrow \text{BaO}(\nu') + \text{N2} \quad : \quad {}^{1}P^{R}_{\nu\nu'}$$

$$\text{Ba} + ON_2(\nu) \rightarrow \text{BaO}^{*}(\nu'') + N_2 \quad : \quad {}^{1,2}P^{R}_{\nu\nu''}$$

$$\text{BaO}(\nu) + N_2 \rightarrow \text{BaO}^{*}(\nu') + N_2 \quad : \quad {}^{1,2}P^{V}_{\nu\nu'}$$

The initial translational energy range scanned relative to the ground state reagents was 0.0 to 0.11 eV.

4. Results and Discussion

4.1 Uncoupled $Ba + ON_2 \rightarrow BaO + N_2$ results

The reaction probabilities ${}^1P_{00}^R$, ${}^1P_{01}^R$, and ${}^1P_{02}^R$ are presented in Figures 10 and 11 as a function of the total energy E and the initial translational energy E_0 for the uncoupled surfaces. The inner and outer arrows on the lower abscissa indicate the total energies at which the vibrational state v' of BaO^* and BaO respectively become accessible. The reaction probabilities ${}^1P_{03}^R$, ${}^1P_{04}^R$, and ${}^1P_{04}^R$ are all less than 3×10^{-3} over the energy range considered. These uncoupled results show that the ${}^1P_{00}^R$ transition is dominant at low collision energies and the reactive transitions $0 \rightarrow 1$ and $0 \rightarrow 2$ become appreciable consecutively with increasing energy. This behavior is characteristic of a repulsive energy surface and based on remarks in Section 2.1 it is not unexpected. Also, we note that the total reaction probability is greater than 0.8 over the collision energy range of 0.0 to 0.11 eV. This may be a bit surprising since the skew angle for this system is 41°.

The energy dependence of these reactive transition probabilities exhibits marked oscillatory structure. Since the reduced mass of this system is so large it might be reasonable to assume that these rapid oscillations are semi-classical in nature and hence that semi-classical theories of reactive scattering could reproduce them.[25]

4.2 Coupled $Ba + ON_2 \rightarrow BaO^*$, $BaO + N_2$ results

The reaction probabilities ${}^1P_{00}^R$, ${}^1P_{01}^R$, and ${}^1P_{02}^R$ are plotted as a function of E and E_0 for the coupled system in Figures 12 and 13.

A comparison of the coupled and uncoupled $^{1}P_{00}^{R}$ results reveals striking similarities between them. Evidently the $^{1}P_{00}^{R}$ transition is very weakly coupled to the excited state surface. The $^{1}P_{01}^{R}$ and $^{1}P_{02}^{R}$ coupled results do, however, appear to be strongly coupled to the upper surface as a comparison between Figures 13 and 11 indicates. The $^{1}P_{02}^{R}$ transition is the most strongly coupled transition in two senses. First, the attenuation of the magnitude of the coupled $^{1}P_{02}^{R}$ probability over the uncoupled one is largest (in absolute terms). Second, the energy dependence of this coupled probability is most affected by the coupling. Interestingly, the coupled $^{1}P_{02}^{R}$ has a lower effective threshold energy than does the uncoupled $^{1}P_{02}^{R}$.

The electronically non-adiabatic transition probability $^{1,2}P_{00}^{R}$ is presented in Figure 14. A comparison of this result with the coupled and uncoupled $^{1}P_{02}^{R}$ results shows some striking similarities. The energy dependence of the $^{1,2}P_{00}^{R}$ curve in the range $0.09 \text{ eV} \leq E \leq 0.12 \text{ eV}$ is quite similar in structure and magnitude to the coupled $^{1}P_{02}^{R}$ curve. However, for E between 0.12 eV and 0.15 eV there is a strong resemblance in the energy dependence of the $^{1,2}P_{00}^{R}$ curve and the uncoupled $^{1}P_{02}^{R}$ one. There is an energy displacement in the peak height locations of these oscillating curves, however.

As a result of the similarities noted above and as seen directly from Figure 14, the threshold energy for the $^{1,2}P_{00}^{R}$ transition probability is considerably above its energetic threshold (0.028 eV). The magnitude of this transition probability is large indicating that for collision energies greater than 0.05 eV the reaction product BaO^{*} is formed with approximately the same probability as the ground state

product BaO, on the average. That this would occur with the 0.05 eV spin-orbit coupling strength is not obvious. It was previously found in model calculations on a fictitious two-state H + H_2 reaction that a 0.05 eV "spin-orbit" coupling strength gave electronically non-adiabatic transition probabilities which were an order-of-magnitude smaller than the electronically adiabatic ones.[20]

The reaction probabilities ${}^{1,2}P_{01}^{R}$ and ${}^{1,2}P_{02}^{R}$ are not shown since they are small compared to ${}^{1,2}P_{00}^{R}$ over the energy range considered. ${}^{1,2}P_{01}^{R}$ never exceeds 0.04 and ${}^{1,2}P_{02}^{R}$ never exceeds 0.008.

4.3 Coupled BaO + N_2 → BaO^* + N_2 results

An interesting process which our calculations can be applied to is the vibrational relaxation of BaO in collisions with N_2 (treated as a structureless mass point) to yield BaO in a lower vibrational state or BaO^*. We present some results on the relative efficiency of the V - T versus V - E (V - T meaning vibration to translation and V - E meaning vibration to electronic excitation) transfer of energy in the BaO + N_2 collisions.

Consider first the transfer of vibrational energy in the processes

$$\mathrm{BaO}(\nu = 4) + \mathrm{N_2} \begin{cases} \rightarrow \mathrm{BaO}^*(\nu') + \mathrm{N_2} \\ \rightarrow \mathrm{BaO}(\nu'') + \mathrm{N_2} \end{cases} .$$

In Figure 15 we have plotted the energy dependence of the transition probabilities ${}^{1}P_{44}^{V}$, ${}^{1}P_{43}^{V}$, ${}^{1,2}P_{41}^{V}$, and ${}^{1,2}P_{42}^{V}$. All other transition

probabilities ${}^{1}P^{V}_{4\nu'}$, ${}^{1',2}P^{V}_{4\nu''}$, and ${}^{1}P^{R}_{4\nu'''}$ are smaller than 0.03 in the energy range shown in this figure except at E = 0.0845 eV where the probability ${}^{1}P^{V}_{42}$ equals 0.176. As seen from this figure either the V - T or V - E transfer process is not very efficient for BaO($\nu = 4$). However, the V - E transfer is substantially more likely than the V - T one. At higher collision energies the V - E process does appear to be increasing in probability.

Analogous results are seen in Figures 16 and 17 where the energy dependence of the transition probabilities ${}^{1}P^{V}_{33}$, ${}^{1}P^{V}_{32}$, ${}^{1',2}P^{V}_{30}$, ${}^{1',2}P^{V}_{31}$, and ${}^{1',2}P^{V}_{32}$ is plotted. The ${}^{1}P^{V}_{32}$ probability is roughly the same in magnitude as ${}^{1',2}P^{V}_{30}$, although the latter probability is larger at the lower energies. For E greater than 0.12 eV the transition probabilities ${}^{1}P^{V}_{32}$ and ${}^{1',2}P^{V}_{31}$ are both appreciable. However, over much of the entire energy range considered the sum $\sum_{\nu'} {}^{1',2}P^{V}_{3\nu'}$ is greater than the sum $\sum_{\nu''} {}^{1}P^{V}_{3\nu''}$ indicating as before that the V - E process is more efficient than the V - T one for this system.

Finally, we consider V - T and V - E processes for the transfer of energy in BaO($\nu = 2$). The transition probabilities ${}^{1}P^{V}_{22}$ and ${}^{1}P^{V}_{21}$ are plotted in Figure 18 as a function of E and ${}^{1',2}P^{V}_{20}$ and ${}^{1',2}P^{V}_{21}$ are plotted in Figure 19. In this case the total transfer of vibrational energy is more efficient than for BaO($\nu = 3$ or $\nu = 4$). At the lower energies ${}^{1}P^{V}_{21}$ and ${}^{1',2}P^{V}_{20}$ are large and approximately equal whereas at the higher energies the transition probabilities ${}^{1',2}P^{V}_{21}$ and ${}^{1}P^{V}_{23}$ (as seen in Figure 16) also become significant contributors to the vibrational energy transfer. Thus, in this case both V - T and V - E processes contribute about equally and significantly to the

vibrational energy transfer of BaO($\nu = 2$) in nonreactive collisions. We also note that the reactive transition probability ${}^1P_{20}^R$ (= ${}^1P_{02}^R$ given in Figure 13) is significant at the higher energies and hence this reaction channel is effective in transferring vibrational energy from BaO($\nu = 2$). This is not an important consideration in collisions of BaO($\nu = 3$ or $\nu = 4$) with N_2 because the reaction probabilities ${}^1P_{30}^R$ and ${}^1P_{40}^R$ are less than 0.06 over the energy range considered.

5. Summary and Conclusions

The electronically adiabatic and non-adiabatic reactions

$$Ba(^1S) + N_2O(x\,^1\Sigma^+) \rightarrow BaO(x\,^1\Sigma^+) + N_2(x\,^1\Sigma_g^+)$$

and

$$Ba(^1S) + N_2O(x\,^1\Sigma^+) \begin{cases} \rightarrow BaO(a\,^3\pi) + N_2(x\,^1\Sigma_g^+) \\ \rightarrow BaO(x\,^1\Sigma^+) + N_2(x\,^1\Sigma_g^+) \end{cases}$$

have been studied within the collinear framework and with N_2 treated as a mass point. Model LEPS potential energy surfaces coupled by a model spin-orbit orbit interaction potential have been employed. The ground state potential surface is of the repulsive type. This probably accounts for the fact that there is little vibrational excitation of the product BaO($x\,^1\Sigma^+$) in the uncoupled calculations for collision energies less than 0.1 eV. The lack of vibrational excitation except at collision energies greater than 0.1 eV seems to correlate with the threshold energy of approximately 0.1 eV for the formation of BaO($a\,^3\pi, \nu' = 0$) in the coupled calculations. That is, vibrational excitation of BaO($x\,^1\Sigma$) and the formation of BaO($a\,^3\pi$) seem to be related

processes. Also, $BaO(a^3\pi, \nu' = 0)$ is formed with a substantial reaction probability ($\gtrsim 0.4$) at collision energies greater than 0.10 eV. This implies that the spin-orbit coupling strength of 0.05 eV is effective in causing large electronically non-adiabatic transitions in this system.

A study of nonreactive vibrational energy transfer in collisions of $BaO(x^1\Sigma^+, \nu = 2, 3, 4) + N_2$ to form $BaO(x^1\Sigma^+, \nu') + N_2$ or $BaO(a^3\pi, \nu'') + N_2$ was also carried out. The total energy range considered was the same as the one considered in the $Ba + N_2O$ studies. It was found that for $\nu = 4$, vibration to electronic energy transfer was more efficient than vibration to translation transfer. For $\nu = 3$ and $\nu = 2$, however, the two transfer processes were found to be comparable in efficiency. The fact that the ground state surface is reactive also enhances the vibration transfer for $\nu = 2$ since the reaction probability to form $Ba + N_2O$ is appreciable at the higher energies considered.

The energy dependence of all the transition probabilities studied showed marked oscillatory structure. This feature would make a comparison between the exact quantum results and approximate semi-classical ones very interesting. Much of the motivation behind doing exact quantum calculations on model systems is to stimulate comparison and development of approximate results and theories. This may accelerate progress in obtaining accurate three-dimensional cross-section calculations from approximate methods on real chemical systems.

Table 1. LEPS parameters for the singlet ground state Ba - O - N_2 potential energy surface.[a]

	$BaO(x^1\Sigma^+)$	$ON_2(x^1\Sigma^+)$	BaN_2[b]
D_i(eV)	3.844	3.644	3.64
r_{ie}(bohr)	4.4598	2.6778	4.4598
β_i(bohr^{-1})	0.70856	1.0	0.70856
Δ_i	0.220	0.08	0.08

[a] The expression for the generalized LEPS function is given by

$$V = Q'_1 + Q'_2 + Q'_3 - (\alpha'^2_1 + \alpha'^2_2 + \alpha'^2_3 - \alpha'_1\alpha'_2 - \alpha'_2\alpha'_3 - \alpha'_1\alpha'_3),$$

where

$$Q'_i = [D_i/4(1+\Delta_i)]\{(3+\Delta_i)\exp[-2\beta_i(r_i - r_{ie})] - (2+6\Delta_i)\exp[-\beta_i(r_i - r_{ie})]\}$$

and where i refers to a given diatom pair.

[b] The parameters given in this column are meaningless for collinear collisions.

Table 2. LEPS parameters for the triplet excited state Ba - O - N_2 potential energy surface.

	$BaO(a^3\pi)$	$ON_2(a^3\pi)$	BaN_2
D_i(eV)	2.63	1.0	2.63
r_{ie} (Å)	4.7244	3.7795	4.7244
β_i(Å^{-1})	0.8202	0.7938	0.8202
Δ_i	0.15	0.45	0.15

Table 3. Parameters for the model spin-orbit coupling surface.[a]

$\gamma = 0.05$ eV
$\beta = 1.1$ bohr^{-1}
$\alpha = 8.0$ bohr^{-2}
$R_{10} = 4.8516$ bohr
$R_{20} = 4.0$ bohr

[a] $V^{so} = \gamma\, \mathrm{sech}[\beta(R_2 - R_{20})]\exp[-\alpha(R_1 - R_{10})^2]$, $R_2 > R_{20}$

$= 0$, $R_2 \leq R_{20}$

References

1. (a) T. Carrington, Chemiluminescence and Bioluminescence edited by M. J. Cormier, D. M. Hercules, and J. Lee (Plenum, New York, 1973), Chapter 1; (b) D. R. Herschbach, ibid., Chapter 3.
2. (a) R. K. Preston and J. C. Tully, J. Chem. Phys. 54, 4297 (1971); (b) J. C. Tully and R. K. Preston, ibid., 55, 562 (1971).
3. J. R. Krenos, R. K. Preston, R. Wolfgang and J. C. Tully, J. Chem. Phys. 60, 1634 (1974).
4. W. H. Miller and T. F. George, J. Chem. Phys. 56, 5637 (1972).
5. T. F. George and T.-W. Lin, J. Chem. Phys. 60, 2340 (1974).
6. (a) T.-W. Lin, T. F. George, and K. Morokuma, Chem. Phys. Lett. 22, 547 (1973); (b) T.-W. Lin, T. F. George, and K. Morokuma, J. Chem. Phys. 60, 4311 (1974).
7. (a) Ch. Ottinger and R. N. Zare, Chem. Phys. Lett. 5, 243 (1970); (b) C. D. Jonah, R. N. Zare, and Ch. Ottinger, J. Chem. Phys. 56, 263 (1972).
8. C. R. Jones and H. P. Broida, J. Chem. Phys. 60, 4369 (1974).
9. R. W. Field, C. R. Jones, and H. P. Broida, J. Chem. Phys. 60, 4377 (1974).
10. C. J. Hsu, W. D. Krugh, and H. B. Palmer, J. Chem. Phys. 60, 5118 (1974).
11. A. Schultz and R. N. Zare, J. Chem. Phys. 60, 5120 (1974).
12. R. W. Field, J. Chem. Phys. 60, 2400 (1974).
13. See, for example J. T. Muckerman, J. Chem. Phys. 54, 1155 (1971).

14. See, for example, A. Chutjian and G. A. Segal, J. Chem. Phys. 57, 3069 (1972).

15. H. H. Michels (private communication) "1st Summer Colloquium on Electronic Transition Laser," (1974).

16. The value of $D_e(BaO(a\,^3\pi))$ given in ref. 12 is 3.6 eV. Our estimate was based on preliminary ab initio calculations of H. H. Michels.

17. A. Kuppermann, Electronic and Atomic Collisions, VII. International Conference on the Physics of Electronic and Atomic Collisions, Abstract of Papers (North-Holland, Amsterdam, 1971), p. 3.

18. (a) G. C. Schatz, J. M. Bowman, and A. Kuppermann, J. Chem. Phys. 58, 4023 (1973); (b) G. C. Schatz and A. Kuppermann, J. Chem. Phys. 59, 964 (1973); (c) J. M. Bowman, G. C. Schatz, and A. Kuppermann, Chem. Phys. Lett. 24, 378 (1974).

19. J. C. Polanyi and J. L. Schreiber, Physical Chemistry--An Advanced Treatise, Vol. VI, Kinetics of Gas Reactions edited by H. Eyring, W. Jost and D. Henderston (Academic Press, New York, to be published), Chapter 9.

20. J. M. Bowman and A. Kuppermann, unpublished results.

21. L. M. Delves, Nuclear Phys. 20, 275 (1960).

22. F. T. Smith, Phys. Rev. A179, 111 (1969).

23. J. Grosser and A. E. De Vries, preprint.

24. J. M. Bowman, Ph.D. Thesis (California Institute of Technology, Pasadena, California, 1974).

25. W. H. Miller, Adv. Chem. Phys. xxv, p. 69, and references cited therein.

Figure Caption

Figure 1: Three-dimensional perspective plot of the ground state singlet potential energy surface of $BaON_2$.

Figure 2: Three-dimensional perspective plot of the excited state triplet potential energy surface of $BaON_2$.

Figure 3: Equipotential contour plot of the ground state singlet $BaON_2$ potential energy surface. The crossing seam is also shown.

Figure 4: Equipotential contour plot of the excited state triplet $BaON_2$ potential energy surface. The crossing seam is also shown.

Figure 5: Potential energy curves of N_2O as a function of the internuclear distance R.

Figure 6: Potential energy curves of BaO as a function of the internuclear distance R.

Figure 7: Vibrational energy spectrum of the $BaO(x\,^1\Sigma^+)$, $BaO(a\,^3\pi)$, and $ON_2(x\,^1\Sigma^+)$ molecules.

Figure 8: Equipotential energy plot of the model spin-orbit coupling potential surface as a function of the two internuclear distances R_1 and R_2. The crossing seam is also shown.

Figure 9: Three-dimensional perspective plot of the model spin-orbit coupling potential.

Figure 10: Reaction probability $^1P_{00}^R$ for the uncoupled reaction as a function of the total energy E and the initial translational energy E_0. The significance of the arrows is given in the text.

Figure 11: Reaction probabilities $^1P_{01}^R$ and $^1P_{02}^R$ for the uncoupled reaction as a function of the total energy E and the initial translational energy E_0.

Figure 12: Reaction probability $^1P_{00}^R$ for the coupled reaction as a function of the total energy E and the initial translational energy E_0.

Figure 13: Reaction probabilities ${}^{1}P_{01}^{R}$ and ${}^{1}P_{02}^{R}$ for the coupled reaction as a function of the total energy E and the initial translational energy E_0.

Figure 14: Reaction probability ${}^{1,2}P_{00}^{R}$ for the coupled reaction as a function of the total energy and the initial translational energy E_0.

Figure 15: Non-reactive probabilities ${}^{1}P_{44}^{V}$, ${}^{1}P_{43}^{V}$, ${}^{1,2}P_{41}^{V}$, and ${}^{1,2}P_{42}^{V}$ for the coupled system as a function of the total energy E.

Figure 16: Non-reactive probabilities ${}^{1}P_{33}^{V}$, ${}^{1}P_{32}^{V}$, and ${}^{1,2}P_{30}^{V}$ for the coupled system as a function of the total energy E.

Figure 17: Non-reactive probabilities ${}^{1,2}P_{31}^{V}$ and ${}^{1,2}P_{32}^{V}$ for the coupled system as a function of the total energy E.

Figure 18: Non-reactive probabilities ${}^{1}P_{22}^{V}$ and ${}^{1}P_{21}^{V}$ for the coupled system as a function of the total energy E.

Figure 19 : Non-reactive probabilities ${}^{1,2}P_{20}^{V}$ and ${}^{1,2}P_{21}^{V}$ for the coupled system as a function of the total energy E.

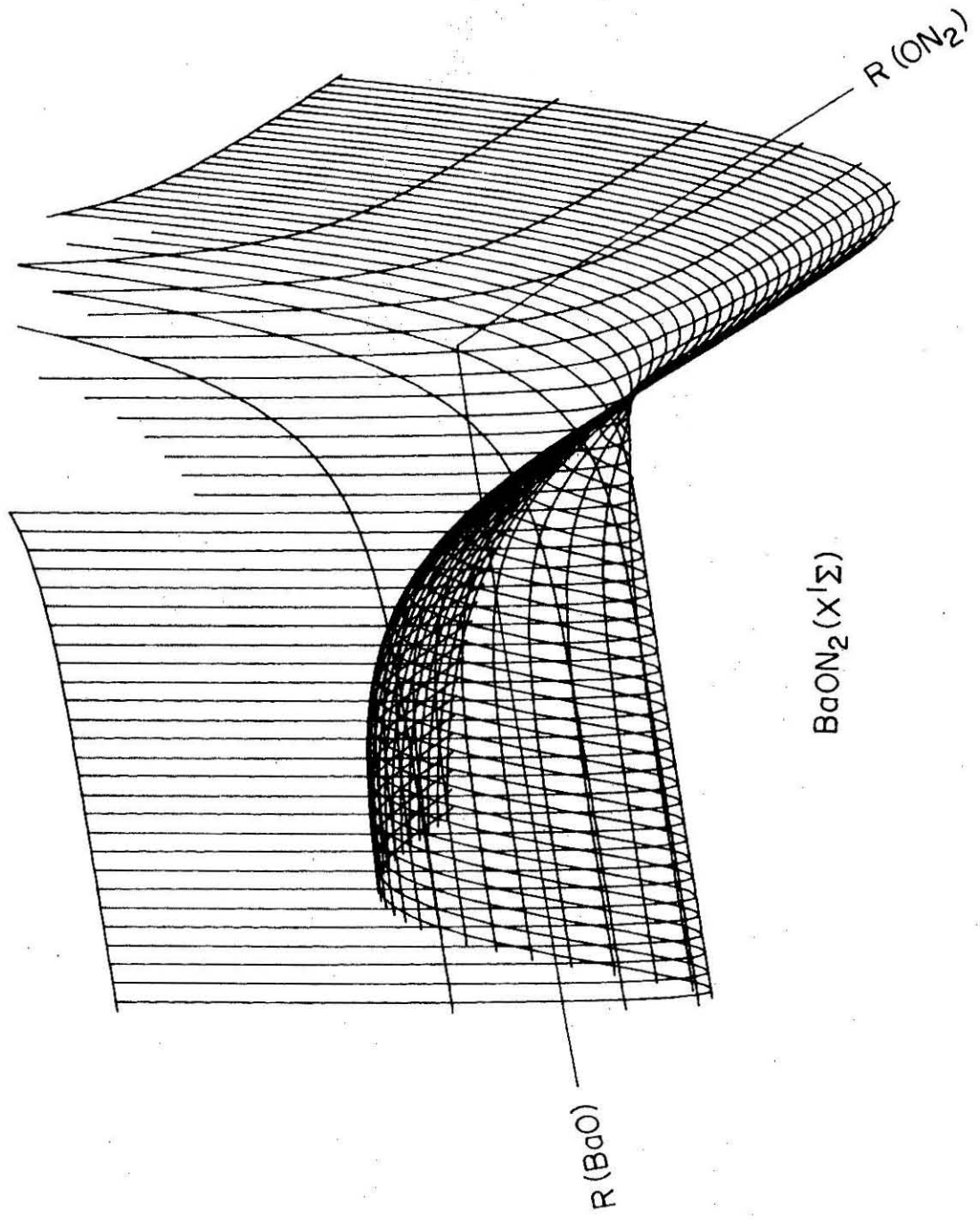

Figure 1

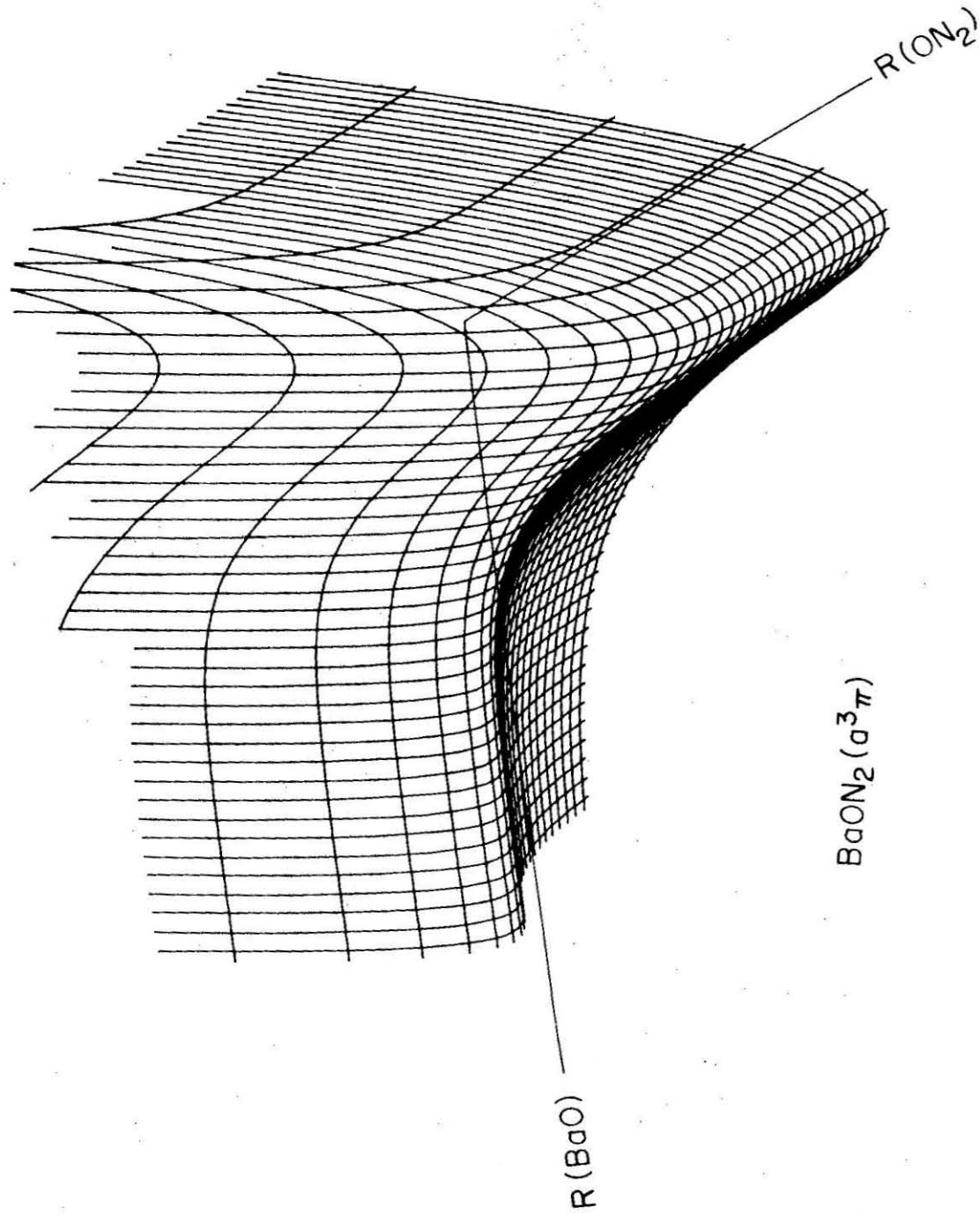

Figure 2

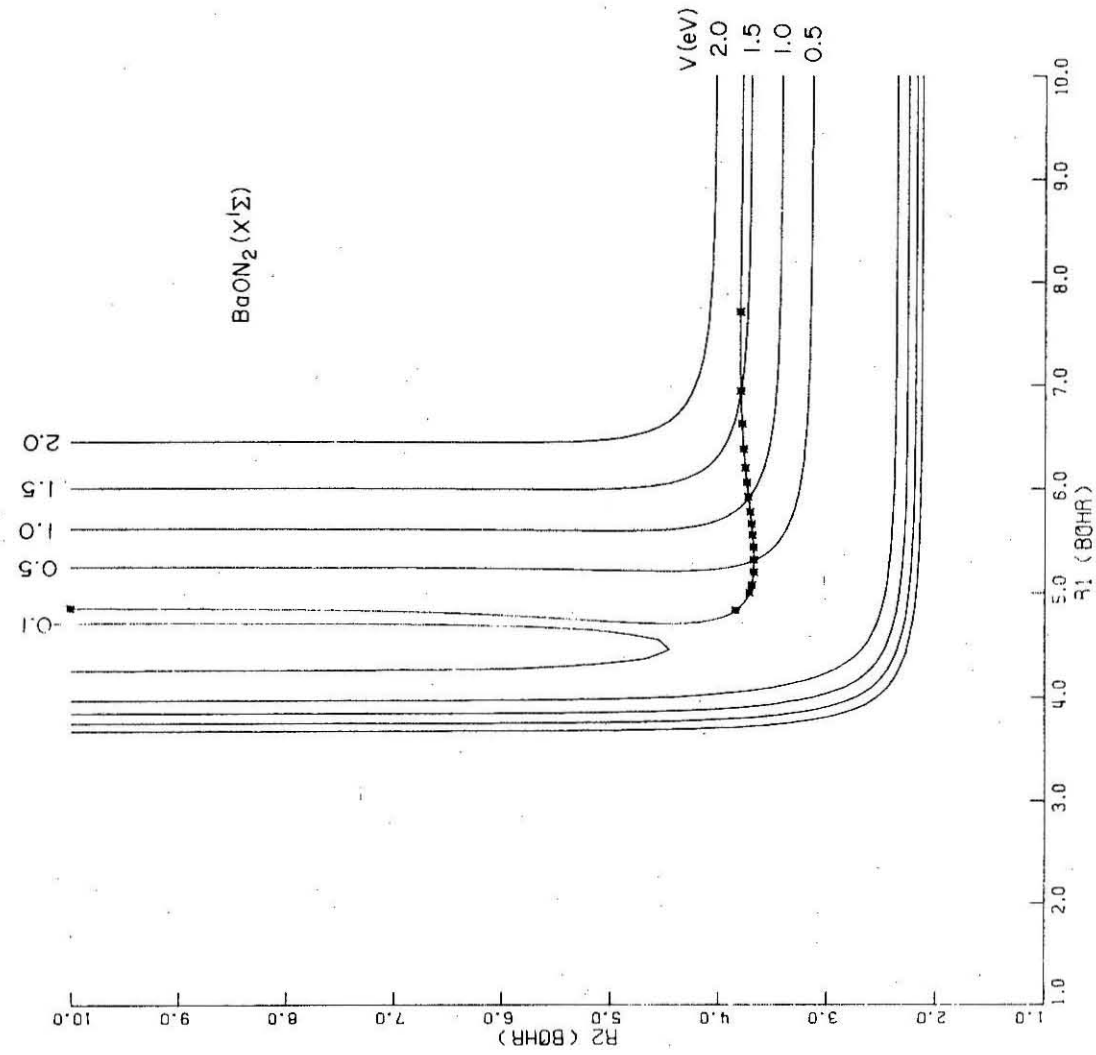

Figure 3

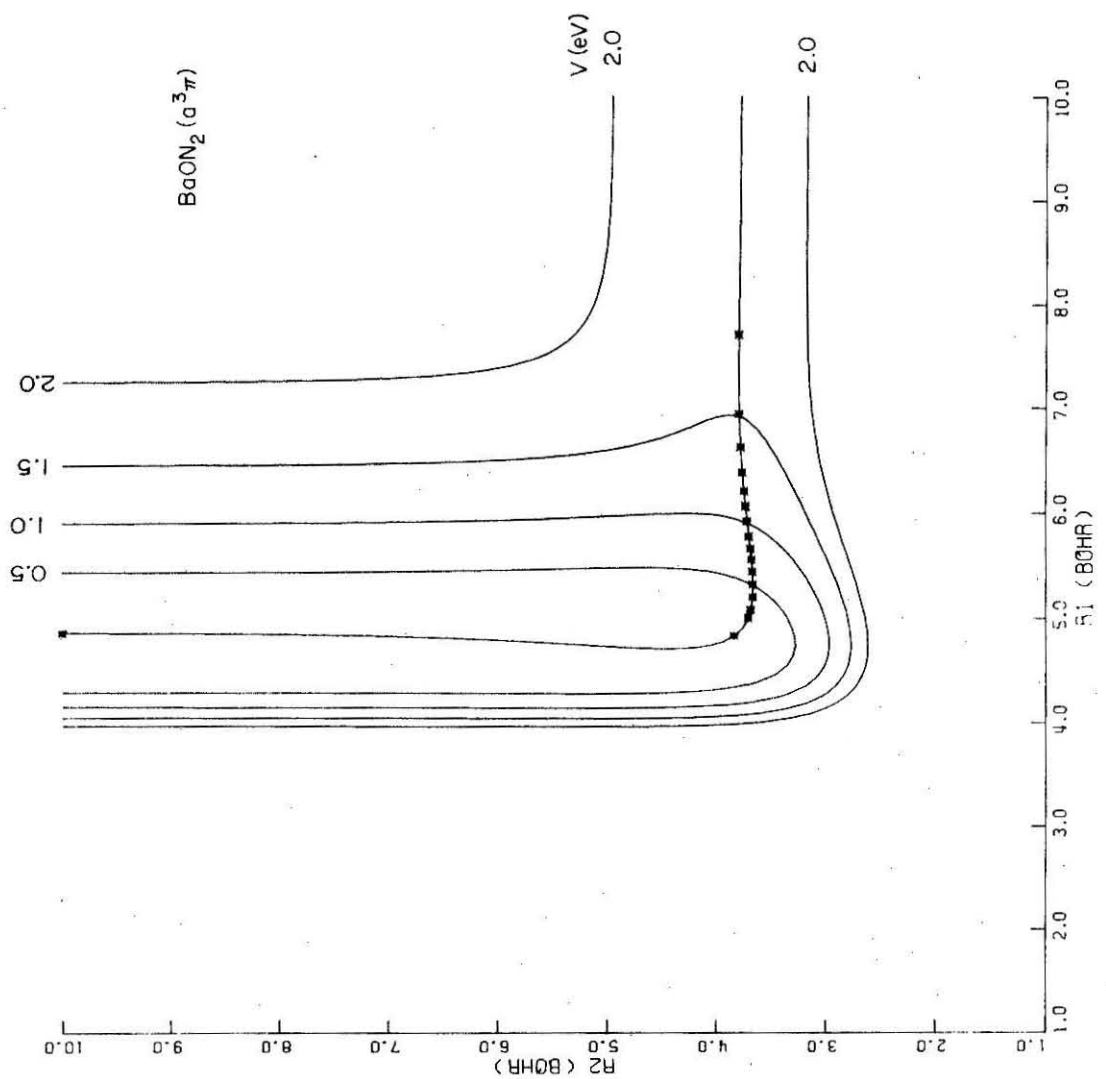
BaON2 (a3π)
V (eV)
2.0
2.0
2.0
1.5
1.0
0.5
R1 (BOHR)
R2 (BOHR)
1.0
2.0
3.0
4.0
5.0
6.0
7.0
8.0
9.0
10.0

Figure 4

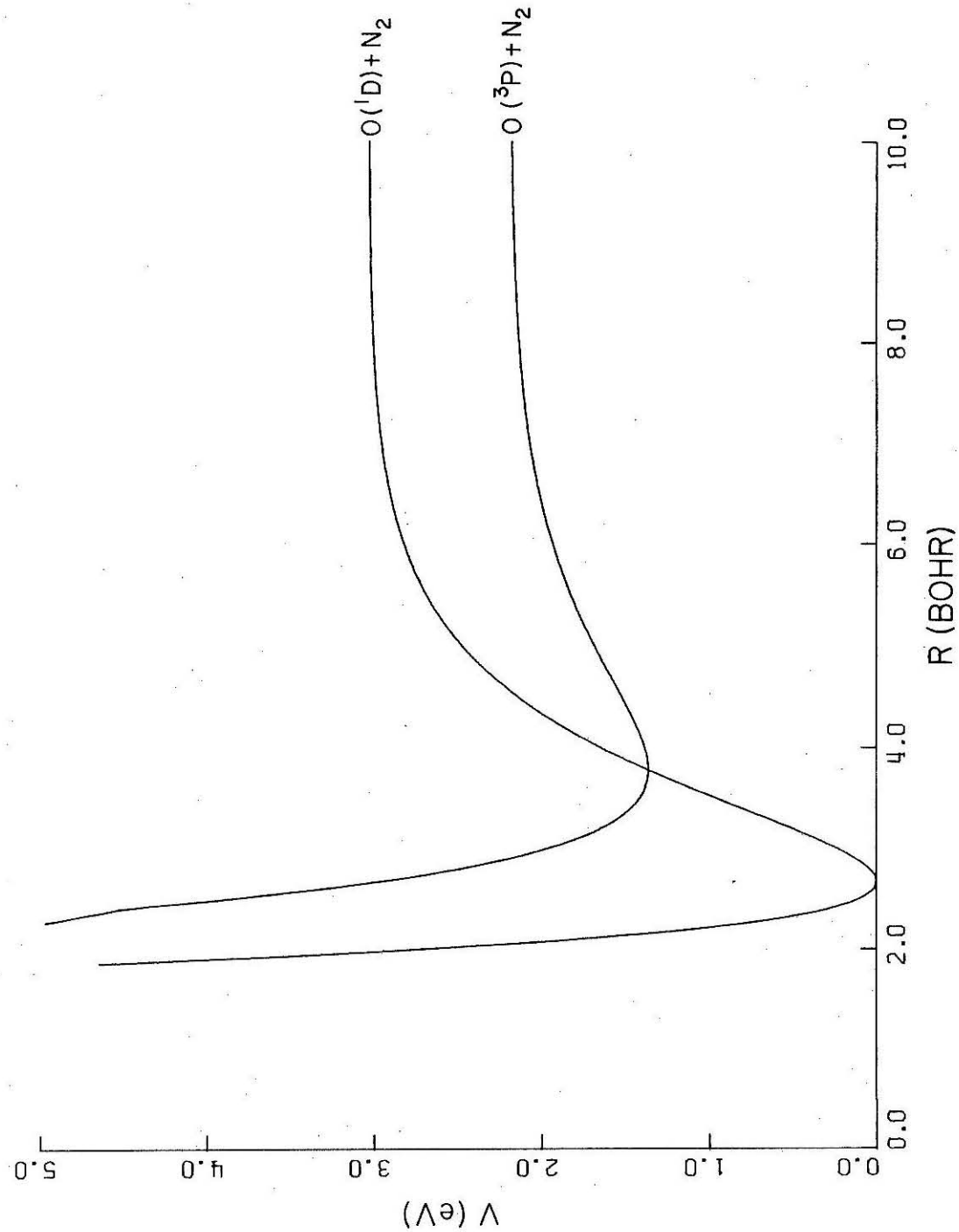

Figure 5

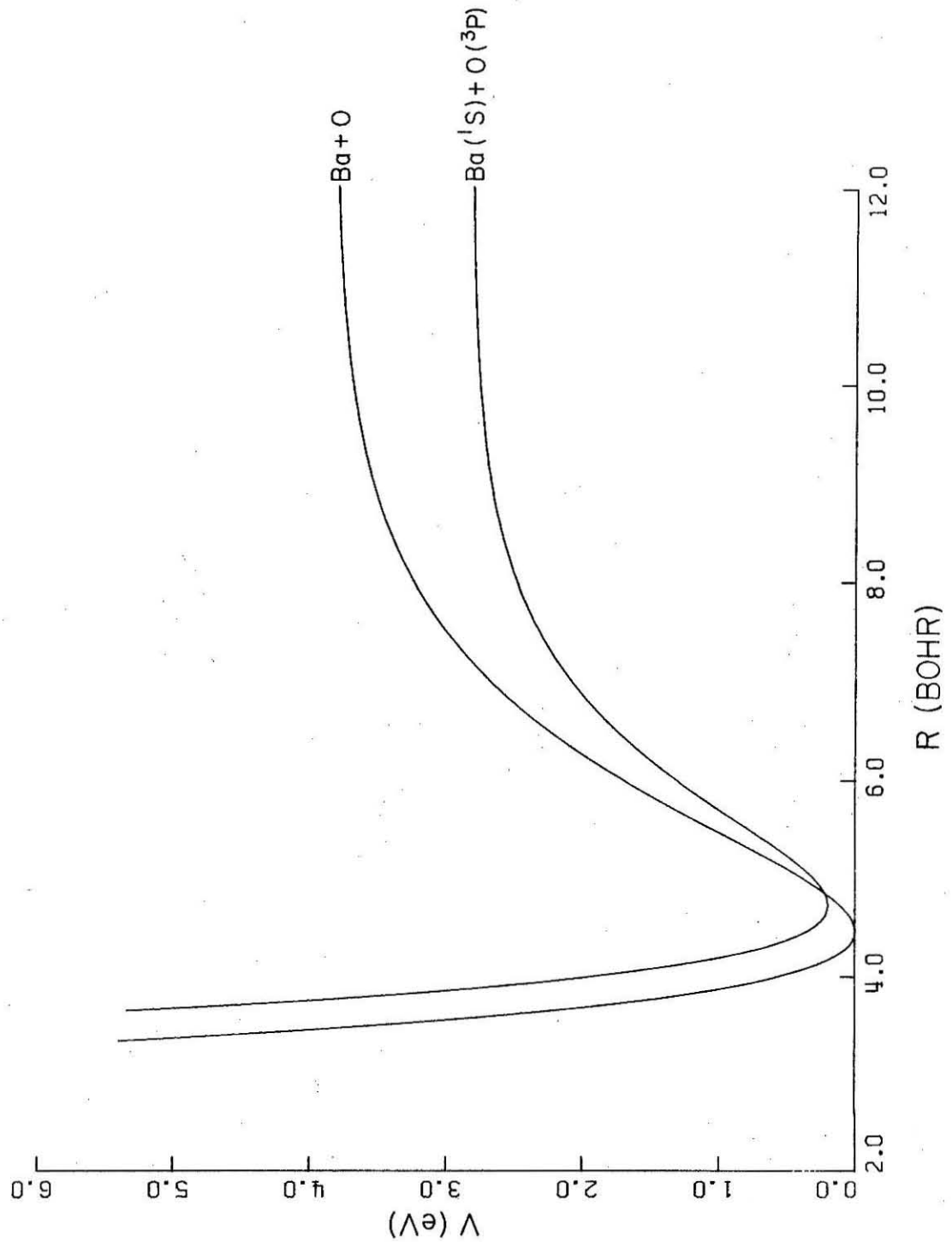

Figure 6

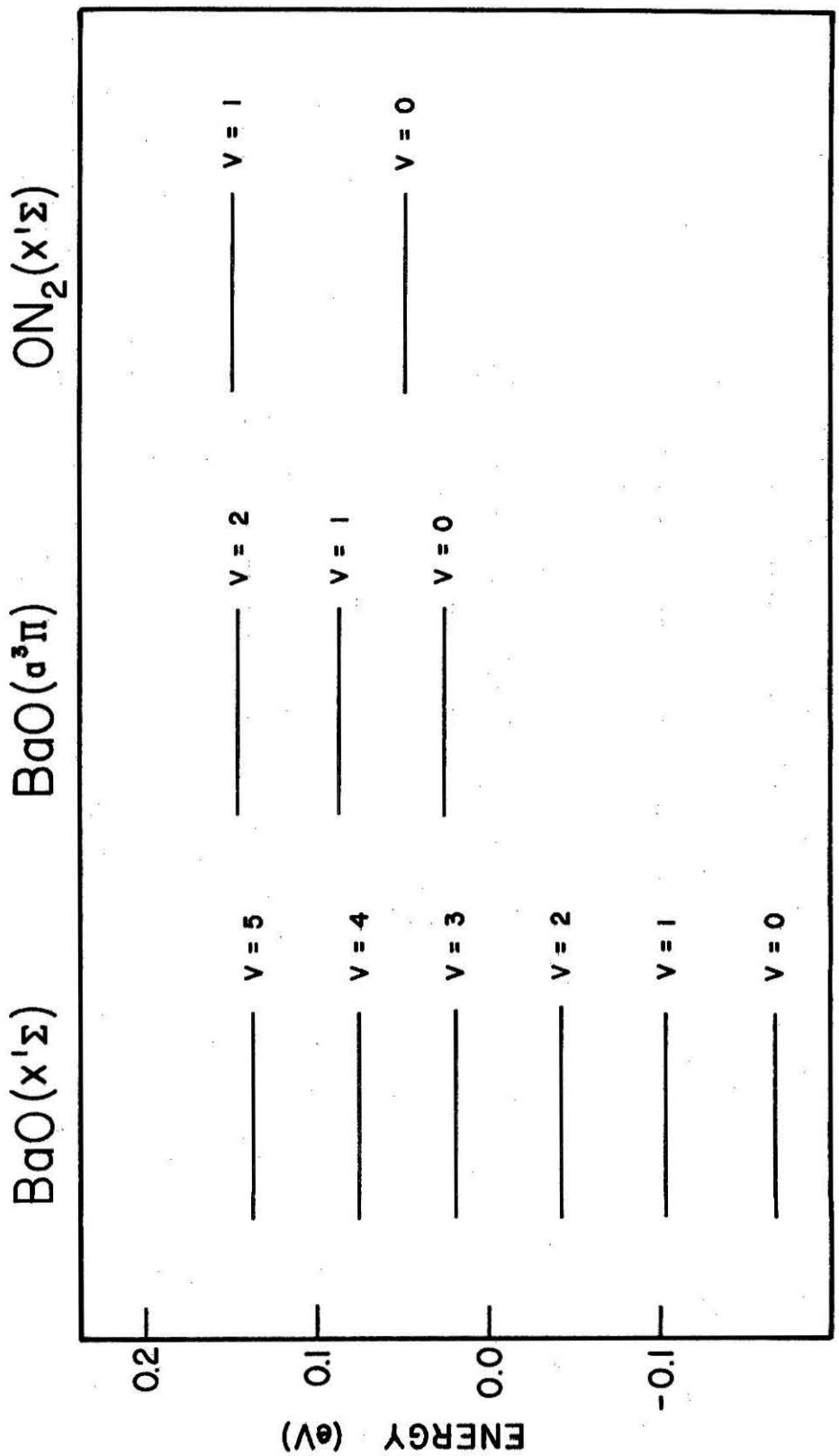
BaO(x'Σ)
BaO(a³Π)
ON₂(x'Σ)
v = 5
v = 4
v = 3
v = 2
v = 1
v = 0
v = 2
v = 1
v = 0
v = 1
v = 0
0.2
0.1
0.0
-0.1
ENERGY (eV)

Figure 7

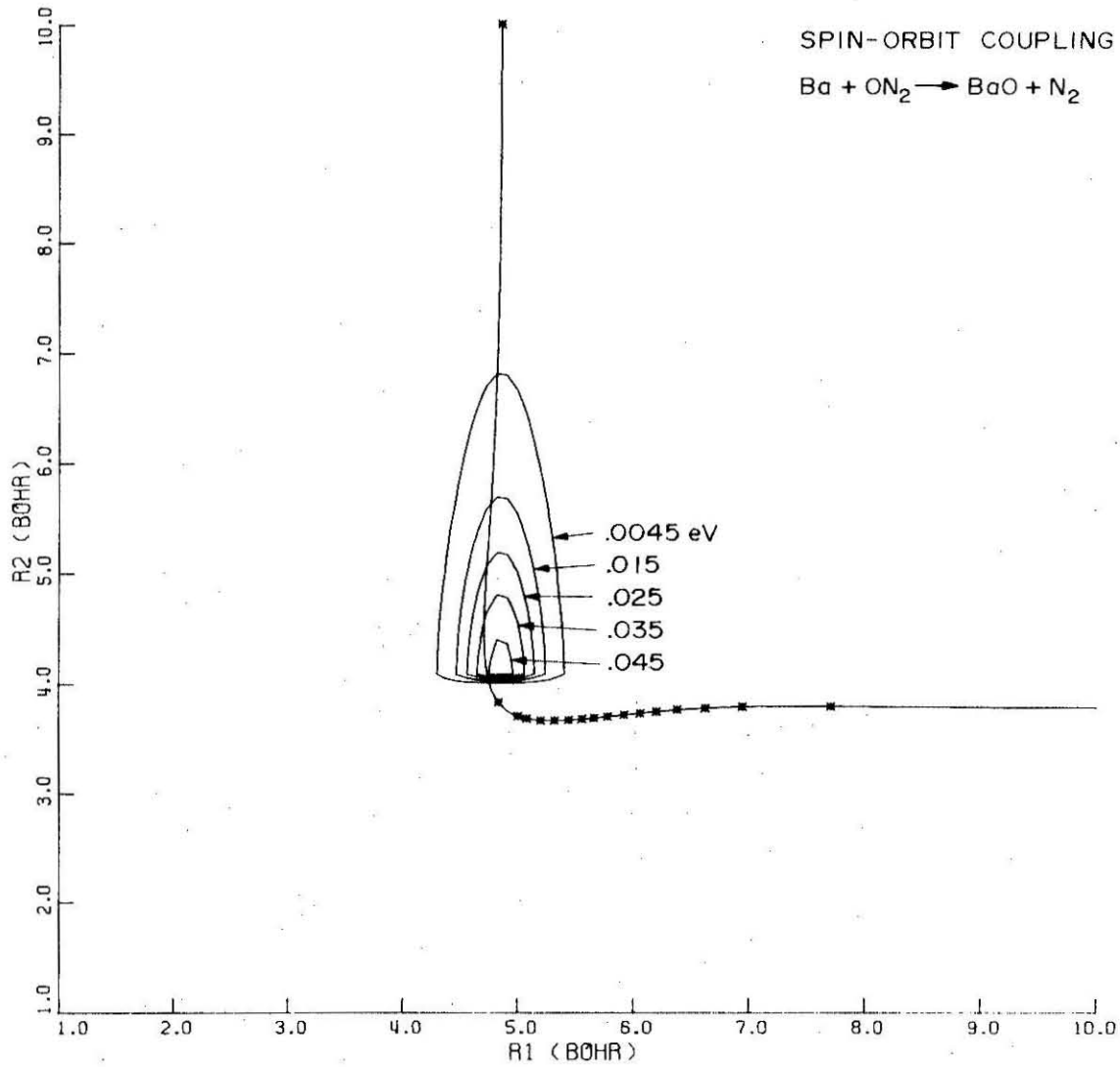
SPIN-ORBIT COUPLING
Ba + ON2 → BaO + N2
.0045 eV
.015
.025
.035
.045
R2 (BOHR)
R1 (BOHR)
1.0
2.0
3.0
4.0
5.0
6.0
7.0
8.0
9.0
10.0

Figure 8

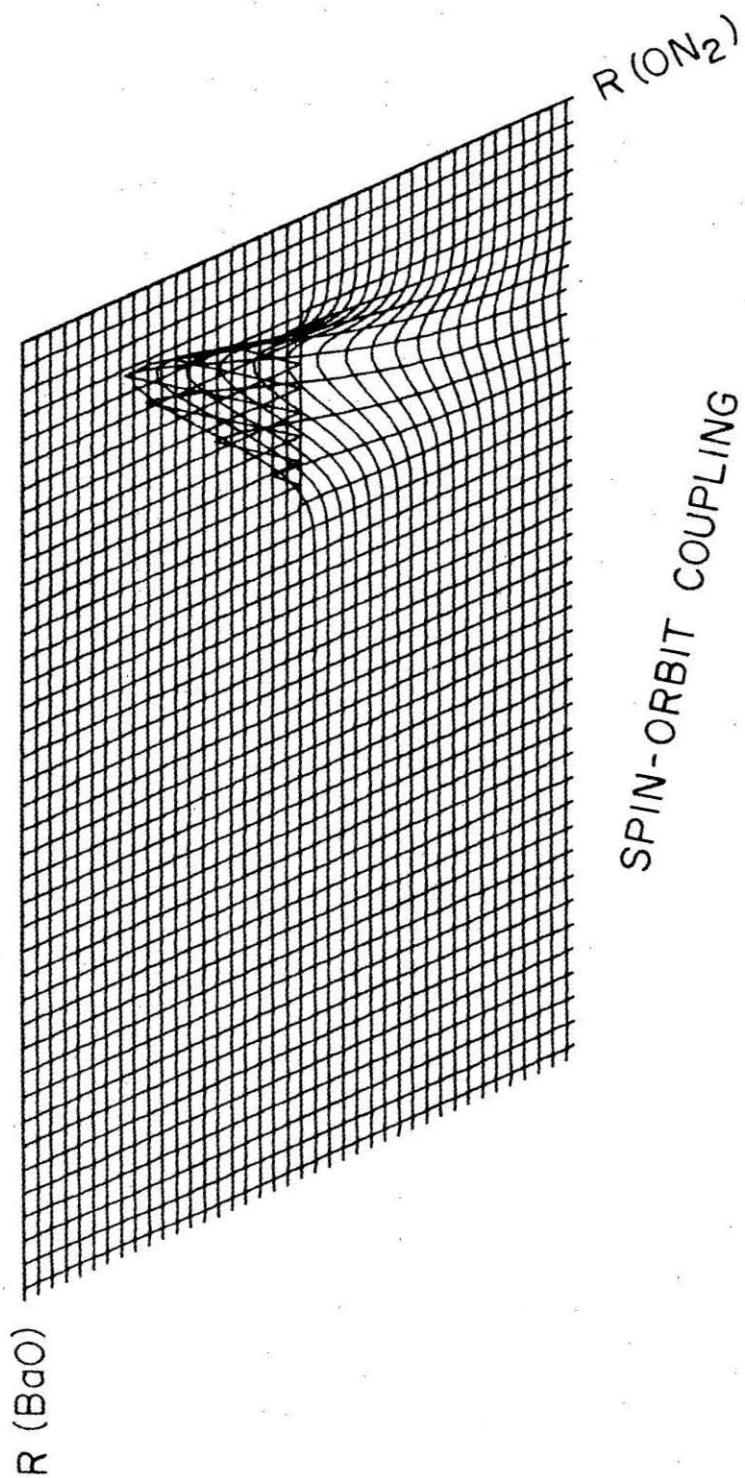

Figure 9

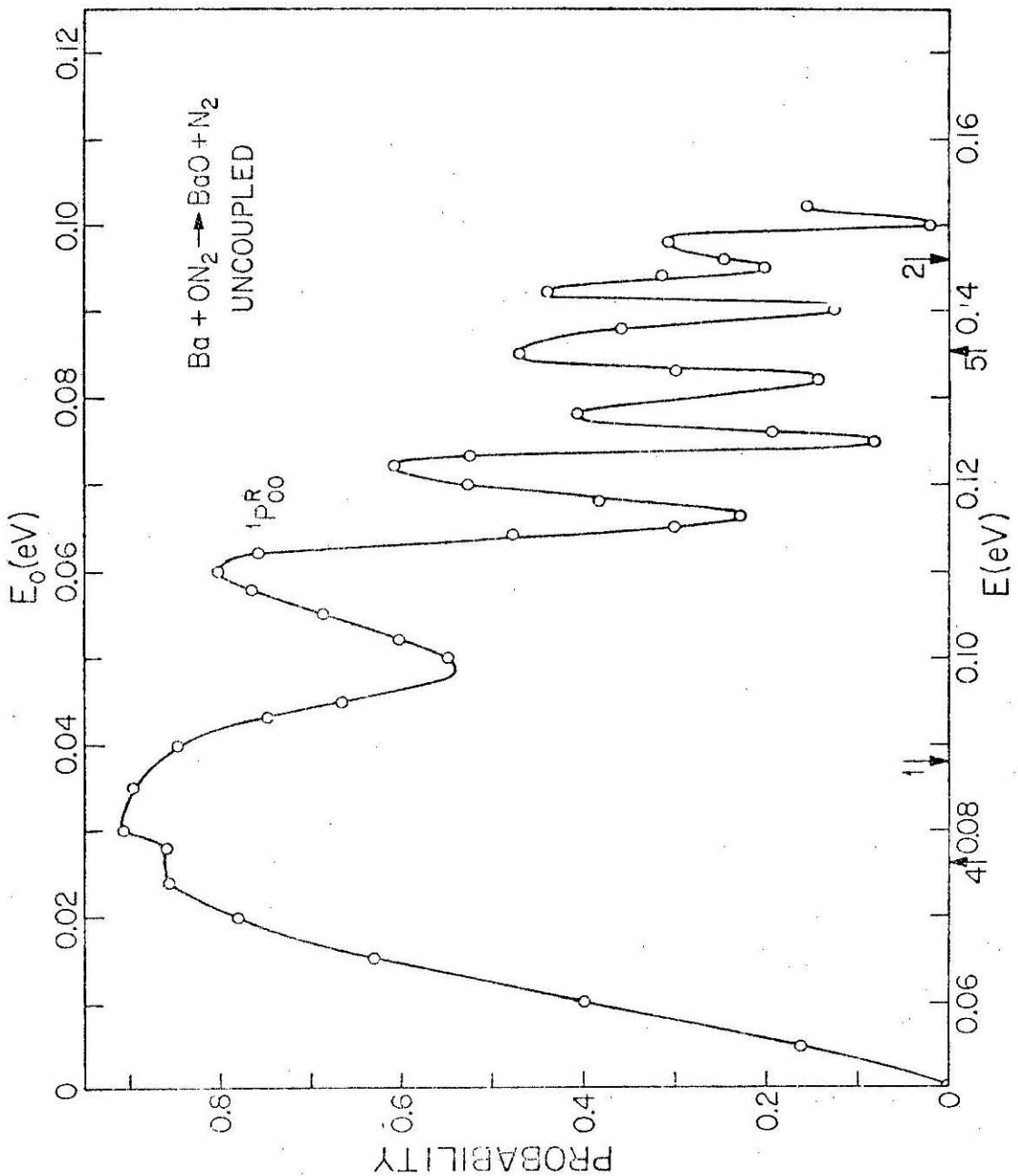
Ba + ON2 → BaO + N2
UNCOUPLED
1P00R
E0(eV)
E(eV)
PROBABILITY
0
0.02
0.04
0.06
0.08
0.10
0.12
0.16
0.2
0.4
0.6
0.8
1
2
4
5

Figure 10

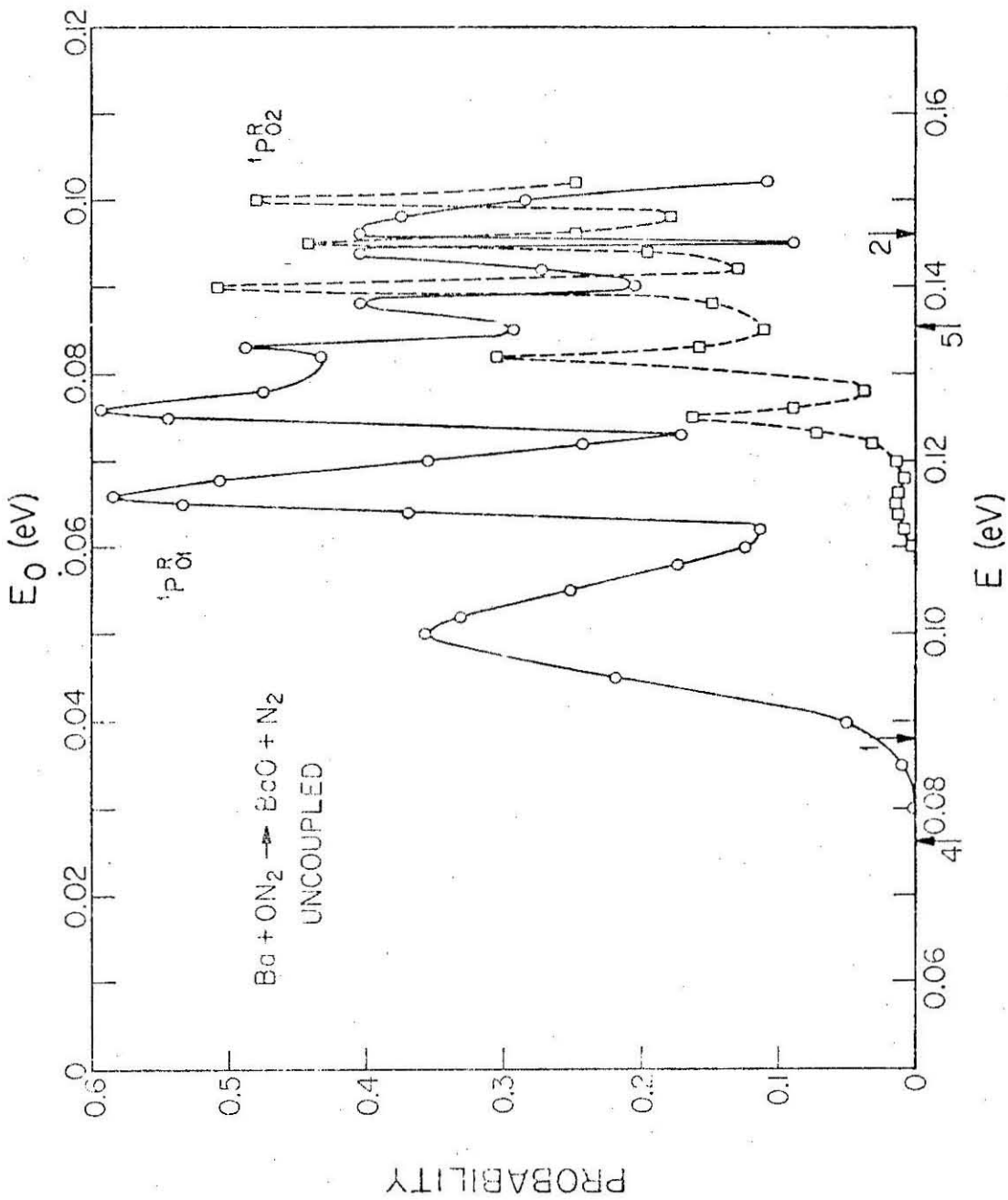
E_0 (eV)
E (eV)
PROBABILITY
$^1P^R_{\delta 1}$
$^1P^R_{\delta 2}$
Ba + ON_2 → BaO + N_2
UNCOUPLED
1
2
4
5

Figure 11

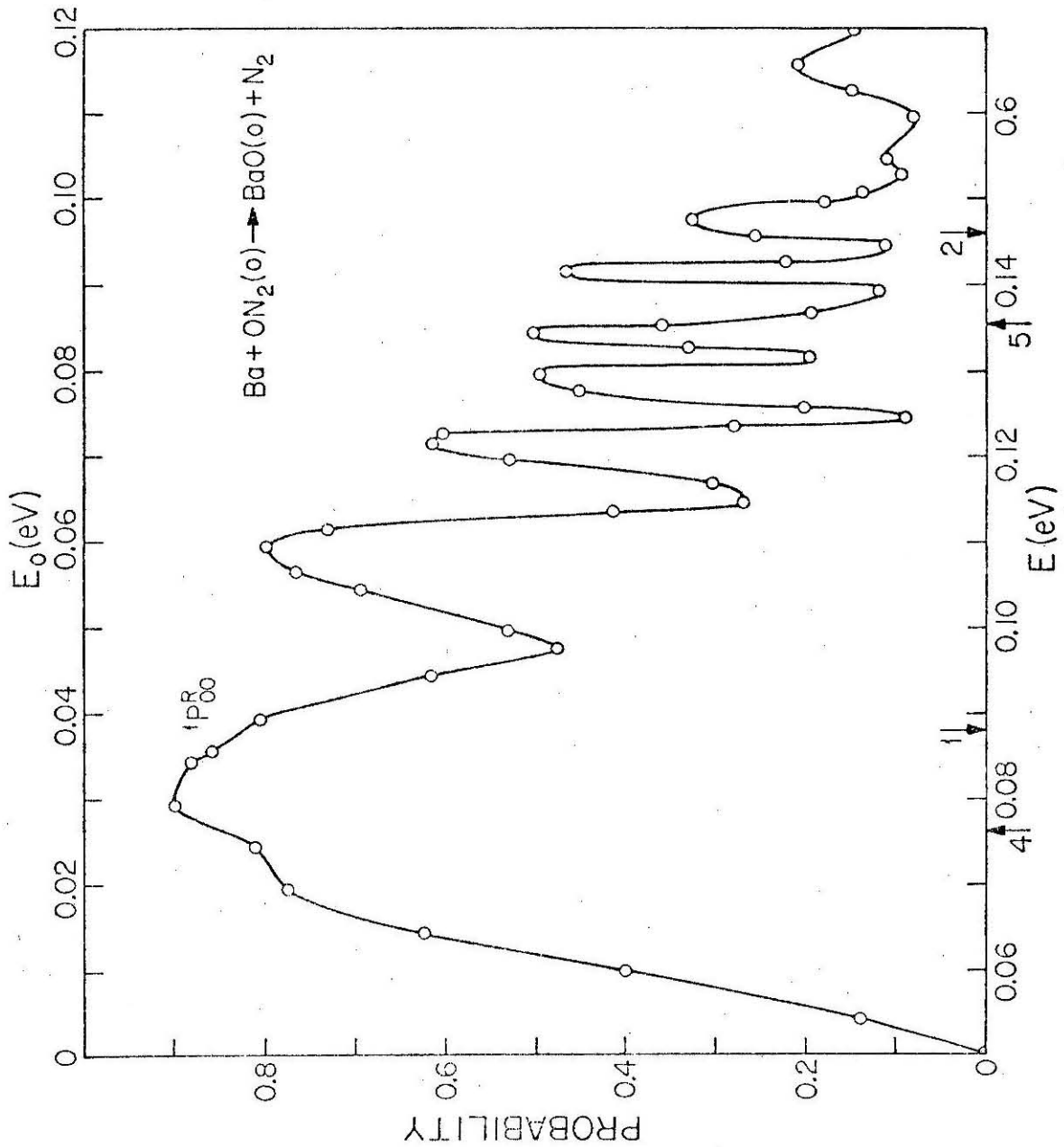
Ba + ON2(o) → BaO(o) + N2
E0(eV)
E (eV)
PROBABILITY
1PR00
0
0.02
0.04
0.06
0.08
0.10
0.12
0.14
0.2
0.4
0.6
0.8
1
2
4
5

Figure 12

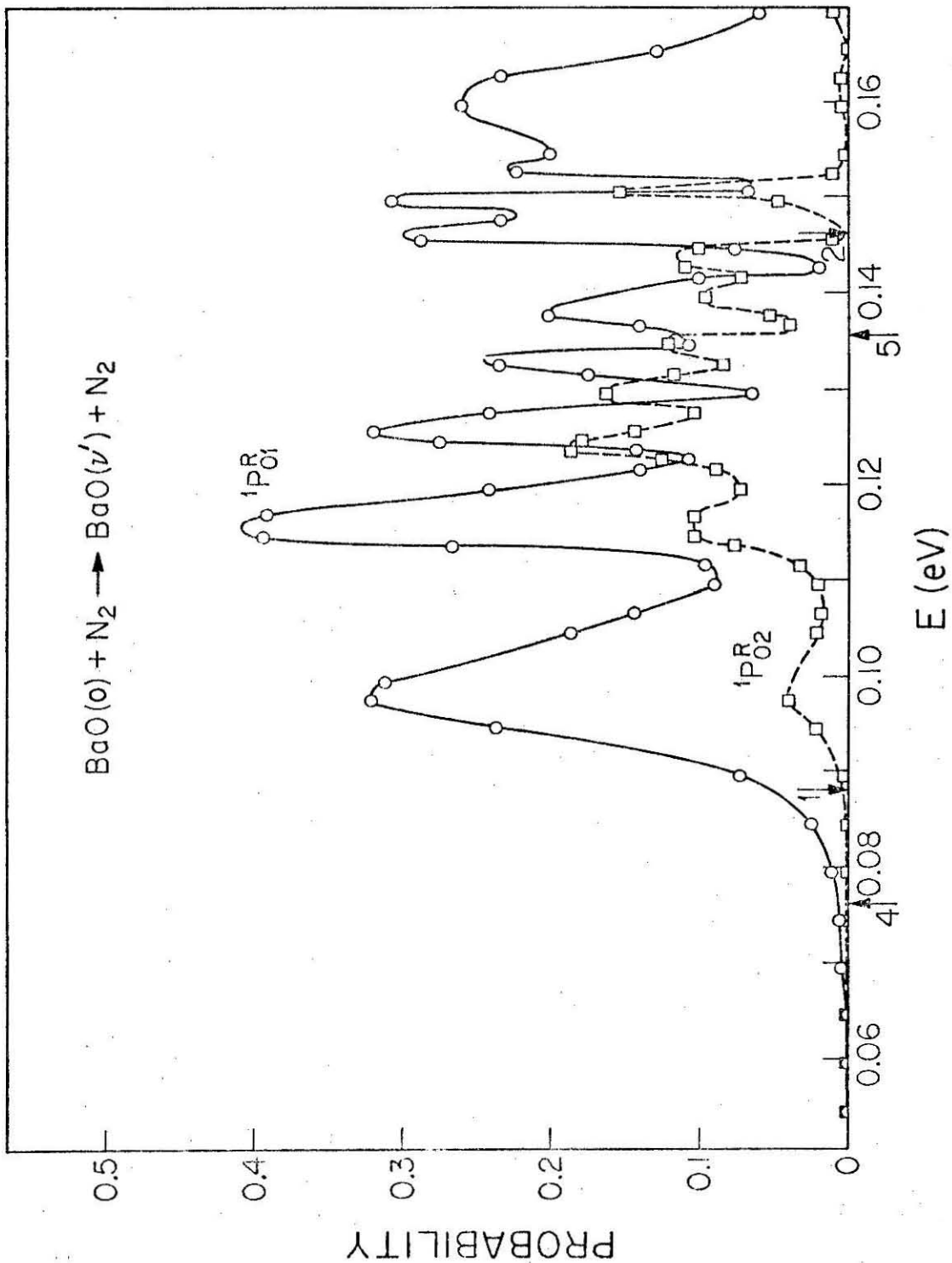
BaO(o) + N2 ⟶ BaO(v′) + N2
1PR01
1PR02
PROBABILITY
E (eV)
0.5
0.4
0.3
0.2
0.1
0
0.06
0.08
0.10
0.12
0.14
0.16
1
2
4
5

Figure 13

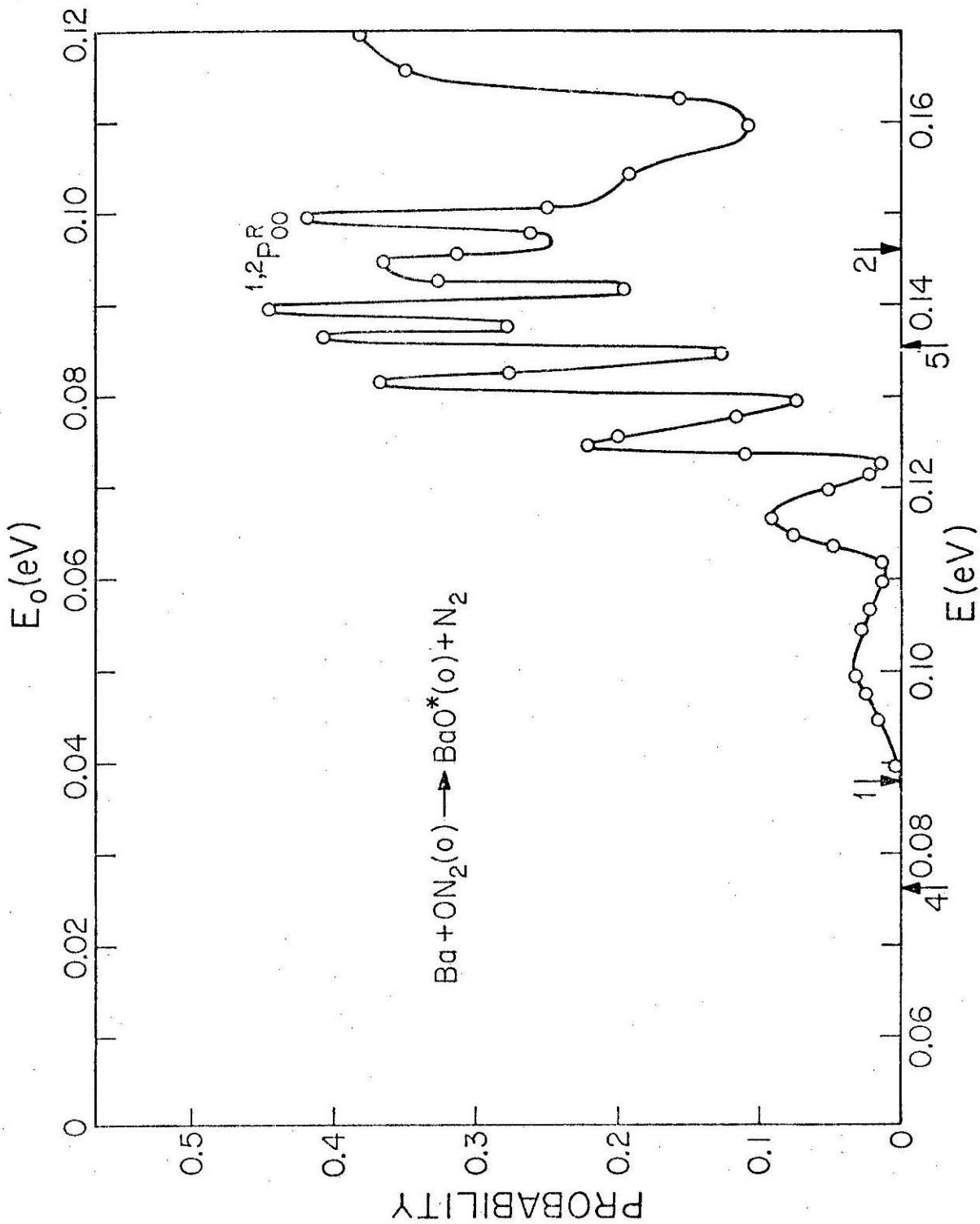
PROBABILITY
0
0.1
0.2
0.3
0.4
0.5
E(eV)
0.06
0.08
0.10
0.12
0.14
0.16
1
2
4
5
E_o(eV)
0
0.02
0.04
0.06
0.08
0.10
0.12
$^{1,2}P_{00}^{R}$
$Ba + ON_2(o) \longrightarrow BaO^*(o) + N_2$

Figure 14

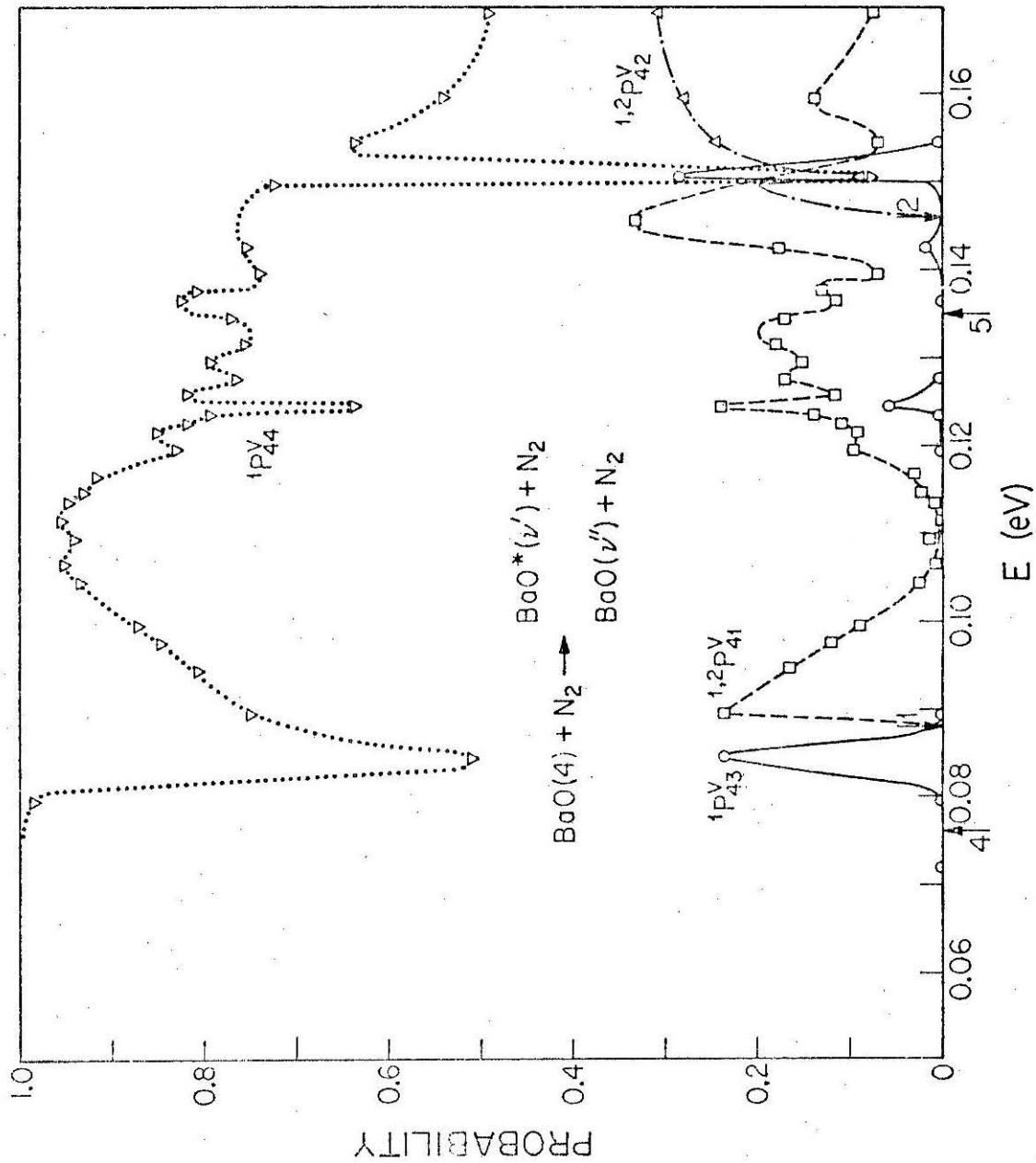
PROBABILITY
1.0
0.8
0.6
0.4
0.2
0
0.06
0.08
0.10
0.12
0.14
0.16
E (eV)
4
5
$^1P^V_{44}$
$^1P^V_{43}$
$^{1,2}P^V_{41}$
$^{1,2}P^V_{42}$
BaO(4') + N_2
BaO*(ν') + N_2
BaO(ν'') + N_2

Figure 15

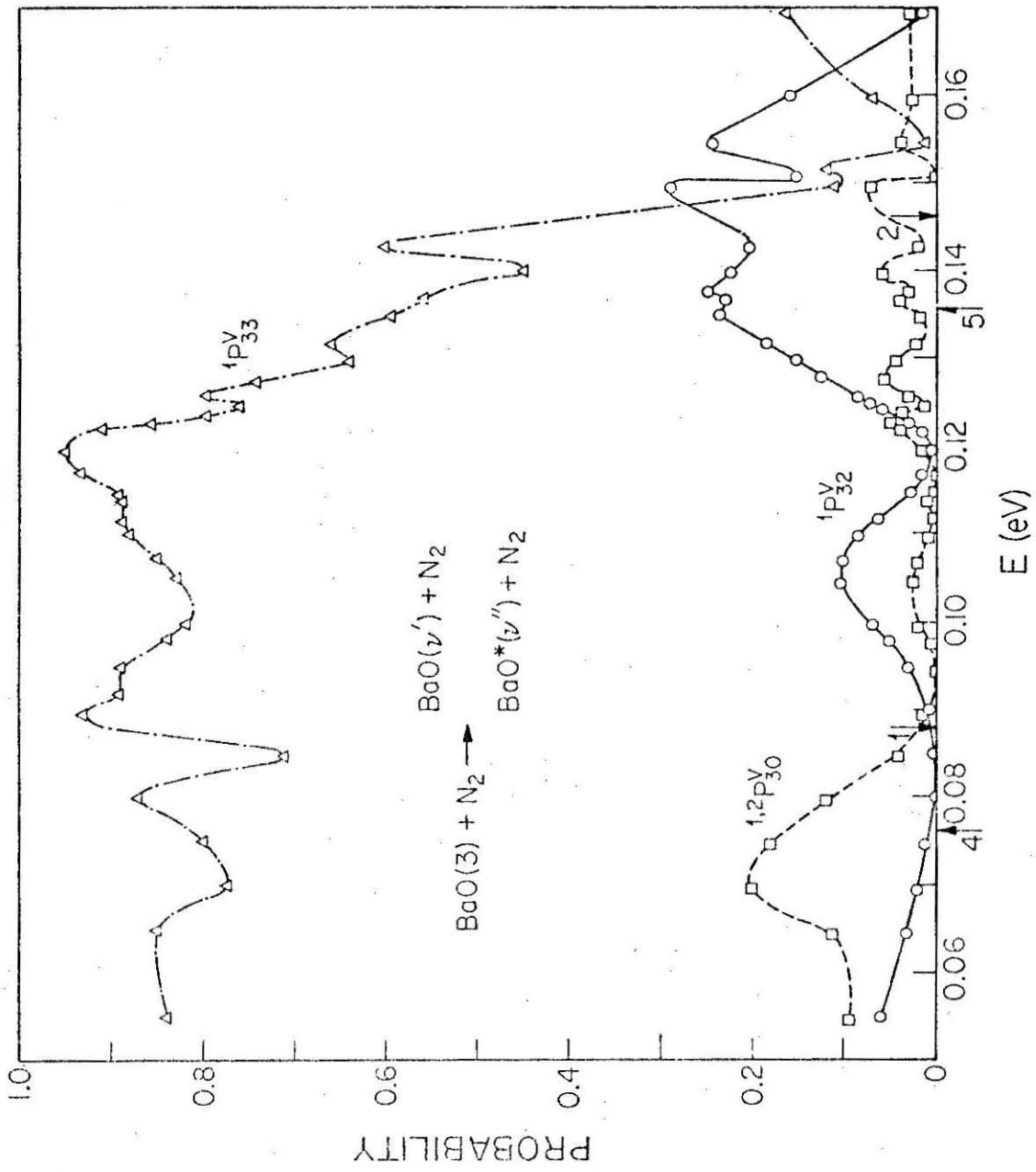
PROBABILITY
1.0
0.8
0.6
0.4
0.2
0
0.06
0.08
0.10
0.12
0.14
0.16
E (eV)
$^1PV_{33}$
$^1PV_{32}$
$^{1,2}PV_{30}$
BaO(3) + N_2
BaO(ν′) + N_2
BaO*(ν″) + N_2
1
2
4
5

Figure 16

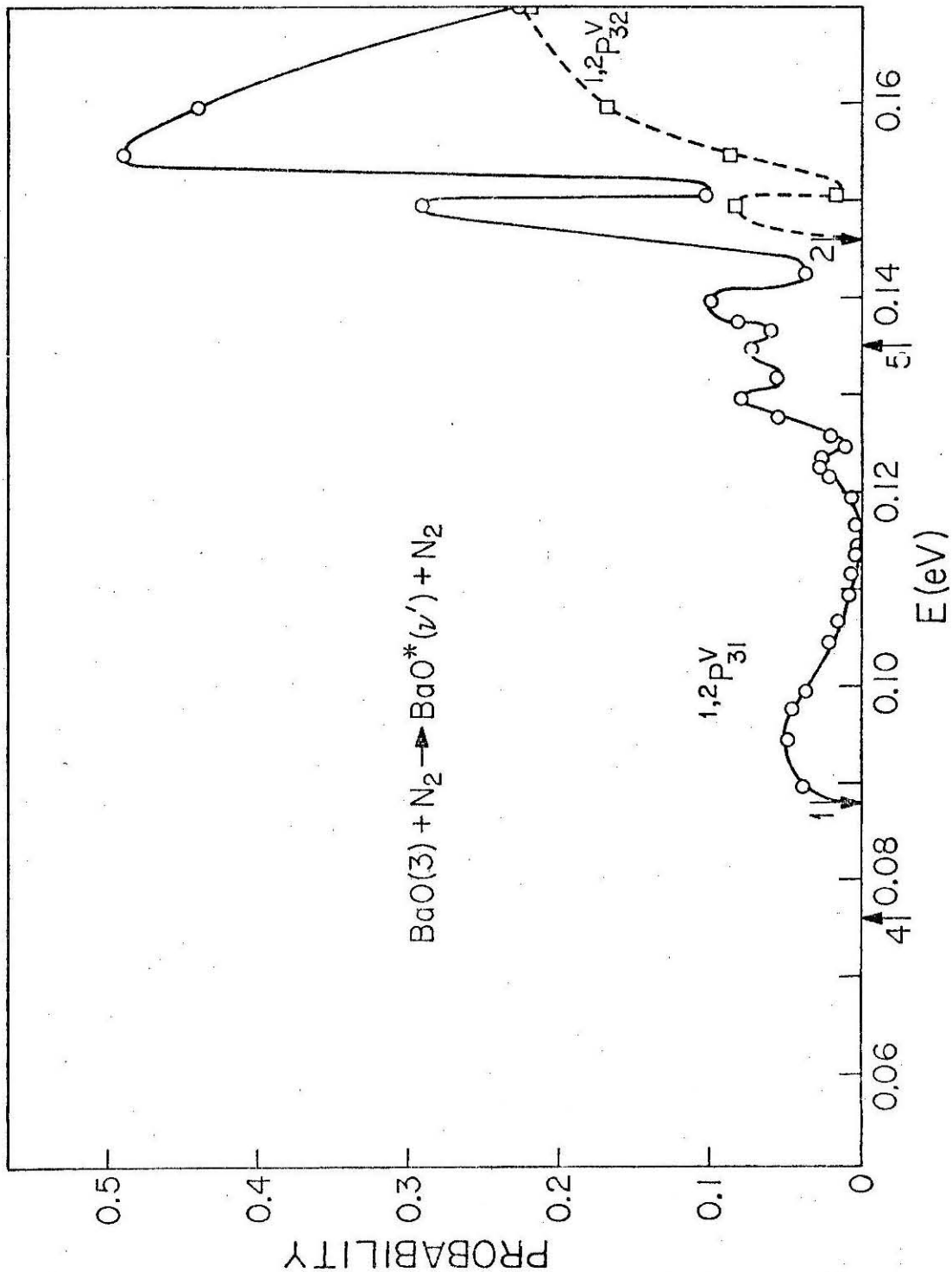
PROBABILITY
0.5
0.4
0.3
0.2
0.1
0
0.06
0.08
0.10
0.12
0.14
0.16
E (eV)
4
1
5
2
$^{1,2}P^{V}_{31}$
$^{1,2}P^{V}_{32}$
$BaO(3) + N_2 \rightarrow BaO^*(v') + N_2$

Figure 17

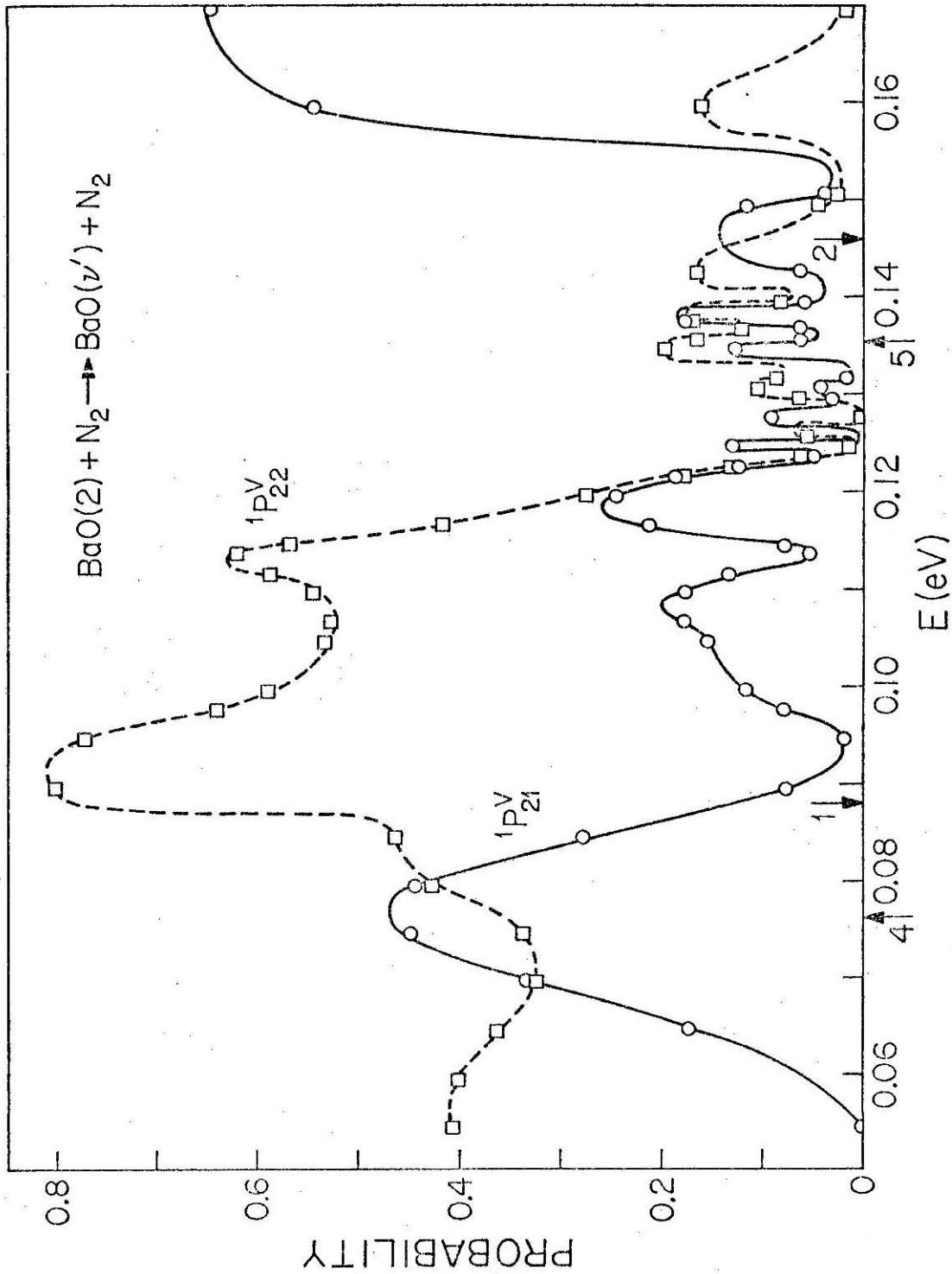
BaO(2) + N2 → BaO(v') + N2
1PV22
1PV21
1
2
4
5
0.06
0.08
0.10
0.12
0.14
0.16
E (eV)
0
0.2
0.4
0.6
0.8
PROBABILITY

Figure 18

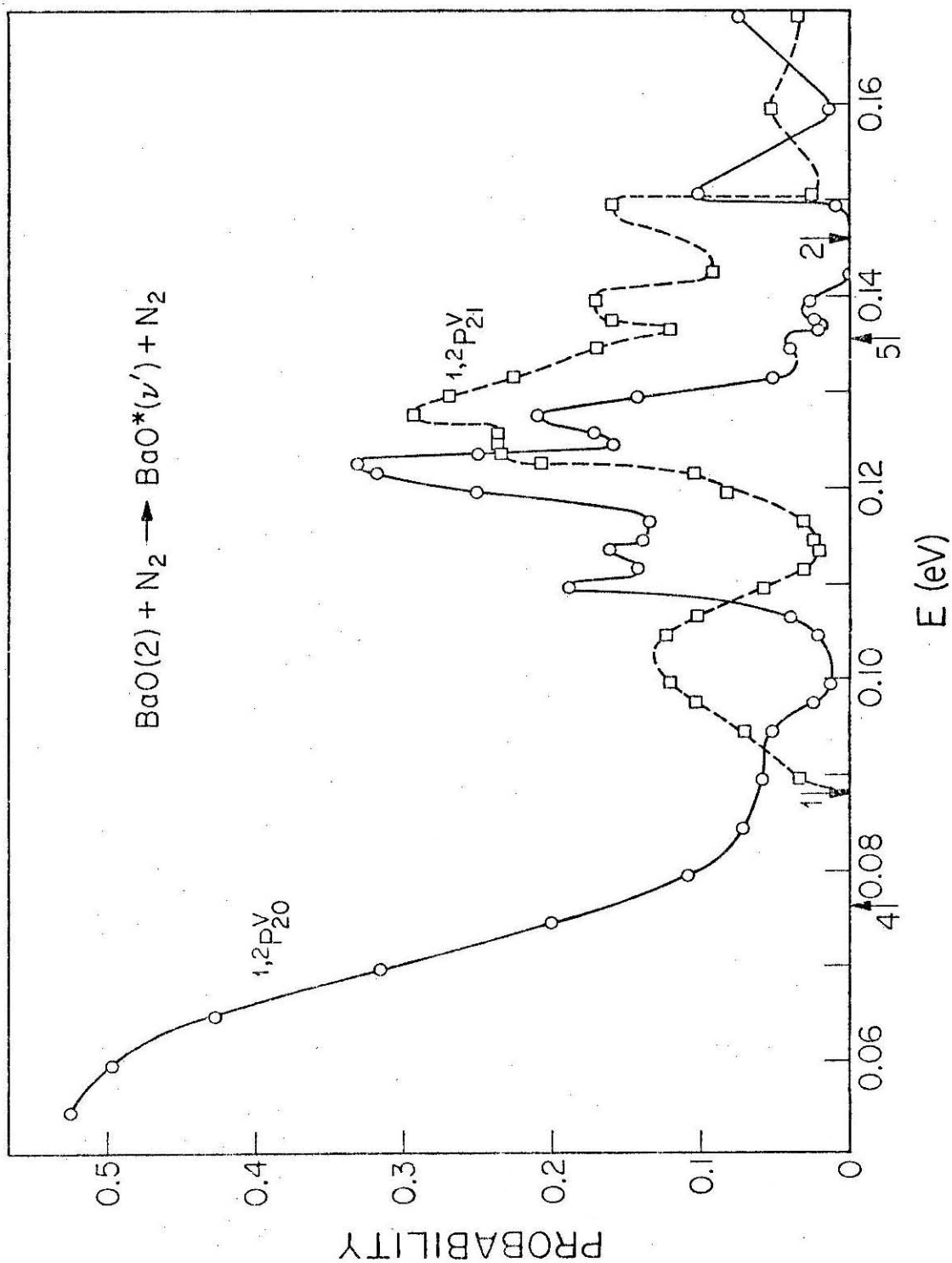
BaO(2) + N2 → BaO*(v') + N2
1,2PV20
1,2PV21
PROBABILITY
E (eV)
0.5
0.4
0.3
0.2
0.1
0
0.06
0.08
0.10
0.12
0.14
0.16
4
1
5
2

Figure 19

Appendix 1: Born-Oppenheimer Coupling Terms in the Two-State Approximation

In this appendix eqs. (33c) - (33e) are derived. The derivation makes use of the assumption that the two-state expansion is complete.

By definition,

$$F_{ij} = \langle \chi_i | \frac{d}{dx} | \chi_j \rangle_{el},$$

$$T_{ij}'' = - \frac{\hbar^2}{2\mu} \langle \chi_i | \frac{d^2}{dx^2} | \chi_j \rangle_{el}.$$

Thus, to derive eqs. (33c) and (33d) we must show that

$$\langle \chi_1 | \frac{d^2}{dx^2} | \chi_2 \rangle_{el} = \frac{dF_{12}}{dx} \tag{A1}$$

$$\langle \chi_2 | \frac{d^2}{dx^2} | \chi_1 \rangle_{el} = - \frac{dF_{12}}{dx} . \tag{A2}$$

According to its definition above

$$\frac{dF_{12}}{dx} = \langle \frac{d\chi_1}{dx} | \frac{d}{dx} | \chi_2 \rangle_{el} + \langle \chi_1 | \frac{d^2}{dx^2} | \chi_2 \rangle_{el}. \tag{A3}$$

The term $\langle \frac{d\chi_1}{dx} | \frac{d\chi_2}{dx} \rangle_{el}$ is identically zero in the two-state approximation. This follows from the fact that

$$\langle \chi_i | \frac{d}{dx} | \chi_i \rangle_{el} = 0 \tag{A4}$$

which state that $\frac{d}{dx} \chi_i$ has a non-zero projection with the state χ_j only ($j \neq i$). Thus, eq. (A1) is proved and eq. (A2) follows from eqs. (11a) and (12a). This completes the proof of eqs. (33c) and (33d).

To prove eq. (33e) we note that from (A4)

$$\frac{d}{dx}\langle\chi_i|\frac{d}{dx}|\chi_i\rangle_{el}=0$$

so that

$$-\langle\frac{d\chi_i}{dx}|\frac{d\chi_i}{dx}\rangle_{el}=\langle\chi_i|\frac{d^2}{dx^2}|\chi_i\rangle_{el}\,. \tag{A5}$$

However, we know that

$$\frac{d\chi_i}{dx}=F_{ij}\chi_j$$

and we have the result that

$$\langle\chi_i|\frac{d^2}{dx^2}|\chi_i\rangle_{el}=-F_{ij}^{\,2}\,. \tag{A6}$$

Finally making use of eqs. (11a) and (12a) we have the result that

$$\langle\chi_1|\frac{d^2}{dx^2}|\chi_2\rangle_{el}=\langle\chi_2|\frac{d^2}{dx^2}|\chi_1\rangle_{el}=-F_{12}^{\,2}$$

and hence

$$T_{11}''=T_{22}''=\frac{\hbar^2}{2\mu}F_{12}^{\,2}$$

which is identical to eq. (33e).

Appendix 2: The Transformation From the Diabatic to the Adiabatic Representations in the Two-State Approximation

To transform from the diabatic equations (35a) and (35b) to the adiabatic ones (34a) and (34b) requires a unitary transformation, $\underline{C}$, of the basis functions $\chi_1^{\,d}$ and $\chi_2^{\,d}$. This matrix transformation can be written as [38]

$$\begin{bmatrix} \chi_1^{\,a} \\ \chi_2^{\,a} \end{bmatrix} = \begin{bmatrix} \cos\alpha & \sin\alpha \\ -\sin\alpha & \cos\alpha \end{bmatrix} \begin{bmatrix} \chi_1^{\,d} \\ \chi_2^{\,d} \end{bmatrix} \tag{A7}$$

where the unitary matrix diagonalizes $\underline{U}^d(x)$ at all x. Hence, the quantity α is a function of x. Before proceeding, we rewrite the diabatic equations in matrix form as follows:

$$\left\{ -\frac{\hbar^2}{2\mu} \begin{bmatrix} \frac{d^2}{dx^2} & 0 \\ 0 & \frac{d^2}{dx^2} \end{bmatrix} + \begin{bmatrix} H_{11} & H_{12} \\ H_{21} & H_{22} \end{bmatrix} - E \begin{bmatrix} 1 & 0 \\ 0 & 1 \end{bmatrix} \right\} \begin{bmatrix} \psi_1^{\,d} \\ \psi_2^{\,d} \end{bmatrix} = 0. \tag{A8}$$

The unitary transformation of this equation by $\underline{C}$ leaves the identity matrix unchanged and by design it diagonalized the $\underline{U}^d$ matrix. Thus, it remains to investigate its action on the kinetic energy operator matrix. By the theorem of representation theory [40] the transformed kinetic energy operator matrix, $\underline{T}'$, is related to the original one $\underline{T}$ by

$$\underline{T}' = \underline{C}\,\underline{T}\,\underline{C}^{\dagger} \,, \tag{A9}$$

where $\underline{C}^{\dagger}$ is the adjoint of $\underline{C}$. Since $\underline{C}$ is real, $\underline{C}^{\dagger}$ is simply the transpose of $\underline{C}$, $\underline{C}^{t}$. Thus, we have three matrix multiplications to perform to obtain $\underline{T}'$, namely

$$\begin{bmatrix} \cos\alpha(x) & \sin\alpha(x) \\ -\sin\alpha(x) & \cos\alpha(x) \end{bmatrix} \begin{bmatrix} \frac{d^2}{dx^2} & 0 \\ 0 & \frac{d^2}{dx^2} \end{bmatrix} \begin{bmatrix} \cos\alpha(x) & -\sin\alpha(x) \\ \sin\alpha(x) & \cos\alpha(x) \end{bmatrix} \tag{A10}$$

It is straightforward to show that the resulting matrix is

$$-2\mu\hbar^2\underline{T}' = \begin{bmatrix} -\gamma^2 + \frac{d^2}{dx^2} & -(\frac{d\gamma}{dx} + 2\gamma\frac{d}{dx}) \\ \frac{d\gamma}{dx} + 2\gamma\frac{d}{dx} & -\gamma^2 + \frac{d^2}{dx^2} \end{bmatrix} \tag{A11}$$

Thus, the transformed coupled equations are given by

$$[-\frac{\hbar^2}{2\mu}\frac{d^2}{dx^2} + \frac{\hbar^2\gamma^2}{2\mu} + E_1(x) - E]\psi_1^d = \frac{\hbar^2}{2\mu}[\frac{d\gamma}{dx} + 2\gamma\frac{d}{dx}]\psi_2^d \tag{A12a}$$

$$[-\frac{\hbar^2}{2\mu}\frac{d^2}{dx^2} + \frac{\hbar^2\gamma^2}{2\mu} + E_2(x) - E]\psi_2^d = -\frac{\hbar^2}{2\mu}[\frac{d\gamma}{dx} + 2\gamma\frac{d}{dx}]\psi_2^d. \tag{A12b}$$

$E_1(x)$ and $E_2(x)$ are the eigenvalues of the $\underline{U}^d$ matrix and within the two-state approximation they are identical to the adiabatic potential curves of eqs. (32a) and (32b). From inspection of eqs. (A12a) and (A12b) and eqs. (32a) and (32b), in order to establish the equivalence of these sets of equations it must be demonstrated that

$$\gamma = F_{12} \quad . \tag{A13}$$

The general proof of eq. (A13) involves much algebra. We shall

demonstrate that it is true at the crossing point of the two diabatic curves H_{11} and H_{22}.

The function γ is related to α by

$$\gamma = \frac{d\alpha}{dx} \quad ,$$

where α is determined by the eigenvalue equation which results from the diagonalization of the $\underline{U}^d$ matrix and is given by

$$\tan 2\alpha(x) = 2H_{12}(x)/[H_{22}(x) - H_{11}(x)] \quad . \tag{A14}$$

Hence, at the crossing point

$$\gamma = \frac{d}{dx}(H_{11}-H_{22})/4H_{12} \quad . \tag{A15}$$

For the two-state approximation it can be shown trivially that

$$F_{12} = \langle \chi_1{}^a | \frac{d}{dx} H^{el} | \chi_2{}^a \rangle / [E_2(x) - E_1(x)] \tag{A16}$$

and from the diagonalization of $\underline{U}^d$ that

$$E_{1(2)} = \frac{H_{11} + H_{22}}{2} \quad (\mp) \sqrt{\tfrac{1}{4}(H_{11}-H_{22})^2 + H_{12}{}^2} \quad . \tag{A17}$$

Thus, at the crossing point

$$E_2 - E_1 = 2H_{12}$$

and hence from eq. (A16)

$$F_{12} = \langle \chi_1{}^a | \frac{d}{dx} H^{el} | \chi_2{}^a \rangle / 2H_{12}. \tag{A18}$$

From eq. (A1) we can express $\chi_1{}^a$ and $\chi_2{}^a$ in terms of $\chi_1{}^d$ and $\chi_1{}^d$

and if we substitute the resulting expressions into (A18) we obtain

$$F_{12} = \sin\alpha\cos\alpha(\langle\chi_1^d|\frac{d}{dx}H^{el}|\chi_1^d\rangle - \langle\chi_2|\frac{d}{dx}H^{el}|\chi_2\rangle)$$

$$+ \cos^2\alpha\ \langle\chi_1^d|\frac{d}{dx}H^{el}|\chi_2^d\rangle - \sin^2\alpha\ \langle\chi_2^d|\frac{d}{dx}H^{el}|\chi_1^d\rangle \quad . \qquad \text{(A19)}$$

Making use of the fact that

$$\langle\chi_i^d|\frac{d}{dx}H^{el}|\chi_j^d\rangle = \frac{d}{dx}\langle\chi_i^d|H^{el}|\chi_j^d\rangle \ , \quad i,j = 1,2 \quad , \text{(A20)}$$

we can rewrite (A19) as

$$F_{12} = \sin\alpha\cos\alpha\frac{d}{dx}(H_{11}-H_{22}) + \cos^2\alpha - \sin^2\alpha\frac{dH_{12}}{dx} \quad . \qquad \text{(A21)}$$

From eq. (A14), at the crossing point, we have that

$$\cot 2\alpha = 0$$

which from the identity

$$\frac{\cos^2\alpha - \sin^2\alpha}{\sin\alpha\cos\alpha} = \cot 2\alpha$$

implies that

$$\cos^2\alpha - \sin^2\alpha = 0$$

and further that

$$\sin\alpha\cos\alpha = \tfrac{1}{2} \quad .$$

Hence from (A15) we have the result that

$$F_{12} = \frac{d}{dx}(H_{11} - H_{22})/4H_{12}$$

which is identical to (A15) establishing that at the crossing point

$$F_{12} = \gamma \quad .$$

This equality is valid for all values of the internuclear distance.

Thus, we have demonstrated that the diabatic and adiabatic representations are equivalent in the two-state approximation.

Appendix 3: The Coupled Differential Equations for the Two-State Atom-Molecule Chemical Reaction

In this appendix we develop the close-coupling technique used to solve the coupled partial differential equations (25a) and (25b) for the electronically non-adiabatic chemical reaction $A + BC \rightarrow AB + C$, $AB^* + C$. As a relevant example we assume that these equations describe the non-adiabatic coupling between a singlet and triplet electronic state denoted respectively by the numbers 1 and 2.

According to the remarks of Section 6 H_{12} is the matrix element of the spin-orbit coupling $\hat{V}^{SO}$ in the basis set χ_i which are eigenfunctions of H^{el} without $\hat{V}^{SO}$. Thus, we rewrite the coupled eqs. (25a) and (25b) as

$$\left[-\frac{\hbar^2}{2\mu}\left(\frac{\partial^2}{\partial x_1^2} + \frac{\partial^2}{\partial x_2^2}\right) + V_1(x_1, x_2) - E \right] \psi_1(x_1, x_2) = -V_{12}^{SO}\, \psi_2(x_1, x_2) \qquad \text{(A22a)}$$

$$\left[-\frac{\hbar^2}{2\mu}\left(\frac{\partial^2}{\partial x_1^2} + \frac{\partial^2}{\partial x_2^2}\right) + V_2(x_1, x_2) - E \right] \psi_2(x_1, x_2) = -V_{12}^{SO}\, \psi_1(x_1, x_2). \qquad \text{(A22b)}$$

V_1 and V_2 are the potential energy surfaces corresponding to the singlet and triplet electronic states and V_{12}^{SO} is the matrix element $\langle \chi_1 | \hat{V}^{SO} | \chi_2 \rangle_{el}$. We require that in the limit of separated reagents and products

$$V_{12}^{SO}(x_1, x_2) \underset{x_1 \rightarrow \infty}{\sim} 0 \qquad \text{(A23)}$$

$$V_{12}^{SO}(z_1, z_2) \underset{z_1 \rightarrow \infty}{\sim} 0 \; . \qquad \text{(A24)}$$

This means that the equations (A22a) and (A22b) uncouple when the

chemical interaction is over. This may not always be rigorously true as the discussion in paper III. 3 points out. However, we shall assume that it is true in order to avoid complications in the scattering analysis of eqs. (A22a) and (A22b) presented in Appendix 4.

In the asymptotic regions of space describing the separated reagents and products eqs. (A22a) and (A22b) become

$$\left[-\frac{\hbar^2}{2\mu}\left(\frac{\partial^2}{\partial x_1^2} + \frac{\partial^2}{\partial x_2^2}\right) + V_1^0(x_2) - E\right] \psi_1(x_1, x_2) = 0 \qquad \text{(A25a)}$$

$$\left[-\frac{\hbar^2}{2\mu}\left(\frac{\partial^2}{\partial x_1^2} + \frac{\partial^2}{\partial x_2^2}\right) + V_2^0(x_2) - E\right] \psi_2(x_1, x_2) = 0 \qquad \text{(A25b)}$$

and analogous equations exist in the (z_1, z_2) coordinates describing the rearrangement channel. We have made use of the fact that

$$V_i(x_2, x_3) \underset{x_3 \to \infty}{\sim} V_i^0(x_2), \quad i = 1, 2$$

as well as eqs. (A23) and (A24). The potentials $V_i^0(x_2)$ describe the unperturbed internal motion of the BC molecule in the ith electronic state. Thus, the general solutions to eqs. (A25a) and (A25b) are given by

$$\psi_1(x_1, x_2) \underset{x_1 \to \infty}{\sim} \begin{cases} \sum_{i=1}^{N1} \left[A_i e^{ik_i^{(1)} x_1} + B_i e^{-ik_i^{(1)} x_1} \right] \phi_i^{(1)}(x_2), & \text{(A26a)} \\ \sum_{j=N1+1}^{\infty} \left[a_j e^{\kappa_j^{(1)} x_1} + b_j e^{-\kappa_j^{(1)} x_1} \right] \phi_j^{(1)}(x_2), & \text{(A26b)} \end{cases}$$

$$\psi_2(x_1, x_2) \underset{x_1 \to \infty}{\sim} \begin{cases} \sum_{i=1}^{N2} \left[C_i e^{ik_i^{(2)} x_1} + D_i e^{-ik_i^{(2)} x_1} \right] \phi_i^{(2)}(x_2), & \text{(A27a)} \\ \sum_{j=N2+1}^{\infty} \left[c_j e^{\kappa_j^{(2)} x_1} + d_j e^{-\kappa_j^{(2)} x_1} \right] \phi_j^{(2)}(x_2) \ . & \text{(A27b)} \end{cases}$$

The BC vibrational functions $\phi_i^{(1)}$ and $\phi_j^{(2)}$ satisfy the following eigenvalue equations

$$\left[-\frac{\hbar^2}{2\mu} \frac{d^2}{dx_2^2} + V_1^0(x_2) - \varepsilon_i^{(1)} \right] \phi_i^{(1)}(x_2) = 0 \ , \qquad \text{(A28a)}$$

$$\left[-\frac{\hbar^2}{2\mu} \frac{d^2}{dx_2^2} + V_2^0(x_2) - \varepsilon_j^{(2)} \right] \phi_j^{(2)}(x_2) = 0 \ . \qquad \text{(A28b)}$$

From these equations and eq. (A25a) and (A25b) we have that

$$E = \begin{cases} \varepsilon_i^{(1)} + \dfrac{\hbar^2 k_i^{(1)^2}}{2\mu} \ , & i = 1, \ldots, N1 \\ \varepsilon_i^{(1)} - \dfrac{\hbar^2 \kappa_i^{(1)^2}}{2\mu} \ , & i = N1+1, \ldots, \infty \\ \varepsilon_i^{(2)} + \dfrac{\hbar^2 k_i^{(2)^2}}{2\mu} \ , & i = 1, \ldots, N2 \\ \varepsilon_i^{(2)} - \dfrac{\hbar^2 \kappa_i^{(2)^2}}{2\mu} \ . & i = N2+1, \ldots, \infty \end{cases}$$

The numbers N1 and N2 refer to the number of open vibrational channels of BC in electronic state 1 and 2 respectively at the total energy E. The number of closed vibrational channels is in practice finite, not infinite as indicated above. For future use we define M1 and M2 as the total number of channels included in the expansion

(A26) and (A27) for the BC molecule in electronic states 1 and 2 respectively. Thus, the corresponding number of closed channels is M1-N1 and M2-N2. An analogous set of equations applies for the rearrangement channels AB + C and AB^* + C.

The close coupling approach to the solution of eqs. (A22a) and (A22b) proceeds by expanding ψ_1 and ψ_2 analogously as in eqs. (A26) and (A27) as follows

$$\psi_1 = \sum_{i=1}^{M1} g_i^{(1)}(x_1)\phi_i^{(1)}(x_2) \tag{A29}$$

$$\psi_2 = \sum_{j=M1+1}^{M1+M2} g_j^{(2)}(x_1)\phi_j^{(2)}(x_2) \quad . \tag{A30}$$

Substitution of eqs. (A29) and (A30) into eqs. (A22a) and (A22b) yields

$$\sum_{i=1}^{M1} \left[-\frac{\hbar^2}{2\mu}\left(\frac{\partial^2}{\partial x_1^2} + \frac{\partial^2}{\partial x_2^2}\right) + V_1(x_1, x_2) - E\right] g_i^{(1)}(x_1)\phi_i^{(1)}(x_2)$$

$$= \sum_{j=M2+1}^{M1+M2} - V_{12}^{SO}\, g_j^{(2)}(x_1)\phi_j^{(2)}(x_2) \ , \tag{A31a}$$

$$\sum_{j=1+M1}^{M1+M2} \left[-\frac{\hbar^2}{2\mu}\left(\frac{\partial^2}{\partial x_1^2} + \frac{\partial^2}{\partial x_2^2}\right) + V_2(x_1, x_2) - E\right] g_j^{(2)}(x_1)\phi_j^{(2)}(x_2)$$

$$= \sum_{i=1}^{M1} -V_{12}^{SO}(x_1, x_2) g_i^{(1)}(x_1)\phi_i^{(1)}(x_2). \tag{A31b}$$

Making use of eqs. (A28a) and (A28b) we rewrite eqs. (A31a) and (A31b) as follows

$$\sum_{i=1}^{M1} \left\{ -\frac{\hbar^2}{2\mu}\frac{\partial^2}{\partial x_1^2} + [V_1(x_1,x_2) - V_1^0(x_2)] - (E - \varepsilon_i^{(1)}) \right\} g_i^{(1)} \phi_i^{(1)}$$

$$= \sum_{j=M1+1}^{M1+M2} -V_{12}^{SO}(x_1,x_2) g_j^{(2)} \phi_j^{(2)} \quad , \quad \text{(A32a)}$$

$$\sum_{j=M1+1}^{M1+M2} \left\{ -\frac{\hbar^2}{2\mu}\frac{\partial^2}{\partial x_1^2} + [V_2(x_1,x_2) - V_2^0(x_2)] - (E - \varepsilon_j^{(2)}) \right\} g_j^{(2)} \phi_j^{(2)}$$

$$= \sum_{i=1}^{M1} -V_{12}^{SO}(x_1,x_2) g_i^{(1)} \phi_i^{(1)} \quad . \quad \text{(A32b)}$$

Now we multiply the left hand side of these equations by $\phi_k^{(1)}$ and $\phi_l^{(2)}$ respectively and integrate with respect to x_2. Making use of the orthonormality of the functions $\{\phi_k^{(1)}\}$ and the functions $\{\phi_l^{(2)}\}$ eqs. (A32a) and (A32b) become

$$\sum_{i=1}^{M1} -\frac{\hbar^2}{2\mu}\frac{d^2}{dx_1^2} g_i^{(1)} \delta_{ki} + (V_1^I)_{ki} g_i^{(1)} - (E - \varepsilon_i^{(1)}) g_i^{(1)} \delta_{ki} =$$

$$= \sum_{j=1+M1}^{M1+M2} (-V_{12}^{SO})_{kj} g_j^{(2)} \quad , \quad \text{(A33a)}$$

$$\sum_{j=M1+1}^{M1+M2} -\frac{\hbar^2}{2\mu}\frac{d^2}{dx_1^2} g_j^{(2)} \delta_{lj} + (V_2^I)_{lj} g_j^{(2)} - (E - \varepsilon_j^{(2)}) g_j^{(2)} \delta_{lj} =$$

$$= \sum_{i=1}^{M1} (+V_{12}^{SO})_{li} g_i^{(1)} \quad , \quad \text{(A33b)}$$

where,

$$(V_1^I)_{ki}(x_1) = \int dx_2 \phi_k^{(1)}(x_2)[V_1(x_1,x_2) - V_1^0(x_2)]\phi_i^{(1)}(x_2), \quad k,i=1,\ldots,M1$$

$$(V_2^I)_{1j}(x_1) = \int dx_2 \phi_1^{(2)}(x_2)[V_1(x_1,x_2) - V_1^o(x_2)]\phi_j^{(2)}(x_2), \quad 1, j=1+M1, \ldots, M1+M2$$

and

$$(V_{12}^{SO})_{kj} = \int dx_2 \phi_k^{(1)}(x_2)\, V_{12}^{SO}(x_1,x_2)\phi_j^{(2)}(x_2), \quad \begin{matrix} k = 1, \ldots, M1 \\ j = M1+1, \ldots, M1+M2 \end{matrix}$$

$$(V_{12}^{SO})_{1i} = \int dx_2 \phi_1^{(2)}(x_2)\, V_{12}^{SO}(x_1,x_2)\phi_i^{(1)}(x_2), \quad \begin{matrix} 1 = M1+1, \ldots, M1+M2 \\ i = 1, \ldots, M1 \end{matrix}$$

We now generalize the notation and write the coupled equations (A33a) and (A33b) in matrix form. First, we note that ψ_1 and ψ_2 given by eqs. (A29) and (A30) are only two of a set of 2(M1 + M2) linearly independent solutions to the coupled "Schrödinger" equations (A22a) and (A22b). Indeed, we have in general

$$\psi_1^m(x_1,x_2) = \sum_{i=1}^{M1} \phi_i^{(1)}(x_2)\, g_{im}^{(1)}(x_1), \quad m = 1, \ldots, M1 \qquad \text{(A34a)}$$

$$\psi_2^n(x_1,x_2) = \sum_{j=1+M1}^{M1+M2} \phi_j^{(2)}(x_2)\, g_{jm}^{(2)}(x_1), \quad n = M1+1, \ldots, M1+M2 \qquad \text{(A34b)}$$

As usual, we have written down only M1 and M2 of the 2M1 and 2M2 set of solutions. We generate the full set by performing forward and backward integrations. Our remarks to this point apply to both sets of integrations independently. We return to this point later. Substitution of eqs. (A34a) and (A34b) into eqs. (A33a) and (A33b) leads to the following equations

$$\sum_{i=1}^{M1} -\frac{\hbar^2}{2\mu}\frac{d^2}{dx_1^2} g_{im}^{(1)} \delta_{ki} + (V_1^I)_{ki} g_{im}^{(1)} - (E - \varepsilon_i^{(1)}) g_{im}^{(1)} \delta_{ki}$$

$$= \sum_{j=1+M1}^{M1+M2} (-V_{12}^{SO})_{kj} g_{jn}^{(2)} \qquad \text{(A35a)}$$

$$\sum_{j=1+M1}^{M1+M2} -\frac{\hbar^2}{2\mu}\frac{d^2}{dx_1^2} g_{jn}^{(2)} \delta_{lj} + (V_2^I)_{lj} g_{jn}^{(2)} - (E - \varepsilon_j^{(2)}) g_{jm}^{(2)} \delta_{lj}$$

$$= \sum_{i=1}^{M1} (-V_{12}^{SO})_{li} g_{im}^{(1)} \quad . \qquad \text{(A35b)}$$

These equations can be written as a matrix differential equation. Indeed, making the following definitions

$$[\underline{U}]_{ij} = \begin{cases} \frac{2\mu}{\hbar^2}(V_1^I)_{ij} , & i,j = 1,\ldots,M1 \\ \frac{2\mu}{\hbar^2}(V_2^I)_{ij} , & i,j = 1+M1,\ldots,M1+M2 \end{cases}$$

$$[\underline{K}^2]_{ij} = \begin{cases} \frac{2\mu}{\hbar^2}(E - \varepsilon_i^{(1)})\delta_{ki} , & i,k = 1,\ldots,M1 \\ \frac{2\mu}{\hbar^2}(E - \varepsilon_j^{(2)})\delta_{lj} , & i,j = 1+M1,\ldots,M1+M2 \end{cases}$$

$$[\underline{U}]_{ij} = \frac{2\mu}{\hbar^2}(V_{12}^{SO})_{ij} , \quad \begin{array}{l} i = 1,\ldots,M1 \\ j = M1+1,\ldots,M1+M2 \\ \text{or} \\ j = 1,\ldots,M1 \\ i = 1+M1,\ldots,M1+M2 \end{array}$$

$$(\underline{G''})_{ij} = \begin{cases} \dfrac{d^2}{dx_1^2}\, g_{ij}^{(1)}\, \delta_{ij}\,, & i,j = 1,\ldots,M1 \\ \dfrac{d^2}{dx_1^2}\, g_{ij}^{(2)}\, \delta_{ij}\,, & \begin{matrix} i = M1+1,\ldots,M1+M2 \\ j = 1,\ldots,M1 \end{matrix} \\ \dfrac{d^2}{dx_1^2}\, g_{ij}^{(1)}\, \delta_{ij}\,, & \begin{matrix} i = 1,\ldots,M_1 \\ j = 1+M1,\ldots,M1+M2 \end{matrix} \\ \dfrac{d^2}{dx_1^2}\, g_{ij}^{(2)}\, \delta_{ij}\,, & i,j = 1+M1,\ldots,M1+M2 \end{cases}$$

and

$$(\underline{G})_{ij} = \begin{cases} g_{ij}^{(1)}\,, & i,j = 1,\ldots,M1 \\ g_{ij}^{(2)}\,, & \begin{matrix} i = M1+1,\ldots,M1+M2 \\ j = 1,\ldots,M1 \end{matrix} \\ g_{ij}^{(1)}\,, & \begin{matrix} i = 1,\ldots,M1 \\ j = 1+M1,\ldots,M1+M2 \end{matrix} \\ g_{ij}^{(2)}\,, & i,j = 1+M1,\ldots,M1+M2 \end{cases}$$

eqs. (A35a) and (A35b) can be written as

$$\underline{G''} + (\underline{K}^2 - \underline{\mathcal{U}})\underline{G} = 0. \qquad \text{(A36)}$$

This matrix differential equation is integrated in the variables (x_1, x_2) up to a point x_1^0 near the region of strong chemical interaction. A standard fourth order Runge-Kutta/Adams-Moulton integrator was used for this purpose and the choice of linearly independent initial conditions as well as a stabilization of the solution matrix was made as described previously.[1]

We now examine the extension of the technique of changing

basis functions $\phi_i^{(1)}$ and $\phi_i^{(2)}$ during the propagation of the solution matrix developed for the one state reactive scattering program.[1] Suppose at some point x_1' (greater than x_1^0) new basis functions $\Phi_i^{(1)}$ and $\Phi_i^{(2)}$ are used in the expansion of ψ_1 and ψ_2. These functions are eigenfunctions of the following reference Hamiltonians:

$$\left[-\frac{\hbar^2}{2\mu}\frac{d^2}{dx_2^2} + V_1(x_1', x_2) - \mathcal{E}_i^{(1)}(x_1')\right]\Phi_i^{(1)}(x_2)=0 \qquad \text{(A37a)}$$

$$\left[-\frac{\hbar^2}{2\mu}\frac{d^2}{dx^2} + V_2(x_1', x_2) - \mathcal{E}_j^{(2)}(x_1')\right]\Phi_j^{(2)}(x_2) = 0 \qquad \text{(A37b)}$$

In order for the matrix differential equation (A36) to be integrated "new" initial conditions for $\underline{G}$ and $\underline{G}'$ must be established. This is accomplished by the requirement that at the interface $x_1 = x_1'$ the total wavefunction and its first derivative must be continuous. Equality requires that

$$\chi_1(\underset{\sim}{r}^{el};x_1'^{(-)},x_2)\psi_1(x_1'^{(-)},x_2) + \chi_2(\underset{\sim}{r}^{el};x_1'^{(-)},x_2)\psi_2(x_1'^{(-)},x_2) =$$

$$\chi 1(\underset{\sim}{r}^{el};x_1'^{(+)},x_2)\psi_1(x_1'^{(+)},x_2) + \chi_2(\underset{\sim}{r}^{el};x_1'^{(+)},x_2)\psi_2(x_1'^{(+)},x_2) \quad , \text{(A38)}$$

where the (+) and (-) superscripts denote that the approach to x_1' is from above and below respectively. Since χ_1 and χ_2 are electronic functions we can multiply eq. (A38) by χ_1^* and integrate with respect to $\underset{\sim}{r}^{el}$ to arrive at

$$\psi_1(x_1'^{(-)},x_2) = \psi_1(x_1'^{(+)},x_2) \quad . \qquad \text{(A39)}$$

Similarly, by multiplying (A38) by χ_2^* and integrating with respect to $\underset{\sim}{r}^{el}$ we secure

$$\psi_2(x_1'^{(-)}, x_2) = \psi_2(x_1'^{(+)}, x_2) \quad . \tag{A40}$$

We note that eqs. (A39) and (A40) are the same for any number of coupled electronic states. Substituting into eq. (A39) the appropriate expansions of ψ_1 in the bases $\phi_i^{(1)}$ and $\Phi_i^{(1)}$ yields

$$\sum_{i=1}^{M1} \Phi_i^{(1)}(x_2) g_{im}^{(1)}(x_1'^{(-)}) = \sum_{j=1}^{M1} \phi_j^{(1)}(x_2) g_{jm}^{(1)}(x_1'^{(+)}) \quad . \tag{A41}$$

(For convenience we have retained the notation $g_{ij}^{(1)}$ in the new expansion of ψ_1; this should not lead to any confusion). Multiplying the left and right hand sides of eq. (A41) by $\Phi_k^{(1)}(x_2)$ and integrating with respect to x_2, we obtain

$$g_{km}^{(1)}(x_1'^{(-)}) = \sum_{j=1}^{M1} S_{kj}^{(1)} g_{jm}^{(1)}(x_1'^{(+)}) \quad , \quad k=1, \ldots, M1 \tag{A42}$$

where

$$S_{kj}^{(1)} = \int dx_2 \, \Phi_k^{(1)}(x_2) \phi_j^{(1)}(x_2) \quad , \quad k, j = 1, \ldots, M1 \quad .$$

In an exactly analogous manner we have that

$$g_{lm}^{(2)}(x_1'^{(-)}) = \sum_{n = M1+1}^{M1+M2} S_{ln}^{(2)} g_{nm}^{(2)}(x_1'^{(+)}) \quad , \tag{A43}$$

where

$$S_{ln}^{(2)} = \int dx_2 \, \Phi_l^{(2)}(x_2) \, \phi_n^{(2)}(x_2) \quad , \quad l, n = M1+1, \ldots, M1+M2 \quad .$$

Now let us examine the consequences of requiring continuity of the total wavefunction at $x = x_1'$. Continuity is guaranteed *if*

$$\frac{\partial \Psi}{\partial x_1}(x_1'^{(-)}, x_2) = \frac{\partial \Psi}{\partial x_1}(x_1'^{(+)}, x_2) \quad . \tag{A44}$$

Thus, according to eqs. (A38) and (A44)

$$\frac{\partial \chi_1}{\partial x_1}(x_1'^{(-)})\psi_1 + \chi_1 \frac{\partial \psi_1}{\partial x_1}(x_1'^{(-)}) + \frac{\partial \chi_2}{\partial x_1}(x_1'^{(-)})\psi_2 + \chi_2 \frac{\partial \psi_2}{\partial x_1}(x_1'^{(-)}) =$$

$$\frac{\partial \chi_1}{\partial x_1}(x_1'^{(+)})\psi_1 + \chi_1 \frac{\partial \psi_1}{\partial x_1}(x_1'^{(+)}) + \frac{\partial \chi_2}{\partial x_1}(x_1'^{(+)})\psi_2 + \chi_2 \frac{\partial \psi_2}{\partial x_1}(x_1'^{(+)}). \tag{A45}$$

However, from eqs. (A39) and (A40) this equation becomes

$$\chi_1 \frac{\partial \psi_1}{\partial x_1}(x_1'^{(-)}) + \chi_2 \frac{\partial \psi_2}{\partial x_1}(x_1'^{(-)}) = \chi_1 \frac{\partial \psi_1}{\partial x_1}(x_1'^{(+)}) + \chi_2 \frac{\partial \psi_2}{\partial x_1}(x_1'^{(+)}). \tag{A46}$$

Proceeding as before, we multiply eq. (A46) by χ_1^* and integrate with respect to $\hat{\mathbf{r}}^{el}$ and then multiply by χ_2^* and integrate with respect to $\hat{\mathbf{r}}^{el}$ to arrive at

$$\frac{\partial \psi_1}{\partial x_1}(x_1'^{(-)}) = \frac{\partial \psi_1}{\partial x_1}(x_1'^{(+)}) \tag{A47a}$$

$$\frac{\partial \psi_2}{\partial x_1}(x_1'^{(-)}) = \frac{\partial \psi_2}{\partial x_1}(x_1'^{(+)}) \quad . \tag{A47b}$$

From these equations and eqs. (34a) and (34b) we have that

$$\frac{dg'^{(1)}_{km}}{dx_1}(x_1^{0\,(-)}) = \sum_{j=1}^{M1} S^{(1)}_{kj} \frac{dg^{(1)}_{jm}}{dx}(x_1'^{(+)}) \quad , \qquad k = 1, \ldots, M1 \tag{A48}$$

$$\frac{dg^{(2)}_{lm}}{dx_1}(x_1'^{(-)}) = \sum_{n=M1+1}^{M1+M2} S^{(2)}_{ln} \frac{dg^{(2)}_{nm}}{dx}(x_1'^{(+)}), \; l=1+M1, \ldots, M1+M2 \tag{A49}$$

Eqs. (A42), (A43), (A48), and (A49) can be cast into matrix form as follows

$$\underline{G}(x_1'^{(-)}) = \underline{S}\,\underline{G}(x_1'^{(+)}) \tag{A50}$$

$$\underline{G}'(x_1'^{(-)}) = \underline{S}\,\underline{G}'(x_1'^{(+)}) \tag{A51}$$

where from its definition the matrix $\underline{S}$ is clearly block diagonal.

We consider next the change of independent variables at the point $x_1 = x_1^0$. Polar coordinates are introduced[1] and the two coupled partial differential equations are given by

$$\left[-\frac{\hbar^2}{2\mu}\left(\frac{1}{r^2}\frac{\partial^2}{\partial\varphi^2} + \frac{\partial^2}{\partial r^2} + \frac{1}{r}\frac{\partial}{\partial r}\right) + V_1(r,\varphi) - E\right]\psi_1(r,\varphi) = -V_{12}^{SO}\,\psi_2(r,\varphi), \tag{A52a}$$

$$\left[-\frac{\hbar^2}{2\mu}\left(\frac{1}{r^2}\frac{\partial^2}{\partial\varphi^2} + \frac{\partial^2}{\partial r^2} + \frac{1}{r}\frac{\partial}{\partial\varphi}\right) + V_2(r,\varphi) - E\right]\psi_2(r,\varphi) = -V_{12}^{SO}\,\psi_1(r,\varphi)\ . \tag{A52b}$$

Making the usual change of functions,[1]

$$\psi_i(r,\varphi) = \frac{1}{r^{\frac{1}{2}}}\,\Phi_i(r,\varphi)\ , \tag{30}$$

eqs. (A52a) and (A52b) can be rewritten as

$$-\frac{\hbar^2}{2\mu}\left(\frac{1}{r^{5/2}}\frac{\partial^2\Phi_1}{\partial\varphi^2} + \frac{1}{4r^{5/2}}\Phi_1(r,\varphi) + \frac{1}{r^{1/2}}\frac{\partial^2\Phi_1}{\partial r^2}\right) + (V_1 - E)\frac{\Phi_1(r,\varphi)}{r^{1/2}} = -V_{12}^{SO}\,\Phi_2(r,\varphi)/r^{1/2}\ , \tag{A53a}$$

$$-\frac{\hbar^2}{2\mu}\left(\frac{1}{r^{5/2}}\frac{\partial^2\Phi_2}{\partial\varphi^2} + \frac{1}{4r^{5/2}}\Phi_2 + \frac{1}{r^{1/2}}\frac{\partial^2\Phi_2}{\partial r^2}\right) + (V_2 - E)\frac{\Phi_2}{r^{1/2}} = -V_{12}^{SO}\,\Phi_1/r^{1/2}\ . \tag{A53b}$$

Multiplying these equations by $r^{\frac{1}{2}}$, we obtain

$$-\frac{\hbar^2}{2\mu}\left(\frac{1}{r^2}\frac{\partial^2}{\partial\varphi^2}+\frac{\partial^2}{\partial r^2}\right)\Phi_1+(V_1-\frac{\hbar^2}{8\mu r^2}-E)\Phi_1=-V_{12}^{SO}\Phi_2\ , \tag{A54a}$$

$$-\frac{\hbar^2}{2\mu}\left(\frac{1}{r^2}\frac{\partial^2}{\partial\varphi^2}+\frac{\partial^2}{\partial r^2}\right)\Phi_2+(V_2-\frac{\hbar^2}{8\mu r^2}-E)\Phi_2=-V_{12}^{SO}\Phi_1\ . \tag{A54b}$$

As usual, we expand Φ_1 and Φ_2 as follows:

$$\Phi_1^m(r,\varphi)=\sum_{i=1}^{M1}\phi_i^{(1)}(r)g_{im}^{(1)}(\varphi)\ , \tag{A55a}$$

$$\Phi_2^m(r,\varphi)=\sum_{j=M1+_1}^{M1+M2}\phi_j^{(2)}(r)g_{jm}^{(2)}(\varphi)\ . \tag{A55b}$$

Inserting (A55a) and (A55b) into (A54a) and (A54b), multiplying through by r^2 and doing the standard multiplying by $\phi_k^{(1)}(r)$ and $\phi_l^{(2)}(r)$ and integrating with respect to r we obtain the following coupled differential equations for $g_{im}^{(1)}(\varphi)$ and $g_{jm}^{(2)}(\varphi)$.

$$\sum_{i=1}^{M1}-\frac{\hbar^2}{2\mu}\frac{d^2}{d\varphi^2}g_{im}^{(1)}\delta_{ki}+g_{im}^{(1)}[(U_1)_{ki}-E_{ki}-\frac{\hbar^2}{8\mu}\delta_{ki}]=\sum_{j=M1+1}^{M1+M2}(-U_{12}^{SO})_{kj}g_{jm}^{(2)}\ , \tag{A56a}$$

$$\sum_{j=1+M1}^{M1+M2}-\frac{\hbar^2}{2\mu}\frac{d^2}{d\varphi^2}g_{jm}^{(2)}\delta_{lj}+g_{jm}^{(2)}[(U_2)_{lj}-E_{lj}-\frac{\hbar^2}{8\mu}\delta_{lj}]=\sum_{i=1}^{M1}(-U_{12}^{SO})_{li}g_{im}^{(1)}\ . \tag{A56b}$$

We have made use of the following in deriving these equations:

$$-\frac{\hbar^2}{2\mu}\frac{d^2\phi_i^{(1)}}{dr^2}+(V_1(r,\varphi_0)-\mathcal{E}_i^{(1)})\phi_i^{(1)}=0\ ,\qquad i=1,\ldots,M1$$

$$-\frac{\hbar^2}{2\mu}\frac{d^2\phi_j^{(2)}}{dr^2} + (V_2(r,\varphi_0) - \mathcal{E}_j^{(2)})\phi_j^{(2)} = 0 \quad , \qquad j = 1+M1, \ldots, M1+M2$$

where $V_1(r,\varphi_0)$ and $V_2(r,\varphi_0)$ are reference potentials referred to a particular value of φ, φ_0 and

$$(U_1)_{ki} = \int dr \phi_k^{(1)}(r)\, r^2 [\, V_1(r,\varphi) - V_1(r,\varphi_0)\,] \phi_i^{(1)}(r) \quad , \qquad k,i=1,\ldots,M1$$

$$(U_2)_{lj} = \int dr \phi_l^{(2)}(r)\, r^2 [\, V_2(r,\varphi) - V_2(r,\varphi_0)\,] \phi_j^{(2)}(r) \quad , \qquad l,j=1+M1,\ldots,M1+M2$$

$$E_{ki} = \int dr \phi_k^{(1)}(r)\, r^2 (E - \mathcal{E}_i^{(1)}) \phi_i^{(1)}(r) \quad , \qquad k,1 = 1,\ldots,M1$$

$$E_{lj} = \int dr \phi_l^{(2)}(r)\, r^2 (E - \mathcal{E}_j^{(2)}) \phi_j^{(2)}(r) \quad , \qquad l,j = 1+M1,\ldots,M1+M2$$

$$(U_{12}^{SO})_{kj} = \int dr \phi_k^{(1)}(r)\, r^2 V_{SO}(r,\varphi) \phi_j^{(2)}(r), \qquad k = 1,\ldots,M1 \quad j = 1+M1,\ldots,M1+M2$$

$$(U_{12}^{SO})_{li} = \int dr \phi_l^{(2)}(r)\, r^2 V_{SO}(r,\varphi) \phi_i^{(1)}(r), \qquad l = M1+1,\ldots,M1+M2 \quad i = 1,\ldots,M1$$

As previously, this set of coupled differential equations can be cast into a matrix equation

$$\underline{G}''(\varphi) + (\underline{K}^2 - \underline{U})\underline{G} = 0 \qquad \text{(A57)}$$

where all of the matrices are the one analogous to those defined in equations preceding eq. (A36) with the exception of the $\underline{K}^2$ matrix. It is given by

$$[\underline{K}^2]_{ij} = \frac{2\mu}{\hbar^2} E_{ij} - \frac{1}{4}\delta_{ij} \quad , \qquad i,j=1,\ldots,M1+M2 \quad .$$

The procedure for changing expansion functions $\phi_i^{(1)}$ and $\phi_j^{(2)}$ at a value of $\varphi = \varphi'$ is identical to the one given previously by eqs. (A42),

(A43), (A48) and (A49).

The matching of the wavefunction at the boundary $x = x_1^0$ and equivalently by $\varphi = 0$ proceeds as follows. At this boundary we require that

$$\chi_1(\underset{\sim}{r}^{el};x_1^0, x_2)\,\frac{\Phi_1(\varphi=0,r)}{r^{1/2}} + \chi_2(\underset{\sim}{r}^{el};x_1^0, x_2)\,\frac{\Phi_2(\varphi=0,r)}{r^{1/2}}$$

$$= \chi_1(\underset{\sim}{r}^{el};x_1^0, x_2)\,\psi_1(x_1^0, x_2) + \chi_2(\underset{\sim}{r}^{el};x_1^0, x_2)\psi_2(x_{10}, x_2) \quad .$$

Multiplying this equation first by χ_1^* and integrating with respect to $\underset{\sim}{r}^{el}$ and then multiplying by χ_2^* and integrating with respect to $\underset{\sim}{r}^{el}$ (and recalling that $\langle \chi_1 | \chi_2 \rangle_{el} = 0$) we arrive at

$$\frac{\Phi_1(\varphi=0,r)}{r^{1/2}} = \psi_1(x_{10}, x_2) \quad , \tag{A58}$$

$$\frac{\Phi_2(\varphi=0,r)}{r^{1/2}} = \psi_2(x_{10}, x_2) \quad . \tag{A59}$$

Each of these equations is identical to the equation found in the previous collinear formulation for electronically adiabatic chemical reactions. Inserting the expansions (A34a), (A34b), (A55a), and (A55b) into eqs. (A58) and (A59) we have

$$\frac{1}{r^{1/2}} \sum_{i=1}^{M1} g_{im}^{(1)}(\varphi=0)\phi_i^{(1)}(r) = \sum_{j=1}^{M1} g_{jm}^{(1)}(x_{10})\phi_j^{(1)}(x_{20} - r) \quad , \tag{A60}$$

$$\frac{1}{r^{1/2}} \sum_{k=1+M1}^{M1+M2} g_{km}^{(2)}(\varphi=0)\phi_k^{(2)}(r) = \sum_{l=1+M1}^{M1+M2} g_{lm}^{(2)}(x_{10})\phi_l^{(2)}(x_{20} - r) \quad . \tag{A61}$$

Note that the origin of the polar coordinate system is the point $(x_1^0, x_2^0)^1$ and we have made use of the fact that

$$x_2 = x_{20} - r\cos\varphi$$
$$= x_{20} - r \qquad (\text{for } \varphi = 0).$$

Proceeding as usual, we multiply eq. (A60) by $\phi_k^{(1)}(r)$ and eq. (A61) by $\phi_n^{(2)}(r)$ and integrate with respect to r, subsequent to multiplying both equations by $r^{\frac{1}{2}}$. Doing this, we secure

$$g_{nm}^{(1)}(\varphi=0) = \sum_{j=1}^{M1} r_{nj}^{1/2}\, g_{jm}^{(1)}(x_1^0) \quad , \tag{A62}$$

$$g_{nm}^{(2)}(\varphi=0) = \sum_{l=1+M1}^{M1+M2} r_{nl}^{1/2}\, g_{lm}^{(2)}(x_1^0) \quad , \tag{A63}$$

where

$$r_{kj}^{1/2} = \int dr\, \phi_k^{(1)}(r)\, r^{1/2}\, \phi_j^{(1)}(r) \quad , \qquad k,j=1,\ldots,M1$$

$$r_{nl}^{1/2} = \int dr\, \phi_n^{(2)}(r)\, r^{1/2}\, \phi_l^{(2)}(r) \quad , \qquad n,l=1+M1,\ldots,M1+M2$$

We similarly match the derivatives (being careful with the formula $x_2 = x_{20} - r\cos\varphi$) and obtain:

$$\frac{dg_{km}^{(1)}}{d\varphi}(\varphi=0) = \sum_{j=1}^{M1} -r_{kj}^{3/2}\, \frac{dg_{jm}^{(1)}}{dx_1}(x_1^0) \quad , \tag{A64}$$

$$\frac{dg_{nm}^{(2)}}{d\varphi}(\varphi=0) = \sum_{l=M1+1}^{M1+M2} -r_{nl}^{3/2}\, \frac{dg_{lm}^{(2)}}{dx_1}(x_1^0) \quad , \tag{A65}$$

where

$$r_{ij}^{3/2} = \begin{cases} \int dr\ \phi_i^{(1)}(r)\, r^{3/2}\, \phi_j^{(1)}(r) \ , & i,j=1,\ldots,M1 \\ \int dr\ \phi_i^{(2)}(r)\, r^{3/2}\, \phi_j(r) \ , & i,j=M1+1,\ldots,M1+M2 \end{cases}$$

Equations (A62) - (A65) in principle establish the initial conditions for propagation of the coupled differential equations (A56). However, it is more convenient numerically to use basis functions $\phi_i^{(1)}$ and $\phi_i^{(2)}$ referenced to a $\varphi > 0$.[1] Thus, overlap matrices between this basis set and the one referenced to $\varphi = 0$ must be computed. With this modification the final equations for the initial conditions are given by

$$g_{im}^{(1)}(\varphi=0) = \sum_{j=1}^{M1} \sum_{k=1}^{M1} S_{ik}^{(1)}\, r_{kj}^{1/2}\, g_{jm}^{(1)}(x_{10}) \ ,$$

$$i = 1,\ldots,M1$$

$$\frac{dg_{im}^{(1)}}{d\varphi}(\varphi=0) = \sum_{j=1}^{M1} \sum_{k=1}^{M1} -S_{ik}^{(1)}\, r_{kj}^{3/2}\, \frac{dg_{jm}^{(1)}}{dx_1}(x_{10}) \ ,$$

$$g_{nm}^{(2)}(\varphi=0) = \sum_{p=1}^{M1+M2} \sum_{l=1}^{M1+M2} S_{nl}^{(2)}\, r_{lp}^{1/2}\, g_{pm}^{(2)}(x_{10}) \ ,$$

$$n=1+M1,\ldots,M1+M2$$

$$\frac{dg_{nm}^{(2)}}{d\varphi}(\varphi=0) = \sum_{p=1}^{M1+M2} \sum_{l=1}^{M1+M2} -S_{nl}^{(2)}\, r_{lp}^{3/2}\, \frac{dg_{pm}^{(2)}}{dx_1}(x_{10}) \ .$$

With initial conditions established the integration of eq. (A56) can be carried out. Details regarding further propagation in the rearrangement coordinate system (φ', r') and (z_1, z_2) are very similar to

the ones given above and are not considered further. The entire procedure generates M1 + M2 linearly independent solutions to the two-coupled Schrödinger equations (A22a) and (A22b). Another set of M1 + M2 linearly independent solutions is generated by performing a "back integration." That is, the above procedure is repeated except it is begun in the product arrangement channel. Details regarding this procedure are given elsewhere.[1]

In Appendix 4 the asymptotic scattering analysis is presented for the two-state problem. Since it is an extension of the single state analysis the description is brief.

References

1. A. Kuppermann, Electronic and Atomic Collisions, VIIth International Conference on the Physics of Electronic and Atomic Collisions, Abstract of Papers (North-Holland, Amsterdam, 1971), p. 3; unpublished results.

Appendix 4: R and S Matrix Scattering Analysis for the Electronic Two-State $A + BC \rightarrow AB + C$, $AB^* + C$ Collinear Chemical Reaction

As discussed in Appendix 3 a total of $2(M1 + M2)$ linearly independent solutions of the Schrödinger equation are generated for the electronic two-state $A + BC \rightarrow AB + C$, $AB^* + C$ collinear chemical reaction. The techniques used to obtain the R matrix[1] and from it the S matrix[1] from this set of solutions are outlined in this appendix.

Since the R-S analysis developed for the electronic two-state problem is a straightforward extension of the one-state analysis given previously[2-4] we give the details only of the modifications of the one-state analysis and simply quote one-state results. Also, a current density analysis of the two-state wavefunction is made and the necessity of a complete electron-nuclear uncoupling is pointed out in order for the following R-S analysis to be valid.

The $\underline{G}$ matrix defined by eq. (A36) of Appendix 3 has dimensions $(M1 + M2) \times (M1 + M2)$. Let us denote the $\underline{G}$ matrix obtained in the forward integration by $\underline{G}^+$ and in the backward integration by $\underline{G}^-$. The jth column of $\underline{G}^{+(-)}$, $G_j^{+(-)}$ has the following elements asymptotically (in terms of real functions)[1-3]

$$g_{ij}^{+(-)}(x_1, x_2) \underset{x_1 \to \infty}{\sim}$$

$$\begin{cases} D_{ij}^{+(-)} \sin(k_i^{(1)} x_1) + \overline{D}_{ij}^{+(-)} \cos(k_i^{(1)} x_1), \\ \qquad\qquad i = 1, \ldots, N1 \\ C_{ij}^{+(-)} \exp(\kappa_i^{(1)} x_1) + \overline{C}_{ij}^{+(-)} \exp(-\kappa_i^{(1)} x_1), \\ \qquad\qquad i = N1+1, \ldots, M1 \\ B_{ij}^{+(-)} \sin(k_i^{(2)} x_1) + \overline{B}_{ij}^{+(-)} \cos(k_i^{(2)} x_1), \\ \qquad\qquad i = M1+1, \ldots, M1+N2 \\ A_{ij}^{+(-)} \exp(-\kappa_i^{(2)} x_1) + \overline{A}_{ij}^{+(-)} \exp(\kappa_j^{(2)} x_1) \\ \qquad\qquad i = M1+N2+1, \ldots, M1+M2 \end{cases}$$

$$g_{ij}^{+(-)}(z_1, z_2) \underset{z_1 \to \infty}{\sim}$$

$$\begin{cases} J_{ij}^{+(-)} \sin(k_i^{(1)'} z_1) + \overline{J}_{ij}^{+(-)} \cos(k_i^{(1)'} z_1), \\ \qquad\qquad i = 1, \ldots, N1' \\ H_{ij}^{+(-)} \exp(\kappa_i^{(1)'} z_1) + \overline{H}_{ij}^{+(-)} \exp(-\kappa_i^{(1)'} z_1), \\ \qquad\qquad i = N1'+1, \ldots, M1 \\ F_{ij}^{+(-)} \sin(k_i^{(2)'} z_1) + \overline{F}_{ij}^{+(-)} \cos(k_i^{(2)'} z_1), \\ \qquad\qquad i = M1+1, \ldots, M1+N2' \\ E_{ij}^{+(-)} \exp(\kappa_i^{(2)'} z_1) + \overline{E}_{ij}^{+(-)} \exp(-\kappa_i^{(2)'} z_2), \\ \qquad\qquad i = M1+N2', \ldots, M1+M2 \end{cases}$$

$$j = 1, \ldots, M1+M2 \quad .$$

N1 and N2 are the number of open vibrational states of the reactant molecule BC in electronic states 1 and 2 respectively and N1′ and N2′ are the number of open vibrational states of the product molecule AB in electronic states 1 and 2 respectively.

In order to construct the R matrix from the matrices of coefficients given above requires the construction of a super matrix $\underline{\delta}$.

This matrix consists of an assembly of many submatrices of certain of the above coefficients. The submatrices are

$$(\underline{D}^{+(-)})_{ij} = D_{ij}^{+(-)}, \quad \begin{array}{l} i = 1, \ldots, N1 \\ j = 1, \ldots, M1 \end{array}$$

$$(\underline{D}'^{+(-)})_{ij} = D_{ij}^{+(-)}, \quad \begin{array}{l} i = 1, \ldots, N1 \\ j = M1+1, \ldots, M1+M2 \end{array}$$

$$(\underline{C}^{+(-)})_{ij} = C_{ij}^{+(-)}, \quad \begin{array}{l} i = N1+1, \ldots, M1 \\ j = 1, \ldots, M1 \end{array}$$

$$(\underline{C}'^{+(-)})_{ij} = C_{ij}^{+(-)}, \quad \begin{array}{l} i = N1+1, \ldots, M1 \\ j = M1+1, \ldots, M1+M2 \end{array}$$

$$(\underline{J}^{+(-)})_{ij} = J_{ij}^{+(-)}, \quad \begin{array}{l} i = 1, \ldots, N1' \\ j = 1, \ldots, M1 \end{array}$$

$$(\underline{J}'^{+(-)})_{ij} = J_{ij}^{+(-)}, \quad \begin{array}{l} i = 1, \ldots, N1' \\ j = M1+1, \ldots, M1+M2 \end{array}$$

$$(\underline{H}^{+(-)})_{ij} = H_{ij}^{+(-)}, \quad \begin{array}{l} i = N1'+1, \ldots, M1 \\ j = 1, \ldots, M1 \end{array}$$

$$(\underline{H}'^{+(-)})_{ij} = H_{ij}^{+(-)}, \quad \begin{array}{l} i = N1'+1, \ldots, M1 \\ j = M1+1, \ldots, M1+M2 \end{array}$$

$$(\underline{B}^{+(-)})_{ij} = B_{ij}^{+(-)}, \quad \begin{array}{l} i = M1+1, \ldots, M1+N2 \\ j = 1, \ldots, M1 \end{array}$$

$$(\underline{B}'^{+(-)})_{ij} = B_{ij}^{+(-)}, \quad \begin{array}{l} i = M1+1, \ldots, M1+N2 \\ j = M1+1, \ldots, M1+M2 \end{array}$$

$$(\underline{A}^{+(-)})_{ij} = A_{ij}^{+(-)}, \quad \begin{array}{l} i = M1+N2+1, \ldots, M1+M2 \\ j = 1, \ldots, M1 \end{array}$$

$$(\underline{A}'^{+(-)})_{ij} = A_{ij}^{+(-)} \quad , \qquad \begin{array}{l} i = M1+N2+1, \ldots, M1+M2 \\ j = M1+1, \ldots, M1+M2 \end{array}$$

$$(\underline{F}^{+(-)})_{ij} = F_{ij}^{+(-)} \quad , \qquad \begin{array}{l} i = M1+1, \ldots, M1+N2' \\ j = 1, \ldots, M1 \end{array}$$

$$(\underline{F}'^{+(-)})_{ij} = F_{ij}^{+(-)} \quad , \qquad \begin{array}{l} i = M1+1, \ldots, M1+N2' \\ j = M1+1, \ldots, M1+M2 \end{array}$$

$$(\underline{E}^{+(-)})_{ij} = E_{ij}^{+(-)} \quad , \qquad \begin{array}{l} i = M1+N2', \ldots, M1+M2 \\ j = 1, \ldots, M1 \end{array}$$

$$(\underline{E}'^{+(-)})_{ij} = E'^{+(-)}_{ij} \quad , \qquad \begin{array}{l} i = M1+N2', \ldots, M1+M2 \\ j = M1+1, \ldots, M1+M2 \quad . \end{array}$$

In terms of these submatrices, the $\underline{\delta}$ matrix is given by

$$\underline{\delta} = \begin{bmatrix} \underline{D}^{+} & \underline{D}^{-} & \underline{D}'^{+} & \underline{D}'^{-} \\ \underline{C}^{+} & \underline{C}^{-} & \underline{C}'^{+} & \underline{C}'^{-} \\ \underline{J}^{+} & \underline{J}^{-} & \underline{J}'^{+} & \underline{J}'^{-} \\ \underline{H}^{+} & \underline{H}^{-} & \underline{H}'^{+} & \underline{H}'^{-} \\ \underline{B}^{+} & \underline{B}^{-} & \underline{B}'^{+} & \underline{B}'^{-} \\ \underline{A}^{+} & \underline{A}^{-} & \underline{A}'^{+} & \underline{A}'^{-} \\ \underline{F}^{+} & \underline{F}^{-} & \underline{F}'^{+} & \underline{F}'^{-} \\ \underline{E}^{+} & \underline{E}^{-} & \underline{E}'^{+} & \underline{E}'^{-} \end{bmatrix} \quad . \tag{A66}$$

This matrix has dimensions 2(M1+M2) x 2(M1+M2) and for the R-matrix analysis its inverse $\underline{\delta}^{-1}$ is required. A matrix, $\underline{\mathcal{S}}$, somewhat analogous to $\underline{\delta}$ is now defined. It is given by

$$\mathcal{D} = \begin{bmatrix} \underline{\bar{D}}^{+} & \underline{\bar{D}}^{-} & \underline{\bar{D}}'^{+} & \underline{\bar{D}}'^{-} \\ \underline{\bar{J}}^{+} & \underline{\bar{J}}^{-} & \underline{\bar{J}}'^{+} & \underline{\bar{J}}'^{-} \\ \underline{\bar{B}}^{+} & \underline{\bar{B}}^{-} & \underline{\bar{B}}'^{+} & \underline{\bar{B}}'^{-} \\ \underline{\bar{F}}^{+} & \underline{\bar{F}}^{-} & \underline{\bar{F}}'^{+} & \underline{\bar{F}}'^{-} \end{bmatrix} \tag{A67}$$

and has dimensions (N1 + N1′ + N2 +N2P) x 2(M1 + M2). The submatrices are exactly analogous to the ones given above with the upper bar inserted. The penultimate step is to form from $\underline{\delta}^{-1}$ a matrix $\underline{C}$ which consists of the open columns of $\underline{\delta}^{-1}$ only and has dimensions 2(M1 + M1) x(N1 + N2 + N1′ + N2′). Finally, a diagonal (N1 + N1′ + N2 + N2′) x (N1 + N1′ + N2 + N2′) matrix $\underline{K}^{\frac{1}{2}}$ is defined by

$$\underline{K}^{\pm\frac{1}{2}} = \begin{bmatrix} \underline{k}^{(1)\pm\frac{1}{2}} & & & \\ & \underline{k}^{(1)',\pm\frac{1}{2}} & & \\ & & \underline{k}^{(2)\pm\frac{1}{2}} & \\ & & & \underline{k}^{(2)',\pm\frac{1}{2}} \end{bmatrix} \tag{A68}$$

where,

$$(\underline{k}^{(1)\pm\frac{1}{2}})_{ij} = k_i^{(1)\pm\frac{1}{2}}\delta_{ij}\,, \qquad i = 1,\ldots,N1$$

$$(\underline{k}^{(1)',\pm\frac{1}{2}})_{ij} = k_i^{(1)',\pm\frac{1}{2}}\delta_{ij}\,, \qquad i = 1,\ldots,N1'$$

$$(\underline{k}^{(2)\pm\frac{1}{2}})_{ij} = k_i^{(2)\pm\frac{1}{2}}\delta_{ij}\,, \qquad i = M1+1,\ldots,M1+N2$$

$$(\underline{k}^{(2)',\pm\frac{1}{2}})_{ij} = k_i^{(2)',\pm\frac{1}{2}}\delta_{ij}\,, \qquad i = M1+1,\ldots,M1+N2'$$

and $k_i^{(1)}$, $k_i^{(2)}$ are given just after eq. (A28b) of Appendix 3 and $k_i^{(1)'}$ and $k_i^{(2)'}$ are the analogous quantities for the rearrangement channel.

δ_{ij} is, in this context, the Kroneker delta function. Then in terms of $\underline{C}$, $\underline{\mathcal{A}}$, and $\underline{K}^{\frac{1}{2}}$ the R-matrix is given by[2,3]

$$\underline{R} = \underline{K}^{\frac{1}{2}} \underline{\mathcal{A}} \underline{C} \underline{K}^{-\frac{1}{2}} \quad . \tag{A69}$$

The R-matrix has dimensions (N1 + N1′ + N2 + N2′) x (N1 + N1′ + N2 + N2′) and in terms of it the S-matrix is given by[1-3]

$$\underline{S} = (\underline{I} - i\underline{R})^{-1}(\underline{I} + i\underline{R}) \quad . \tag{A70}$$

Finally, the probability matrix $\underline{P}$ which gives the probability for the system of reactants in a given initial state i to undergo a transition to a final state f, e.g. reactive and electronically non-adiabatic is given by

$$P_{if} = |S_{fi}|^2 \quad . \tag{A71}$$

We consider now a current density analysis of the scattering wavefunction given in the traveling wave representation. Thus,

$$\Psi_I(\underset{\sim}{r}^{el}, x_1, x_2) \underset{x_1 \to \infty}{} \chi_1^a(\underset{\sim}{r}^{el}; x_1, x_2)\Big[e^{-ik_I^{(1)}x_1}\phi_I^{(1)}(x_2) + \sum_{i=1}^{N1}\left(\frac{k_I^{(1)}}{k_i^{(1)}}\right)^{\frac{1}{2}} S_{iI} e^{ik_{iI}^{(1)}x_1}\phi_i^{(1)}(x_2)\Big] + \chi_2^a(\underset{\sim}{r}^{el}; x_1, x_2) \sum_{i=N1+N1'+1}^{N1+N1'+N2}\left(\frac{k_I^{(1)}}{k_i^{(2)}}\right)^{\frac{1}{2}} S_{iI} e^{ik_{iI}^{(2)}x_1}\phi_i^{(2)}(x_2) \quad , \tag{A72}$$

where I denotes the initial state of the reactants and i denotes the final state of the reactants. Eq. (A72) is the scattered wave for non-reactive scattering which is sufficient for consideration of the properties current density vector $\underset{\sim}{j}(\underset{\sim}{r}^{el}, x_1, x_2)$. Note we have dropped the closed

channels since they necessarily make a zero contribution to $\underset{\sim}{j}(\underset{\sim}{r}^{el}, x_1, x_2)$.

By definition $\underset{\sim}{j}(\underset{\sim}{r}^{el}, x_1, x_2)$ is given by[5]

$$\underset{\sim}{j}(\underset{\sim}{r}^{el}, x_1, x_2) = \frac{\hbar}{\mu} I_m \left(\Psi_I^* \underset{\sim}{\nabla} \Psi_I\right) , \tag{A73}$$

where in the collinear case

$$\underset{\sim}{\nabla} = \frac{\partial}{\partial x_1} x_1 + \frac{\partial}{\partial x_2} x_2 + \alpha \underset{\sim}{\nabla}_{el} ; \tag{A74}$$

α is a dimensionless mass ratio chosen so that the definition of $\underset{\sim}{j}$ given by (A73) is correct. We assert that the contributions made by $\frac{\partial}{\partial x_2} x_2$ and $\alpha \underset{\sim}{\nabla}_{el}$ to $\underset{\sim}{j}$ are identically zero. This is so because the $\underset{\sim}{r}^{el}$ and x_2 motions are presumed to be bound. Thus, we need consider the $\frac{\partial}{\partial x_1} x_1$ term only. Performing the necessary differentiations and multiplications yields the following terms;

$$\chi_1^{a*} \chi_1^a \left\{ -ik_I \left|\phi_I^{(1)}(x_2)\right|^2 + \sum_{i=1}^{N1} \sum_{j=1}^{N1} ik_{iI}^{(1)} \left(\frac{k_I^{(1)}}{k_{jI}^{(1)}}\right)^{\frac{1}{2}} \left(\frac{k_I^{(1)}}{k_{iI}^{(1)}}\right)^{\frac{1}{2}} S_{jI}^* S_{iI} \right.$$

$$\left. e^{i(k_{iI}^{(1)} - k_{jI}^{(1)})x_1} \phi_i^{(1)} \phi_j^{(1)} \right\} +$$

$$\chi_2^{a*} \chi_2^a \sum_{i,j=N1+N1'+1} \sum ik_{iI}^{(2)} \left(\frac{k_I^{(1)}}{k_{iI}^{(2)}}\right)^{\frac{1}{2}} \left(\frac{k_I^{(1)}}{k_{jI}^{(2)}}\right)^{\frac{1}{2}} S_{jI}^* S_{iI} e^{i(k_{jI}^{(2)} - k_{iI}^{(2)})x_1} \phi_i^{(2)} \phi_j^{(2)} +$$

$$\chi_1^{a*} \chi_2^a \{\quad\} + \chi_2^{a*} \chi_1^a \{\quad\}' + \chi_1^{a*} \frac{\partial \chi_1^a}{\partial x_1} \{\quad\}'' + \chi_1^{a*} \frac{\partial \chi_2^a}{\partial x_1} \{\quad\}''' +$$

$$\chi_2^{a*} \frac{\partial \chi_1^a}{\partial x_1} \{\quad\}'''' + \chi_2^{a*} \frac{\partial \chi_2^a}{\partial x_1} \{\quad\}''''' \quad .$$

In order to secure the scattering flux, these terms must be integrated with respect to $\underset{\sim}{r}^{el}$ and x_2. Doing the x_2 integration first yields for the

quantities multiplying $\chi_1^{a*}\chi_1^a$ and $\chi_2^{a*}\chi_2^a$ very familiar expressions for the flux associated with electronic states 1 and 2 separately and we note that the remaining terms are non-vanishing. Finally, we consider the $\underset{\sim}{r}^{el}$ integration. Making use of the fact that the χ_i^a form an orthonormal set of functions we have that

$$\underset{\sim}{J}(x_1) = \frac{\hbar}{\mu}\Big[-k_I^{(1)} + \sum_{i=1}^{N1} k_I^{(1)} |S_{iI}|^2 + \sum_{j=N1+N1'+1}^{N1+N1'+N2} k_I^{(1)} |S_{jI}|^2\Big] +$$

$$\frac{\hbar}{\mu} I_m\Big[\langle\chi_1^a|\frac{\partial\chi_1^a}{\partial x_1}\rangle_{el}\{\quad\}'' + \langle\chi_1^a|\frac{\partial\chi_2^a}{\partial x_1}\rangle_{el}\{\quad\}''' +$$

$$\langle\chi_2^a|\frac{\partial\chi_1^a}{\partial x_1}\rangle_{el}\{\quad\}'''' + \langle\chi_2^a|\frac{\partial\chi_2^a}{\partial x_1}\rangle_{el}\{\quad\}''''''\Big] .$$

Very curiously we see that $\underset{\sim}{J}$ contains terms in addition to the usual expected contributions, i.e., the terms given explicitly; terms which contain Born-Oppenheimer coupling terms (cf. eq. (12a) of Section 2). It has been shown previously that the terms $\langle\chi_i^a|\frac{\partial\chi_i^a}{\partial x_1}\rangle_{el}$ vanish identically, however, the terms $\langle\chi_i^a|\frac{\partial\chi_j^a}{\partial x_1}\rangle_{el}(i \neq j)$ do not in general vanish. In fact we have that $\{\quad\}''' = \{\quad\}''''''^*$ and from previous results (eq. (11a) of Section 2) that $\langle\chi_1^a|\frac{\partial\chi_2^a}{\partial x_1}\rangle_{el} = -\langle\chi_2^a|\frac{\partial\chi_1^a}{\partial x_1}\rangle_{el}^*$, hence we have that

$$\underset{\sim}{J} = \frac{\hbar}{\mu}\Big[-k_I^{(1)} + \sum_{i=1}^{N1} k_I^{(1)} |S_{iI}|^2 + \sum_{j=N1+N1'+1}^{N1+N1'+N2} k_I^{(1)} |S_{jI}|^2\Big] +$$

$$\frac{\hbar}{\mu} 2I_m \langle\chi_1^a|\frac{\partial\chi_2^a}{\partial x_1}\rangle_{el}\{\quad\}''' .$$

Thus, we stress that the terms involving $\langle \chi_1^a | \frac{\partial \chi_2^a}{\partial x_1} \rangle_{el}$ do not necessarily vanish. However, we can argue that they do indeed vanish since if they do not this implies that the two-state coupled equations would remain coupled asymptotically. This we have assumed does not happen and, interestingly, we find here that this assumption must be reiterated in order for the scattering analysis we have performed to be valid. Thus, the vanishing of $\langle \chi_1^a | \frac{\partial \chi_2^a}{\partial x_1} \rangle_{el}$ asymptotically is not a new assumption, although it is an essential one for our scattering analysis. Therefore, $\underset{\sim}{J}(x_1)$ becomes simply

$$\underset{\sim}{J}(x_1)_{x_1 \to \infty} \frac{\hbar}{\mu} \left[-k_I^{(1)} + \sum_{i=1}^{N1} k_I^{(1)} |S_{iI}|^2 + \sum_{j=N1+N1'+1}^{N1+N1'+N2} k_I^{(1)} |S_{jI}|^2 \right] .$$

A similar analysis of $\underset{\sim}{J}$ can be made in the rearrangement channel with the result that

$$\underset{\sim}{J}(z_1)_{z_1 \to \infty} \frac{\hbar}{\mu} \left[\sum_{k=N1+1}^{N1'} k_I^{(1)} |S_{kI}|^2 + \sum_{l=N1+N1'+N2+1}^{N1+N1'+N2+N2'} k_I^{(1)} |S_{lI}|^2 \right] .$$

From conservation of flux we must have that

$$\underset{\sim}{J}(x_1 \to \infty) + \underset{\sim}{J}(z_1 \to \infty) = 0 \quad ,$$

and as a result that

$$\sum_{i=1}^{N1+N1'+N2+N2'} |S_{iI}|^2 = 1 \quad .$$

This confirms one property of the S-matrix.[1]

References

1. N. F. Mott and H. S. W. Massey, The Theory of Atomic Collisions (Oxford, London, 1965), pp. 388 - 394.
2. (a) D. G. Truhlar and A. Kuppermann, J. Chem. Phys. 56, 2232 (1972); (b) D. G. Truhlar, Ph.D. Thesis, California Institute of Technology (Pasadena, California, 1970), pp. 214 - 218.
3. A. Kuppermann, to be published.
4. D. J. Diestler and V. McKoy, J. Chem. Phys. 48, 2941, 2951 (1968).
5. L. M. Delves, Nuclear Phys. 20, 275 (1960).

PROPOSITION I

Abstract

Exact quantum calculations of the collinear $H^+ + H_2 \rightarrow H_2 + H^+$ reaction using a realistic and modified potential energy surface have revealed sharp resonant behavior in the reaction probability. We argue that the reaction is vibrationally adiabatic, and hence that these resonances are due to the presence of a one-mathematical dimensional potential well along the reaction coordinate. We propose to calculate these resonant energies and widths approximately by making use of several bound-state stabilization methods (which have been successfully tested previously on one-dimensional well problems) to compute the resonant wavefunctions and energies. Some preliminary results are presented.

Exact quantum calculations of the collinear $H^+ + H_2(\nu=0) \rightarrow H_2(\nu'=0) + H^+$ reaction have revealed striking resonant behavior in the energy dependence of the P_{00}^R reaction probability.[1] In one set of calculations, using a modified H_3^+ potential energy surface, two resonances occur at collision energies of 0.236 eV and 0.406 eV. The respective widths are approximately 0.01 eV and 0.005 eV. Another set of calculations, making use of the realistic Preston and Tully DIM H_3^+ potential surface,[2] were performed and many resonances were found. The calculation of the reaction probability in both cases required much computer time due to the many basis functions used in the close-coupling type solution of the two-mathematical dimensional Schrödinger equation. Since the H_3^+ surface (unmodified) contains a deep well (-3.39 eV) relative to the separated reagents and products it seems reasonable that it is the major source of the resonant behavior. The modified surface has a well depth of 1.0 eV.

In natural collision coordinates (for collinear collisions) the H_3^+ motion can be decomposed into motion along and transverse to a reaction coordinate.[3] In the adiabatic approximation it is assumed that these two degrees of freedom are uncoupled.[4-7] Thus, the two-mathematical dimensional scattering problem can be reduced to a one-mathematical dimensional one. Neglecting curvature of the reaction path the Schrödinger equation for the scattering motion, given in terms of the reaction coordinate s, is

$$\left[-\frac{\hbar^2}{2\mu} \frac{d^2}{ds^2} + V(s) + \mathcal{E}_0(s) - E \right] \psi(s) = 0 \quad . \tag{1}$$

V(s) is the potential energy along the reaction coordinate, $\mathcal{E}_0(s)$ is the local vibrational eigenvalue of the motion transverse to the reaction coordinate, μ is the reduced mass of the H_3^+ system (in a suitable mass-weighted coordinate system) and E is the total energy of the H_3^+ system. The potential V(s) is shown in Figure 1 for the H_3^+ DIM surface (labeled by $\alpha = 0.0$) and for the modified surface (labeled by $\alpha = 0.5$).

Within the adiabatic approximation we propose to compute the resonance energies and widths associated with modified and unmodified V(s) potentials given in eq. (1). Such a calculation would represent the first attempt to find the resonances and widths associated with a chemical reaction in this way. Before outlining the details of the methods proposed to do this, a justification of the adiabatic approximation is made.

The reaction probability P_{00}^R for both the modified and unmodified potential surfaces remained substantial, i.e., greater than 0.6 and 0.8 for the two surfaces respectively even though other reactive channels were open. This, indicates that the reaction is reasonably adiabatic asymptotically and hence gives some justification for assuming a high degree of adiabaticity in the strong interaction region as well.

A stabilization method to compute the resonances and widths for one-dimensional scattering equations (of which eq. (1) is an example) based on the finite-difference boundary-value method (FDBVM) has recently been given by Truhlar.[8] Briefly, the method calls for the discretization of the second order differential equation (1) by a finite difference approximation, making the wavefunction obey an arbitrary boundary condition at some value (in our case two values) of the inde-

pendent variable (typically the boundary conditions are $\psi(s_1) = \psi(s_2) = 0$) and then solving the resulting eigenvalue/eigenvector equation. The boundary conditions are then changed a few times and a scan for "stable" eigenvalues is made. Such eigenvalues correspond approximately to resonance energies. Also Hazi and Taylor[9] have shown that the width associated to a given resonance Γ can be approximated by the following expression:

$$\frac{d\epsilon_i}{ds_1} \approx - \frac{2\epsilon_i}{s_1 + (2\hbar^2 k_r/\mu\Gamma)} \qquad (2)$$

where ϵ_i is the ith stable eigenvalue and $k_r = (2\mu\epsilon_i)^{\frac{1}{2}}/\hbar$. Truhlar has made use of (2) with success with the FDBVM.[10]

Another independent method (though related to the above one) to calculate resonance energies and widths was proposed by Hazi and Taylor.[9] In this method, which we propose to use also, a basis set of N_1 L^2 functions is chosen appropriately for the problem under consideration. The Hamiltonian is diagonalized within this basis set and eigenvalues and eigenfunctions are obtained. The number of functions in the basis set is then changed several times and, as before, stable eigenvalues are sought. Expression (2) can be used to calculate Γ. For the potentials shown in Figure 1 an appropriate L^2 basis set would be harmonic oscillator wavefunctions.[11]

In Table 1 we present some preliminary results on eigenvalue stabilization for the unmodified potential V(s). The potential V(s) was determined at 150 points and then a spline fit was made at a total of 700 points. The FDBVM was used to find eigenvalues for four sets of

boundary conditions. The step size in the finite difference discretization was 0.035 bohr. This should yield accuracy in the eigenvalues shown to 2 - 3 significant digits. As seen in the table (and indicated by asterisks(*)) there are four stable eigenvalues: (0.030, 0.028, 0.027, 0.024), (0.041, 0.040, 0.043, 0.043), (0.106,0.101, 0.096, 0.088), and (0.139,0.138, 0.139, 0.139). Taking the average for the four sets we conclude that four resonances should occur in the H_3^+ system at collision energies of 0.027 eV, 0.042 eV, 0.098 eV, and 0.139 eV. The exact quantum results, though not very well resolved, show resonances at approximately 0.014 eV, 0.03 eV to 0.04 eV, 0.100 eV, 0.140 eV, and higher energies. There appears to be some encouraging agreement between the approximate and exact results. However, we feel that more approximate calculations are required, especially on the modified V(s) potential. In that case there are two very well resolved exact quantum oscillations which afford an excellent opportunity for testing the approximate methods described above.

Table 1. Stabilization of eigenvalues for unmodified V(s) for H_3^+ system using the finite-difference-boundary-value method.

s_1=0.0 s_2=22.77[a]	s_1=1.0098 s_2=21.73	s_1=2.052 s_2=20.69	s_1=3.095 s_2=19.64
0.00706[b]	0.00933	0.00003	0.00630
0.01226	0.01860	0.01333	0.02367*
0.01928	0.02816*	0.02739*	0.04317**
0.02956*	0.03986**	0.04250**	0.06454
0.04046**	0.05360	0.05891	0.08777***
0.05153	0.06864	0.07671	0.11284
0.06357	0.08452	0.09603***	0.13921****
0.07697	0.10135***	0.11680	0.16736
0.09128	0.11925	0.13885****	0.19697
0.10630***	0.13817****	0.1622	0.22809
0.12211	0.15815	0.18670	0.26066
0.13876***	0.17900	0.21236	0.29458
0.15624	0.20078	0.23914	
0.17442	0.22345	0.26703	

[a] Boundary conditions in bohr.

[b] Energy eigenvalues in eV.

References

1. J. M. Bowman and A. Kuppermann, unpublished results.
2. R. K. Preston and J. C. Tully, J. Chem. Phys. 54, 4297 (1971).
3. R. A. Marcus, J. Chem. Phys. 45, 4495 (1966).
4. R. A. Marcus, J. Chem. Phys. 46, 959 (1967).
5. R. E. Wyatt, J. Chem. Phys. 51, 3489 (1968).
6. D. G. Truhlar and A. Kuppermann, J. Amer. Chem. Soc. 93, 1840 (1971).
7. J. M. Bowman, A. Kuppermann, J. T. Adams, and D. G. Truhlar, Chem. Phys. Lett. 20, 229 (1973).
8. D. G. Truhlar, Chem. Phys. Lett. 15, 783 (1972).
9. A. U. Hazi and H. S. Taylor, Phys. Rev. A1, 1109 (1970).
10. D. G. Truhlar, Chem. Phys. Lett. 26, 377 (1974).
11. L. Pauling and E. B. Wilson, Introduction to Quantum Mechanics (McGraw-Hill, New York, 1935), Chapter III.

Figure Captions

Figure 1: Comparison of the modified ($\alpha = 0.5$) and unmodified ($\alpha = 0.0$) H_3^+ potential energy surfaces along the reaction coordinate, i.e., the (same) minimum energy path.

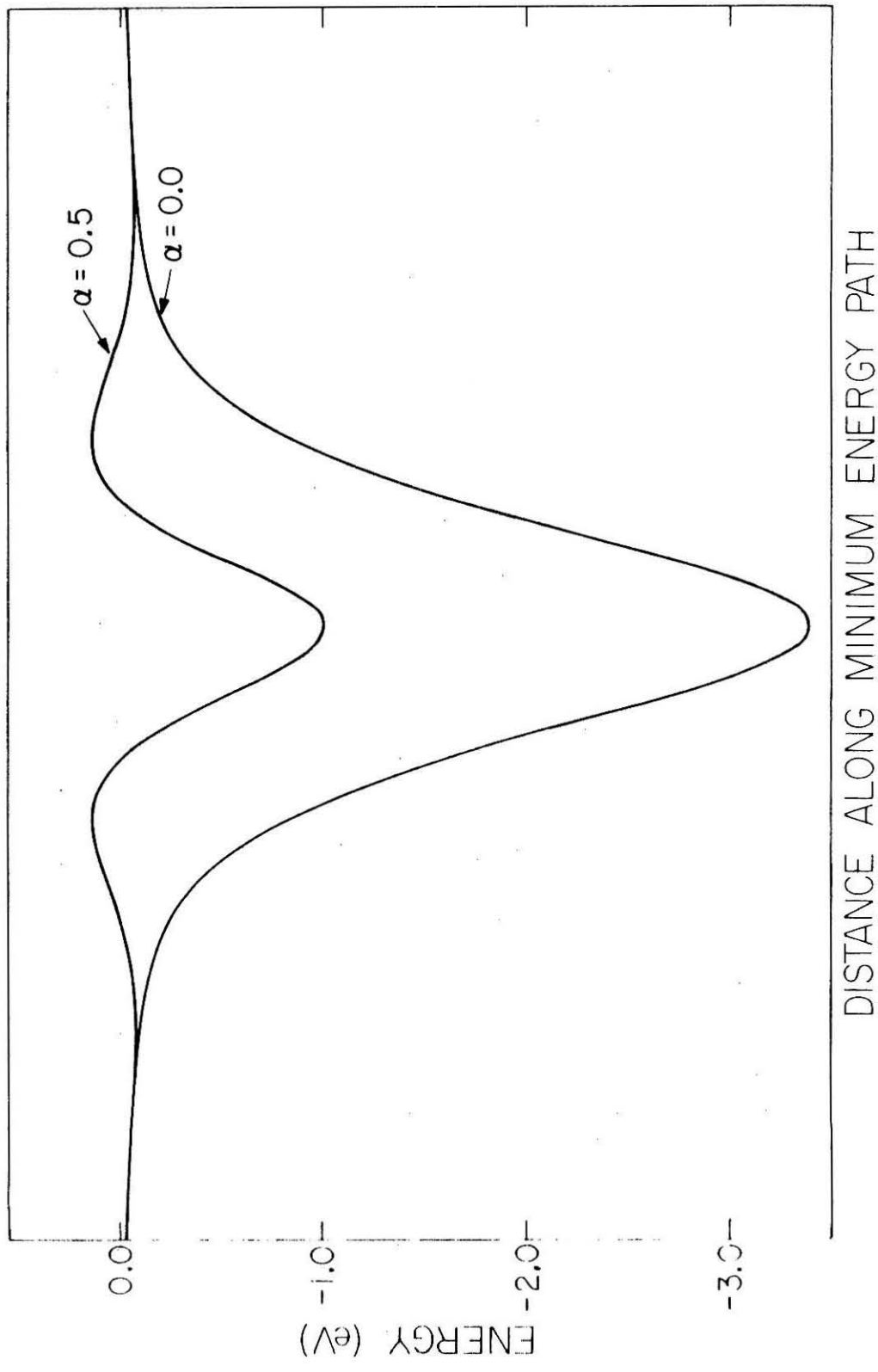
α = 0.5
α = 0.0
0.0
-1.0
-2.0
-3.0
ENERGY (eV)
DISTANCE ALONG MINIMUM ENERGY PATH

Figure 1

PROPOSITION II

Abstract

It is proposed that a three-body Ar potential energy surface be calculated within the Thomas-Fermi-Dirac method as modified and extended by Gordon and Kim. This potential energy surface, heretofore unavailable, would be useful in assessing the importance of non-separable three-body forces in the theory of liquids.

It is well-established that for liquid Ar both microscopic as well as thermodynamic properties are appreciably affected by a non-separable three-body potential. This was convincingly demonstrated in recent molecular dynamics calcuations by Barker, Fisher, and Watts.[1] In these calculations several thermodynamic properties of liquid Ar were calculated, these included the total energy and pressure as a function of temperature and volume. Agreement with experiment was good when a three-body potential was included in the calculations.

Sherwood and Prausnitz[2,3] in numerical calculations of the third virial coefficient for Ar found that three-body contributions were significant although they did not obtain very good agreement with experiment. To quote from their conclusion section: "The third virial coefficient is more sensitive to the shape of the potential function than is the second coefficient.... The calculated contribution from nonadditive attractive forces [the ones considered by Sherwood and Prausnitz] is very significant.... The size of the correction raises the question of the importance of three-body repulsive forces [i.e., short range forces]...."[3]

The three-body potential used by Sherwood and Prausnitz and Barker et al. is of the Axilrod-Teller form[4]

$$V_{123} = \nu\,(r_{12}r_{23}r_{13})^{-3}(1 + 3\cos\Theta_1\cos\Theta_2\cos\Theta_3),$$

where r_{ij} are the distances between any two Ar atoms and Θ_i are the interior angles of the triangle formed by the three Ar atoms. The parameter ν is related to the polarizability of the Ar atom α and the long range two-body C_6 parameter by the expression[5]

$$\nu = \tfrac{3}{4}\,\alpha\, C_6 \quad .$$

This potential is the long-range three-body potential and cannot be expected to be accurate when there is some overlap between any two Ar charge densities. Therefore, the potential at short range must be calculated from a different approach. A full Hartree-Fock or configuration interaction calculation would be prohibitively costly and probably unnecessary. We propose to calculate the short-range and the long-range Ar_3 potential energy surface within the Thomas - Fermi-Dirac (TFD) method[6] as applied by Abrahamson and co-workers[7] and as recently modified by Gordon and Kim.[8]

In calculations of the short-range Ar_2 potential Abrahamson assumed that the total electron density ρ could be written approximately as the sum $\rho = \rho_1 + \rho_2$ where ρ_i is the (known) charge density associated with the ith isolated unperturbed Ar atom. With this assumption the application of the TFD method is relatively simple.[9] Comparisons with experiments and other potentials indicated that the TFD potential with the assumed form for ρ gives an accurate representation of the short-range repulsive part of the Ar_2 potential.[7a] Recently, Gordon and Kim,[8] making the same assumptions as previously about the additivity of the densities ρ_i, extended the TFD idea by including a correlation term in ρ taken from the uniform electron gas model.[10] The Ar_2 potential they obtained included the attractive well and overall was in reasonably good agreement with results from previous semi-empirical calculations and molecular beam experiments.

We propose to use the TFD method as extended by Gordon

and Kim to calculate the Ar_3 potential energy surface. Briefly, to calculate the interaction energy at a given value of the internuclear distances R_{12}, R_{13}, and R_{23} requires an integration of the energy density which can be written as

$$E(\rho_{123}) = E_c(\rho_{123}) + E_T(\rho_{123}) + E_{ex}(\rho_{123}) + E_{corr}(\rho_{123}) \quad .$$

E_c, E_T, E_{ex}, and E_{corr} are respectively the bulk coulomb, kinetic, exchange, and correlation energies. The interaction energy is given by

$$V(R_{12}, R_{13}, R_{23}) = \int d^3r_1 \, d^3r_2 \, d^3r_3 \, E(\rho_{123})\rho(123)$$

where $\underset{\sim}{r}_i$ is the radius vector of the ith Ar nucleus and $\rho_i(\underset{\sim}{r}_i)$ is the associated electron density. In the expression above for the interaction energy the nine-fold integration indicated above can be reduced to at most a three-fold integration. Such integrations can be carried out efficiently using the quadrature methods of reference 8. To generate an extensive Ar_3 potential energy surface in this way would not require substantial amounts of computer time. Also, an accurate Ar density is available from Hartree-Fock claculations on Ar.[11]

Once the Ar_3 potential is generated the non-separable three-body term would be determined by subtracting from the Ar_3 potential the summed two-body potentials. The resulting three-body potential could be compared to the Axilrod-Teller one and possibly spliced on to it to generate a complete short-range and long-range three-body potential.

In addition to a re-calculation of the third virial coefficient the two- and three-body radial distribution functions $g^{(2)}$ and $g^{(3)}$ could be calculated for liquid Ar. The experiments of Mikolaj and Pings[12] revealed a linear dependence on the density of $g^{(2)}$. This indicated that the three-body potential in liquid Ar was non-negligible. Rushbrooke and Silbert[13] and Rowlinson[14] then extended the hyper-netted chain theory and the Percus-Yevick theories of liquids to include triplet potentials. Thus, the ab initio calculations of $g^{(2)}$ and $g^{(3)}$ is possible given that the three-body potential is known.

References

1. J. A. Barker, R. A. Fisher, and R. D. Watts, Mol. Phys. 21, 657 (1971).
2. A. E. Sherwood and J. M. Prausnitz, J. Chem. Phys. 41, 413 (1964).
3. A. E. Sherwood and J. M. Prausnitz, J. Chem. Phys. 41, 429 (1964).
4. B. M. Axilrod and E. Teller, J. Chem. Phys. 11, 229 (1943).
5. (a) T. Midzuno and T. Kihara, J. Phys. Soc. Japan 11, 1045 (1956); (b) T. Kihara, Advan. Chem. Phys. 1, 267 (1958).
6. H. A. Bethe and R. W. Jackiw, Intermediate Quantum Mechanics (W. A. Benajmin, New York, 1968), 2nd Edition, Chapter 5.
7. (a) A. A. Abrahamson, Phys. Rev. 130, 693 (1963); (b) A. A. Abrahamson, R. D. Hatcher, and G. H. Vineyard, Phys. Rev. 121, 159 (1961).
8. R. G. Gordon and Y. S. Kim, J. Chem. Phys. 56, 3122 (1972).
9. Ordinarily the density ρ must be found from a non-linear first-order differential equation, cf. ref. 6, p. 85.
10. See, for example, A. L. Fetter and J. D. Walecka, Quantum Theory of Many-Particle Systems (McGraw-Hill, New York, 1971), Chapters I and IV.
11. T. L. Gilbert and A. C. Wahl, J. Chem. Phys. 47, 3425 (1967).
12. P. G. Mikolaj and C. J. Pings, J. Chem. Phys. 46, 1401, 1412 (1967).

13. G. S. Rushbrooke and M. Silbert, Mol. Phys. 12, 505 (1967).

14. J. S. Rowlinson, Mol. Phys. 12, 513 (1967).

PROPOSITION III

Abstract

It is proposed to make use of vibrational adiabaticity in three-dimensional classical trajectory calculations to decrease the computer time for such calculations by as much as a factor of five. Such a reduction is necessary if quasi-classical forward and reverse reaction cross-sections are to be calculated efficiently.

The classical trajectory method has been used as reliable guide to the details of bimolecular reactions, e.g. reaction cross-section, vibrational energy distributions, etc.[1] However, the expense in computer time is quite large. As an example, consider the computer costs of the recently studied reaction $F + H_2 (D_2) \rightarrow FH (D) + H (D)$.[2] Typically, for each value of the collision energy and for H_2 in a given rovibrational state 500 - 1000 trajectories are performed. A reasonably complete study including several rotational states for the ground vibrational state and a scan of 10 collision energies would require $\approx 2 \times 10^4$ trajectories. The time to compute a trajectory varies according to the computer used. However, the way in which trajectory calculations have been carried out has been unvarying since 1965.[3] A time of 5 seconds per trajectory on a CDC 6600 has been reported.[2c] In another study[2e] the time was 20 seconds per trajectory on a CDC 7600, due mainly to the procedure for calculating the FD_2 potential surface. Taking the former time as typical, a total of $\approx 10^5$ seconds $\approx 3 \times 10^2$ hours of CDC 6600 time is required to make an adequate study of the $F + H_2 (D_2)$ reaction.

There are obviously two factors which cause the computer time to be so exhorbitant. The first is the number of trajectories to be performed and the second is the time per trajectory. The former factor is probably immutable. However, there are several ways to improve the second one. The time per trajectory is essentially determined by the length of the trajectory. For reactions like $F + H_2$ the integration is typically started when the F - H distance is of the order of 10 bohr

and terminated at roughly the same distance. Thus, a trajectory length of say 18 bohr is probably typical. The rationale for choosing the initial and final distance is based on there being a negligible interaction potential between F and H_2 at these distances.

We propose to reduce the computer time per trajectory by a factor of five by decreasing the length of the trajectory by a factor of five. We assert and propose to test that the F + H_2 reaction is to a good approximation vibrationally adiabatic except in a small region of configuration space where the curvature of the reaction path is large. This region of space is roughly 3 bohr along the reaction coordinate; hence a factor of 6 decrease in the length of the trajectory results and a concomitant decrease in computer time.

We would perform the trajectory calculations by starting and terminating the trajectory just before and after the region of strong non-adiabaticity. The final vibrational and rotational action variables would be calculated. From the fact that the reaction is adiabatic away from the region of the numerical integration it would be straightforward to perform the asymptotic scattering analysis even though the trajectory might be many bohr interior to the actual asymptotic region. A speed-up of classical trajectory calculations by a factor of five would help to make reverse quasi-classical trajectory calculations[3] feasible. In these calculations perhaps several times as many trajectories would have to be performed as compared with standard forward quasi-classical trajectory calculations. However, as recently shown in collinear calculations of the F + H_2 and F + D_2 reactions[4] the differences between forward and reverse results can be significant and hence

both should be done.

Several studies of vibrational adiabaticity in classical trajectory calculations have been carried out for the H + H_2 reaction.[5,6] Although the focus was on vibrational adiabaticity of the product H_2 some results were given as a function of the reaction coordinates. The results generally indicated that although the reaction was not very adiabatic the vibrational action showed little variation with s outside of a region of roughly 2 bohr straddling the saddle point of the potential energy surface.[5] Such results are encouraging, however, not necessarily applicable to a highly exothermic reaction like F + H_2. Thus, a vibrational adiabatic analysis should be carried out for this reaction and to determine if a speed-up of a factor of five in performing the classical trajectories can be achieved. If it can, we would propose to do the reverse three-dimensional quasi-classical trajectory calculations on the F + H_2 reaction by making use of the vibrational adiabaticity in the reaction except near the saddle-point region of the potential energy surface.

Finally, we note that while the above procedure may be valid for the vibrational degrees of freedom it may not be for the rotational ones. Depending on the desired output of the calculation this might not be very important. However, it should be studied and the extent of adiabaticity determined.

References

1. For a recent review, see D. L. Bunker, Methods of Comp. Phys. 10, 287 (1971).
2. (a) J. T. Muckerman, J. Chem. Phys. 54, 1155 (1971); (b) ibid. 56, 2997 (1972); (c) R. L. Jaffe and J. B. Anderson, J. Chem. Phys. 54, 2224 (1971); ibid. 56, 682 (1972); (d) R. L. Wilkins, J. Chem. Phys. 56, 912 (1972); (e) N. C. Blais and D. G. Truhlar, J. Chem. Phys. 58, 1090 (1973).
3. M. Karplus, R. N. Porter, and R. D. Sharma, J. Chem. Phys. 43, 3259 (1965).
4. J. M. Bowman, G. C. Schatz, and A. Kuppermann, Chem. Phys. Lett. 24, 378 (1974).
5. S.-F. Wu and R. A. Marcus, J. Chem. Phys. 53, 4020 (1970).
6. S.-F. Wu and R. A. Marcus, J. Chem. Phys. 56, 3519 (1972).

PROPOSITION IV

Abstract

It is proposed to solve the classical equations of motion pertinent to electron scattering by H and He at intermediate collision energies, i.e., $E_c \gtrsim 30$ eV. Such an approach is capable of describing direct and exchange collisions. A study of the transitions $H(1^2S) + e^- \rightarrow H(2^2S) + e^-$, and $He(1^1S) + e^- \rightarrow He(2^1S) + e^-$, $He(2^3S) + e^-$ is proposed and the possibility of utilizing semi-classical quantization of initial and final states is explored.

The use of classical mechanics in electron scattering by atoms has been very limited. Approximate classical impulse treatments of the ionization of H(1S) and (2S) by electron impact have been given.[1-3] Agreement with first-order Born claculations was good for collision energies greater than several Rydbergs. To our knowledge no other modern classical treatment of electron scattering has been attempted. This is a little surprising since there is presently no universally applied quantum approach to electron scattering. This is especially true for the intermediate collision energy range, e.g. 50 eV - 100 eV where first-order Born treatments are not reliable. Recent interest in the Glauber[4, 5] and other so-called Eikonal approximations[6] points clearly to the interest in a reliable, efficient means of doing intermediate range electron scattering calculations. Unfortunately for a system with more than two electrons, e.g. e^- + He these Eikonal approximations become rapidly inefficient.

The deBroglie wavelength of a 50 eV and 100 electron is 3.3 bohr and 2.3 bohr respectively. It may be argued that these wavelengths are small compared to the distance over which the coulomb potentials changes appreciably, i.e., say greater than 10 - 20 eV for much of the effective range of these potentials. Thus, a purely classical approach to the scattering of electrons might give a reasonably accurate description of some aspects of electron scattering in this intermediate energy range. This assertion is based on two facts in addition to the rough WKB criterion just given.[7] One is that within the classical framework the scattering of the electron by the full and rigorous interaction potential can be calculated exactly for all impact energies. This in-

cludes direct and exchange (reactive) scattering. An exact quantal treatment of the scattering has not been carried out except at very low energies and for elastic scattering[8] because of the great numerical difficulties.

We propose to carry out exact classical trajectory calculations of the total and differential cross-sections for the following collision processes:

$$e^- + H(1S) \rightarrow e^- + H(2S) \quad \text{(direct and exchange)}$$

$$e^- + He(1^1S) \rightarrow e^- + He(2^1S),\ e^- + He(2^3S) \ .$$

These calculations will be quasi-classical in the sense that the H and He atoms will be initially in approximate semi-classical 1S and 1^1S eigenstates respectively. The prescription for forming the H atom 1S state from the Bohr-Sommerfeld rules is well-known[9] as is the fact that the resulting energy eigenvalues are in exact agreement with the rigorous quantum ones. A description a lá Bohr-Sommerfeld of the $He(1^1S)$ has recently been given.[10] There it was found that the Bohr-Sommerfeld energy eigenvalue is 4.3 eV greater than the exact one. Quantization of the final state of the H or He atom is not proposed for reasons discussed later. A crude assignment of a final state can be made in the following way. A classical trajectory which transfers an amount of energy ΔE to the atom contributes to the atomic transition closest in energy to the energy of the initial atomic state plus ΔE. More sophisticated methods of assignment are possible based on a calculation of the action variables n' and k[11] for hydrogen and (approximately) for He also. Since the collision energies we propose to consider

are much in excess of the thresholds for the transitions given above, we feel that the results of the trajectory calculations will not be very sensitive to the scheme used to assign final states.

Our interest in the collision process $e^- + He(1^1S) \rightarrow e^- + He(2^1S)$ is motivated by the very interesting experimental results which show a rising differential cross-section (DCS) for scattering angles greater than 45°. Between 0° and 45° the DCS decreases monotonically by three orders of magnitude.[12] This striking behavior of DCS is not predicted at all by a variety of methods used to calculate the $1^1S \rightarrow 2^2S$ transition, e.g. Born approximation. The Glauber approximation calculations[13] does reproduce the qualitative behavior of the observed DCS, however, the quantitative agreement is poor. It is probable that the behavior of this DCS is a dynamical effect not associated to a quantum effect such as a resonance since the shape of this DCS is seen at impact energies of 29.1 eV and 40 eV. Thus, we feel confident that the classical approach outlined above will reproduce the experimental results, at least qualitatively.

We have examined the possibility of applying the semi-classical theories of Miller and Marcus[14] to the electron scattering processes given above. These theories provide a rigorous semi-classical description of both the initial and final states. Hence, the difficulty associated with "quantizing" the final in the quasi-classical approach is overcome. However, an investigation of these methods revealed a serious conceptual problem associated with the usual Bohr-Sommerfeld description of the H(1S) state (an analogous problem exists in Miller's description of the $He(1^1S)$ state[10].) To illustrate this difficulty,

consider the Bohr-Sommerfeld description of the H(1S) state. As is well known this state results from the quantization rule[11]

$$p_\theta = k\hbar, \quad k = 1 \tag{1}$$

where p_θ is the classical angular momentum of the electron. The quantization associated with radial motion is given by[15]

$$\oint p_r dr = n'\hbar, \quad n' = 0 \tag{2}$$

where p_r is the radial momentum and $\oint$ signifies an integration over one complete oscillation. The trouble is associated with the eq. (2). Since $n' = 0$ it appears as though the r-motion can be ignored. This is the origin of the idea of circular Bohr orbits. In fact it cannot be ignored, as a rigorous semi-classical description of the wavefunction immediately indicates. The correct semi-classical wavefunction is needed in the semi-classical theory.[16] Unfortunately the semi-classical wavefunction coupled with eq. (2) predicts that the probability of finding the electron with any value of r between its classical turning points is a <u>non-zero</u> constant. Clearly, this makes no physical sense. Indeed, the source of the problem is the fact that Bohr orbits violate the semi-classical uncertainty principle, $[p_r, r] = i\hbar$. According to the Bohr theory $[p_r, r] = 0$. Thus, the quantization condition (2) must be modified to take account of the uncertainty principle (perhaps by replacing n' by $n' + \frac{1}{2}$) if the semi-classical method is to be used in electron scattering applications to hydrogen and helium collisions.

References

1. M. Grzinski, Phys. Rev. 115, 374 (1959).
2. D. Banks, L. Vriens, and T. F. M. Bonsen, J. Phys. B (London) 2, 976 (1969).
3. K. C. Mathur, A. N. Tripathi, and S. K. Joshi, Phys. Rev. 184, 242 (1969).
4. R. Glauber, Lectures in Theoretical Physics (Wiley, New York, 1959), Vol. 1, p. 315.
5. See, for example, H. Tai, R. H. Bassel, E. Gerjuoy, and V. Franco, Phys. Rev. 1, 1819 (1970).
6. See, for example, J. C. Y. Chen, L. Hambro, A.-L. Sinfailam, and K. T. Chung, Phys. Rev. 7, 2003 (1973).
7. L. I. Schiff, Quantum Mechanics, third edition (McGraw-Hill, New York, 1955), p. 271.
8. C. Schwartz, Phys. Rev. 124, 1468 (1961).
9. M. Born, Atomic Physics, eighth edition (Blackie, London, 1969), pp. 103-113.
10. W. H. Miller, J. Chem. Phys. 56, 38 (1972).
11. See ref. 9, pp. 118-120.
12. For a review of the experimental results see, S. Trajmar, Phys. Rev. 8, 191 (1973).
13. A. C. Yates and A. Tenney, results quoted in ref. 12.
14. For a review, see W. H. Miller, Adv. Chem. Phys. XXV, 69 (1974).
15. See ref. 11, Appendix XIV.
16. J. M. Bowman and A. Kuppermann, Chem. Phys. 2, 158 (1973).

PROPOSITION V

Abstract

An exact quantum study of the collinear reactions

$$F(^2P_{3/2}) + H_2 \rightarrow HF + H$$
$$F(^2P_{1/2}) + H_2 \rightarrow HF + H$$
$$F(^2P_{1/2}) + H_2 \rightarrow F(^2P_{3/2}) + H$$

is proposed. We intend to make use of our existing quantal program to perform the calculations and to compare the results with the approximate pseudo-semi-classical ones of Tully. Also, an approximate quantum factorization of the problem is suggested.

The reaction of F with H_2 is of great interest since it is the pumping reaction in the HF chemical laser. This has stimulated much experimental and theoretical work in understanding the details of the $F + H_2$ reaction.

It has recently been pointed out that in the absence of spin-oribt coupling only one collision in three of $F + H_2$ has a chance of leading to reaction.[1] This is due to the fact that only one of the P orbitals of flourine bonds with the H atom to give a reactive potential energy surface.[2] Thus, the reasonable suggestion that rate constants and reaction cross-sections computed by trajectory methods should be scaled down by a factor of three was made.[1] This statistical argument is based on a neglect of spin-orbit coupling in the fluorine atom and hence the argument is only approximately valid.[3]

Very recently approximate semi-empirical "diatomics-in-molecules" calculations of the relevant $F + H_2$ potential energy surfaces and the spin-orbit coupling between them have been reported.[4] The reactions represented by these surfaces are:

(i) $F(^2P_{3/2}) + H_2 \rightarrow FH + H$

(ii) $F(^2P_{1/2}) + H_2 \rightarrow FH + H$

(iii) $F(^2P_{1/2}) + H_2 \rightarrow F(^2P_{3/2}) + H.$

Reaction (i) can proceed (electronically) adiabatically, however, reaction (ii) cannot. It must non-adiabatically "jump" to the electronic surface associated with reaction (i). The coupling which affects such a non-adiabatic transition is the spin-orbit interaction between $F(^2P_{3/2})$ and $F(^2P_{1/2})$, enhanced by collisions with H_2. Reaction (iii) is included

since it represents a non-reactive collision which is nevertheless electronically non-adiabatic.

We propose to calculate, quantum mechanically, the transition probabilities for reactions (i) - (iii) for collinear collisions. We shall make use of a computer program recently developed[5] to perform the calculations. There are several reasons for performing such a calculation. First, no quantum calculations of electronically non-adiabatic reactions have been reported. Second, several approximate semi-classical dynamical theories of such reactions have recently been developed[6-8] but remain untested against exact quantum calculations. An approximate version of one of these theories has been applied to reactions (i) - (iii) recently.[9] A third reason has to do with the nature of the spin-orbit interaction. The coupling is apparently strongest in the near asymptotic region of the reagent channel.[4] This suggests that the quantal description can, to a good approximation, be divided into two steps. The first would involve a calculations of the "jumping" probability amplitude which would be unrelated to the reaction probability amplitude. Then, given the amplitude to be "found" in a particular surface the calculation of the reaction probability could be carried out. Symbolically, the amplitude for reaction (ii) could be written as

$$T_{fi} = \sum_{j} \tau_{fj} t_{ji} \qquad (1)$$

where t_{ji} represents the amplitude to make an electronically non-

adiabatic transition from the initial state i to any intermediate state j, i.e., a vibrational state of H_2 and τ_{fj} represents the amplitude for reaction to occur from the jth state to the final state f of the product HF. Such a factorization could be tested by exact quantum calculations and if found valid, would be an extremely useful representation of electronically non-adiabatic chemical reactions.

Another point to be explored by exact quantum calculations is the choice of representation, i.e., diabatic or adiabatic[10] in which the non-adiabatic coupling is to be expressed. The diatomics-in-molecules approach can be formulated in either representation; the one chosen in reference 4 is the adiabatic one. In this representation the non-adiabatic coupling is affected by nuclear momentum operators acting on the electronic wavefunctions.[11] Such coupling is usually difficult to calculate in ab initio molecular quantum mechanics computations of the electronic wavefunctions, whereas the diabatic coupling is usually less difficult to calculate. Thus, we propose to do our quantum calculations in both representations. A possible difficulty in using the diabatic representation arises, however, due to the fact that the diabatic coupling does not vanish in the limit of infinite separation of the F and H_2 reagents. In a similar context, Mies has argued for a mixed diabatic-adiabatic representation,[12] wherein the coupling at infinity does vanish. We propose to investigate the possibility of using such a representation and hence avoid this coupling at infinite separation of the reagents. Another motivation for performing the quantum calculations in both the adiabatic and diabatic representa-

tions is to see in which representation eq. (1) is a better approximation.

References

1. D. G. Truhlar, J. Chem. Phys. 56, 3189 (1972).
2. N. C. Blais and D. G. Truhlar, J. Chem. Phys. 58, 1090 (1973).
3. J. T. Muckerman and M. D. Newton, J. Chem. Phys. 58, 3191 (1972).
4. J. C. Tully, J. Chem. Phys. 59, 5122 (1973).
5. J. M. Bowman and A. Kuppermann, unpublished results.
6. J. C. Tully and R. K. Preston, J. Chem. Phys. 55, 562 (1971).
7. W. H. Miller and T. F. George, J. Chem. Phys. 56, 5637 (1972).
8. T. F. George and Y.-W. Lin, J. Chem. Phys.
9. J. C. Tully, J. Chem. Phys. 60, 3042 (1974).
10. F. T. Smith, Phys. Rev. 179, 111 (1969).
11. See, for example, ref. 10 and references cited therein.
12. F. H. Mies, Phys. Rev. 7, 942, 957 (1973).